Mechanistic Studies on Three Areas of Organic Chemistry -

A Combined Computational and Experimental Approach

Simon Rohrbach

PhD Thesis

Department of Pure and Applied Chemistry at the University of Strathclyde

2019

I - Declaration of Ownership

This Thesis is the result of the author's original research. It has been composed by the author and has not been previously submitted for examination which has let to the award of a degree.

Date: 21/09/2019

II - Acknowledgements

This section is without any doubt going to be the most often read part of this These. So, I better make it entertaining.

All the chemistry knowledge that allowed me to write this Thesis comes from my chemistry teachers (meaning: I have not really done much but listened to them...). So, thank you, Mister Grossen for my first proper explosion, Mister Juchler - eventually, I also learnt some English (although, the dialect is almost as aboriginal as is your Haaslitiitsch dialect) - , Mister Frey - I still can't decide whether I like chemistry more because of explosives or drugs... - , Prof. Jürg Hulliger - it took me another eight years to learn how to practically solve the Schrödinger equation you suggested me to solve in my first semester at the University - , and Prof. Philippe Renaud - your career advice and support is invaluable, thank you a lot. Foremost of all, I am grateful to Prof. John Murphy for taking me in his research group and letting me choose from a delicious "menu" of projects. Thank you for your guidance and support. Many thanks also to Prof. Tell Tuttle for your help with one of these menus, the DFT soup.

I am also grateful for all critical inputs from Dr. Rushabh Shah. It was a great lesson, not only in terms of science but also in terms of how to listen to criticism. A decisive breakthrough of my work was made at GSK under your coaching. Thanks to Prof. Nick Tomkinson for the best safety advice ever ("Good idea to make enough material for the rest of your PhD. But don't forget, you also need enough fingers for the rest of your PhD") and a nice chat whenever we met while cycling to work. Many thanks to Patricia Keating for support with mass spectrometry and sharing the passion for GC (and also for not giving me hell when blowing the filament - again...). Thanks to Craig Irving for all your support and training on the NMR instruments.

A special thanks to all the members of the JAM group! To Giuseppe for the "seriousness" and to Allan for counterbalancing it. Thanks to Andrew for being truly serious - especially when extinguishing fires. Thanks to Norman for being my witness. I forgive you that you were better dressed than I was...)). Thanks to Florimond, to Polly for really good sounds in the lab (not the usual Barry White...) and to Mark for giving me a demonstration of the chaos theory - you should consider applying to the Cronin group... Thanks to Daniela, Kenny, Krystian, and Travis. You are really good guys to work with.

Many thanks to ARCHIE-WeSt and to Richard and Karina for letting me burn up 1'000'000'000 core hours in six month (which is the standard allocation of a research group per year). Now I understand why MP2 sucks. Here a couple of boilerplate phrases (but important ones!): I thank the EPSRC UK National Mass Spectrometry Facility at Swansea University for high-resolution mass spectrometry analysis. I challenged you guys with some tough samples but you always made them fly (that was not boilerplate). I also thank The University of Strathclyde and GSK for funding.

Finally, I would like to express my deep gratitude to the people who are close to me. Thanks

to my mother and father, to whom I owe everything I have. Thanks to my brother for being the smart and humble one of us. Thank you Olena, my dear wife, for your love and support. Through you I feel at home here. Also, thank you, Shroeddy, my fluffy friend, for generating cosiness wherever you go.

Thank you Venerable Geshe Kelsang Gyatso Rinpoche for giving deep meaning to my life, a role model to aspire to, and clear instructions in how to train the mind. Thank you Gen Kelsang Zamling, Gen Kelsang Machig and Gen-la Kelsang Kunsang for introducing me to the fundamentals of Buddhist philosophy such that it touched my heart. Thank you Gen Kelsang Tubchen for all your support and explanations and your pure example. Thank you Fi, Annabel, Jon, Sue, Kelsang Drolkar, Simon (I am looking forward to meet you again on the 15th at 6:30 am), Rob, Brenda and William, and Tommy (smashing washing - now I spelled it correctly). I feel very happy to have met you.

May this work benefit others.

III - Publications

Electron-Transfer and Hydride-Transfer Pathways in the Stoltz-Grubbs Reducing System (KO*t*Bu/Et_3SiH)

A. J. Smith, A. Young, S. Rohrbach, E. F. O'Connor, M. Allison, H.-S. Wang, D. L. Poole, T. Tuttle, J. A. Murphy, *Angew. Chem. Int. Ed.* **2017**, *56*, 13747–13751.

Concerted Nucleophilic Aromatic Substitution Reactions

Simon Rohrbach, Andrew J. Smith, Jia Hao Pang, Darren L. Poole, Tell Tuttle, Shunsuke Chiba, John A. Murphy, *Angew. Chem. Int. Ed.* **2019**, in press, DOI 10.1002/anie.201902216.

Neutral Organic Super Electron Donors Made Catalytic

S. Rohrbach, R. S. Shah, T. Tuttle, J. A. Murphy, *Angew. Chem. Int. Ed.* **2019**, *58*, 11454–11458.

Silylation of Amines with the KO*t*Bu-Et_3SiH Reagent System

F. Palumbo, S. Rohrbach, T. Tuttle, J. A. Murphy, manuscript in preparation. (Chapter 3)

Concerted vs. Stepwise Mechanism of the S_NAr Reaction

S. Rohrbach, T. Tuttle, J. A. Murphy, manuscript in preparation. (Chapter 4)

Arene Reduction Reactions with the KO*t*Bu-Et_3SiH Reagent System

S. Rohrbach, T. Tuttle, J. A. Murphy, manuscript in preparation. (Chapter 3)

IV - Abstract

This Thesis contains three results chapters. The underlying aim of these project chapters is to gain a detailed understanding of reaction mechanisms and to develop new synthetic methods based on this knowledge. The three results chapters come under the following titles.

Organic Super Electron Donors Made Catalytic (Chapter 2)

Neutral organic super electron donors are versatile and powerful reducing agents. So far, however, it has not been possible to use such electron donors in a catalytic sense. Also, many of these donors show significant limitations when applied in radical cascade reactions. This limitation is due to the fact that these donors form relatively long-lived radical cation species upon oxidation, which interfere with the desired radical reaction. The reason for this behaviour is, that the established classes of neutral organic electron donors are (potential) *double* electron donors. To address these shortcomings, this Thesis reports ways to generate and utilise neutral organic *single* electron donors (Scheme IV-I). According to the envisaged scheme, the organic single electron donor **(i)** is generated as an intermediate in a radical chain reaction. The hydrogen abstraction from **(iii)** by the generated radical, •R', is the chain propagation step. It becomes evident that the scheme harbours the possibility to use the single electron donor **(i)** catalytically. The aminal **(iii)** is regenerated from the benzimidazolium salt **(ii)** and a hydride source. Sodium borohydride was found to be the ideal hydride source.

The protocol was used to perform a range of 5-*exo*-*trig* radical cyclisation reactions and its applicability is demonstrated. Based on a combined experimental and computational approach, a plausible initiation pathway based on oxygen in the air is proposed.

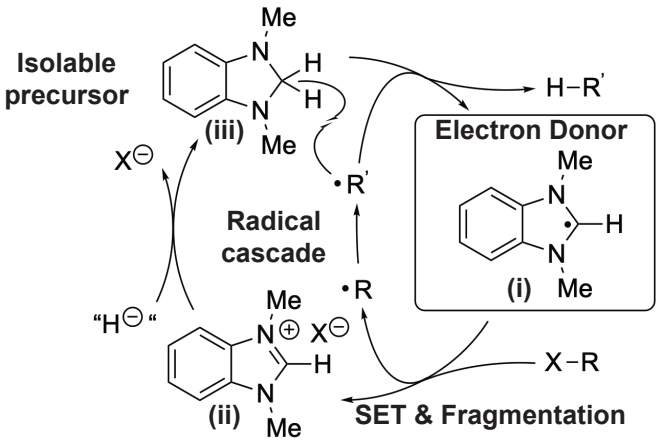

Scheme IV-I The proposed scheme for catalytic use of an organic single electron donor **(i)**.

The KO*t*Bu-Et_3SiH Reagent System (Chapter 3)

The combination of silanes and potassium *tert*-butoxide allows for various different transformations. Accordingly, several mechanistic pathways and key reactive species have been proposed to account for the different reactions in the literature (Figure IV-I). Hydride transfer mechanisms have been suggested to involve the silicate **(iv)**, which is in equilibrium with potassium hydride **(v)** and silyl ether **(vi)**. Plausible radical and single electron transfer mechanisms involve **(vii)** and **(viii)**. Finally, hydrogen atom transfer mechanisms via **(ix)** cannot be fully excluded as alternatives for many of the discussed mechanisms. The formidable challenge is to probe these different domains of reactivity separately with suitable substrates. Based on a combined approach of experimental and computational investigations, strong indications are reported for single electron transfer reactivity (presumably with species **(viii)** acting as the single electron donor) and hydride transfer mechanisms. Additionally, plausible mechanisms for the silylation reaction of amines **(x)** to give the silylated species **(xi)** are proposed based on computational studies (Scheme IV-II).

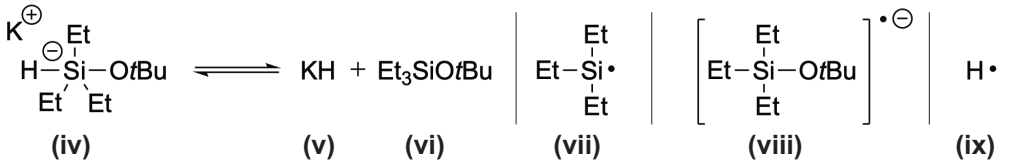

Figure IV-I Proposed key species that are responsible for the reactivity of the KOtBu-Et_3SiH reagent system.

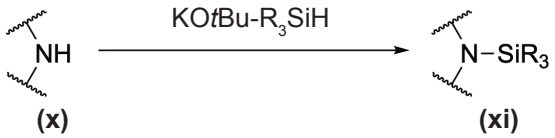

Scheme IV-II What is the mechanism of the silylation reaction of simple amines with the KO*t*Bu-Et_3SiH (or more generally the KO*t*Bu-Silane) reagent system?

Concerted vs. Stepwise S_NAr Mechanism (Chapter 4)

Over the last decades, more and more reports accumulated in the literature that suggested certain S_NAr reactions follow a concerted pathway. These days, the combined impact of these investigations has reached a critical momentum and it seems appropriate to fundamentally question the long established mechanistic picture of the S_NAr reaction. High level computational (wave-function based) methods are here employed to benchmark DFT functionals, based on whether these correctly predict the mechanism of a S_NAr reaction to be stepwise or concerted. A reliable functional is then used to establish trends, which show what aspects (nucleophile, counter cation, leaving group, aromatic system) of the reaction at hand influence its mechanistic propensity, and in what way. Eventually this allowed estimation of when an S_NAr reaction follows a concerted and when a stepwise pathway is taken.

V - Terms and Abbreviations

1,2-DCE	1,2-Dichloroethane
1,4-DMP	1,4-Dimethylpiperazine
Ac	Acetyl
acac	Acetylacetone
ACN	Acetonitrile
AIBN	Azobisisobutyronitrile
Ar	Aryl
ATR	Attenuated total reflectance
b.p.	Boiling point
BHAS	Base-promoted homolytic aromatic substitution
CI	Chemical ionisation
cS_NAr	Concerted nucleophilic aromatic substitution
Cy	Cyclohexyl
d.r.	Diastereomeric ratio
DABCO	1,4-Diazabicyclo[2.2.2]octane
DBU	1,8-Diazabicyclo[5.4.0]undec-7-ene
DCM	Dichloromethane
$dF(CF_3)ppy$	3,5-Difluoro-2-[5-(trifluoromethyl)-2-pyridinyl-*N*]phenyl
DFT	Density functional theory
DIAD	Diisopropyl azodicarboxylate
DMA	*N,N*-Dimethylacetamide
DMAP	*p*-Dimethylaminopyridine
DMBI	1,3-Dimethyl-2-phenylbenzimidazoline
DMF	*N,N* -Dimethylformamide
DMPU	1,3-Dimethyl-3,4,5,6-tetrahydro-2(1H)-pyrimidinone
DMSO	Dimethyl sulfoxide
DTBP	*Di-tert*-butyl peroxide
dtbpy	4,4'-*Di-tert* -butyl-2,2'-dipyridyl
E1	Unimolecular elimination
E1cB	Elimination unimolecular conjugate base
E2	Bimolecular elimination
$E_{1/2}$	Half-wave potential
$E_{p/2}$	Half-peak potential
E_p^{ox}	Oxidation peak potential
EI	Electron ionisation

ESR	Electron spin resonance
Et	Ethyl
eV	Electron volt
EWG	Electron-withdrawing group
Fc	Ferrocene
FID	Flame ionisation detectors
GC	Gas chromatography
HOMO	Highest occupied molecular orbital
HRMS	High resolution mass spectrometry
IRC	Internal reaction coordinate
KHMDS	Potassium bis(trimethylsilyl)amide
LC	Liquid chromatography
LED	Light emitting diode
LUMO	Lowest unoccupied molecular orbital
Me	Methyl
MS	Mass spectrometry
Ms	Methansulfonyl
*μ*W	Microwave
n.d.	Not detected
NBS	*N*-Bromosuccinimide
*n*Bu	*n*-Butyl
NCS	*N*-Chlorosuccinimide
NIS	*N*-Iodosuccinimide
NMR	Nuclear magnetic resonance
o/n	Overnight
Oct	*n*-Octyl
p*K*a	Negative of the common logarithm of the acid dissociation constant
PEG	Polyethylene glycol
Ph	Phenyl
Piv	Pivaloyl
ppb	Parts per billion
ppm	Parts per million
PRC	Polarity reversal catalyst
PTFE	Polytetrafluoroethylene
RT	Room temperature
SCE	Saturated calomel electrode
SED	Super electron donor
SET	Single electron transfer
S_N1	Unimolecular nucleophilic substitution
S_N2	Bimolecular nucleophilic substitution
S_NAr	Nucleophilic aromatic substitution
SOMO	Singly occupied molecular orbital
STAB	Sodium triacetoxyborohydride

*t*BME	*tert*-Butyl methyl ether
*t*Bu	*tert*-Butyl
TDAE	Tetrakis(dimethylamino)ethylene
THF	Tetrahydrofuran
TLC	Thin-layer chromatography
TMS	Tetramethylsilane
TTF	Tetrathiafulvalene
TTMSS	Tris(trimethylsilyl)silane

VI - Table of Contents

1. Introduction

This Thesis encompasses three topics, which are the development of a potent single electron donor that can be used in a catalytic sense (Chapter 2), investigations of the various mechanistic pathways accessible to the KO*t*Bu-Et_3SiH reagent system (Chapter 3) and theoretical studies of the concerted nucleophilic aromatic substitution mechanism (Chapter 4). Accordingly, the following literature overview is subdivided in three sections to cover the relevant literature for the three following chapters. In the first part, neutral organic electron donors are reviewed (Section 1.1 to Section 1.4). In the second part an overview of the relevant literature examples of the KO*t*Bu-Et_3SiH reagent system (Section 1.5) is given and in the last part a critical analysis of literature reports on cS_NAr reactions is given (Section 1.6).

1.1. Properties of Organic Electron Donors

1.1.1 Overview

The potential of organic molecules to engage in redox reactions has received more and more attention during the last decades. For example, with the dawn of photoredox catalysis, it became critical to understand the oxidation and reduction potentials of the species involved in the reaction.[1]

Attempts to find organic molecules with exceptionally negative redox potentials led to the fascinating discovery of so-called organic “super electron donors” (SED), which are capable of injecting an electron into the π-system of benzene rings.

In the following, an overview of neutral organic electron donors from simple and weakly reducing aliphatic amines up to the most reducing known representatives is given. The emphasis lies on the properties of the electron donors under thermal conditions rather than photochemical conditions. Following a discussion of the properties of organic electron donors, their applications in bond-forming and bond-breaking reactions are reviewed. Of particular interest, in light of this thesis, is the applicability of super electron donors in reductive radical reactions.

In their review on organic electron donors, Broggi et al. classified the relevant species into six groups based on key structural motifs (Figure 1-1):[2]

i. Amines (for example DABCO **1**)
ii. Tetrathiafulvalenes (for example **2**)
iii. Tetraaminoethylenes (for example **3**)
iv. Tetraazafulvalenes (for example **4**)
v. Bispyridinylidenes (for example **5**)
vi. Further Organic Electron Donor Scaffolds

Up to the bispyridinylidenes, this ordering is roughly in line with increasing reducing power.

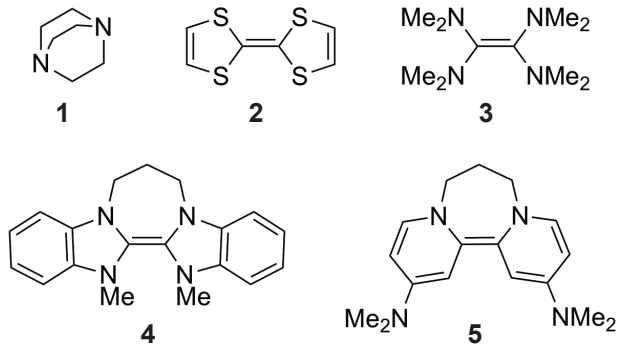

Figure 1-1 Classes of organic electron donors.

The amine electron donors are the weakest class of electron donors. They are typically used in large excess at elevated temperatures and can only reduce a limited range of substrates. Moreover, some structurally privileged amines can play key roles as redox shuttles in photochemical reactions or overall oxidative processes. Tetrathiafulvalenes have one key representative, compound **2**, which can be used in radical-polar crossover reactions.[3] The class of tetraaminoethylenes has one representative as well that stands out - TDAE **3** - and that finds application in several interesting reductive bond-forming reactions.[4,5] However, the substrate scope is limited to a few classes of electron-poor structures. Tetraazafulvalenes and bispyridinylidenes typically can reduce iodobenzene derivatives and can convert them to the aryl anion through the transfer of two electrons. Only in a few cases can evidence of radical intermediates be found.[6-8]

When this thesis was written, the record-holding donor in terms of oxidation potential belonged to the group of bispyridinylidenes.[9] However, it should be noted that the reduction power achieved with compounds belonging to the group of tetraazafulvalenes and bispyridinylidenes can be very similar.

There are further scaffolds which can give rise to highly reductive organic compounds that cannot be grouped together with one of the above-mentioned scaffolds. In the following, representatives of the six classes of electron donors are introduced in more detail.

1.1.2 Electrochemical Properties of Aliphatic Amines

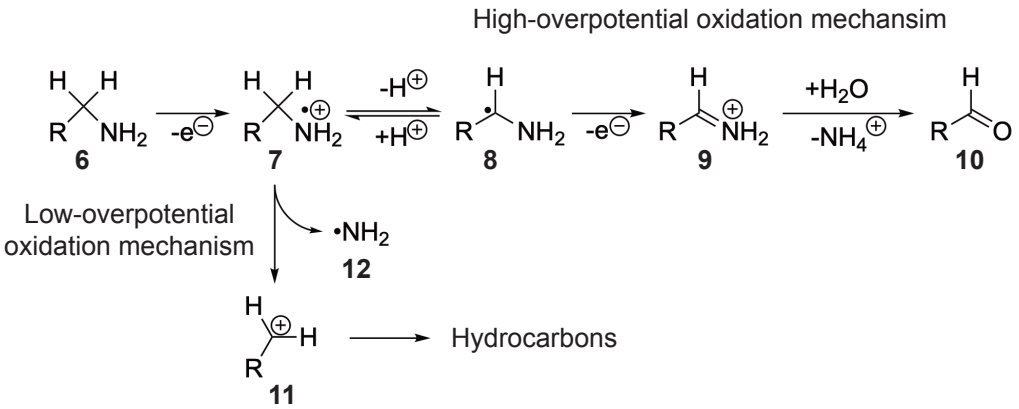

Scheme 1-1 Electrochemical oxidation of aliphatic amines.

Most of the neutral organic electron donors contain nitrogen-based functional groups that are key to their reactivity. In these electron donors, the nitrogen atoms are part of a π-system in one way or another. The focus of this section, in contrast, lies on fully saturated amines. Amines typically react as bases (Lewis or Brønsted) or nucleophiles. Less commonly but intriguingly, they can participate in redox reactions. There are very few examples of such amines that can give rise to significantly stable radical cations when oxidised. DABCO **1** appears to be a particularly privileged structure in this regard.

The oxidation of aliphatic amines has been studied extensively with electrochemical techniques.[10,11] Typically amines undergo irreversible oxidation at electrodes due to rapid decomposition of the radical cation species. A high- and a low-overpotential oxidation mechanism have been suggested (Scheme 1-1).[10] The initial oxidation of the primary amine **6** gives the radical cation **7**, which is in equilibrium with the nitrogen-stabilised radical **8**. At high overpotential, species **8** is oxidised further to the iminium cation intermediate **9**, which, after hydrolysis gives the aldehyde product **10** and an ammonium ion. When less positive potentials are applied, the decomposition reaction can show significant branching at the intermediate **7**. This intermediate can fragment into the carbocation **11** and the aminyl radical **12**. Then the carbocationic intermediate **11** can either react with the solvent as an electrophile or lose a proton. The aminyl radical **12** is likely subject to further oxidation. Analogous decomposition pathways have been proposed to operate with other amines which feature α-hydrogen atoms.[10,11]

The electrochemical behaviour of DABCO **1** stands in sharp contrast to these general oxidation mechanisms of aliphatic amines. McKinney and Geske were among the first who realised the special electrochemical properties of this compound, i.e. the relatively long half-life of several seconds of the radical cation species.[12] From the EPR spectrum, McKinney and Geske deduced that the cation has the same symmetry as the neutral DABCO molecule (D_{3h}).[12]

What makes the DABCO-radical cation so exceptionally stable? Two different aspects of the structure of DABCO were pointed out by McKinney and Geske, on the basis of which its electrochemical properties can be discussed.[12] In the more simple picture, the remarkable stability of the DABCO radical cation arises as a result of the spacial proximity of the two nitrogen atoms. Hence, the effect would solely depend on the distance between the nitrogen atoms (2.55 Å of DABCO[13,14]). The more elaborate picture considers through-bond interactions of the nitrogen atoms as a key factor in the stabilisation of the radical-cation state. These through-bond stabilising effects would critically depend on the geometry of the motif, i.e. the hyperconjugation between the nitrogen lone-pairs and the adjacent carbon-carbon bonds. In the case of DABCO, the lone pairs on the nitrogen atoms and the σ*-orbitals of the three

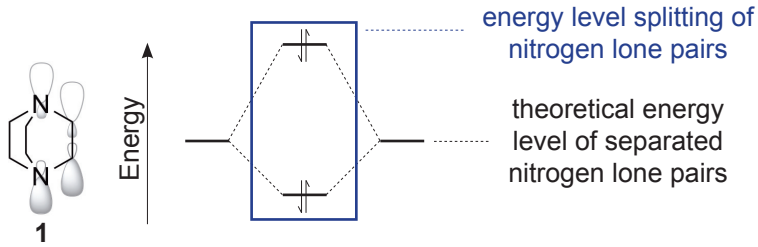

Figure 1-2 The nitrogen lone-pair orbitals align with the σ*-orbitals of the carbon-carbon bonds in DABCO.

carbon-carbon bonds are all aligned in the same direction (Figure 1-2).

In the neutral DABCO molecule, the lone-pair orbitals are split into two energy levels. The low ionisation potential indicates that the energy of the HOMO is raised compared to other amines. Further, the HOMO - HOMO-1 splitting is large compared to other structurally related diamines. This underlines that the efficient electronic communication of the nitrogen atoms occurs through the ethylene bridges and not through space.[15]

Calculations have shown that, upon oxidation of DABCO, the carbon-carbon bond distance significantly increases, while the carbon-nitrogen bond shortens and the carbon-carbon-nitrogen angle decreases.[16] These structural changes show that the interaction of the nitrogen lone-pairs and the σ*-orbitals of the carbon-carbon bonds is accentuated in the DABCO radical cation. While the splitting of the lone-pair orbitals is energy-raising in the neutral form of DABCO, it is overall stabilising in the radical cation form.

The decomposition pathways of the DABCO-radical cation **13** have been examined in detail for the electrochemical oxidation (Scheme 1-2).[17] It was found that at least three processes run in parallel. These are one first-order decay of the radical cation (Pathway 1) and two second-order decay processes (Pathways 2 and 3). The (pseudo) first-order decay process is a hydrogen abstraction by the DABCO-radical cation **13** from an abundant hydrogen source such as the solvent or the electrolyte (in their study, the authors used acetonitrile and tetrabutylammonium chloride, respectively). The two second-order processes involve two DABCO-derived species. In Pathway 2, a neutral molecule of DABCO **1** and a DABCO-radical cation **13** undergo either a hydrogen transfer (Pathway 2a) or a proton transfer (Pathway 2b). The products of both processes are the same, namely protonated DABCO **14** and the DABCO α-aminoalkyl radical **15**. The third pathway involves two molecules of the DABCO-radical cation **13**. These undergo a hydrogen-transfer disproportionation to give protonated DABCO **14** and the diradical **16**. A computational investigation of the latter species suggests that the two spin-carrying orbitals are, indeed, orthogonal to each other.[17]

The remarkable electrochemical properties of DABCO **1** led to its use as a redox shuttle in several instances.[18,19]

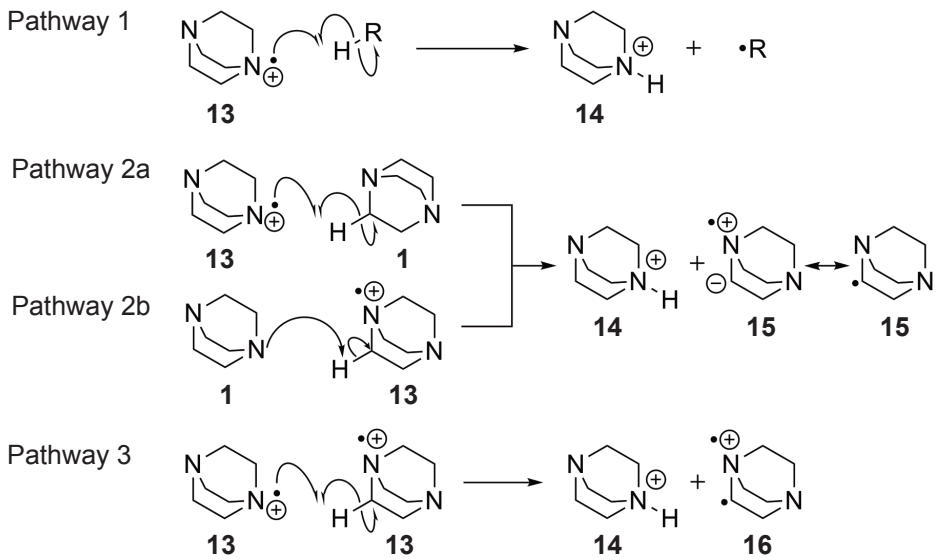

Scheme 1-2 Three decay processes have been discussed for the DABCO-radical cation.

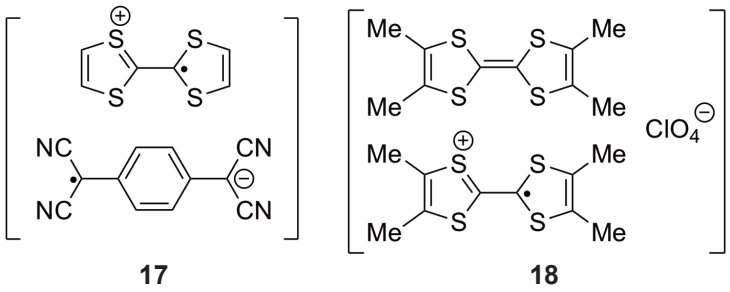

17 **18**

Figure 1-3 Tetrathiafulvalene structures are building blocks in many organic conductors.

1.1.3 Electrochemical Properties of Tetrathiafulvalenes

Tetrathiafulvalenes received considerable attention mainly due to their electronic properties. The charge-transfer compound **17**, for example, is a milestone in the development of organic conductors. Also the salt **18** is remarkable as it shows superconductivity.[20]

The archetype compound of the tetrathiafulvalene (TTF) class is **2** (Figure 1-4). Compound **2** was first synthesised by Wudl et al. after the intriguing electrochemical properties of other tetrathiafulvalene analogues fostered interest in the compound class.[21] Later on the discussion of the reactivity of tetrathiafulvalenes will mainly focus on compound **2**. But first it is worthwhile to take a look at a simple series of tetrathiafulvalene species with significantly different oxidation potentials.

Based on the four compounds in Figure 1-4, it is possible to illustrate two structural features that critically influence their oxidation potential. If the π-system of the molecules is extended by fused benzene rings, the oxidation potential becomes more positive. This can be seen from comparison of the oxidation potentials of **2**[2] with **19**[22] and from comparison of **20**[23] with **21**.[24] The other key characteristic is the quinone-derived central ring in **20** and **21**. Both compounds exhibit a more negative oxidation potential than their analogues, which lack the central quinone-derived ring, **2** and **19**, respectively. There are two reasons why the quinone-derived motif leads to more negative oxidation potentials. First, the accumulated charge in the cationic state is spatially more separated and delocalised over a larger π-system. Second, the central ring in **20** and **21** gains aromaticity upon oxidation. As will become evident from later discussions, these features outlined here are general and apply also to other classes of neutral organic electron donors.

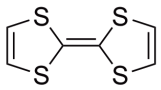

2
0.32 V (0.71 V)

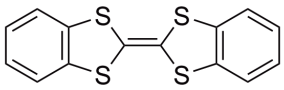

19
0.62 V (0.97 V)

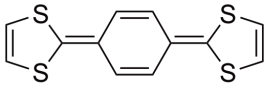

20
-0.11 V (-0.04 V)

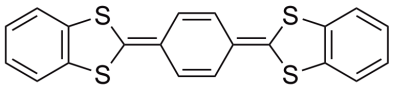

21
0.06 V (0.33 V)

Figure 1-4 Oxidation potentials are reported *vs.* SCE in ACN with the exception of **19**, which was analysed in DMF. The second oxidation potential is shown in brackets.

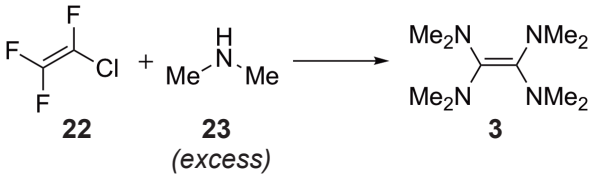

22 **23** (*excess*) **3**

Scheme 1-3 TDAE can be obtained by treating chlorotrifluoroethylene with dimethylamine.

1.1.4 Synthesis and Electrochemical Properties of Tetraaminoethylenes

The synthesis of the parent compound of the tetraaminoethylene class, TDAE **3**, was first described by Pruett et al. During their studies they found that chlorotrifluoroethylene **22** was converted to TDAE **3** when it was treated with an excess of dimethylamine **23** (Scheme 1-3). The authors noticed that the compound produces chemiluminescence in contact with air, which indicated its interesting reactivity.[25]

A comprehensive study of the compound class became possible when Wanzlick et al. described an alternative entry to the tetraaminoethylene core structure (Scheme 1-4).[26-28] The thermodynamic and kinetic characteristics of the equilibrium depicted in Scheme 1-4 were later reviewed by Alder et al.[29] Despite the fact that a range of tetraaminoethylenes has been examined, no compound from this class found as many synthetic applications as a reducing agent as the parent compound TDAE.[2]

It was reasoned that, in compounds such as **25,** the extended π-system lowers the energy of the first antibonding orbital, which happens to be the HOMO.[28] Another reason may be that the phenyl group substituents in **25** are inductively less electron-donating than are the methyl groups in TDAE **3**. Consequently, molecules with aromatic substituents as **25** are generally weaker electron donors than TDAE **3**. Therefore they never got the importance of TDAE **3** as reducing agents. Indeed, it is not their property as reducing agents, that species such as **25** became famous for but the equilibria they participate in with their monomers **24** and the carbene-nature of **24** (Scheme 1-4).[27]

TDAE shows reversible electrochemical behaviour.[2] Depending on the solvent, either two one-electron redox events or one two-electron redox event can be observed. In acetonitrile, two redox events can be resolved ($E_{1/2}$ = -0.78 V and -0.61 V vs. SCE).[30,31] These two redox waves coalesce in the more polar solvent DMF to one wave at $E_{1/2}$ = -0.62 V vs. SCE.[30] The electrochemical behaviour demonstrates that TDAE can be engaged in single electron transfer reactions.[2]

1.1.5 Synthesis of Tetraazafulvalenes

The tetraazafulvalenes (Scheme 1-5) are the nitrogen analogues of the tetrathiafulvalenes (Figure 1-4) and are typically synthesised from the imidazole- or benzimidazole-derived

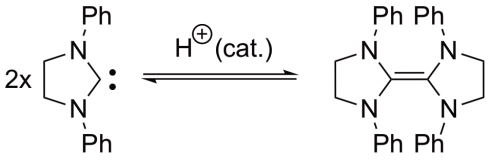

24 **25**

Scheme 1-4 An example of a Wanzlick-carbene **24** and the equilibrium it can participate in.

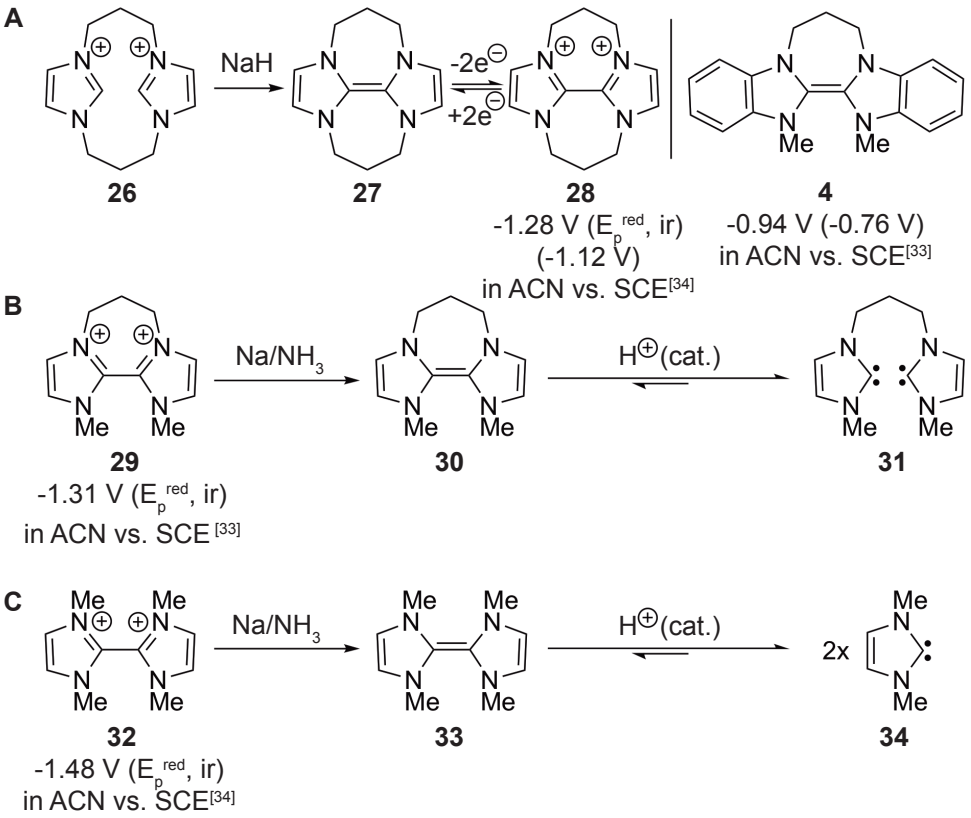

Scheme 1-5 The more flexibly the two imidazole units are tethered the more unstable the corresponding electron donors are. If a second redox event is observed, the more positive value is given in brackets. (ir) means irreversible and the peak potential of the reduction wave is given.

carbenes. In one of his early reports on carbenes, Wanzlick pointed out that imidazole-derived carbenes are significantly more stable than the ones derived from the more saturated counterpart imidazoline.[27,29] Consequently, the proton-catalysed equilibrium between imidazole-derived carbenes (and their benzimidazole analogues) and the corresponding dimers is shifted towards the monomers. Hence, electron donors belonging to the class of tetraazafulvalenes typically feature one or two bridging alkyl chains that hold the two subunits together and thereby shift the equilibrium towards the dimerised carbenes. The doubly propylene-bridged electron donor **27** is accessible from the dication **26** via carbene intermediates and can be isolated in solid form (Scheme 1-5 A).[32] Similar to the case of TDAE, one two-electron redox wave was observed for the redox couple **27**/**28** in the polar solvent DMF. The system shows good electrochemical reversibility ($E_{1/2}$ = -1.20 V vs. SCE in DMF).[33]

In contrast to **27**, the electron donors **30** and **33** were found to be accessible only via reduction of the dication precursors **29** and **32**, which already have a central σ-bond in place (Scheme 1-5 B and C). Once formed, **30** and **33** were found to equilibrate quickly to the carbene species **31** and **34** with a half-life of hours and minutes, respectively.[35] The fast dissociation to the carbenes **31** and **34** may be the reason why it was not possible to form the electron donors **30** and **33** in an electrochemical set-up while this approach was successful with compound **27**.[36] Clearly, the bottle-neck in the synthesis of **30** and **33** is the final step. In

contrast, the most demanding part in the synthesis of **27** is the formation and purification of the macrocyclic precursor **26**.[35]

1.1.6 Synthesis and Electrochemical Properties of Bispyridinylidenes

The bispyridinylidenes are a diverse class of electron donors harbouring structures such as **35**,[37] **36**,[38] **37**[39] and **38**[40] with intriguing electrochemical properties (Figure 1-5). The record-holding electron donor **40**[9] in terms of its oxidation potential to date belongs to this compound class, too, as do the three previous record holders **38**, **5**[7] and **39**.[41]

The radialene **35** introduced and studied by Rheingold et al. is not as strongly reducing as other representatives of this compound class.[37] In fact, it stands out as a redox active organic molecule for another reason. The compound shows one reversible four- and one two-electron redox wave in cyclic voltammetry experiments. It is the first organic molecule which shows a four-electron redox step for a single electrochemically active centre. The four-electron reduction happens between the fully oxidised state (charge +6) and the dicationic state. The four-electron reduction of the fully oxidised state is accompanied by large structural changes. It has been suggested that these structural changes are at the heart of a potential inversion that makes the transfer of the last three electrons more favourable than the transfer of the first electron.[37]

The viologen **36** has been investigated in detail as well as its radical cationic and its dicationic derivatives. It is one of few examples where a crystal structure was recorded for the

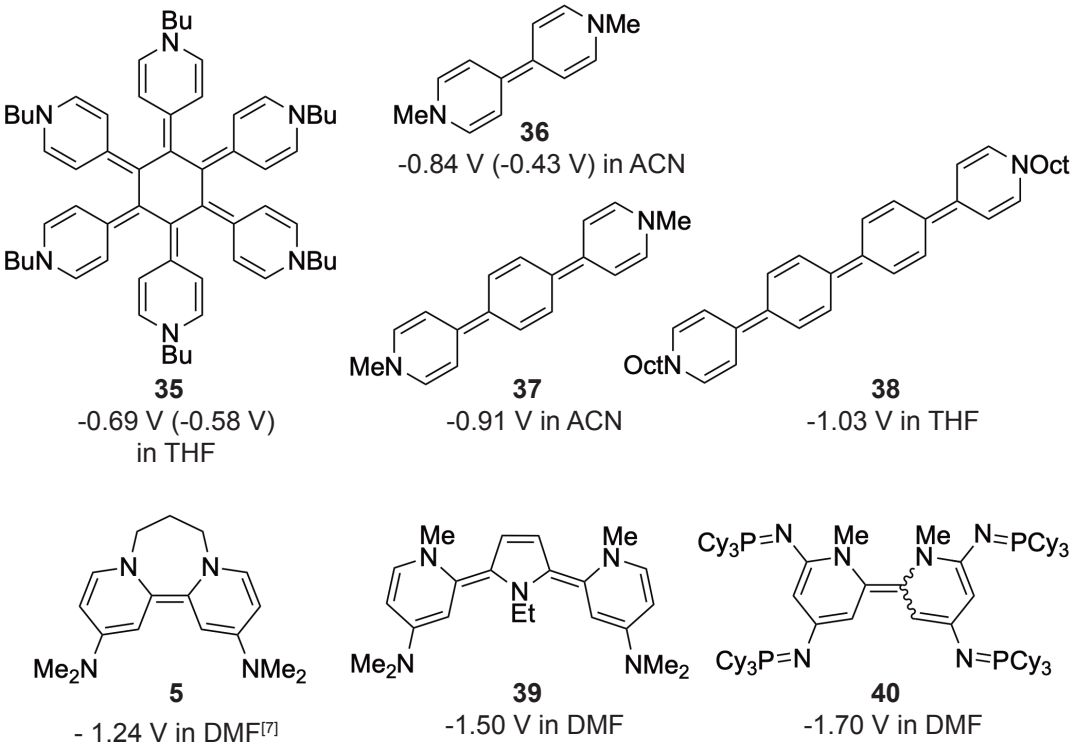

Figure 1-5 Important representatives of the bispyridinylidene electron donor class. Values for $E_{1/2}$ are vs. SCE. If a second redox event is observed, the more positive value is given in brackets.

radical cation oxidation state (with hexafluorophosphate as the counter anion). Strikingly, the compound undergoes partial disproportionation in the crystal as was concluded i. a. from the fact that the molecule exists in two different structures in the crystal.[38] It is also noteworthy that the first and the second oxidation potential of **36** are relatively far apart on the potential scale with a difference of *ca.* 0.4 V. For comparison, compound **4** with a comparable first oxidation potential shows also two redox waves. These are, however, less than half as far apart with a separation of 0.18 V.[33] The large separation of the two redox waves of compound **36** is also in contrast to the electrochemical behaviour of the analogous, extended viologens **37** and **38**. Both extended viologens show only one two-electron redox event. Moreover, the extended viologens become successively more reducing as the number of rings in the molecule increases. It has been reasoned that the extended viologens **37** and **38** are more reducing than parent compound **36** because, upon oxidation, not only two but three and four rings gain aromaticity, respectively - i.e. the aromatic driving force behind the oxidation process increases with the increasing number of rings. An additional factor is that in the oxidised form of **36**, the accumulated positive charge concentrates on a comparatively small structure. The charge is better separated in the oxidised forms of **37** and **38**.[40]

Initially developed as an n-dopant for organic semiconductors, **38** was found to be the strongest neutral organic reducing agent at the time of its characterisation. The electronic structure of **38** posed some questions. There is an indication from ^{1}H-NMR and EPR studies and X-ray diffraction experiments that the compound does not only exist in closed shell form - both in solution and in the solid state. It has been suggested that open shell singlet or triplet states can be populated under ambient conditions (Scheme 1-6).[40] Later the problem was revisited by Raman spectroscopy and computational studies.[42] Indeed, it was demonstrated that a triplet diradical state is accessible in the solid state and in solution under ambient conditions. The reason why an EPR experiment does not give conclusive results for compound **38** while Raman spectroscopy does, was thought to be due to the different timescales of the events the two techniques probe. The vibrational motion probed by Raman is short compared to the lifetime of the singlet or triplet state. In other words, intersystem crossing does not occur on the timescale of the Raman experiment. Consequently, singlet and triplet vibrational motions can be resolved. On the longer EPR timescale, however, the system undergoes multiple intersystem crossing events, which lead to a massive broadening of the EPR signals.[42] There are a number of compounds that show similarly intriguing electronic structure.[43]

Further increase of the reducing power was achieved by adding electron-donating substituents to the pyridine core, which leads for example to electron donors consisting of DMAP

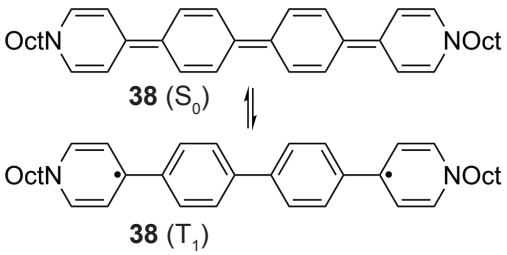

Scheme 1-6 The singlet ground state and excited triplet state of **38** are both populated at ambient conditions.

moieties such as **5**.[7] Compound **5** marked a milestone in the development of the bispyridinylidene electron donors. One of the key features that make the electron donor **5** so attractive, is the short and relatively easy synthesis (Scheme 1-7). The formation of the precursor salt **42** is achieved in one step from 1,3-diiodopropane and DMAP **41**. In the second step the central double-bond is formed in an analogous way to how most tetraazafulvalene donors are generated. Treatment of the precursor salt **42** with a base yielded the target compound. It was suggested that a carbene intermediate **43** resulted after the first deprotonation, which nucleophilically attacks the neighbouring pyridinium moiety. A second deprotonation of **44** leads down to the product **5**.[7] The ready accessibility of the donor certainly fostered its extensive study.

Several analogues of the DMAP-derived electron donor **5** were examined by Murphy et al. based on the successful synthesis of **5** (Scheme 1-7). Modification of the alkyl linker and simple substitutions of the dimethylamine groups, however, did not bring significant increases of donor strength.[44] Modification in the core structure, in turn, proved to be more rewarding. The compound **39** was found to be significantly more reducing than **5**.[41] Analogous to the series of viologens, **36** - **38**, it was reasoned that the more negative oxidation potential of **39** was due to the gain of aromaticity in three rings instead of just two rings as in compound **5**. Unfortunately, it was not possible to record conclusive NMR spectra of the reduced form of **39**. The EPR spectra were inconclusive as well.[41] This is most likely because open-shell configurations are populated, similarly to what was observed with the extended viologen **38** (Scheme 1-6).[41,42]

Dyker et al. examined the effect of electron donating substituents on the fundamental bis-pyridine core in more detail. Eventually, they came up with the rather exotic phosphine imine group, -N=PCy_3, which is superior to the dimethylamine group -NMe_2 as an electron-donating (+M) substituent.[45] Amongst other interesting compounds, the study culminated in the development of **40**, which is the strongest ground-state organic reducing agent to date.[9]

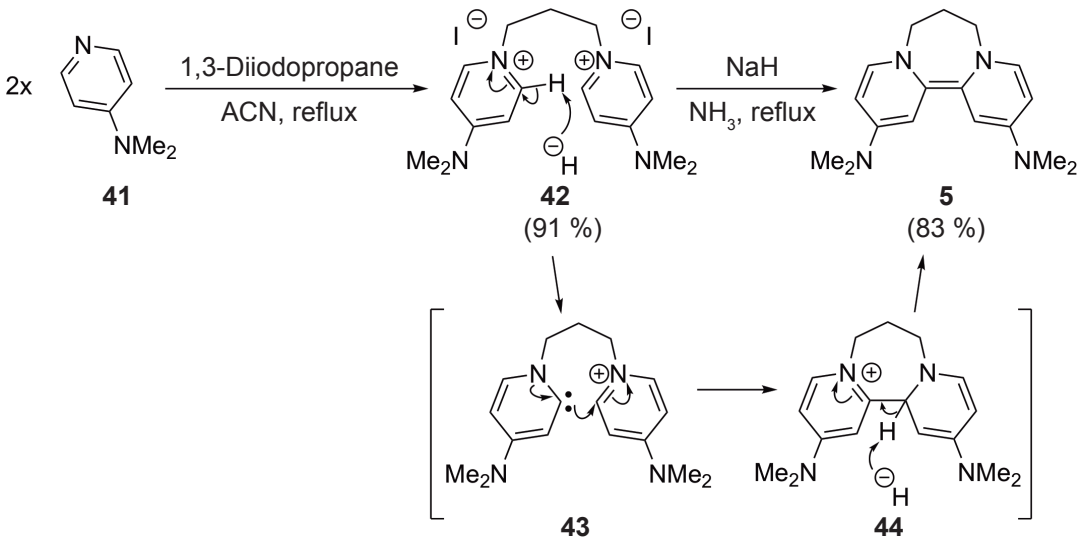

Scheme 1-7 The short synthesis of electron donors built from two DMAP units was an important step in the development of bis-pyridine electron donors.

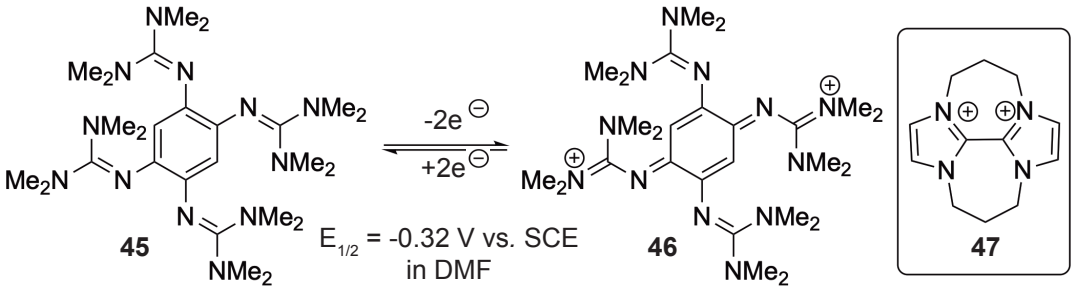

Scheme 1-8 It has been proposed that - in apolar solvents - **45** can compete with the strongest electron donors. In the dicationic form **46** the charge is more delocalised than for example in **47**.

1.1.7 Further Organic Electron Donor Scaffolds

The electron donor **45** (Scheme 1-8) was found to be only moderately reducing, based on its redox potential in acetonitrile.[46] While the gain in aromaticity was found to be a critical feature of the tetraazafulvalene and bispyridinylidene donors,[47] the compound **45** seems to lose aromaticity upon oxidation.[46] Computational studies suggested, however, that **45** may be more reducing than the imidazole donor **27** in apolar solvents with a dielectric constant $\varepsilon < 3$ (for example toluene or 1,4-dioxane). In the dication **46**, the positive charge is more delocalised than it is in **47**. As a result the dication **46** depends to a lesser extent on stabilisation by the solvent than does the dication **47**.[46]

The porphyrin derivative **48**[48] is interesting as it shows antiaromatic properties in its reduced form and aromatic properties once it is oxidised (Figure 1-6). Apparently, the central ethylene unit is rather small, such that the porphyrin scaffold cannot adopt a planar conformation in either the reduced form or the oxidised form. Hence, although antiaromaticity doubtlessly manifests in the ^{1}H-NMR spectrum, the bending of the molecule observed by X-ray diffraction experiments is not only due to a Jahn-Teller distortion.[48]

All donors introduced so far, but the simple amines, rely on one or more electron-rich carbon-carbon double-bonds. An alternative to that very central motif was made accessible by

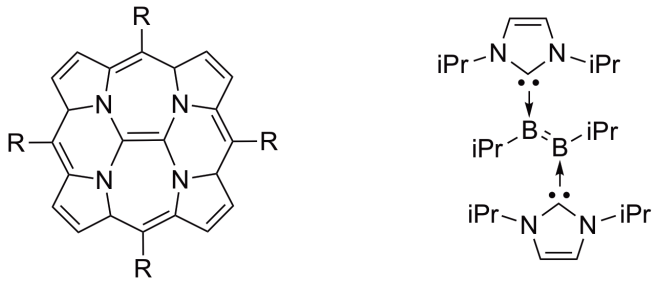

Figure 1-6 A negative redox potential can also be found for molecules which do not belong to the above-introduced, typical electron donor structures. The compound **49** shows a one-electron redox wave only.

Robinson et al. when they isolated and characterised the first neutral compound with a formal boron-boron double bond.[49] Their research paved the way for the development of highly reducing species like **49**. It is noteworthy that this compound undergoes a single electron oxidation only, and that the unpaired spin in the cationic form is mainly associated with the boron-boron core.[50] The localisation of the radical on the two boron atoms is in agreement with computational studies which show that the HOMO is mainly centred on these atoms.[49] More recently, Jiao et al. reported the formation of highly reducing species by treating a diboron substrate with a Lewis base.[51]

1.1.8 Factors Influencing the Strength of Electron Donors

In the previous sections, some aspects of the structure-activity relationship of the electron donors were touched already. In this section a more comprehensive discussion is given of how the molecular architecture determines the reducing power of these compounds. The neutral organic electron donors beyond simple amines typically have one key feature in common: an electron-rich central carbon-carbon double bond.

The Effect of the Heteroatoms in the Electron Donor Core

The series of chalcogen derivatives of **50** has been characterised (Figure 1-7 A), however, no simple trend emerged.[52,53] Two characteristics of the elements have a contrary effect on the oxidation potential of the electron donor molecule. With decreasing electronegativity of the element X, the compound **50** should become more reducing. However, as the electronegativity decreases the atomic number increases. As a consequence, the orbital overlap between the lone-pairs on element X and the carbon-carbon π-bond becomes poorer. This second trend of poorer orbital overlap counteracts the first trend of decreased electronegativity. The overlay

A

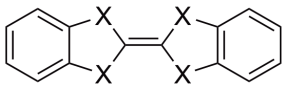

50

	X	$E_{1/2}$ in DCM vs. SCE
50a	O	0.57 V (E_p^{ox}, ir)[52,56]
50b	S	0.71 V (1.14 V)[53]
50c	Se	0.78 V (1.17 V)[53]
50d	Te	0.71 V (1.05 V)[53]

B

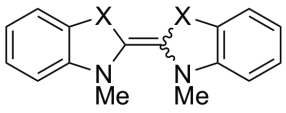

51

	X	$E_{1/2}$ in ACN vs. SCE
51a	NMe	-0.91 V[54]
51b	O	-0.26 V (E_p^{ox}, ir) (0.11 V)[54]
51c	S	-0.21 V (-0.04 V)[54]

C

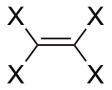

	X	$E_{1/2}$ in ACN vs. SCE
3	NMe_2	-0.75 V (-0.61 V)[30,31]
52	OMe	0.71 V (E_p^{ox}, ir)[55]

Figure 1-7 The effect of different heteroatoms on the electron donor scaffolds such as **50** has been investigated. If a second redox event is observed, the more positive value is given in brackets. (ir) means irreversible and the peak potential of the oxidation wave is given.

of these two effects is responsible for the non-linear trend that is observed in the chalcogen series.[53] According to the same line of reasoning, it follows that nitrogen is a more suitable heteroatom than is oxygen for building highly reducing electron donor molecules (Figure 1-7 B). Indeed, a large decrease of the oxidation potential is observed if the two oxygen atoms in **51b** are replaced with nitrogen to give **51a**.[54] The sulfur analogue **51c** is slightly less reducing than **51b**,[54] which reproduces the trend that was already observed for scaffold **50**.[52,53] The difference of the reduction potential between TDAE **3** and its methoxy analogue **52** is another impressive illustration of the effect of nitrogen vs. oxygen in the electron donor core (Figure 1-7 C). In fact, the oxidation potential of **3**[30,31] seems to be much more negative than the oxidation potential of **52** (however, it should be noted that the oxidation potentials of the two compounds cannot be directly compared since **52** shows an irreversible electrochemical behaviour).[55]

The Importance of Gaining Aromaticity

If the heteroatom in the donor core allows for efficient orbital overlap with the adjacent carbon-carbon π-system, an additional important effect can become operational that further increases the reducing power of these molecules. The effect is based on the gain of aromaticity upon oxidation in heterocycles adjacent to the central electron-rich double-bond of the electron donors (Figure 1-8).[47] It is the reason behind the large difference of reducing power between TDAE **3** and electron donor **27**. Upon oxidation of **27** to **55**, the π-system of the molecule becomes aromatic, while no gain in aromaticity can occur during the oxidation of **3**. In the benzimidazole-derived electron donor **4**, the π-system is already partially aromatic. Thus, the effect of gaining aromaticity upon oxidation to **54**, while still noticeable, is less pronounced compared to **27**.[47]

The Effect of Substituents on the Electron Donor Core

The effect of decorating the electron donor core with electron-withdrawing or electron-donating

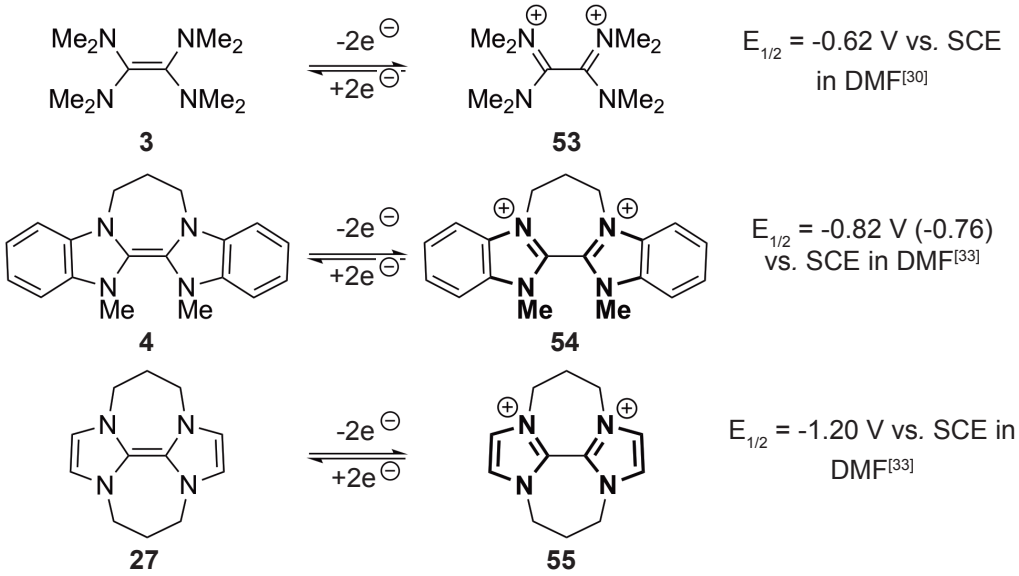

Figure 1-8 The gain of aromaticity in the heterocyclic cores of organic electron donors (such as in **54** and **55**) is a key driving force behind the reducing power of these molecules (rings that gained aromaticity upon oxidation are drawn in bold).

A

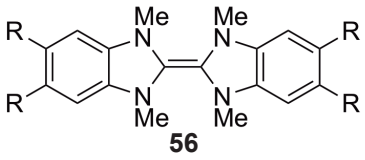

56

	R	$E_{1/2}$ in ACN vs. SCE
56a	-OMe	-1.07 V
56b	-H	-0.90 V
56c	-Br	-0.73 V (-0.64 V)
56d	-Cl	-0.69 V

B

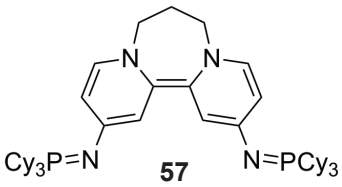

57

$E_{1/2}$ = -1.50 V (-1.29 V)
in DMF vs. SCE[45]

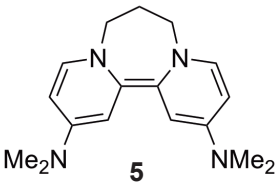

5

$E_{1/2}$ = -1.24
in DMF vs. SCE [7]

Figure 1-9 Substituents on the heterocyclic core of the electron donors can significantly tune their reduction power. If two separate oxidation waves are observed the second oxidation potential is given in brackets.

substituents is straightforward; conjugative electron-donating substituents (such as -OMe in **56a**) make the electron donor more reducing. This correlation can be nicely illustrated based on the electron donor core **56** (Figure 1-9 A).[57]

As mentioned previously, Dyker et al. studied the effect of different substituents on the oxidation potential of bispyridinylidene electron donors systematically. They found a good correlation between the oxidation potential as determined by cyclic voltammetry and the Hammett coefficient σ_p^+ for these substituents. Indeed, this correlation allowed them to suggest a refined value for the σ_p^+ coefficient of the studied tricyclohexylphosphine imide substituents. This substituent was found to be an exceptionally strong π-electron donor. The corresponding bis-pyridine electron donor **57** has a more negative first oxidation potential than the DMAP-derived donor **5** by 0.26 V (Figure 1-9 B).[45]

The Effect of (Torsional) Flexibility of the Electron Donor Core Subunits

The nature of the linking alkyl chain between the two halves of the electron donor influences the geometry and, thereby, its properties. Although the effect of the length of the linker chain on the reduction potential is rather small, it can be consistently observed in several instances. The more torsional flexibility the two halves of the donor core have, the more negative is the first oxidation potential of the electron donor (Figure 1-10). For example, in the series of **58** - **59** the oxidation potential increases with increasing length of the alkyl linker.[33] An analogous trend can be observed for the reduction potential of the oxidised salts of the imidazole-derived electron donors **28**, **29** and **32** (Scheme 1-5).[2] An extrapolation of this trend leads to the structure **60** (Figure 1-10). This open-shell species can be regarded as a model of an imidazole-derived donor which is twisted by 90° such that the two π-systems have no overlap. Based on calculated gas-phase ionisation potentials the species **60** is predicted to be a stronger reducing agent than **27** by 0.3 eV.[58] Recently, other examples have been published which impressively illustrate the effect of torsional flexibility on the redox potential.[59]

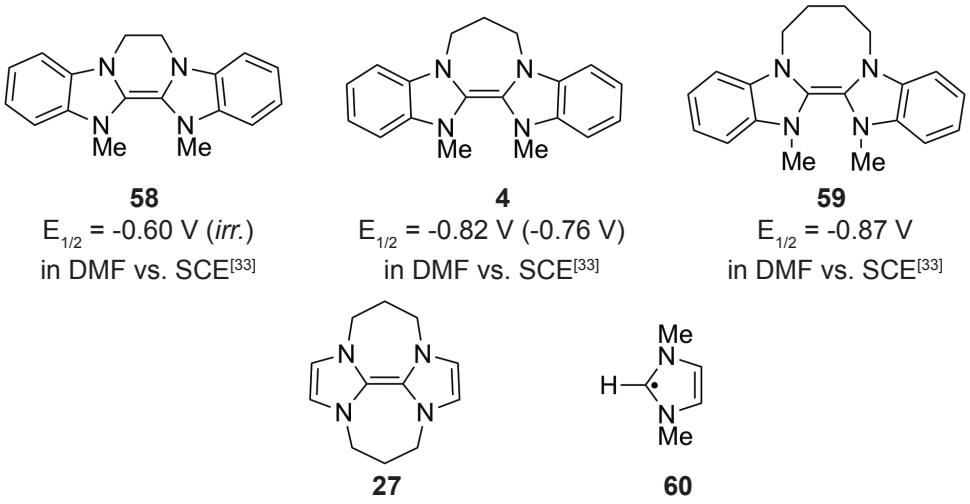

Figure 1-10 The more torsional flexibility the two subunits of the electron donors have, the more reducing the molecule is in general.

Other Factors Influencing the Reduction Reactions with Organic Electron Donors

The solvent obviously affects the strength of reducing agents. Moreover, the oxidation potential of different organic electron donor molecules depends to a different extent on solvation.[60] For example, this has been discussed based on electron donor **45** (Scheme 1-8, Chapter 1.1.7).[46]

Besides the interaction of the electron donor molecule with the solvent, its interaction with the substrate is decisive for the overall reaction. Generally, it is assumed that the organic electron donors form only a weak complex with their substrates. Consequently, the electron transfer is typically regarded as an outer-sphere process where Marcus theory can be applied.[61] A comparison of the normal potentials of TDAE **3** and the benzimidazole-derived electron donor **4** indicates the importance of specific interactions between the electron donor and the substrate. The 0.2 V difference between the redox potential of the two compounds appears to be too small to fully account for the striking difference of their reactivity (Scheme 1-9). Namely, in contrast to TDAE **3**, the electron donor **4** is capable of reducing iodoarenes to aryl radicals.[47,62] It has been suggested that the difference in reactivity is rooted in the ability of **4** to be responsive to π-π-stacking interactions with its substrate.[62] However, based on electrochemically determined reduction potentials, the benzimidazole-derived donor **4** would not be expected to be capable of the reduction of iodoarenes at all (iodoarenes are reduced at ca. -2.2 V vs. SCE[63]). Again π-π-stacking interactions are thought to be crucial for the reduction to proceed.[62] The importance of π-π-stacking interactions has been accounted for in a refined theoretical approach.[64]

Another key point of the reduction of iodoarenes is that the single electron transfer is followed by an irreversible cleavage of the carbon-iodine bond. The importance of such an irreversible reaction following a challenging electron transfer can be illustrated by the selective reaction of the substrate **63** over the product **65** in the reaction presented in Scheme 1-10. Both compounds show similar first reduction potentials in an electrochemical measurement.

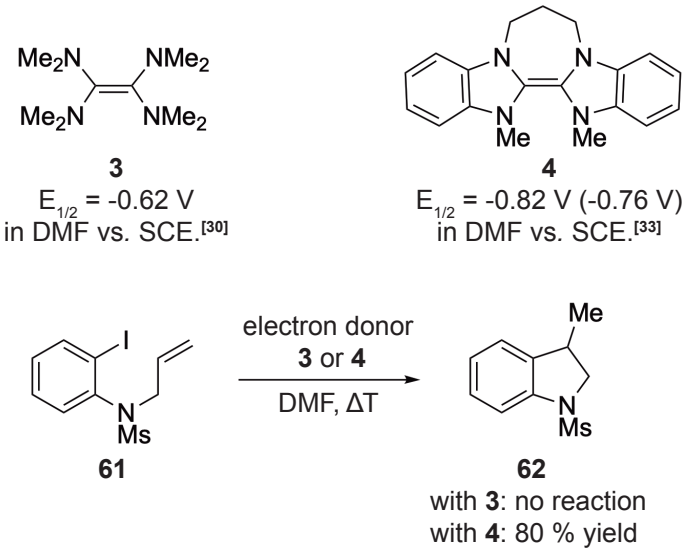

Scheme 1-9 The different reactivity of **3** and **4** is thought not only to be based on the difference in their redox potential but also in the different ability of the two compounds to engage in π-π-stacking interactions with its substrate.

[32] The radical anion **67** derived from the ketone **65**, however, cannot undergo an efficient irreversible reaction which would drive the reduction reaction forward. Therefore, the radical anion **67** has no other option than to transfer an electron back to an oxidised molecule of the electron donor or to the substrate **63** or get oxidised upon work-up.[32] Originally, the substrate **63** was designed with the aim to demonstrate that the donor **27** is capable of reducing aryl iodides to aryl anions. Indeed, the only plausible way to arrive at the cyclised product **65** includes the aryl anion intermediate **64**.[32]

As the iodoarenes are reduced in a first SET, the question arises why the donor **27** is capable of a second reduction while the donor **4** is not.[32,47] The standard potential of an aryl radical was estimated from experimental data to be close to 0.0 V vs. SCE.[66] More recently, the reduction of aryl radicals has been revisited theoretically. Based on these studies it was suggested that the experimentally derived value for the reduction potential around 0.0 V vs. SCE might be too positive by as much as 0.8 V.[67] The theoretically determined standard potential of aryl

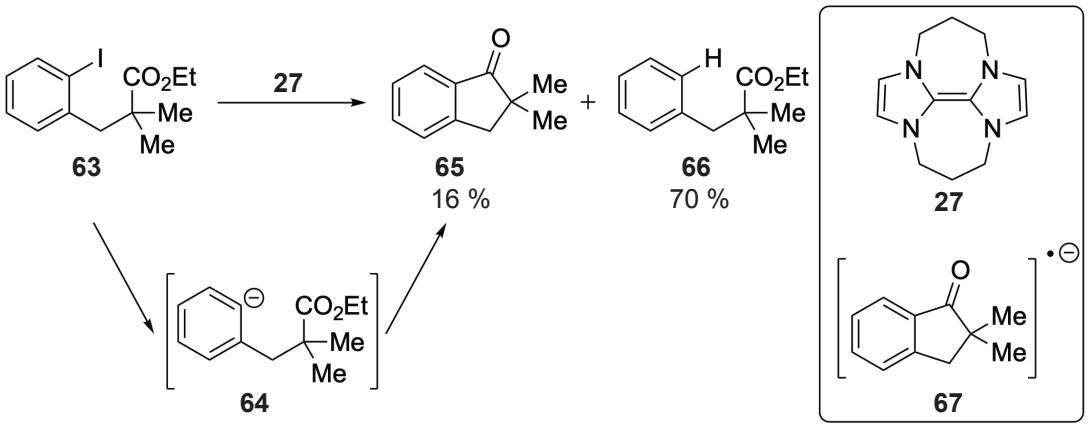

Scheme 1-10 The donor **27** is capable of reducing iodoarenes such as **63** to the aryl anion.

radicals (-0.77 V vs. SCE[67]), however, is still slightly more positive than the standard potential of the benzimidazole-derived donor **4** (-0.82 V vs. SCE[33,65]). Hence, even with the modified value for the reduction potential of aryl radicals the different selectivities of the donors **4** and **27** cannot be fully explained. Calculations on the structure of the radical cation intermediates of the two electron donor molecules showed that the radical cation of **4** is already significantly twisted about the central carbon-carbon bond (the torsion angle was found equal to 26°), while the radical cation of **27** is clearly more planar (the torsion angle was found equal to 12°).[32] It was suggested that favourable π-π-stacking interactions between the relatively planar radical cation of **27** and the aryl radical are still possible, which facilitates a second single electron transfer. With the more twisted radical cation of **4**, the π-π-stacking interactions with the substrate are no longer sufficiently developed to allow for a second single electron transfer.[32]

1.2. Reactions of Organic Electron Donors

This section gives an overview of the chemical transformations that have been achieved with some of the above-introduced electron donors. The discussion of synthetic applications will be limited to amines, tetraaminoethylenes, tetrathiafulvalenes, tetraazafulvalenes, and bispyridinylidenes. For the class of tetraazafulvalenes, it is the parent compound **2**, which has received the most thorough investigation of its use in synthesis. For the class of tetraaminoethylenes, it is TDAE **3**, which is the most important representative from a synthetic perspective. Thus, the examples given for these two classes of electron donors will focus on these two species. Among the tetraazafulvalene donors, it is the benzimidazole donor **4**, which differs significantly from related species in terms of its reactivity. The other tetraazafulvalene donor that has been extensively examined is the doubly bridged imidazole-derived electron donor **27**. For the bispyridinylidene electron donors it is the DMAP-derived electron donor **5** that was most widely applied in synthesis.

1.2.1 Reactivity of Amines as Reducing Agents

Although there are several reports on reductive dehalogenation of alkyl halides with amines as the reducing agent, examples where this chemistry has been used to achieve reductive radical cyclisations are scarce. Ishibashi et al. pioneered the use of piperazine **69** as a solvent and reducing agent in radical cyclisations starting from 2,2,2-trichloroacetamides (Scheme 1-11). Piperazine **69** stands out from a range of primary, secondary and tertiary amines that were screened in an initial study.[68] To date, typically 5-*exo-trig* cyclisations or 6-*exo-trig*

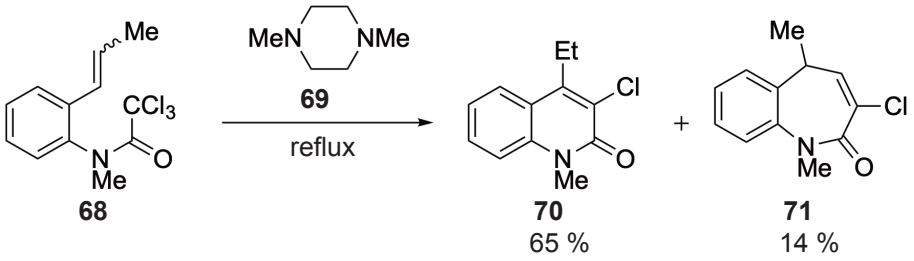

Scheme 1-11 2,2,2-Trichloroacetamides can be reduced in boiling **69** to give a radical intermediate, which engages in a 6-exo-trig cyclisation. After a branching neophyl rearrangement, H-abstraction and elimination of HCl the products are delivered.

cyclisations have been performed with this reagent. As can be seen from the given example in Scheme 1-11, the termination of the radical cascade by hydrogen abstraction that eventually leads to the formation of product **70**[69] competes with a neophyl rearrangement, which leads to the by-product **71**. For comparison, the branching is less favourable (i.e. shows a lower efficiency for the formation of either product) with the well-established tributyltin hydride/AIBN system. Hence, for some substrate classes, amine reagents may offer advantages over more typically used reagents.[69] The reactivity of amines as electron donors is, however, not yet fully understood. For example, it has been observed that the performance of **69** critically depends on its water content (an optimum was identified around 0.2 equiv. to 5.0 equiv. with respect to **69**). This phenomenon still awaits an explanation.[70]

Ishibashi et al. also published examples where triethylamine and tripropylamine were used to reduce diphenyl disulfide to the sulfur-centred radical. These radicals were successfully used to form carbon-sulfur bonds by trapping them with alkynes.[71]

Amines can also engage in electron transfer reaction with the buckminsterfullerene C_{60} **72** (Scheme 1-12).[72] Typically, the radical cations of primary and secondary amines immediately recombine with the fullerene radical anion after the single electron transfer. Amines that give rise to stable radical cations such as TDAE **3** can form charge-transfer complexes with fullerene. The base DBU **73** shows an intermediate behaviour insofar as it gives rise to a charge-transfer complex **74** with a half-life of ca. 1 h in benzene at room temperature. The complex decays via a radical-radical recombination, which leads to the final product **75**.[72] This example demonstrates that **73** can give rise to a significantly stable radical cation upon oxidation.

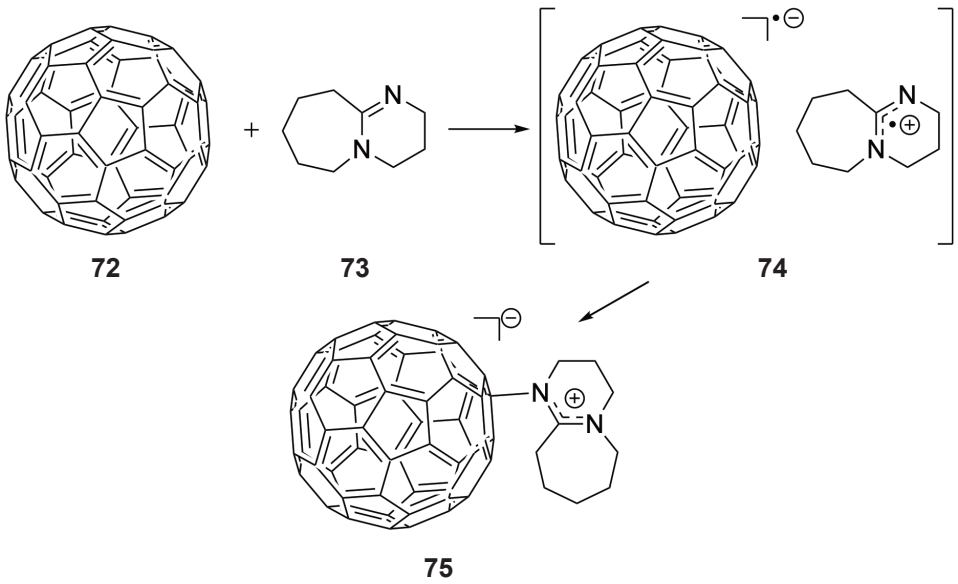

72 **73** **74** **75**

Scheme 1-12 The buckminsterfullerene **72** can be reduced with DBU **73** via a transient charge-transfer complex **74** to the final product **75**.

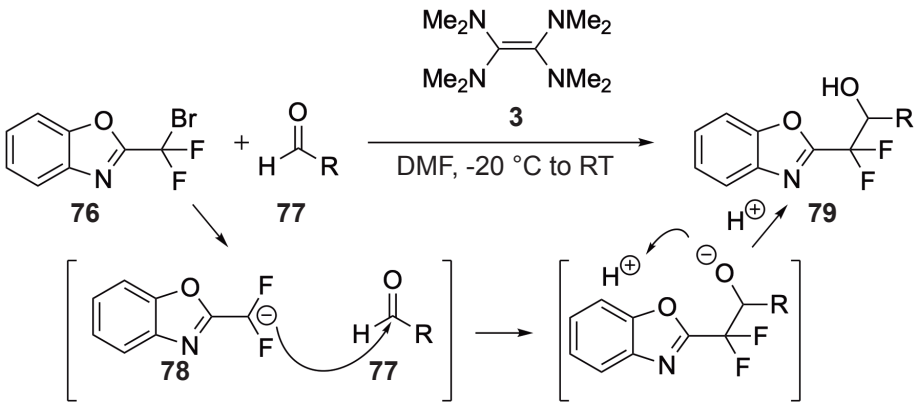

Scheme 1-13 A typical application of TDAE **3** is the generation of difluoro-carbanions, which can be trapped by electrophiles such as aldehydes.

1.2.2 Reactivity of TDAE as a Reducing Agent

TDAE **3** has been employed in an impressive diversity of reductive bond-forming reactions, despite it being a rather weak electron donor.[2] As the compound only reacts with fairly electron-poor substrates, a virtue was made of the necessity and a typical application of TDAE became the generation of difluoro-carbanions such as **78** (Scheme 1-13). Typically, in addition to the two geminal fluorine atoms, a third stabilising group is required, such as the electron-deficient aromatic system in **76** or a carbonyl group.[4] Under certain conditions it was possible to reduce trifluoroiodomethane CF_3I to the trifluoromethyl anion[4] or benzylic halogen bonds to the benzyl anions[2] and to engage these anions in bond-forming reactions with appropriate electrophiles. Most frequently, carbonyl groups are used as electrophiles such as aromatic or aliphatic aldehydes, ketones and α-ketoesters. Further, a range of examples is given where sulfonyl aldimines and thiocyanates act as electrophiles.[2] In several instances, light activation of TDAE has been shown to improve its reactivity.[4]

As becomes clear from these examples, TDAE **3** reduces electron-poor substrates to the anion. But is it also possible to engage this reducing agent in a single electron transfer reaction to access radical species? Reactions that can only proceed via radical intermediates are simple tests for single electron transfer reactivity. Such a reaction is presented in Scheme 1-14. The formation of **81** indicates the generation of a radical intermediate derived from **76**.[30, 4]

Nishiyama et al. reported the TDAE-mediated synthesis of 1,2,3,4-tetrahydronaphthalenes

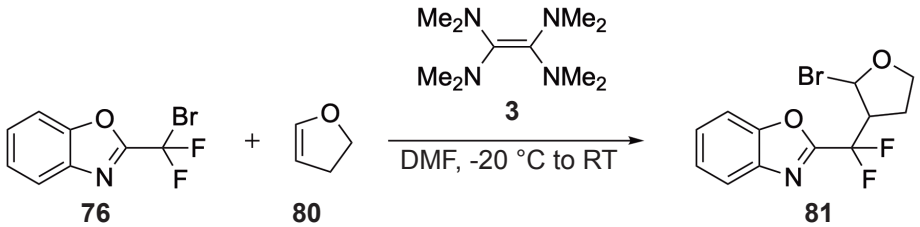

Scheme 1-14 Evidence for the stepwise single electron transfer from TDAE **3** to its substrates comes from reactions where only the radical intermediate can react forward to a stable product.

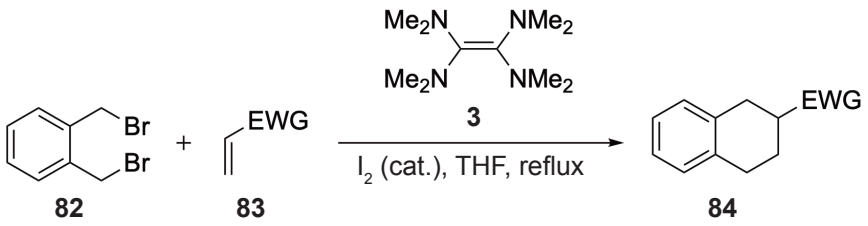

Scheme 1-15 A radical mechanism has been proposed for the TDAE-mediated synthesis of **84** but an ionic reaction cannot be ruled out.

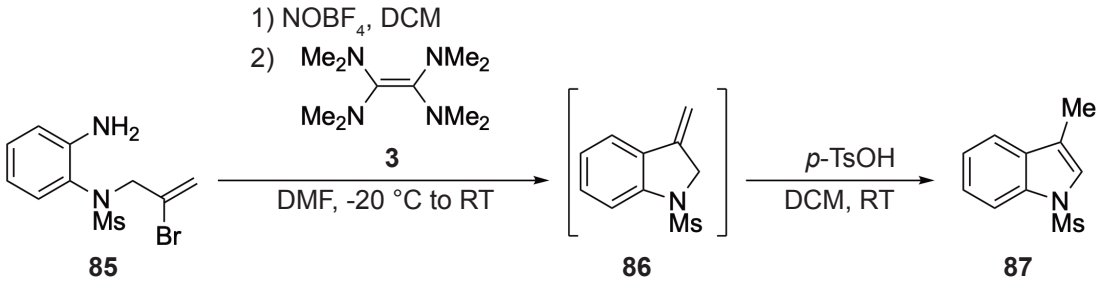

Scheme 1-16 The Murphy indole synthesis relies on a radical cascade that terminates itself by expulsion of the unpaired spin in a fragmentation step. The intermediate **86** can readily be isomerised to the final product **87**.

84 starting from the dibromo-species **82** and the Michael acceptor **83** (Scheme 1-15). Radical intermediates were proposed but no rigorous evidence was given.[73]

Classical radical chemistry with TDAE **3** was performed by Murphy et al. with diazonium salts as the electron acceptors (Scheme 1-16, the diazonium salt is synthesised in situ in the first step). In this study, it was found that TDAE **3** does not contribute to the termination of the radical cascade in any productive way. Thus, it was necessary to design substrates with radical leaving groups such as the bromine atom in compound **85** in order to achieve productive, high-yielding radical cyclisation reactions. As a consequence of the nature of the substrates, the radical cascade produced intermediates such as **86**, which can readily be isomerised to the indole product **87**.[5] This synthetic approach to indoles is known as the ”Murphy indole synthesis”.[74]

1.2.3 Reactivity of Tetrathiafulvalene 2 and the Radical Polar Crossover Reaction

In contrast to TDAE **3**, some organic electron donors are prone to interact with the reactive species they generate in a controlled fashion. This characteristic is particularly pronounced in the class of tetrathiafulvalene electron donors and it opens doors to interesting transformations (Scheme 1-17). Murphy et al. explored reaction sequences where aryl radicals were generated from diazonium salts with tetrathiafulvalene **2**. The diazonium salts were typically formed in situ from the aniline (such as **88**). After a radical cascade, the product radical is trapped by the tetrathiafulvalene-derived radical cation to give the intermediate **89**. The tetrathiafulvalene moiety is then displaced by a nucleophile in a final S_N1-type reaction. In the example shown in Scheme 1-17, the hydroxyl group of **90** acts as an internal nucleophile. It was found possible to form five- and six-membered rings with internal nucleophiles. Larger rings, however, could

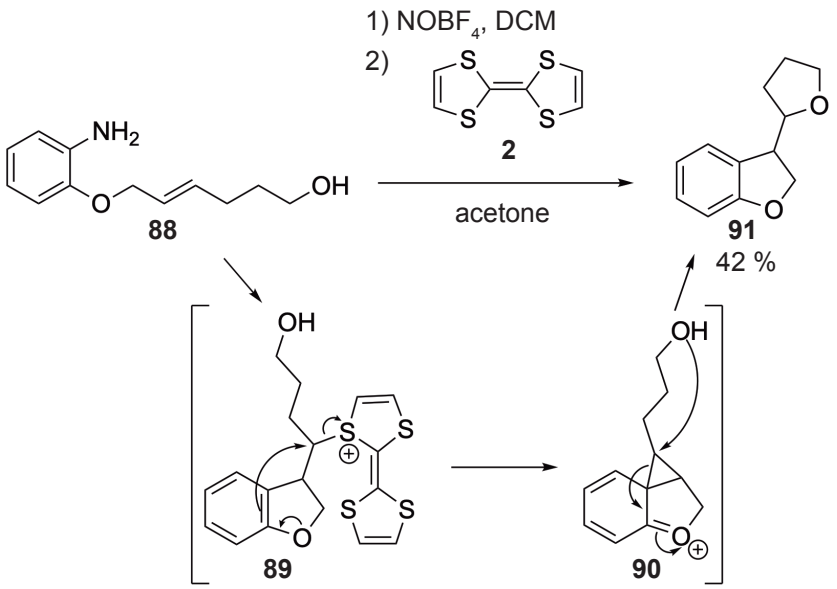

Scheme 1-17 The radical-polar crossover reaction requires crucial assistance of an electron rich neighbouring group for the S_N1-type displacement of the tetrathiafulvalene moiety.

not be accessed efficiently.[3] External nucleophiles were also successfully employed in this type of reaction. For example, nucleophilic solvents, such as methanol or acetonitrile or traces of water in acetone, were used to displace the tetrathiafulvalene moiety.[75] Since the polar displacement joins so seamlessly onto the radical cascade the term ”radical-polar crossover reaction” has been coined for these sequences.[75] Good reviews on this subject are given by Broggi et al.[2] and in more detail by Murphy.[76]

The polar part of the reaction, i.e. the nucleophilic displacement of the tetrathiafulvalene-moiety, turned out to be the crucial step of this transformation. In fact, it imposes some restrictions on the substrate scope. In order to better understand the polar step of the reaction and the limitations that come with it, a series of experiments was performed.[75] It was demonstrated that the assistance of an electron-rich neighbouring group is crucial for the nucleophilic displacement step, especially when it occurs at secondary centres instead of tertiary centres. The displacement of the tetrathiafulvalene-moiety from primary centres was not observed. [77] Because the nucleophilic displacement heavily depends on the assistance of an electron donating group, it appears appropriate to draw a delocalised carbocation intermediate like **90** rather than a localised cation at the carbon atom where the tetrathiafulvalene moiety was attached to initially (Scheme 1-17). Since tetrathiafulvalene **2** is not formally consumed in the reaction it could be used catalytically. Indeed, it was possible to run reactions with substoichiometric amounts of **2** as was demonstrated on one example.[75,78]

Theoretical studies of the tetrathiafulvalene radical cation showed that the spin-density was highest on the sulfur atoms, which helped to rationalise the formation of a sulfonium salt intermediate **89**.[75] Indeed, for the majority of examples, the intermediate carbon-centred radicals recombined with the tetrathiafulvalene radical cation at the sulfur atom.[2,76] When tetrathiafulvalene **2** was studied in radical 1,5-hydrogen atom transfer reactions with substrate **92**, however, it was found that the radical-radical recombination occurs at an internal carbon atom of

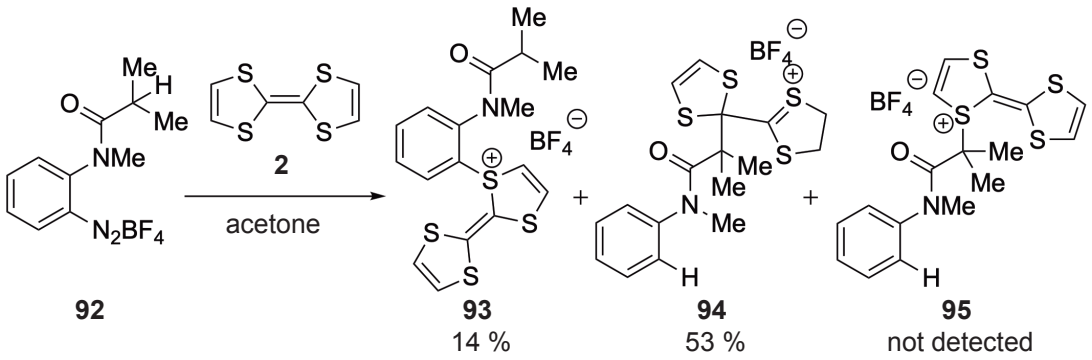

Scheme 1-18 The 1,5-hydrogen atom transfer reaction gave an unexpected carbon-carbon bond formation between the intermediate radical and the tetrathiafulvalene radical cation.

the tetrathiafulvalene radical cation (Scheme 1-18).[79] The formation of **94** rather than **95** was explained by the destabilizing effect which the carbonyl group would exert on the α-sulfonium group in **95**. The fact that the formation of **95** becomes energetically less favourable was assumed to manifest in an increase of the energy barrier towards this product.[79]

Another point worth noting about the reaction in Scheme 1-18 is the by-product **93**. It illustrates one major drawback of tetrathiafulvalene in radical-polar crossover reactions. The radical-radical recombination with the tetrathiafulvalene radical cation may prematurely terminate the radical cascade. With the aim of circumventing this problem, several dithiadiazafulvalene analogues of **2**, such as **96**, were examined (Figure 1-11).[80] It was expected that, due to steric interactions with the protruding side-chains on the nitrogen atoms, the radical-radical recombination would be slowed down. It was found that the novel compound class not only has more negative reduction potentials than tetrathiafulvalene. The compounds also showed slower trapping of radicals. Although there is evidence that the novel compounds can terminate a radical cascade, it was not possible to engage the corresponding intermediates in nucleophilic displacements as was possible for the tetrathiafulvalene-mediated reactions.[80]

Despite its conceptual beauty, the radical-polar crossover reaction suffers from considerable limitations of the substrate scope. Moreover, the approach is closely tied to the reactivity of the tetrathiafulvalene core. The limited scope of the original reaction with **2** and the difficulties in developing this reagent further may be responsible for the fact that the reaction has not found wider applications.[2]

1.2.4 Reactivity of the Benzimidazole-Derived Electron Donor 4

The synthetic utility of organic electron donors such as **4** was recognised and expanded among others by Murphy et al. The benzimidazole-derived electron donor **4** was the first neutral organic compound found capable of reducing aryl iodides to radicals (Scheme 1-19). For

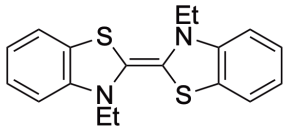

96

Figure 1-11 Dithiadiazafulvalenes such as **96** were found to be unable to replicate the reactivity of tetrathiafulvalene **2** in radical polar crossover reactions.

example, the substrate **97** was reduced to the radical intermediate **98**, which engaged in a 5-*exo*-*trig* cyclisation to give the product **99** in good yield (Scheme 1-19 A). It was also possible to synthesise indole cores following the same strategy as shown in Scheme 1-16. But with the electron donor **4**, more convenient to use aryl iodides, such as **100**, also become viable substrates (in contrast to having to form diazonium salt intermediates). The indoline intermediate **101** was isomerised in situ to the indole product **102**. Further, it was possible to apply the procedure to aliphatic iodides (Scheme 1-19 C). For example, the primary iodide **103** was efficiently reduced to the alkyl radical, which gave the product **104** after cyclisation and hydrogen abstraction.[6] The last reaction is noteworthy as the substrate **103** is also susceptible to nucleophilic substitutions at the iodide, as well as elimination of the iodide to afford an alkene. But the compound **103** was only observed to undergo reductive cyclisation under the applied conditions.

Initially, it was not clear whether the electron donor **4** is capable of reducing aryl or even alkyl radicals to the corresponding anions. In order to firmly establish the proposed radical mechanism, diagnostic substrates were treated with **4** (Scheme 1-20).[6] The two reactions would lead to products that are characteristic either of radical intermediates or (alkyl) carbanion intermediates. The treatment of substrate **105** with the electron donor **4** (Scheme 1-20 A) may lead to the radical intermediate **106**. This radical could then abstract a hydrogen from the solvent or the electron donor and give the product **107**. Alternatively, it could receive an additional electron in a second single electron transfer step, which would lead to **108**. This intermediate would be expected to give the alkene **109** after expulsion of methoxide. The compound **109** was, however, not detected. Similarly, compound **110** can lead to a radical intermediate that

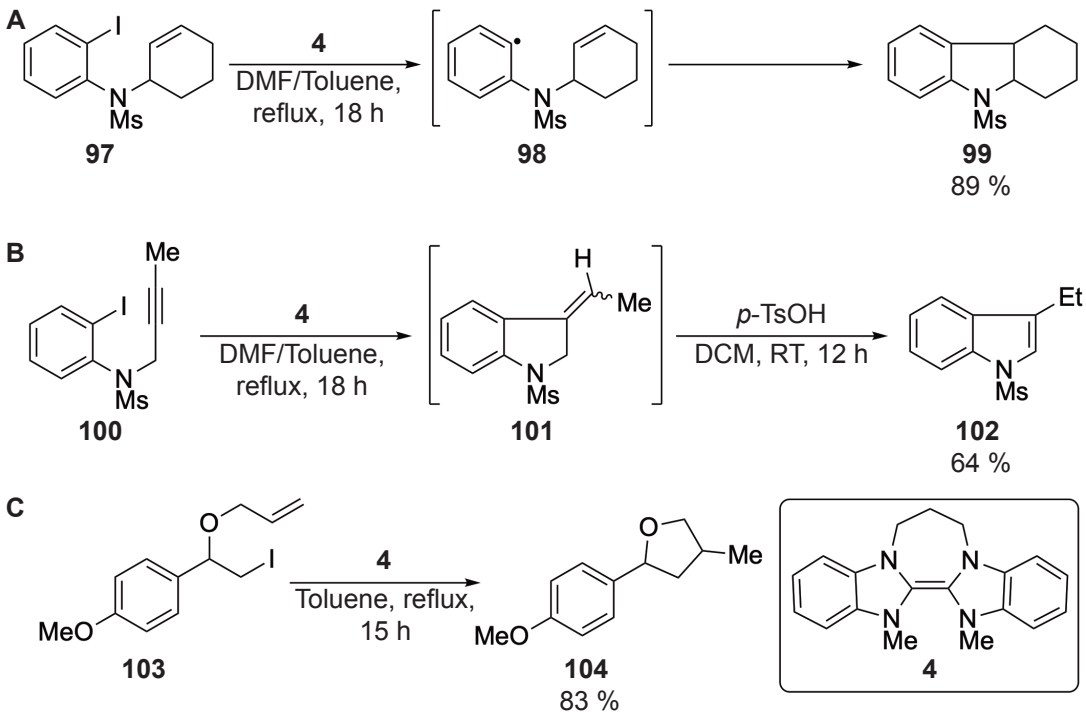

Scheme 1-19 The electron donor **4** was successfully employed in typical radical cyclisations. For the reactions in **A** and **B** the electron donor was conveniently formed *in situ*.

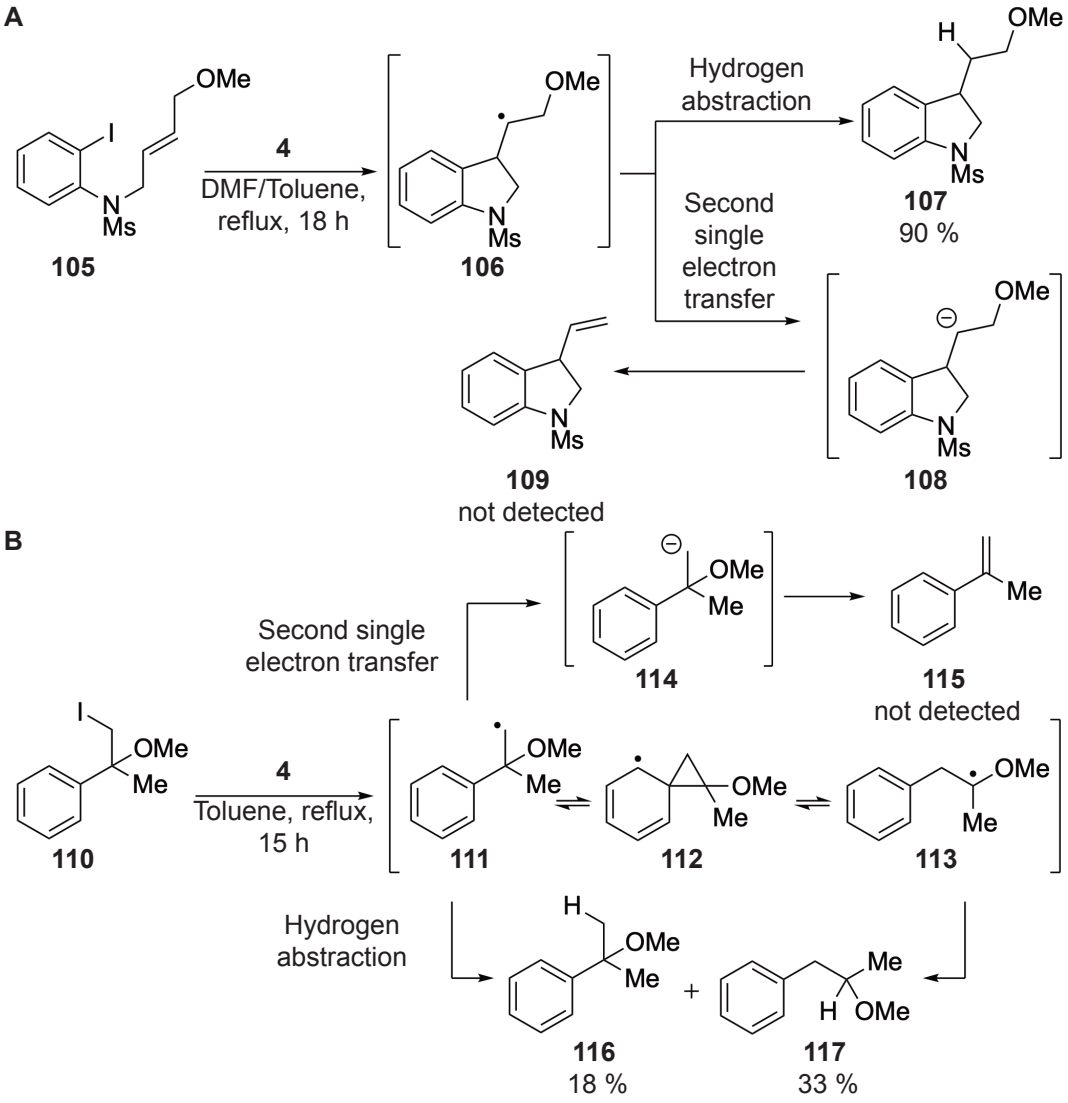

Scheme 1-20 Initially, it was not clear whether the donor **4** is capable of reducing aryl radicals or alkyl radicals to anions. In the reactions **A** and **B**, no indication for the conversion of alkyl radicals to the carbanion was found.

can undergo neophyl rearrangement, which eventually leads to the two compounds **116** and **117**. If a second single electron transfer to the radical **111** occurred, one would expect the formation of **115**. Again, the diagnostic product for the carbanionic intermediate **114** could not be detected. Instead, the isolation of **116** and **117** gave clear evidence for the neophyl rearrangement taking place. Altogether these results strongly indicate the presence of radical intermediates only, alkyl radicals are unlikely to be further reduced to alkyl anions with electron donor **4**.[6]

A second single electron transfer to an aryl radical is expected to be easier than a second single electron transfer to an alkyl radical. The high-yielding cyclisations presented in Scheme 1-19 **A** and **B**, and in Scheme 1-20 **A** strongly suggest that aryl radicals are formed from the aryl iodide substrates and not aryl anions. However, as was observed with TDAE **3**, the choice of the substrate and reaction conditions may affect which intermediates (radicals or anions) can react onwards (Chapter 1.2.2). Hence, it was necessary to directly probe for the formation

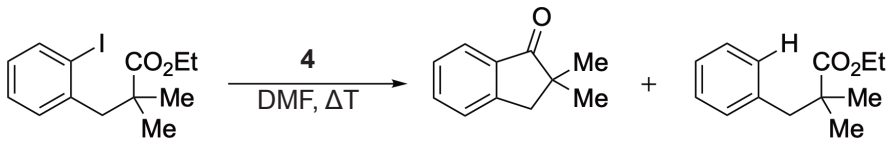

63 **65** not detected **66** 67 %

Scheme 1-21 The electron donor **4** was probed for its ability to form aryl anions from aryl iodides. No evidence for these species was found, which would have manifested in the formation of **65**.

of aryl anion intermediates (Scheme 1-21). When treated with **4** the substrate **63** is converted to the dehalogenated product **66** in good yield. The product **65**, which is diagnostic for aryl anion intermediates was, however, not detected.[32] With the imidazole-derived electron donor **27**, in contrast, the substrate **63** gave a positive test result (i.e. product **65** was formed) for the aryl anion intermediate (Scheme 1-10, Chapter 1.1.8).[32]

As the radical nature of the cyclisation was supported by strong experimental evidence and the formation of aryl anions seems unlikely, the remaining open question about the reactions with electron donor **4** was the source of the hydrogen atom in the radical cascade termination step. In isotope labelling experiments in DMF-d_7 the solvent was ruled out as a hydrogen source.[32] Thus it was suggested that the donor molecule itself acts as a hydrogen source either in its reduced form or in one of its cationic forms.[62]

After the initial mechanistic studies, the substrate scope of the electron donor **4** was explored. Soon its limitations became apparent. The donor was able to quantitatively reduce 9-chloroanthracene **118a** (X = Cl, Scheme 1-22). But the reaction of the more challenging substrate, 9-cyanoanthracene **118a** (X = CN) gave a significantly lower yield of **119**.[81] The electron donor **4** then clearly reached its limits when it was engaged in the reduction of aryl bromides (Scheme 1-23). While aryl iodide substrate **120a** gave good yields of product **121**, the bromide analogue **120b** gave significantly lower yields even after extensive optimisation of the reaction conditions.[82]

Besides as a reducing agent in classical radical cyclisation cascades, the electron donor **4** was also examined as an initiator for polymerisation reactions (Scheme 1-24).[83] The compound **4** was found capable of injecting electrons into the π-system of ethyl methacrylate **122**. The substrate was converted quantitatively, but only relatively short oligomers **123** were obtained. A radical polymerisation mechanism was suggested for the reaction.[83] The monomer

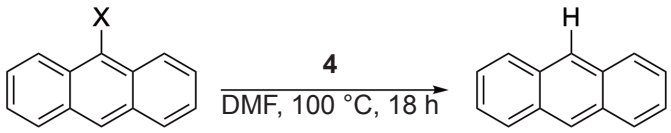

118a (X = Cl)
118b (X = CN)

119
from **118a**: 99 %
from **118b**: 60 %

Scheme 1-22 9-Chloroanthracene was quantitatively reduced by electron donor **4** and 9-cyanoanthracene was reduced in fair yield.

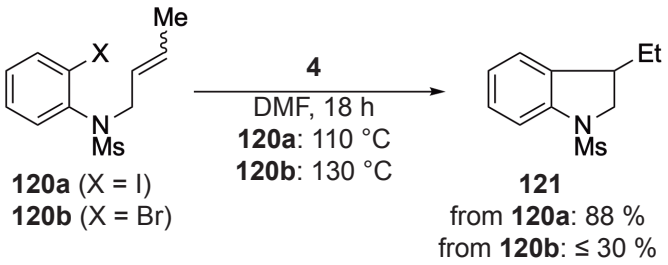

120a (X = I)
120b (X = Br)

121
from **120a**: 88 %
from **120b**: ≤ 30 %

Scheme 1-23 The electron donor **4** was significantly less efficient at reducing aryl bromides compared to aryl iodides.

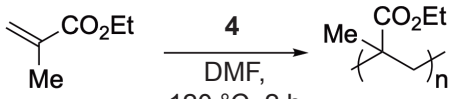

122 **123**

Scheme 1-24 The electron donor **4** was investigated as a possible initiator for the polymerisation reaction of **122**. Oligomers of low molecular weight were formed. A radical polymerisation mechanism was suggested for the reaction.

ethyl methacrylate **122** is the only substrate reported to be reduced by **4** that does not feature an aromatic system.

1.2.5 Reactivity of the Imidazole-Derived Electron Donor 27

The tetraazafulvalene donor **27**, featuring two imidazole units, was the first neutral organic compound that reduced aryl iodides to aryl anions (Chapter 1.1.1). The donor was further examined on its capacity to reductively cleave sulfones (Scheme 1-25).[84] Indeed, it was found to be an efficient reducing agent for such transformations with interesting and useful selectivities. For example, the mildly activated sulfone **124** was reduced to **125** in good yield while, from the analogous alkyl sulfone **126**, the reduced product **127** was not obtained (Scheme 1-25 A and B). Computational studies show that the LUMO of compound **124** has a node through the carbon-sulfur bond that will be broken. For the compound **126** this is not the case. The good chemoselectivity of **27** allowed for the selective reduction of dialkyl disulfones **128** to the monosulfone compounds **129** (Scheme 1-25 C).[84]

Based on computational studies, it has been suggested that the fragmentation of the nitrogen-sulfur bond occurs concomitantly with the first single electron transfer step and that this step is the rate-limiting one. The reactive sulfones **124** and **128** in Scheme 1-25 fragment into the alkyl radical and a sulphinate anion in silico. It was suggested that the resulting alkyl radicals are further reduced to the anion.[84]

Tosylamides, where the nitrogen atom is part of a π-system, were reduced as well, but more forcing conditions were required. For example, tosylated indole **130** was reduced to the indole **131** in high yield (Scheme 1-26 A), while no reaction was observed with tosylated piperidine **132** even after prolonged reaction time (Scheme 1-26 B).[84]

The electron donor **27** was also effective in reducing naphthyl bromide and anthracenyl chloride to the corresponding hydrocarbon products.[32] Further, compound **27** was found to be remarkably basic. It underwent a proton-deuterium exchange of the imidazole ring protons in acetonitrile-d_3 at room temperature.[65]

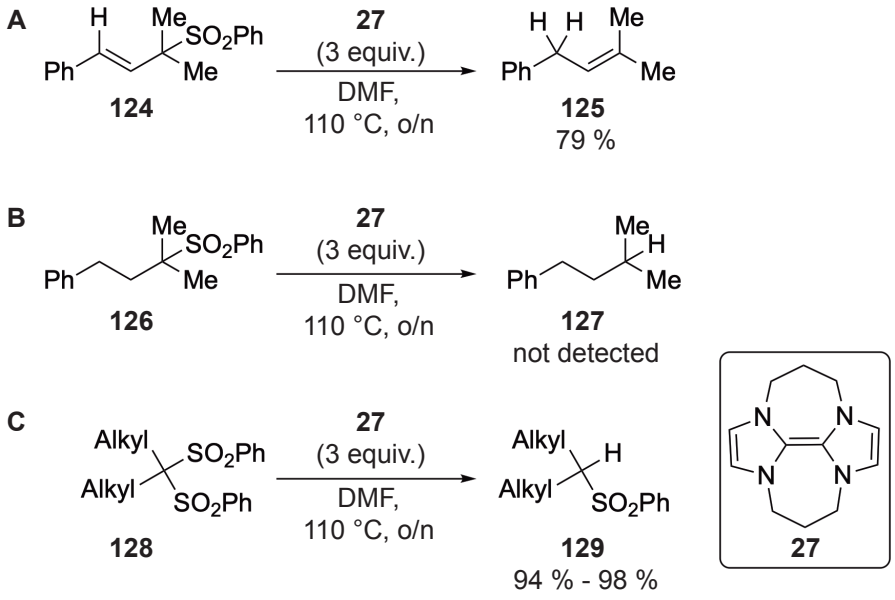

Scheme 1-25 The imidazole donor **27** was found to be a mild, effective and selective reducing agent for alkyl phenyl sulfones.

1.2.6 Reactivity of the DMAP-Derived Electron Donor 5

The DMAP-derived electron donor **5** has been used for the reductive cleavage of a range of functional groups. First, it was demonstrated that the compound is capable of reducing aryl iodide substrates to aryl anions (Scheme 1-27 A). The same approach was followed as before (Scheme 1-10, Scheme 1-21) with a slightly modified probing substrate **134**. Indeed, treatment of **134** with the electron donor **5** at room temperature furnished the product **135** in good yield. The yield gives a lower limit for the conversion of the aryl iodide to the aryl anion because the by-product **136** could either arise from anionic intermediates or radical intermediates. Further, the electron donor was capable of reducing aryl bromide **137** in good yields to **138** under more forcing conditions (Scheme 1-27 B). The carbon-sulfur bond in substrates such as **139** was also susceptible to reductive cleavage by the electron donor **5** and the product **140** was obtained almost quantitatively (Scheme 1-27 C).[7]

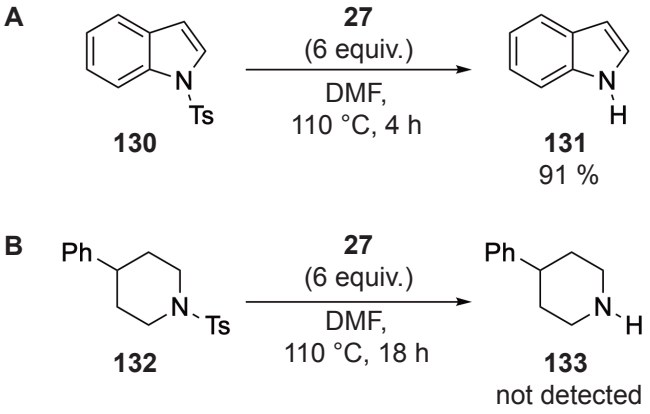

Scheme 1-26 Activated tosylamides were viable substrates for the donor **27**.

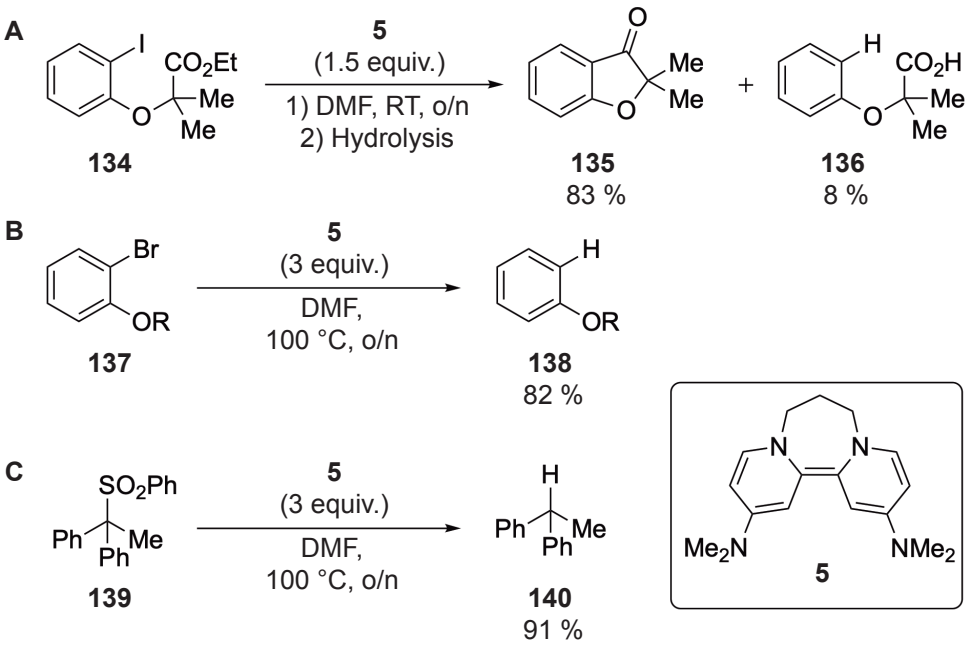

Scheme 1-27 It was demonstrated that the DMAP-derived electron donor **5** reduces aryl iodides to aryl anions in good yield. The donor is also capable of reducing aryl bromides and sulfones efficiently.

The reductive cleavage of the nitrogen-oxygen bond in Weinreb amides was achieved in low to moderate yield with **5** (Scheme 1-28).[85] The study unveiled an interesting dependence of the presence of a phenyl ring in the substrate and the proximity of this phenyl group to the Weinreb amide function on the reaction yield. The experimental findings were substantiated with DFT calculations. It was shown that for the substrates **141a-b** the LUMO is at least partially associated with the Weinreb amide. The corresponding reduced products **142a-b** were obtained in good yield under mild conditions (Scheme 1-28 A). For the substrates **141c-e**, the LUMO was no longer associated with the Weinreb amide but localised fully on the phenyl ring. Fair yields of the reduced products **142c-e** could only be achieved when the reaction temperature was increased to 100 °C (Scheme 1-28 B). When no phenyl ring was present, as is the case in the substrate **143**, even at high temperature and with a large excess of the electron donor **5**, only moderate yields of reduced product **144** were achieved (Scheme 1-28 C). Two explanations were given for the observed trend. Both are based on the assumption that the initial single electron transfer is the rate-limiting step. First, it was proposed that in the initial single electron transfer, an electron is transferred into the LUMO and from there on into the σ*-orbital that is associated with the nitrogen-oxygen bond. Spacial proximity of these two orbitals would certainly facilitate the promotion of the electron. Second, it was pointed out that the donor may complex with substrates that have extended π-systems via π-π-stacking interactions (see also Chapter 1.1.8). Such interactions are expected to encourage a single electron transfer step.[85]

The oxygen-carbon bond in acyloin condensation products **145** was reductively cleaved with electron donor **5** in moderate to high yields to give products **146** (Scheme 1-29 A).[86] A good leaving group was a prerequisite for this reaction to be feasible. When the hydroxy group is acetylated, an alternative reaction pathway becomes accessible (Scheme 1-29 B). The

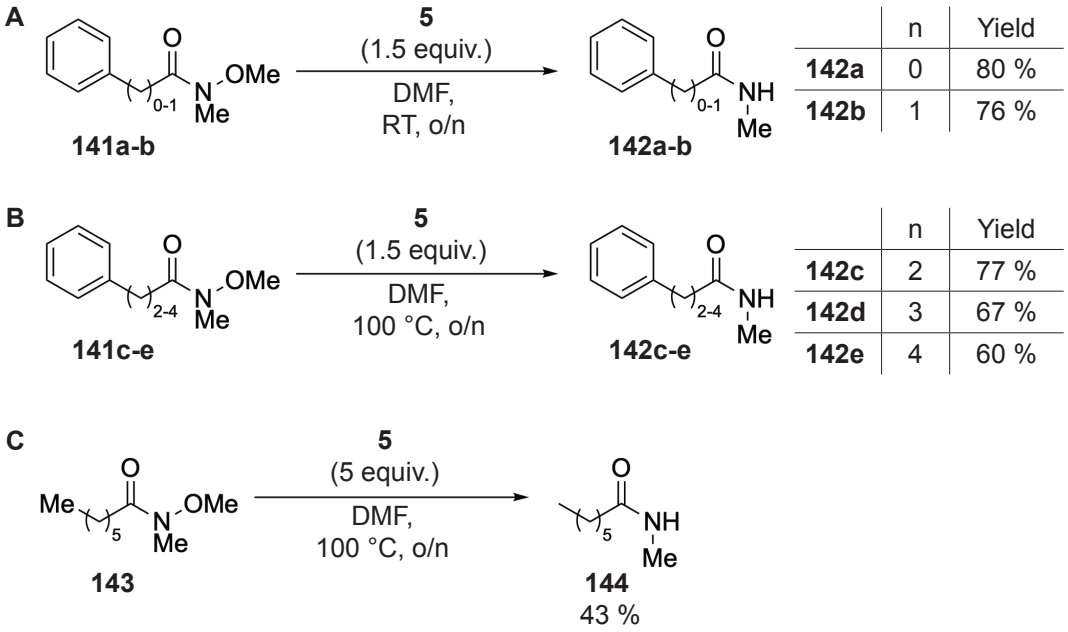

Scheme 1-28 On the basis of the reductive nitrogen-oxygen bond cleavage with Weinreb amides, the assisting effect of a phenyl group in the substrate molecule was demonstrated.

electron donor **5** can act as a base and convert the substrates **147** into the α,β-unsaturated γ-lactones **148**. Only aliphatic substituents R^1 and R^2 were tolerated in the latter, base-catalysed transformation.[86]

Both triflate esters and triflamides were reductively cleaved with donor **5**.[8] On the basis of the aliphatic and aromatic triflate esters **149** and **151**, respectively, (Scheme 1-30) some key reactivity patterns of the electron donor can be highlighted. The selective oxygen-sulfur bond cleavage of the aliphatic triflate esters **149** to give the alcohols **150** is unprecedented (Scheme 1-30 A). Moreover, the example illustrates that the compound **5** is more reductive

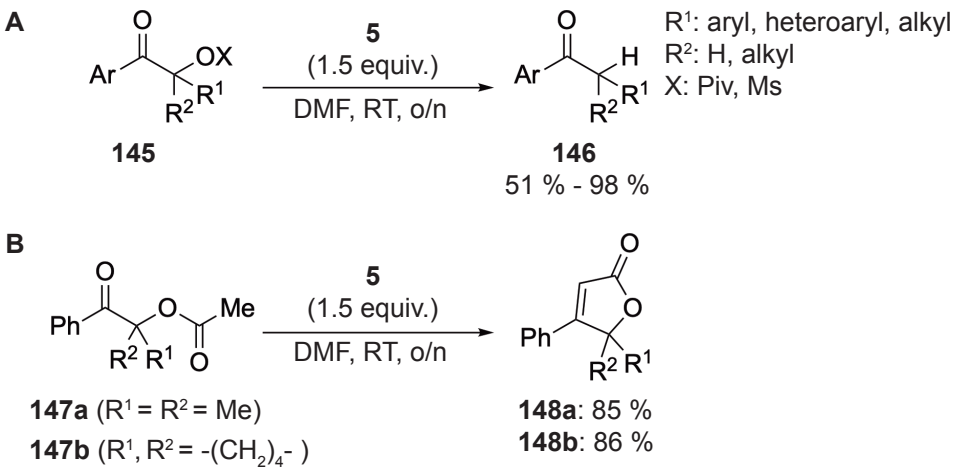

Scheme 1-29 A The reductive elimination of the hydroxy group in acyloin coupling products is possible if the hydroxy group is turned into a good leaving group. **B** If the hydroxy group is acetylated, the electron donor can act as a base and lead to the formation of α,β-unsaturated γ-lactones.

than nucleophilic - it reduces a challenging substrate but it does not touch a very good electrophile. In the series of substrates **149**, the proximity of an aromatic system to the triflate function has little effect on the reaction. Indeed, computational investigations showed that the LUMO is always associated with the sulfonate function regardless of the length of the alkyl linker. This is in contrast to what has been found with the series of Weinreb amides (Scheme 1-28). It indicates that the proximity of aromatic systems to the reactive functional group in the substrate molecule can - but does not always - critically assist reduction reactions with neutral organic electron donors. The aromatic triflate ester **151** was reduced to the phenol **152** in high yield (Scheme 1-30 B). The isomerisation of the double-bond in the side-chain of the compound **152** is another manifestation of the electron donor's basicity.[8]

The question of the hydrogen atom source in the above discussed reactions has been tackled in detail for the electron donor **5** and the imidazole donor **27**. It was found that in both cases the major source is the hydrogen atoms on the heterocycles next to the nitrogen atom.[82]

1.2.7 Radical Trapping and One-Carbon Extrusion

When primary iodides or bromides were treated with the electron donor **27** under standard conditions, it was noted that traces of an aldehyde were formed. When the crude material was subjected to an acidic work-up it was possible to isolate the aldehyde **154** and **156** from the substrates **153** and **155**, respectively (Scheme 1-31). The additional carbon atom could stem from the solvent and indicate the formation of an alkyl anion, which would nucleophilically attack DMF. However, from the reaction with **155** performed in *N,N*-dimethylacetamide (DMA) the solvent was ruled out as a source of the new carbon atom (Scheme 1-31 B). With DMA as the electrophile, one would expect the ketone **157** to be formed. Instead, the formation of the aldehyde **156** was observed again, while **157** was not detected. This finding only leaves the donor itself as the possible source of the new carbon atom.[87] Hence, the formation of an intermediate **158** was proposed (Scheme 1-32 - they reaction pathways that may lead to this intermediate will be discussed later, see Scheme 1-35).[87] The structure would be in equilibrium with the carbene **159**, which may transform into **160** via a proton transfer. Nucleophilic

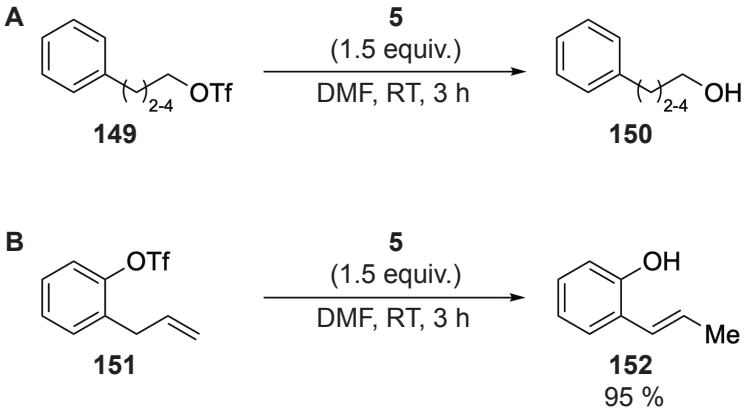

	n	Yield
150a	2	91 %
150b	3	93 %
150c	4	85 %

Scheme 1-30 The electron donor shows interesting selectivities towards aliphatic triflate esters. The carbon-sulfur bond is selectively cleaved. Aromatic triflate esters may be reduced in the same way.

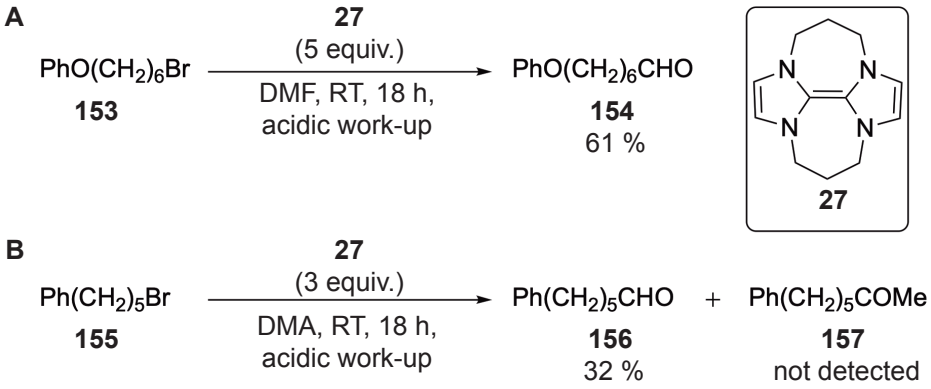

Scheme 1-31 When alkyl iodides or alkyl bromides are treated with the electron donor **27** one-carbon homologated aldehydes can be isolated.

attack of the enamine function onto the iminium function would then lead to **161**, which upon acidic work-up could liberate **162**. The latter compound can undergo decarboxylation, which gives the observed aldehyde **163**.[87]

The proposed mechanism postulates a disproportionation of oxidation states between the two imidazolium units in order to reach the oxidation state of the carbonyl carbon atom. In principle, a second molecule of the electron donor **27** could reduce **159** to **164**, which upon hydrolysis would give the aldehyde as well (Scheme 1-32). To test for this possibility the compound **165** was treated with electron donor **27** (Scheme 1-33). After an acidic work up that would hydrolyse **166**, no aldehyde **167** was detected. The fact that, from **165**, product **167** is not obtained, indicates that the electron donor **27** is unlikely to be able to reduce the imidazolium compound **159** to the corresponding 2,3-dihydroimidazoline **164** (Scheme 1-32).[87]

To better back-up the proposed mechanism, a substrate class was designed, that would give an alternative product to the homologated aldehyde compounds. Moreover, this alternative product would be characteristic for the adduct **158** or one of the structures that **158** is

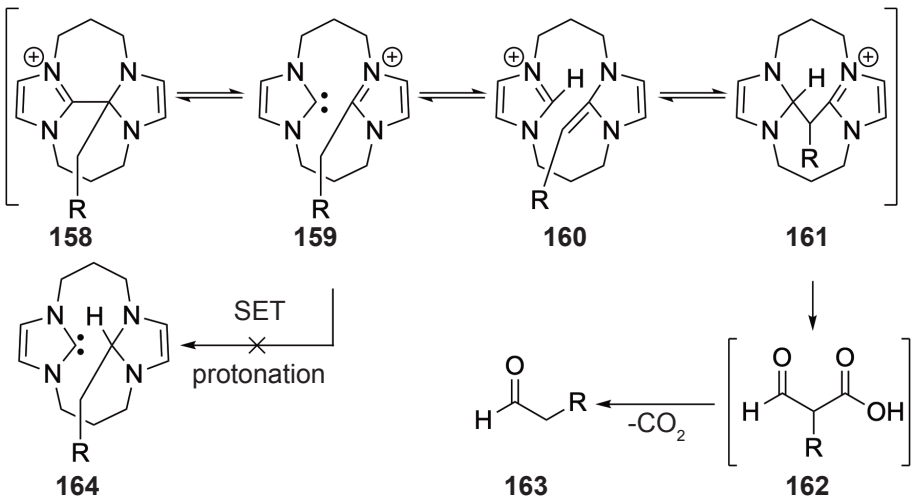

Scheme 1-32 A plausible mechanism leads from the adduct species **158** to the one-carbon homologated aldehyde product **163**.

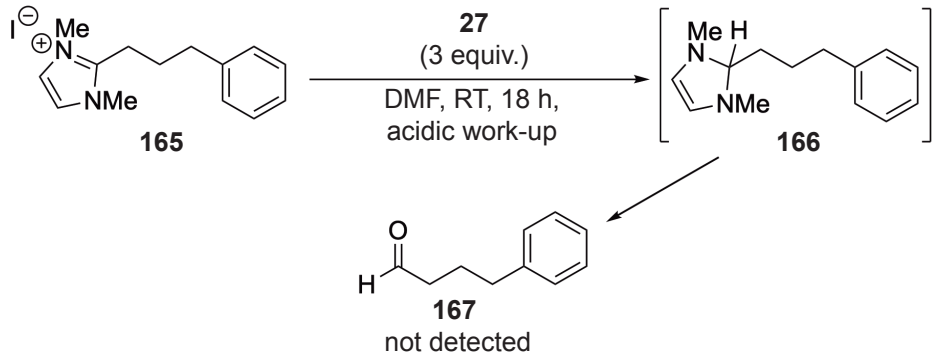

Scheme 1-33 Reduction and protonation of imidazolium compounds with the electron donor **27** is not possible under the examined conditions.

in equilibrium with (Scheme 1-32). The ether **168** is such a probe substrate (Scheme 1-34).[88] The structure **169** corresponds to the structure **160** in Scheme 1-32. The intermediate **169** can eliminate methanolate R^1O^- (overall this is an E1cB-elimination process). This route is an alternative to the intramolecular nucleophilic bond formation, which leads from **160** to **161** in Scheme 1-32. In a second E1cB-elimination, the second alcohol R^2OH **175** is formed. It seems unlikely that the alcohols are liberated via an E2 mechanism where the donor would act as a base (it was shown for the DMAP-derived electron donor **5** that an E2 reaction with alcohols does not occur).[88] The remaining best explanation is the one shown and it requires the intermediate **169** or **160**, respectively.[88]

How are intermediates like **158** (Scheme 1-32) or **169** (Scheme 1-34) formed? Three plausible pathways were discussed (Scheme 1-35). First, the electron donor **27** could act as a nucleophile towards the substrate **176** (Path 1). Second, the two radicals **177** and **178** formed

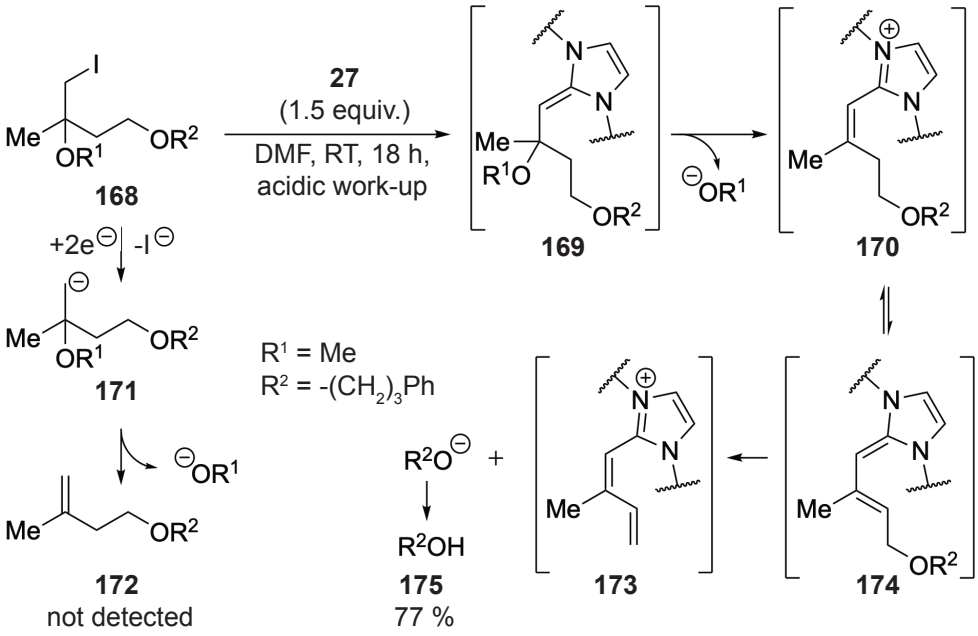

Scheme 1-34 Evidence for the mechanism as proposed in Scheme 1-32 was obtained with 1,3-diether substrates and the diagnostic liberation of the alcohol R^2OH.

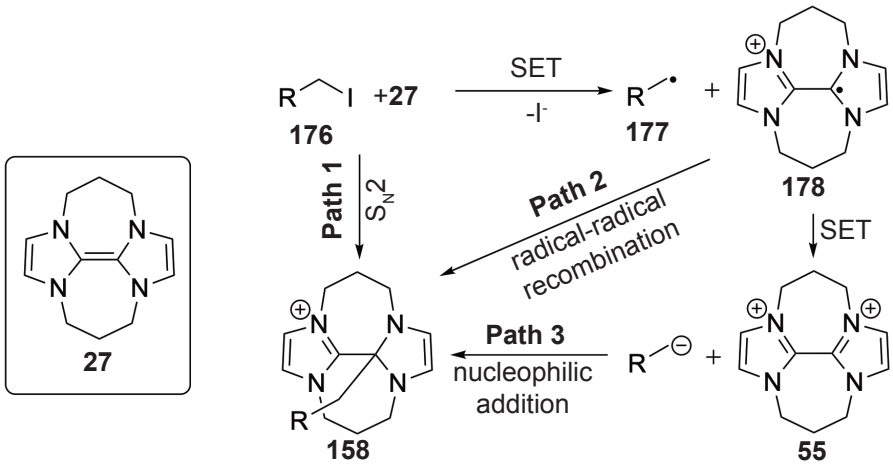

Scheme 1-35 Three pathways for the formation of the adduct species **158** were discussed.

after the first single electron transfer step could recombine (Path 2). Third, after a second single electron transfer the ion pair **55** and a carbanion would form, which could then collapse to the neutral species **158** (Path 3). With the probe molecule **168**, it was possible to shed some light on this question. If **168** was reduced to the anion **171**, one would expect the formation of **172** after the expulsion of an alkoxide anion (Scheme 1-34). This compound, however, was not detected.[88] Hence, Path 3 was ruled out as the mechanism behind the formation of **158**. However, based on the results with probe molecule **168**, it was not possible to rule out either Path 1 or Path 2. Further evidence, that will be discussed in the next paragraph in a slightly different context, suggested that the radical-radical recombination Path 2 is more likely. In brief, characteristic products that originated from donor-substrate adducts **158** were observed *after* a radical cyclisation of the substrate. Overall there is strong indication for the presence of radical intermediates and, as a consequence, that the adduct **158** can form via radical-radical recombination according to Path 2.[87]

The reactivity of electron donor **27** discussed above is unique insofar as a carbon atom is transferred from the electron donor to its substrate. But the initial recombination step of the donor molecule with its substrate also finds its counterpart in reactions with the benzimidazole-derived electron donor **4** and the DMAP-derived electron donor **5**. For these two electron donors the recombination does, however, not lead to a one-carbon homologation of the substrate. The two compounds **4** and **5** have been studied[88] with an analogous approach as exemplified for **27** above. It is worthwhile to directly compare the results for the three electron donor species reacting with the same substrate **179** (Scheme 1-36). When the substrate **179** is treated with one of the electron donors **4**, **5**, and **27**, three products can form. Compound **180** arises in a direct reduction either via the aryl radical and hydrogen abstraction or via the aryl anion and protonation. For the formation of **181** and **182**, a radical cyclisation is required. If the product radical abstracts a hydrogen atom, the compound **181** is obtained. However, if the product radical recombines with the donor radical cation, the alcohol **182** can be liberated according to a similar mechanism to the one shown in Scheme 1-34 and Scheme 1-35.[88]

One way of looking at the data in Scheme 1-36 is to note that the formation of products **181** and **182** requires a radical cyclisation. The relative amount of alcohol **182** on the sum of

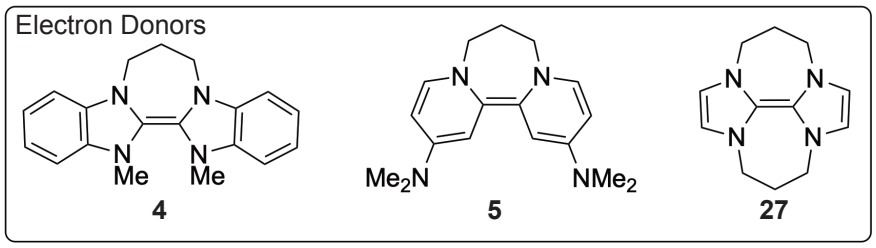

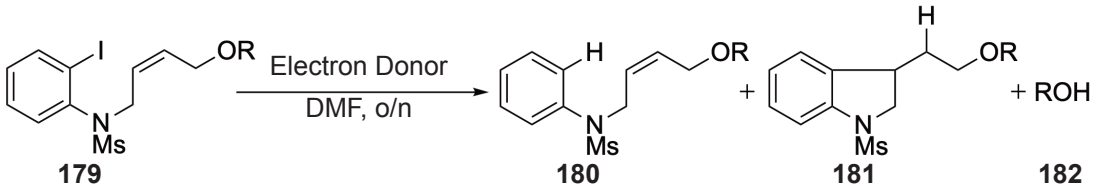

Electron Donor \ Product	**180**	**181**	**182**	**182** / (**181** + **182**) x 100 %
4	13 %	34 %	8 %	19 %
5	14 %	not detected	3 %	100 %
27	27 %	8 %	35 %	81 %

Scheme 1-36 The formation of the alcohol **182** indicates recombination between the electron donor and its substrate after the radical cyclisation step.

the 'radical cyclisation products' **181** + **182** gives an estimate of the fraction of radicals that are trapped by the electron donor. It becomes obvious that the electron donors **27** and **5** are particularly prone to radical trapping as the relative amount of alcohol **182** on total 'radical cyclisation products' is particularly high. The benzimidazole donor **4** instead, leads mainly to the formation of the cyclised product **181**. It should be noted, however, that also this electron donor recombines at least with a fraction of the radicals it generates (i.e. with 19 % of the alkyl radicals that are formed after the radical cyclisation). Hence, the trapping of alkyl radicals is a recurring theme among organic super-electron donors.[88]

It was difficult to explain the different extents of radical trapping by the different electron donor molecules. It was noted that the gain in aromaticity upon radical-radical recombination may be different for the three radical cations **183**, **184** and **178** (Figure 1-12). The driving force from gaining aromaticity would be lowest for the benzimidazole donor for the same reasons that make it the least reducing electron donor in this series (Chapter 1.1.8). The less favourable thermodynamics of the recombination for this donor could manifest in a higher energy barrier for this process.[88] The unpaired spin in the radical cation **183** can be delocalised over a larger ring system than in **184** or **178**. This may explain the greater kinetic stability of **183** and thus its greater reluctance to recombine with alkyl radicals. The radical cations derived from the electron donors are likely to accumulate in the reaction mixture. They eventually reach levels where the trapping of the low-abundant alkyl radicals derived form the substrate becomes efficient. Hence, the process likely is an example of the persistent radical effect (also referred to as Fischer-Ingold effect).[89,90]

With the above electron donors, the radical trapping reaction led to unwanted by-products.

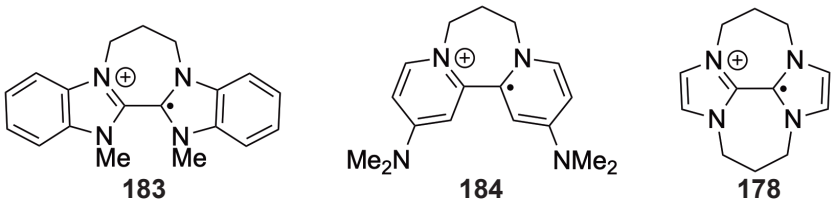

Figure 1-12 Radical cations derived from the electron donors **4**, **5, and 27**.

However, a similar radical trapping event can be desirable in other contexts. By deprotonating 2-azaalyls **185**, Walsh et al. formed highly reducing anion species **187** (Scheme 1-37 A).[91] These anions were able to donate an electron to an aryl or alkyl halide substrate **186**. Upon fragmentation of the carbon-halogen bond, an aryl or alkyl radical **189** was generated, respectively. This radical was trapped with high efficiency by the neutral radical **188**, which was derived from the azaallyl substrate. Detailed mechanistic investigations - for example with probe substrates such as **192** (Scheme 1-37 B) - allowed the radical nature of the process to be established and the proposed radical-radical recombination step to be substantiated.[91] Later a similar study was published that employed aryl nitriles as substrates, instead of aryl halides.[92]

1.3. Comments on Reductive Radical Reactions with Organic Super Electron Donors

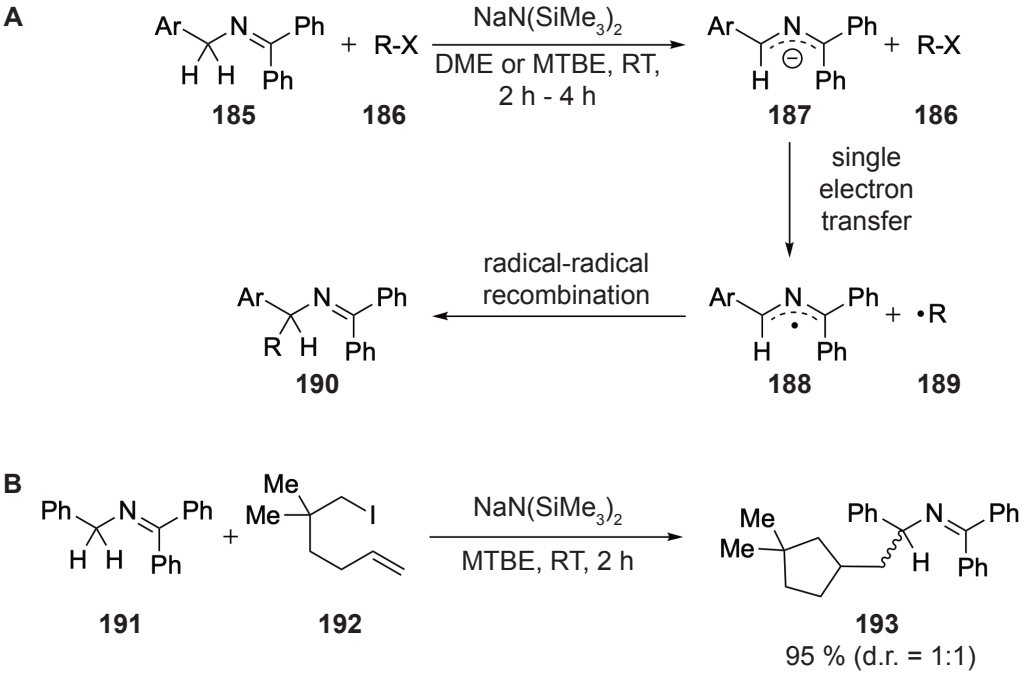

Scheme 1-37 While radical recombination reactions are problematic with neutral organic super electron donors, the same effect can be synthetically useful in related systems.

The classical reagents for hydrogen atom transfer reactions are trialkyltin hydrides and tris(trimethylsilyl)silane (TTMSS). Both reagents experienced widespread application in radical chemistry and have proved to be extremely useful hydrogen atom sources. However, they both suffer from significant drawbacks. The tin reagents are highly toxic and their by-products are difficult to remove. The silane reagent suffers from its high costs. Thus, much effort was made to find alternatives. Murphy et al. pioneered the use of hypophosphites and diethylphosphine oxide[93] in radical bond forming reactions.[94] Other developments include catecholborane, complexes of borane with N-heterocyclic carbenes, complexes of trialkylboranes with water and a range of organometallic complexes.[95] Borohydrides, too, have been used as hydrogen atom donors. Typical radical reactions with borohydrides require photoactivation by UV-irradiation.[96]

Most of these reagents involve a hydrogen atom abstraction as the chain-propagating step. There are very few examples where a single electron transfer lies at the heart of the chain propagation step. One example is given by Studer et al. where alcoholates act as hydrogen atom donors (their α-hydrogen atom is abstracted in the course of the reaction).[97] Although many of the introduced reagents for reductive radical reactions have their particular advantages, no reagent is without drawback or limitations. Thus, the need for alternatives still exists and it is worthwhile to take a look at where neutral organic electron donors take their place amongst these reagents.

As became clear from the discussion of radical – radical cation recombination reactions (Chapter 1.2.7) with the imidazole-derived electron donor **27** and the DMAP-derived electron donor **5**, it is not possible to profit from their electron donor properties in radical reactions when alkyl radicals are involved. The benzimidazole-derived electron donor **4**, in contrast, shows a much lower tendency to recombine with alkyl radicals. In an attempt to combine the superior electron donor strength of **27** or **5** with the favourably slow reactivity towards radicals of the benzimidazole donor's radical cation, hybrid electron donors were synthesised (Scheme 1-38). Their redox potentials were intermediate between the potentials of the parent electron donor compounds. Compound **194** and **195** showed fully reversible electrochemical behaviour and two consecutive one-electron waves were resolved. Compound **196** showed partially irreversible behaviour and only one redox event was observed.[65]

The hybrid donors were assayed with the aryl iodide **197**, which can either be directly reduced to compound **198** via a radical or an anionic intermediate. Alternatively, the substrate can undergo a reductive radical cyclisation reaction to form **199** (Scheme 1-38). The electron donor **195** is clearly superior to the other two examples in terms of the yield of cyclised product but also in terms of the total recovery of material. The most likely way of material loss is radical – radical cation recombination (Chapter 1.2.7). However, no direct proof is given for the nature of the side-reactions that lead to loss of material. Overall, the approach of merging different subunits to create 'hybrid' electron donors was quite successful. Compared to the benzimidazole-derived electron donor **4**, the 'hybrid' electron donor **196** is 0.27 V more reducing while retaining the good performance in radical cyclisation reactions.[65]

Although successful, the mix-and-match approach introduced above does not solve the fundamental issue of using organic super electron donors in reductive radical reactions. The vast majority of organic electron donors introduced so far are potential *double* electron donors - most of the exceptions belong to the class of simple and only moderately reducing amines. What is needed in radical reactions is a potent organic *single* electron donor. One example

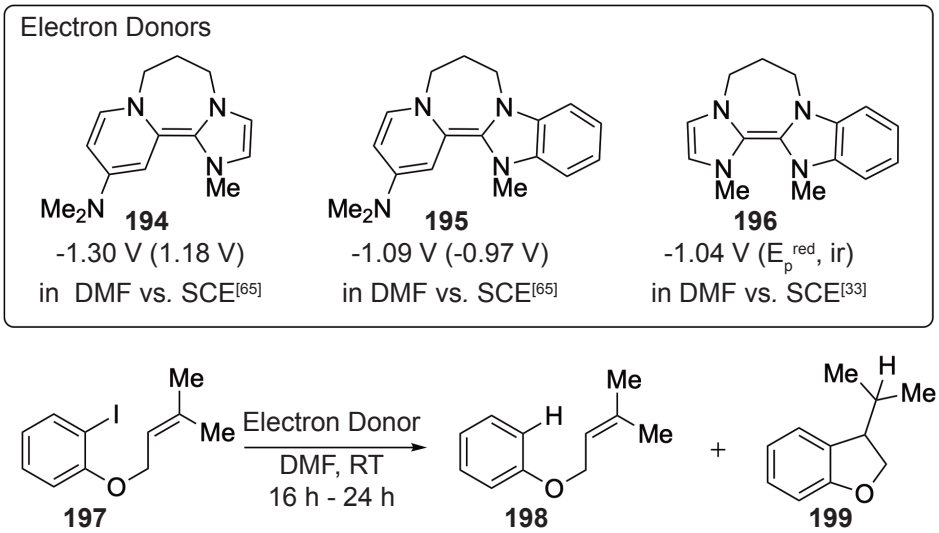

Electron Donor \ Product	197	198	199	total recovery of material
194	not detected	59 %	not detected	59 %
195	6 %	12 %	74 %	92 %
196	12 %	17 %	25 %	54 %

Scheme 1-38 The redox potentials of the hybrid electron donors were found to be intermediate between the parent compounds. If a second redox event is observed the more positive value is given in brackets. (ir) means irreversible and the peak potential of the reduction peak potential of the corresponding salt is given. The performance of the hybrid electron donors **194** - **196** in radical cyclisation reactions was analysed.

(although only studied theoretically) of such a single electron donor was already encountered earlier on, namely structure **60** (Figure 1-13). It essentially corresponds to one half of the imidazole-derived electron donor **27**. Recently, related radical species such as **201** and **202** have been investigated by cyclic voltammetry. Compounds, such as **202**, have even been isolated and characterised by X-ray diffraction analysis and EPR experiments.[98] It is quite exceptional that radical species as reactive as **201** and **202** can be obtained in solid form. In general, open-shell species like **60** will only transiently exist. The radical species **201** and **202** were generated by reducing the precursor salt with potassium naphthalide. An alternative precursor may be the aminal species as, for example, aminal **200** for **60**.

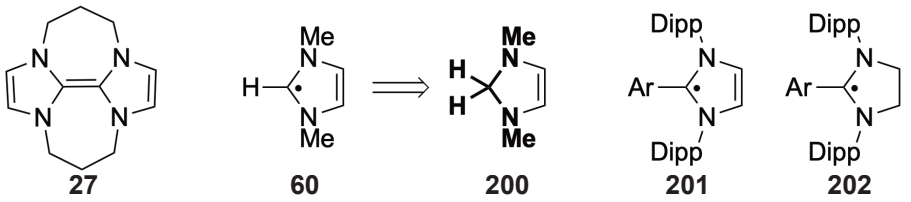

Figure 1-13 Aminals are potential precursors of single electron donors.

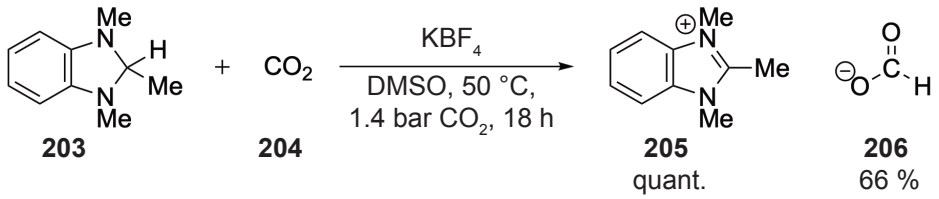

Scheme 1-39 The reduction of CO_2 to formate by 2,3-dihydrobenzimidazole **203** was proposed to proceed via a hydride transfer.

In the context of reduction reactions, aminals are typically discussed as hydridic reducing agents. In a very recent study, for example, it was demonstrated that the 2,3-dihydrobenzimidazole derivative **203** is able to reduce CO_2 to formate (Scheme 1-39).[99] Based on a computational model [the DFT method used was M06/6-31+G(d,p)/PCM(DMSO)] a plausible mechanism was put forward, where a hydride from the aminal function is transferred to CO_2 in a single step. In the same study, in a separate reaction step, it was shown that **203** can be electrochemically regenerated from **205**.[99]

Chikashita et al. employed 2,3-dihydrobenzimidazole compounds and related structures in typical hydride reduction reactions.[100,101] However, the question about the mechanism became more challenging when 2,3-dihydrobenzimidazole derivative **207** was used to selectively reduce a range of α-halocarbonyl compounds **208** to the corresponding carbonyl compounds **210** (Scheme 1-40 A). From most of these reactions it was possible to isolate the salt **209**. Since the compound **207** was found not to reduce carbonyl functional groups, it was hypothesised that it might be an interesting reducing agent to convert acid chlorides to aldehydes. Indeed, **207** was also found to cleanly reduce acid chlorides to aldehydes (Scheme 1-40 A).[102] Based on relative reaction rates of different α-halocarbonyl compounds, it was suggested that **207** acts as a hydride source.[102]

Tanner et al. later demonstrated that at least for the reaction of **207** with α-halocarbonyl compounds, a radical mechanism is operative (Scheme 1-41).[103] When the reduction reaction

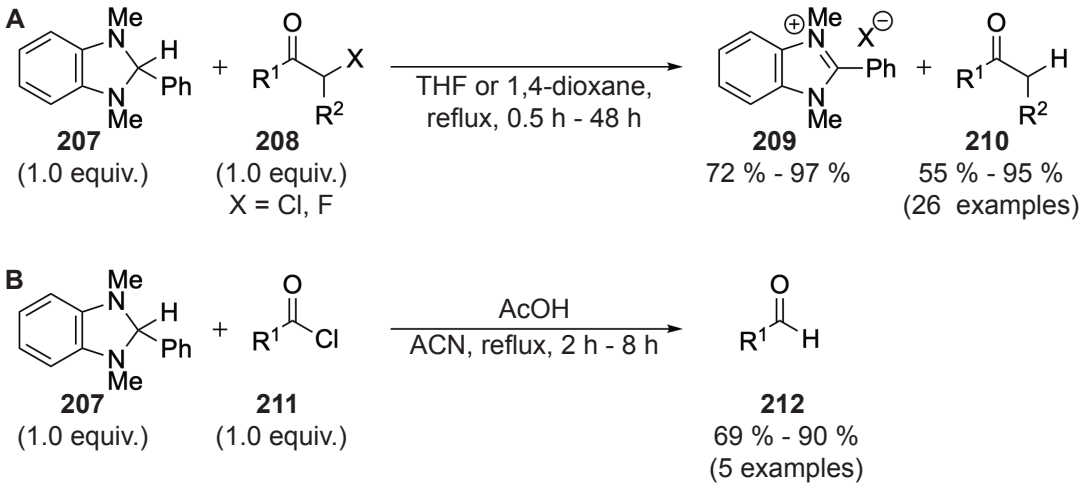

Scheme 1-40 The 2,3-dihydrobenzimidazole **207** derivative was effective at reducing α-halocarbonyl compounds **208** to the carbonyl compounds **210** and acid chlorides **211** to aldehydes **212**.

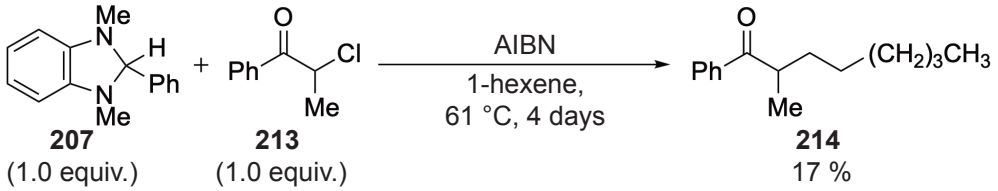

Scheme 1-41 When the reduction of **213** by **207** was performed in 1-hexene as a solvent the addition product **214** was formed, which can only arise form radical intermediates.

of the substrate **213** with the 2,3-dihydrobenzimidazole reagent **207** was performed in 1-hexene as a solvent, the addition product **214** was formed. The product **214** can only arise from radical intermediates. Further experiments with radical initiators and inhibitors substantiated the radical nature of this reduction reaction. Based on these findings, a radical chain reaction mechanism was proposed (Scheme 1-42).[103] After an initiation step, the radical **216** is formed from **207**. This open-shell species can act as a single electron donor towards the substrate **208**. Thereby the salt **209** is formed, together with the radical **215**. This radical abstracts a hydrogen atom from another molecule of **207** in the chain propagation step. This gives the product **210** and regenerates the single electron donor species **216**.[103] An analogous mechanism has previously been proposed for reduction reactions with NADH model compounds[104] and NADH itself (if reacting in solution, but not if bound to the enzyme as a co-factor).[105] The reactivity of **207** has been further explored by Tanner et al. since, and the proposed mechanism was additionally substantiated.[106-109]

Another enzymatic co-factor that is generally discussed as a hydridic reducing agent is 5,10-methylenetetrahydrofolate.[110] Possible model compounds for this co-factor are imidazolidines[110] such as **217**. Wanzlick et al. demonstrated that this compound can be oxidised

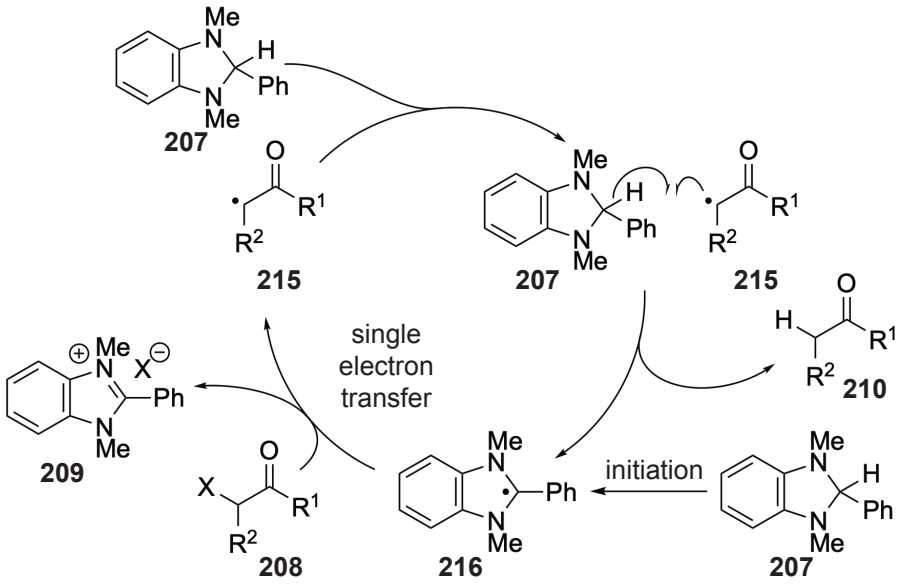

Scheme 1-42 In the reduction of **208** with **207**, the open-shell single electron donor species **216** was proposed as a key intermediate in the radical chain reaction.

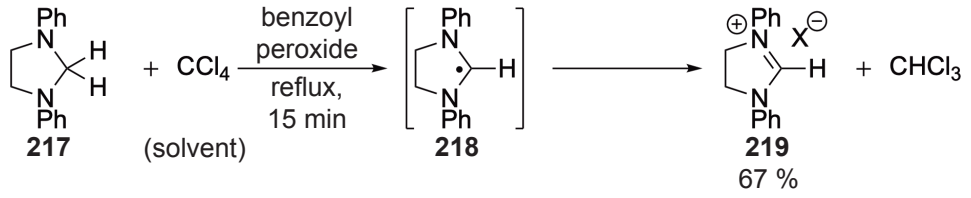

Scheme 1-43 For the mechanism of the oxidation reaction of **217** with carbon tetrachloride a radical intermediate **218** was proposed.

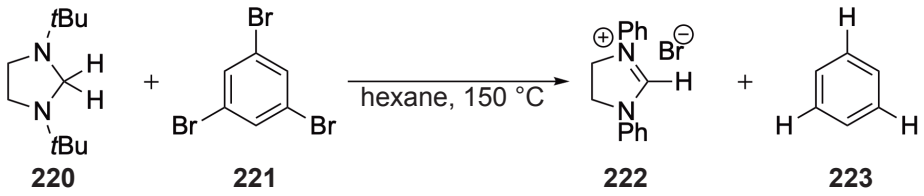

Scheme 1-44 The imidazolidine **220** is able to reduce 1,3,5-tribromobenzene **221** to benzene.

with carbon tetrachloride to give **219** and chloroform (Scheme 1-43). A radical mechanism was suggested as the main reaction pathway.[111] Later, Denk et al. showed that aminals related to **217** can act as potent reducing agents.[111,112] For example, it was possible to reduce 1,3,5-tribromobenzene **221** to benzene with the imidazolidine **220** (Scheme 1-44).[110]

These results suggest that aminals can be interesting reducing agents. Moreover, a radical chain mechanism, as suggested by Tanner et al. (Scheme 1-42),[103] may be accessible for a wider class of aminals. Hence, this compound class potentially harbours many precursors of single electron donors than can be exploited in reductive radical reactions. Although 2,3-dihydrobenzimidazole derivatives have been studied in detail[113] and used, for example, in combination with light activation,[114-118] a more general discussion of the application of aminals as precursors of ground-state electron donors, such as **216**, could not be found in the literature.

1.4. Upconversion of Reducing Power

The discussion of aminals as precursors of single electron donor species implies that a mildly reducing precursor **224** can be converted into a potential single electron donor **225** by homolytic fragmentation of a carbon-hydrogen bond (for example by hydrogen abstraction by a radical) (Scheme 1-45). Similar reactions recently have been discussed under the title ‘Upconversion of Reductants’.[119] In typical electron transfer reduction reactions, the reducing agent is present in the reaction mixture in stoichiometric amounts from the beginning. In stark contrast, upconversion of reducing power requires that the reducing species is formed continuously during the reaction. Typically, this happens in a catalytic cycle that can be conveniently described with the notion of the electron as a catalyst.[120]

A representative example of upconversion of reducing power is shown in Scheme 1-46.[121] After an initial single electron transfer to the substrate **226** the labile N-O bond fragments to give the anion **228** and the oxygen-centred radical **229**. The benzylic hydrogen atoms are particularly acidic due to the unpaired spin on the oxygen atom. The subsequent proton transfer

Scheme 1-45 Hydrogen abstraction from **224** turns the compound into a potential single electron donor. Overall the system becomes more reducing.

between **228** and **229** is a typical example of a radical enhanced deprotonation.[122,123] The generated ketyl radical **230** is highly reducing - much more reducing than the radical anion of the substrate **227**. The radical **230** first transfers the electron onto **231**. The radical anion **233** then engages in the chain-propagating single electron transfer to another molecule of substrate.[121]

During the autocatalytic decomposition of **226**, a highly reducing species **230** is generated from a less reducing species **227**. A general scheme to define and measure the extent of the upconversion of reducing power over a reaction sequence has been suggested (Figure 1-14).[119] The scheme is based on the comparison of two analogous reactions - one with n electrons in the system (referred to as 'neutral reaction' in Figure 1-14) and one with n+1 electrons (referred to as 'radical anion reaction' in Figure 1-14). It follows that, if the n+1 electron reaction is less exergonic than the n electron reaction, upconversion of reducing power occurred. The extent of the upconversion can be measured as the difference between the Gibbs free energy of the two analogous reactions. This difference in the Gibbs free energy is related to the difference between the redox potential ΔE of the precursor and the product by $\Delta G_{Upconversion} = -F\Delta E$, where F stands for the Faraday constant.[119] As an extension of the scheme, the opposite

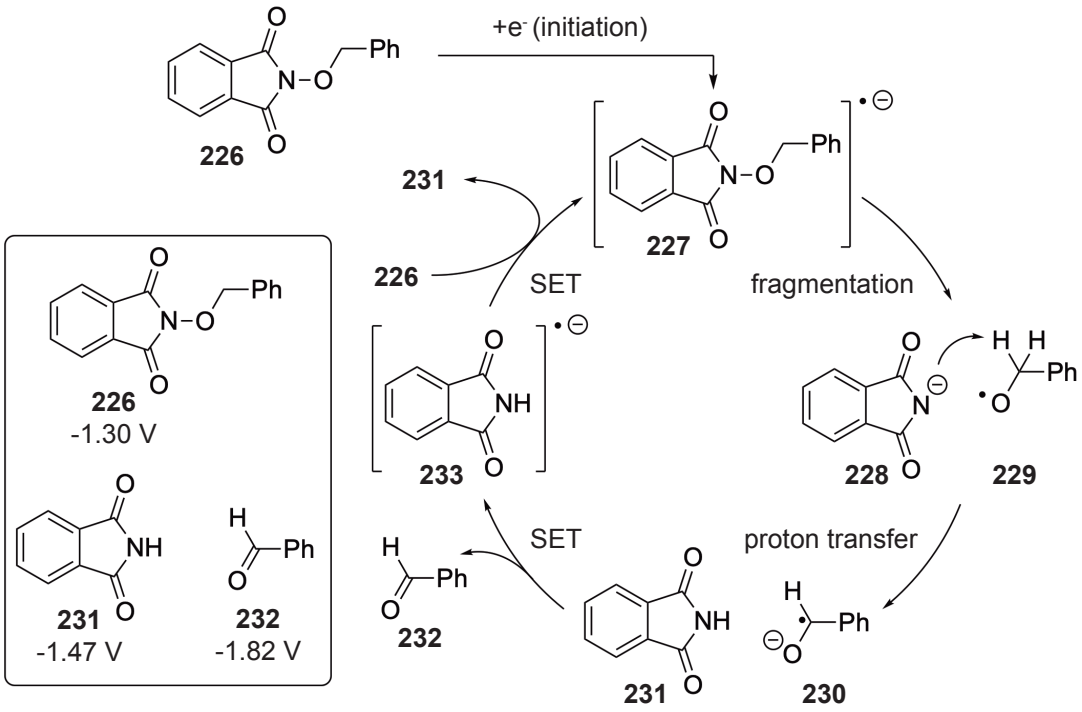

Scheme 1-46 The decomposition of **226** under electrochemical conditions was observed to be autocatalytic. The E_p^{red} values (in DMF vs. SCE) are given for the three key intermediates of the cycle.

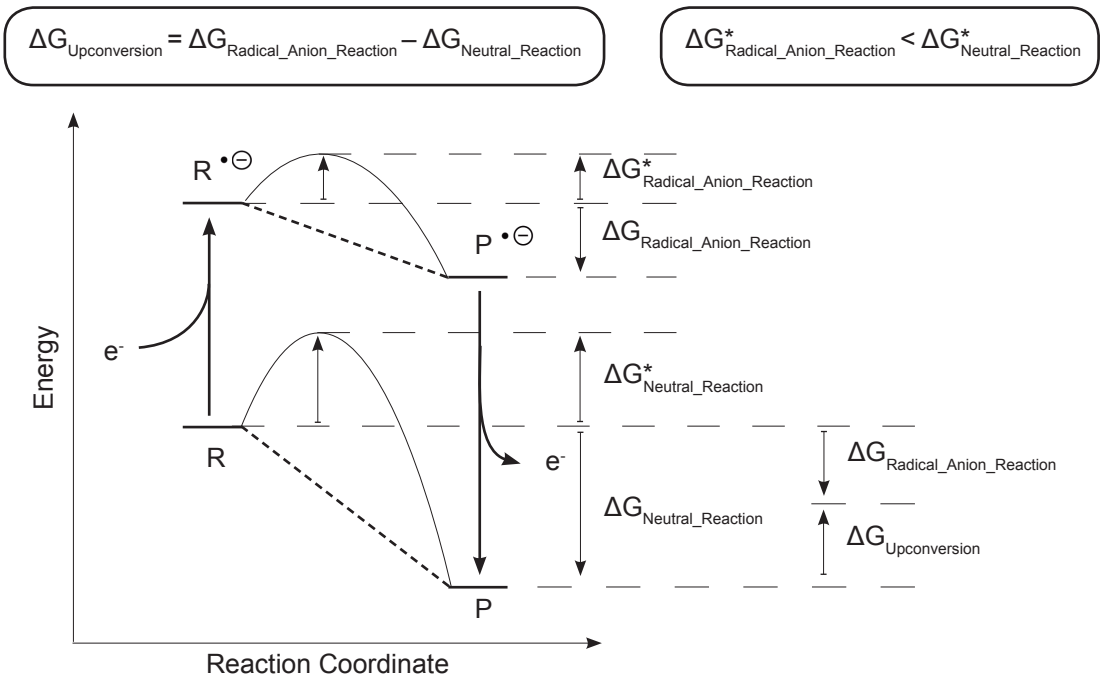

Figure 1-14 A general scheme to define and measure the upconversion of reducing power during a reaction has been suggested.[119]

case, when the n+1 electron reaction is more exergonic than the n electron reaction, can be regarded as upconversion of oxidation power. Also, in principle it is possible to generalise the scheme further and to compare an n electron reaction to its n+x electron counterpart. In this more general situation, the difference in the $\Delta G_{Upconversion}$ is related to ΔE by $\Delta G_{Upconversion} = -xF\Delta E$, where x stands for the number of transferred electrons. For example, if the upconversion of reduction power in the formation reaction of the classical dimeric electron donors **235** is to be discussed, x = 2 is required (Scheme 1-47). In this case, the n+2 electron reaction starts from the precursor **234** and leads to the neutral electron donor molecule **235**. The n electron reference reaction starts from the radical cation species and leads to the dication **237**, which is the oxidised form of the electron donor **235**.

Upconversion of reducing power can be found in very different examples and the impression may arise that it is a specialised phenomenon. This is not the case. On the contrary, it is a widespread phenomenon that is at the heart of the mechanism of some important reaction classes.[119] For example, upconversion of reducing power drives many $S_{RN}1$ reactions[124] and BHAS reactions.[125] The generally accepted reaction mechanism of the BHAS reaction is shown in Scheme 1-48 for the formation of biphenyl.[125] In the initiation step, an electron is injected into **238**. The resulting radical anion **239** undergoes fragmentation. The phenyl radical **240** then adds onto a molecule of benzene, which leads to the cyclohexadienyl radical **241**. The methine hydrogen atom shown in **241** is relatively acidic due to the presence of the unpaired spin in the molecule. Consequently, it undergoes facile deprotonation to give the radical anion **242**. Species **242** engages in the chain-propagating single electron transfer step, which regenerates the radical anion **239** and forms the product biphenyl **243**. Focusing on the most elementary step, upconversion of reducing power occurs when the cyclohexadienyl radical **241** is deprotonated to give the radical anion **242**. One can also choose to analyse the

n+2 Electron Reaction

234 235

n Electron Reaction (hypothetical reference reaction)

236 237

Scheme 1-47 The scheme to measure upconversion of reducing power can be applied to the classical double electron donors. In this case, the difference of the number of electrons between the two corresponding reactions is two electrons and not one as in the original scheme.

whole reaction sequence in terms of upconversion of reducing power. To do so, the reduction potentials of **238** and **243** are compared. It was found that **238** with X = I is easier to reduce than biphenyl **243**. Hence, it is expected that the radical anion **242** can efficiently transfer an electron to another molecule of substrate **238**. Hence, also for the scope of the whole reaction sequence from **239** to **243**, upconversion of reducing power occurs. The situation is different, however, for the substrate **238** with X = Br. Then the chain-propagating electron transfer from **242** to another molecule of substrate is uphill, as comparison of the reduction peak potential of the corresponding compounds suggests. There is no upconversion of reducing power occurring over the whole reaction sequence, which means that the chain propagating electron

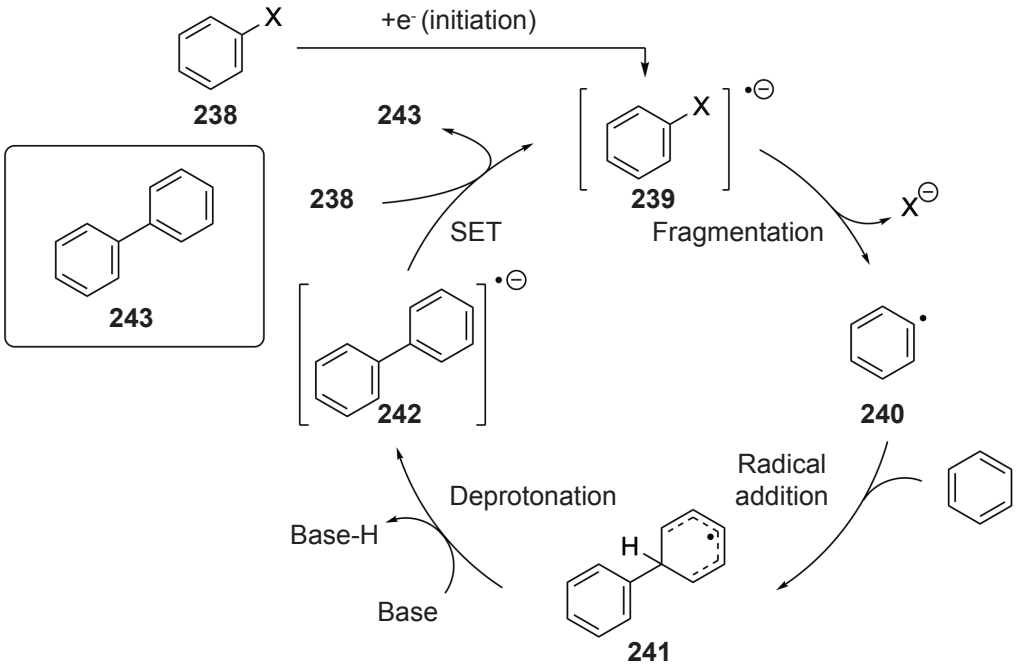

Scheme 1-48 In the BHAS reaction, upconversion of reducing power occurs when the intermediate **241** is deprotonated.

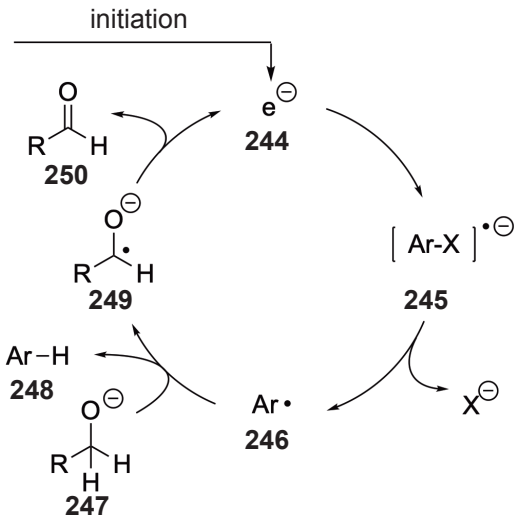

Scheme 1-49 Upconversion of reducing power was achieved by converting alcoholates into ketyl radicals.[97]

transfer is less efficient. Consequently, the yield for the reaction with bromobenzene is lower compared to the reaction with iodobenzene. However, the deprotonation step from **241** to **242** is still the same. Thus, although there is no upconversion of reducing power over the whole reaction sequence, there is upconversion of reducing power occurring during this elementary step.[119] In BHAS reactions, upconversion of reducing power also is a key characteristic of the initiation step[126,127] and possible radical proliferation mechanisms.[128]

Studer et al. turned alcoholates into highly reducing ketyl radicals to drive a reductive dehalogenation chain reaction (Scheme 1-49).[97] The mechanism of the reaction is drawn with the notion of the electron as a catalyst.[120] The key step is the hydrogen atom abstraction from the alcoholate **247** by the aryl radical **246** to give the ketyl radical **249**. During this step, the reduction potential of the system increases. Indeed, the ketyl radical is a strong enough electron donor to reduce aryl iodide and aryl bromide substrates efficiently.[97] In a similar study, highly reducing radical anion intermediates were generated from the solvent 1,4-dioxane. With this reagent system, it was possible to reduce aryl bromides and aryl chlorides.[129]

Examples of upconversion of oxidation power have been reported, for example, by Bauld et al.[130] Upconversion of oxidation power also plays a crucial role in the recently reported hole-catalysed Newman-Kwart reaction.[131,132]

1.5. The KO*t*Bu-Et$_3$SiH Reagent System

1.5.1 Synthetic Applications Reported by Grubbs et al.

With the aim to find a reagent system that is able to reductively decompose lignin into its building blocks, Grubbs et al. investigated various transition metal complexes, hydrogen sources and alkoxide bases.[133] Using the lignin model compound **251**, several reagent combinations were identified that were able to reduce aryl ethers. They all contained triethylsilane and potassium *tert*-butoxide. Surprisingly, control reactions without transition metal complexes showed that these two reagents alone were capable of reductively cleaving the carbon-oxygen

Table 1-1 Reductive cleavage of aryl ethers with KO*t*Bu-Et_3SiH reagent system

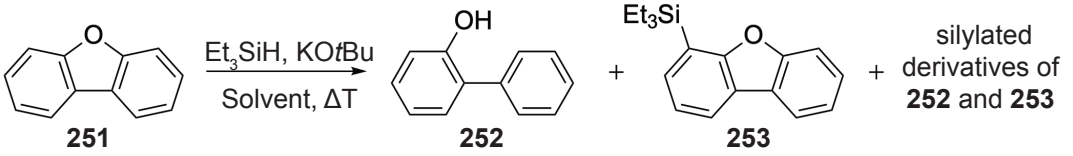

251 **252** **253**

Entry	Et_3SiH equiv.	KO*t*Bu equiv.	Solvent	Temp.	**252**	**253**	Silylated derivatives of **252** and **253**
1	5	5	Toluene	100 °C	63	10	24
2	3	3	Mesitylene	165 °C	85	3	7
3	3	3	Mesitylene + 1,4-cyclohexadiene	165 °C	95	-	-

bond in **251**. Hence, the reactivity of combinations of only triethylsilane and potassium *tert*-butoxide was further investigated (Table 1-1). When **251** was treated with triethylsilane and potassium *tert*-butoxide in toluene at 100 °C, the reduced product **252** was obtained along with other silylated compounds such as **253** (Entry 1). At higher temperatures the distribution of products was shifted towards the desired compound **252** at the expense of silylated products (Entry 2). Although the mechanism of the reaction was unknown at that time, it was proposed that the silylated products arise via a radical mechanism. To shut down these radical pathways, 1,4-cyclohexadiene was added to the reaction as a co-solvent. The result was the exclusive formation of the desired product **252** (Entry 3).[133]

A range of aryl and alkyl ethers was found to be susceptible to reductive cleavage by the KO*t*Bu-Et_3SiH reagent system. In the case of naphthyl ethers, a trace amount of hydrogenated naphthalene was detected. Otherwise the reduction of aromatic systems was not observed. The silylation at aromatic rings was observed to be reversible under the applied reaction conditions.[133]

As the formation of **253** in Table 1-1 already suggests, the reagent system KO*t*Bu-Et_3SiH may be developed further to achieve silylation of aromatic systems. Indeed, that was accomplished by Grubbs et al. two years after their initial publication on this reagent system (Scheme 1-50).[134-136] Using substoichiometric amounts of potassium *tert*-butoxide and performing the reaction at moderate temperature, the silylation of a range of indoles **254** at the C2-position was achieved with good regioselectivity and yield (Scheme 1-50 A). But not only indoles were viable substrates. A range of other heterocycles was silylated with equally good regioselectivity and yield (Scheme 1-50 B). Also, benzylic positions were found to be viable to silylation with this protocol (Scheme 1-50 C).[134] By changing potassium *tert*-butoxide for either sodium hydroxide or potassium hydroxide, the silylation of terminal alkynes became possible (Scheme 1-51).[137]

Closely related to their initial publication on the KO*t*Bu-Et_3SiH reagent system (Table 1-1), Grubbs et al. described the reductive desulfurisation of a range of aryl thioethers (Scheme 1-52).[138] The two carbon-sulfur bonds in **265** were reductively cleaved. Indeed, sulfur was cleanly removed from all the investigated substrates. In the case of the 2-naphthalenethiol, **266**, in addition to the expected product naphthalene **267**, a trace amount of hydrogenated

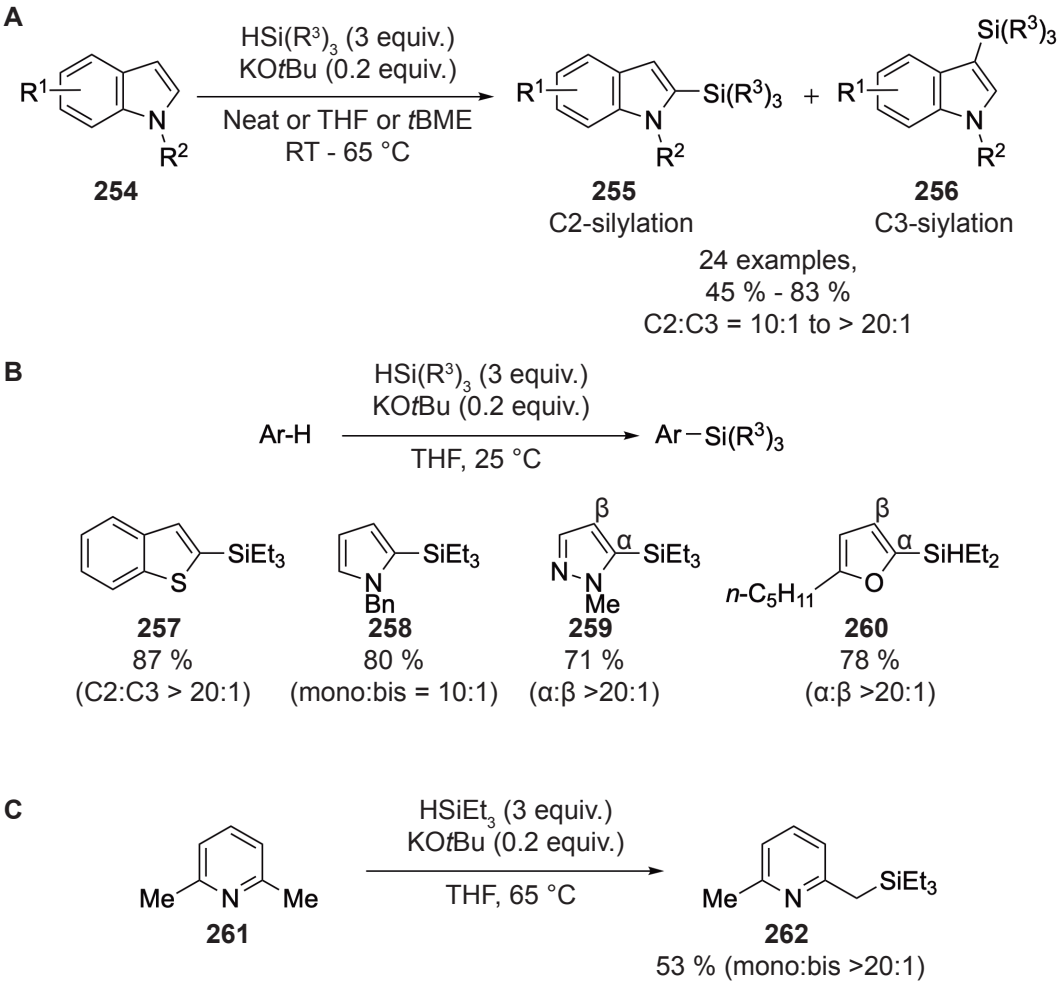

Scheme 1-50 Selective C2-silylation of a range of indoles was achieved with the KO*t*Bu-Et_3SiH reagent system. Also other heterocycles were silylated with good regioselectivity and yield as were benzylic positions in some substrates.

naphthalene **268** was detected. The authors suggested that this protocol might potentially find application for the desulfurisation of fuels.[138]

1.5.2 Proposed Mechanisms

It has become apparent that the reaction outcomes of the KO*t*Bu-Et_3SiH reagent system can be quite diverse. Either silylation of the substrate is observed or reductive defunctionalisation

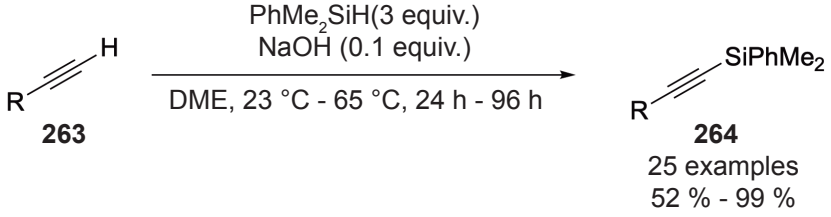

Scheme 1-51 The silylation of terminal alkynes was achieved by treating the substrates with a hydroxide base and a silane reagent.

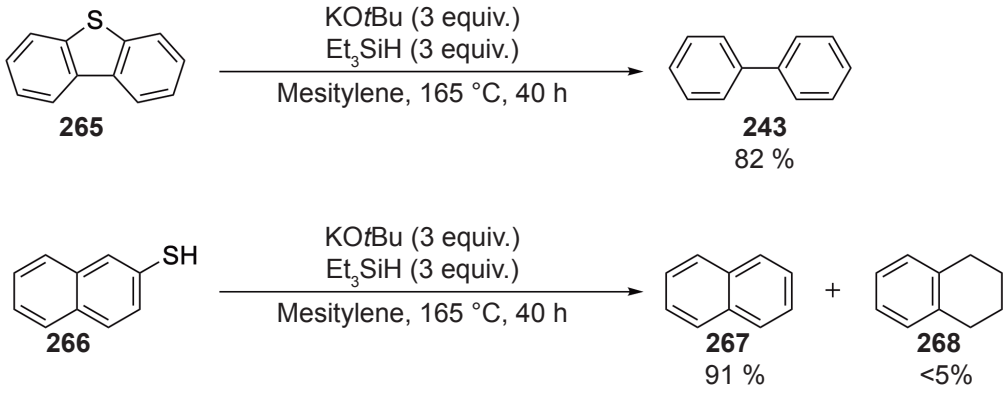

Scheme 1-52 The defunctionalisation of thioaryl substrates was achieved with the KO*t*Bu-Et_3SiH reagent system.

occurs. These diverse outcomes suggest that several mechanistic pathways are accessible to the reagent system. Moreover, the desired reactivity can be selected by carefully choosing the reaction conditions. Substoichiometric amounts of base and low temperatures favour silylation, while stoichiometric amount of base and high temperatures favour reductive defunctionalisation.

Tanner et al. described the multifaceted nature of pentavalent silicon species three decades ago.[139] For example, when the probe substrate **269** was treated with a silane and a fluoride source it was observed that the main reactivity of the system is hydride reduction, which led to the formation of **270** (Scheme 1-53). The hydridic nature of hypervalent silane species has been well studied and found many synthetic applications.[140] The by-product **271**, however, is unlikely to be formed via a hydridic reduction pathway. This product is characteristic of single electron transfer reduction of the substrate **269**. Indeed, the formation of **271** was fully suppressed when the radical quenching agent 1,4-dinitrobenzene **272** was added to the reaction. It was also observed by Tanner et al. that oxygen did not inhibit the reactivity but increased the concentration of radical species in the system.[139] Hence, oxygen in air may serve as an initiator in this and related reactions. Analogous observations were made by Corriu et al. with a pentavalent silicon species. These authors successfully isolated potassium tetraethoxyhydrosilane $(EtO)_4SiHK$ and analogues thereof.[141] It was demonstrated that this reagent typically reacts as a hydridic reducing agent but it was also found to be able to engage in single electron transfer reactions toward benzylic halides.[142]

These two aspects, radical and ionic transformations, accessible to hypervalent silicon species were discussed in detail by Grubbs et al. for the KO*t*Bu-Et_3SiH reagent system based on

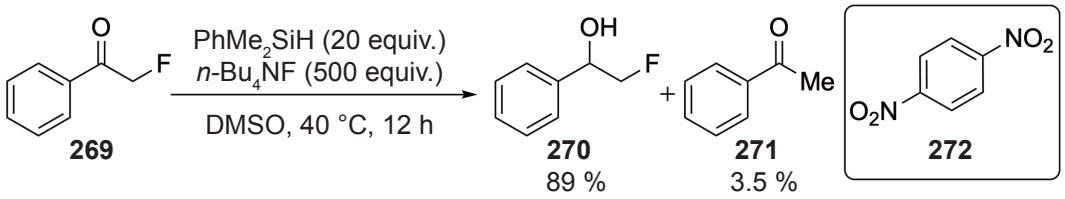

Scheme 1-53 Strong indications for single electron transfer reactions of a silane/Lewis base system was obtained with well-validated probe substrates such as **269**.

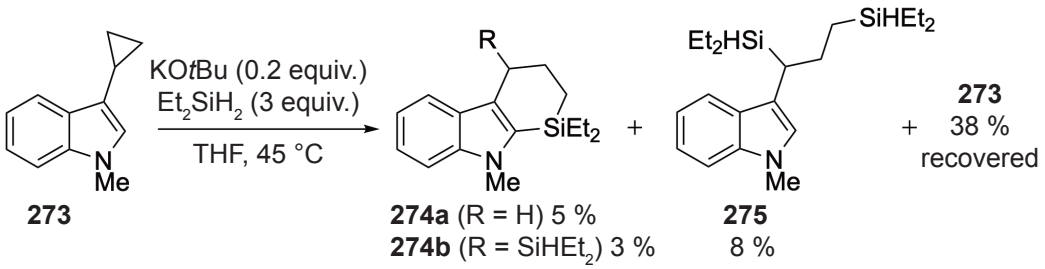

Scheme 1-54 Radical clock experiments suggest that radical intermediates are involved in the silylation reactions of heterocycles.

the indole silylation reaction.[143,144] By deuterium labelling experiments, it was shown that the hydrogen atom which is replaced by a silyl group, quantitatively ends up as molecular hydrogen.[143] Experiment and DFT calculations concordantly showed that, in general, the silylation on the more electrophilic site of the heterocycle is kinetically favoured. For the indole silylation it was additionally shown that the kinetic product, which is silylated at the 2-position, is not the thermodynamic product. Exposure of C2-silylated indoles led to the formation of the C3-silylated isomer.[143]

Evidence for radical intermediates was obtained from radical clock experiments (Scheme 1-54). When subjected to the KO*t*Bu-Et_3SiH system, the cyclopropyl group in **273** ring-opened to give rise to several products. Although, these products are formed in low yields, their presence clearly demonstrates that radical species are generated in the reaction. Hence, radical species may also contribute to the productive silylation reaction.[143]

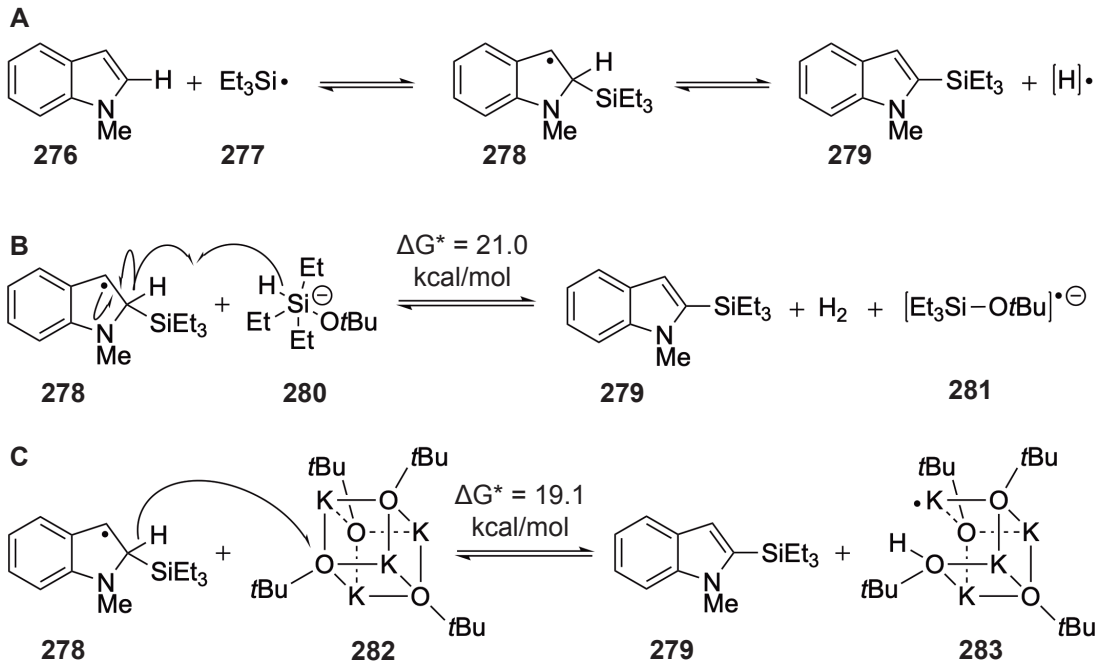

Scheme 1-55 In the proposed radical mechanism for the silylation of heterocycles with the KO*t*Bu-Et_3SiH reagent system, the rate-determining step was found to be the hydrogen abstraction from **278**.

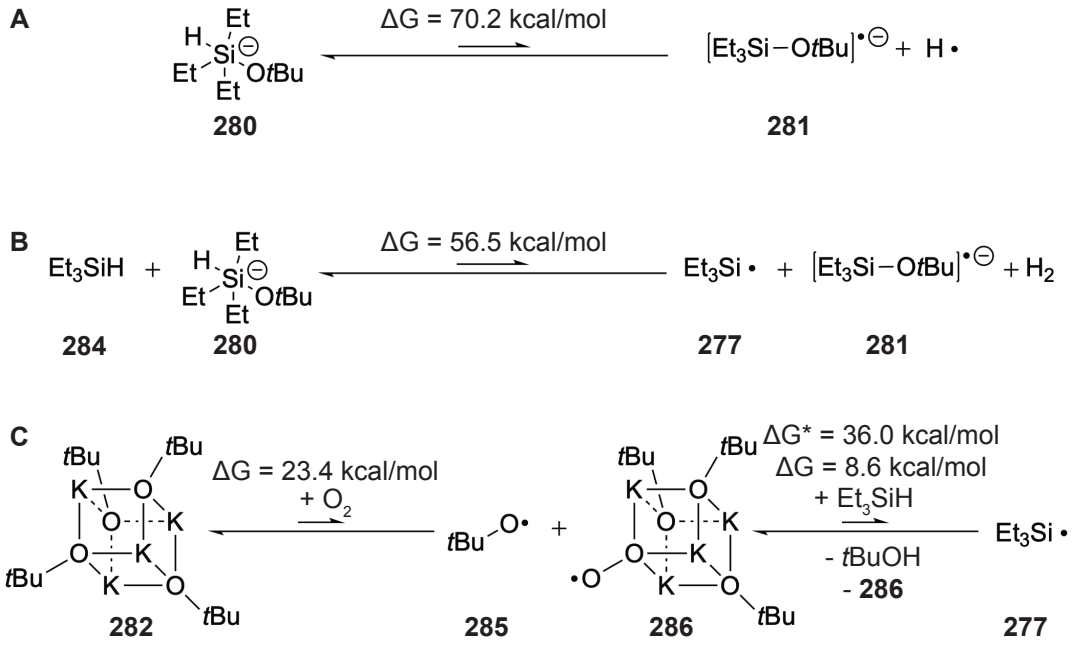

Scheme 1-56 Different initiation mechanisms have been proposed to trigger radical cascades in the KO*t*Bu-Et_3SiH reagent system.

The radical mechanism requires the silyl radical **277** to be formed (Scheme 1-55 A). This species adds onto the indole substrate **276** at the C2 or C3 position (only the C2 addition is shown). The subsequent elimination of hydrogen from the intermediate **278** was found to be the rate-determining step (by DFT calculations). One possible step for the hydrogen abstraction involves the pentavalent silicon species **280** (Scheme 1-55 B). Together with the radical **278**, species **280** can lead to the expulsion of molecular hydrogen and the formation of product **279** as well as the radical anion **281**. The radical anion **281** is proposed to fragment to the triethylsilyl radical **277** and *tert*-butoxide. Thereby the radical chain would be propagated. Alternatively, the potassium *tert*-butoxide tetramer **282** (it was suggested that the tetrameric representation of KO*t*Bu is more appropriate in this context than a monomeric representation) was found capable of abstracting the hydrogen atom from **278** as well (Scheme 1-55 C). This would lead to the product **279** and the potassium *tert*-butoxide-derived complex **283**. This complex was proposed to react with triethylsilane to form molecular hydrogen and to give back the silyl radical **277**.[143]

The remaining unknown step of these proposed radical chain mechanisms is the initiation mechanism. Two possible initiation processes were discussed.[143] The first mechanism involves a homolytic fragmentation of the silicon-hydrogen bond in **280** (Scheme 1-56 A). By DFT calculations this step, however, was found to be very endergonic. A modification of this initiation approach, which involves triethylsilane, turned out to be energetically seriously uphill, too (Scheme 1-56 B). Finally, a mechanism involving oxygen - which may always be contained in the reaction mixture on ppm-levels - was identified. This mechanism showed an acceptable energy profile for an initiation process (Scheme 1-56 C). In the course of this possible mechanism, a *tert*-butoxyl radical **285** is formed. In separate experiments with typical radical initiators, however, it was found that initiators, which give rise to the radical **285** directly cannot

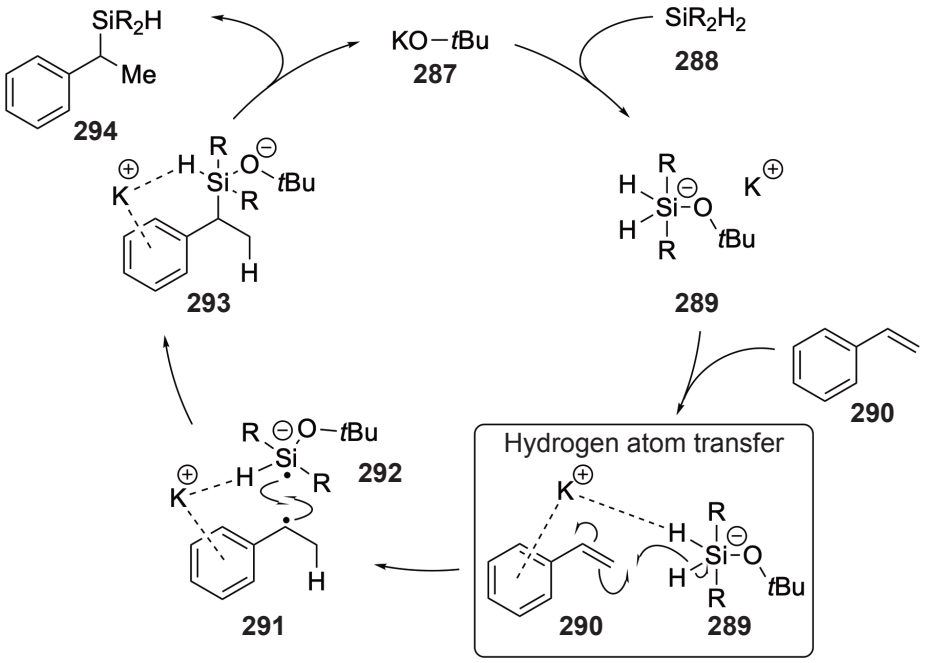

Scheme 1-57 Based on experimental and computational mechanistic studies a hydrogen atom transfer has been proposed as the key step in the silylation of styrene analogues.

replace potassium *tert*-butoxide. Moreover, such initiators do have a deleterious effect on the reaction, even when potassium *tert*-butoxide is present.[143] Thus, no fully convincing initiation mechanism of possible radical chain reactions with the KO*t*Bu-Et_3SiH system could be identified so far.

Even though radical reactions accessible to the KO*t*Bu-Et_3SiH reagent system are not fully understood yet, radical processes have been suggested for the desulfurisation of aryl thioether substrates and the reductive cleavage of the carbon-oxygen bond in aryl ethers.[138]

Very recently, the silylation of alkenes was reported. Based on innovative (and not yet commonly accessible) DFT methods, radical-clock experiments, radical trapping studies and EPR spectroscopy results, a hydrogen atom transfer mechanism was proposed as the key step (Scheme 1-57).[145] The catalytic cycle starts with potassium *tert*-butoxide **287**. This base complexes the silane reagent **288** to give **289**. This species can engage in a hydrogen atom transfer towards the styrene substrate **290**. The benzylic radical **291** then recombines with the silyl radical anion **292** to give the adduct **293**, which dissociates into the product **294** and potassium *tert*-butoxide **287**. From the DFT model it was found that the complexation of the aromatic system to the potassium cation is crucial to render the hydrogen atom transfer step energetically accessible.[145]

An ionic process for the silylation of heterocycles has been considered as well as radical processes (Scheme 1-58).[144] The key step in the ionic process is the deprotonation of the heterocycle. Monitoring the reaction by mass spectrometry showed that the ion **295** is only formed after an initial lag period (hence, it is unlikely to be an artefact of the ionisation method) and only in reactions with the KO*t*Bu-Et_3SiH reagent system. In particular, KO*t*Bu in the absence of Et_3SiH was unable to generate this anion. Therefore, it was proposed that a hydride species generated from KO*t*Bu and Et_3SiH is acting as the base.[144] Indeed, the generation of hydride

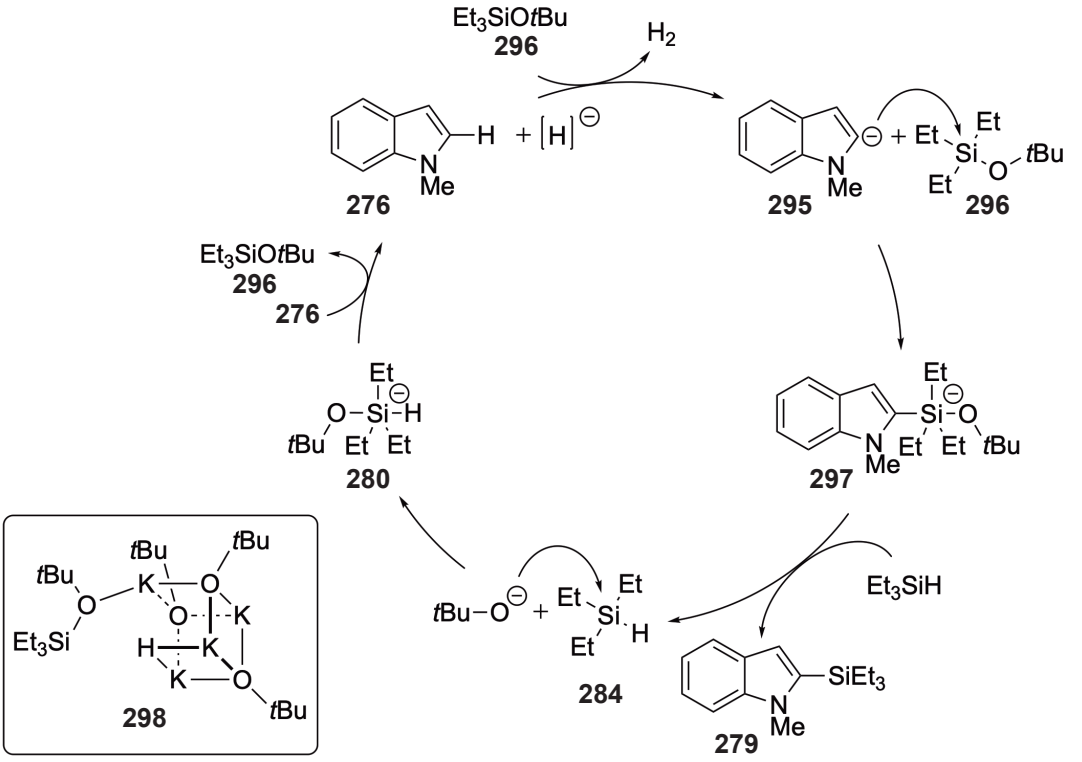

Scheme 1-58 An ionic mechanism has been proposed for the silylation of various heterocycles. Here the mechanism is shown based on the example of indole **276**.

species from silanes when treated with strong nucleophiles has precedents in the literature.[146] Once formed, the anion **295** attacks **296**. The collapse of the pentavalent silicon intermediate **297** leads to the formation of product **279** and generates *tert*-butoxide. The latter nucleophile is proposed to propagate the chain by attacking triethylsilane to give **280**, which can regenerate the hydride species and **296**. Thereby, the catalytic cycle of the hydride-mediated deprotonation-silylation of indole is closed. The effect of counter cations was discussed on several levels. First, it was pointed out that the complexation of the heterocycle by a potassium cation may crucially support the deprotonation. Second, instead of a naked hydride anion, a hydride species **298** derived from a potassium *tert*-butoxide tetramer was considered. In DFT calculations, this structure was found to be a competent base for the deprotonation of indole **276**.[144]

1.5.3 Analogous Dehydrogenative Silylation Mechanisms to the Ionic Mechanism Proposed by Grubbs et al. for the KO*t*Bu-Et$_3$SiH Reagent System

Analogous to the proposed formation of **298**, the formation of highly reactive main group metal hydrides with silanes as the hydrogen source is known. For example, calcium hydride complexes and strontium hydride complexes have been successfully synthesised and applied in the hydrosilylation of conjugated alkenes.[147,148] More closely related to the KO*t*Bu-Et$_3$SiH chemistry reported by Grubbs et al. is the silylation of alkynes via a calcium hydride complex **304** (Scheme 1-59 A).[149] The silane **300** was reacted with the alkyne **301** in the presence of the catalyst **299** under mild conditions to give the silylated alkyne product **302** in high yield. Based on a previously published mechanism for the corresponding reaction with an ytterbium catalyst,[150,151] a mechanism has been proposed for the calcium-catalysed silylation (Scheme

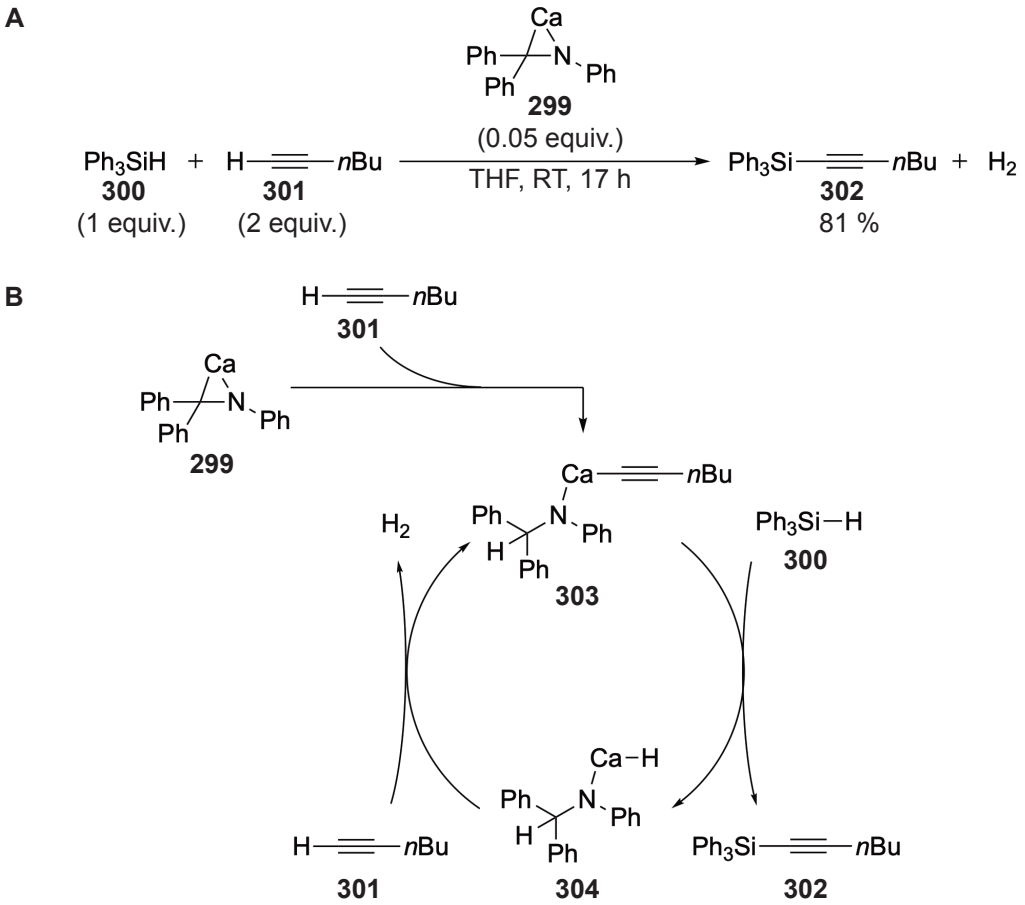

Scheme 1-59 The silylation of terminal alkynes has been achieved with a calcium catalyst and a calcium hydride intermediate has been proposed to play a key role in the deprotonation of the alkyne substrate.

1-59 B).[149] The catalyst **299** is activated by the addition to the alkyne **301** to give **303**. This calcium alkynilide attacks the silane reagent **300**, which leads to the formation of product **302** and the calcium hydride species **304**. This calcium hydride corresponds to the hydride intermediate **298** proposed by Grubbs et al. (Scheme 1-58). The calcium hydride intermediate **304** deprotonates the alkyne substrate **301** to close the catalytic cycle.[149]

The catalyst **299** was also studied for the dehydrogenative silylation of amines.[149] Indeed, a range of alkaline earth metal hydride catalysts[152-154] has been investigated for this reaction. For their barium hydride catalyst, Sarazin et al. presented a plausible reaction mechanism based on kinetic studies, kinetic isotope experiments and DFT calculations (Scheme 1-60).[154] The reaction mechanism starts with a ligand exchange from **307** to **308**, which is endergonic by 12.9 kcal/mol. In the next step, which has a low barrier of activation and is almost thermoneutral, the nitrogen-silicon bond is formed to give the intermediate **309**. The subsequent hydride transfer from silicon to barium is the rate-limiting step (the transition state energy is +19 kcal/mol relative to the reference point **307**). This step and the following ligand exchange are both exergonic and lead to the barium hydride intermediate **311**. Expulsion of hydrogen then gives back the initial structure **307** and closes the catalytic cycle. Attempts to find a concerted mechanism for the formation of the nitrogen-silicon bond and formation of molecular hydrogen

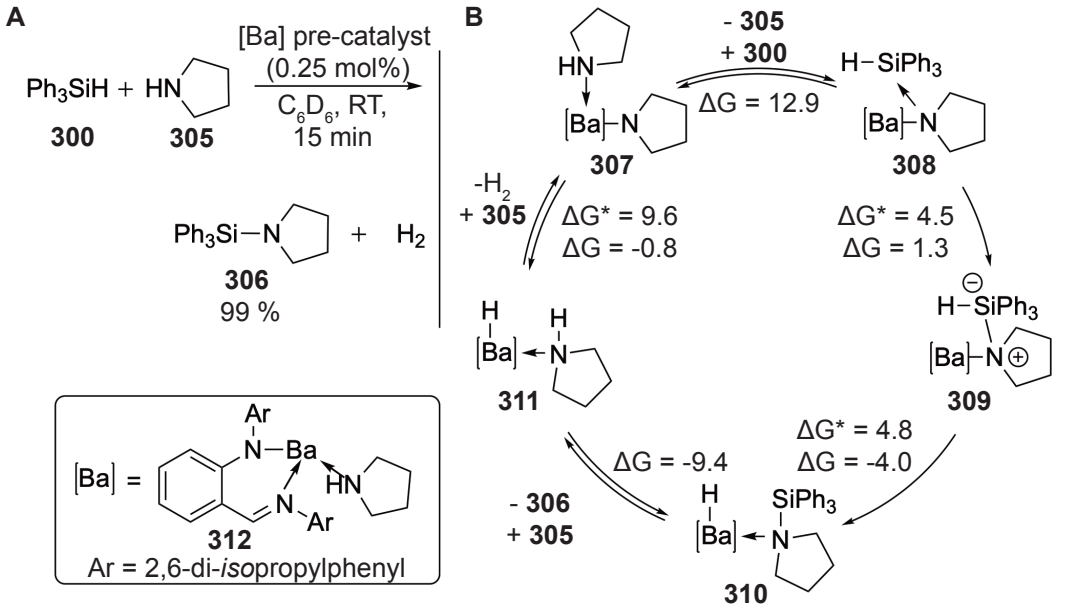

Scheme 1-60 Based on DFT calculations a detailed mechanism for the dehydrogenative silylation of amines with the barium catalyst **312** has been suggested. Energies are reported in kcal/mol.

by DFT methods were unsuccessful. This fruitless search has been interpreted as an indication that such a concerted mechanism would have an inaccessible, high energy transition state.[154] In a related example with a magnesium catalyst, a similar mechanism was proposed. The only difference to the barium-hydride system was the rate limiting step. With the magnesium catalyst, this step was unlikely to be the hydride migration but more likely the nucleophilic attack of the magnesium amide on the silane.[152,154]

The alkaline earth catalysts discussed above are generally rather sophisticated compounds that are newly designed and typically highly sensitive to air and humidity. Contrasting these advanced catalysts, simple alkaline metal hydrides were found to be effective catalysts for the dehydrogenative coupling of silanes and amines, too.[155-158] Fink reported the successful dehydrogenative silylation mediated by catalytic amounts of sodium hydride (Scheme 1-61).[155] Treating amines **313** with silanes **314** in the presence of a catalytic amount of an alkali metal

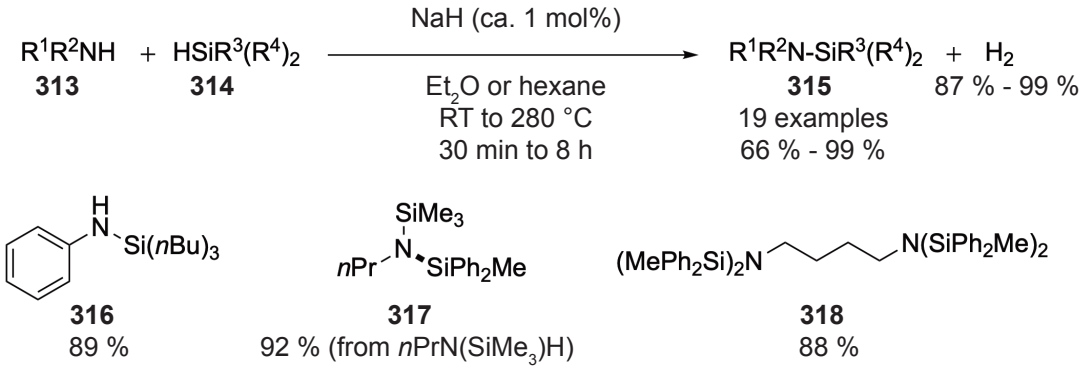

Scheme 1-61 A very efficient dehydrogenative silylation protocol of amines uses sodium hydride in catalytic amounts.

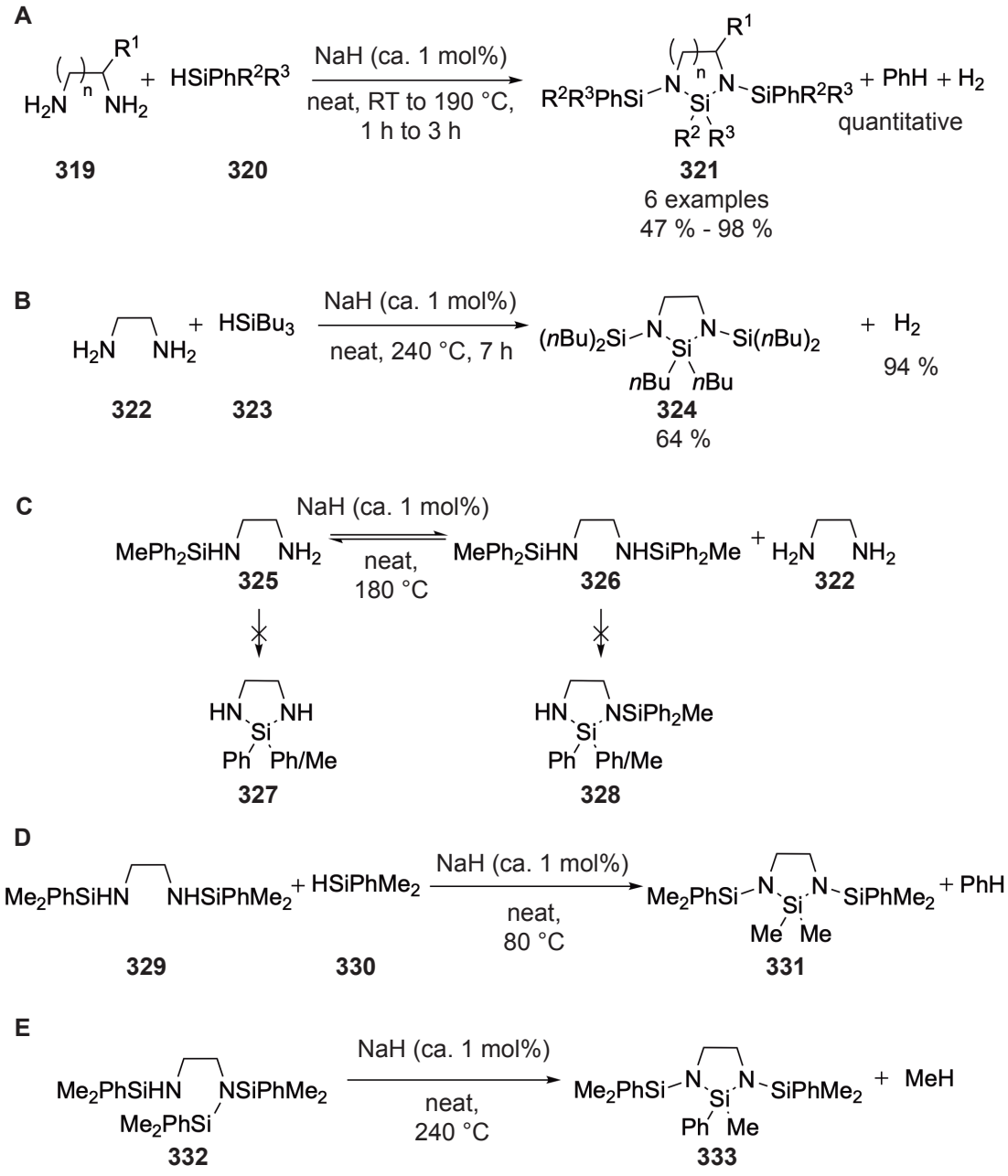

Scheme 1-62 If 1,2-diamines and 1,3-diamines are treated with three equivalent of silane in the presence of sodium hydride, five- and six-membered diazasilolidines are obtained.

hydride - mainly sodium hydride was used - gave the silylated amines **315** in high yields. Generally, the reactions were found to give clean products - stoichiometric amounts of hydrogen was the only by-product. Monosilylation of primary amines was achieved with high chemoselectivity when equimolar amounts of both reagents were used (for example in the synthesis of **316**). That does not imply that di-silylation was not achievable. For example, a second silylation of a silylamine gave **317** and a four-fold silylation of 1,4-butanediamine gave **318**.[155]

The polysilylation of 1,2-diamines and 1,3-diamines **319** harboured some surprise (Scheme 1-62 A).[156] Instead of linear products analogous to **318**, cyclic compounds **321** were obtained. The formation of the ring implies that the silane reagent must lose a second substituent,

besides hydride. Indeed, if phenylsilane **320** was used as a reagent, benzene was isolated in quantitative yield from the reactions. Also trialkylsilanes, such as **323**, were found to undergo this type of cyclisation reaction (Scheme 1-62 B). In addition to the isolation of product **324**, *n*-butane was detected. Mechanistic investigations showed that mono- and bis-silylated 1,2-diamines, **325** and **326**, do not undergo cyclisation (Scheme 1-62 C). Only equilibration between **325** on one side and **326** and **322** on the other side was observed. When the di-silylated 1,2-diamine **329** was treated with silane **330** in the presence of sodium hydride at moderate temperature, it readily gave **331** accompanied by the formation of benzene (Scheme 1-62 D). The hypothetical intermediate **332** was able to cyclise to **333** under the reaction conditions but only at much higher temperatures (Scheme 1-62 C). Moreover, this time not benzene was formed as a by-product, but methane. This observation indicates that the reaction with compound **332** does not exactly mirror the situation when **329** is treated with **330**.[156]

The activation of the silane species in the above reactions occurs by a nucleophilic attack on the silane. Hence, it is not surprising that a catalytic amount of a nucleophile instead of a hydride can mediate such reactions. For example, a catalytic amount of fluoride was found capable of inducing an efficient dehydrogenative silylation of amines.[159] The hydrodefluorination

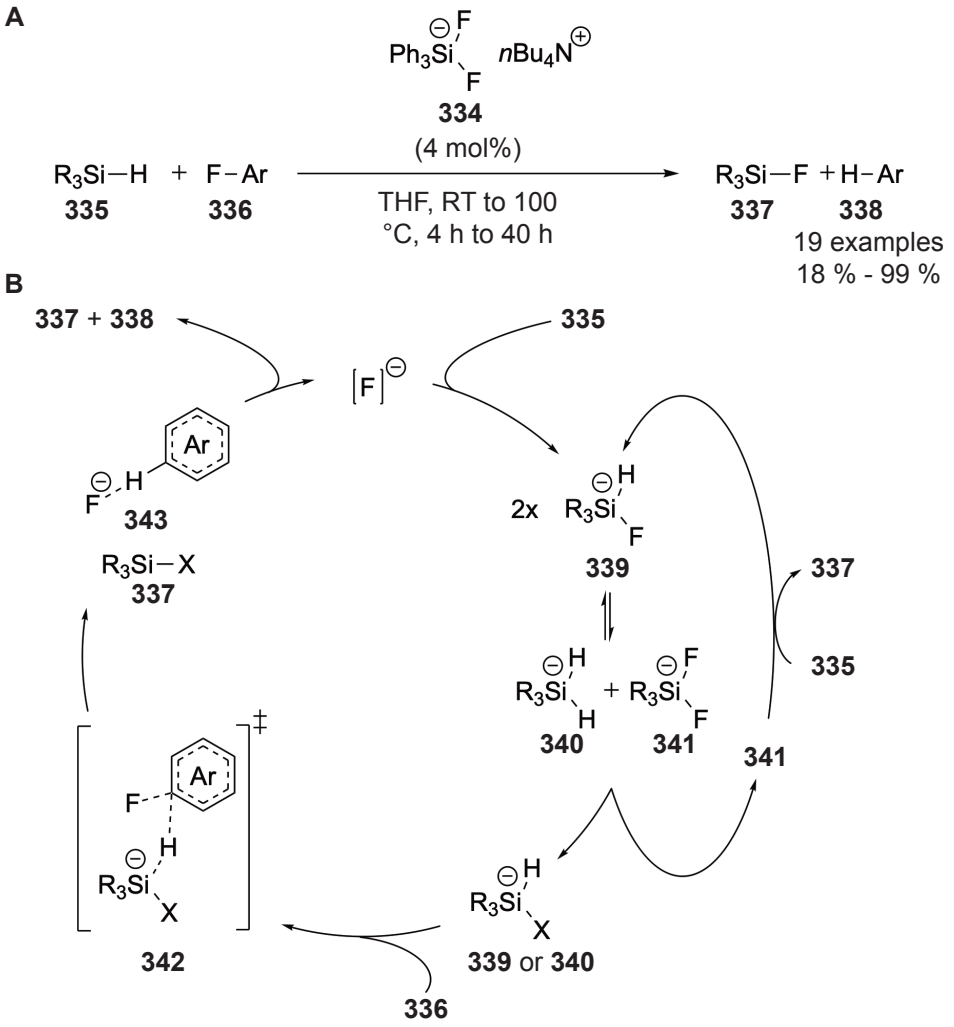

Scheme 1-63 For the fluoride-catalysed hydrodefluorination of polyfluoroarenes, the pentavalent silicon hydrides **339** and **340** were proposed as key reactive intermediates.

of polyfluoroarenes follows a similar principle (Scheme 1-63 A).[160] It was found that with a catalytic amount of a fluoride source **334** and silane **335** as a reducing agent, regioselective hydrodefluorination was achieved for a range of polyfluoroarenes **336**. Based on DFT calculations, a catalytic cycle was proposed (Scheme 1-63 B). Formally, the first step is the attack of a fluoride anion on silane **335** to give the pentavalent silicate hydride **339**. This species can undergo disproportionation to **340** and **341**. Difluorosilicate **341** can react with another molecule of **335** to regenerate **339**. Both species, **339** and **340**, were found capable to perform the following hydrodefluorination reaction (based on the DFT calculations). The displacement of fluoride from the aromatic substrate proceeds via the transition state **342**. Remarkably, no Meisenheimer intermediate was found for this nucleophilic aromatic substitution, *i.e.* the proposed S_NAr pathway is concerted. During the S_NAr displacement, compound **337** is formed together with the complex **343**. The complex **343** dissociates to give the product **338** and to (formally) regenerate the fluoride anion.[160] Catalytic dehydrogenative reactions with silanes have recently been reviewed.[161]

1.6. The Concerted S_NAr Reaction Mechanism

1.6.1 Background

Some nucleophilic aromatic substitutions have been found to proceed via a concerted pathway as has been seen in the last example of the previous section, for example (Scheme 1-63). This finding stands in contrast to the generally accepted stepwise mechanism[162] of the S_NAr reaction that proceeds via a Meisenheimer intermediate. In fact, the example of the concerted S_NAr from Scheme 1-63 is not an isolated case but stands in a long list of examples of S_NAr reactions that have been claimed to proceed via a concerted pathway. It seems that S_NAr reactions can either proceed via a Meisenheimer intermediate or via a concerted mechanism based on the nature of the aromatic system, the nucleophile and the leaving group (Scheme 1-64).

An important reason for why the stepwise mechanism of the S_NAr reaction has been widely accepted, is that for some S_NAr reactions, the presence of intermediates (i.e. Meisenheimer intermediates) have been convincingly demonstrated (Figure 1-15). The first examples of isolable intermediates from S_NAr reactions were given by Meisenheimer in his seminal study on nitroarenes. There, the compound **344** was documented for the first time among other, similar examples.[163] Later, an analogous intermediate, **345**, was unambiguously characterised by X-ray diffraction analysis.[164] A remarkable number of stable Meisenheimer intermediates such as **346**, **347** and **348** has been characterised and reported over time. A review of these reports has been provided by Beletskaya et al.[165]

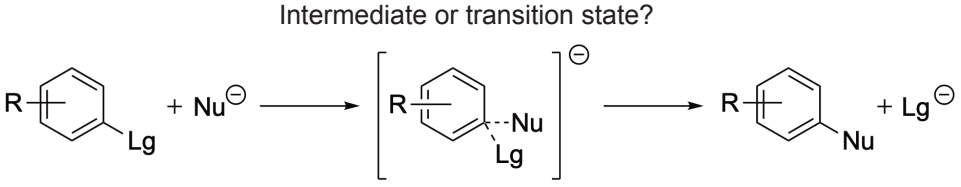

Scheme 1-64 The generally accepted mechanism of the S_NAr reaction proceeds via Meisenheimer intermediate. However, in many cases a concerted mechanism may be operative.

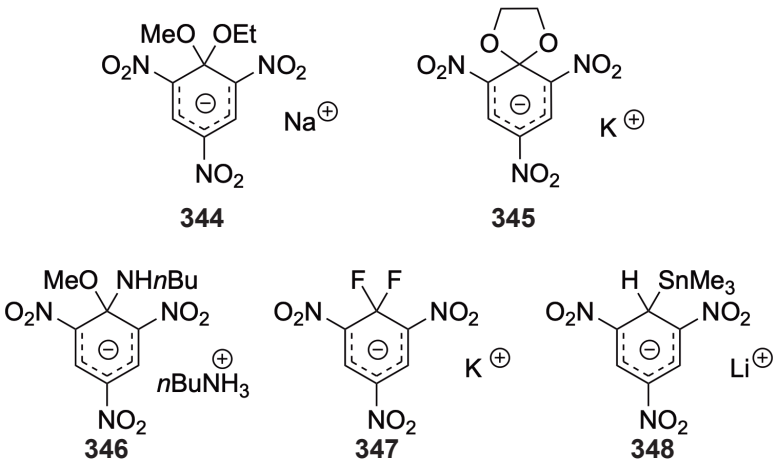

Figure 1-15 Several Meisenheimer intermediates have been characterised.

1.6.2 Experimental Evidence Indicative of Possible Concerted S_NAr Mechanisms

To convincingly demonstrate the absence of a Meisenheimer intermediate in the S_NAr reaction pathway is much more difficult. The limit of experimental chemical accuracy is generally regarded to be 1-2 kcal/mol.[166] If a Meisenheimer intermediate has a lower barrier for the onwards reaction than 2 kcal/mol, it still has a significant life-time in the range of 10^{-12} s, but may evade detection by conventional experimental methods. Thus, it is very hard to convincingly demonstrate by experiment that an S_NAr reaction follows a concerted pathway. The reaction may appear as being concerted while it actually follows a stepwise mechanism.

Williams et al. demonstrated how far one can go in elucidating the mechanism of the S_NAr reaction by rigorous kinetic investigations in conjunction with quantitative structure-activity relationship analysis. In several of Williams' studies, it was found that the accumulated data is best in agreement with a concerted mechanism.[167-170] For example, the reaction of pyridines **349** with triazine substrates **350** was found to likely proceed via a concerted S_NAr mechanism (Scheme 1-65).[169] The electronic nature of **349** and **350** was systematically varied by changing R^1 and R^2, respectively. In short, it was observed that the basicity of the nucleophile **349** as well as the basicity of the leaving group **352** has a significant effect on the reaction rate. It was concluded that this observation was best in agreement with a concerted mechanism.[169]

No other claims of concerted S_NAr reactions have been based on comparably rigorous, experimental studies as those examples published by Williams above. This is partly because many of the commonly encountered S_NAr reactions do not lend themselves to analogous studies. In most cases either the nucleophile or the leaving group is a simple entity such as a halogen atom or a hydride. This makes systematic variation of their electronic properties by derivatisation impossible and Bønsted-correlations, as used by Williams, cannot be established. Many authors therefore turned to Hammett correlations, where the electronic nature of the aromatic system of the electrophile is changed (nucleophile and leaving group are kept constant). The slope of the Hammett correlation served as an indication for whether the S_NAr reaction under scrutiny follows a concerted or stepwise mechanism. According to this line of reasoning, a flat slope - little accumulation of negative charge on the aromatic ring during the rate-determining step -indicates a concerted mechanism, while a steep slope - significant accumulation of negative charge on the aromatic ring during the rate-determining step - indicates

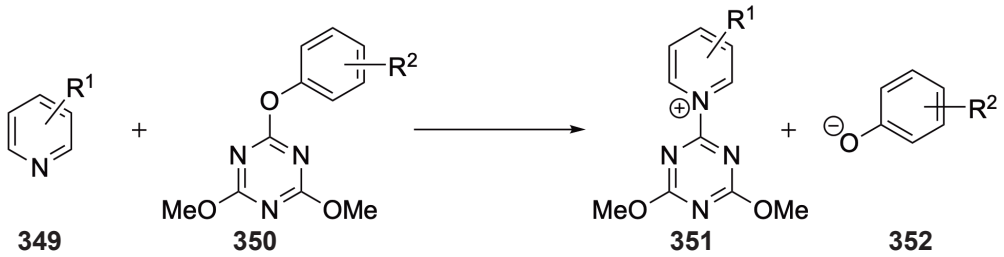

Scheme 1-65 By systematically varying the electronic nature of R^1 and R^2, Williams et al. found that both, the nature of the nucleophile and the nature of the leaving group, have a substantial effect on the rate limiting transition state of this class of reactions.

a stepwise mechanism. This approach relies on the intuitive reasoning that, for an S_NAr pathway with a Meisenheimer intermediate, more negative charge accumulates in the π-system during the rate-determining step than for a corresponding concerted pathway. Although reasonable, this approach lacks a solid theoretical foundation. It is also problematic for another reason. The slope of the Hammett correlation depends on the temperature[171] and possibly other factors (as mentioned in the study by Fry and Pienta[172] for example). Thus, it becomes difficult to compare the slopes of different Hammett correlations obtained from different experimental conditions (which unfortunately does not prevent many authors from doing it). Also, it is important to emphasize in this context, that a change in slope of the Hammett correlation indicates the change in the nature of the rate limiting step - the reverse statement, however, does not hold.

For S_NAr reactions, typically Hammett ρ-values in the range of $+3 < \rho < +9$ have been reported (usually a stepwise mechanism has been implied for these examples and no further investigations were performed).[162,171,173,174] For an S_NAr reaction where a concerted mechanism has been suggested, many of the measured Hammett ρ-values fall in the range from 0 to 2[169,170, 172,175] but may reach values up to 4.5.[176] It becomes clear that, in addition to not being theoretically sound, the judgement of the S_NAr mechanism based on ρ-values lacks any reliable reference values.

1.6.3 Computational Investigations of the S_NAr Mechanism

It follows from the above discussion that the typical experimental tools available to organic chemists to elucidate reaction mechanism are of limited use in order to decide whether a particular example of an S_NAr reaction follows a concerted or a stepwise mechanism. Computational approaches, in contrast, can give a clear indication of the reaction mechanism of a particular example. The main challenge with computational tools, however, is to establish their validity.[177] The examples of (proposed) concerted S_NAr reactions can be grouped into intermolecular and intramolecular reactions. In both cases a broad range of nucleophiles and leaving groups were combined. In the following, a few selected examples are presented to highlight key points and to show trends, as far as this is possible.

Examples of Intermolecular Concerted S_NAr Reactions

Jacobsen et al. combined computational investigations and sophisticated NMR experiments to pin down the nature of the mechanisms of three examples of S_NAr transformations (Scheme

1-66) all of which feature either a C-F bond formation or scission.[178] By NMR, the kinetic isotope effect (KIE) of $^{12}C/^{13}C$ at the *ipso*-carbon was measured. A remarkable signal enhancement in the NMR experiment was achieved by not measuring the relative signal intensity of the *ipso*-^{13}C-carbon atom directly. Instead, the ^{19}F satellite signal (arising from $^{2}J_{^{13}C\text{-}^{19}F}$) was compared with the ^{19}F singlet (if the *ipso*-carbon is ^{12}C) to deduce the $^{12}C/^{13}C$-ratio in the product or remaining starting material. Hence, a fluoride atom attached to the *ipso*-carbon atom either in the substrate (fluoride as a leaving group - Scheme 1-66 A) or in the product (fluoride as a nucleophile - Scheme 1-66 B and C) is a prerequisite for this method to work. If the $^{12}C/^{13}C$-ratio were to be measured directly, impractically long acquisition times and large amounts of material would be required. The measured KIE without contextualisation provides no insight in relation to the nature of the mechanism (i.e. the two reactions in Scheme 1-66 A and B have the same experimental KIE of 1.035). The required context is provided by the computational method. [The DFT method used for all the geometry optimisations was B3LYP-D3(BJ)/6-31+G(d)/PCM(solvent). Based on these structures, various methods were evaluated for the KIE prediction]. For every reaction, the maximal (for the hypothetical concerted S_NAr pathway) and minimal (for the hypothetical stepwise S_NAr pathway) value of the KIE were calculated. For the reaction of **353** with **354** (Scheme 1-66 A) it was found that the measured KIE reached only 47 % of the theoretical maximal value. It was concluded that this reaction follows a stepwise mechanism. The reaction of **357** with **358** (Scheme 1-66 B), in contrast, showed a KIE that was 87 % of the theoretical value and it was concluded that it follows a concerted mechanism. For the reaction of **361** with **358** (Scheme 1-66 C) the experimental KIE reached 73 % of the theoretical maximum. Thus, the mechanism for the S_NAr of **361** lies somewhere

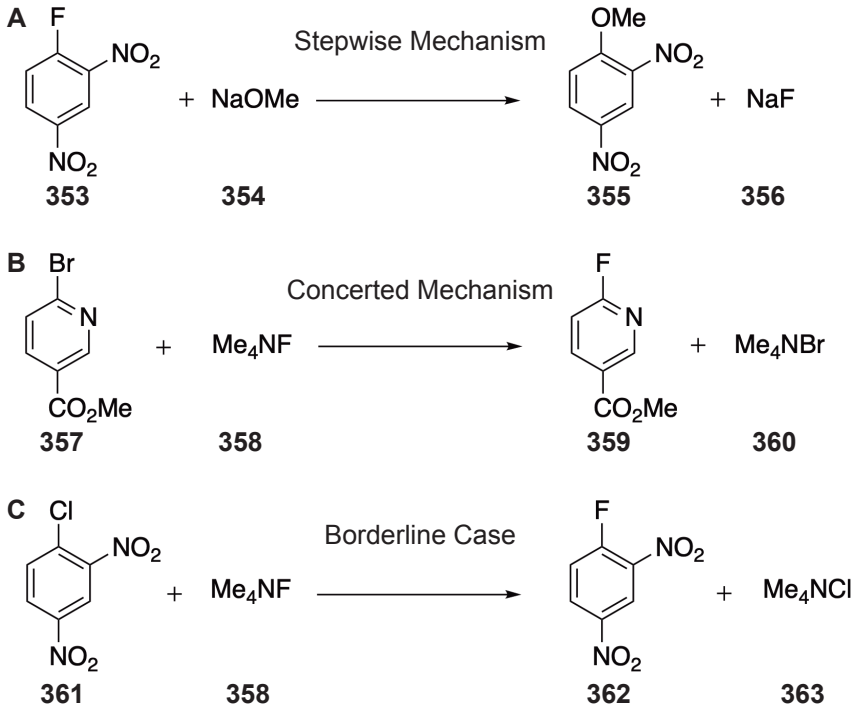

Scheme 1-66 Three different examples of S_NAr reactions have been investigated in detail with a combined computational and experimental approach to elucidate the exact nature of the mechanism - concerted or stepwise.

between the mechanism followed by **353** and **357**. It was described as a borderline case that could not be clearly assigned either to the concerted or the stepwise regime of the S_NAr reaction.[178]

The work by Jacobsen et al. was important in raising the general awareness that the S_NAr reaction can proceed via a concerted mechanism.[179] Moreover, based on computational investigations of a range of simple S_NAr examples, it was pointed out that probably many S_NAr reactions proceed via a concerted pathway.[178] Their study underlines the power of computational approaches in answering this question. Indeed, looking at the work by Jacobsen et al. more critically, it becomes evident that the experimental study did not add any additional information to the computational data. In fact, the interpretation of the experimental data may change if a different computation method would produce a different result. Critically, the computational method that was used for the all-decisive structure optimisation was not validated in any way (in contrast to the methods used to calculate the KIE, which were properly benchmarked, but all relied on the initially generated geometries).

Glukhovtsev et al. computationally investigated the identity reaction of halobenzene with the halide series (Scheme 1-67).[180] [The main method was B3LYP/6-31+G(d)/gas phase. As a benchmark method MP2/6-31+G(d) was used for geometry optimisation in conjunction with frequencies obtained from HF/ 6-31+G(d) or B3LYP/6-31+G(d)]. It was found that the reaction of fluorobenzene **364** with fluoride proceeds via a Meisenheimer intermediate. The three other halobenzene substrates **366**, in contrast, were found to undergo a concerted S_NAr identity reaction.[180]

Uggerud et al. expanded the above study by Glukhovtsev et al. to identity reactions of second- (NH_2^-, OH^-, F^-), third- (PH_2^-, SH^-, Cl^-) and fourth-row (AsH_2^-, SeH^-, Br^-) nucleophiles (Scheme 1-68).[181] Also, a more diverse array of substituents R^1 and R^2 was included in the study. [The DFT method used was OPBE/6-311++G(d,p)/gas phase]. A Meisenheimer intermediate was observed for all three second-row nucleophiles. For both nucleophiles X = NH_2^- or F^- substituents R^1 as different as NH_2 and NO_2 were analysed (R^2 = H). For the hydroxide nucleophile, X = OH^-, two examples were investigated with R^1 = H and R^1 = NO_2 (R^2 = H). For the third- and fourth-row nucleophiles, concerted mechanisms were found in several instances. In general, a concerted mechanism was predicted for more electron-rich aromatic systems. A step-wise mechanism with a Meisenheimer intermediate would only become favourable as electron-withdrawing groups are attached to the aromatic ring. For example, the reaction with X = Cl^- with R^1 = NO_2 and R^2 = H was predicted to follow a concerted mechanism while the reaction with the same nucleophile and R^1 = R^2 = NO_2 follows a stepwise mechanism.[181]

To structure their results, Uggerud et al. used the ionisation energy of the 1s orbital at the

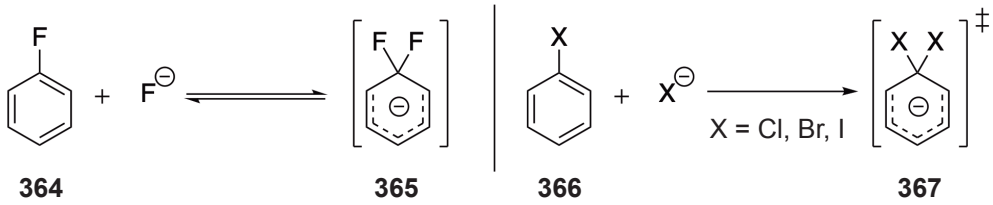

364 **365** **366** **367**

Scheme 1-67 The identity reactions of the halide series with halobenzene was found to proceed via a concerted S_NAr mechanism for X = Cl, Br, I and stepwise for X = F.

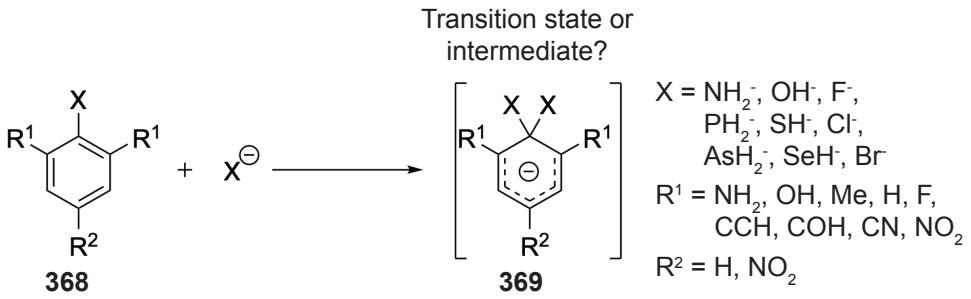

Scheme 1-68 A broad range of identity S_NAr reactions was investigated by DFT methods to establish general trends for nucleophiles and the electronic nature of the aromatic ring.

ipso-carbon as a descriptor. It was found that this energy (as calculated by DFT) correlates well with the relative energy of the Meisenheimer intermediate/Meisenheimer-like transition state structure for all investigated identity reactions.[181] The obtained data also suggests that there is no break in the correlation when the changeover from a stepwise to a concerted S_NAr mechanism occurs. However, only a few data points are available that span both mechanistic regimes and it is not clear whether this observation is significant.

Sun and DiMagno report a fluorodechlorination reaction and a fluorodenitration reaction of aryl chlorides and nitroaryl compounds, respectively.[182] Computational studies were performed for the fluorodenitration reaction. [The DFT method used was B3LYP/6-311++G(d,p)/PCM(ACN)]. A range of *para*-substituted nitroaryl compounds was analysed and grouped according to the Hammett parameter. A good linear correlation was obtained. It was observed that for substituents with a Hammett constant $\sigma_p^- \leq 0$ (i.e. H and more electron-donating substituents) the reaction proceeds via a concerted mechanism (Meisenheimer-like transition state).[182] Similar to the study by Uggerud et al., no change in slope of the Hammett correlation was observed when the mechanism changed from stepwise to concerted. This observation adds to the concerns discussed above for using the Hammett correlation as an indicator of the nature of the S_NAr mechanism.

Based on their computational model, Sun and DiMagno observed a dramatic rate-deceleration of the fluorination reactions when going from the gas phase to the solution phase. This effect has been explained by the large solvation energy of the fluoride anion.[182] A more detailed computational investigation of ion pairing, explicit hydration and solvent polarity was undertaken by Pliego and Piló-Veloso for the fluorodechlorination reaction of 4-chlorobenzonitrile.[183] The computational model predicted the reaction to follow a concerted mechanism for all variations that were examined. [The DFT method used was B3LYP/6-31(+)G(d)/PCM(various solvents)]. By varying the solvent polarity, it was found that for a given fluoride salt there is a solvent with ideal polarity, which just allows for the dissociation of the ion pair but does not solvate the fluoride ion too strongly.[183] Recently, Silva and Pliego examined the S_NAr displacement of bromide from substrates such as **370** with various nucleophiles (Table 1-2).[184] [Geometry optimisations were performed with X3LYP/6-31+G(d)/PCM(solvent). Refined electronic energies were obtained from single-point calculations with M08-SO/def2-TZVPP+ on the optimised geometries]. In all cases, a Meisenheimer-like transition state **371** was found. Interestingly, the electron-donating methoxy substituent had an accelerating effect if placed in the *meta*-position.[184] This indicates that the σ-inductive effects outweigh the π-conjugative

Table 1-2 Interesting effects on the activation energy of *meta*- and *para*-substituents were observed in computational models for the S_NAr replacement of bromide with methoxide.

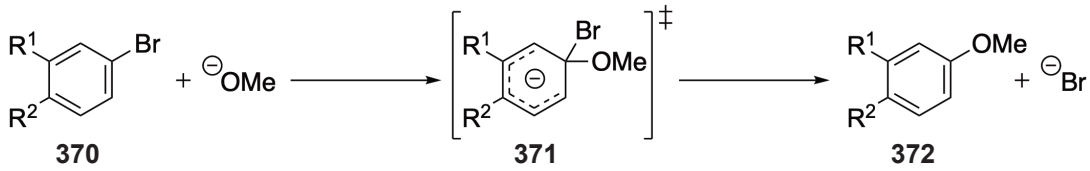

Entry	R^1	R^2	ΔG* (kcal/mol)
1	H	H	27.05
2	H	OMe	28.43
3	OMe	H	25.75

effects in this example.

For the above examples, no change in mechanism was observed when changing the solvent or solvent model, or even when going from gas phase to solution phase. These may be due to the fact that the investigated examples are very clearly located in the concerted S_NAr domain. However, it has been suggested that subtle changes in the environment of the S_NAr displacement, such as a change in the medium, may affect the nature of the mechanism for borderline examples.[185] Such a borderline case has been identified by Tanaka et al. (Scheme 1-69).[186] [The DFT method used was B3LYP/6-31G(d)/gas phase]. For their computational model, the authors found that the *ortho*-substituted product **374** is formed via a step-wise mechanism, while the *para*-substituted product **375** is formed in a concerted addition-displacement step. It was reasoned that hydrogen bonding interactions from the incoming ammonia nucleophile with the nitro group critically add to the stability of the Meisenheimer intermediate such that it actually becomes a local minimum on the potential energy surface. These interactions also lower the overall energy barrier towards the formation of **374**. Hence, this product is formed preferentially, which is, indeed, what has been observed experimentally.[186]

Examples of Intramolecular Concerted S_NAr Reactions

There is a range of S_NAr displacement reactions that occur intramolecularly (i.e. the S_NAr reaction step follows first order kinetic rate laws). These can be further subdivided into those reactions that give rise to the formation of a new ring or to those that proceed via a spiro-transition state. An example of a reaction of the first kind has been reported by Hartley et al.

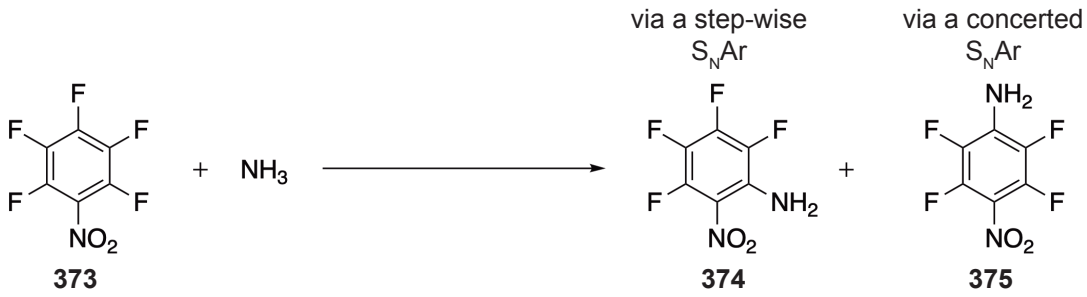

Scheme 1-69 Subtle changes in the environment of the S_NAr displacement may induce it to follow a concerted or a stepwise mechanism.

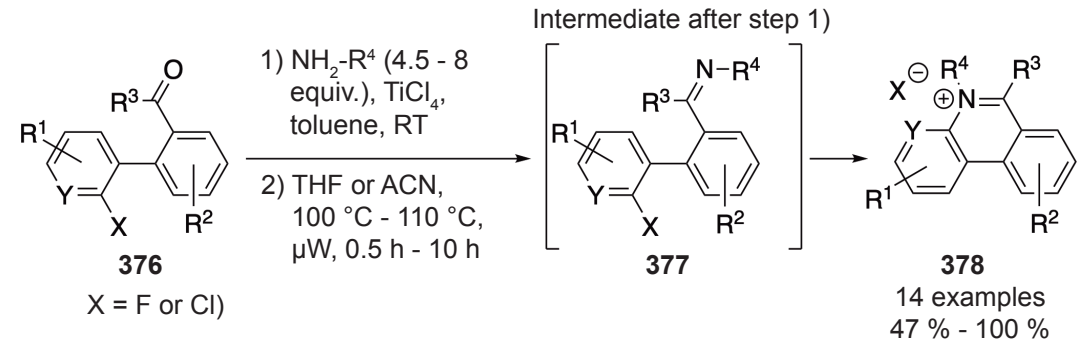

Scheme 1-70 The cyclisation of **377** was found to proceed via a concerted S_NAr mechanism.

(Scheme 1-70).[187] The imines **377** were formed in situ and were smoothly transformed into the phenanthridinium salts **378** by heating in a microwave oven. A range of electronically very different substituents was tolerated as for example R^1 = *p*-NO_2 or R^1 = *p*-OMe. Computational studies suggested that the S_NAr proceeds via a concerted mechanism, regardless of the nature of R^1 (or R^2) substituent (other substituents were kept constant in the computational study). [The DFT method used was M06-2X/def2-TZVP+/SMD(ACN)].[187]

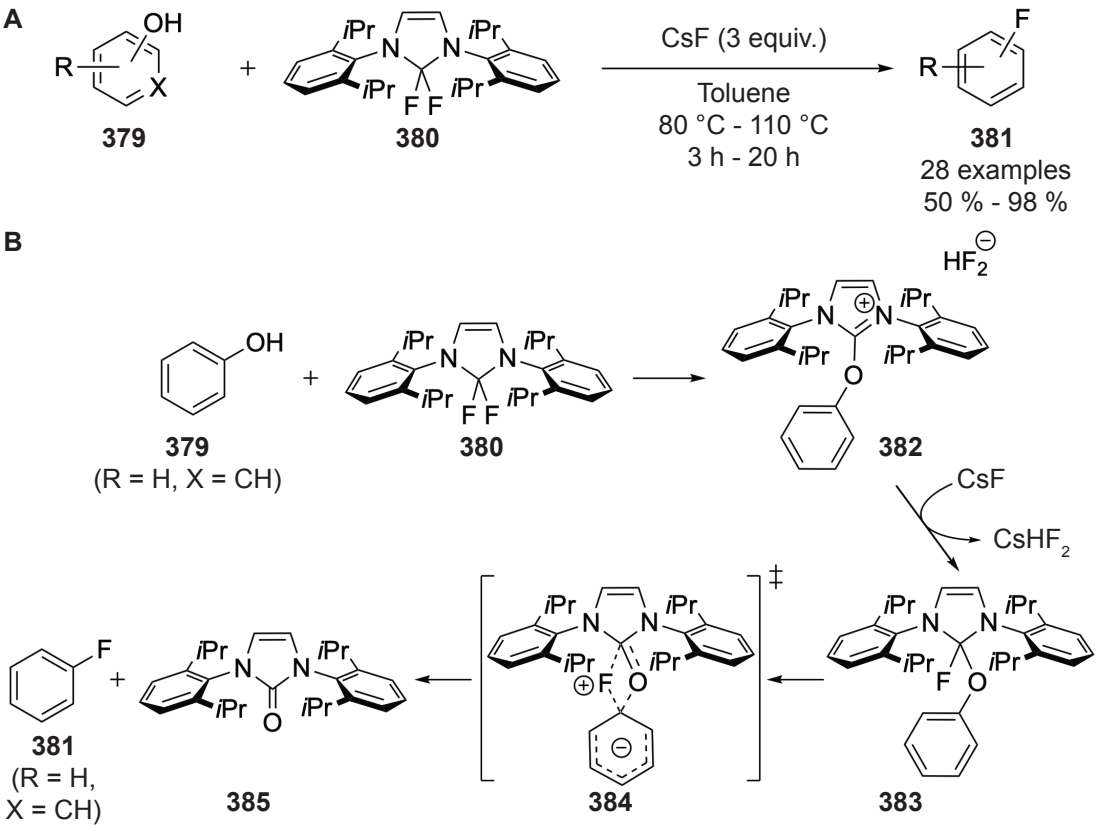

Scheme 1-71 The key step in the phenol deoxyfluorination reaction with PhenoFluor **380** is an intramolecular concerted S_NAr displacement.

In S_NAr reactions that proceed via a spiro-transition state, no new ring is formed in the product. One of the most famous examples of this class of transformations certainly is Ritter's deoxyfluorination reaction with PhenoFluor **380** (Scheme 1-71).[188-190] A broad range of phenols **379** with very different electronic nature (for example, R = *p*-NO_2 or R = *p*-NH_2) was found to undergo fluorination efficiently with **380** to give the aryl fluorides **381** in high yields (Scheme 1-71 A).[188] The proposed mechanism (Scheme 1-71 B) was substantiated by the independent synthesis and characterisation of **383**. Computational studies showed that the S_NAr displacement starting from this intermediate proceeds in a concerted fashion via a single transition state **384** to the aryl fluoride product **381** and the urea by-product **385**. [The DFT method used was B3LYP/6-31G(d)/PCM(toluene)].[189]

The similarity of the deoxyfluorination reaction to the Newman-Kwart rearrangement and similar transformations was pointed out.[189] Indeed, the Newman-Kwart rearrangement was suggested to proceed via single-step S_NAr mechanism that involves a four-membered cyclic transition state (Scheme 1-72 A).[191,192] The Newman-Kart rearrangement is closely related to the Schönberg rearrangement (Scheme 1-72 B) and the Chapman rearrangement (Scheme 1-72 C). Based on comparable Hammett ρ-values it has been suggested that the three reactions probably follow a similar, concerted mechanism.[193] Computational studies for the Newman-Kart rearrangement[194,195] supported the initial suggestion[191,192] that this reaction may follow a concerted pathway. In a computational study it was also found that the scope of the Newman-Kwart rearrangement can be expanded to vinylic systems, in principle (Scheme 1-73).[194] [The computational method used was B3LYP/6-31+G(d,p) for geometry optimisation. Single point energies were calculated with MP2/6-31+G(d,p). All calculations were performed in the gas phase]. For example, the activation enthalpy of the aromatic substrate **392** and the vinylic substrates **394** and **396** was found to be equally high (Scheme 1-73 A *vs.* B and C). The aliphatic substrate **398**, in contrast, exhibited a much higher activation enthalpy (Scheme 1-73 D). Indeed, the geometry of the transition of substrate **398** showed that the

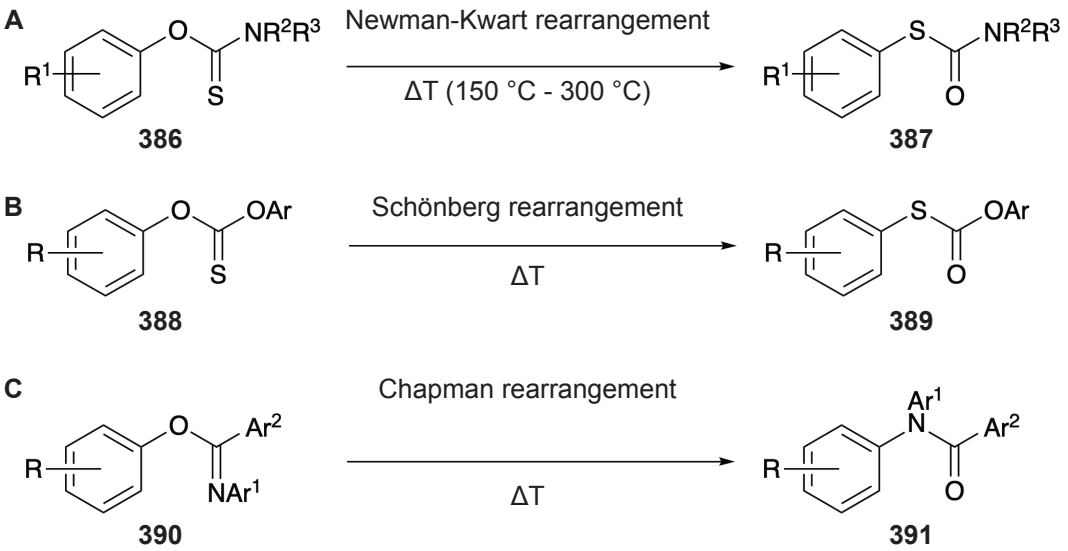

Scheme 1-72 The Newman-Kwart, Schönberg, and Chapman rearrangement typically require high temperatures to proceed.

carbon-oxygen bond is almost fully dissociated while the carbon-sulfur bond did not yet form to a significant extent. Hence, the mechanism for the rearrangement of **398** is reminiscent of an S_N1 reaction. For all four examples shown in Scheme 1-73, a concerted rearrangement pathway was identified.[194]

An hole-catalysed version of the Newman-Kwart rearrangement was introduced more recently by Nicewicz et al.[196] According to these protocols, the rearrangement of the substrate is induced by a single electron oxidation step. The dramatically decreased activation barrier allows the hole-catalysed Newman-Kwart rearrangement to proceed under much milder conditions.[196] Based on computational studies, it was shown that this modified Newman-Kwart rearrangement proceeds via a concerted pathway akin to the original reaction.[132,197]

The above reactions with a four-membered spirocyclic transition state have all been suggested to proceed via a concerted mechanism. Indeed, no example was found where evidence for Meisenheimer intermediate was presented for this class of reactions. For the analogous rearrangement reactions with a five-membered spirocyclic transition state, in contrast, a Meisenheimer intermediate was identified in several computational studies.[198-201] Based on the Smiles-reaction of **400** it was demonstrated that the choice of the computational method can affect the nature of the reaction profile (i.e. stepwise vs. concerted) (Scheme 1-74).[177] [For all investigated methods the 6-31+G(d,p) basis set was used. Solvent effects were accounted for with the PCM(methanol) solvent model]. With the high-level reference method CCSD(T)// MP2(SDQ) it was found that the structure **401** is a minimum on the potential energy surface. Hence, according to the reference calculation, the Smiles rearrangement of **400** proceeds in a stepwise fashion via a Meisenheimer intermediate. It should be noted that the energy profile exhibits a shallow minimum, i.e. the intermediate is stabilised by only 0.9 kcal/mol with respect to the first transition state. Thus, the reaction of **400** can be regarded as a mechanistic boarder-line case.[177]

Different DFT methods were then investigated for their ability to reproduce the energy profile obtained with the reference method. The Minnesota functionals M06 and M06-2X, and the ωB97X functional were found to predict a stepwise reaction mechanism in accordance with

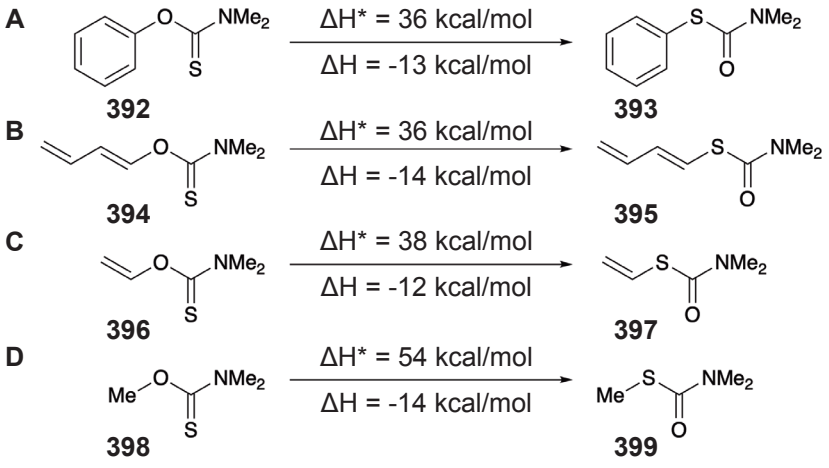

Scheme 1-73 In a computational study it was demonstrated that the scope of the Newman-Kwart rearrangement can in principle be expanded to vinylic systems.

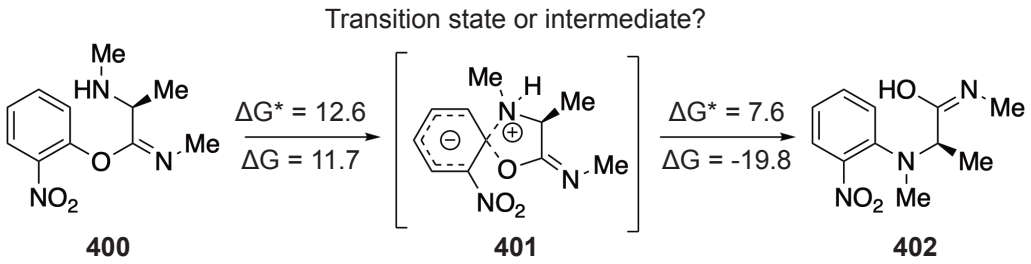

CCSD(T)//MP4(SDQ):	intermediate (reference method)
M06 and M06-2X:	intermediate
ωB97X:	intermediate
B3LYP:	transition state

Scheme 1-74 The choice of the DFT functional affects the nature of the reaction profile. For all methods the 6-31+G(d,p) basis set was used with PCM(methanol) solvent model. The energies obtained with reference method are given (in kcal/mol).

the reference method. The very popular B3LYP functional, in contrast, predicted the reaction to follow a concerted mechanism. Thus, according to the B3LYP calculation the structure **401** corresponds to a transition state.[177] The study underlines that the computational model needs to be carefully validated if a realistic reaction profile is to be established. This is particularly true if a boarder-line case is investigated where the reaction pathway exhibits a shallow minimum for the Meisenheimer intermediate.

One example where a concerted mechanism has been put forward for the Smiles-rearrangement is shown in (Scheme 1-75).[202] In this variant of the Julia-Kocieński reaction, the Smiles-rearrangement is an essential step. The aldehyde **403** reacts with the anion **404** to give the alkoxide intermediate **405**. This intermediate undergoes the Smiles-rearrangement to **407**, which decays spontaneously to the alkene **408**. The underlying mechanism has been studied in detail with computational methods. [The DFT method used was B3LYP/6-311+G(d,p)/PCM(solvent)]. The effect of coordinating counter cations and different solvents on the *cis/trans* selectivity was rationalised. It was also found that the Smiles-rearrangement step follows a concerted mechanism in all examined cases (different solvents and counter ions). It was noted that, in the transition state **406**, no significant amount of negative charge is transferred onto the tetrazole ring. Instead, the negative charge is directly transferred from the attacking alkoxide nucleophile to the sulfur atom of the leaving group.[202]

The multi-component reaction of pyridine **409**, benzyne **410** (generated in situ) and *N*-methyl isatin **413** harbours a Smiles-rearrangement as a key step, too (Scheme 1-76).[203] According to a plausible mechanism, pyridine **409** attacks benzyne **410**, which leads to the zwitterion **411**. After a proton transfer the carbene **412** is formed. This carbene nucleophilically adds on to isatin **413** to give the intermediate **414**. The intermediate **414** spontaneously undergoes the Smiles-rearrangement via the transition state **415** to give the product **416**. The computational model predicts this rearrangement to follow a concerted pathway. [The DFT method used was B3LYP/6-311++G(d,p)/IEFPCM(THF)].[203]

From above examples it becomes evident that the concerted S_NAr reaction mechanism is likely to be a widespread phenomenon that occurs in a diverse range of S_NAr reactions. Due to the diversity of the reported examples, it is not straightforward to extract simple guidelines that would allow one to estimate when a S_NAr reaction follows a concerted and when a stepwise

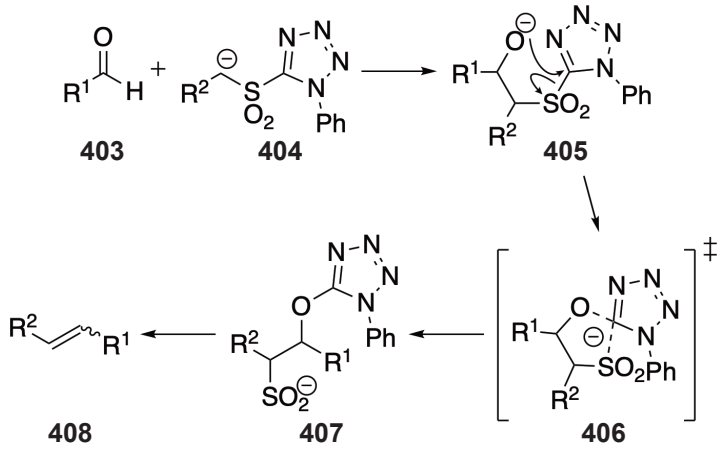

Scheme 1-75 The Smiles-rearrangement at the heart of the Julia-Kocieński was found to proceed via a concerted mechanism.

mechanism. It also became clear that it is challenging to experimentally show that a given set of S_NAr reactions proceeds via a concerted mechanism. While experimental investigations always rely on establishing trends over a range of examples, computational investigations can give a well-defined answer for a single S_NAr reaction. But the validity of the computational method needs to be carefully established. So far, such a careful validation has only been reported for the Smiles-rearrangement[177] but not for a general intermolecular S_NAr reaction.

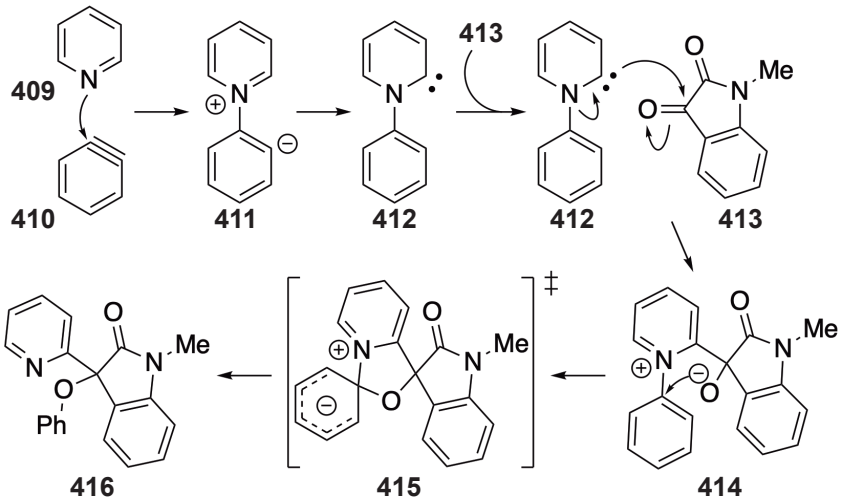

Scheme 1-76 The Smiles-rearrangement in the three-component reaction of pyridine **409**, a benzyne precursor and N-methyl isatin **413** was found to follow a concerted mechanism according to the computational model employed.

2. Organic Super Electron Donors Made Catalytic

2.1. Background

A major drawback of neutral organic super electron donors is that these molecules suffer from significant side-reactions when used in radical transformations. This tendency is linked to the fact that most of the electron donors discussed so far can give rise to relatively long-lived radical cations. The radical cation species is prone to recombine with reactive alkyl radicals when it accumulates in the reaction mixture. This process likely follows the principle of the persistent radical effect[89,90] and has been discussed in detail in the introduction (see Chapter 1.2.7). The recombination of the electron donor-derived radical cation with other radical species is, in general, undesired. A possible way to avoid such side-reactions is to design neutral organic *single* electron donors such as **417** (Scheme 2-1). Upon oxidation, a closed shell species **418** is obtained. Compared to quasi-persistent radical cationic intermediates, this closed shell benzimidazolium by-product would have a low tendency to interfere with the desired radical cascade.

Obviously, the required single electron donor species **417** is highly reactive and, due to its radical nature, it would no longer be easily accessible as a bulk material. Thus, single electron donors such as **417** would need to be generated in situ from a stable precursor. As expounded in Chapter 1.3, aminals are a promising compound class of such precursor molecules.

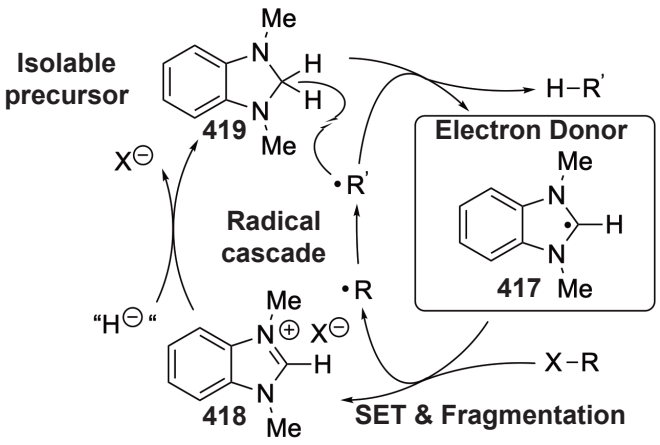

Scheme 2-1 The proposed scheme for how to use an organic single electron donor **417** catalytically.

Accordingly, **419** is the simplest, logical precursor of **417**.

According to the envisaged scheme, the organic single electron donor **417** is generated as an intermediate in a radical chain reaction. The hydrogen abstraction from **418** by the generated radical, •R', is the chain propagation step. The fact that **417** is generated in a radical chain is a distinguishing feature of the proposed process to the previously established protocols with double electron donors. Although these electron donors are typically formed in situ from a stable cationic precursor in the presence of a base[35] or from a zwitterionic carboxylate precursor,[204] they do not take part in a chain reaction.

It also becomes evident that the scheme harbours the possibility to use the single electron donor **417** catalytically. The aminal **419** can, in principle, be regenerated from the benzimidazolium salt **418** and a hydride source. Ideally, the organocatalyst would allow use of a mild, cheap and non-toxic hydride species as a terminal reducing agent. Through the action of the organocatalyst, a hydride source could be used to drive a radical cascade that would otherwise not engage in radical reactions.

When analysing the proposed reaction from the perspective of upconversion of reducing power (Chapter 1.4), it becomes apparent that this must happen on two different levels. Clearly, when going from **419** to **417**, upconversion of reducing power must be achieved. If not, **419** would react directly with the substrate via a single electron transfer or would not react at all. Further, when comparing the whole sequence from **418** to **417**, upconversion of reducing power must be achieved for the same reason (i.e. otherwise the hydride source would react directly with the substrate via a single electron transfer or would not react at all). Thus, in the proposed cycle, the organocatalyst not only converts a hydride equivalent from the terminal reducing agent to a single electron reductant. Also the net reducing power of the terminal reducing agent is increased. This overall upconversion of reducing power is possible, because the reactions from **418** to **419** and from **419** to **417** are both exergonic. They provide the energetic driving force to "pump up" an electron into an energetically high lying orbital (the principle depicted in Figure 1-14 applies).

This chapter is structured as follows. As became apparent from the introduction (Chapter 1.3), aminals such as **419** have received limited attention as potential hydrogen sources in radical reactions. Consequently, it was necessary to first study the reactivity of **419** separately (as will be discussed in Chapter 2.2.1 and Chapter 2.2.2). Once optimal conditions were established for this reaction, it was possible to develop the protocol further and to find conditions where **417** was used catalytically (Chapter 2.2.4). The scope of reductive radical cyclisation reactions with the conditions using stoichiometric amounts of **419** and with catalytic amounts of **418** was then investigated (Chapter 2.3). Finally, other heterocycles were explored for their ability to act as single electron donor precursors or as catalysts, according to the mechanism in Scheme 2-1 (Chapter 2.4).

2.2. Developing a Catalytic Electron Donor Protocol

2.2.1 Preliminary Experiments - Deiodination

(A detailed description of the following experiments can be found in Chapter 5.3.3).

In order to understand the fundamental reactivity of 1,3-dimethyl-2,3-dihydro-1*H*-benzo[*d*]imidazole **419** in radical reactions, the simple deiodination reaction of 4-iodobiphenyl **420** was

Table 2-1 Optimisation for the Deiodination Reaction

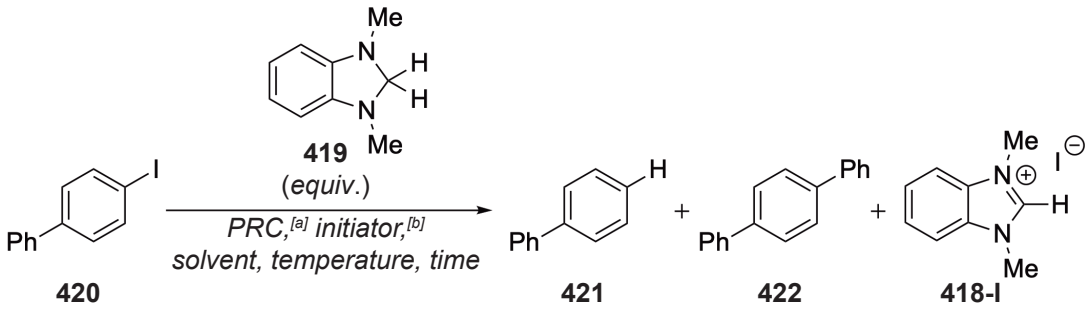

Entry	419 (equiv.)	PRC[a] (equiv.)	Initia-tor[b]	Solvent	Temp.	Time (h:min)	Yield of 421[c]
1	2.0	none	LP	benzene	70 °C	16:00	22 %[d]
2	2.0	none	DBP	benzene	80 °C	16:00	20 %[d]
3	2.0	none	DTBP	benzene	130 °C	16:00	65 %[e,f]
4	2.0	0.05	LP	benzene	70 °C	16:00	75 %[e]
5	2.0	0.05	DTBP	benzene	130 °C	16:00	81 %[e,g]
6	**2.0**	**none**	**air**	**none**	**RT**	**38:00**	**91 %**[e,h]
7	1.1	none	air	none	45 °C	18:00	78 %
8	1.1	none	air	DMSO	45 °C	18:00	89 %
9	1.1	none	air	ACN	45 °C	18:00	84 %
10	1.5	none	air	ACN	45 °C	6:00	90 %
11	2.0	none	air	ACN	45 °C	6:00	99 %
12	**2.0**	**none**	**air**	**ACN**	**55 °C**	4:00	**99 % (92 %)**[e]
13	1.1	none	air	Acetone	45 °C	18:00	82 %
14	1.1	none	air	1,4-dioxane	45 °C	18:00	76 %
15	1.1	none	air	EtOAc	45 °C	18:00	73 %
16	1.1	none	air	DMF	45 °C	18:00	66 %
17	1.5	none	air	DMF	45 °C	6:00	83 %
18	2.0	none	air	DMF	45 °C	6:00	90 %
19	**2.0**	**none**	**air**	**DMF**	**55 °C**	**4:00**	**95 %**
20	1.1	none	air	DCM	45 °C	18:00	59 %
21	1.1	none	air	Cyclohexane	45 °C	18:00	55 %
22	1.1	none	air	THF[i]	45 °C	18:00	28 %

[a] *n*-Dodecanethiol was used as a polarity reversal catalyst (PRC).

[b] LP: lauroyl peroxide; DBP: dibenzoyl peroxide; DTBP: di-*tert*-butyl peroxide. For all the initiators other than air, 0.2 equiv. were used. When air was used as an initiator, the reaction was left open to air for the whole reaction period via a needle.

[c] The yield was determined by HPLC vs. 1-phenylpyrrolidin-2-one as internal standard unless mentioned otherwise.

[d] The conversion (product / {product + substrate} x 100 %) was determined by ^{1}H-NMR.

[e] Isolated yield.

[f] Additionally, 20 % of *p*-terphenyl **422** and 51 % of **418-I** were isolated.

[g] Additionally 15 % of *p*-terphenyl **422** and 36 % of **418-I** were isolated.
[h] Additionally 49 % of **418-I** was isolated.
[i] THF, without stabiliser, was used.

chosen as a model system (Table 2-1). Initially, the reaction was performed in benzene and different radical initiators were examined (Entries 1 - 3). The temperatures were chosen such that the half-life time $t_{1/2}$ of the radical initiators was approximately 3 h for each experiment.[205] Clearly, *di-tert*-butyl peroxide (DTBP) gave the best results from these three initiators (Entry 3). From the experiment with DTBP, *p*-terphenyl **422** and the benzimidazolium salt **418-I** were also isolated. Since the aminal hydrogen atoms are relatively hydridic (2,3-dihydrobenzimidazoles have been used as hydride sources, indeed, see Chapter 1.3) it was natural to investigate the effect of a polarity reversal catalyst. The underlying principle of polarity reversal catalysis and its applications have been studied in detail, mainly by Roberts et al.[206-208] The thiol acts as a relay between the radical **424** and the aminal hydrogen atom that is to be abstracted from **419** (as illustrated in Figure 2-1 following the general principle explained by Roberts[206]). The direct hydrogen atom abstraction by the nucleophilic radical **424** from the hydridic aminal **419** suffers from a high activation barrier because of a polarity mismatch between the two species (orange curve). The hydrogen abstraction by **424** from the protic thiol **423** is much faster. The generated electrophilic thiyl radical **425** is then competent in abstracting the hydridic hydrogen atom from **419** (blue curve). For the study presented here, *n*-dodecanethiol was selected as a polarity reversal catalyst. In two reactions with different initiators, the *n*-dodecanethiol was found to have a pronounced positive impact. In the reaction with lauroyl peroxide, a 75 % yield was achieved (Entry 4) compared to 22 % conversion in the analogous reaction without the thiol (Entry 1). Similarly, with DTBP, the yield increased from 65 % (Entry 3) to 81 % (Entry 5) due to the effect of the thiol. In the further investigation of the reaction conditions the PRC was excluded first. It was assumed that other factors influencing the reaction outcome would

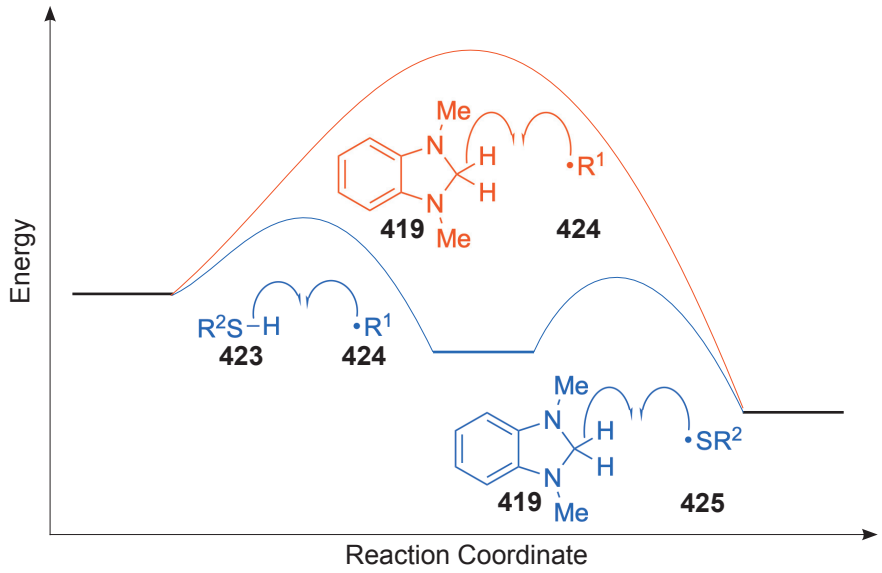

Figure 2-1 In the polarity reversal catalysis approach, one slow - because of a polarity mismatch between the hydrogen atom and the incoming radical - hydrogen atom transfer step is replaced by two fast - polarity matched - hydrogen atom transfer steps.

manifest more pronouncedly in its absence.

Through serendipity, it was observed that the reaction proceeds when open to air under highly concentrated conditions. Hence, the substrate **420** and reducing agent **419** were reacted neat at room temperature open to air (Entry 6) and a high yield of reduced product **421** was obtained. However, effective mixing was no longer possible under neat conditions, since the substrate **420** is solid at room temperature and since the reaction generated **418-I**, which is a solid too. In order to remove this potential source of variability, a suitable solvent was sought for the reaction. The initially used solvent, benzene, was no longer considered as an option, because of its toxicity and because it gives rise to the *p*-terphenyl by-product **422**. For the initial solvent screen, the amount of **419** was decreased from 2.0 equiv. to 1.1 equiv., the time was limited to 18 h and a moderate reaction temperature of 45 °C was chosen. For comparison, a neat reaction with these parameters was performed (Entry 7). It was found that the reaction in DMSO (Entry 8), ACN (Entry 9) and acetone (Entry 13) gave a slightly higher yield of reduced product than the neat reaction. The solvents - listed according to decreasing performance - 1,4-dioxane (Entry 14), EtOAc (Entry 15), DMF (Entry 16), DCM (Entry 20), cyclohexane (Entry 21) and THF (Entry 22) gave yields that were lower than for the neat reference reaction.

Finally, it was investigated how the reactions with a solvent and left open to air respond to an increase in temperature and an increase in equivalents of **419**. The investigation was performed for the solvents ACN (Entries 9-12) and DMF (Entries 16-19). By increasing the ratio of **419** to 2.0 equiv. and the temperature to 55 °C, an almost quantitative yield was achieved in ACN after a conveniently short reaction time of 4 h (Entry 12). A comparable result was achieved with DMF as the solvent (Entry 19).

It becomes apparent that the deiodination reaction of **420** with **419** is quite flexible. It works well under neat conditions and in a number of solvents. Conveniently short reaction times of a few hours can be achieved at moderate temperatures. Also the salt by-product **418-I** can readily be separated from the desired reaction product. Importantly, the reaction can be initiated by oxygen in the air. Hence, the protocol can be dramatically simplified, compared to reactions with the previously established electron donors (see Chapter 1.2.4 to Chapter 1.2.6 for examples), which require handling under strictly inert atmosphere and dry conditions. For the further development of the protocol, it was decided to retain the initiation by oxygen in air.

2.2.2 Optimisation for Reductive Radical Cyclisation Reactions with 419

(A detailed description of the following experiments can be found in Chapter 5.3.4).

The deiodination reaction discussed above served as a stepping stone towards the carbon-carbon bond formation in a reductive radical cyclisation reaction. The cyclisation leading from substrate **426** to product **427** was selected as a model system to study this class of reactions with reducing agent **419** (Table 2-2). Based on the results of the deiodination reaction discussed above, the temperature of 55 °C, the loading of aminal **419** (2.0 equiv.), and the mode of initiation (reactions left open to air) were selected as ideal. These parameters would give a conveniently fast reaction rate and a simple reaction set-up. The reactions were monitored by GC-FID in order to get a better understanding of their time courses. In Table 2-2, the time when the reaction reached full conversion is given.

A number of solvents were investigated (Entries 1-6). The concentration of **426** was chosen as 0.5 M and 0.2 equiv. of polarity reversal catalyst (PRC) were included for this screen. It

Table 2-2 Optimisation of the Reductive Cyclisation Reaction of 426

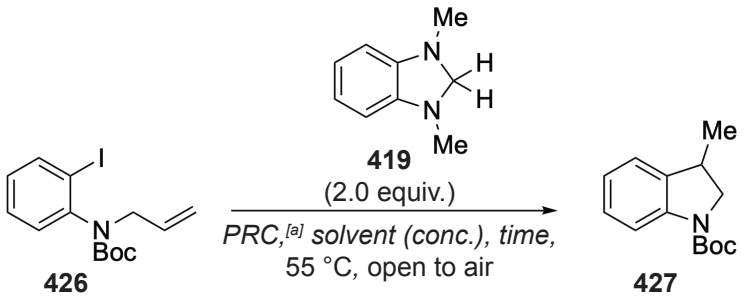

Entry	PRC[a] (equiv.)	Solvent	Concentration	Time[b] (h:min)	Yield of 427[c]
1	**0.2**	**DMF**	**0.5 M**	**0:50**	**87 % (86 %)[d]**
2	0.2	ACN	0.5 M	1:15	75 %
3	0.2	Cyclohexane	0.5 M	4:00	65 %
4	0.2	Toluene	0.5 M	4:00	66 %
5	0.2	THF[e]	0.5 M	3:00	69 %
6	0.2	*t*BuOH	0.5 M	>4:00	46 %[f]
7	0.2	DMF	0.1 M	0:15	77 %
8	1.0	DMF	0.1 M	0:05	81 %
9	0.05	DMF	0.5 M	1:00	76 %
10	none	DMF	0.5 M	2:00	64 % (65 %)[d]
11	0.05	ACN	0.5 M	1:30	69 %
12	none	ACN	0.5 M	2:00	58 %
13[g]	0.2	DMF	0.5 M	>6:00	62 %[h]

[a] *n*-Dodecanethiol was used as a polarity reversal catalyst (PRC).

[b] The reaction progress was monitored by GC-FID and the time when the reaction reached full conversion is given.

[c] Yield determined by GC-FID vs. 1-phenylpyrrolidin-2-one as internal standard, unless mentioned otherwise.

[d] Isolated yield in brackets.

[e] THF without stabiliser was used.

[f] Yield of remaining starting material was 45 % by GC-FID vs. 1-phenylpyrrolidin-2-one as internal standard.

[g] The reaction was degassed by purging with nitrogen and was kept under a nitrogen atmosphere.

[h] 22 % of remaining starting material was measured by GC-FID vs. 1-phenylpyrrolidin-2-one as internal standard.

was expected that the presence of the PRC would be more important for this model substrate because after the cyclisation the alkyl radical intermediate is less reactive compared to the aryl radical intermediate obtained in the simple dehalogenation reaction. It was found that the reaction performed best in DMF (Entry 1). With this solvent, the highest final yield was obtained

and also the shortest time until the reaction reached full conversion. An only slightly inferior result was obtained with ACN (Entry 2). The other solvents gave clearly slower reaction rates and lower yields of product.

Next, the concentration of the reaction was lowered from 0.5 M (Entry 1) to 0.1 M (Entry 7). Somewhat surprisingly, the reaction time markedly decreased by ca. a factor of three. The yield of product for reaction in Entry 7, however, was significantly lower than in the reference reaction (Entry 1). The reason behind these two observations - higher reaction rate and lower yield of desired product - is not fully understood at present. An ansatz to an explanation may be that at lower concentration, a side-reaction becomes accentuated. That would lead to faster consumption of starting material while giving a decreased yield of product. However, no by-product could be isolated and characterised. Hence, the interpretation of this result remains speculative. In an attempt to increase the yield of the reaction at 0.1 M concentration, the loading of *n*-dodecanethiol was increased from 0.2 equiv (Entry 7) to 1.0 equiv. (Entry 8). Indeed, the yield of product increased slightly. Moreover, the reaction rate became even faster, giving full conversion of substrate in only 5 min.

Stoichiometric amounts of the thiol polarity reversal catalyst are, however, not desirable. Ideally, the amount of thiol should be as small as possible. Therefore, it was investigated whether the amount of thiol could be decreased compared to the so far best conditions (Entry 1). With 0.05 equiv. of thiol (Entry 9), a drop in yield and a slightly increased reaction time was observed. A further drop in yield and increase in reaction time occurred when the reaction was performed in the absence of the polarity reversal catalyst altogether (Entry 10). An analogous trend - although slightly less pronounced - of decreasing yield and increasing reaction time with a decrease of thiol loading was observed in ACN as the solvent (Entry 2, 11 and 12).

Finally, the effect of the presence of air on the reaction was investigated (Entry 13). Under a nitrogen atmosphere, the reaction time dramatically increased by more than a factor of six. This finding substantiates the hypothesis that oxygen in the air acts as an initiator for the reaction.

As observed before for the deiodination of **420**, the reaction is quite flexible insofar as it tolerates various solvents and conditions. The responses to changes of solvent, the concentration, and loading of thiol are significant but not dramatic (the yield of product generally varies by less than 30 %). This indicates that the protocol is inherently robust. The conditions in Entry 1 were selected as ideal for reductive radical cyclisation reactions with aminal **419**.

2.2.3 Computational Studies on the Initiation by Oxygen

(A detailed description of the following DFT calculations can be found in Chapter 5.3.5).

Initiation by oxygen in the air requires that the aminal **419** is oxidised by oxygen. A possible mechanism of the initiation has been investigated with computational methods (Figure 2-2). The first possibility that was considered is a single electron transfer from the aminal **419** to oxygen (Variant A). The energy barrier was calculated according to Nelsen's four-point method,[209] which is an implementation of Marcus theory.[61,210] The energy barrier for the single electron transfer was found to be 29.5 kcal/mol. The process was overall endergonic by 28.9 kcal/mol. The resulting aminal radical cation **428** can transfer a proton to the superoxide anion **429** to give the benzimidazoyl radical **417** and hydroperoxyl radical **430**. This proton transfer is almost thermoneutral. As an alternative, the direct hydrogen abstraction of a hydrogen atom from aminal **419** by oxygen has been considered (Variant B). Although a transition state

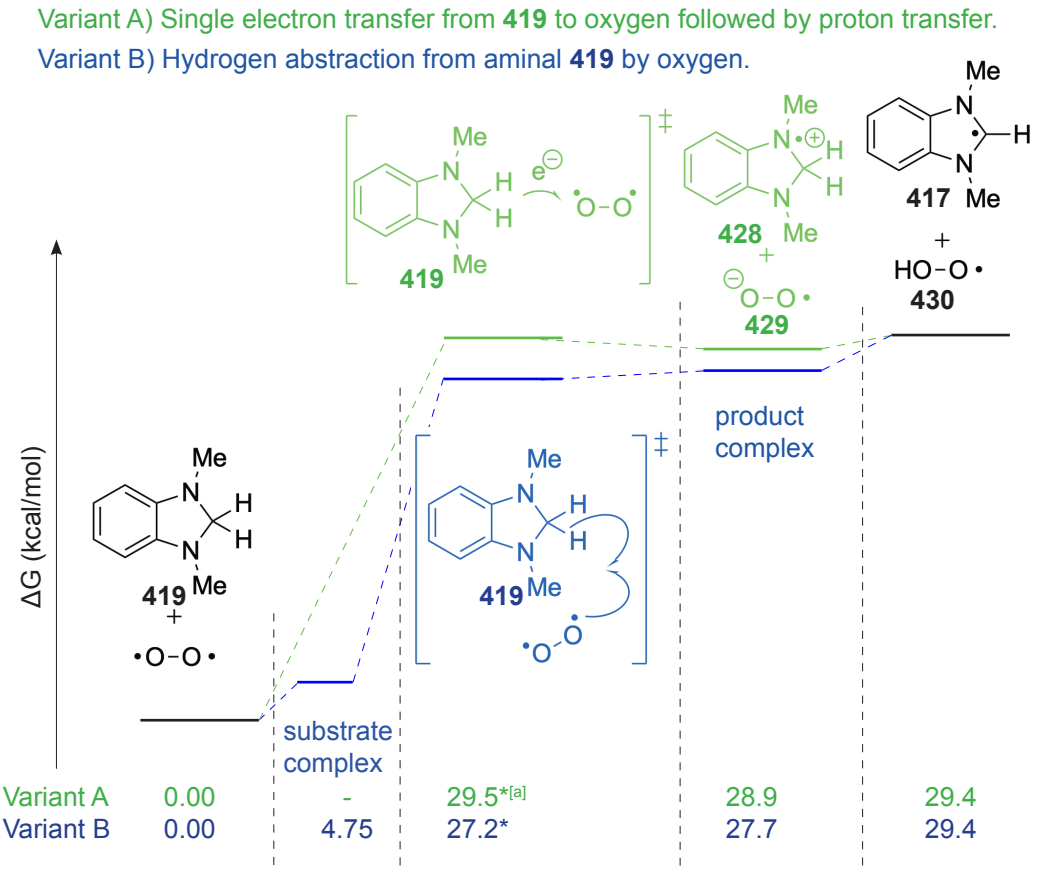

Figure 2-2 Oxidation of **419** by oxygen. Level of theory: UM06-2X/6-311++G(d,p)/cpcm(DMF). (*) Transition state energies are marked with an asterisk. [a] Calculated by Nelsen's four-point method[209] based on Marcus theory.[61, 210]

structure was successfully identified, the process is effectively barrier-less - after the thermal energy corrections have been made, the transition state energy turns out to be slightly lower than the energy of the product complex. Decomplexation of the reaction products leads to the same end-point as reached in Variant A. Overall, the two energy profiles are very similar. They both show a negligible barrier while being strongly endergonic.

In light of the pronounced endergonic nature of the oxidation of **419** it becomes critical to identify a subsequent reaction step that can drive the initiation process forwards. An efficient forward reaction of either of the three products, **417**, superoxide or hydroperoxyl radical, could fulfill this requirement.

First, the hydrogen abstraction by the peroxide species **429** or **430** from another molecule of aminal **419** was considered (Scheme 2-2). Two sets of values are reported in this scheme. The first set of Gibbs free energies refers to the separated aminal **419** and peroxide species. The second set of energies is given with respect to the reference from Figure 2-2, i. e. two separate molecules **419** and one molecule of oxygen. It becomes clear that the superoxide radical anion **429** is not able to abstract a hydrogen atom from the aminal **419** efficiently in any case. The situation is different with the hydroperoxyl radical **430**. This species is sufficiently reactive to

419 **417**

Peroxide Species	ΔG* (kcal/mol)	ΔG*[a] (kcal/mol)	ΔG (kcal/mol)	ΔG[a] (kcal/mol)
429 (X = O^-)	31.4	60.8	15.5	44.9
430 (X = OH)	12.5	41.9	-4.37	25.0

Scheme 2-2 Hydrogen abstraction from **419** by peroxide species **429** or **430**. Level of theory: UM06-2X/6-311++G(d,p)/cpcm(DMF). (*) Transition state energies are marked with an asterisk. [a] Calculated relative to the reference point in Figure 2-2.

abstract a hydrogen atom from **419** in a mildly exergonic reaction. Measured with respect to the beginning of the initiation process the activation energy is, however, high at 41.9 kcal/mol. This barrier appears to be too high for an effective initiation process (a detailed computational study on organic super electron donors as initiators for base-promoted homolytic aromatic substitution reactions gives a set of reference values for initiation processes of radical chain reactions that is linked to experiments).[64]

The most simple onward reaction of peroxide species **429** and **430** did not lead to an obvious step that would drive the initiation process forward. Hence, the attention was focused on the onward reaction of the benzimidazoyl radical **417** (Scheme 2-3). The oxidation of **417** by oxygen is almost barrier-less and strongly exergonic. Therefore this is a very likely process to drive the initiation reaction forward. The overall barrier at 29.8 kcal/mol is reasonable for an initiation reaction.[64] The strong exothermicity of this single electron transfer step makes the initiation process less endergonic overall. Importantly, once **417** is removed from the equilibrium, the hydroperoxyl radical **430** is free to react as in Scheme 2-2 and thereby adding additional driving force to the reaction. The reaction of **417** with iodobenzene has a substantially higher

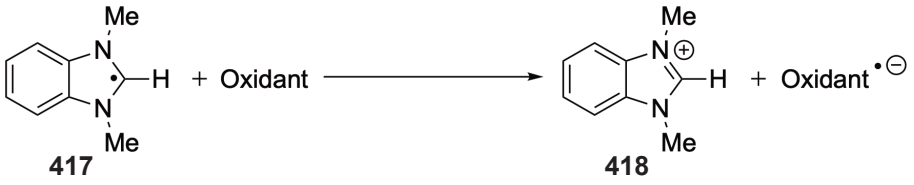

417 **418**

Oxidant	ΔG* (kcal/mol)	ΔG*[a] (kcal/mol)	ΔG (kcal/mol)	ΔG[a] (kcal/mol)
Oxygen	0.43	29.8	-20.6	8.80
Iodobenzene	12.4	41.8	-12.2	17.3

Scheme 2-3 Hydrogen abstraction from **419** by peroxide species **429** or **430**. Level of theory: UM06-2X/6-311++G(d,p)/cpcm(DMF). (*) Transition state energies are marked with an asterisk.These were calculated by Nelsen's four-point method[209] based on Marcus theory.[61, 210] [a] Calculated relative to the reference point in Figure 2-2.

Table 2-3 Development of the Catalytic Electron Donor Protocol

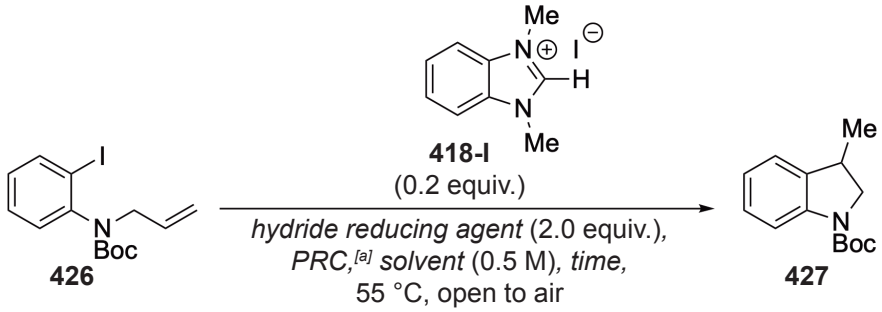

Entry	Hydride Reducing Agent	Loading of 418-I (equiv.)	PRC (equiv.)[a]	Solvent	Time (h:min)[b]	Yield of 427[c]
1	**$NaBH_4$**	**0.2**	**0.2**	**DMF**	**4:00**	**84 %**
2	**$NaBH_4$**	**0.2**	**0.2**	**DMF**	**3:40**[d]	**83 %**[e]
3	$NaBH_4$	0.05	0.2	DMF	4:00[f]	61 %[g]
4	$NaBH_4$	0.2	none	DMF	4:00	8 %
5	$NaBH_4$	0.2	0.2	ACN	4:00	40 %
6	$NaBH_4$	0.2	none	ACN	4:00	3 %
7	$NaBH_4$	0.2	0.2	*t*BuOH	4:00	20 %
8	$NaBH_4$	0.2	0.2	THF	4:00	18 %
9	$NaBH_4$	0.2	0.2	Toluene/ *t*BuOH	4:00	35 %
10	$NaBH_4$	0.2	0.2	Toluene/ water	4:00	27 %
11	$Na(AcO)_3BH$	0.2	0.2	DMF	4:00	40 %
12	$Na(AcO)_3BH$	0.2	none	DMF	4:00	7 %
13	$Na(AcO)_3BH$	0.2	0.2	ACN	4:00	7 %
14	$Na(AcO)_3BH$	0.2	none	ACN	4:00	1 %
15	$Na(AcO)_3BH$	0.2	0.2	*t*BuOH	4:00	6 %
16	$Na(AcO)_3BH$	0.2	0.2	THF	4:00	5 %
17	$Na(AcO)_3BH$	0.2	0.2	Toluene/ *t*BuOH	4:00	4 %
18	$Na(AcO)_3BH$	0.2	0.2	Toluene/ water	4:00	0 %
19	$Na(AcO)_3BH$	0.2	0.2	DMF	30:00	35 %[h]
20	$Na(AcO)_3BH$[i]	0.2	0.2	DMF	20:00	8 %[j]
21	$NaBH_3CN$	0.2	0.2	DMF	20:00	2 %[k]
22	$NaBH_4$	none	0.2	DMF	20:00	9 %[l]
23	$NaBH_4$	none	2.0	DMF	5:00	64 %
24	$NaBH_4$	none	none	DMF	20:00	0 %[m]

[a] *n*-Dodecanethiol was used as a polarity reversal catalyst (PRC).

[b] Time for which the reaction was heated at 55 °C.

[c] Yield determined by GC-FID vs. 1-phenylpyrrolidin-2-one as an internal standard unless mentioned otherwise.

[d] The reaction reached full conversion after 3 h.
[e] Isolated yield.
[f] The reaction reached full conversion after 4 h.
[g] Yield determined by ^{1}H-NMR vs. 1,3,5-trimethoxybenene as internal standard. No remaining starting material was detected.
[h] Yield of remaining starting material was 65 % by GC-FID vs. *n*-dodecane as internal standard.
[i] 8 equiv. of $Na(AcO)_3BH$ were used.
[j] The reaction was monitored by ^{1}H-NMR. The yield was determined vs. 1,3,5-trimethoxybenene as internal standard. The yield of remaining starting material was 43 % vs. the same internal standard.
[k] Yield of remaining starting material was 98 % by GC-FID vs. *n*-dodecane as internal standard.
[l] Yield determined by ^{1}H-NMR vs. 1,3,5-trimethoxybenene as internal standard. Yield of remaining starting material was 87 % vs. the same internal standard.
[m] The product was not detected by ^{1}H-NMR. Yield of remaining starting material was quantitative vs. 1,3,5-trimethoxybenene as internal standard.

barrier than the reaction with oxygen. Therefore, iodobenzene is not a suitable oxidising agent for the initiation process - as a part of the downstream radical chain reaction, however, the electron transfer from **417** to iodobenzene is very accessible.

In conclusion, a simple and plausible initiation pathway based on oxygen and **419** has been identified. It was also found that oxygen reacts much faster with the single electron donor **417** than iodobenzene (and most likely other aryl iodide substrates). Consequently, in the reaction vessel, oxygen will be consumed first. After the oxygen levels are low the productive radical chain reaction will become dominant. In addition to starting the radical reaction this “self-deoxygenation” of the reaction mixture helps to protect the desired radical chain reaction from side-reactions with oxygen.

2.2.4 Optimisation of the Catalytic Electron Donor Protocol

(A detailed description of the following experiments can be found in Chapter 5.3.6).

As can be seen from the results above, the reductive radical reactions with **419** are well-behaved and high-yielding. Building on this promising basis, it was intended to form **419** in situ from a catalytic amount of the salt **418-I**. Again the reductive radical cyclisation of substrate **426** was chosen as a model reaction. The investigation was started, based on the optimal conditions identified for the reaction with stoichiometric amounts of **419** (see Table 2-2 Entry 1). In order to make the protocol catalytic, the 2.0 equiv. of **419** were replaced by a substoichiometric amount of its precursor salt **418-I** and a stoichiometric amount of a hydride reducing agent (Table 2-3). A series of solvents and solvent mixtures was investigated with both sodium borohydride (Entries 1, 5, 7-10) and sodium triacetoxyborohydride (STAB) (Entries 11, 13 and 15-18) as the hydridic, terminal reducing agents. The experiments in this solvent screen were stopped after 4 h of reaction time. For all solvents tested, sodium borohydride clearly gave better results than STAB. DMF again stood out as the solvent of choice with both hydride reagents (Entries 1 and 11). Indeed, with sodium borohydride in DMF a very comparable yield

was achieved (Table 2-3 Entries 1 and 2) to the previously achieved yield with stoichiometric amounts of **419** (Table 2-2 Entry 1). In contrast to the previous optimisation studies, where the differences between various solvents were moderate, the yields obtained with the catalytic conditions fluctuate strongly when going from one solvent to another.

The conditions in Table 2-3 Entry 1 were identified as optimal and were confirmed by repeating the experiment on slightly larger scale and closely monitoring the reaction progress over time (Entry 2). The reaction reached full conversion after 3 h and the cyclised product was isolated in 83 % yield.

Lowering the amount of the polarity reversal catalyst from 0.2 equiv. to 0.05 equiv. led to a significant drop in yield (Entry 1 vs. Entry 3). At the same time, the turnover number of the catalyst increased to ca. 12 (mol/mol) compared to ca. 4 (mol/mol) in Entry 2.

The effect of the absence of *n*-dodecanethiol on the reaction under catalytic conditions was investigated in several instances. When no thiol was used (Entries 4, 6, 12 and 14) the yield dropped dramatically compared to the analogous reactions with the thiol (Entries 1, 5, 11 and 13, respectively).

STAB is a considerably milder reducing agent than sodium borohydride. Hence, a protocol based on STAB as the terminal hydridic reducing agent holds the promise of a higher functional group tolerance compared to a sodium borohydride based protocol. Therefore, attempts were made to improve the initial results obtained with STAB (Entry 11). However, prolonged heating (Entry 19) or increased amounts of STAB (Entry 20) did not lead to higher yields of product. On the contrary, opposing the initial expectation of achieving a milder protocol with STAB slow decomposition of starting material was observed with the latter conditions (Entry 20). Sodium cyanoborohydride was investigated as a milder alternative to sodium borohydride, too, (Entry 21) but without success.

Finally, a series of control reactions was performed (Entries 22 - 24). When no catalyst **418-I** was added (Entry 22) to the reaction, the yield dropped by almost an order of magnitude compared to the reference reaction (Entry 1). The origin of the formation of the small amount of product **427** in reaction of Entry 22 was further investigated. By increasing the amount of thiol to 2.0 equiv., the yield of **427** increased to 64 % (Entry 23). The result demonstrates that the combination of *n*-dodecanethiol and sodium borohydride is able to promote the radical cyclisation reaction. This observation is interesting in its own right but it was not further investigated here. Performing the reaction in the absence of both **418-I** and the thiol led to no formation of **427** at all. These observations show that in the catalytic electron donor protocol, potentially two different mechanisms may contribute to the formation of product **427**. Under the optimal conditions of Entry 1, however, the major reaction pathway critically relies on the presence of the catalyst **418-I**.

The catalytic protocol showed stronger dependence on the conditions such as the nature of the solvent and the presence of the polarity reversal catalyst than the previously developed protocol with stoichiometric amounts of **419**. Considering that for the reaction catalysed by **418-I** two processes - the radical chain reaction and the catalytic cycle - must work in concert, the higher sensitivity to deviations from optimal conditions is not surprising. Pleasingly, the optimal conditions (Entries 1 and 2) gave comparably high yields to the optimal conditions identified for the reaction with stoichiometric amounts of **419**.

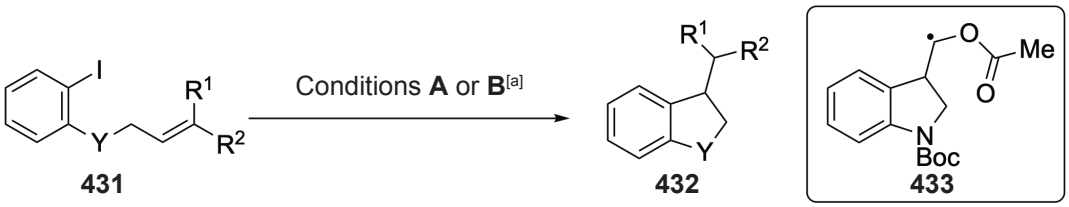

			A	B
431a	R^1= Me, R^2 = Me, Y = NBoc	**432a**	64 %	77 %
431b	R^1= H, R^2 = OAc, Y = NBoc	**432b**	22 %	-
431c	R^1= H, R^2 = C(O)OMe, Y = NBoc	**432c**	86 %	-
431d	R^1= H, R^2 = H, Y = O	**432d**	72 %[b]	67 %[c]

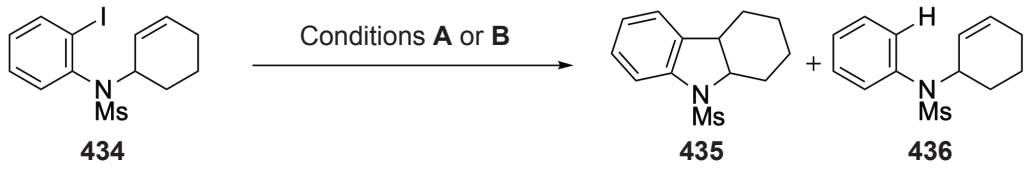

			A	B
434		**435**	87 %	62 %[d]

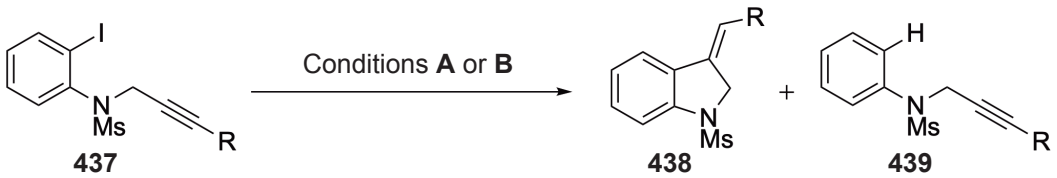

			A (*E*/*Z*)	B (*E*/*Z*)
437a	R = Me	**438a**	84 % (2/8)	62 % (3/7)[e]
437b	R = Cy	**438b**	90 % (3/7)	83 % (2/8)

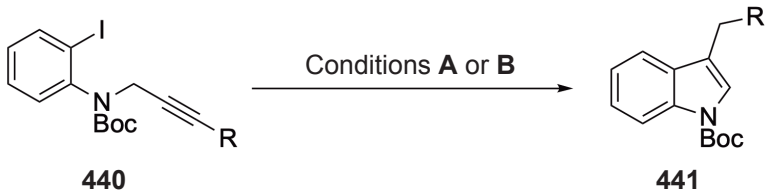

			A	B
440a	R = CH_2OTBDPS	**441a**	79 %	53 %
440b	R = H	**441b**	36 %	36 %

Scheme 2-4 The scope of both the stoichiometric protocol with **419** and the catalytic protocol with **418-I** was studied based on a number of radical cyclisation reactions. [a] Conditions **A**: **419** (2.0 equiv.), *n*-dodecanethiol (0.2 equiv.), DMF (0.5 M), 55 °C, open to air. Conditions **B**: **418-I** (0.2 equiv.), $NaBH_4$ (2.0 equiv.), *n*-dodecanethiol (0.2 equiv.), DMF (0.5 M), 55 °C, open to air. [b] Yield determined by ^{1}H-NMR vs. 1,3,5-trimethoxybenzene as an internal standard. [c] Yield determined by ^{1}H-NMR vs. 1,3,5-trimethoxybenzene as an internal standard. Additionally, the product was isolated in 60 % yield (volatile!). [d] The directly reduced by-product **436** was isolated in 11% yield. [e] The directly reduced by-product **439a** (R = Me) was isolated in 14 % yield.

2.3. Investigation of the Substrate Scope

2.3.1 Reductive Radical Cyclisation Reactions

(A detailed description of the following experiments can be found in Chapter 5.3.7).

The substrate scope for reductive radical cyclisation reactions was examined for both, the protocol with stoichiometric amounts of **419** and the protocol with catalytic amounts of **418-I**. In Scheme 2-4 the results of these protocols are directly compared.

The 5-*exo*-*trig* cyclisation of substrates **431a**, **431d** and **434** with an electron-neutral alkene radical trap worked well according to both protocols. In particular, the products **432a** and **432d** were obtained in very similar yields from the reaction performed either with stoichiometric amounts of **419** or catalytic amounts of **418-I**. Only in the case of **434** was the cyclised product **435** obtained in substantially lower yield from the catalytic protocol **B** compared to the stoichiometric protocol **A**. From the catalytic reaction also, the directly reduced by-product **436** was isolated in 11 % yield.

The substrate **431c** with an electron-poor alkene gave high yields of cyclised product when treated according to the stoichiometric protocol **A**. An electron-rich alkene, such as the enol ester in substrate **431b**, however, was not tolerated well, leading to a low yield of cyclised product **432b**. A likely reason for this poor outcome may be that the electron-rich radical intermediate **433** is not competent in sustaining the radical chain. Unfortunately, it was not possible to isolate further products, which could have shed light on side-reactions from the complex reaction mixture.

The 5-*exo*-*dig* cyclisation of the substrates **437a** and **437b** were both high-yielding when performed according to the stoichiometric protocol **A**. Following the catalytic protocol **B**, the reaction of the substrate **437a** was accompanied by the formation of the directly reduced by-product **439a** (R = Me) in 14 % yield. No such by-product was observed in the reaction of substrate **437b** when subjected to the catalytic protocol and the cyclised product **438b** was obtained in 83 % yield - close to the result achieved following the stoichiometric protocol.

The 5-*exo*-*dig* reactions with **440a** and **440b** did not give the indoline products but the indole products **441a** and **441b** as the double-bond isomerised during the isolation of these compounds. According to conditions **A**, the product **441a** was obtained in high yield and according to the conditions **B** a somewhat lower but still synthetically useful yield of 53 % was achieved. The substrate **440b**, in contrast, gave a low yield of **441b** when treated according to either protocol, **A** or **B**. This indicates that a terminal alkyne radical trap may not be compatible with these protocols.

In general, good yields were obtained with both protocols for the reductive radical cyclisation reactions tested here. As a general trend, it can be seen that the catalytic conditions give slightly lower yields of cyclised products. In two cases it was possible to isolate a directly reduced, non-cyclised by-product. These observations indicated that the catalytic protocol is more prone to side-reactions.

Next, the scope of alkyl halide substrates **442** was investigated for the protocol with stoichiometric amounts of aminal **419** (Scheme 2-5). While the alkyl iodide **442a** gave a high yield of cyclised product **443**, the same product was obtained in slightly lower yield from the alkyl bromide substrate **442b**. The alkyl chloride compound **442c** was found not to be a viable substrate at all, i. e. no product **443** was formed when **442c** was treated with aminal **419**. From this reaction, remaining starting material (70 %) was recovered.

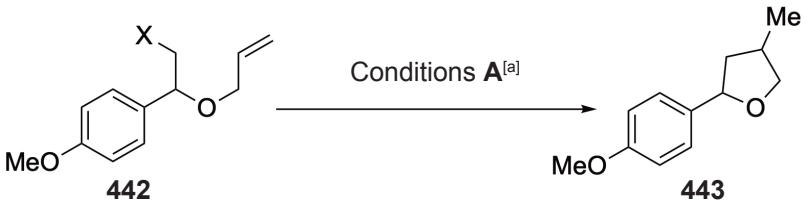

442 443

			Yield (d.r.)
442a	X = I	**443**	87 % (4:1)
442b	X = Br	**443**	67 % (4:1)
442c	X = Cl	**443**	0 %[b]

Scheme 2-5 The scope of alkyl halides was tested for the stoichiometric protocol **A** based on substrate **442**. [a] Conditions **A**: **419** (2.0 equiv.), *n*-dodecanethiol (0.2 equiv.), DMF (0.5 M), 55 °C, open to air. [b] 70 % of recovered starting material **442c**.

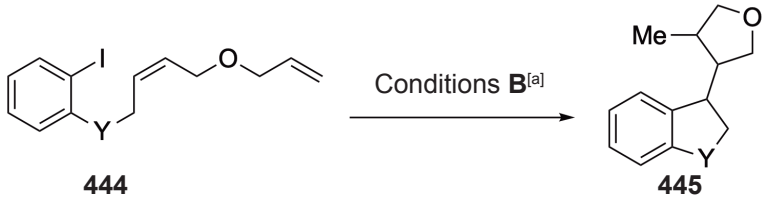

444 445

			Yield (d.r.)
444a	Y = NBoc	**445a**	51 % (7:1)
444b	Y = O	**445b**	62 % (5:2:1:1)

Scheme 2-6 The catalytic protocol **B** was challenged with two more complex radical cyclisation cascades. [a] Conditions **B**: **418-I** (0.2 equiv.), $NaBH_4$ (2.0 equiv.), *n*-dodecanethiol (0.2 equiv.), DMF (0.5 M), 55 °C, open to air.

Finally, the catalytic protocol was challenged with more complex radical cyclisation cascades (Scheme 2-6). The substrates **444** can undergo two consecutive 5-*exo*-*trig* cyclisation steps leading to the tricyclic products **445**. From both substrates, **444**, the desired product was obtained in satisfactory yield. Moreover, in the case of substrate **444a**, the product **445a** was obtained with good diastereoselectivity. It should be noted that the diastereoselectivity in these reactions is under substrate control. Simple guidelines to predict the diastereoselectivity of radical cyclisation reactions have been proposed by Beckwith, Schiesser and Houk.[211,212] These results demonstrate that the catalytic protocol is also competent when applied to more advanced multistep radical cascade reactions.

2.3.2 Reductive Cleavage of the N-O Bond in Weinreb Amides

(A detailed description of the following experiments can be found in Chapter 5.3.9 - Chapter 5.3.11).

The reductive N-O bond cleavage in Weinreb amides with neutral organic electron donors has been reported previously (see Chapter 1.2.6).[85] To investigate the reactivity of these more challenging-to-reduce substrates with aminal **419**, the standard reaction protocol was adapted

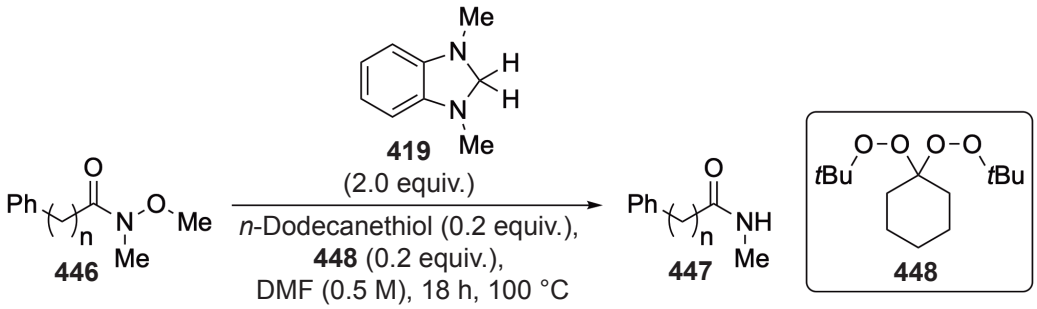

446a	n = 0	**447a**	94 % (93 %)[a]
446b	n = 1	**447b**	not detected[b]

Scheme 2-7 Investigation of the reductive N-O bond cleavage in Weinreb amides. [a] Yields in brackets have been determined by ^{1}H-NMR vs. 1,3,5-trimethoxybenezene as internal standard. [b] The product **447b** was not detected by either ^{1}H-NMR spectroscopy or GC-MS analysis. The yield of remaining starting material **446b** was 79 % as determined by ^{1}H-NMR vs. 1,3,5-trimethoxybenezene as internal standard.

(Scheme 2-7). Instead of oxygen in the air, the peroxide **448** was used as initiator and the reaction was performed at 100 °C ($t_{1/2}$ of **448** at this temperature is ca. 10 h)[213] instead of at

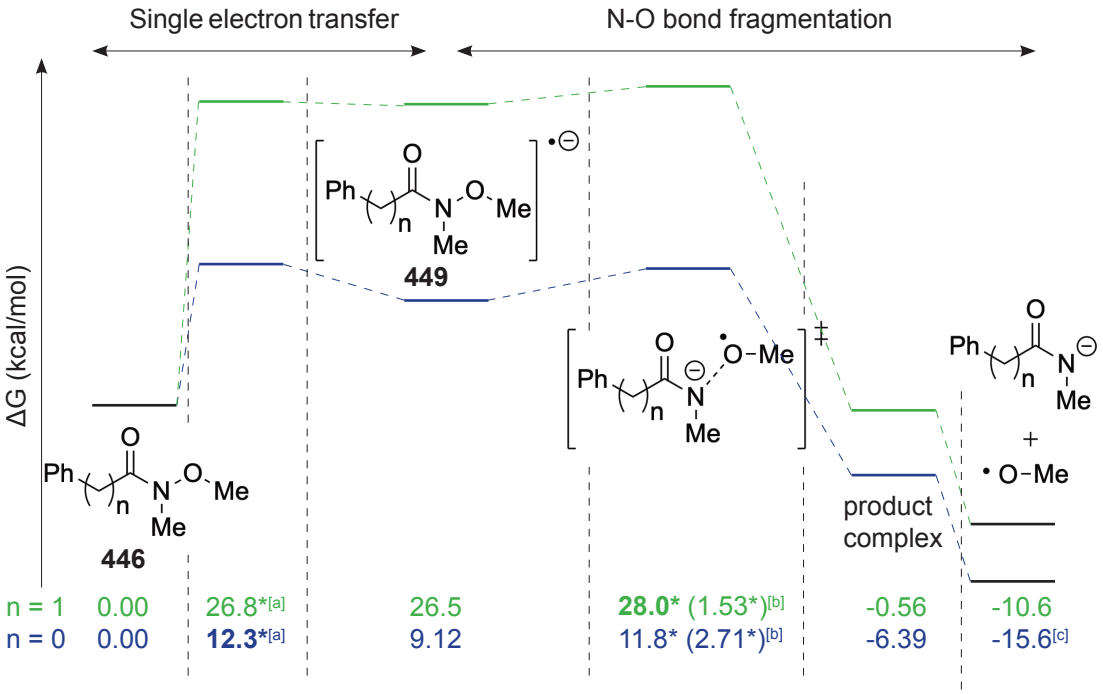

Figure 2-3 Reductive N-O bond cleavage in Weinreb amide substrates **446**. Level of theory: UM06-2X/6-311++G(d,p)/cpcm(DMF). (*) Transition state energies are marked with an asterisk. [a] Calculated by Nelsen's four-point method[209] based on Marcus theory.[61, 210] [b] The value in brackets is measured with respect to the radical anion **449**. [c] The alternative fragmentation to a aminyl radical and a methoxide anion is energetically less favourable by > 16 kcal/mol.

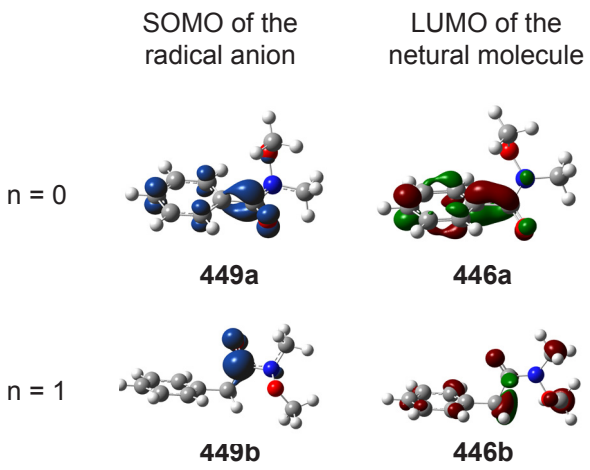

Figure 2-4 Visualisation of the SOMOs of the radical anions **449** (left column) and the LUMOs of the neutral compounds **446** (right column).

55 °C. It was found that the N-O bond in substrate **446a** was readily cleaved to give the amine **447a** in high yield. With the benzylic Weinreb amide substrate **446b**, however, no cleavage of the N-O bond was observed (i.e. the amide **447b** was not detected). This striking discrimination between the two substrates **446** is in principle in line with the trend that was previously observed (see Chapter 1.2.6),[85] but it is much more pronounced. For comparison, in the previous study, the substrate **446b** was reduced only slightly less efficiently than the substrate **446a** under identical conditions. A marked decrease in yield was only observed when the alkyl linker between the Weinreb amide function and the aromatic system was two methylene units in length or longer.

To better understand the sharp discrimination between substrate **446a** and **446b**, the energy profile for the single electron transfer and subsequent N-O bond fragmentation was calculated (Figure 2-3). It was found that there is a pronounced difference in the energy profile of the reductive N-O bond cleavage for **446a** and **446b**. While the overall energy barrier for the reduction of **446a** (n = 0) is achievable, this is no longer the case with substrate **446b** (n = 1). The difference between the two substrates roots in the initial single electron transfer step. For substrate **446b**, this step is much more endergonic than for substrate **446a**. The subsequent fragmentation of the N-O bond is strongly exergonic and shows a low relative energy barrier in both cases of $\Delta G^*_{rel} < 3$ kcal/mol.

When looking at the spin density distribution in the two radical anions **449**, a fundamental difference becomes apparent (Figure 2-4). While the unpaired electron in **449a** is distributed over the amide function and the aromatic system, the spin is fully localised on the amide function in **449b**. This is only in apparent contradiction to the findings presented in the introduction (see Chapter 1.2.6)[85] In that study the authors analysed and commented on the LUMO of the neutral compound. This orbital, however, corresponds to the SOMO in the radical anion only in a first approximation. From the visualisation of the LUMOs of the two neutral molecules **446**, it becomes apparent that in the case of **446b** the localisation of the LUMO significantly deviates from the localisation of the SOMO of the radical anion. Clearly - and in accordance with what has been reported previously - the LUMO is distributed over the amide function and the aromatic system. This analysis shows that it is problematic to discuss the electronic structure of the radical anion based on the frontier orbitals of the neutral counterpart. It also gives a nice

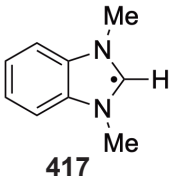

417

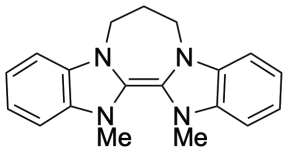

4

Method	$E_{1/2}$ of 417 (V vs. SCE)	$E_{1/2}$ of 4 (V vs. SCE)
UM06-2X/6-31+G(d,p)/cpcm(DMF)	-1.86	-0.762
UB3LYP/6-31+G(d,p)/cpcm(DMF)	-1.78	-0.911
CV experiment	-1.84[a]	-0.82[b]

Figure 2-5 Based on the redox potential electron donor, electron donor **417** is by 1 V more reducing than the parent electron donor **4**. [a] Measured in ACN.[113] [b] Measured in DMF.[33]

visual explanation for why the reduction of **446a** is much easier than the reduction of **446b**; in the radical anion **449a**, the additional electron is delocalised over the amide function and the aromatic ring while in **449b** the electron is fully located on the amide function.

The Weinreb amides **446** were found not to be suitable substrates for the catalytic conditions **B**, since - not surprisingly - hydride reduction to the corresponding alcohols outran any other reaction. Still, in case of substrate **446a**, small amounts of amide product **447a** were detected (see Chapter 5.3.9 for details).

2.3.3 Benchmark

(A detailed description of the following experiments can be found in Chapter 5.3.12).

From electrochemically determined redox potentials, it can be estimated that the single electron donor **417** is approximately 1 V more reducing than the parent benzimidazole-derived electron donor **4** (Figure 2-5). A computational investigation of the redox potentials based on a method used by Nicewicz et al.[214] is in agreement with these experimental findings. This difference of reduction potential is massive, especially for two structurally so closely related compounds. It is, however, not entirely surprising and can be rationalised following the argument in Chapter 1.1.8. An analogous finding was published by Giri et al.[58] From their computational study, it follows that the open-shell species **60** has a distinctly lower ionisation potential than the related dimeric electron donor **27** (Figure 2-6).[58]

The key question is how far the decreased redox potential of **417** with respect to **4** translates

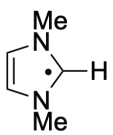

60

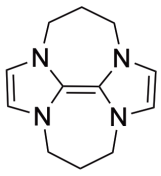

27

Figure 2-6 An analogous difference of reduction power, as found with the electron donor couple **417** and **4**, was identified by Giri et al. for the species **60** and **27**.

Table 2-4 Comparison of the effective reducing power of three different neutral organic electron donors

Reducing Agents

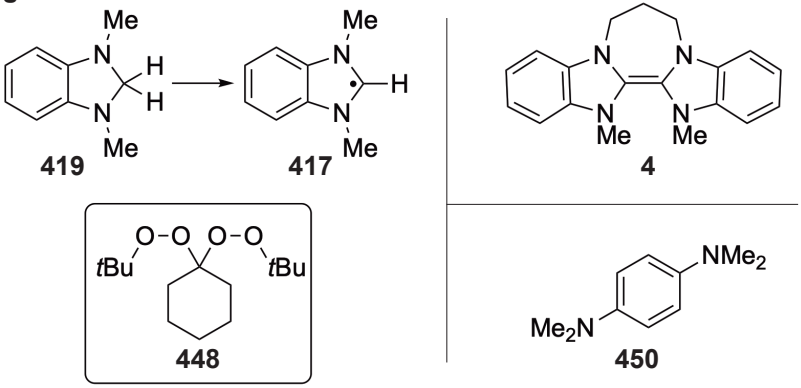

Reference Reactions

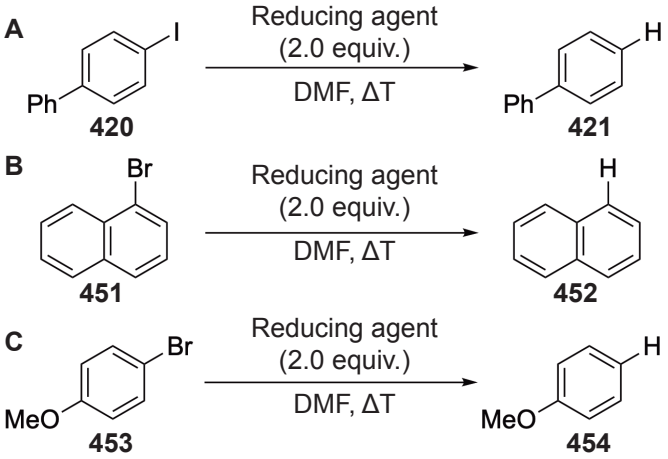

Entry	Reducing Agent	Reaction (substrate)	Initiator	Temp.	Time	Yield of Reduced Product[a]
1	**419**	**A (420)**	air	55 °C	4 h	95 %[b]
2	**419**	**B (451)**	air	55 °C	4 h	80 %
3	**419**	**C (453)**	air	55 °C	4 h	40 %
4	**419**	**B (451)**	**448**	100 °C	20 h	94 % (74 %)[c]
5	**419**	**C (453)**	**448**	100 °C	20 h	42 %
6	**4**	**A (420)**	none	100 °C	20 h	66 %
7	**4**	**B (451)**	none	100 °C	20 h	< 1 %
8	**4**	**C (453)**	none	100 °C	20 h	4 %
9	**450**	**A (420)**	air	55 °C	4 h	not detected

[a] The yield was determined by GC-FID vs. 1,3,5-trimethoxybenezene as internal standard unless mentioned otherwise.

[b] This entry is copied from Table 2-1 Entry 19. The yield was determined by HPLC vs. 1-phenylpyrrolidin-2-one as internal standard.

[c] Isolated yield is given in brackets.

into higher reactivity. Only comparing the redox potential as measured by cyclic voltammetry of the two electron donors neglects the fact that their abundance in the actual reduction reaction is quite different. Namely, electron donor **4** is present in stoichiometric amounts while electron donor **417** is formed only in traces at any time. According to the Nernst equation[215] the electrochemical driving force of a reducing agent depends on its standard potential as well as on the ratio of the activity of the reduced species and the oxidised species of the redox couple. Hence, it is not a priori clear whether the protocol with **417** will be more reducing than an analogous protocol with **4**.

To better understand the effective reduction potential of **417** and to compare it to **4**, a series of benchmarking reactions was performed (Table 2-4). Judged from electrochemical studies, the reduction of the aryl iodide **420** is the easiest reaction in the series.[216] The reduction of the two aryl bromide substrates **451** and **453** becomes increasingly difficult.[217] As has been seen at the very beginning of this section, the electron donor **417** derived from aminal **419** is competent in reducing the aryl iodide substrate in almost quantitative yield (Table 2-4 Entry 1, copied from Table 2-1 Entry 19). It was also possible to reduce the aryl bromide substrate **451** in good yield (Entry 2). The more challenging-to-reduce electron-rich 4-bromoaniosle substrate **453** was still reduced in respectable yield of 40 % (Entry 3). Only a slight increase in yield of the reduced products was observed when the aryl bromide substrates **451** and **453** were reacted with **419** at higher temperature, for a longer time and with the peroxide initiator **448** (Entries 4 and 5).

When the three reactions were repeated with the electron donor **4** only the aryl iodide substrate was reduced (Entry 6), albeit in lower yield than the previously achieved yield with **419** (Entry 1). The two aryl bromide substrates only gave trace amounts of reduced product when treated with electron donor **4** (Entries 7 and 8). Clearly, the newly introduced reduction protocol based on aminal **419** is more powerful than the protocol based on the structurally related and previously established[6] electron donor **4**.

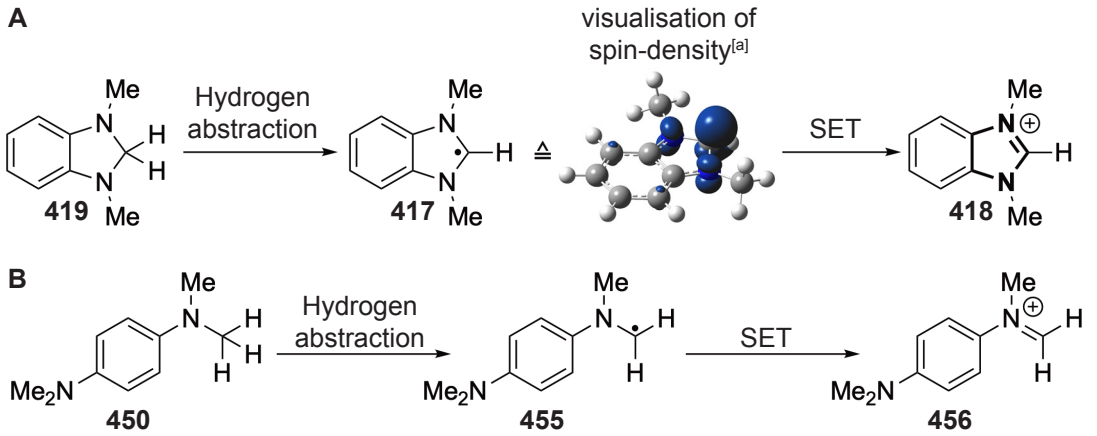

Scheme 2-8 A) The aminal **419** can give rise to **417** with a radical centre that is in the α-position to two nitrogen atoms. Upon single electron transfer (SET) the oxidised product **418** gained aromaticity compared to **417**. B) The diamine potentially can give rise to radical **455** which is, however, not as privileged as is **417**. [a] Level of theory: UM06-2X/6-311++G(d,p)/cpcm(DMF).

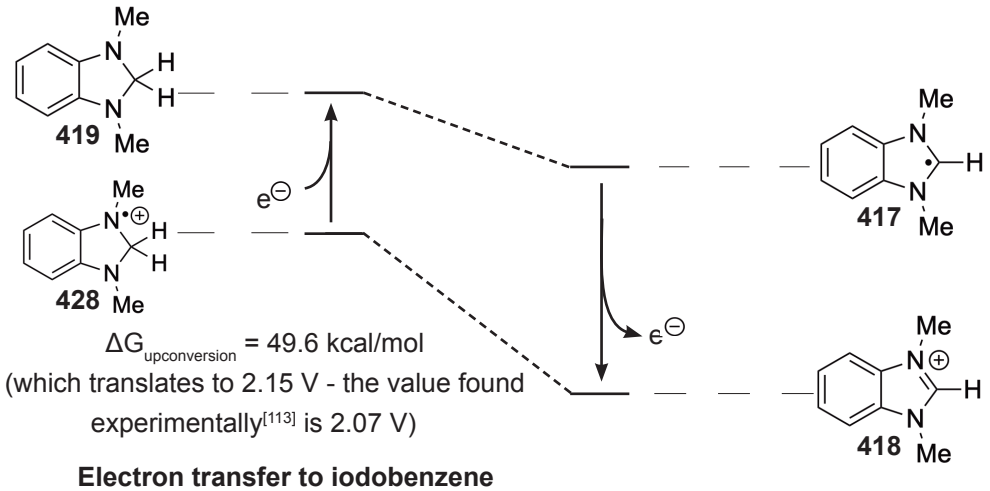

Electron transfer to iodobenzene

Reducing agent	ΔG* (kcal/mol)[a]	ΔG (kcal/mol)
419	41.0	37.4
417	12.4	-12.2

Figure 2-7 Remarkable upconversion of reducing power is achieved when going from the aminal **419** to the open-shell species **417**. This upconversion of reducing power manifests in the fact that **417** is able to reduce iodobenzene while **419** clearly is not. Level of theory: UM06-2X/6-311++G(d,p)/cpcm(DMF). [a] Calculated by Nelsen's four-point method[209] based on Marcus theory.[61,210]

Finally, experimental support was sought to substantiate the hypothesis that **419** does not act as an electron donor in its own right in these reactions. To do so, the electronically similar diamine **450** was selected to contrast the reactivity of **419**. It was found that **450** was incapable of reducing the easiest-to-reduce substrate **420** in the series (Entry 9). This implies first that the aryl diamine **419** is unlikely to act as a single electron donor towards this substrate directly. It is only by turning into the open-shell species **417** that the molecule becomes highly reducing (Scheme 2-8 A). The radical **417** is electron-rich as the unpaired spin is neighboured by two nitrogen atoms. Upon single electron transfer, the oxidised product **418** gains aromaticity with respect to **417**. Second, the experiment indicates that even if an analogous hypothetical reaction pathway for the diamine **450** occurred, it would not lead to a comparably privileged, electron-rich radical species that would gain aromaticity upon oxidation (Scheme 2-8 B). The radical **455** is only neighboured by one nitrogen atom and the oxidation product **456** did not gain aromaticity with respect to **455**.

One can also look at the difference between the aminal **419** and the open-shell species **417** from the perspective of upconversion of reducing power (see Chapter 1.4). Applying the scheme presented in Figure 1-14 to this system (Figure 2-7) indicates that the achieved upconversion is $\Delta G_{upconversion}$ = 49.6 kcal/mol. This value is derived from computations. It translates to a difference between the redox potential of **419** and **417** of 2.15 V. This figure is in good agreement with the experimentally found difference in redox potentials of 2.07 V.[113] This massive increase in reducing power manifests in the fact that **417** shows favourable kinetics and thermodynamics for the single electron transfer to iodobenzene, while **419** clearly does not (Figure 2-7).

In light of the results presented in Table 2-4, it was somewhat surprising to find that with

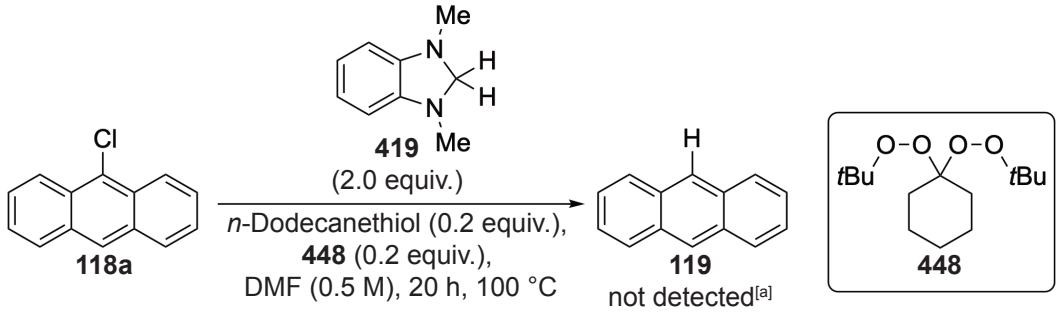

Scheme 2-9 The aryl chloride substrate **118a** could not be reduced with **419**. [a] The reaction was analysed by ^{1}H-NMR spectroscopy. No product was detected. The yield of remaining starting material was quantitative as determined by ^{1}H-NMR spectroscopy vs. 1,3,5-trimethoxybenzene as internal standard.

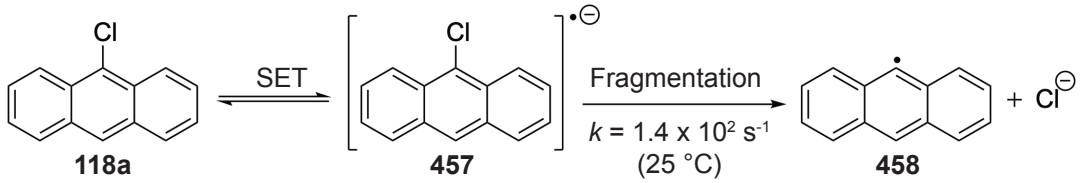

Scheme 2-10 The radical anion **457** is long-lived with respect to fragmentation. This may allow for re-oxidation pathways to outrun the irreversible fragmentation towards **458**.

419, it was not possible to reduce 9-chloroanthracene **118a** - a substrate that was previously reported to be reduced quantitatively by the electron donor **4** in the same solvent, at the same temperature and with a slightly shorter reaction time (see Chapter 1.2.4).[81] Electrochemical studies indicate that **118a** is easier to reduce[218] than the aryl bromide substrates from Table 2-4 (estimated based on the reduction peak potential).[217] A distinguishing feature of **118a** is that it can give rise to a relatively long-lived radical anion species **457** with respect to fragmentation to the aryl radical **458** and a chloride anion (the first order rate-constant for the fragmentation of **457** is $k = 1.4 \times 10^2$ s^{-1} at 25 °C, Scheme 2-10).[218] Hence, it appears possible that the radical anion **457** is re-oxidised more quickly back to the neutral starting material **118a** (e.g. by the radical initiator) than it can fragment forward to **458**.

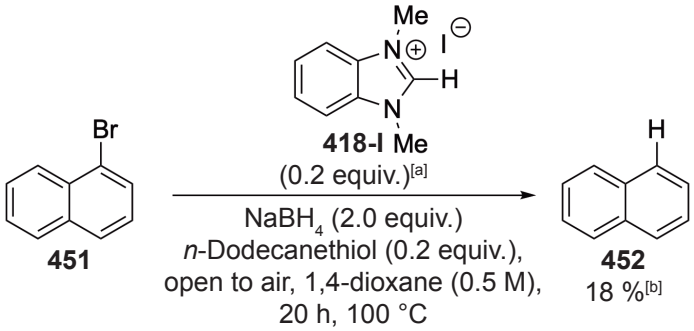

Scheme 2-11 The reduction of **451** can also be achieved according to a modified catalytic protocol. [a] In a blank reaction without **418-I**, no **452** was detected by ^{1}H-NMR. [b] Isolated as an inseparable mixture with 71 % of remaining starting material **451**.

It becomes apparent that the low abundance of **417** and the requirement for (oxidative) initiation comes along with some restrictions. The reduction reaction with **419** depends on an efficient, irreversible fragmentation of a bond to drive the reaction forward. If this prerequisite is fulfilled, the challenging-to-reduce substrates that did not react when treated with the parent electron donor **4** can be reduced now.

The reduction of aryl bromide **451** was attempted under catalytic conditions (Scheme 2-11). For this reaction, 1,4-dioxane was chosen as the solvent instead of DMF. There is a risk of a violent runaway reaction with high concentrations of sodium borohydrides in DMF at elevated temperatures.[219] Treating **451** with sodium borohydride and the catalyst **418-I** at 100 °C for 20 h only gave a low yield of the reduced product naphthalene **452**. In fact, no catalytic turnover was achieved. In a blank reaction without the organocatalyst **418-I** no reduced product **452** was detected. This result indicates that with the catalytic conditions, a radical chain reaction can no longer be sustained with substrates than are more difficult to reduce than aryl iodide.

2.4. Expanding the Scope of SET Precursors and Catalysts

The proposed principle of how to use an organic super electron donor in a catalytic sense has been demonstrated, based on the dihydrobenzimidazole / benzimidazolium catalytic cycle. Potentially, this concept can be extended to other scaffolds that function in the same way as an organocatalyst. Of particular interest was to investigate the possibility to use imidazole and dihydropyridine scaffolds as catalysts. The corresponding open-shell species **60** (Scheme 2-12) and **465** (Table 2-6) are expected to be even more reducing than **417**. The required dihydro precursors **220** (Scheme 2-12) and **464** (Table 2-6), however, are no longer readily accessible due to their high reactivity. Therefore accessing these species as intermediates in a catalytic cycle appeared to be a promising approach to utilise the high reducing power of the derived single electron donors. This section details the investigations that have been made

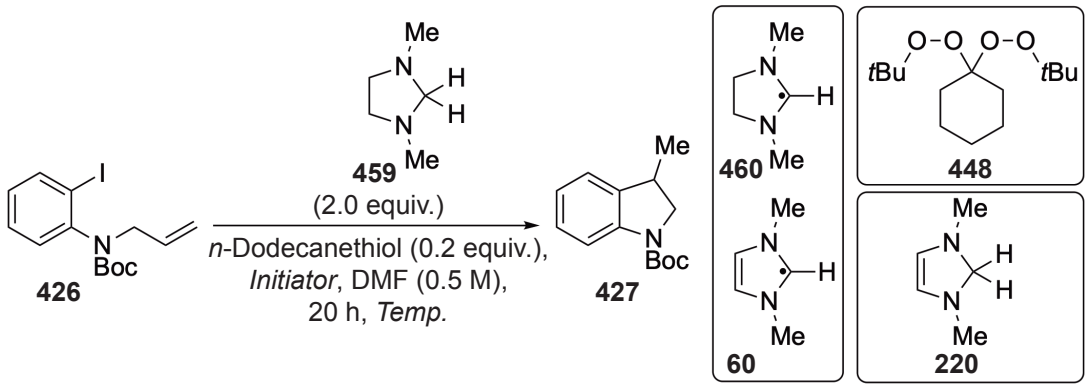

Entry	Initiator	Temp	Yield of 427[a]	Remaining 426[a]
1	Oxygen in the air	55 °C	12 %	72 %
2	**448**	100 °C	93 % (94 %)[b]	not detected

Scheme 2-12 The simple aminal **459** is an effective reducing agent for the radical cyclisation of **426**. [a] Yields were determined by ^{1}H-NMR vs. 1,3,5-trimethoxybenezene as an internal standard. [b] Isolated yield.

towards this end.

Initially it was attempted to synthesise the dihydroimidazole **220**. It was possible to form the compound in solution but it turned out to be difficult to isolate the material in neat form due to its high air and moisture sensitivity.[220-222] Thus, it became quickly clear that this material is very unlikely to ever find application as an easy-to-handle reducing agent. As an alternative, the fully saturated analogue **459** was investigated. This compound is bench-stable and can conveniently be handled open to air. Compound **459** was used as a stoichiometric reducing agent in the previously employed model radical cyclisation reaction of substrate **426** (Scheme 2-12). When the reaction was performed at 55 °C and open to air, only a small yield of cyclised product **427** was formed while the major part of starting material **426** remained unreacted (Entry 1). Repeating the experiment at 100 °C, with the initiator **448** instead of oxygen, led to a massive improvement of the yield (Entry 2).

A very similar aminal has previously been used by Denk et al. for the dehalogenation of various aryl halide substrates.[111,112,110] However, evidence for the nature of the mechanism (i. e. a hydride transfer vs. hydrogen abstraction and single electron transfer) was not given. The experiment in Scheme 2-12 unequivocally demonstrates the radical nature of the reduction process. The experiment also shows that a potent single electron donor species can be derived from a simple aminal function. But clearly, the electron donor **460** derived from **459** is less potent than **417**. The reason for the lower reactivity lies in the absence of aromatic driving

Table 2-5 Attempts to reduce 1-bromonaphthalene 451 with the imidazolium iodide catalyst 461.

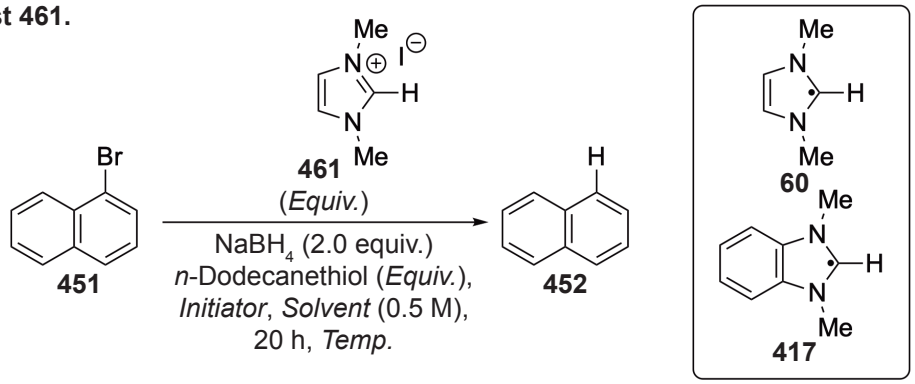

Entry	Solvent	Temp.	461 (equiv.)	PRC (equiv.)	Initiator	Yield of 452[a]
1	DMF	55 °C	0.2	0.2	air	11 %
2	1,4-Dioxane	100 °C	0.2	0.2	**448**	7 %
3	1,4-Dioxane	100 °C	0.2	0.2	air	25 %
4	1,4-Dioxane	75 °C	0.2	0.2	air	19 %
5	1,4-Dioxane	55 °C	0.2	0.2	air	21 %
6	1,4-Dioxane	55 °C	1.0	0.2	air	20 %
7	1,4-Dioxane	55 °C	1.0	1.0	air	30 %
8[b]	1,4-Dioxane	55 °C	none	0.2	air	< 1 %

[a] Yields were determined by GC-FID vs. 1,3,5-trimethoxybenzene as internal standard.
[b] Blank reaction without **461**.

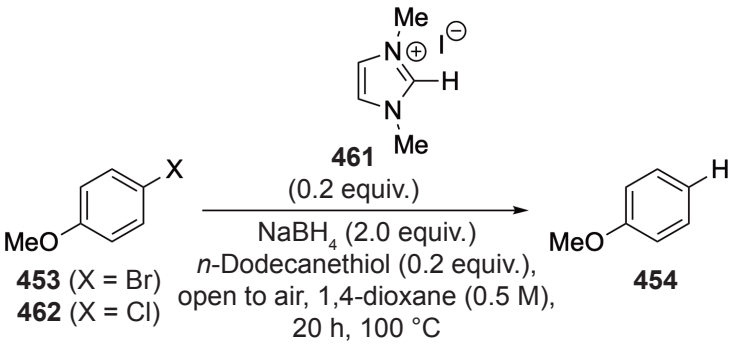

		Yield of 454[a]
453	X = Br	30 %
462	X = Cl	< 1 %

Scheme 2-13 Challenging the catalyst **461** with two aryl halide substrates that are difficult to reduce. [a] Yields were determined by GC-FID vs. 1,3,5-trimethoxybenzene as internal standard.

force for the oxidation of **460**. Previously, this aromatic driving force was found to be an important factor in the reducing strength of organic super electron donors (see Chapter 1.1.8).

Isolation of **220** is challenging and the use of a saturated analogue goes at the expense of reducing power. But isolation of **220** may not be necessary if it was possible to form it in situ analogous to what has been achieved with the catalytic protocol and the benzimidazolium salt **418-I**. Since **60** is expected to be the stronger single electron donor than **417**, the relatively challenging-to-reduce aryl bromide substrate **451** was selected for the initial exploration of the catalyst **461** (Table 2-5). The reduced product **417** was formed only in low yield in DMF as the solvent at 55 °C (Entry 1). By switching to 1,4-dioxane as the solvent it became possible to run the reaction at higher temperatures (as mentioned before, high concentrations of $NaBH_4$ in DMF at elevated temperatures are potentially hazardous).[219] Performing the reaction at 100 °C with the peroxide radical initiator **448** let to no improvement of the yield (Entry 2). Actually, the yield was slightly lower than in the previous reaction. However, when using oxygen in the air as the initiator, a substantial increase in yield of the reduced product **452** to 25 % was observed (Entry 3). It was found possible to decrease the temperature to 75 °C or 55 °C without a significant decrease in yield (Entries 4 and 5). It was noticed that the yield of reduced product was never significantly higher than 20 % - i.e. the yield approximately equalled the amount of 'catalyst'. Therefore, the effect on the reaction of using stoichiometric loading of **461** was investigated. However, no increase in yield of **452** was observed with 1.0 equiv. of the imidazolium salt **461** (Entry 6). Increasing at the same time also the amount of *n*-dodecanethiol from 0.2 equiv. to 1.0 equiv led to a slight increase in yield from 20 % (Entry 6) to 30 % (Entry 7). Finally, a blank reaction was performed in the absence of the organocatalyst **461**. Only trace amounts of product were detected in this experiment (Entry 8).

It can be seen that, in principle, reduction of aryl bromide **451** with sodium borohydride mediated by the imidazolium salt **461** is possible. However, no significant catalytic turnover was achieved. Therefore this heterocycle does probably not act as a catalyst is this reaction. There are several possible reasons why the reaction does not perform well. First, the dihydroimidazole **220** is prone to decomposition,[220-222] which may quickly lead to removal of the

Table 2-6 Attempts to use the pyridinium salt 463 as an organocatalyst.

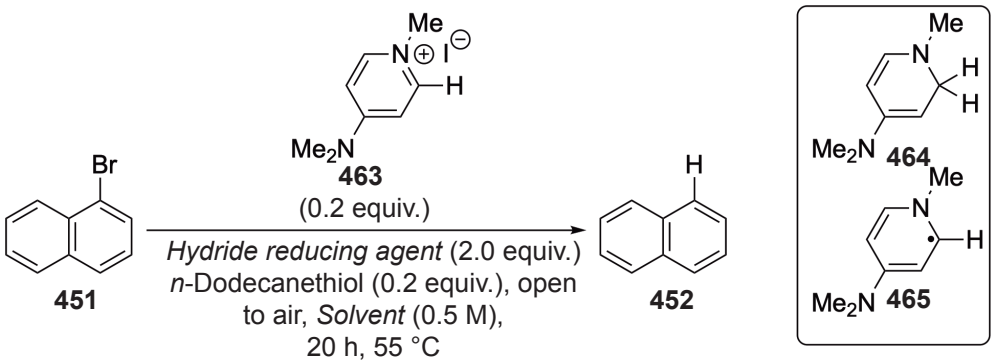

Entry	Solvent	Hydride reducing agent	Yield of 452[a]
1	DMF	$NaBH_4$	2 %
2	1,4-Dioxane	$LiAlH_4$	63 %
3[b]	1,4-Dioxane	$LiAlH_4$	29 %

[a] Yields were determined by GC-FID vs. 1,3,5-trimethoxybenzene as internal standard.
[b] Blank reaction without catalyst **463**.

organocatalyst from the reaction mixture. Second, the hydride transfer from sodium borohydride to **461** may be too slow. Therefore the amount of **220** in the reaction mixture may not be sufficient to sustain the radical chain process.

Finally, it was attempted to use the pyridinium salt **463** as an organocatalyst (Table 2-6). Upon reduction with an appropriate hydride reducing agent, the dihydropyridine **464** would be formed, which in turn would serve as a precursor of the single electron donor **465**. An initial attempt with sodium borohydride as the hydride source gave only trace amounts of the reduced product **452** (Entry 1). By using the much stronger hydride reducing agent, lithium aluminium hydride, the reduced product was formed in good yield (Entry 2). However, when a blank reaction was performed without the organocatalyst **463** still significant amounts of naphthalene **452** were formed (Entry 3). This indicates that the strong hydridic reducing agent needed to generate the dihydropyridine **464** can reduce the aryl bromide substrate on its own to a significant extent. The ca. 30 % difference in yield between Entry 2 and Entry 3 indicate that no significant catalyst turnover is achieved in the reaction with **463**. This may be for the same reasons as given before for the reactions with the imidazolium salt **461**.

2.5. Summary and Conclusion

The dihydrobenzimidazole **419** has been established as a useful reducing agent for reductive radical cyclisation reactions of aryl iodide substrates. The reaction conditions are mild and the reaction convenient to set up as dry conditions or inert atmosphere are not required. In fact, if the reaction is left open to air, no additional radical initiator is required. Oxygen in the air is proposed to start the radical chain reaction and a plausible mechanism has been established, based on computational studies. The conditions were further developed such that **419** was generated in situ from a catalytic amount of the benzimidazolium salt **418-I**. For

these catalytic conditions, sodium borohydride was identified as a suitable terminal and hydridic reducing agent. From this hydridic reagent, a single electron donor is generated through the action of the organocatalyst **418-I** (see also Scheme 2-1). The reactivity of stoichiometric amounts of aminal **419** was directly compared with the reactions where **418-I** was used as a catalyst over a range of substrates. It was found that both protocols perform well. But the catalytic protocol gives slightly lower yields and has a stronger tendency to form by-products.

It is difficult to quantify the upconversion of reducing power (see Chapter 1.4) that is achieved when going from sodium borohydride to the single electron donor **417** due to the difficulty of determining a reliable redox potential for sodium borohydride.[223,224] The effect of upconversion of reducing power is evident from the observed reactivity, though. High yielding reduction reactions were achieved in the presence of the organocatalyst, but not in its absence. These experiments underline that **417** is a potent single electron reducing agent and, indeed, much more potent than the corresponding, dimeric electron donor **4**. The low abundance of the reducing species **417**, however, requires the electron transfer itself either to be strongly exergonic or then to be followed by a fast and irreversible reaction. This condition is fulfilled for aryl iodide substrates. The catalytic protocol is limited in its applicability towards the reduction of aryl bromides. A possible reason is that no efficient chain reaction can be established.

Finally, first investigations were made to expand the chemistry investigated with **419** and **418-I** on other nitrogen heterocycles. It was found that the simple and fully saturated aminal **459** was able to act as an efficient reducing agent towards an aryl iodide substrate at elevated temperatures. Attempts to use imidazolium salt **461** and pyridinium salt **463** as catalysts were only partially successful as no significant conversion could be achieved. The reason for the absence of turnover with these compounds may root in their high reactivity, which leads to rapid decomposition of the catalyst. Alternatively, hydride delivery to the cationic form may be inefficient, such that the corresponding dihydro species is not sufficiently abundant to sustain the radical chain reaction.

2.6. Outlook

From the results presented in this chapter several possible future lines of investigation arise. One obvious focus of research is the identification of other simple heterocycles that can act as catalysts in the way of **418-I**. The main goal of such a study would be to better understand what characteristics of a heterocycle make it a good organocatalyst for the upconversion of a hydride reagent's reducing power. The ambition would be to find a catalyst that works with an even milder hydridic reducing agent than **418-I** and still gives rise to a potent single electron donor. It is apparent that two properties of the heterocycle need to be balanced. On the one hand, the cationic form needs to be efficiently reduced by the hydride reagent, i.e. it needs to be sufficiently electrophilic (i.e. electron-deficient). On the other hand, the corresponding radical (analogous to **417**) needs to be a strong electron donor and therefore electron-rich. To level these conflicting requirements on the catalyst one may play with σ-electron-withdrawing substituents (to favour hydride delivery to the cationic form of the catalyst) and π-electron-donating substituents (to enhance the reduction potential of the derived open-shell electron donor). Such substituents may be used to decorate, for example, the benzimidazole scaffold.

Also exploring scaffolds beyond the benzimidazole, imidazole and pyridine cores may be interesting and rewarding. As has been demonstrated in this chapter, simple aminals are potential precursors of single electron donors. These may also turn out to be effective catalysts

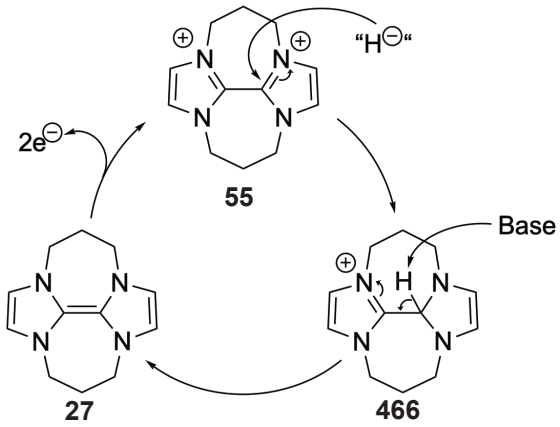

Scheme 2-14 A possible scheme to use the previously established dimeric super electron donors in a catalytic sense.

in the sense of **418-I**. The number of potentially interesting structures is huge. Due to the simplicity of the chemistry, it seems straightforward to develop a computational model to predict the suitability of a given structure to act as a catalyst. This would enable an efficient first screen of several compounds and potentially allow guidelines to be established for the further elaboration of promising candidates.

One may also move in a slightly different direction and investigate the possibility to make the previously established dimeric electron donors catalytic. In addition to a hydride reducing agent, such a catalytic cycle would also require a base (Scheme 2-14). The dication **55** may be reduced by a suitable hydride agent to the intermediate **466**. Deprotonation by a base then gives the electron donor **27**, which, upon double electron oxidation, returns to the initial dication **55**.

3. The KO*t*Bu-Et_3SiH Reagent System

3.1. Background

The combination of silanes and potassium *tert*-butoxide allows for various different transformations. Accordingly, several mechanistic pathways have been proposed to account for the different reactions. Especially from the relevant publications by Grubbs, Stoltz et al.[133-138,143,144] and Jeon et al.[145] a number of key species emerge (Figure 3-1, see also Chapter 1.5). Broadly speaking, the experiments suggest ionic and radical reaction pathways to be accessible. Ionic mechanisms depend on the formation of a hydride species. For example, complexation of potassium *tert*-butoxide to triethylsilane leads to **280**.[144] This species then is in equilibrium with potassium hydride **467** and the silyl ether **296**. In their computational studies, Grubbs et al. either represented the hydride equivalent as a naked hydride anion or as a potassium hydride - potassium *tert*-butoxide composite (see also Scheme 1-58).[144] An obvious middle way in the representation of the hydride equivalent is as potassium hydride **467**.

The proposed radical pathways in the KO*t*Bu-Et_3SiH system hinge on the presence of the silyl radical **277**. This species has been proposed to be involved in various pathways, some of which lead to the radical anion **281**.[143] Finally, and as mainly advocated by Jeon et al.,[145] hydrogen atom transfer (HAT) steps may be key in the reaction of certain substrates with the KO*t*Bu-Et_3SiH system. The hydrogen atom **468** may serve as a model for HAT processes.

From the species presented in Figure 3-1, the radical anion **281** stands out as a potentially very powerful single electron donor. As remarkable as it looks on paper, this species has been considered as a by-product only in previous discussions. It follows that the reagent system may show three aspects of reactivity: 1) single electron transfer chemistry, 2) radical addition reaction (i.e. hydrogen atom transfer or silyl radical chemistry) and 3) hydride reactions (i.e. deprotonation or hydride reduction steps). The formidable challenge is to probe these three domains of reactivity separately with suitable substrates. This will help to deepen the understanding of the intriguing chemistry accessible to the KO*t*Bu-Et_3SiH reagent system. The prime goal of this work was to probe for single electron transfer chemistry and hydride-mediated pathways.

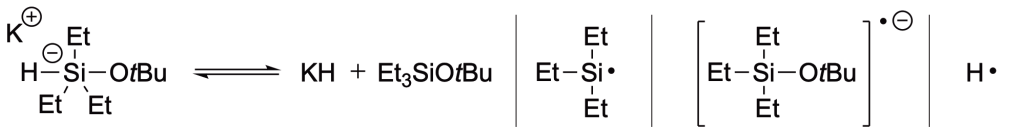

Figure 3-1 Proposed key species that are responsible for the reactivity of the KO*t*Bu-Et_3SiH reagent system.

3.2. Electron-Transfer and Hydride-Transfer Pathways in the KO*t*Bu-Et_3SiH Reagent System

3.2.1 Reductive Cleavage of Aryl Ethers

(A detailed description of the following experiments can be found in Chapter 5.4.2).

Aryl ethers were the first substrate class to which Grubbs et al. applied the KO*t*Bu-Et_3SiH reagent system.[133] The reductive cleavage of aryl ethers via single electron transfer reduction with alkali metals is well documented.[225-229] This short literature survey clearly showed that single electron transfer chemistry would be consistent with Grubbs' initially published results on the aryl ether cleavage with the KO*t*Bu-Et_3SiH reagent system. In order to explore this aspect of the reagent system in more detail, a series of aryl ethers was synthesised and exposed to the reagent system.

Initially, it was found that the reaction temperature can be lowered to 130 °C (compared to 165 °C as used by Grubbs et al.[133]) if the reaction is performed under neat conditions.[230] These conditions were then applied to simple benzylic aryl ethers (Scheme 3-1). Both substrates **469** and **472** were consumed to a high degree, but only small amounts of identifiable products were formed. The low boiling point of these products as well as the complex nature of the reaction mixture made it impossible to isolate them. It was reasoned that the large number of benzylic hydrogen atoms in the substrates **469** and **472** may make them susceptible to side-reactions. Hence, in the further design of probe substrates, such positions were avoided. Also, in order to promote the proposed single electron transfer processes, a larger aromatic system was chosen, which would be easier to reduce.

An interesting class of substrates was identified in the naphthyl ether compounds **474**, **479** and **482** (Scheme 3-2). When subjected to the Et_3SiH-KO*t*Bu reagent system, the expected

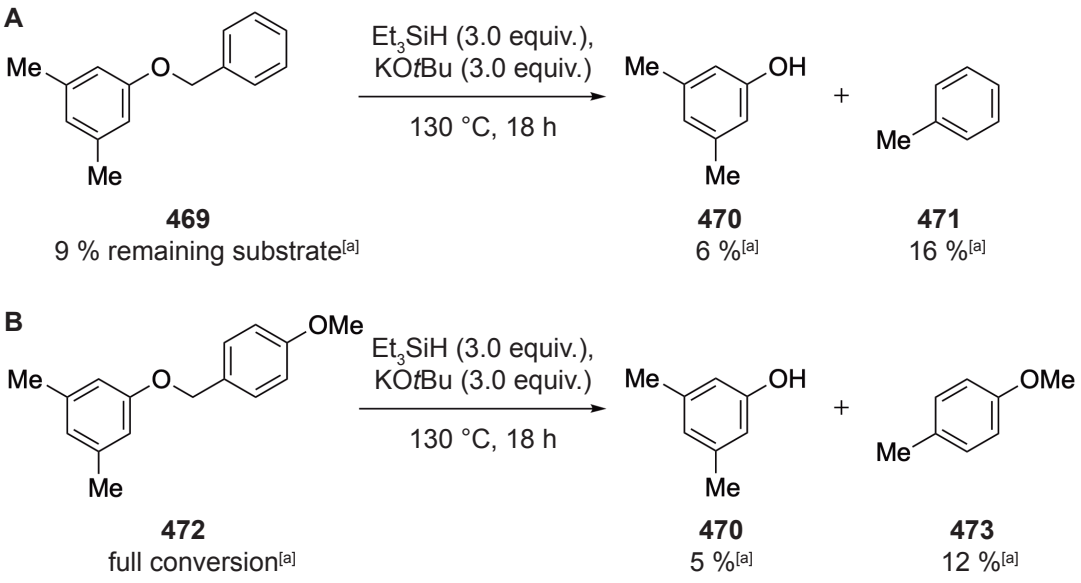

Scheme 3-1 Initial model compounds to investigate the aryl ether cleavage gave low yields of reduced products only. [a] Yield was determined by ^{1}H-NMR vs. 1,3,5-trimethoxybenzene as internal standard.

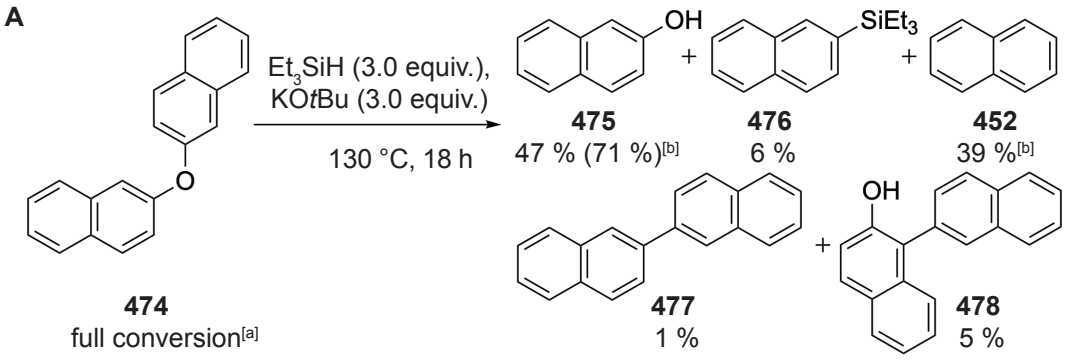

Blank (no Et_3SiH): quant. recovery of **474**

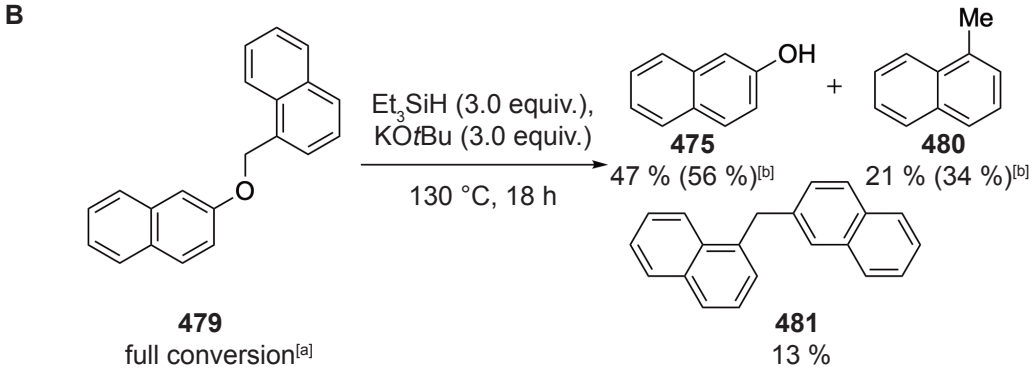

Blank (no Et_3SiH): quant. recovery of **479**
Blank (no KO*t*Bu): 93 % recovery of **479**

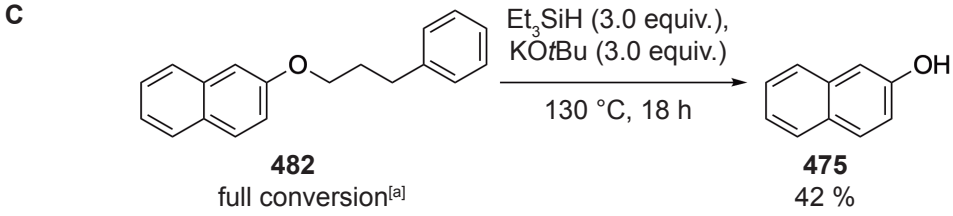

Blank (no Et_3SiH): quant. recovery of **482**

Scheme 3-2 Besides the expected naphthol product, a number of intriguing rearranged products were isolated from the reactions of naphthyl ethers **474**, **479** and **482** with the Et_3SiH-KO*t*Bu reagent system. [a] No remaining substrate was detected by ^{1}H-NMR. [b] Yield was determined by ^{1}H-NMR vs. 1,3,5-trimethoxybenzene as internal standard.

2-naphthol product **475** was formed in approximately equal yield from all of the three substrates. Moreover, a number of products were isolated - albeit in low yields - that suggest the presence of 2-naphthyl radicals. For example, it is difficult to think of a mechanism to account for the formation of **477** and **478** that does not involve a 2-naphthyl radical. Indeed, it appears very likely that a 2-naphthyl radical adds onto naphthalene **452** or 2-naphthol **475**, which upon oxidation (e.g. during work-up and isolation), gives the products **477** and **478**, respectively. The formation of a 2-naphthyl radical, in turn, is a tell-tale sign of a single electron transfer

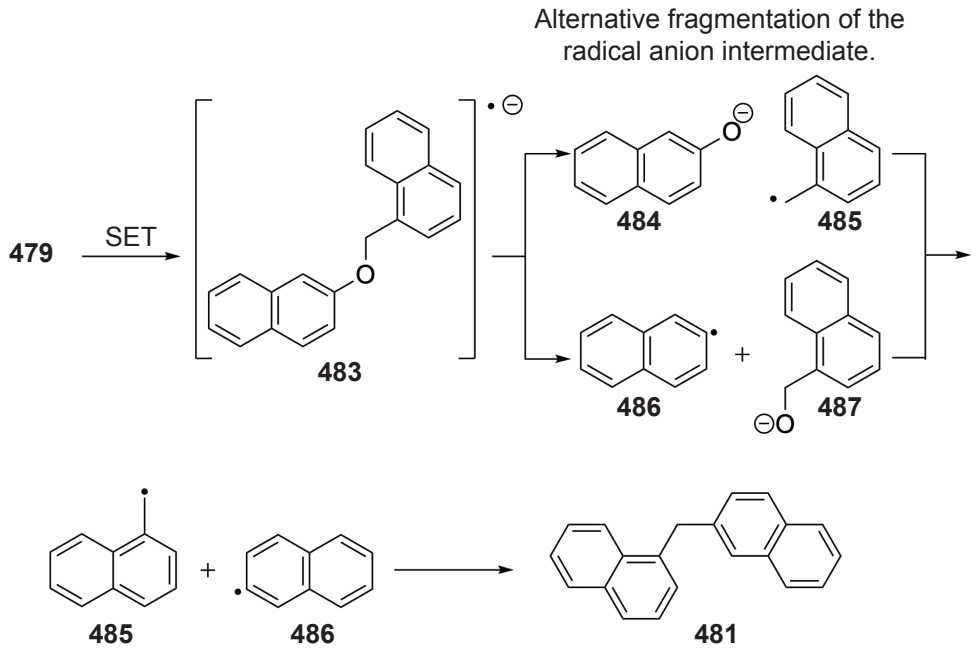

Scheme 3-3 A proposed mechanism for the formation of **481** involves the recombination of the highly reactive aryl radical **486** with the more stable benzylic radical **485**.

reduction of the substrate. Similarly, the product **481** likely forms via radical intermediates (Scheme 3-3). The regioselectivity in the fragmentation of aryl ether radical anions can be quite poor.[229] Thus, both radical species **485** and **486** may be formed. Compared to the aryl radical **486**, the benzylic radical is relatively stable. Although **485** is far from being a persistent radical, its abundance relative to **486** may increase in the reaction mixture such that the recombination between **485** and **486** becomes efficient (akin to the persistent radical effect).[89,90]

The aryl ether series was further expanded to the menthol-derivatives **488**, **489** and **493** (Scheme 3-4). The 2-naphthol ether **488** was completely consumed after 18 h of reaction time and the 2-naphthol product was isolated in 66 %. No product derived from the aliphatic part of the substrate could be isolated. In sharp contrast, the phenol ether **489** only reached 50 % conversion based on recovered substrate after 18 h. Also the regioselectivity of the ether cleavage in **489** was different to **488**. From the reaction with the former substrate, the major alcohol product was menthol **491**, while phenol **490** and its silylated derivative **492** were formed in smaller amounts. Finally, the fully aliphatic ether **493** turned out not to be reactive under the applied Et_3SiH-KO*t*Bu conditions and the substrate was recovered quantitatively from the reaction.

Since the stereochemistry in the aliphatic part of **488** and **489** is not identical, it is not possible to directly compare the outcome of the reactivity of these substrates. Nevertheless, it can be noted that the reactivity decreases pronouncedly as the aromatic system gets smaller. This observation is consistent with a single electron transfer as the key step in the cleavage of the carbon-oxygen bond.

The energy profile of the electron transfer and carbon-oxygen bond cleavage was calculated for the model compound **495** (Scheme 3-5). (A detailed description of the following computational results can be found in Chapter 5.4.4). The model **495** was chosen to closely mirror the

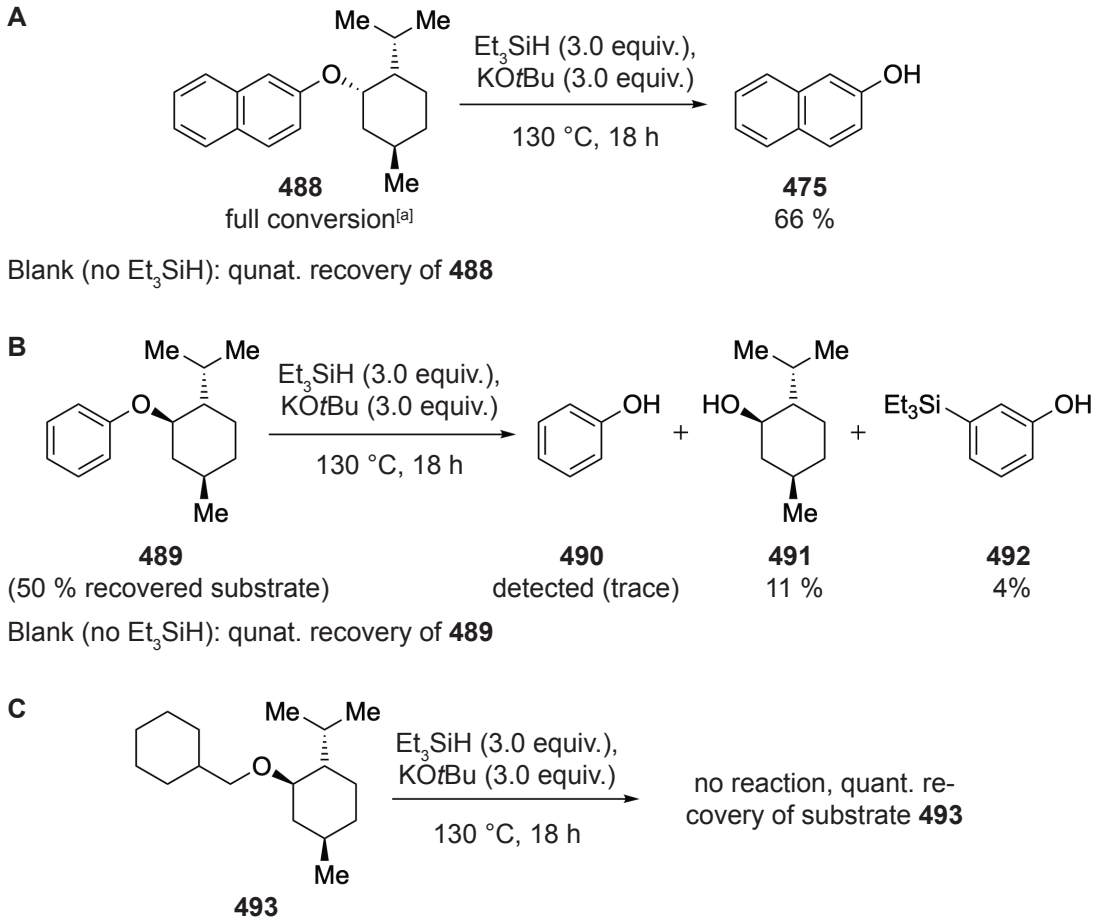

Scheme 3-4 A series of menthol derivatives was subjected to the Et_3SiH-KO*t*Bu system. [a] No remaining substrate was detected by ^1H-NMR.

substrate **488**. Instead of the triethylsilane species **281**, the trimethyl analogue **494** was used in the calculation. The single electron transfer from **494** to **495** was found to be strongly exergonic and to have a very accessible energy of activation. The subsequent fragmentation of the radical anion **496** showed a higher but still readily accessible barrier of 22.5 kcal/mol. Three alternative mechanisms were computationally investigated, too. The displacement of the isopropyl residue on **495** with a silyl radical via the transition state **499** showed an inaccessibly high barrier of 42.4 kcal/mol. An equally high barrier was found for the ether cleavage via the transition state **500**. This pathway was investigated as a model system for possible hydrogen atom transfer reactivity. In light of the inaccessibly high activation energy of transition state **500**, this process can be safely ruled out as part of the reductive cleavage reaction of **495** and analogues. Finally, the attack of potassium hydride on the ether **495** was investigated. This hypothetical reaction pathway also exhibits an insurmountably high activation energy of transition state **501** and can thus be ruled out as a major reaction pathway.

Overall the gathered information strongly suggests that single electron transfer processes are accessible to the KO*t*Bu-Et_3SiH reagent system and play a major role in the reductive cleavage of aryl ether substrates. Computationally, the energy profile for a single electron transfer and subsequent fragmentation of the carbon-oxygen bond was found to be accessible. Other pathways based on previously proposed reactive species that may be accessible to

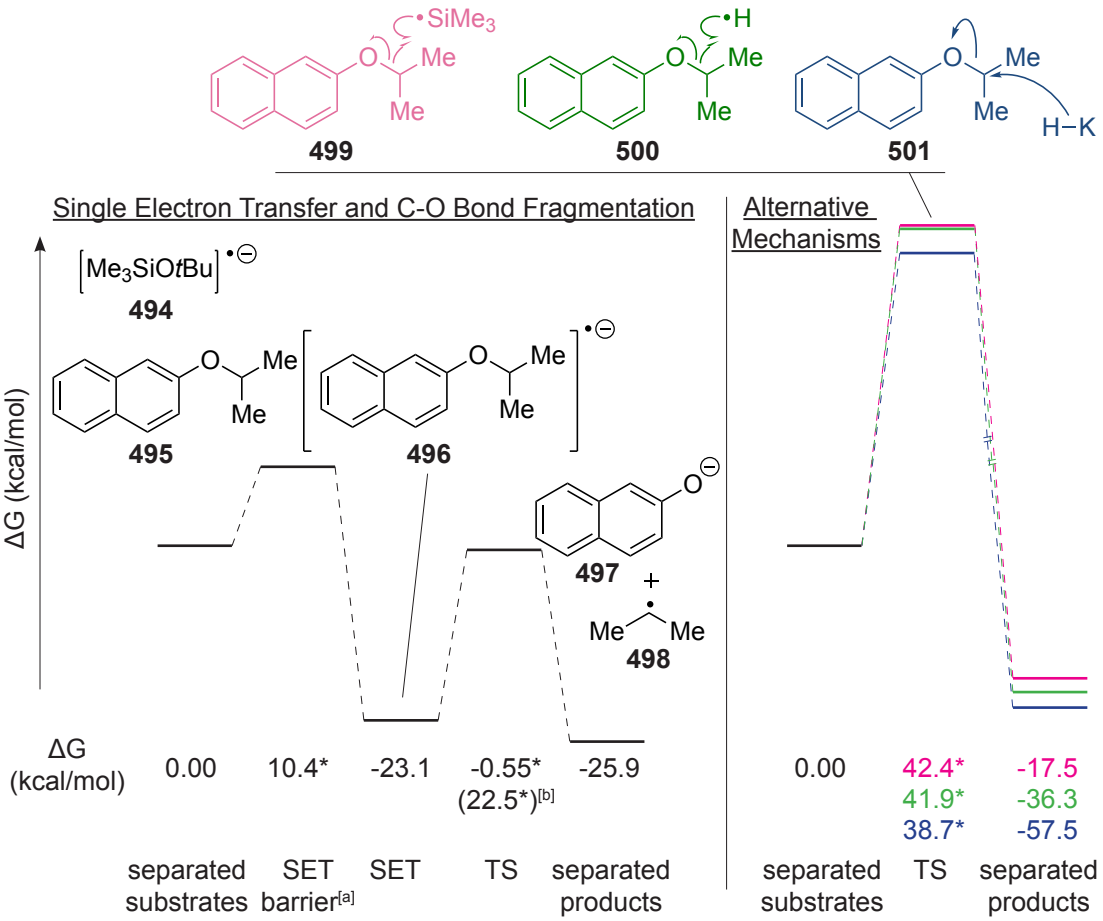

Scheme 3-5 [a] Calculated according to Nelsen's four-point method.[209] [b] Barrier height is relative to the preceding intermediate **496**.

the KO*t*Bu-Et_3SiH reagent system were considered too. These were, however, found to exhibit inaccessibly high energy barriers. These findings are in line with the observations made for the reductive cleavage of carbon-nitrogen bonds in *N*-benzyl indole substrates (experimental work by Andrew J. Smith and computational studies by Allan Young).[231]

3.2.2 Arene Reduction

(A detailed description of the following experiments can be found in Chapter 5.4.5).

In two instances, Grubbs et al. reported the formation of small quantities of hydrogenated naphthalene products derived from naphthyl substrates when treated with the KO*t*Bu-Et_3SiH reagent system (see Chapter 1.5.1).[133,138] This is reminiscent of Birch-type reduction processes and understanding the processes that lead to these by-products may give further insights into the intriguing reactivity of this reagent system. Hence, it was decided to investigate the reduction of aromatic systems with the KO*t*Bu-Et_3SiH reagent system in detail.

The reduction of anthracene **119** was chosen as a starting point (Table 3-1). Since the KO*t*-Bu-Et_3SiH was shown to lead to the silylation of aromatic systems (see Chapter 1.5.1), which has also been observed under the conditions applied here (Scheme 3-2 A and Scheme 3-4

Table 3-1 Reduction of Anthracene with the KO*t*Bu-Et_3SiH Reagent System

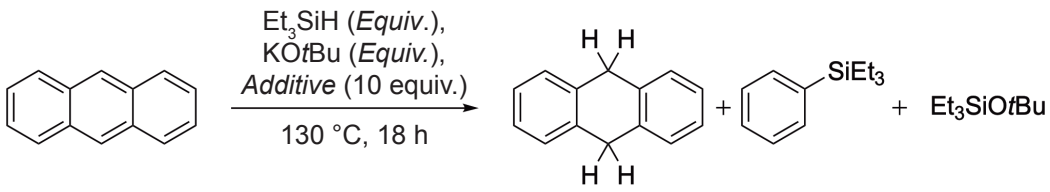

119 **502** **503** **296**

Entry	Additive (10 equiv.)	Equiv. of KO*t*Bu and Et_3SiH	Yield of 502	Yield of 119	By-Product (Yield)
1	Benzene	30	62 %	20 %	**503** (31 %)[a,b]
2	Cyclohexene	30	59 %	21 %	**296** (9 %)[c]
3	Cyclohexane	30	80 %	6 %	**296** (21 %)[c]
4	-	30	85 %	5 %	**296** (22 %)[c]
5	-	3	26 %	61 %	-

[a] The yield of **503** was calculated with respect to the amount of benzene.
[b] *tert*-Butoxytriethylsilane **296** was detected by GC-MS analysis of the crude product.
[c] The yield of **296** was calculated with respect to the amount of Et_3SiH.

B), initially an excess of an additive was added to the reaction (Entry 1 - 3). It was reasoned that the additive would scavenge silyl radicals and thereby make the analysis of the anthracene-derived products easier. In fact, anthracene would be the easiest-to-reduce component in the reaction mixture and therefore mainly engage in reductive processes. The hope was to separate silylation pathways and reduction pathways in this way. A 30-fold excess of KO*t*Bu and Et_3SiH was used with respect to anthracene, which equates to a 3-fold excess with respect to the additive. With benzene as the additive, the reduced product 9,10-dihydroanthracene **502** was obtained in good yield and remaining anthracene **119** was recovered (Entry 1). As expected, silylated benzene **503** was also formed and isolated in 31 % yield (calculated with respect to the initial amount of benzene). The result with cyclohexene as the additive was very similar (Entry 2). The only difference was that no by-product derived from the cyclohexene additive could be isolated. To investigate the effect of the additive, the reaction was performed with cyclohexane as a less interfering additive (Entry 3) and without an additive at all (Entry 4). Somewhat surprisingly, the yield of product **502** increased by ca. 20 % in these two reactions (with respect to Entries 1 and 2). No silylated anthracene derivatives could be identified in either reaction and only small quantities of remaining substrate were recovered. Clearly, an additive is not required to protect the anthracene substrate from side-reactions.

Finally, it was attempted to perform the reaction with three equivalents of KO*t*Bu and Et_3SiH with respect to anthracene (Entry 5). However, only a small quantity of 9,10-dihydroanthracene **502** was isolated and most of the substrate **119** was recovered from this reaction. This shows that a large excess of the KO*t*Bu-Et_3SiH reagents is required to drive this reduction reaction forward. The reason may be that the negatively charged intermediate anthracene species are in equilibrium with the silyl-derived reducing agent. There is no obvious way in which the negative charge that builds up on the anthracene core during the reaction could be

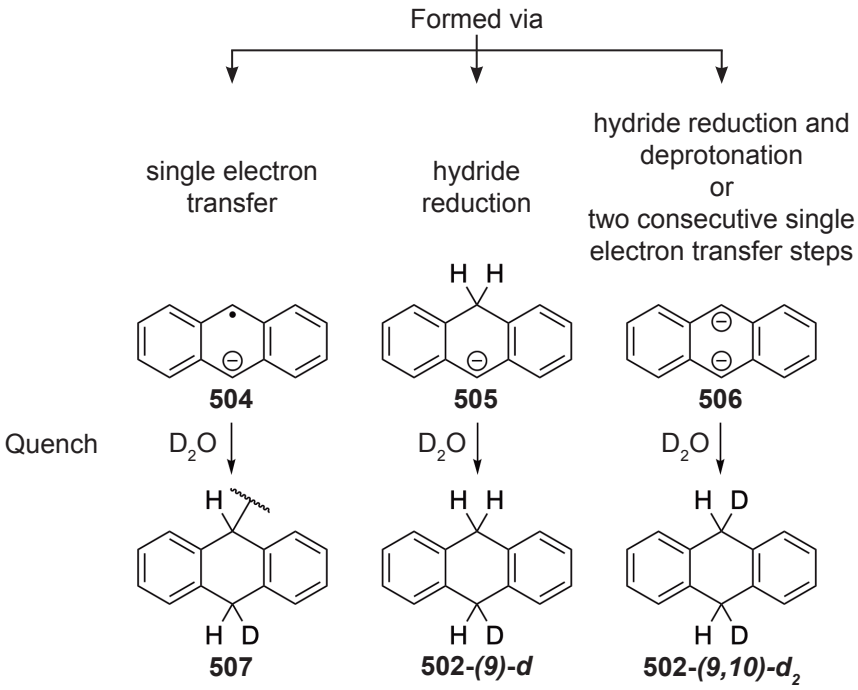

Figure 3-2 Possible anionic intermediates in the reduction of anthracene and expected deutero-derivatives arising from quenching the reaction with deuterium oxide.

stabilised. Protonation likely occurs only during the work-up.

Knowing the nature of the negatively charged anthracene intermediates could give valuable information about the reduction process. In Figure 3-2, anionic anthracene species are shown that are potentially formed in the reaction of anthracene with KO*t*Bu and Et_3SiH. Additionally, the derivatives of these compounds are shown that are expected to be obtained upon quenching the reaction with deuterium oxide.

The radical anion **504** is the typical Birch reduction intermediate. It is, however, unlikely that this structure is the predominant species in the reaction mixture with the KO*t*Bu-Et_3SiH reagent system. Upon work-up, **504** is unlikely to give rise to the isolated product 9,10-dihydroanthracene **502** but would either give rise to derivatives such as **507** or be oxidised back to anthracene. The intermediate **505** may be formed via hydride reduction of anthracene. Upon quenching with deuterium oxide the mono-deuterated compound **502-*(9)-d*** would be formed. The analogous reduction of anthracene cores with lithium aluminium hydride has previously been reported.[232] Also the reduction of anthracene itself with potassium hydride has previously been observed.[233] Finally, the anthracene dianion **506** may be formed to some extent, either by deprotonation of **505** or by a second single electron transfer to **504**. Upon quenching with deuterium oxide one would expect to obtain the di-deuterated compound **502-*(9,10)-d_2***.

When the reduction reaction of anthracene with the KO*t*Bu-Et_3SiH reagent system was quenched with deuterium oxide, the major deuterated product was **502-*(9,10)-d_2*** (Scheme 3-6). Careful analysis of the mass spectrometry data indicated, however, the presence of more highly deuterated analogues such as the tri- and possibly also the tetra-deuterated compound, **502-*(9,9,10)-d_3*** and **502-*(9,9,10,10)-d_4***, respectively. This observation indicated that multiple proton-deuterium exchanges can occur during the work-up. Indeed, when the non-deuterated

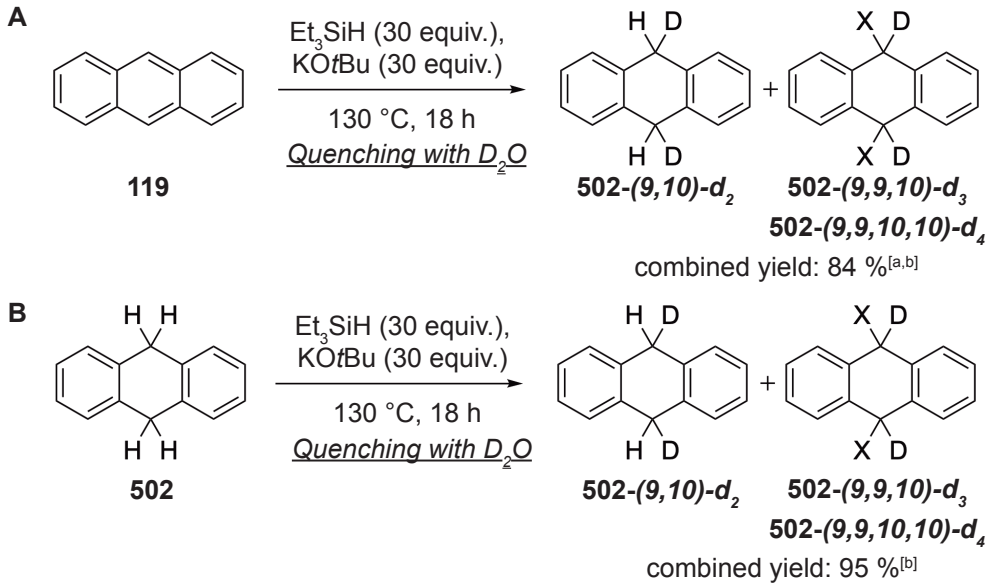

Scheme 3-6 Quenching the reaction mixture of anthracene and the KO*t*Bu-Et_3SiH reagent system with deuterium oxide leads to deuterated products. [a] Additionally 7 % of remaining starting material was isolated. [b] Analysis of the mixture of deuterated derivatives of **502** suggests the presence of the di-, tri- and potentially tetra-deuterated material.

substrate **502** was subjected to the reaction conditions and quenched with deuterium oxide, the same mixture of deuterated analogues was obtained. Thus, it becomes clear that quenching the reaction mixture with deuterium oxide cannot give information about the anionic intermediate of anthracene reduction.

With DFT methods, two mechanisms for the reduction of anthracene were investigated (computational studies by Allan Young).[231] It was found that the single electron transfer from the radical anion **494** (as a model of **281**) to anthracene was strongly exergonic but suffered from an insurmountably high activation barrier. At first, this result was counter-intuitive. Closer inspection showed that the reorganisation energy of the system is remarkably small. The combination of the pronounced exothermicity and the small reorganisation energy lets the electron transfer fall in the Marcus inverted region. Since the single electron transfer pathway was ruled out based on this result, a hydride reduction pathway was investigated and was found to exhibit an accessible energy profile. These findings suggest that hydride pathways may play a role in the reduction of anthracene and possibly also in the reduction of other aromatic systems.[231] But an alternative mechanism involving hydrogen atom transfer cannot be ruled out at this stage.[145]

Next, several aromatic substrates were subjected to the KO*t*Bu-Et_3SiH reagent system (Scheme 3-7). Phenanthrene **508** and naphthalene **452** gave the hydrogenated products **509** and **510**, respectively, although in much lower yield compared to the reaction of anthracene (Table 3-1 Entry 4). In the case of phenanthrene, a significant amount of an intractable mixture of by-products was observed. In the case of the reduction of naphthalene, a substantial amount of substrate remained unreacted. This observation is in line with the expectation that it is more difficult to reduce naphthalene than it is to reduce anthracene, i.e. the postulated anionic intermediate **511** is less stable than the corresponding anthracene derived anion **505**.

The reduction of stilbene **512** was high-yielding and gave the reduced product **513** almost quantitatively. Interestingly, when starting from diphenylacetylene **514**, the same product **513** was obtained as the major product of the reaction. Even though the yield of **513** is lower starting from **514**, the reaction is remarkable since two equivalents of hydride are transferred to the substrate. Finally, also acridine **515** and quinoline **517** were reduced under the applied KO*t*Bu-Et_3SiH conditions. The dihydroacridine **516** was obtained in comparable yield to the

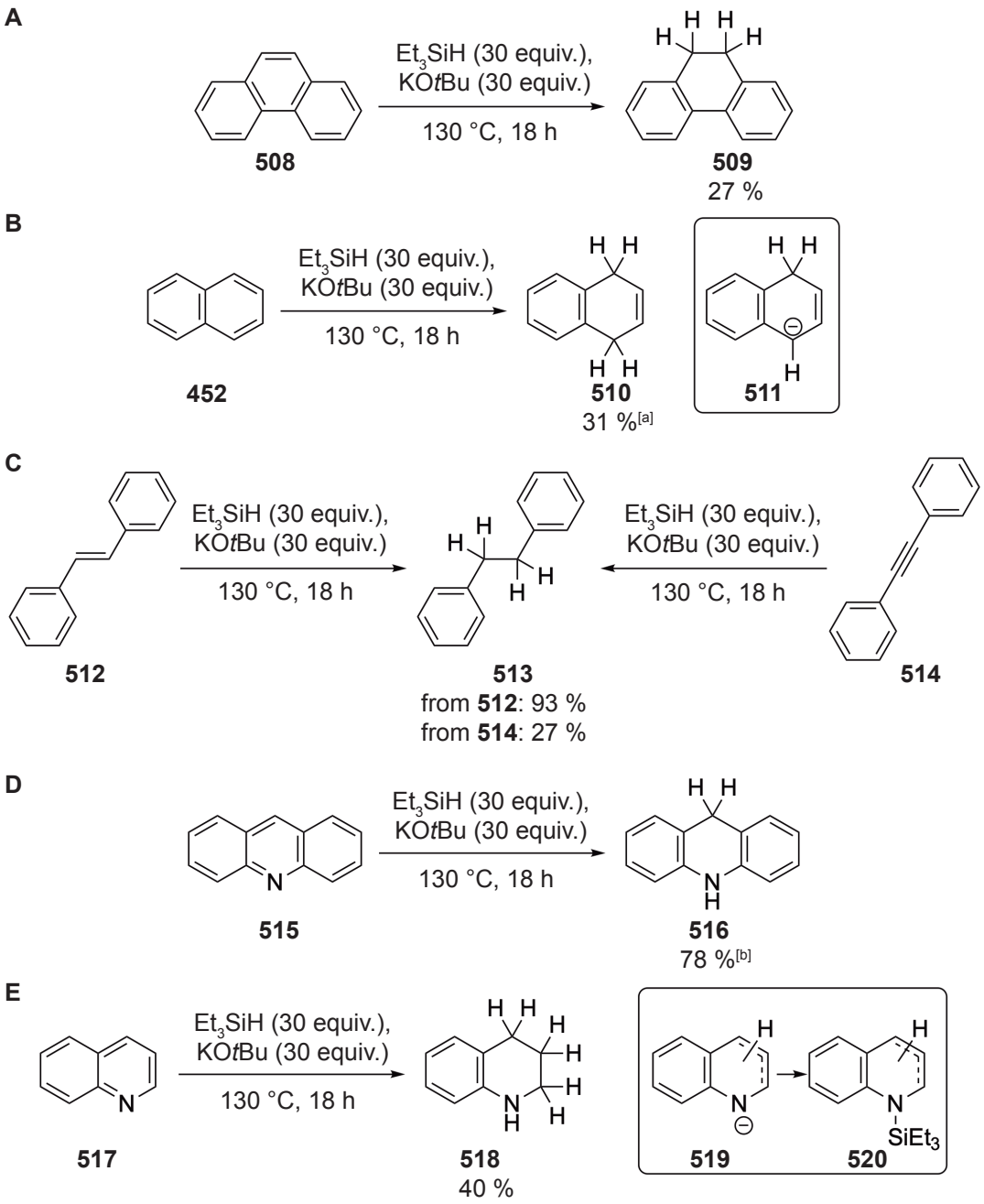

Scheme 3-7 A series of aromatic compounds has been subjected to reduction with the KO*t*Bu-Et_3SiH reagent system. [a] The yield was determined by ^{1}H-NMR vs. 1,3,5-trimethoxybenzene as internal standard. Additionally 42 % of remaining naphthalene were measured. [b] Additionally 12 % of acridine **515** were recovered.

dihydroanthracene **502** (Table 3-1 Entry 4). The quinoline **517**, in contrast, did not give the dihydro product analogous to the reduction of naphthalene. Instead, the tetrahydroquinoline **518** was obtained as the major reaction product. The key question is why the reduction of naphthalene stops after one hydride equivalent has been transferred on the substrate while the reduction of quinoline can proceed such that, in total, two hydride equivalents are transferred on the substrate. A possible explanation may be that the anionic intermediate **519** derived from quinoline is sufficiently nucleophilic to get silylated (for examples of analogous silylation reactions see Chapter 1.5.3). Thereby the neutral species **520** may be formed, which can potentially be further reduced. The silyl group likely is removed from the substrate upon work-up and purification. The anion **511** derived from naphthalene, in contrast, may not be sufficiently nucleophilic to get silylated. Consequently the negative charge cannot be stabilised and the reduction stalls at the dihydro stage.

Going further, the reaction of simple anthracene derivatives, exposed to the KO*t*Bu-Et_3SiH conditions, was investigated (Scheme 3-8). The reduction of 9-cyanoanthracene **521** gave the corresponding dihydro compound **522** only in low yield. The major reaction product was the methyl analogue **523**, which was obtained as an inseparable mixture with small quantities of **502** and **524**. The reaction of the amide **525** overall gave a similar outcome. With this substrate, not even small amounts of product, still containing the amide function, could be isolated. Instead, the compound **523** was again the major reaction product and was isolated as a mixture with minor quantities of **502** and **524**. The three compounds together gave an essentially quantitative mass balance.

There are two noteworthy points about these two reactions. First, the complete reduction of either functional group to give **523** requires the cleavage of a (benzylic) carbon-heteroatom bond. Such a cleavage likely involves silylated intermediates in order to stabilise the negative charge that builds up on the heteroatom during the preceding reduction of the functional group. A proposed mechanism is exemplified for the 9-cyanoanthracene substrate **521** (Scheme 3-9). First, the nitrile group likely is converted to the disilylated amine intermediate **528** via the subsequent delivery of two hydride equivalents. Then a hydride adds onto the aromatic system to give the anionic intermediate **529**. This intermediate may expel the amide **530** to form then neutral compound **531**, which is further reduced to the anion **532**. Upon protonation during quenching the reaction, the intermediate **532** gives the observed compound **523**.

The second remarkable aspect of the reactions in Scheme 3-8 A and B is the formation of the by-products **502** and **524** in roughly equimolar amounts. This requires the cleavage of a carbon-carbon bond. In order to obtain information about the reduction stage of the functional group at which this bond cleavage occurs, the methyl anthracenes **526** and **527** were subjected to the KO*t*Bu-Et_3SiH reagent system. In neither case were products derived via a carbon-carbon bond cleavage detected (by inspection of the crude reaction product by ^1H-NMR spectroscopy). The corresponding dihydroanthracene products **523** and **524** were obtained almost quantitatively and only traces of unreacted starting material were recovered. This observation suggests that the carbon-carbon bond cleavage in the reactions of **521** and **525** occurs before the corresponding functional group is fully reduced to a methyl residue. A plausible mechanism is outlined for the 9-cyanoanthracene substrate **521** (Scheme 3-10). After hydride addition onto the substrate **521** the anion **533** may expel cyanide to give anthracene **119**. Anthracene is then further reduced to **502** while the cyanide anion adds to another molecule of **521**. The corresponding adduct **534** can then be further reduced to the

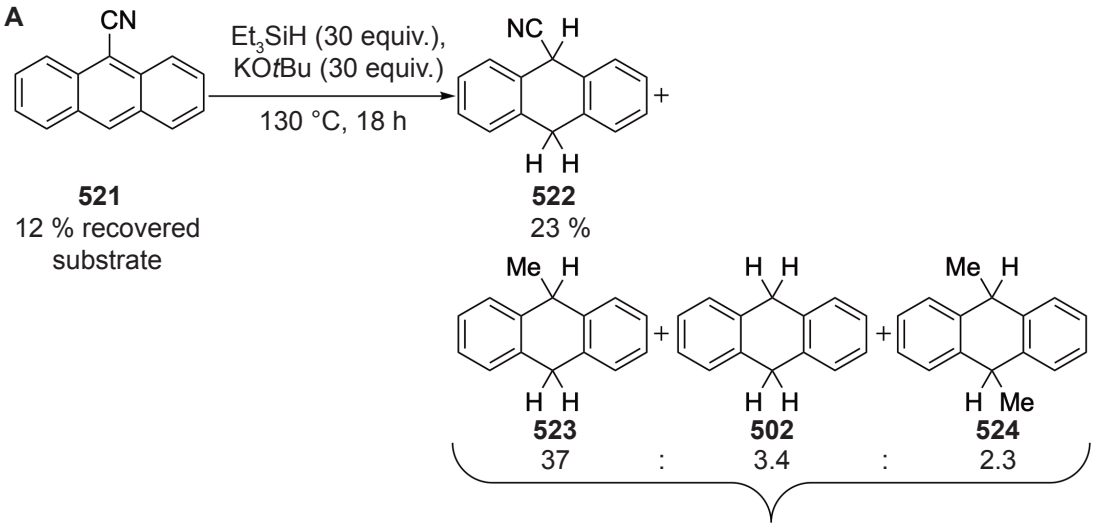

Scheme 3-8 Reduction of anthracene derivatives with the KO*t*Bu-Et_3SiH reagent system.

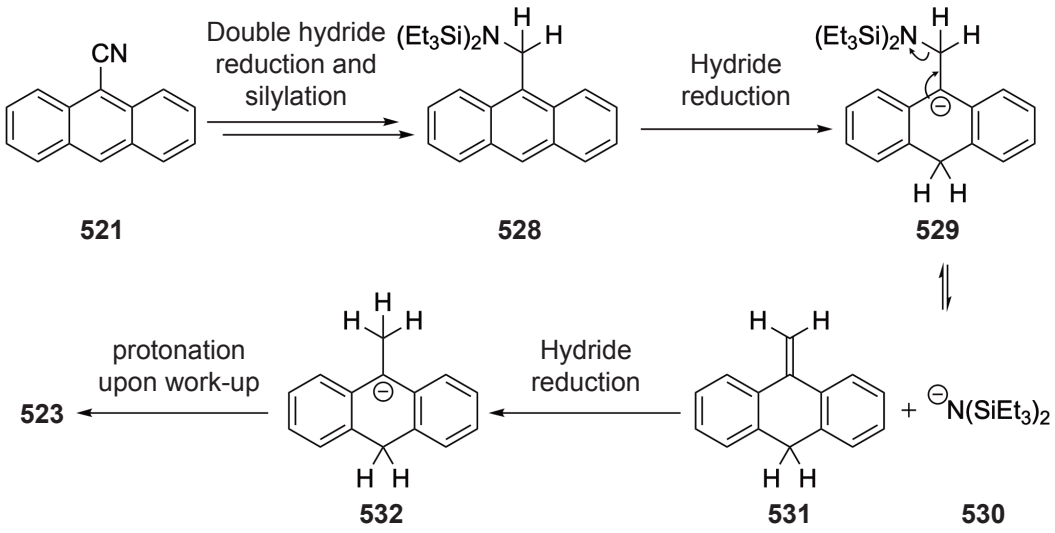

Scheme 3-9 The proposed mechanism for the reduction of the nitrile group requires a double silylation at the nitrogen in order to stabilise the negative charge that builds up on this heteroatom.

isolated product **524**.

The proposed mechanism is in line with the observation that no carbon-carbon bond cleavage occurs during the reduction of the substrates **526** and **527**. This makes good sense as, compared to cyanide or the acyl anion (from the amide), the methyl anion is a much worse leaving group.

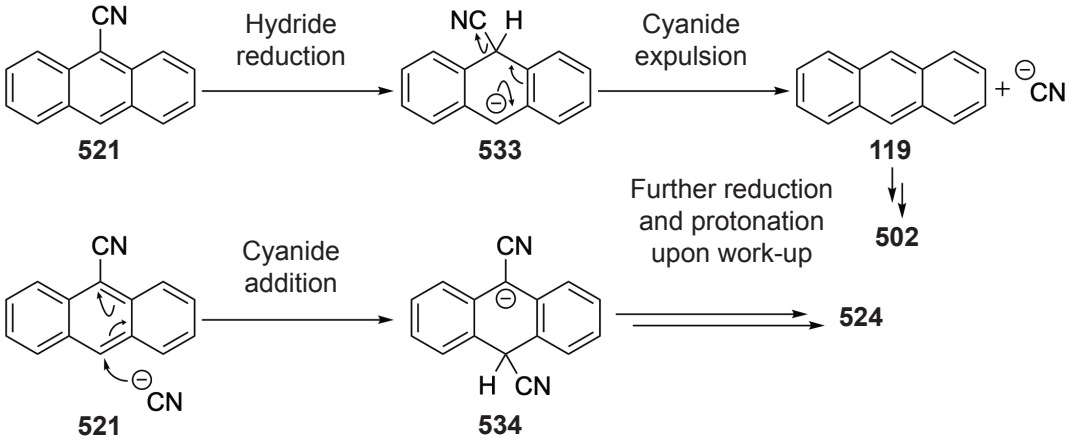

Scheme 3-10 The proposed mechanism for the formation of products **502** and **524** from **521**.

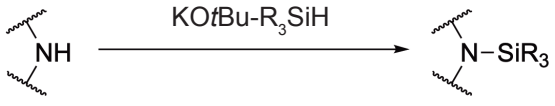

535 **536**

Scheme 3-11 Is the KO*t*Bu-Et_3SiH (or more generally the KO*t*Bu-Silane) reagent system able to silylate simple amines?

3.3. Silylation of Amines

As became clear from the results above, the KO*t*Bu-Et_3SiH reagent system is a powerful reductant. Several mechanisms appear to be accessible. These are single electron transfer steps and hydride reduction reactions. Depending on the substrate and conditions, hydrogen atom-mediated processes may also play a role.[145] In most cases described in Chapter 3.2, the reduction process stopped after the first single electron transfer or after one hydride equivalent had been transferred onto the substrate. However, a number of examples was identified where multiple hydride equivalents were transferred (e.g. the reduction of **514**, **517**, **521** and **525**). In these cases, the question arises of how the accumulation of negative charge on the substrate is stabilised. In light of the strong basicity of the reaction mixture, a simple protonation step does not appear plausible. Instead, silylation of anionic intermediates may play a crucial role of stabilising intermediates in the reduction process. In fact, many elegant silylation protocols were reported that rely on a silane reagent as the silicon source. In combination with a base or a strong nucleophile as a catalyst, clean silylation of very diverse substrates was achieved (Chapter 1.5.3). It was thus natural to investigate the ability of the KO*t*Bu-Et_3SiH system to silylate nucleophilic substrates. Amines were chosen for this investigation as a simple and relevant substrate class and as likely intermediates in the reduction process of **517**, **521** and **525** (Scheme 3-11). The proposed mechanism of such silylation reactions was investigated by DFT methods. The experimental work mentioned in this section was performed by Fabrizio Palumbo.[234]

3.3.1 Silylation of Simple Amines

(A detailed description of the following computational studies can be found in Chapter 5.4.7).

For the initial computational studies, trimethylsilane was used as a model for triethylsilane. Based on the ionic silylation mechanism discussed in the introduction (Chapter 1.5.3), it was proposed that in the first step the amine is deprotonated. But the direct deprotonation of the aliphatic amine **537** with potassium *tert*-butoxide **287** was found to be strongly endergonic and thus not feasible (Figure 3-3). Further, it was not possible to locate a transition state for a concerted hydride transfer and deprotonation step involving the pentavalent silicate **540** and the amine **537** (when a potassium counter cation was included). Corresponding attempts resulted in the collapse of the input structure to **541** and potassium hydride **542** upon optimisation. Further optimisation led to a transition state where potassium hydride performed the deprotonation. Therefore it appears plausible to represent the hydride equivalent, that is formed when potassium *tert*-butoxide attacks silane, as potassium hydride. Indeed, the computational model suggests that the formation of potassium hydride from potassium *tert*-butoxide and trimethylsilane is accessible (Figure 3-4). After the addition of potassium *tert*-butoxide

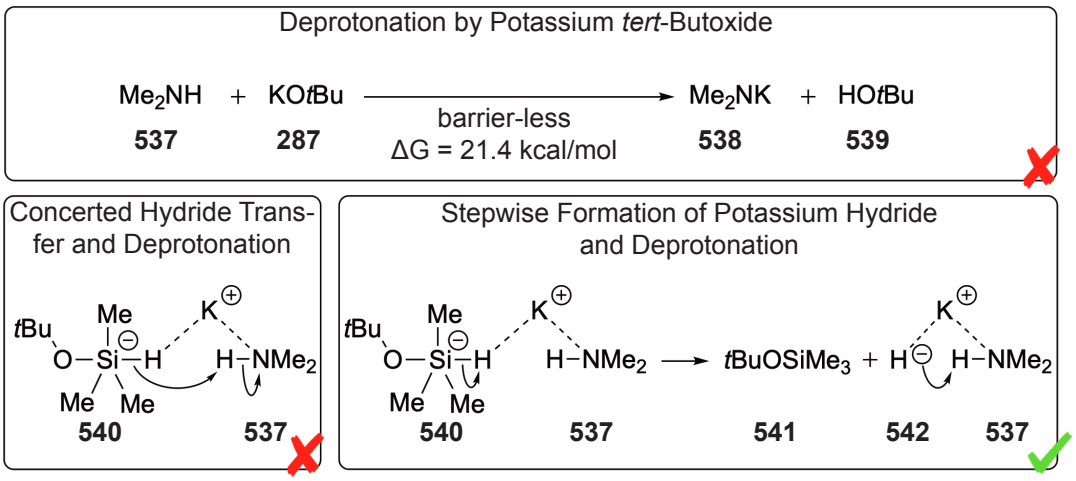

Figure 3-3 The key deprotonation step of the amine substrate.

to the silane, the intermediate **540a** is formed, where the potassium cation coordinates to the pentavalent silicate species via the oxygen atom. Rearrangement of the potassium cation to coordination of this species via the silicon hydride leads to the structure **540b**, which is directed towards the elimination of potassium hydride. This elimination is the rate-limiting step and is accessible with an energy barrier of 19.4 kcal/mol. Overall, the reaction is moderately endergonic. This indicates that only small amounts of potassium hydride are generated at any time in the reaction mixture.

Experimentally, it was found that the silylation of amines is high yielding and clean when the amine is treated with an excess of silane and a catalytic amount of potassium *tert*-butoxide. [234] The fact that the reaction proceeds with catalytic amounts of base was a key observation that helped to identify the proposed, general mechanism (Scheme 3-12). This mechanism is

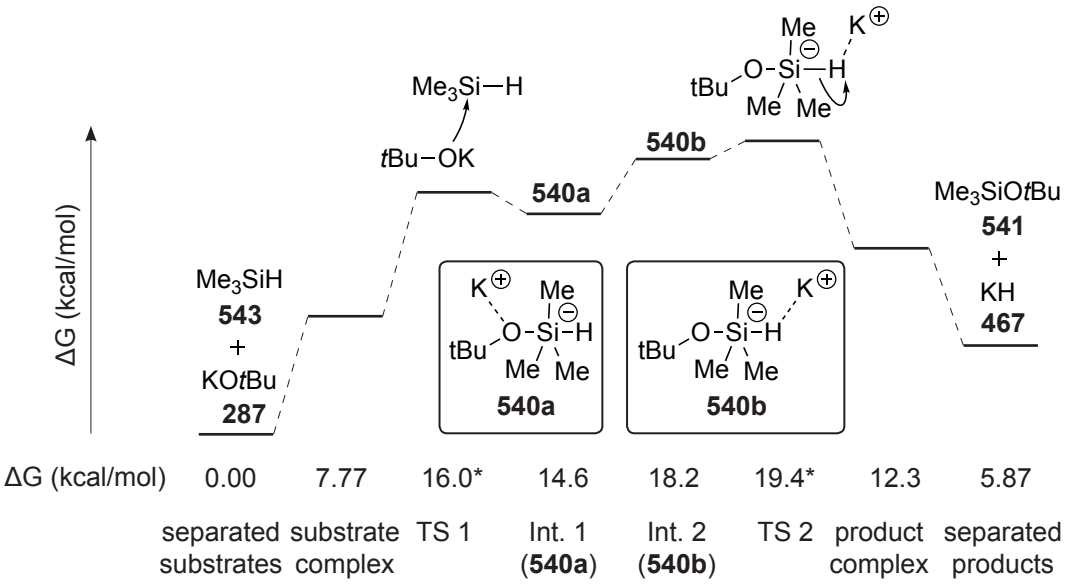

Figure 3-4 The energy profile for the formation of potassium hydride from potassium *tert*-butoxide and trimethylsilane is accessible. (*) The asterisk indicates transition state energies.

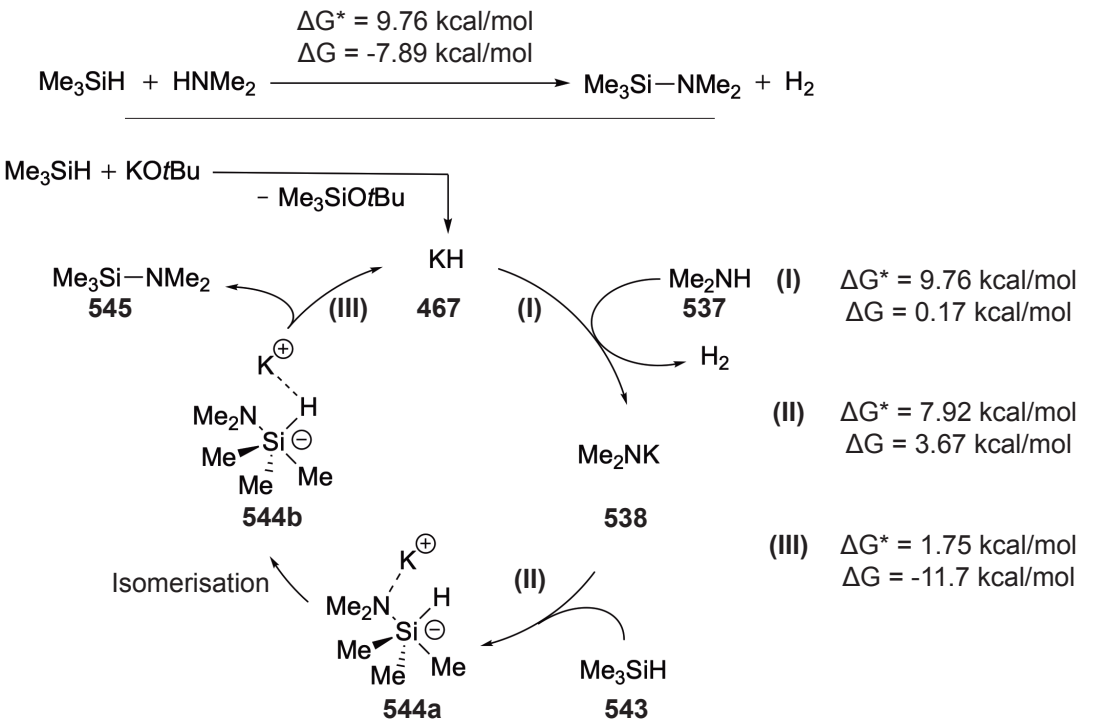

Scheme 3-12 The proposed, general mechanism for the silylation of amines is catalytic in potassium hydride (which is generated from potassium *tert*-butoxide and the silane).

catalytic in potassium hydride **467**, which is formed during the initiation process as detailed in Figure 3-4. Once formed, potassium hydride **467** can efficiently deprotonate the aliphatic amine **537** (Step **(I)**). In stark contrast to the direct deprotonation of the amine with potassium *tert*-butoxide (Figure 3-3), the deprotonation with potassium hydride is nearly thermoneutral. The generated potassium amide **538** is proposed to attack trimethylsilane **543** in Step **(II)** (analogously to the attack of potassium *tert*-butoxide on trimethylsilane during the initiation process - Figure 3-3). This leads to the pentavalent silicate intermediate **544a** (Scheme 3-12), which rearranges to **544b** via a pseudorotation and then expels potassium hydride (Step **(III)**). Thereby the silylated product **545** is formed and the catalytic cycle is closed. The rate limiting step for this simple example is the deprotonation of the amine with potassium hydride (Step **(I)**). Overall, this reaction pathway is very accessible (i.e. activation barriers are low) and exergonic.

For the Steps **(II)** and **(III)** of the catalytic cycle in Scheme 3-12, two additional variations were investigated. The detailed energy profiles are shown in Figure 3-5. The lowest energy pathway is Path C where the potassium amide **538** attacks the silane **543** equatorially with respect to a methyl group. This attack angle leads to the intermediate **544a** and eventually **544b**. An alternative attack angle (Path B) where the nucleophile adds to the silane equatorially with respect to the hydride leads to the intermediates **544c** and **544d**. These are energetically less stable than the corresponding intermediates **544a** and **544b**. Additionally, Path B also exhibits a higher activation energy than Path A. Finally, the attack of the potassium amide **538** on the silyl ether **541** instead of the silane **543** was investigated (Figure 3-5, Path A). This pathway, too, comes with a higher activation energy than Path C. Importantly, Path A does not directly

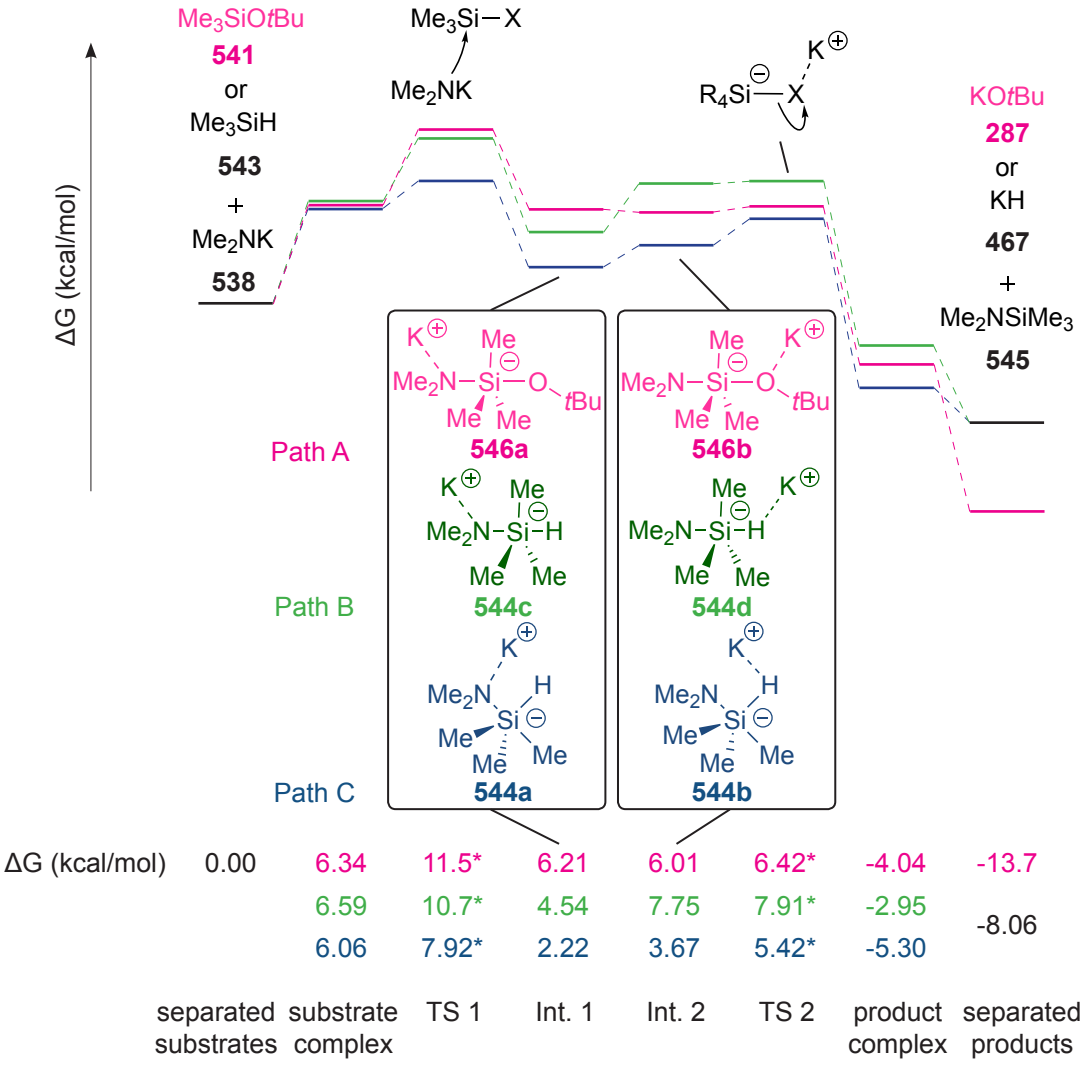

Figure 3-5 The energy profile for obvious variants of the steps **B** and **C** in the catalytic cycle shown in Scheme 3-12. (*) The asterisk indicates transition state energies.

regenerate potassium hydride but gives potassium *tert*-butoxide instead. In order to propagate the chain, potassium *tert*-butoxide is required to react with silane **543** to regenerate potassium hydride (Figure 3-4). Therefore, in this case the rate limiting step of the reaction will be the elimination of potassium hydride from **540b**.

Experimentally, it was observed that some primary amines were silylated only once although in principle double silylation could occur, while others were silylated twice (Scheme 3-13).[234] This observed chemoselectivity was intriguing. In order to understand why the silylation of primary amines stops after the first silylation in some cases, energy profiles for the second silylation step of some aliphatic silyl amines were calculated. First, it was noticed that the deprotonation of **548** (R^1=R^2=Me) was actually more favourable than the deprotonation of **537** (Scheme 3-14) both kinetically and thermodynamically. This observation is in line with the lower p*K*a of silylated amines compared to fully aliphatic amines.[235] Therefore, the decisive step of the double silylation must occur further downstream on the reaction pathway (Figure

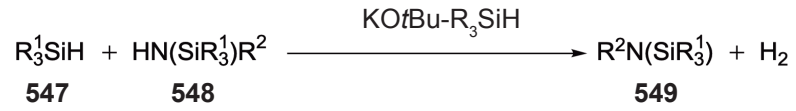

Scheme 3-13 The double silylation of primary amines has never been observed.

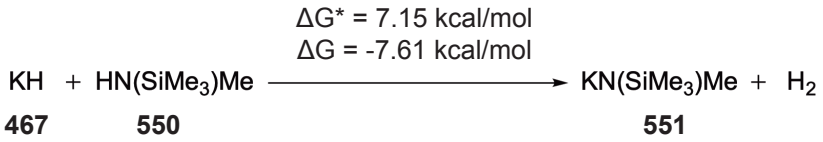

Scheme 3-14 The deprotonation of silyl amines with potassium hydride is favourable and exergonic.

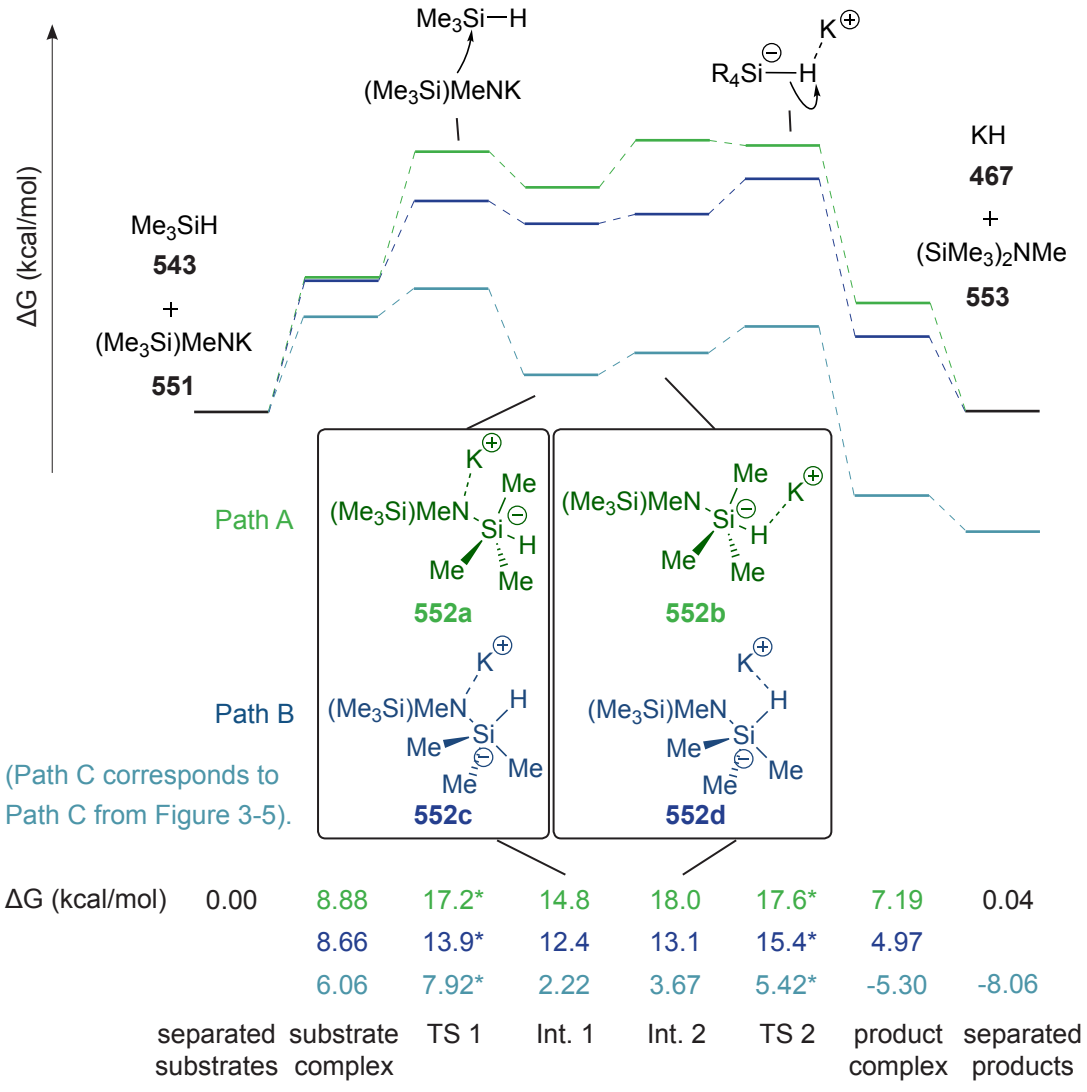

Figure 3-6 The energy profiles for the second silylation of with are shown (Path A and B). For comparison Path C is a replication of Path C from Figure 3-5. (*) The asterisk indicates transition state energies.

3-6). Indeed, the silylation of the potassium salt **551** exhibits a higher activation barrier (Path A and B) than the silylation of the potassium salt **538** (Path C, see also Path C in Figure 3-5). This activation barrier is, however, still very accessible. Further, it was found that the second silylation step of the substrate **551** is essentially thermoneutral. But that does not rule out the reaction from occurring since the generated potassium hydride will be rapidly consumed by the reaction with another amine **550** - the deprotonation step will drive the whole reaction sequence forward. Clearly, the simplified model where aliphatic residues are all approximated as methyl groups suggests that double silylation of primary aliphatic amines is in general possible. The model cannot explain why, in certain substrates, the process stops after the first silylation (vide infra).

In an attempt to improve the model, the tri*methyl*silanyl groups were replaced for tri*ethyl*silanyl groups. This structural change had little effect on the energy profile of the deprotonation step, leading from the amine **554** to the potassium amide **555** (Scheme 3-15). Indeed, it was anticipated that the increased steric bulk of the ethyl groups on the silicon residue would mainly manifest during the attack of the potassium amide **555** on the silane **284** (or the corresponding *tert*-butoxytriethylsilanyl ether **296**). The energy profiles for these steps are shown in Figure 3-7. With triethylsilane as the silicon species, both Path B and C become kinetically equally favourable although the nature of the rate limiting step is different. For Path B the rate limiting step is the addition of the potassium amide **555** onto the silane reagent **284**, while in Path C the rate limiting step is the elimination of potassium hydride **467** from the intermediate **557d**. The silylation via the *tert*-butoxytriethylsilane ether **296** shows the least accessible energy profile. An analogous observation was already made previously (see Figure 3-5). For comparison, also the energy profile of the double silylation with trimethylsilane (Path B in Figure 3-6) is shown in Figure 3-7 as Path D. It becomes evident that the second silylation with triethylsilane is both kinetically and thermodynamically slightly less favourable than the corresponding second silylation with the trimethylsilane reagent. However, the activation energy of slightly more than 19 kcal/mol is still accessible. Also, the exergonicity of the deprotonation step is sufficient to drive the whole process forward. Consequently, the improved model based on the experimentally used[234] silicon reagent triethylsilane **284** still does not give an explanation for why the double silylation is not observed in some cases.

From close inspection of the transition states leading to the intermediates **557a** and **557c**, it became clear that for larger aliphatic residues on the amine there is a potential steric clash with the ethyl groups of the silyl groups. A particularly pronounced clash was anticipated if the aliphatic amine residue is branched at the α-carbon atom.

To better understand the steric effect of the aliphatic residue of the amine on reaction outcome, the energy profiles for the second silylation of silylated *n*-propylamine **559 (R = *n*Pr)** and the analogous *i*-propylamine **559 (R = *i*Pr)** were calculated (Figure 3-8). It was found that, for the *n*-propylamine analogue, the rate-determining step is the elimination of potassium hydride for both investigated pathways (Path A via **560a** and **560b** or Path B via **560c** and **560d**). Importantly, the rate limiting step in Path B appears still accessible with an activation energy of 22.5 kcal/mol. This value is 3.4 kcal/mol higher than the activation barrier for the second silylation with the methylamine analogue **555** (Path E). The energy profiles for the *i*-propylamine **559 (R = *i*Pr)** analogue, in contrast, are clearly less accessible. The activation energy for the rate limiting step in Path C equals 27.6 kcal/mol. This value is 8.5 kcal/mol higher than the rate limiting step in the reaction of the methylamine analogue **555** (Path E). Indeed, the activation

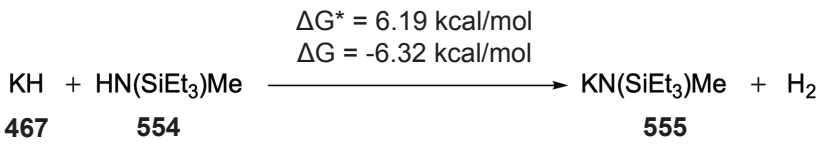

Scheme 3-15 The deprotonation of silyl amine **554** with potassium hydride is favourable and exergonic.

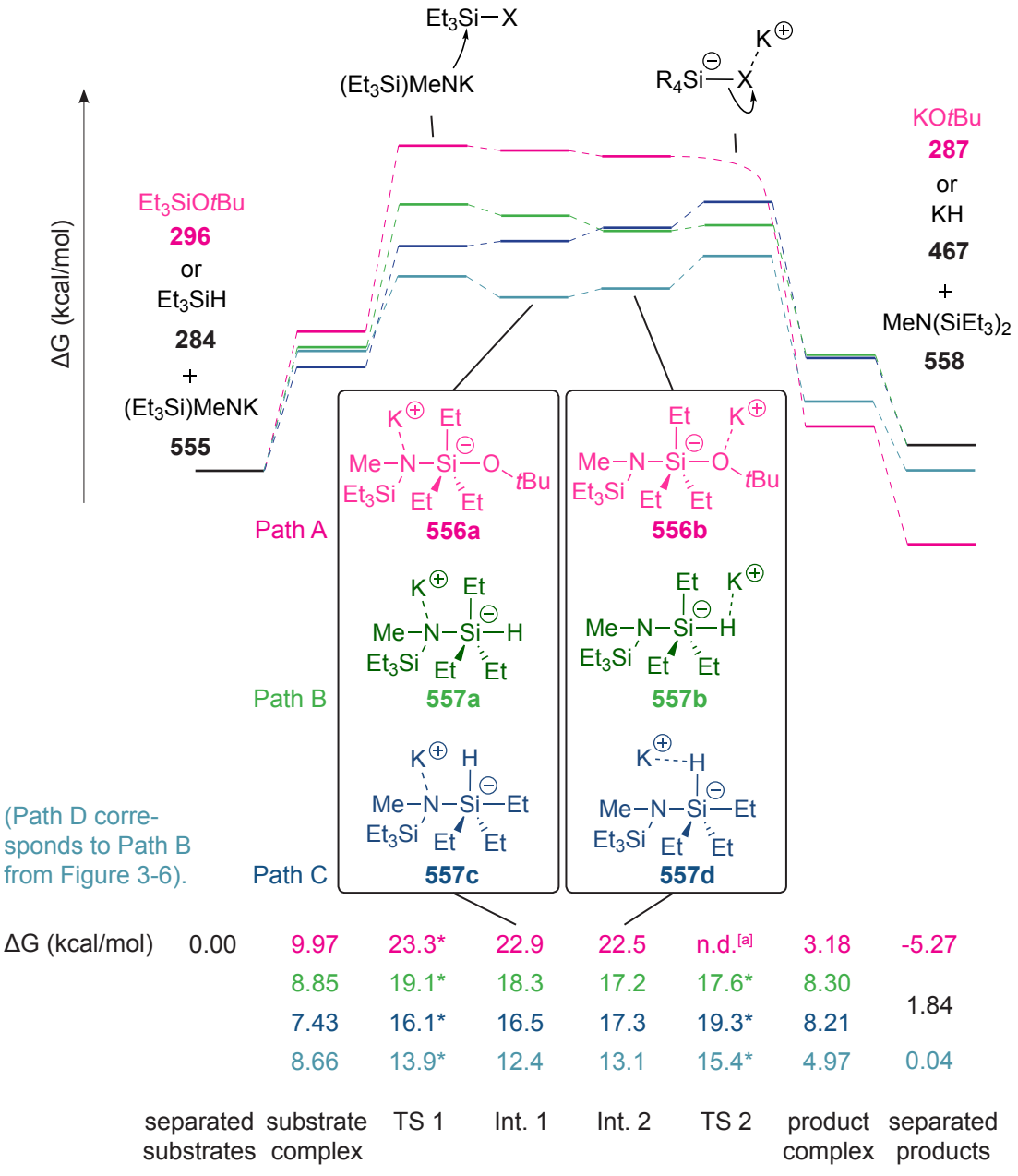

Figure 3-7 The energy profile for the second silylation of an aliphatic amine with triethylsilane is shown. (*) The asterisk indicates transition state energies. [a] Barrier-less elimination of potassium *tert*-butoxide.

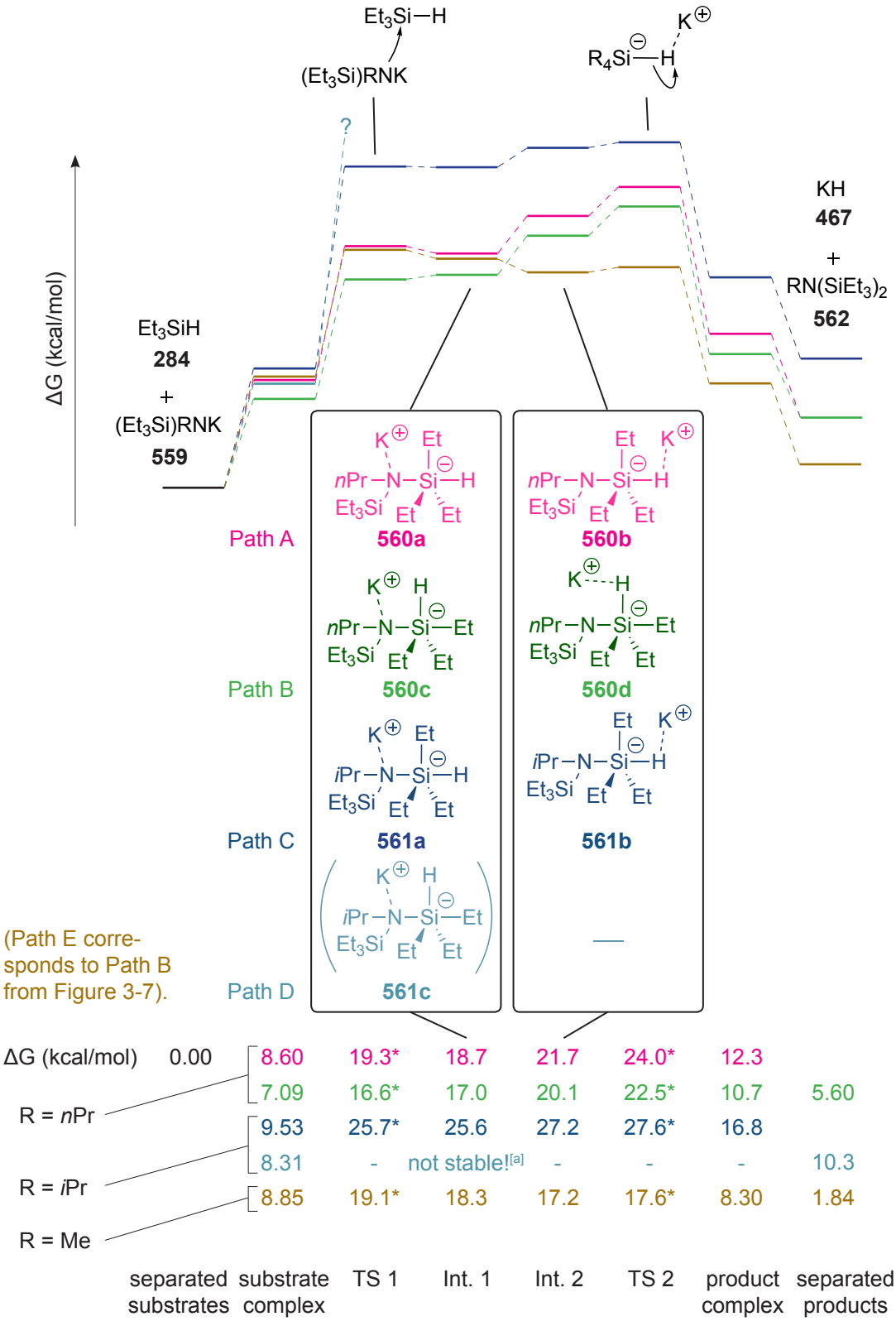

Figure 3-8 The energy profile for obvious variants of the steps **B** and **C** in the catalytic cycle shown in Scheme 3-12. (*) The asterisk indicates transition state energies. [a] Neither the transition state TS 1 nor the structure Int. 1 could be optimised. All attempts to optimise either structure resulted in convergence towards the substrate complex.

barrier of 27.6 kcal/mol is in agreement with no product formation being observed with a closely related amine that is branched at the α-carbon of its aliphatic residue (the reaction temperature was 130 °C).[234] Another tell-tale sign that the second silylation of **559 (R = *i*Pr)** is energetically difficult is the fact that no stable structure for intermediate **561c** (on Path C) could be found (no local minimum on the hyper energy surface corresponding to **561c** could be found). Upon optimisation, the initial guess structure fragmented back to triethylsilane **284** and the potassium amide **559 (R = *i*Pr)**.

According to these computational results, the double silylation of primary aliphatic amines in principle can occur with the KO*t*Bu-Et_3SiH reagent system. This observation is in agreement with literature reports on related silylation reactions of primary amines where double silylation was achieved (Chapter 1.5.3).[155] It is also in agreement with one class of substrates that were exposed to the KO*t*Bu-Et_3SiH reagent system (see **3.3.2** below).[234] It becomes also clear that steric effects play a crucial role for the second silylation of a primary amine. Steric bulk of the aliphatic residue (i.e. branching at the α-carbon) of the substrates that were investigated experimentally[234] is the likely reason for the absence of doubly silylated products in these reactions. It will be interesting to see whether double silylation of sterically less encumbered primary amines is actually possible - as the computational model predicts. Such substrates have not yet been exposed to the KO*t*Bu-Et_3SiH reagent system but will definitely be an interesting test case for the validity of the computational model employed here.

In addition to aliphatic amines, a number of anilines were successfully silylated with the KO*t*Bu-Et_3SiH reagent system.[234] Potassium salts of anilines were expected to be significantly less nucleophilic than their aliphatic counterparts. It was therefore necessary to establish whether or not the proposed reaction mechanism for the silylation of aliphatic amines is still plausible with aniline substrates. As a model system, the parent compound **563** was chosen in combination with trimethylsilane as a silicon source. As expected, the deprotonation of **563** with potassium hydride shows a very low activation barrier and is strongly exergonic (Scheme 3-16). With potassium *tert*-butoxide, the formation of the potassium anilide **564** is almost barrier-less and essentially thermoneutral. Thus, for aniline substrates, the silylation reaction can be initiated by direct deprotonation with potassium *tert*-butoxide. A corresponding pathway was found not to be an accessible for aliphatic amine substrates (Figure 3-3).

Analogous to the investigations of the potassium amide nucleophiles, three obvious pathways for the silylation of the potassium anilide **564** were investigated (Figure 3-9). Following Path A or Path B, it was found that the addition of **564** onto trimethylsilane **543** has a very similar energy barrier for the rate limiting step of (20 - 21) kcal/mol. These activation barriers are accessible and are actually very similar to the activation barrier found for the reaction of trimethylsilane with potassium *tert*-butoxide (Figure 3-4). Next the silylation of **564** with *tert*-butoxytrimethylsilane **541** was simulated and found to be kinetically more favourable than the silylation via Me_3SiH **543**. This observation marks a difference to the reaction of the aliphatic potassium amide species that were investigated previously. The aliphatic potassium amides were found to show lower activation energies in the reactions with **543** compared to **541**. The combination of these findings implies that the silylation reaction of potassium anilides preferentially proceeds via Path C (Figure 3-9) if **541** is available. Alternatively, the reaction can proceed via Path A and B.

It also becomes evident that the silylation of potassium anilides is kinetically more difficult than the silylation of aliphatic potassium amides via any mechanism (for comparison, the most

563 **564**

	X = H	X = O*t*Bu
ΔG* (kcal/mol)	2.71	0.25
ΔG (kcal/mol)	-18.2	0.07

Scheme 3-16 The deprotonation of aniline with either potassium hydride or potassium *tert*-butoxide is kinetically favourable.

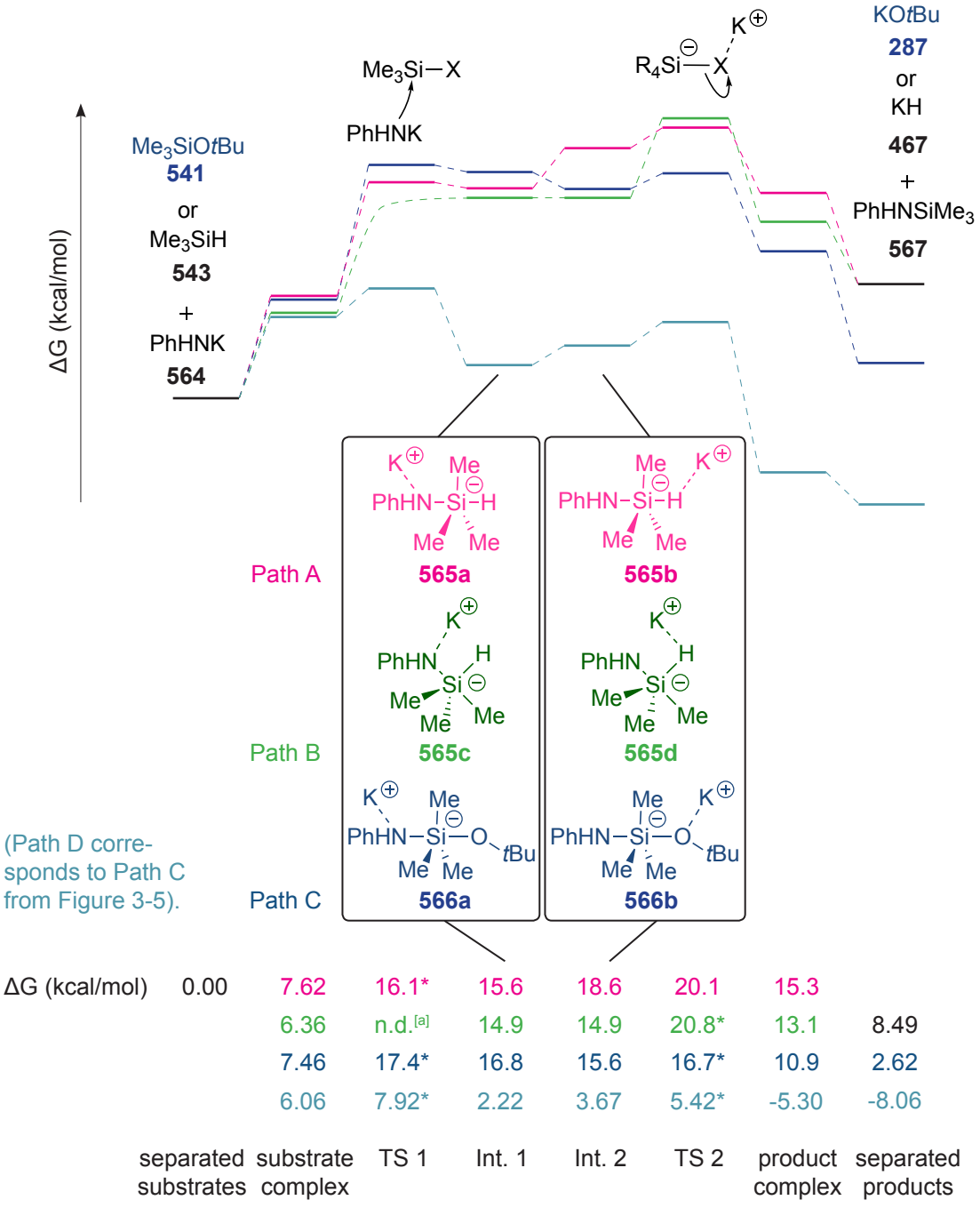

Figure 3-9 The energy profile for the silylation of potassium anilide **564** with trimethylsilane or *tert*-butoxytrimethylsilane is shown. (*) The asterisk indicates transition state energies. [a] Barrier-less addition of **564** onto trimethylsilane.

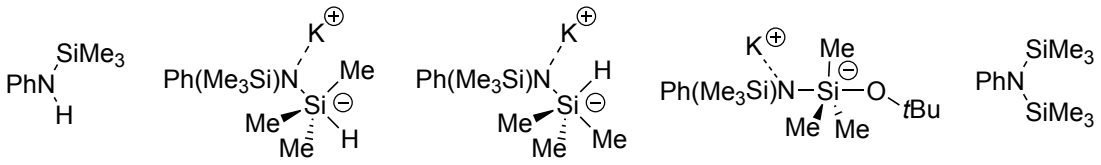

567 **568a** **568b** **569** **570**

Figure 3-10 The addition of potassium anilide **564** to trimethylsilane or *tert*-butoxytrimethylsilane did not lead to a stable intermediate.

accessible energy profile for the silylation of potassium dimethylamide from Figure 3-5 is inset in Figure 3-9). Experimentally, it was found that aliphatic amines reacted more rapidly than aniline substrates in side-by-side reactions. In direct competition experiments where both substrates were contained in the same reaction mixture, however, aniline substrates were found to out-compete aliphatic amines.[234] The first observation is in agreement with the finding that the maximal activation barrier for the silylation of aniline **563** is higher than the maximal activation barrier for the silylation of aliphatic amine **537**. The second observation is perfectly in line with the fact that anilines are more acidic than aliphatic amines. Thus, the anilide is preferentially formed over the amide. Therefore it is the anilide that gets silylated in a direct competition experiment.

Finally, the possibility of a second silylation of the monosilylated aniline **567** was investigated (Figure 3-10). For the formation of each of the intermediates **568a**, **568b** or **569**, neither a stable structure could be identified nor a transition state that would lead to their formation. A similar observation has previously been made with structure **561c** (Figure 3-8). The finding indicates that there is no accessible pathway leading to the formation of **570**, which is in agreement with the experimental work. No doubly silylated products were detected when primary anilines were exposed to the KO*t*Bu-Et_3SiH reagent system.[234]

3.3.2 Cyclisation and Expulsion of Alkyl Potassium Species

When aliphatic 1,2-diamine species such as **571** were subjected to the KO*t*Bu-Et_3SiH reagent system, cyclic products such as **572** were obtained (Scheme 3-17).[234] A similar observation was previously reported by Fink (Chapter 1.5.3).[156] The result is noteworthy as one silyl residue not only suffers loss of a hydride but also an alkyl group. The proposed mechanism (Scheme 3-12) can be easily adapted to this situation. The only change is that instead of potassium hydride, the expelled potassium alkyl species now propagates the chain reaction. At the moment it is not clear at what stage the ring closure occurs. It may occur at any stage of the silylation process - after the first, the second or the third silyl group has been transferred

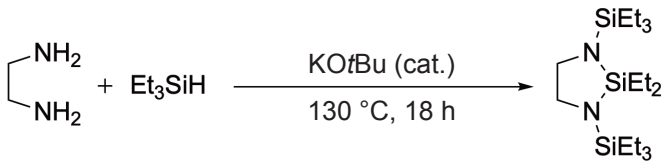

571 **284** **572**

Scheme 3-17 Treatment of aliphatic 1,2-diamines with the KO*t*Bu-Et_3SiH reagent system lead to the formation of cyclic products.

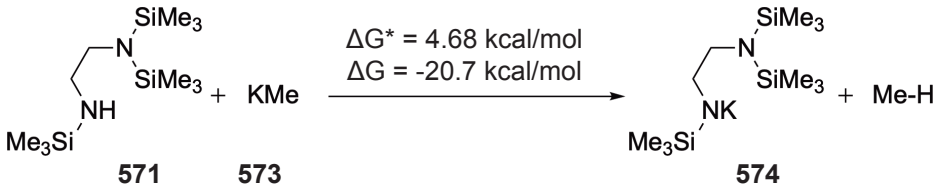

Scheme 3-18 The deprotonation of silyl amines with potassium methyl is favourable and exergonic.

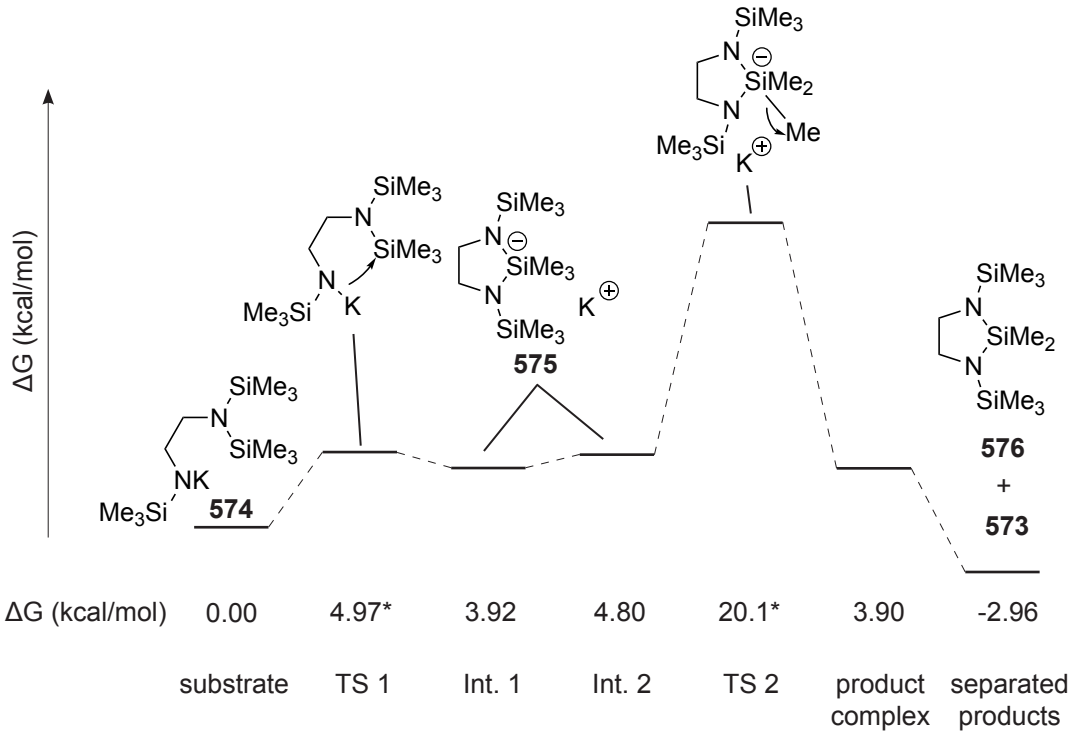

Figure 3-11 The energy profile for the cyclisation reaction towards **572**. The intermediate structure **575** exists in two closely related conformers Int. 1 and Int. 2. (*) The asterisk indicates transition state energies.

onto the diamine substrate. The exact sequence that is followed may actually depend on the backbone structure of the 1,2-diamine and the nature of the silane reagent.

To understand the principal feasibility of the process, it was decided to consider the ring closure step as the last step in the sequence (i.e. after three silyl groups have been attached to the diamine substrate). The energy profile of the model reaction between 1,2-diamine **571** and trimethylsilane **543** has been calculated. The deprotonation of **571** with methyl potassium **573** has - not surprisingly - a low barrier and is strongly exergonic (Scheme 3-18). The potassium amide **574** then readily forms the cyclic intermediate **575**. Two closely related conformations of this intermediate were found along the reaction coordinate. The conformation Int. 2 leads on to the transition state for the expulsion of methyl potassium **573**. This gives the cyclic product **572**. The expulsion of **573** clearly is the most difficult step in the sequence but it is accessible with an activation energy of 20.1 kcal/mol.

3.4. Summary and Conclusion

Several mechanistically different reaction pathways are accessible to the KOtBu-Et_3SiH reagent system. With the choice of suitable substrates, these pathways can be addressed and probed selectively. Ideally, reaction products are formed that are specific for a certain mechanism. Additionally, computational methods can be used to provide a reference, which indicates what reaction pathways are accessible for a certain substrate. Such a combined experimental and computational approach gave strong evidence for single electron transfer reactivity to be at the heart of the reductive aryl ether cleavage. This study is in close agreement with observations made for the reductive cleavage of *N*-benzyl indole substrates (experimental work by Andrew J. Smith and computational studies by Allan Young).[231] It provides additional evidence that the KO*t*Bu-Et_3SiH reagent system can give rise to a potent single electron donor species.

The examination of the reactivity of aromatic hydrocarbons and aromatic heterocycles in conjunction with computational investigations (computational studies by Allan Young)[231] provided evidence for hydride-mediated reductive pathways. The corresponding results have been part of a publication.[231] During the investigation of this substrate class, it became evident that, in certain cases, the reduction can proceed beyond the delivery of one hydride equivalent. This observation raised the question of how anionic intermediates are stabilised, since no obvious proton source is available in the KO*t*Bu-Et_3SiH reagent system (as for example in Birch-type reduction systems).

Inferring from the literature, the KO*t*Bu-Et_3SiH reagents system may be able to silylate sufficiently reactive nucleophiles. In more complex reduction processes, such as the reduction of functional groups, silylation may play a crucial role in stabilising anionic intermediates and thereby allow them to be further reduced. To investigate this possible aspect of the reagent system, amines were chosen as a simple yet relevant substrate class. Computationally, energy profiles for a number of substrates were derived. The knowledge gained from these studies helped to guide the experimental studies and to interpret the experimental results

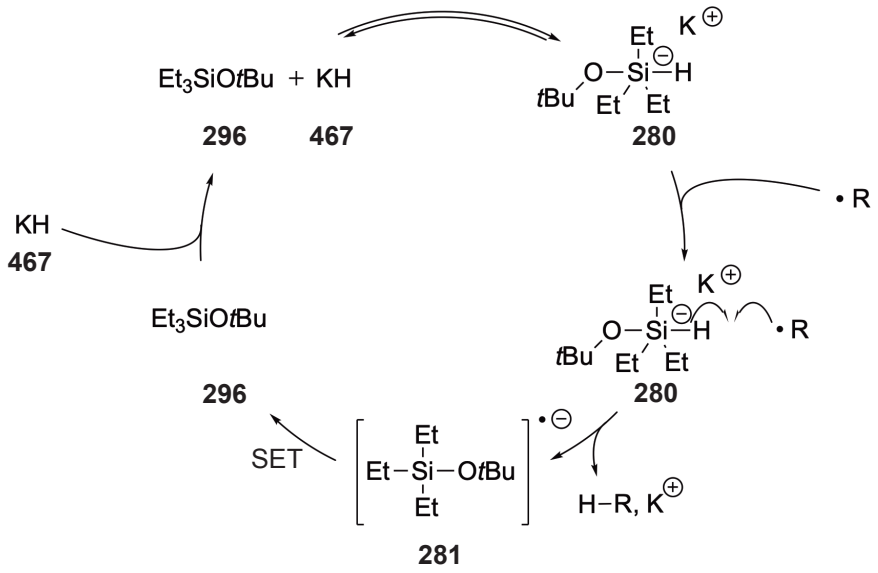

Scheme 3-19 Can the proposed single electron donor **281** be made catalytic?

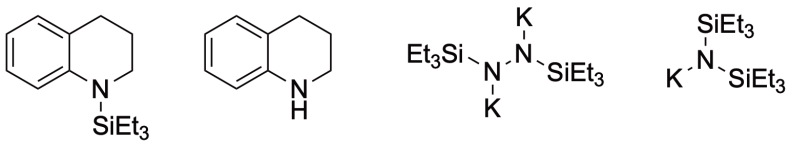

577 **518** **578** **579**

Scheme 3-20 Silylated species are likely to be key intermediates in multistep reduction processes of the KO*t*Bu-Et_3SiH reagent system. Direct evidence of their existence is needed.

(experimental work by Fabrizio Palumbo).[234]

3.5. Outlook

A key proposed species is **281**. So far, no direct evidence for its existence has been presented. Therefore, accessing **281** in a different way (other than by treating triethylsilane with potassium *tert*-butoxide at elevated temperature) would provide valuable information about its exact nature. One alternative access route to **281** is shown in Scheme 3-19. The silyl ether **296** and potassium hydride **467** are likely in equilibrium with **280**. Hydrogen abstraction from **280** by a radical species would lead to the proposed single electron donor **281**. Upon single electron transfer from **281** to a substrate molecule, the silyl ether **296** would be regenerated. This outlined sequence shows that **281** can be accessed from **296**, in principle. A sufficiently strong hydride reagent is required as well as a source of radicals. Following the outlined scheme, it may be possible to use catalytic amounts of **296**. Thereby, a very similar system to the concept presented in Chapter 2 would be obtained. Using **296** in a catalytic sense would provide strong evidence for the intermediate **281**.

A separate line of investigation may aim at identifying silylated intermediates from reduction reactions with the KO*t*Bu-Et_3SiH reagent system. A candidate is **577** as the likely precursor of **518** (Scheme 3-20). The study of the interplay of reductive pathways and silylation of anionic intermediates may culminate in the reduction of molecular nitrogen. Species such as **578** or **579** are obvious products of the potential nitrogen reduction reaction. They would give rise to ammonia or hydrazine upon work-up.

4. Concerted vs. Stepwise S_NAr Mechanism

4.1. Background

As detailed in Chapter 1.6, the classical stepwise mechanism of the S_NAr reaction appears to be not the only possible mechanism. Over the last decades, more and more reports accumulated in the literature that suggested certain S_NAr reactions follow a concerted pathway. These days, the combined impact of these investigations has reached a critical momentum. It seems appropriate to fundamentally question the long established mechanistic picture of the S_NAr reaction.

Probing the mechanism of the S_NAr reaction is challenging, however. Experimentally, complex structure-activity relationship studies need to be performed. This approach has been followed by Williams et al. in several thorough studies.[167-170,236,237] Although the concept behind these studies is elegant and intuitive, it becomes apparent that the approach is limited to certain suitable model systems. With computational tools, in contrast, it is straightforward to determine the energy profile of any imaginable S_NAr reaction. However, the question arises whether the computational method is reliable.[177] Many claims of concerted S_NAr reactions in the literature were based on DFT calculations but only rarely was the validity of the method established.

Because of these challenges, the exact nature of the S_NAr mechanism has only been investigated for isolated examples. A coherent picture of when S_NAr reactions follow a stepwise or a concerted mechanism has not yet been drawn. The aim of the work presented in this chapter was two-fold. First, a reasonable computational model was established that allowed the mechanism of a given S_NAr reaction to be classified as either stepwise or concerted. Based on that model, trends were then identified of what types of S_NAr reactions follow which mechanistic pathway.

4.2. The Transition from a Stepwise to Concerted S_NAr Mechanism

4.2.1 Concept

Computationally, the energy profile of any S_NAr reaction can be established. This allows us to classify S_NAr reactions based on their mechanism - concerted or stepwise. To go further and to establish trends, the reactions need to be parametrised. Broadly speaking, one expects a S_NAr reaction to depend on three intrinsic components: the nucleophile, the leaving group and the aromatic system. There are numerous parameters that would allow any of these three aspects to be described. For the description of the aromatic system, a particularly intuitive and widespread measure exists - the Hammett substituent constants. In fact, Hammett

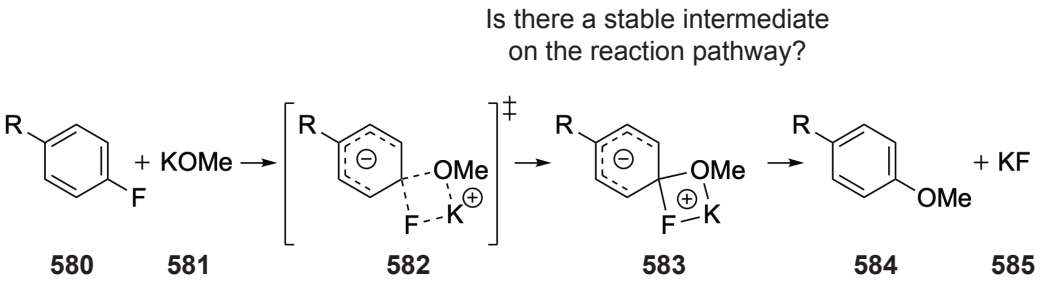

Mechanims	stepwise S_NAr			concerted S_NAr	
-R	-CN	-COMe	$-CO_2Me$	$-CF_3$	-CCH
σ_p^-	1.00	0.84	0.75	0.65	0.53

Figure 4-1 Illustration of the concept based on a simple S_NAr model reaction [M06-2X/6-311++G(d,p)/cpcm(DMF)].

correlations have been applied to S_NAr reactions in many instances and, usually, a good linear regression was observed (Chapter 1.6). Here, instead of analysing the slope of the linear regression, it was examined whether there is a sharp turning point from a stepwise to a concerted mechanism as the aromatic systems becomes more electron-rich (i.e. the ring substituents become less electron-withdrawing - this corresponds to a less positive value of the σ_p^- substituent constant). The Hammett σ_p^- substituent constant was chosen because it was demonstrated previously that the activation energies of S_NAr reactions show good correlation with that parameter.[171, 173] Moreover, a sharp mechanistic turning point on the σ_p^- scale has previously been reported for one single class of S_NAr reactions (Chapter 1.6).[182] The values of the σ_p^- constants were taken from the landmark review by Hansch et al.[238] A selection of *para*-substituents and their associated σ_p^- constants can be found in Table S30 (Chapter 5.5.2).

To establish a proof of concept - and to illustrate the idea - the S_NAr displacement of fluoride in *para*-substituted fluorobenzenes **580** with potassium methoxide **581** was investigated (Figure 4-1). Based on the M06-2X/6-311++G(d,p) level of theory it was observed that a transition from a stepwise to a concerted mechanism occurs if the *para*-substituent becomes less electron-withdrawing than the carbomethoxy ester group. An intermediate **583** was found after the transition state **582** for the examples with -R = -CN, -COMe, and $-CO_2Me$. For the examples with -R = $-CF_3$ and -CCH, instead, the collapse of the transition state **582** led directly to the formation of the products **584** and **585**. The mechanistic turning point can be conveniently described numerically based on the σ_p^- substituent constants. To do so, one can consider the least electron-withdrawing substituent for which the reaction still follows a stepwise energy profile and the most electron-withdrawing substituent for which the reaction still follows a concerted energy profile. Then the average of the two substituent constants is calculated (Equation 4.1). In this equation $\sigma_{p,1}^-$ is the Hammett parameter of the most electron-withdrawing substituent where the S_NAr reaction still follows a concerted pathway and $\sigma_{p,2}^-$ is the Hammett parameter of the least electron-withdrawing substituent for which the reaction still follows a stepwise mechanism. This value $\Delta\sigma_p^-$ gives an estimate for how sharply the mechanistic turning point is projected onto the Hammett σ_p^- scale.

$$\Delta\sigma_p^- = \frac{\left(\sigma_{p,1}^- - \sigma_{p,2}^-\right)}{2}$$ Equation 4.1

The turning point itself can be expressed by introducing the value τ (Equation 4.2) where $\sigma_{p,2}^-$ is the substituent constant for the most electron-withdrawing residue where the S_NAr reaction still proceeds via a concerted mechanism.

$$\tau_p^- \equiv \sigma_{p,2}^- + \Delta\sigma_p^-$$ Equation 4.2

Accordingly, the turning point found for the S_NAr reaction in Figure 4-1 can be quantified as $\tau_p^- = 0.70 \pm 0.05$.

These preliminary results indicate that for a given combination of nucleophile, leaving group and aromatic system, a τ_p^- value can be identified where the S_NAr mechanism changes from stepwise to concerted. This allows for a simple and intuitive discussion of the boundary between the two mechanistic domains. However, before venturing into a broader computational survey of S_NAr reactions, it is critical to validate the used method.

4.2.2 Computational Model

The computational model was chosen and validated by comparing the performance of a variety of DFT functionals against the results of a high-level wavefunction-based method for a test-set of S_NAr reactions. A satisfactorily well performing functional was identified for the further study of S_NAr reaction mechanisms.

Benchmarking

The S_NAr reaction from Figure 4-1 was used as a test case to identify a DFT functional that would predict the mechanistic turning point on the Hammett σ_p^- scale reliably (Figure 4-2). To establish a benchmark result the energy profiles of the four model reactions were calculated with the second-order Møller-Plesset perturbation theory method MP2. MP2 is a wave-function based method and was the most reliable method that was affordable in terms of computational resources (memory requirements and time) for the studied system (number of atoms, electrons, and size of the basis set). The method predicted a sharp turning point for the S_NAr mechanism from stepwise to concerted with $\tau_p^- = 0.92 \pm 0.08$. Importantly, the result was the same if either basis set, 6-311++G(d,p) or aug-cc-pVTZ, was used.

A number of DFT functionals was then applied to the same S_NAr model reactions. For all DFT calculations the 6-311++G(d,p) basis set was used. In Figure 4-2 the DFT functionals were clustered into four groups: hybrid functionals based on Becke's three parameter and/or Lee-Yang-Parr functional, members from the Minnesota family, representatives of the Perdew-Burke-Ernzerhof functional class, and methods derived from Becke's B97 functional.

None of the tested DFT methods was able to reproduce the MP2 result exactly and to predict the same mechanistic turning point. Most functionals, however, gave a result that was satisfactorily close to the MP2 result. Three functionals predicted a mechanistic turning point that was two increments or more ($\Delta\tau_p^- \geq 0.22$) away from the MP2 turning point. Importantly, from

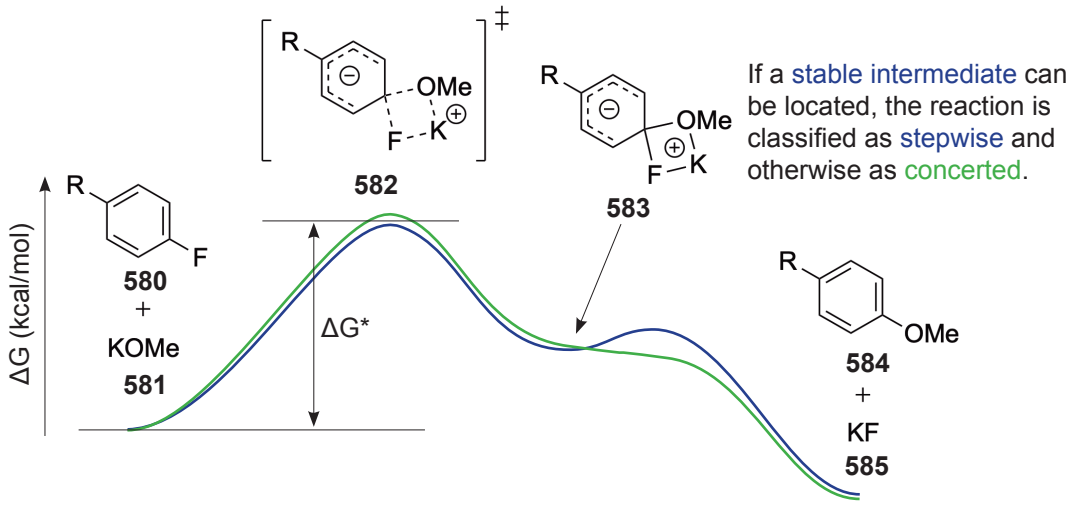

		MP2		B3 and LYP					Minnesota				PBE			B97			
Method		MP2[a]	MP2	B3PW91	B3LYP	B3LYP-D3(BJ)	CAM-B3LYP	BHandHLYP	M06L	M06	M06-2X	M11	PBE0	PBE0-D3(BJ)	HSE1PBE	B97D	ωB97	ωB97X	ωB97XD
-R	σ_p^-																		
$-NO_2$	1.27				s	s						s							
$-COCF_3$	1.09	s	s	s	s	c	s	s	s	s	s	s	s	s	s	c	s	s	s
-CN	1.00	s	s	c	c	c	c	c	c	c	s	c	c	c	c	c	c	c	c
-COMe	0.84	c	c	c	c	c	c	s	c	s	s	c	c	s	c	c	s	c	c
$-CO_2Me$	0.75	c	c	c	c	c	c	c	c	c	s	c	c	c	c	c	c	c	c
$-CF_3$	0.65										c								
-CCH	0.53										c								
Result (Y/N)				✓	✓	✗	✓	✗	✓	✗	✗	✓	✓	✗	✓	✗	✗	✓	✓

Figure 4-2 The mechanistic transition point on the Hammett σ_p^- scale was calculated with a number of different methods in order to identify a suitable DFT functional. For all tested methods, the 6-311++G(d,p) basis set and cpcm solvent model for DMF was used, unless mentioned otherwise. 's' stands for 'stepwise SNAr mechanism', 'c' stands for 'concerted S_NAr mechanism'. [a] The aug-cc-pVTZ basis set was used.

the investigated functionals, the widely used functional B3LYP with D3-dispersion correction - B3LYP-D3(BJ), as used, for example, by Jacobsen et al.[178] - and the M06-2X functionals were among the worst-performing ones.

Four functionals were not able to predict the mechanistic turning point as sharply as the MP2 method, i.e. they produced an alternating pattern of concerted and stepwise mechanisms as the electronic nature of the *para*-substituent changes. These were the BHandHLYP, M06, PBE0-D3(BJ) and ωB97 functionals. These were consequently ruled out as suitable functionals for the following study.

As an additional measure of the performance of the DFT functionals, their ability to correctly

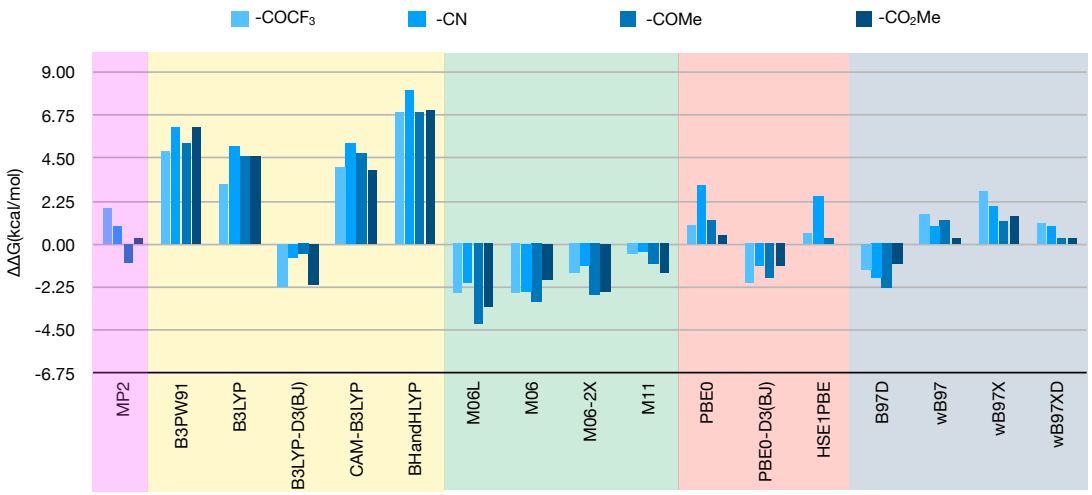

Figure 4-3 The activation energy of the rate limiting step of the S_NAr reaction from Figure 4-2 has been calculated by different DFT methods. For all tested methods the 6-311++G(d,p) basis set and cpcm solvent model for DMF was used. The deviation of these results from the MP2/aug-cc-pVTZ reference calculation is shown.

Table 4-1 Statistical Evaluation of the Functional Performance

Method	STD	MSD	MAD	Absolute Max. Deviation
ωB97XD	0.74	0.64	0.64	1.09
M11	0.96	-0.85	0.85	1.49
ωB97	1.11	1.00	1.00	1.56
MP2[a]	1.17	0.53	1.02	1.89
HSE1PBE	1.31	0.85	0.85	2.55
PBE0-D3(BJ)	1.58	-1.53	1.53	2.04
B3LYP-D3(BJ)	1.59	-1.38	1.38	2.19
B97D	1.67	-1.59	1.59	2.31
PBE0	1.75	1.46	1.46	3.05
ωB97X	1.97	1.87	1.87	2.78
M06-2X	2.03	-1.93	1.93	2.63
M06	2.52	-2.48	2.48	3.01
M06L	3.09	-2.99	2.99	4.13
B3LYP	4.41	4.35	4.35	5.15
CAM-B3LYP	4.53	4.50	4.50	5.29
B3PW91	5.64	5.61	5.61	6.15
BHandHLYP	7.25	7.23	7.23	8.10

The table gives a more detailed analysis of the results shown in Figure 4-3. STD: standard deviation; MSD: mean signed deviation; MAD: mean absolute deviation. The functionals are colour-coded according to their ability to predict the mechanistic turning point τ satisfactorily (see Figure 4-2). [a] The same basis set - 6-311++G(d,p) - was used as for the DFT methods.

reproduce the activation energy of the rate limiting step was investigated. As reference values, the MP2/aug-cc-pVTZ results were taken. The results are shown in Figure 4-3 and Table 4-1. The MP2 method with the smaller 6-311++G(d,p) basis set still gave a result that is reasonably close to the MP2/aug-cc-pVTZ result. The B3 and LYP-based assembly of functionals in general seriously overestimated the activation energy. Only when dispersion correction was included [B3LYP-D3(BJ)] was a close reproduction of the MP2 reference results achieved. The members of the Minnesota functional family all underestimated the activation energy. The M06-2X functional showed a standard deviation close to 2 kcal/mol, while the range-separated hybrid functional M11 showed a standard deviation of less than 1 kcal/mol. The functionals in the PBE0 and B97 group all showed good to excellent performance.

In conclusion, from the nine DFT functionals that were found to predict the mechanistic turning point τ satisfactorily well (see Figure 4-2), four also gave a good prediction of the rate limiting energy barrier with a standard deviation of < 2 kcal/mol. Overall, the M11 and ωB97XD functionals were the two top-runners and the more modern M11 functional was selected for the further study.

The method to test for the presence of a Meisenheimer intermediate so far was to start an optimisation from the transition state geometry that was slightly distorted along the imaginary mode. The optimisation can either converge to a Meisenheimer intermediate or directly to the product complex. Although experience showed that this method is able to detect very shallow local minima on the potential energy surface, it was necessary to establish its validity for the situation at hand. The question of particular concern was whether this method might fail to detect very fleeting Meisenheimer intermediates.

The mechanistic classification based on the M11 functional from Figure 4-2 was expanded by one example and validated by internal reaction coordinate (IRC) scans (Table 4-2). For the three reactions that were found to follow a concerted mechanism, the second transition state (elimination of the fluoride leaving group) was identified. IRC scans were performed starting from the rate limiting transition states. For the stepwise reaction with -R = -$COCF_3$ the IRC scan identified the Meisenheimer intermediate as a local minimum on the potential energy surface. This is in accordance with the initial classification of this example as a stepwise S_NAr reaction. Also, for the three concerted reactions where no intermediate was detected during the optimisation of the transition state structure towards the product complex, an IRC scan was performed. In the case of the reaction with -R = -CN and -R = -COMe, the IRC scan located an intermediate that apparently corresponds to a Meisenheimer intermediate. A frequency calculation identified the intermediate structure for the -R = -CN example as a true minimum. This was not the case for the structure with -R = -COMe (imaginary modes were found in the frequency calculation). Any attempt to identify a transition state for the expulsion of the fluoride leaving group from these two hypothetical intermediate structures failed. Bond scans were performed with a step size of 0.00125 Å to search for a candidate structure for the transition state, but no maxima along the expected reaction coordinate were found in either case. Hence, the stationary points found by the IRC scan for these two examples are better described as inflection points rather than as true local minima on the potential energy surface. For the example with -R = -CO_2Me, the result from the IRC scan is in agreement with the initial classification of the reaction.

It can be concluded that the approach of optimising a transition state geometry towards the product complex is a sufficiently sensitive method for finding Meisenheimer intermediates. The

Table 4-2 Validation of the Method for the Classification of the Reaction Mechanism

-R	σ_p^-	Mechanism[a]	Int1[b]	IRC[c]	TS2[d] (kcal/mol)
$-NO_2$	1.27	stepwise	yes	-	1.61
$-CHC(CN)_2$	1.20	stepwise	yes	-	3.01
$-COCF_3$	1.09	stepwise	yes	MI	1.37
-CN	1.00	concerted	no	MI	not found[f]
-COMe	0.84	concerted	no	(MI)[e]	not found[f]
$-CO_2Me$	0.75	concerted	no	PC	-

[a] As classified in Figure 4-2.

[b] The result is 'yes' if the optimisation from the transition state structure converged to a Meisenheimer intermediate and 'no' if it converged directly to the product complex.

[c] An internal reaction coordinate (IRC) scan was performed, starting from the rate limiting transition state TS1 in forward and reverse direction, until a stationary point was found. The result is 'MI' if a stationary point was found that corresponds to a Meisenheimer intermediate and 'PC' if the scan ran in the forward direction directly to the product complex.

[d] The energy barrier of the second transition state is given relative to the Meisenheimer intermediate.

[e] Imaginary modes were found in a frequency calculation for the stationary point structure identified by the IRC.

[f] Bond scans were performed with a step size of 0.00125 Å to search for a candidate structure for the transition state, but no maxima along the expected reaction coordinate were found.

method has the advantage over IRC scans that it is computationally more effective and does not falsely classify very flat regions on the potential energy surface as intermediates. Indeed, the results from the IRC scans demonstrated that the potential energy surface of S_NAr reactions close to the mechanistic turning point is - not surprisingly - very flat.

Comparison to Literature Reports

In addition to benchmarking the DFT functionals against the results from high-level ab initio calculations (i.e. the MP2 results), their predictions were compared with experimental data. First, the activation energy as calculated by the M11/6-311++G(d,p)/cpcm method was compared to the activation energy measured experimentally for one example[239] (Scheme 4-1). The predicted activation energy deviated by only 1 kcal/mol from the experimental[239] value. This result gives additional confidence in the DFT method. However, it is not the accurate determination of barrier heights that is crucial for the study ahead, but the correct prediction of the existence or absence of a Meisenheimer intermediate in the reaction pathway.

There is very limited purely experimental - and at the same time convincing - evidence for concerted S_NAr mechanisms in the literature for reasons explained in the introduction (Chapter 1.6). Williams et al. made the most substantial contribution to the field in this respect.[167, 168, 169, 170] Therefore it was an obvious step to calculate energy profiles for some of the reactions, which Williams et al. suggested to proceed via a concerted mechanism. The displacement of

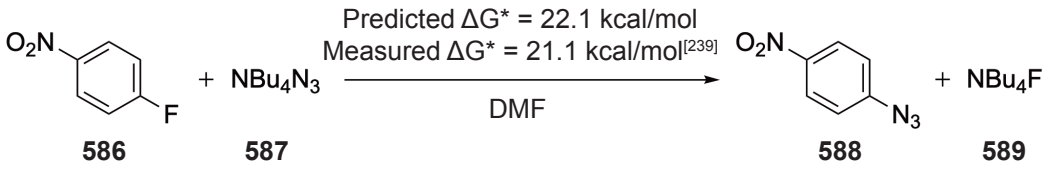

Scheme 4-1 Comparison of predicted and measured activation energy. The mechanism was found to be stepwise. Level of theory: M11/6-311++G(d,p)/cpcm(DMF).

phenolates **594** from a triazine-derivative **590** with amine nucleophiles **591**[169] was chosen as a reference case (Table 4-3). In apparent contradiction to the claim of these reactions to be concerted,[169] a Meisenheimer intermediate was identified for all examined cases. The energy of the Meisenheimer intermediate (MI) is given with respect to the substrate complex formed between **590** and **591**. The transition state energies are given with respect to the Meisenheimer intermediate and are of major concern for the following discussion.

The reaction was performed in an aqueous solvent system of water-dioxane 9:1.[169] There are no parameters available to model this solvent system directly. As a reasonable approximation, the solvent model for water was chosen in the calculation.

The displacement of phenolate **594a** with DMAP as the nucleophile showed a kinetically very short-lived Meisenheimer intermediate **592a** (Entry 1). The relative barrier for the expulsion of the phenolate leaving group **594a** equals 1.15 kcal/mol. To assess the effect of explicit solvation, four water molecules were included in the calculation of the energy profile of this reaction (Entry 2). The effect of these additional molecules on the energy profile was moderate. The relative energy of the Meisenheimer intermediate slightly increased. Also, the intermediate became slightly more stable with an energy barrier for the expulsion of the leaving group **594a** being 2.24 kcal/mol instead of 1.15 kcal/mol. This result shows that explicit solvation does not have a critical effect on the energy profile of this reaction.

Only moderate changes in the energy profile were observed with the two other phenolate leaving groups **594b** and **594c** (Entries 3 and 4). When going from DMAP to the morpholine nucleophile, the rate limiting step changed from the addition of the nucleophile (TS1) to the expulsion of the leaving group (TS2) (Entries 5 and 6). Still, the kinetic stability of the Meisenheimer intermediate was very low. The energy barrier is less than 2 kcal/mol for the decay of this intermediate to the substrate complex.

The computational results stand in apparent contradiction to the interpretation of the kinetic studies that were performed by Williams et al. for this class of S_NAr reactions.[169] Closer inspection of the computational results showed, however, that in the majority of cases the relative stability of the Meisenheimer intermediate is lower than 2 kcal/mol - thus below the typically accepted threshold of chemical accuracy.[166] In that sense, the computational results support the interpretation of Williams' kinetic data. Following conventional experimental approaches, these S_NAr reactions appear to proceed via a concerted mechanism. With computational tools, however, it is possible to detect much shallower minima on the potential energy surface than with conventional experiments. Thereby, a reaction that appears to be concerted in the experiment can correctly be revealed to exhibit fleeting intermediates along its path.

Table 4-3 Energy profiles for S_NAr reactions where experimental evidence suggests a concerted mechanism.[a]

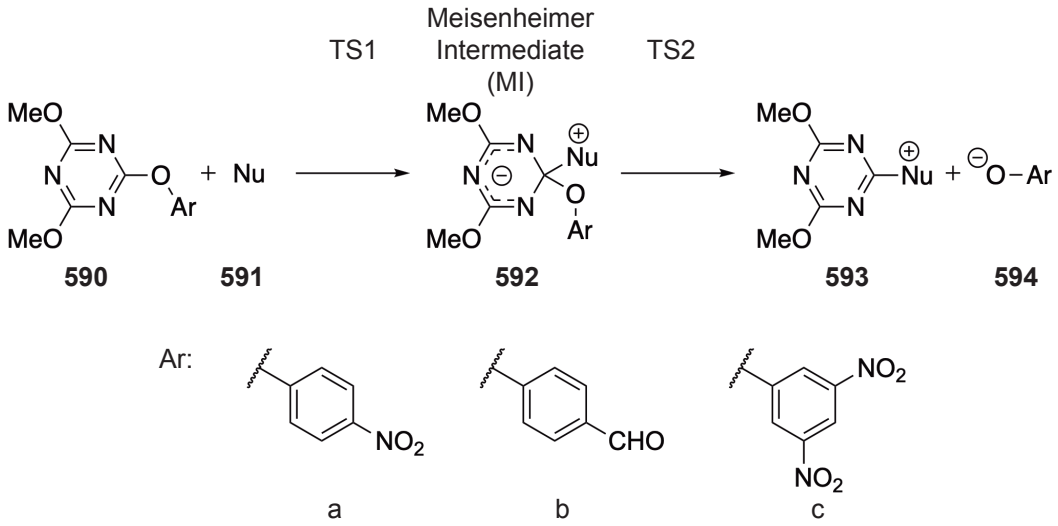

Entry	Nu	Ar	TS1 w.r.t. MI (kcal/mol)I[b]	MI[c] (kcal/mol)	TS2 w.r.t. MI (kcal/mol)[b]
1	DMAP	a	1.90	14.5	1.15
2	DMAP[d]	a	2.85	16.6	2.24
3	DMAP	b	2.19	15.0	1.89
4	DMAP	c	4.06	12.3	0.25
5	Morpholine[e]	a	1.31	11.7	6.38
6	Morpholine[e]	a	1.95	11.0	5.05

[a] Level of theory: M11/6-311++G(d,p)/cpcm(H_2O).
[b] Measured with respect to the Meisenheimer intermediate.
[c] Measured with respect to the substrate complex.
[d] Four explicit molecules of water were included in the calculation.
[e] The energy profiles with two different attack angles of the nucleophile were modelled for the same reaction.

4.2.3 Understanding the Mechanistic Transition Point of S_NAr Reactions

With a validated and efficient computational approach at hand, it became possible to systematically investigate when a S_NAr reaction follows a concerted and when a stepwise mechanism.

The Mechanistic Transition Point in Cross- and Identity-Displacement Reactions

To gain a broad overview of the two mechanistic domains, three classes of S_NAr reactions were investigated. These are the halide displacement with potassium methoxide (Figure 4-4), halide-halide exchange reactions (Table 4-4) and the analogous chalcogen-chalcogen exchange reactions (Table 4-5).

The displacement of four halides with potassium methoxide **581** from benzene-derived

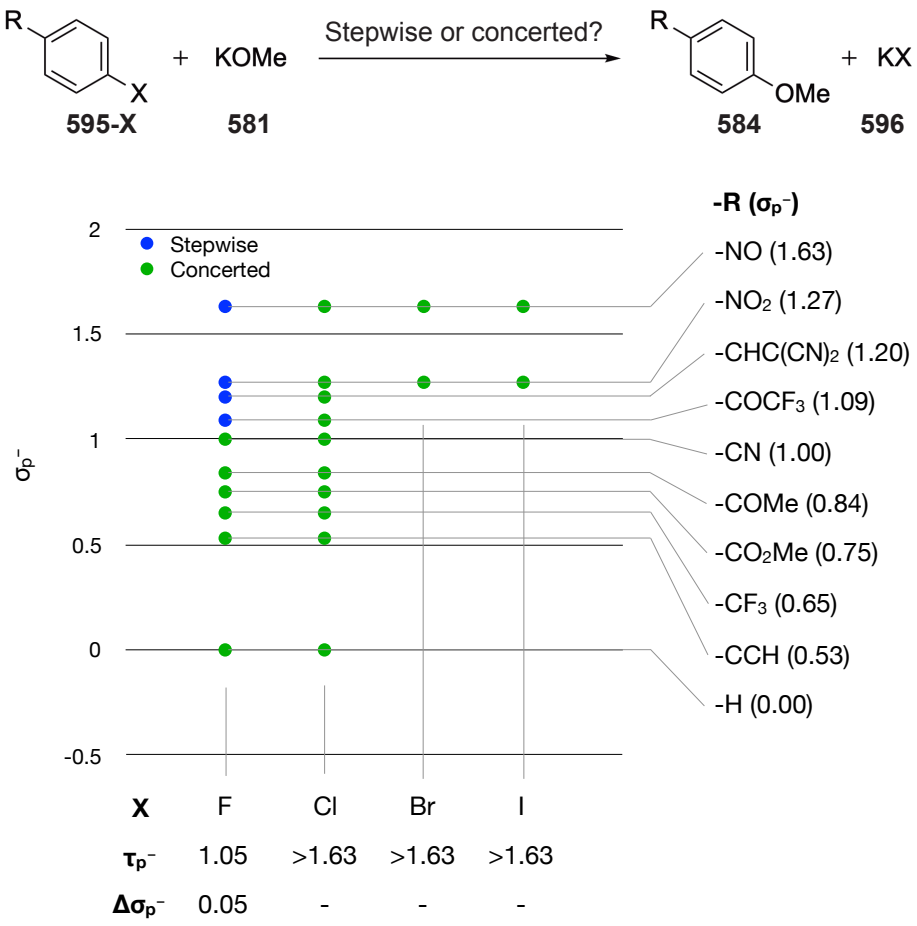

Figure 4-4 The mechanistic transition point for the halide displacement by potassium methoxide was investigated. Level of theory: M11/6-311++G(d,p)/cpcm(DMF).

substrates **595** was investigated (Figure 4-4). Only for the fluoride series was the mechanistic turning point identified, with τ_p^- = 1.05. (For the same series of reactions, the M06-2X functional gave τ_p^- = 0.70 in preliminary studies. Benchmarking the DFT functionals properly then showed that the M06-2X functional significantly underestimates the mechanistic turning point - see above.) For the displacement of chloride, bromide and iodide the mechanistic turning point could not be identified. These reactions all showed a concerted energy profile even with the most electron-withdrawing *para*-nitroso substituent that was included in the σ_p^- scale.

A similar picture was obtained for the halide exchange reactions (Table 4-4). Only for the fluoride identity reaction was a mechanistic turning point identified (τ_p^- = 0.59). For all other combinations of halides, a concerted energy profile was observed even for the examples with the *para*-nitroso substituent. Obviously the mechanistic turning point for these reaction series lies beyond the applied σ_p^- scale.

An analogous study to the halide exchange reactions was performed for the chalcogenide exchange reactions (Table 4-5). The nucleophilic displacement of the chalcogen residue in the substrate **597-X** by the potassium chalcogenide nucleophile **598-Y** served as a model system. In contrast to the halide exchange reaction, the mechanistic turning point for most of the chalcogen exchange reactions actually fell onto the applied σ_p^- scale. Clearly, the

Table 4-4 Halogen-Halogen Exchange Reactions

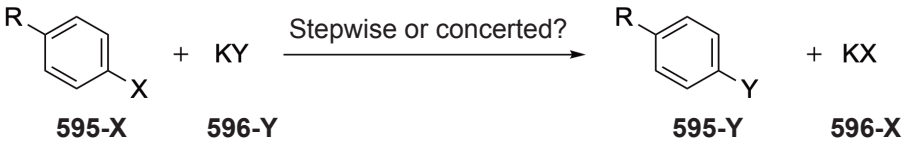

595-X **596-Y** **595-Y** **596-X**

τ_p^- values for the halogen-halogen exchange reactions

KY \ -X	-F	-Cl	-Br	-I
KF	0.59[a]	>1.63[b]	>1.63	>1.63
KCl		>1.63	>1.63	>1.63
KBr			>1.63	>1.63
KI				>1.63

[a] The S_NAr reaction mechanism changes from stepwise to concerted when going from the *para*-substituent -CF_3 (σ_p^- = 0.65) to -CCH (σ_p^- = 0.53).
[b] The *para*-nitroso substituent marks the upper limit (σ_p^- = 1.63) of the applied σ_p^- scale.

Table 4-5 Chalcogen Exchange Reactions

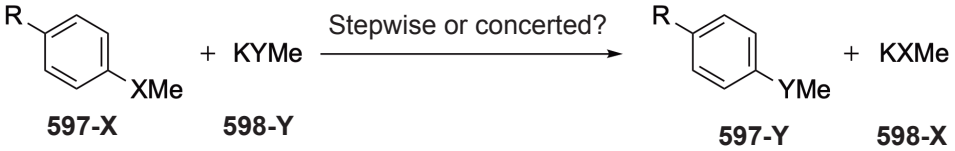

597-X **598-Y** **597-Y** **598-X**

τ_p^- values for the chalcogen-chalcogen exchange reactions

KYMe \ -XMe	-OMe	-SMe	-SeMe
KOMe	<-0.77[a]	0.27	0.64
KSMe		0.31	0.92
KSeMe			0.70

[a] The full set of the σ_p^- values that was used can be found in Table S30 (Chapter 5.5.2).

chalcogen-chalcogen exchange reactions have a much more pronounced tendency to proceed via a stepwise mechanism. In fact, the identity reaction of methoxide proceeded via a Meisenheimer intermediate even for the most electron-donating *para*-substituent that was investigated. With increasing atomic number of the chalcogens, the identity reaction showed a decreased tendency to proceed via a stepwise S_NAr reaction (i.e. the value of τ_p^- increases from <-0.77 for methoxide, to 0.31 for methanethiolate, to 0.70 for methaneselenolate). Likewise, the tendency of the displacement reaction of a methane chalcogenide by potassium

methoxide to follow a stepwise mechanism decreases with increasing atomic number of the displaced chalcogenide (i.e. the value of τ_p^- increases from <-0.77 for methoxide, to 0.27 for methanethiolate, to 0.64 for methaneselenolate).

Clearly, a concerted mechanism is favoured for the chalcogen exchange reaction by the participation of larger (i.e. softer) chalcogens. The analogous statement holds true for the halide exchange reaction. The halides chloride, bromide and iodide all strongly favour a concerted mechanism, either in the halide exchange reaction or in an exchange reaction with potassium methoxide. Only for the S_NAr reactions involving fluoride was a stepwise energy profile found to have significant importance. Because of this finding and because fluoride is the prototype leaving group for S_NAr reactions, the further discussion will focus mainly on S_NAr displacements of fluoride.

Effect of the Counter Cation and Explicit Solvation

So far, only the potassium cation has been considered as a counter cation in the examined model systems. The effect of the counter cation on the S_NAr mechanism was studied, based on the displacement of fluoride from **580** with different alkali metal methoxide salts **599** (Figure 4-5). As a general trend, the stepwise mechanism becomes more dominant with increasing

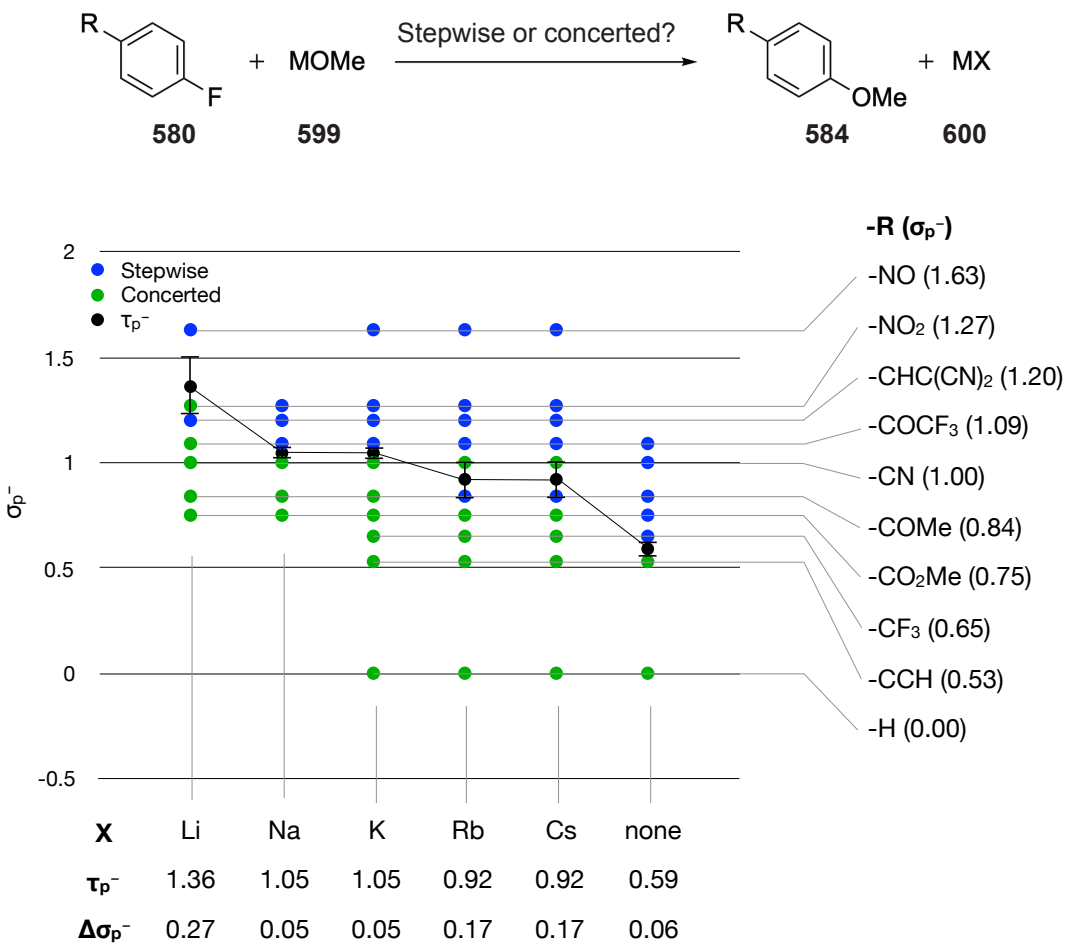

Figure 4-5 The mechanistic transition point for the displacement of fluoride by alkali metal methoxide salts was investigated. Level of theory: M11/6-311++G(d,p)/cpcm(DMF).

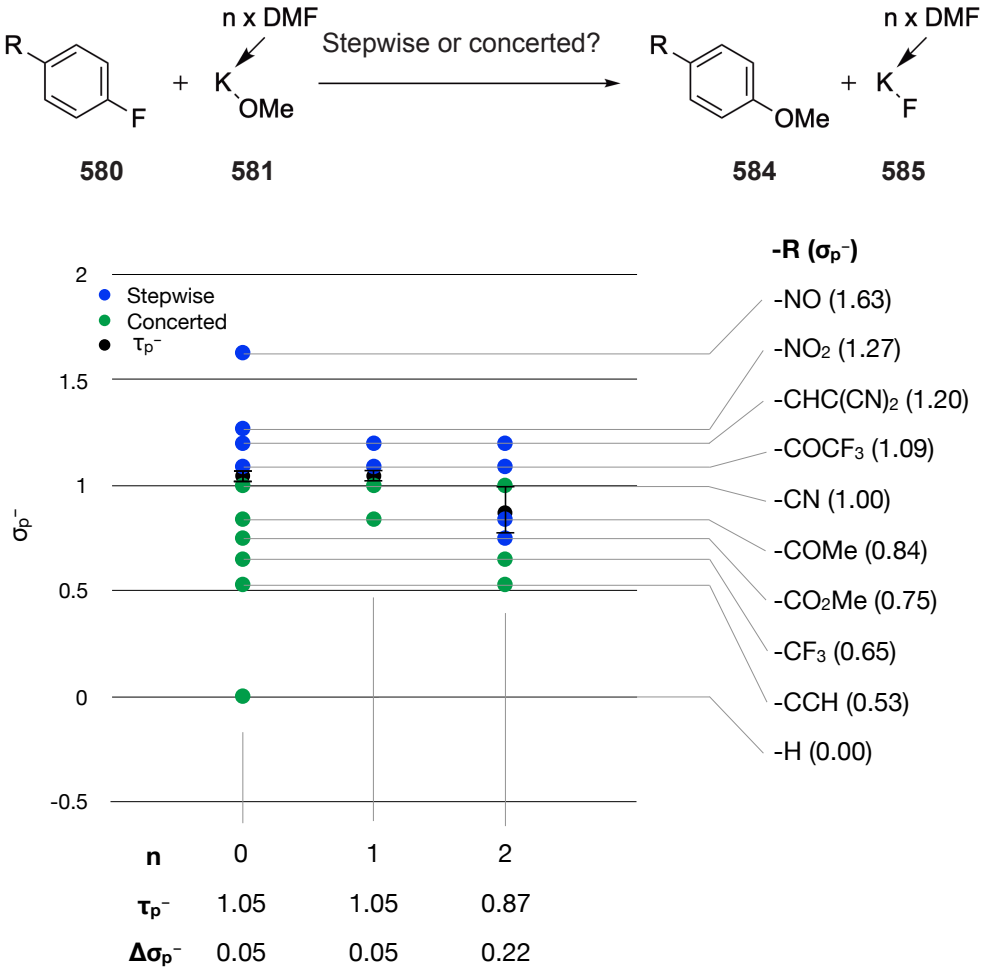

Figure 4-6 The effect of including explicit DMF solvent molecules coordinating to potassium on the mechanistic turning point was investigated for the displacement of fluoride with potassium methoxide. Level of theory: M11/6-311++G(d,p)/cpcm(DMF).

size of the counter cation, i.e. the value for τ_p^- decreases as the counter cation becomes softer. This trend culminates in the extreme case where no counter cation is present at all. Closer inspection of the data showed that there is no or only a small difference between the reactions with the cations sodium, potassium, rubidium and caesium. Only the boundary cases with lithium as a counter cation, on the one hand, and without a counter cation at all, on the other hand, show a pronounced change of the τ_p^- value.

There is an intuitive explanation for the observed trend. The better the counter cation can stabilise the negative charge on the fluoride leaving group, the more strongly a concerted reaction mechanism will be favoured. This observation is in agreement with the trend of decreasing lattice energy of alkali fluoride salts with increasing atomic number of the alkali cation (i.e. weaker bonding between the fluoride anion and the alkali metal cation).[240]

The ability of the alkali counter cation to coordinate to the leaving fluoride anion can have an effect on the mechanistic turning point as became apparent from the above discussion.

In order to refine the understanding of coordination effects, explicit solvent molecules were added to the computational model as ligands of the alkali metal cation (Figure 4-6). It was assumed that the ability of the counter cation to coordinate the fluoride leaving group may decrease if its coordination sphere gets increasingly saturated with other ligands. It was found that the addition of one explicit solvent molecule in the model system did not evoke any shift in τ_p^-. The addition of a second molecule of DMF led to a significant blurring of the mechanistic turning point, which manifests in an increase of $\Delta\sigma_p^-$ from 0.05 to 0.22. Also, the value τ_p^- decreased slightly by 0.18 units. However, since the mechanistic turning point is no longer sharp, it is not clear whether this decrease of τ_p^- is actually significant.

Overall, including explicit solvent molecules did not produce a dramatically different prediction of the mechanistic turning point. A similar observation has already been made in Chapter 4.2.2 (Table 4-3). Hence, relatively weakly coordinating ligands of the alkali metal cation do not seem to have a significant effect on the mechanistic turning point τ_p^-. This result also has practical implications. It suggests that relying on the implicit solvation model alone is a reasonable - and computationally much more effective - approximation.

Effect of the Nucleophile and the Aromatic System

Keeping the fluoride leaving group, the potassium cation and the aromatic core constant, the mechanistic turning point was investigated for different nucleophiles (Figure 4-7). It was found that potassium methanethiolate **601b**, potassium azide **601c** and the two carbon nucleophiles **601d** and **601f** all have the same mechanistic turning point τ_p^- as potassium methoxide. The only exception is the addition of nucleophile **601e** on **580**. This series of S_NAr reactions favours a concerted mechanism more (τ_p^- = 1.36) than the other investigated reaction series (τ_p^- = 1.05). Closer inspection of the geometries of the rate limiting transition states including nucleophile **601e** showed that steric repulsion may be at the heart of this pronounced tendency to follow a concerted mechanism (Figure 4-8). One of the hydrogen atoms of the phenyl group of the nucleophile approaches the plane of the aromatic system of **580 (R = NO_2)** as closely as 2.3 Å in the transition state. This steric clash makes a Meisenheimer intermediate less energetically favourable and pushes the reaction towards a concerted pathway. How steric effects can influence the mechanistic pathway of S_NAr reactions will be discussed in more detail later in this chapter. The average $\overline{\tau_p^-}$ over all six nucleophiles was 1.10 ± 0.12 for the substrate series **580**.

The observation that a number of very different nucleophiles showed the same mechanistic turning point was surprising. In order to investigate whether this observation is general, τ_p^- was calculated for two additional aromatic systems - **603** and **604** - and the nucleophiles **601a - d** (Figure 4-9 and Figure 4-10). For the pyridine series **603**, the variation of τ_p^- among the four nucleophiles **601a - d** was somewhat larger than in the benzene series. The average was slightly lower with a value of 0.93 ± 0.14. For the naphthalene series **604**, the three nucleophiles **601a - c** showed a similar value of τ_p^- with an average $\overline{\tau_p^-}$ of 0.77 ± 0.10. The nucleophile **601d**, in contrast, massively deviated from this average value. In fact, the S_NAr reaction with this nucleophile favoured a stepwise S_NAr reaction even with electron-donating substituents such as *para*-methyl or *para*-NHAc residues. Presumably, π-π-stacking interactions or steric effects between the nucleophile and the aromatic system lead to this pronounced difference to the other nucleophiles. Therefore the reaction series of **601d** with **604** was regarded as an anomaly and not included in the calculation of $\overline{\tau_p^-}$.

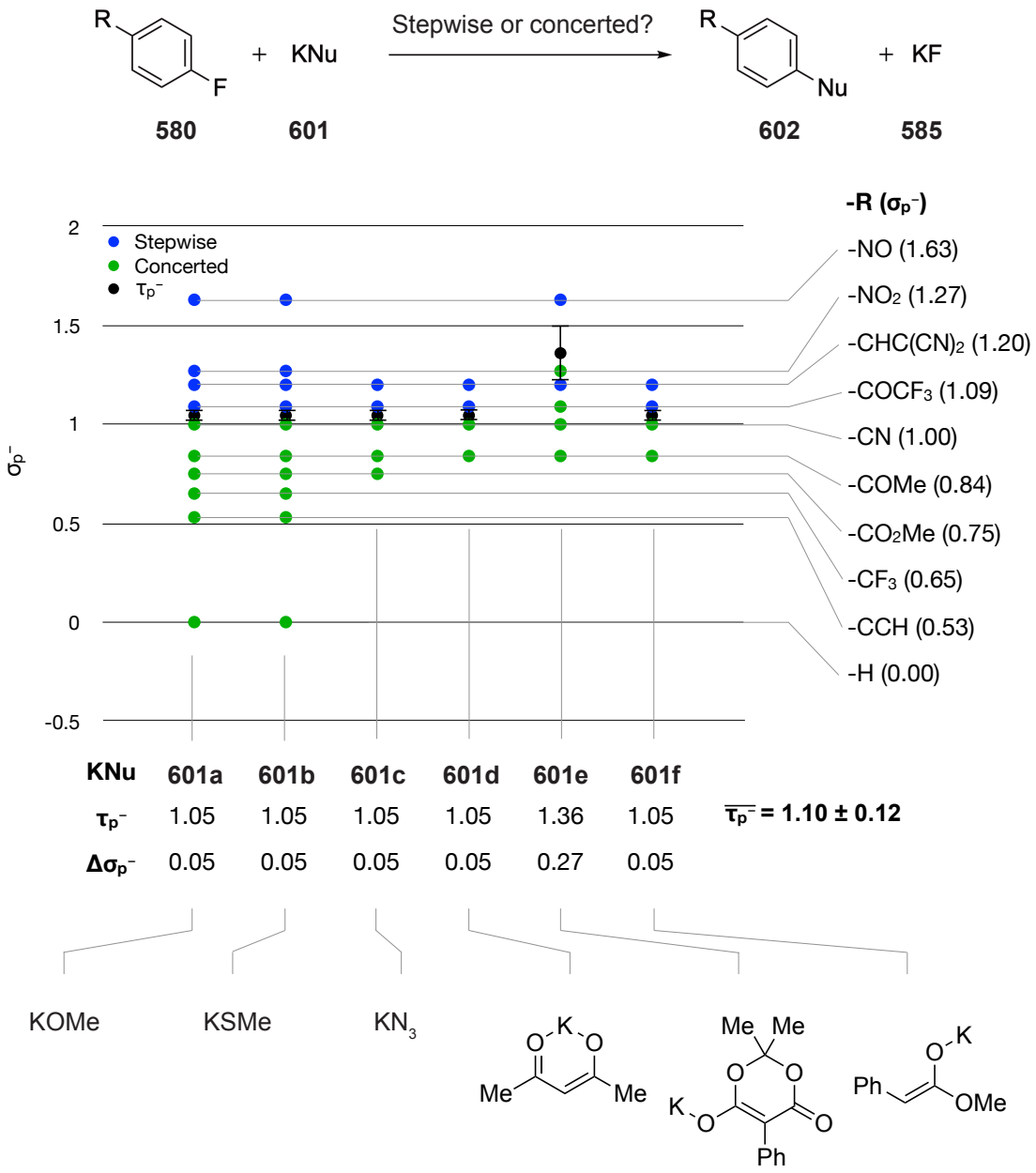

Figure 4-7 The mechanistic turning point was investigated for the S_NAr reaction of several different nucleophiles and *para*-substituted fluorobenzene **580**. Level of theory: M11/6-311++G(d,p)/cpcm(DMF).

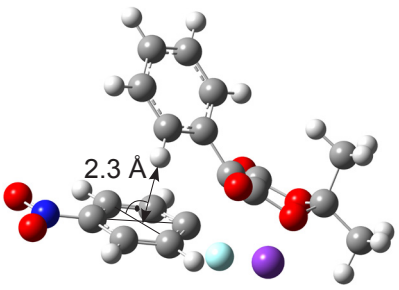

grey: carbon
white: hydrogen
red: oxygen
deep blue: nitrogen
light blue: fluorine
purple: potassium

Figure 4-8 Transition state for the S_NAr reaction between **580** (R = NO_2) and the nucleophile **601e**. Level of theory: M11/6-311++G(d,p)/cpcm(DMF).

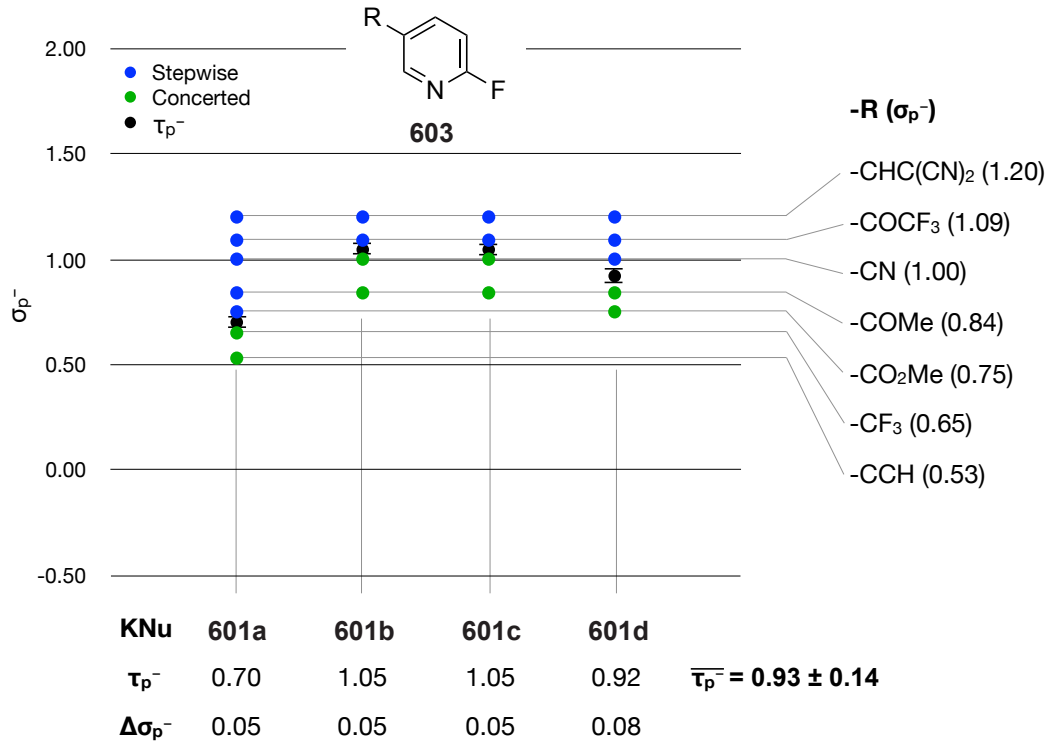

Figure 4-9 The mechanistic turning point was investigated for the S_NAr reaction of several different nucleophiles and 4-substituted 2-fluoropyridine **603**. Level of theory: M11/6-311++G(d,p)/cpcm(DMF).

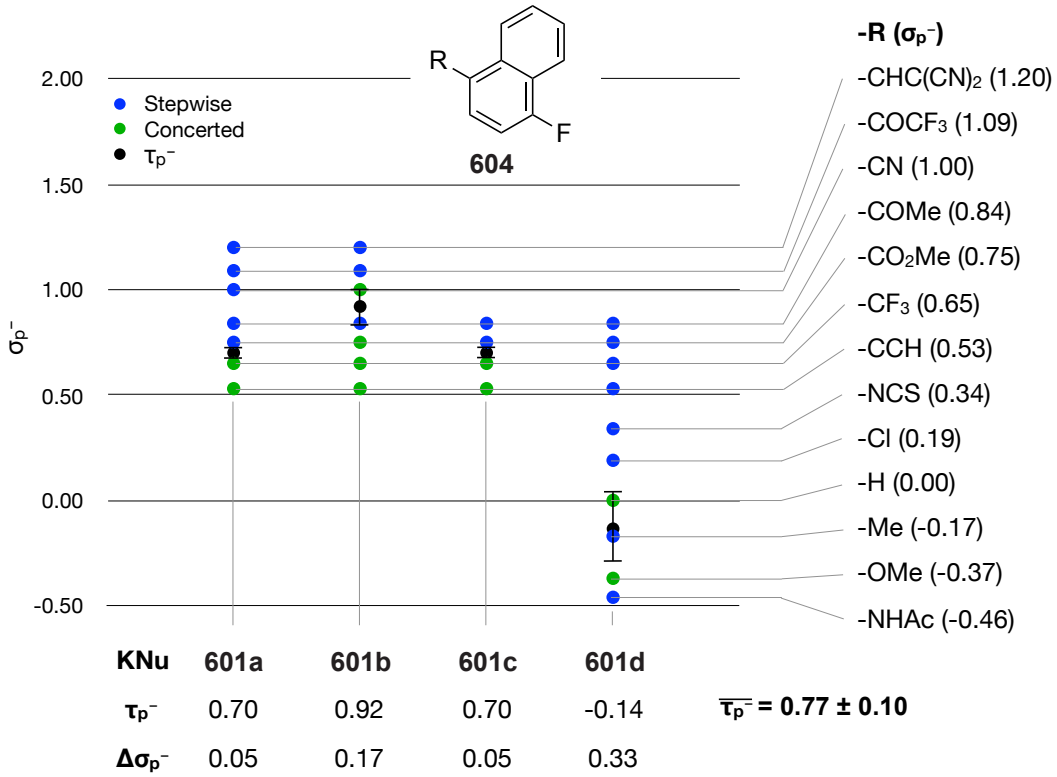

Figure 4-10 The mechanistic turning point was investigated for the S_NAr reaction of several different nucleophiles and 4-substituted 1-fluoronaphthalene **604**. Level of theory: M11/6-311++G(d,p)/cpcm(DMF).

With the exception of the reactions between **601d** and **604** it can be noted that there is relatively little variation between different nucleophiles attacking the same aromatic substrate, i.e. the observation made for the system **580** was essentially reproduced with **603** and **604**. The mechanistic turning point does not seem to depend on the nucleophile strongly, i.e. the value τ_p^- is mainly characteristic for the aromatic system (with a fluoride leaving group). Thus, in principle, it is sufficient to examine the mechanistic turning point with one nucleophile only to characterise the mechanistic preference of a given aromatic system.

When comparing the average $\overline{\tau_p^-}$ values of the aromatic systems **580**, **603** and **604** it was noticed that introducing a nitrogen atom in the ortho position of the ring (**603**) or extending the aromatic system (**604**) appeared to render a stepwise mechanism more favourable (i.e. $\overline{\tau_p^-}$ for **603** and **604** was lower than $\overline{\tau_p^-}$ for **580**). In order to understand whether this is just a random fluctuation or actually part of a trend, two additional series of S_NAr reactions were

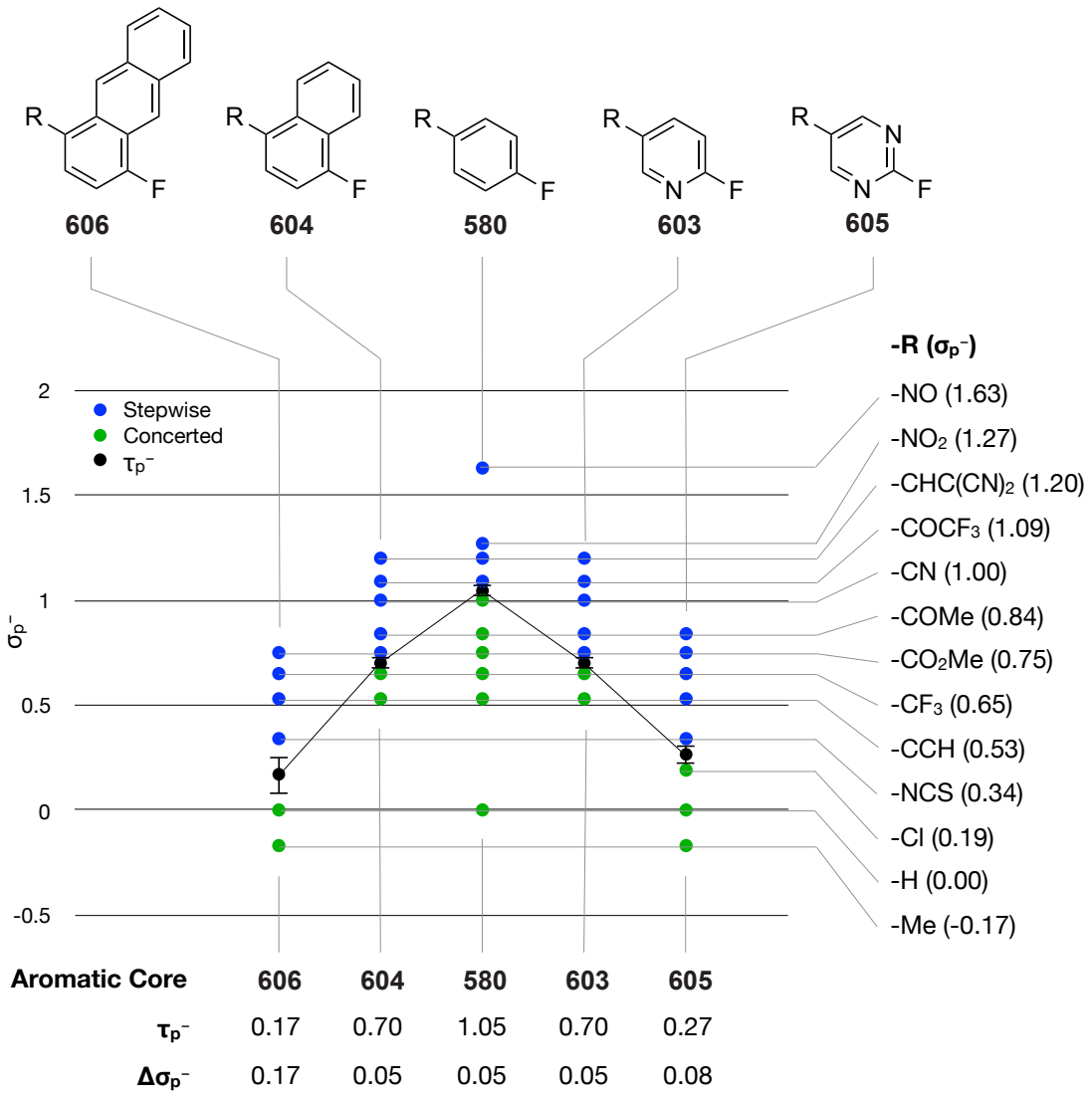

Figure 4-11 The mechanistic turning point was investigated for the S_NAr reaction of several different aromatic cores and the potassium methoxide nucleophile. Level of theory: M11/6-311++G(d,p)/cpcm(DMF).

investigated with potassium methoxide as the nucleophile and the aromatic systems **605** and **606** (Figure 4-11). It can be seen that a stepwise reaction profile became more favoured as either the aromatic system was extended (going from **580** to **604** to **606**) or nitrogen atoms were introduced (going from **580** to **603** to **605**). The effect of one additional fused benzene ring equalled approximately the effect of one additional nitrogen atom.

Both, an additional fused ring and a nitrogen atom in the ring, help to stabilise the negative charge that accumulates on the aromatic system during the addition of the nucleophile. The better the aromatic core on its own is able to stabilise this negative charge, the less the stabilisation of a (potential) Meisenheimer intermediate depends on the electron-withdrawing nature of the *para*-substituent.

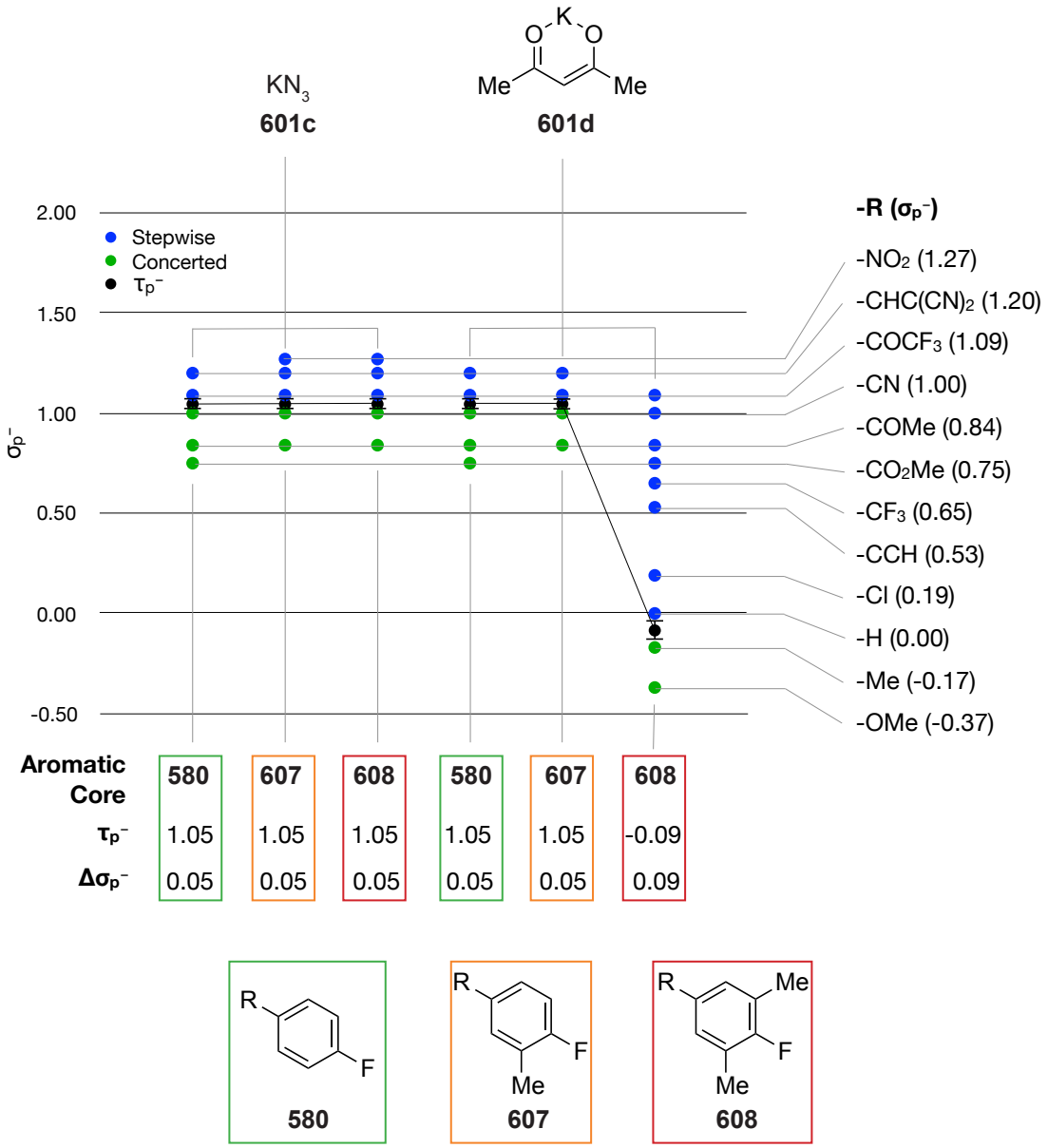

Figure 4-12 Steric effects on the S_NAr mechanistic turning point were investigated by comparing a slim with a bulky nucleophile. Level of theory: M11/6-311++G(d,p)/cpcm(DMF).

Steric Effects

For two cases so far, indication was found that, in addition to the electronic characteristics of the system, steric effects may influence the mechanistic turning point (see Figure 4-8 and Figure 4-10). From the above discussion, it also follows that the electronic nature of nucleophiles does not have a significant effect on τ_p^-. This allows us to investigate steric effects by choosing a bulky and a slim nucleophile. Any significant difference in τ_p^- between these two nucleophiles for the attack at the same series of substrates can then be attributed to steric effects.

Such a comparison was made for the nucleophiles **601c** and **601d** based on the aromatic substrates **580**, **607** and **608** (Figure 4-12). When going from **580** to **607** to **608**, the small nucleophile **601c** does not show any response to the increasing steric bulk and slightly more electron-rich aromatic core. The value τ_p^- remains constant throughout this series. With the sterically more bulky nucleophile **601d**, the situation is different. While there is no difference in τ_p^- between **601c** and **601d** for the substrates **580** and **607**, the value of τ_p^- sharply decreases for the reaction of **601d** when a second *ortho*-methyl group is present as in **608**.

This result shows that steric bulk on the aromatic system can force the S_NAr reaction to follow a stepwise mechanism even if a concerted reaction profile would be expected based on the electronic nature of the substrate. As follows from the combination of the nucleophile **601d** and the aromatic system **608**, the steric bias on the mechanism can be massive. The introduction of the second methyl group induced a larger change in τ_p^- than did the expansion of the aromatic core from benzene to anthracene, for example (Figure 4-11). While changes of the electronic nature of the aromatic system affect the S_NAr reaction of various nucleophiles approximately equally, steric changes affect mainly bulky nucleophiles like **601d**.

The Structure Activity Relationship

The slope of the Hammett correlation for series of S_NAr reactions was often used in the literature as an indicator for the nature of the mechanism. Usually a low value of the slope was considered characteristic of a concerted mechanism. As detailed in the introduction (Chapter 1.6), this line of reasoning is problematic.

In Figure 4-13, the linear correlation of the activation energy vs. σ_p^- for three reaction series is shown. The slopes of these correlations are directly proportional to the slope of standard Hammett correlations. Hence, conclusions based on a relative comparison are the same for either correlation - the activation energy vs. σ_p^- or the standard Hammett correlation. In general, the linear regression for the correlations shown in Figure 4-13 was satisfactory with a value of $R^2 \geq 0.90$. It can be seen that the reaction series of potassium methoxide with **595-F** and with **595-Cl** have a very similar slope. The mechanistic turning point τ_p^- for these two reaction series, however, is quite different (see also Figure 4-4). The reaction series of potassium azide with **595-F**, in contrast, has the same value of τ_p^- as the reaction series of potassium methoxide with **595-F** but the slopes of these two correlations are different (see also Figure 4-7). Obviously, there does not seem to be a connection between the slope of these correlations and the mechanistic preference of the S_NAr reaction series.

Next, the changes in the geometry of the rate-limiting transition states of the S_NAr displacement for the series **595-X** (for X = F, Cl) with potassium methoxide was analysed (Figure 4-14). It can be seen that the investigated distances and angles change in a very similar way between the two series (i.e. the slopes of the correlations of the four investigated parameters

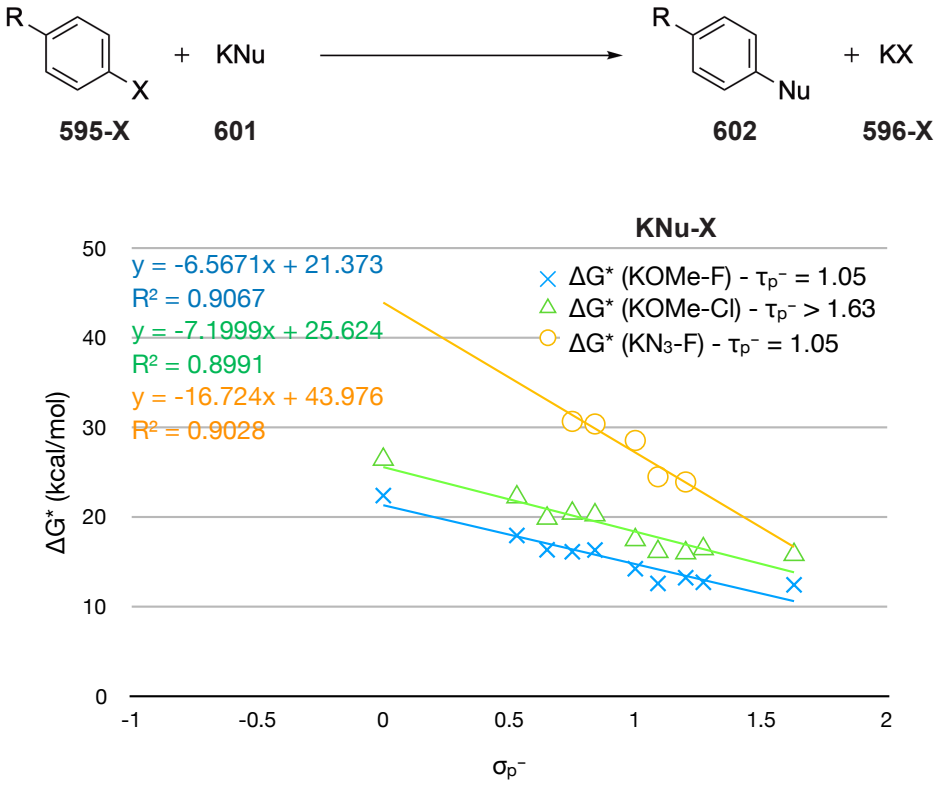

Figure 4-13 What information about the S_NAr mechanism is contained in the activation energy of the rate limiting transition state? Level of theory: M11/6-311++G(d,p)/cpcm(DMF).

are nearly the same). Further, also the absolute values of d_1, a_1 and a_2 are very similar (as expected, there is a large difference in the distance d_2 between the two series, which reflects the length difference {ca. 0.4 Å}[241] between the carbon-fluorine and the carbon-chlorine bond). Again, the change of mechanism from stepwise to concerted is not reflected in the change of any of the investigated parameters.

These observations underline the concerns that were raised in the Introduction regarding the mechanistic information - stepwise or concerted - that is contained in the slope of the Hammett correlation. It becomes evident that in general *the rate limiting step does not contain information about the nature of the S_NAr mechanism*. The mechanistic choice depends on the features of the kinetically more easily broken (or formed) bond. In light of this conclusion it makes perfect sense that the reaction series of different nucleophiles with the same aromatic system have roughly the same value of τ_p^- (see Figure 4-7). In all these apparently different reactions, the key step where the nature of the mechanism is decided is the same - the expulsion of the fluoride leaving group.

4.3. A Complex Case Study

The results of the previous section (Chapter 4.2) allow many S_NAr reactions in the literature to be identified that likely follow a concerted mechanism. A series of such reactions has been chosen for further investigations of the mechanism (Scheme 4-2).[242-244] The choice was

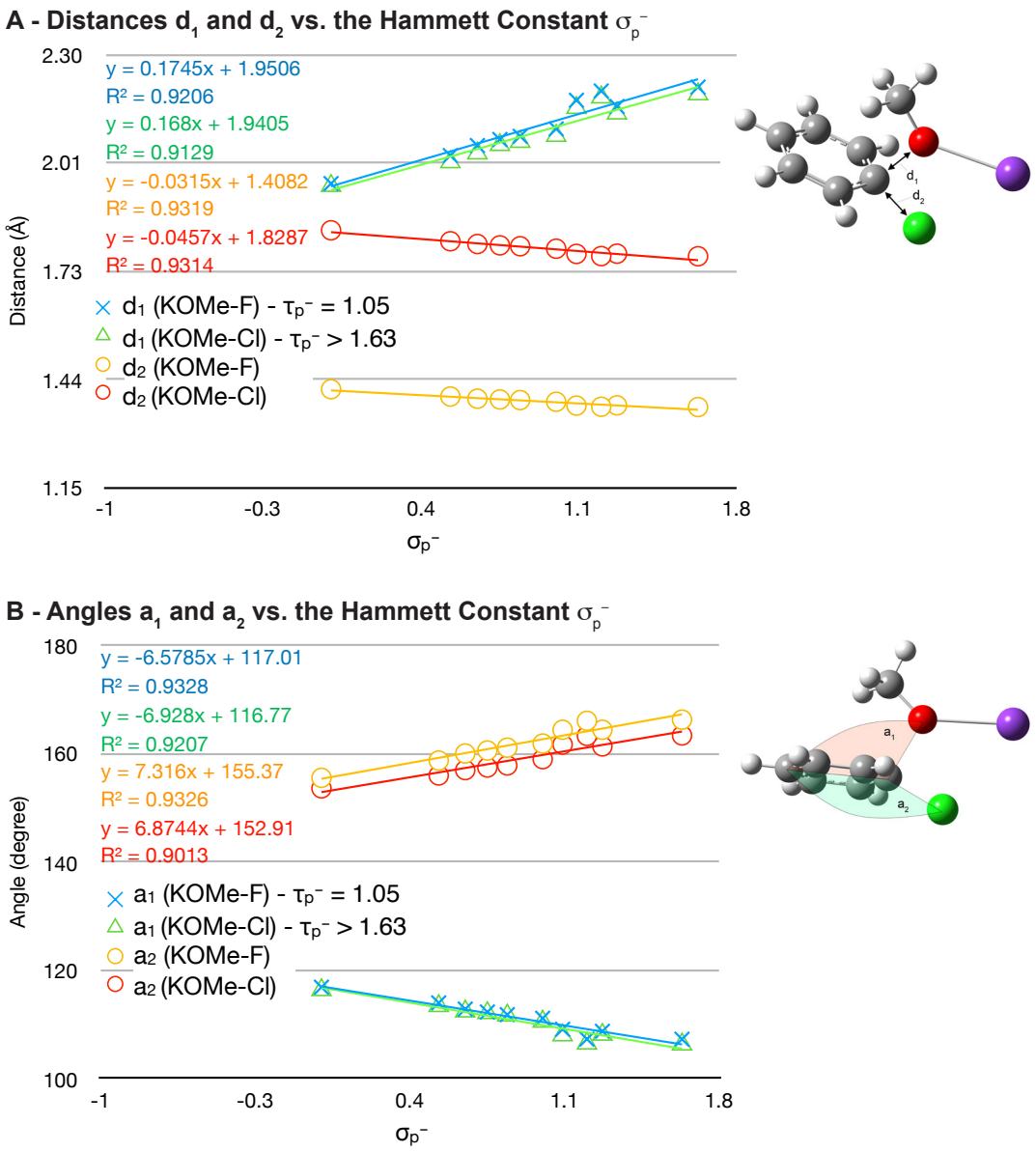

Figure 4-14 Geometry change of the transition state structure vs. the Hammett substitution constant σ_p^- for the displacement of fluoride and chloride with potassium methoxide in the series **595-X**. The distances and angles, which are measured, are illustrated based on the chloride example **595-Cl** with R = H. Level of theory: M11/6-311++G(d,p)/cpcm(DMF).

made based on three main criteria: 1) the mechanism is unknown, 2) the described transformations are potential examples of concerted S_NAr reactions and 3) are mechanistically intriguing as other reaction pathways may be accessible. A systematic investigation of the mechanisms of these reactions has not yet been published. Various candidate mechanisms have been considered possible such as a S_NAr pathway, BHAS-type mechanisms, $S_{RN}1$-type mechanisms or a mechanism including benzyne intermediates.[242- 244]

Due to the potentially complex nature of the mechanism of these reactions, it was decided to use the versatile M06-2X functional[245] that was also used in previous chapters. As expected, the S_NAr energy profile of all examples did not show a Meisenheimer intermediate, i.e.

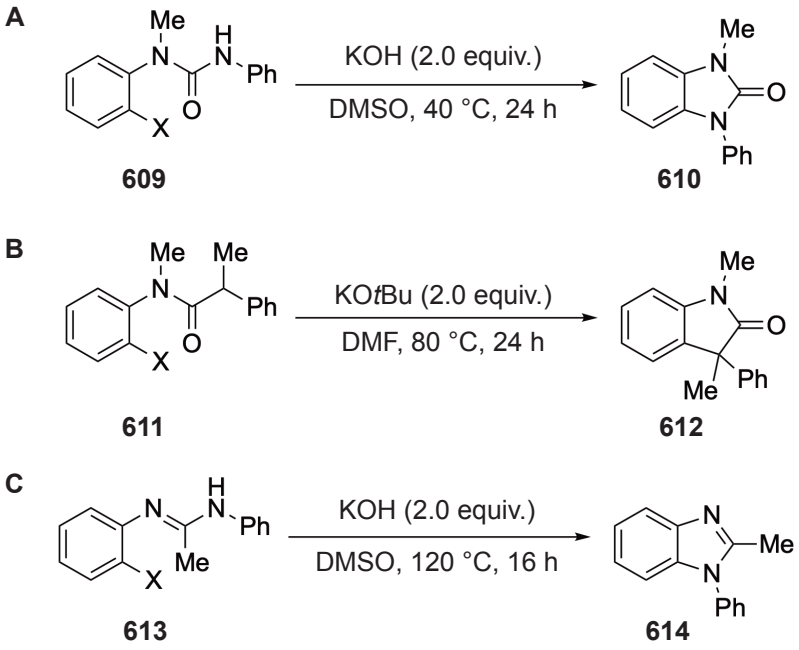

Scheme 4-2 Three transformations where the mechanism is unknown, intriguing and may potentially follow a concerted S_NAr pathway (A,[242] B,[243] C[244]).

the potential S_NAr reaction profiles were all concerted (Table 4-6). However, the activation energies that were found are relatively high in some cases. For the substrate **615**, the activation energy appears to be accessible for the fluoride and iodide example and maybe for the bromide example. The barrier found for the chloride example of 30.0 kcal/mol appears to be too high for an efficient reaction pathway. With substrate **616**, all halide derivatives have a S_NAr barrier that appears to be accessible. For substrate **617**, all halide derivatives have

Table 4-6 S_NAr Energy Profiles

	A		B		C	
	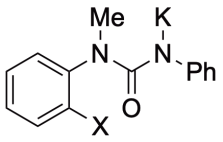		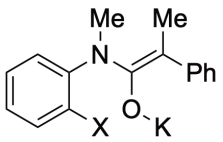		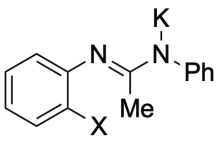	
	615		**616**		**617**	
	610 + KX		**612** + KX		**614** + KX	
X	**ΔG* (kcal/mol)**	**ΔG (kcal/mol)**	**ΔG* (kcal/mol)**	**ΔG (kcal/mol)**	**ΔG* (kcal/mol)**	**ΔG (kcal/mol)**
F	24.7	-33.8	25.6	-46.4	29.0	-35.6
Cl	30.0	-52.4	26.8	-66.7	33.8	54.0
Br	27.1	-60.3	22.1	-75.9	30.0	-61.4
I	24.1	58.8	21.2	-74.7	32.6	-58.6

Table 4-7 Benzyne Pathway Energy Profiles

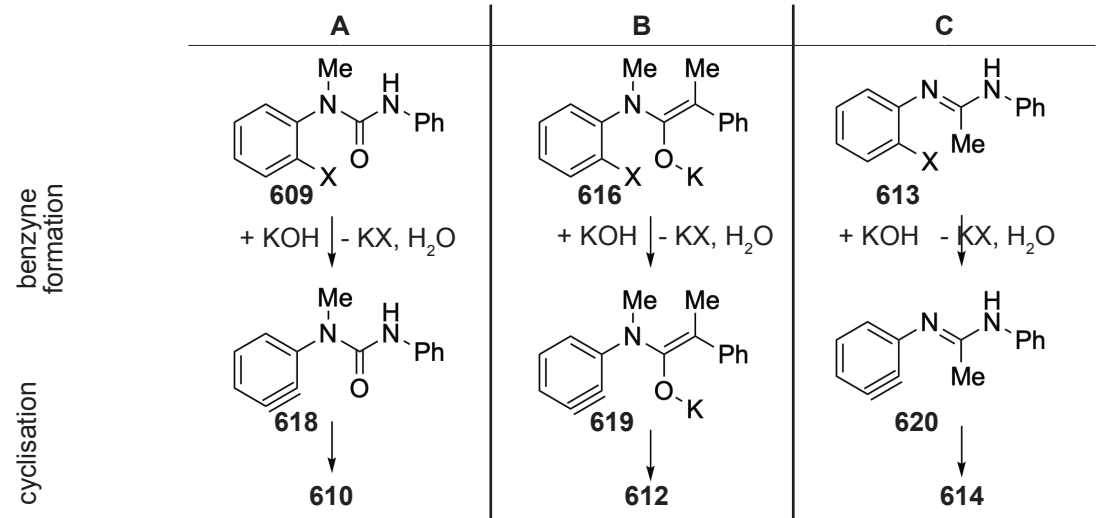

	X	ΔG* (kcal/mol)	ΔG (kcal/mol)	ΔG* (kcal/mol)	ΔG (kcal/mol)	ΔG* (kcal/mol)	ΔG (kcal/mol)
benzyne formation	F	41.7	36.5	41.1	-86.5[a]	42.5	26.8
	Cl	28.2	16.7	27.8	-71.3[a]	28.8	15.1
	Br	20.3	8.76	20.6	-80.0[a]	21.0	7.29
	I	23.8	12.3	22.3	-78.5[a]	22.3	10.3
cyclisation	-	8.22	-86.8	barrier-less	see above[a]	9.44	-88.9

[a] No stable structure for the isolated benzyne intermediate **619** was found. The structures spontaneously collapsed to the final product **612**.

a barrier that suggests that the S_NAr pathway cannot be the major route to the product **614**. Clearly, S_NAr reaction pathways cannot be the only mechanistic pathways accessible to these substrates.

Next, energy profiles for pathways leading to the products **610**, **612** and **614** via benzyne intermediates were investigated (Table 4-7). It should be noted that computationally the formation of the benzyne intermediates is a stepwise process involving a deprotonation followed by the elimination of the halide in all cases. Since this detail is not critical for the discussion at hand, in Table 4-7 the overall values for ΔG* and ΔG are given for the formation of the benzyne intermediates. All computational details are given in Chapter 5.5.5 to reconstruct the full energy profile. Similarly, the cyclisation step is followed by deprotonation and protonation steps, which are omitted for clarity. The energy barrier for the actual cyclisation step - which is rate limiting - is given together with the overall Gibbs free energy.

From the data in Table 4-7, it follows that the benzyne pathway can be ruled out for all substrates with X = F. The chloride substrates are borderline cases. For substrates **609** and **613** with X = Cl, the benzyne pathway is slightly more favourable than the S_NAr pathway and vice versa for the substrate **616** with X = Cl. For the bromide and iodide derivatives of **609** and **613**, the benzyne mechanism is clearly more accessible than the S_NAr pathway. For the

Table 4-8 BHAS and $S_{RN}1$ Pathways

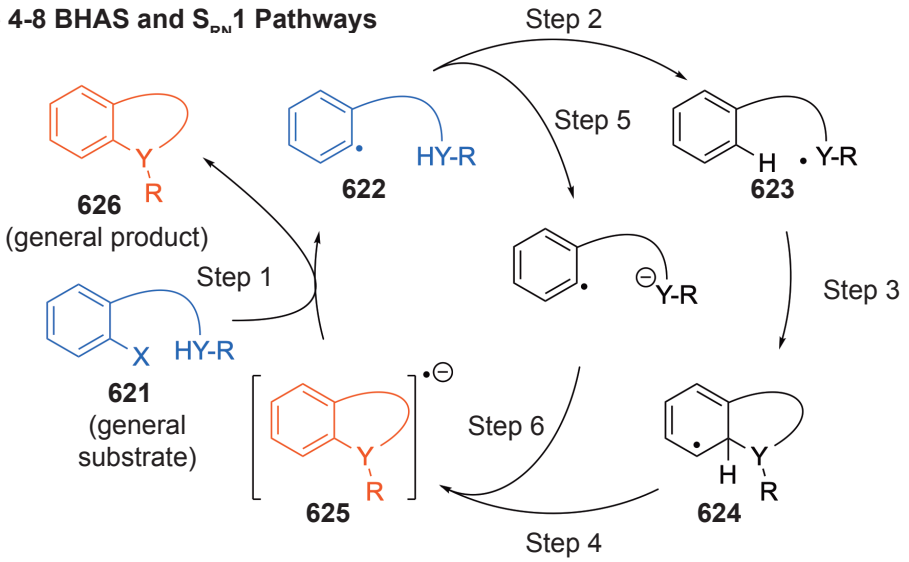

		substrate	A		B		C	
			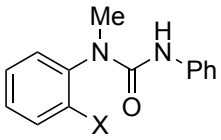		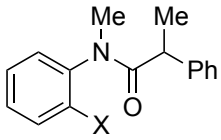		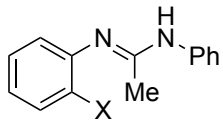	
			609		611		613	
	Step	X	ΔG* (kcal/mol)	ΔG (kcal/mol)	ΔG* (kcal/mol)	ΔG (kcal/mol)	ΔG* (kcal/mol)	ΔG (kcal/mol)
SET[b]	1	F	12.3[a]	-6.70	8.97[a]	0.11	6.99[a]	-20.5
		Cl	3.19[a]	-30.6	6.07[a]	-30.6	3.71[a]	-33.3
		Br	3.41	-42.5	3.12	-39.0	3.80[a]	-42.1
		I	2.19	-38.22	2.64	-36.5	4.03[a]	-39.0
BHAS	2	-	8.13	-18.1	5.63	-26.1	6.85	-18.4
	3	-	**22.8**	-0.07	**18.1**	1.88	**25.8**	3.58
	4	-	barrier -less	-16.4	7.69	-9.72	0.30	-24.4
$S_{RN}1$	5	-	barrier -less	-14.9	barrier -less	-7.02	barrier -less	-15.4
	6	-	**5.85**	-22.5	barrier -less	-36.2	**8.12**	-23.0

[a] The single electron transfer and the fragmentation of the carbon-halogen bond was found to be a stepwise process. The overall energies are given. All computational details are given in Chapter 5.5.5 to reconstruct the full energy profile.

[b] The single electron transfer (SET) step is the same for both the BHAS and the $S_{RN}1$ pathway.

bromide and iodide derivatives of **616**, instead, both mechanisms are approximately equally favourable.

Finally, two radical mechanisms were investigated (Table 4-8). These are a BHAS-pathway[125] and an $S_{RN}1$[124] mechanism. It can be seen that for all three examples both pathways

Table 4-9 Initiation of the BHAS and $S_{RN}1$ Pathways

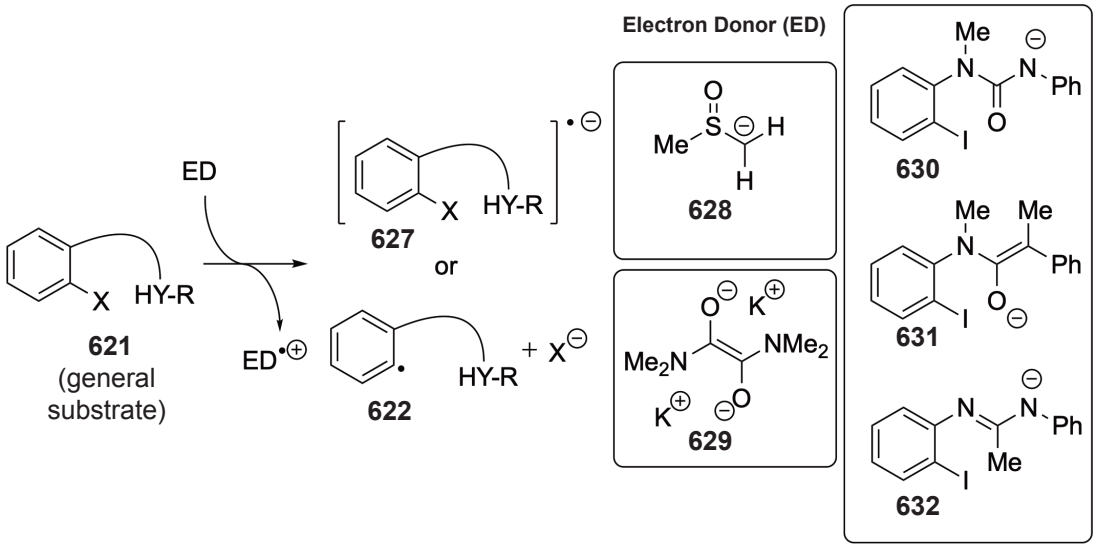

		substrate	A		B		C	
			609		611		613	
ED[a]	X		ΔG* (kcal/mol)	ΔG (kcal/mol)	ΔG* (kcal/mol)	ΔG (kcal/mol)	ΔG* (kcal/mol)	ΔG (kcal/mol)
628 or **629**	F		70.9[b]	63.6	30.3[b]	20.9	49.1	49.0
	Cl		51.8[b]	50.7	33.4[b]	23.5	48.4	48.2
	Br		30.2[c]	15.2	0.42[c]	-19.6	47.9	47.8
	I		29.7[c]	19.4	1.80[c]	-17.1	48.6	48.4
630 or **631** or **632**	F		126[b]	79.2	53.9	53.0	65.7[c]	62.7
	Cl		83.7[b]	66.3	56.9	55.7	72.3[c]	61.9
	Br		37.2[c]	30.8	13.4	12.6	70.8[c]	61.6
	I		37.9[c]	35.0	16.4	15.1	71.8[c]	62.2

[a] The appropriate electron donor (ED) is chosen for each example A-C: **628** for A and B; **629** for C; **630** for A; **631** for B; **632** for C. After the single electron transfer either the radical anion **627** is obtained or spontaneous fragmentation occurred to give **622** and the halide anion. All computational details are given in Chapter 5.5.5 to reconstruct the full energy profile.

[b] After the single electron transfer the radical anion **627** is obtained.

[c] After the single electron transfer a complex between the radical **622** and the halide anion is obtained.

have a very accessible energy profile but clearly the $S_{RN}1$ pathway is more favourable (the activation energies of the rate limiting steps are printed in bold). Somewhat surprisingly, the single electron transfer and carbon-halogen bond cleavage step (Step 1) was found to be accessible also for the fluoride examples. The author is not aware of examples of BHAS or $S_{RN}1$

Table 4-10 Overview of Plausible Mechanisms

substrate / X	A 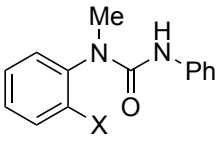 **609**	B 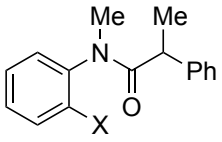 **611**	C 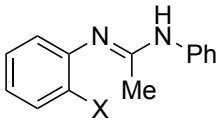 **613**
F	concerted S_NAr ($S_{RN}1$?)	concerted S_NAr ($S_{RN}1$?)	concerted S_NAr ($S_{RN}1$?)
Cl	Benzyne mechanism (concerted S_NAr)	$S_{RN}1$	Benzyne mechanism (concerted S_NAr, $S_{RN}1$)
Br	$S_{RN}1$	$S_{RN}1$	Benzyne mechanism ($S_{RN}1$)
I	$S_{RN}1$	$S_{RN}1$	Benzyne mechanism ($S_{RN}1$)

reactions that successfully employed aryl fluoride substrates. Although the energy profile for the reactions of the aryl fluoride substrates appear to be accessible in these cases, a very efficient fragmentation of the corresponding radical anion intermediates may be required in order to sustain the chain processes (i.e. to prevent side-reactions of the radical anion). A similar case was discussed earlier (Chapter 2.3.3).

Both the BHAS mechanism and the $S_{RN}1$ mechanism critically depend on an initiation process (which has not been included in Table 4-8). The initiation process would generate the first radical species **622**. Hence, although for all cases both a BHAS and an $S_{RN}1$ mechanism are accessible, these chain reactions may not be started if there is no accessible initiation process. Therefore, several plausible initiation mechanisms were investigated for each example (Table 4-9). It can be seen that the anions **630**, **631** or **632** are, in general, not sufficiently strong electron donors to transfer an electron to a substrate molecule. Only with the substrates **631** with X = Br or X = I this initiation mechanism is possible. (For simplicity, only the iodide derivatives were investigated as potential electron donors. The other halide derivatives are expected to show a similar behaviour).

The dimsyl anion **628** may be able to initiate a BHAS or $S_{RN}1$ reaction with the substrate **609** with X = Br and X = I but not in any other case. Previously the dimsyl anion has been demonstrated to be competent initiator for BHAS or $S_{RN}1$ reactions but only after activation with blue LED irradiation.[245] For the reaction of substrate **611**, DMF was used as a solvent. DMF has previously been shown to be a competent initiator for BHAS reactions, most likely by forming dimers such as **629**.[246] Indeed, it was found that this dimer is a sufficiently strong electron donor to act as an initiator also in the reactions of substrate **611**.

It should be noted that only the obvious initiation pathways have been considered so far. The presence of alternative initiation pathways cannot be ruled out. These may depend on small impurities in the substrates or trace amounts of oxygen, for example.

In Table 4-10, the plausible mechanisms for each substrate class are summarised. When two mechanisms have similarly favourable profiles, the alternative (and slightly less accessible)

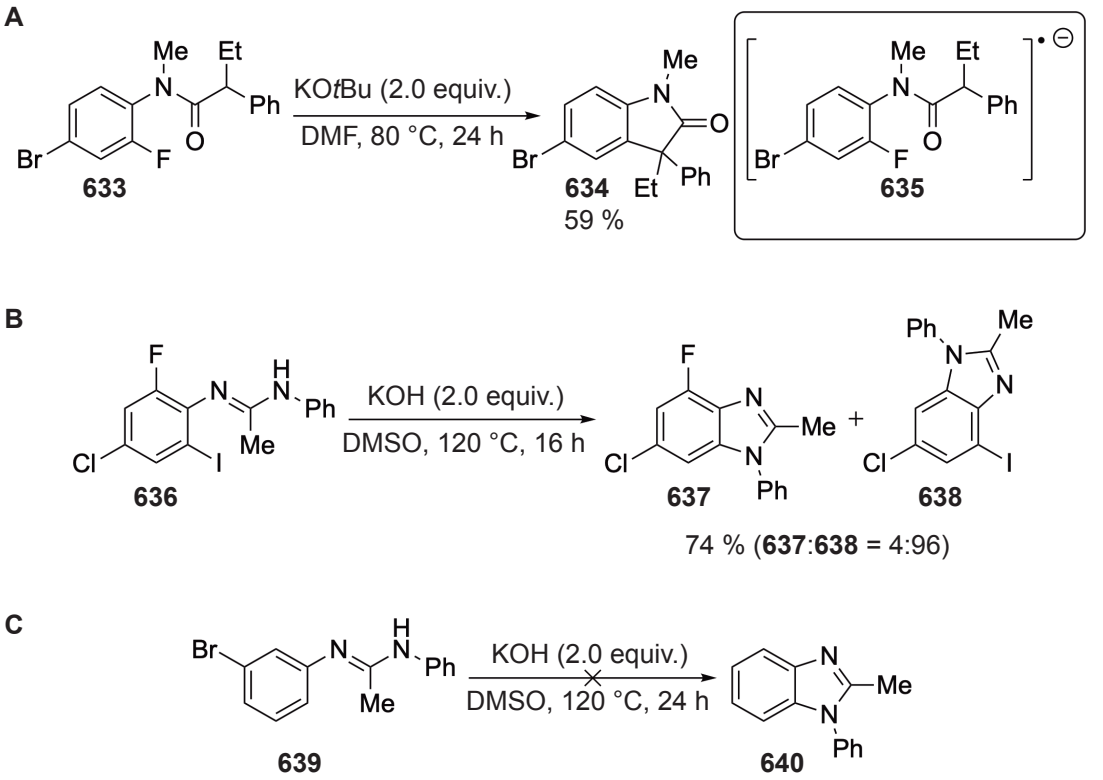

Scheme 4-3 Selected literature results published by Bolm et al. (Reaction A;[243] Reactions B and C[244]).

mechanism is given in brackets. Also, radical pathways cannot be ruled out even for the reactions where no obvious initiation pathway was found. It can be seen that for all fluoride substrates a concerted S_NAr reaction is the most plausible mechanism. For the other halide substrates, it is either a benzyne mechanism or a $S_{RN}1$ process that is likely to be the predominant reaction pathway. Pleasingly, the reported examples for the substrates **609**, **611** and **613** - and additional derivatives thereof - are generally in agreement with the proposed mechanism.[242,243,244] In some instances, the experimental results help clarify which mechanism is operating if two pathways appear accessible based on the computational data (Scheme 4-3 A). For example, substrate **633** cannot give rise to the product **634** via a $S_{RN}1$ mechanism. The hypothetical radical anion intermediate **635** of a $S_{RN}1$ pathway would fragment at the carbon-bromine bond and not at the carbon-fluorine bond - as was required to give rise to the product **634**.

Substrate **636** turned out to be a very interesting one (Scheme 4-3 B). The major product of the reaction was **638**, which must have formed via concerted S_NAr reactions for the same reasons as given above. Additionally, small amounts of **637** were formed. The product **637** may either form via a benzyne pathway or a $S_{RN}1$ mechanism. Bolm et al. suggested that a benzyne mechanism was unlikely to be accessible for substrates like **636** (Scheme 4-3 C). This conclusion was based on the observation that the substrate **639** did not give rise to the product **640**. If a benzyne intermediate was formed at least small amounts of **640** should be detectable.[244]

4.4. Summary and Conclusion

The M11 functional, in combination with the 6-311++G(d,p) basis set, was found to be a suitable method to investigate the mechanism of S_NAr reactions. With this method in hand, a number of S_NAr reactions were investigated. It was found that S_NAr reactions where chloride, bromide or iodide are displaced, typically proceed via a concerted mechanism. In the halide series, stepwise S_NAr reactions are usually only observed with the fluoride leaving group. Whether an S_NAr reaction displacing fluoride follows a stepwise or a concerted mechanism primarily depends on the electron-withdrawing nature of the *para*-substituents on the aromatic system. Additionally, the size of the aromatic system, the presence of nitrogen heteroatoms and steric effects influence the mechanistic choice of the reaction. Also, the nature of the counter cation has a moderate effect on the mechanistic preference of the reaction.

Importantly, for a given aromatic system and fluoride as the leaving group, the mechanistic turning point does not vary much for different nucleophiles. In fact, the choice of the S_NAr mechanism depends on the bond-cleavage which is kinetically easier. In the cases of reactions with fluoride as the leaving group, this step is the expulsion of the fluoride anion. This observation clearly shows that it is very difficult to obtain information about the mechanism of an S_NAr reaction series from Hammett correlations or in general from classical kinetic studies. The reaction step that is typically observable experimentally is the rate limiting step. The critical and kinetically much faster step cannot usually be observed or inferred. Hence, the mechanistic nature of S_NAr reactions can only readily be assessed by computational means.

4.5. Outlook

The major parameters influencing the mechanistic choice of S_NAr reactions have been discovered and investigated except for one: the effect of steric bulk on the side of the nucleophile. The result obtained with the nucleophile **601e** (Figure 4-8) indicates that sterically more bulky nucleophiles may bias the S_NAr mechanism towards a concerted pathway. Therefore, it will be interesting to investigate the change of the mechanistic turning point for the series of potassium methoxide, potassium ethoxide, potassium *iso*-propoxide and potassium *tert*-butoxide nucleophiles. An alternative series of nucleophiles is shown in Figure 4-15 that would be suitable for the same purpose.

A nice possibility to demonstrate the multifaceted mechanisms that are accessible in the reactions reported by Bolm et al.[242, 243, 244] can be found in substrates such as **636**. Under standard conditions, only small amounts of the $S_{RN}1$ product are formed. By including an organic additive in the reaction mixture (such as a small amount of DMF[246]) the much more accessible $S_{RN}1$ pathway may be initiated. Thereby the product ratio of **637**:**638** = 4:96 may

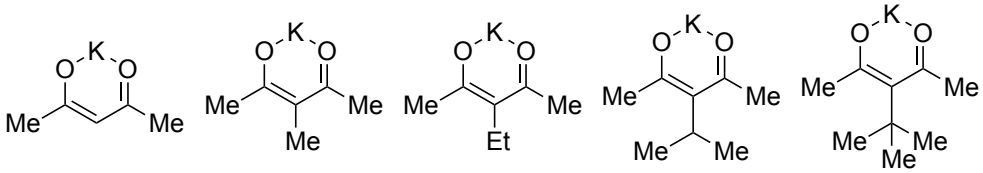

601d **641** **642** **643** **644**

Figure 4-15 A possible series of nucleophiles to assess the effect of steric bulk on the side of the nucleophile.

be switched completely - even if all other reaction parameters are kept the same. This experiment would give additional support for the proposed mechanisms and it would open doors for an elegant control of the chemoselectivity of the reaction.

5. Supporting Information

5.1. Specifications

All reagents and solvents were obtained from commercial suppliers and were used without further purification unless mentioned otherwise.

Thin Layer Chromatography was performed on silica gel pre-coated aluminium plates (60 Å, F254 UV indicator) purchased from Merck. The thin layer chromatograms were analysed by UV (254 nm, UVP mineralight UVG-11 lamp) and staining either with basic $KMnO_4$ [$KMnO_4$ (6 g), K_2CO_3 (40 g), NaOH (5 mL, 10% w/w) in water (600 mL)] or an ethanolic solution of phosphomolybdic acid [phosphomolybdic acid hydrate (10 g) in ethanol (100 mL)].

Flash Column Chromatography purification was performed with 35-70 µm particle size silica gel 60 Å (200-400 mesh) purchased from Prolabo.

NMR spectra were measured on a Bruker AV400 instrument. Spectra were recorded in chloroform-d_1, acetonitrile-d_3, tetrahydrofuran-d_8 or dimethyl sulfoxide-d_6. The frequency was locked against the deuterated solvent signal and the final spectra were referenced against the residual non-deuterated solvent signal (for ^{1}H spectra) or the deuterated solvent signal (for ^{13}C spectra). Chemical shifts are reported as δ (ppm) with respect to tetramethylsilane. The following multiplet abbreviations are used: s = singlet, d = doublet, t = triplet, q = quartet, quint = quintet, sext = sextet, sep = septet, m = multiplet, br = broad. The processed spectra can be found in the Appendix. In cases where yields were measured by ^{1}H-NMR spectroscopy, the internal standard 1,3,5-trimethoxybenezene was used and the T_1 delay time was set to 30 s.

Infrared spectra were recorded on an Agilent Technologies 5500a FTIR with ATR system.

HPLC analysis was performed on a Waters XBridge C18 column (50 mm x 4.6 mm, 3.5 µm) at 30 °C with a flow-rate was 3.0 mL/min. The gradient as stated in Table S1 was used with mobile phases A {10 mM $(NH_4)HCO_3$ aq at pH 10} and B {acetonitrile}. The injection volume was 10 µL. Yields were measured against an internal standard as specified. The response factor was determined according to standard procedures.

Table S1 HPLC gradient

Time (min:s)	% A	% B
0.00	99	1
0.10	99	1
4.00	3	97
5.00	3	97
5.01	99	1
7.00	99	1

LC-MS analysis was performed on an Agilent 6130 dual source LC-MS with 1200 series LC and UV at 254 nm. Ionisation was performed with dual ESI and APCI source in positive and negative ionisation mode. The LC was equipped with an Agilent Poroshell 120 LC column (EC, C18, 2.7 µm, 4.6 mm x 75 mm) at 40 °C with a flow rate of 1.0 mL/min. The gradient as stated in **Table S2** was used with mobile phases A {5 mM $(NH_4)HCO_3$ in water} and B {5 mM $(NH_4)HCO_3$ in acetonitrile}. The injection volume was 10 µL.

Table S2 LC-MS gradient

Time (min:s)	% A	% B
0.00	95	5
1.48	95	5
8.50	0	100
13.50	0	100
16.50	95	5
18.00	95	5

GC-(EI)MS analysis was performed on an Agilent Technologies 7890A GC system connected to an Agilent Technologies 5975C inert XL EI/CI MSD triple axis-mass detector. The GC was equipped with a Rxi-5Sil MS column (30 m x 0.25 mm x 0.25 µm). Helium was used as the carrier gas (1.0 mL/min flow rate). The injector temperature was 320 °C and was operated in splitless mode. The oven program as stated in Table S3 was used.

Table S3 GC-(EI)MS oven program

Time (min:s)	Temperature
0.00	40 °C
4:00	40 °C
18:00	320 °C (20 °C / min)
28:00	320 °C

GC-FID analysis was performed on an Agilent Technologies 7890A GC system. The GC was equipped with an Agilent Technologies HP-5 column (30 m x 0.32 mm x 0.25 µm). Helium was used as the carrier gas (2.0 mL/min flow rate). Yields were measured against an internal standard as specified. The response factor was determined according to standard procedures. The injector temperature was 320 °C and was operated in splitless mode. The oven program as stated in Table S4 was used.

Table S4 GC-FID oven program

Time (min:s)	Temperature
0.00	40 °C
5:00	40 °C
18:00	320 °C (20 °C / min)
23:00	320 °C

ESI-MS (direct injection) analysis was performed on a Thermo Finnigan LCQ Duo device

operating at 4000 kV. The sample was injected as a solution in methanol at a rate of 20 µL/min - 40 µL/min.

HRMS was performed at the Swansea University, Wales, in the EPSRC National Mass Spectrometry Centre. Accurate mass measurements were obtained using the specified ionisation mode with a LTQ Orbitrap XL mass spectrometer.

Melting points were determined using a Gallenkamp Griffen Melting Point Apparatus.

5.2. General Computational Methods

Software used was Gaussian09[247] (both Revisions A.02 or D.01 were used) in combination with GaussView 5.0.9[248] for all calculations.

DFT Methods employed the functional as specified in combination with Pople triple-ζ basis set 6-311++G(d,p)[249-252] for all atoms up to the atomic number Z=18. For larger atoms (these mainly applied to counter cations K^+, Rb^+ and Cs^+ and the halogen atoms bromine and iodine) the appropriate MWB relativistic pseudo-potential and associated basis set was used.[253] Solvation effects were accounted for by the solvent reaction field method using the conductor-like polarisable continuum model (CPCM) unless mentioned otherwise.[254,255]

Nelsen's four-point method[209] is based on Marcus theory.[61,210] The assumption is made that the reorganisation energy of the solvent can be neglected. The Equation 5.1 gives an estimate for the energy barrier ΔG* associated with an electron transfer.

$$\Delta G^* = \frac{\lambda}{4}\left(1 + \frac{\Delta G}{\lambda}\right)^2 \qquad \text{Equation 5.1}$$

ΔG is the Gibbs free energy associated with the electron transfer. λ stands for the internal reorganisation energy and is calculated according to Equation 5.2).

$$\lambda = \frac{\lambda(a_{tot}) + \lambda(b_{tot})}{2} \qquad \text{Equation 5.2}$$

Here $\lambda(a_{tot})$ and $\lambda(b_{tot})$ stand for the reorganisation energy of the electron acceptor and electron donor, respectively. If these are treated in the same calculation (i.e. if they are modelled as a complex) only one term is needed.[64] The reorganisation energy of one species can be expressed by Equation 5.3).

$$\lambda(a_{tot}) = \lambda(a_S) + \lambda(a_P) \qquad \text{Equation 5.3}$$

The subscript indicates the state of the structure 'a', i.e. either in product state (a_P) or substrate state (a_S). These individual contributions are given by Equation 5.4 and 5.5, respectively.

$$\lambda(a_P) = E_{a_P}(R_{a_S}) - E_{a_P}(R_{a_P}) \qquad \text{Equation 5.4}$$

$$\lambda(a_S) = E_{a_S}(R_{a_P}) - E_{a_S}(R_{a_S}) \qquad \text{Equation 5.5}$$

These equations are read as follows. For example, $E_{ap}(R_{as})$ stands for the energy of the structure in the geometry of 'a_S' with the electronic structure of 'a_P'. To calculate this energy, the fully optimised geometry of the substrate 'a_S' is required {in the notion of Equation 5.4 and 5.5 this would be expressed as $E_{as}(R_{as})$}. Then a frequency calculation is preformed on this geometry (denoted R_{as}) but with the electronic configuration of the product 'a_P'. Importantly, no geometry optimisation is performed in this type of calculation and it is normal to observe imaginary frequencies. The results of Equation 5.4 and 5.5 are always positive.

5.3. Experimental Details for Chapter 2 "Organic Super Electron Donors Made Catalytic"

5.3.1 General Experimental Procedures

General Procedure A - Dihydrobenzimidazole Protocol

The reaction vessel was charged with the substrate (0.600 mmol, 1.0 equiv.). Then 1,3-dimethyl-2,3-dihydro-1*H*-benzo[*d*]imidazole **419** (185 mg, 1.20 mmol, 2.0 equiv.) was added as a solution in DMF (1.2 mL) followed by dodecanethiol (29.3 µL, 0.12 mmol, 0.2 equiv.). The reaction vessel was left open to air via a needle. The reaction was heated to 55 °C and monitored by an appropriate technique (^{1}H-NMR, GC-MS, TLC) as stated for each example. When the reaction was found to have reached full conversion, it was poured onto water/brine (100 mL, 2:1). The reaction mixture was extracted with ethyl acetate (4 x 20 mL). The combined organic phases were washed with brine (1 x 50 mL), dried over $MgSO_4$ and concentrated in vacuo. Purification by flash column chromatography gave the pure product.

General Procedure B - Catalytic Protocol

The reaction vessel was charged with the substrate (0.600 mmol, 1.0 equiv.). Then DMF (1.2 mL) was added followed by 1,3-dimethyl-1*H*-benzo[*d*]imidazol-3-ium iodide **418-I** (32.9 mg, 0.12 mmol, 0.2 equiv.), dodecanethiol (29.3 µL, 0.12 mmol, 0.2 equiv.) and $NaBH_4$ (45.4 mg, 1.20 mmol, 2.0 equiv.) in this sequence. The reaction vessel was left open to air via a needle. The reaction was heated to 55 °C and monitored by an appropriate technique (^{1}H-NMR, GC-MS, TLC) as stated for each example. When the reaction was found to have reached full conversion, it was poured onto water/brine (100 mL, 2:1). The reaction mixture was extracted with ethyl acetate (4 x 20 mL). The combined organic phases were washed with brine (1 x 50 mL), dried over $MgSO_4$ and concentrated in vacuo. Purification by flash column chromatography gave the pure product.

5.3.2 Specific Experimental Procedures

1,3-Dimethyl-1*H*-benzo[*d*]imidazol-3-ium iodide 418-I

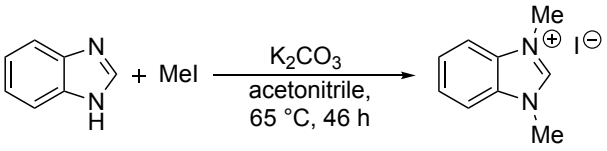

645 **418-I**

The reaction was performed in a controlled laboratory reactor equipped with a condenser. The reaction was kept under nitrogen. No precautions were taken to exclude humidity. The reaction vessel was charged with 1*H*-benzo[*d*]imidazole **645** (35.4 g, 300 mmol, 1.0 equiv.) and acetonitrile (350 mL). Then potassium carbonate (41.5 g, 300 mmol, 1.0 equiv.) was added followed by the slow addition of iodomethane (74.7 mL, 1.20 mol, 4.0 equiv.) over *ca.* 5 min. The suspension was heated to 65 °C (jacket temperature) for 46 h. The reaction was monitored by HPLC and was found to have reached full conversion after that time. The reaction was filtered while it was still hot. The filter cake was washed with warm acetonitrile (100 mL) and warm dichloromethane (200 mL). The crude product was obtained as a wine-red solid (87.9 g). The crude product was dissolved in acetonitrile (300 mL) and water (24 mL) at 65 °C. Upon slow cooling, white crystals formed, which were isolated by filtration. The filter cake was washed with acetonitrile (2 x 20 mL) and acetone (2 x 20 mL) until the material was white. The product 1,3-dimethyl-1*H*-benzo[*d*]imidazol-3-ium iodide **418-I** (58.5 g, 214 mmol, 71 %, crop 1) was obtained as a white crystalline solid. The mother liquor was concentrated to give a wine-red solid (31.0 g). Crystallisation of the material from the mother liquor from hot acetonitrile (90 mL) and water (6 mL) followed by washing with acetonitrile (2 x 10 mL) and acetone (2 x 10 mL) gave the product 1,3-dimethyl-1*H*-benzo[*d*]imidazol-3-ium iodide **418-I** (8.82 g, 32.2 mmol, 11 %, crop 2) as a white crystalline solid. In total 1,3-dimethyl-1*H*-benzo[*d*]imidazol-3-ium iodide **418-I** (67.4 g, 246 mmol, 82 %) was obtained. **^{1}H-NMR** (400 MHz, DMSO-d_6) δ 9.67 (s, 1H), 8.05 – 7.98 (m, 2H), 7.73 – 7.67 (m, 2H), 4.09 (d, *J* = 0.6 Hz, 6H). **^{13}C-NMR** (101 MHz, DMSO-d_6) δ 143.1, 131.6, 126.4, 113.4, 33.2. **LC-(ESI+)-MS** [*m/z*] (0.630 min): 147 (imidazolium cation). **mp** = 190 °C - 193 °C (lit. mp = 190 °C - 192 °C).[256] Ion current analysis showed < 0.1 % (w/w) potassium content. The NMR spectra are in agreement with the previously reported data.[257]

1,3-Dimethyl-2,3-dihydro-1*H*-benzo[*d*]imidazole 419

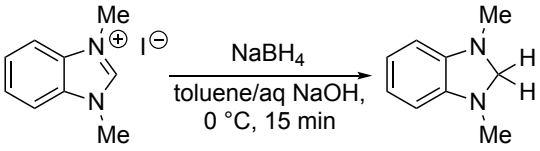

418-I **419**

The reaction was kept under nitrogen. The solution of sodium borohydride (757 mg, 20.0 mmol, 1.0 equiv.) in aqueous NaOH (0.01 M, 20 mL) and toluene (20 mL) was cooled to ice bath temperature. Then 1,3-dimethyl-1*H*-benzo[*d*]imidazol-3-ium iodide **418-I** (5.48 g, 20.0 mmol, 1.0 equiv.) was added in small portions over *ca.* 2 min. The reaction was stirred at ice bath temperature for 15 min before it was diluted with water (120 mL) and *tert*-butylmethyl

ether (100 mL). To the crude reaction was added brine (60 mL) and the phases were separated. The aqueous phase was extracted with *tert*-butylmethyl ether (3 x 80 mL). The combined organic phases were dried over $MgSO_4$ and $Al(OH)_3$ (for *ca.* 5 min) and concentrated *in vacuo* first at room temperature then at 45 °C to a volume of *ca.* 1 mL. Then the crude product was passed over $Al(OH)_3$ and concentrated further under a flow of nitrogen to give 1,3-dimethyl-2,3-dihydro-1*H*-benzo[*d*]imidazole **419** (2.53 g, 16.8 mmol, 84 %, average of three experiments on the same scale, see Table S5) as a pale yellow oil. No further purification was required. For storage over days or longer, the material was kept under nitrogen at 4 °C.**^{1}H-NMR** (400 MHz, THF-d_8) δ 6.52 (dd, *J* = 5.5, 3.2 Hz, 2H), 6.32 (dd, *J* = 5.4, 3.2 Hz, 2H), 4.24 (s, 2H), 2.66 (s, 6H). **^{13}C-NMR** (101 MHz, THF-d_8) δ 144.6, 119.7, 106.7, 81.3, 34.7. **^{1}H-NMR** (400 MHz, Chloroform-*d*) δ 6.71 – 6.65 (m, 2H), 6.43 (dd, *J* = 5.4, 3.2 Hz, 2H), 4.34 (s, 2H), 2.74 (s, 6H). **^{13}C-NMR** (101 MHz, Chloroform-*d*) δ 143.3, 119.3, 106.3, 80.4, 34.6. (Chloroform-*d* was passed over $Al(OH)_3$ and $MgSO_4$ before use). **^{1}H-NMR** (400 MHz, DMSO-d_6) δ 6.58 – 6.51 (m, 2H), 6.40 (dd, *J* = 5.4, 3.2 Hz, 2H), 4.24 (s, 2H), 2.65 (s, 6H). **^{13}C-NMR** (101 MHz, DMSO-d_6) δ 143.2, 118.6, 105.9, 79.6, 34.1. **LC-ESI(+)-MS** [*m/z*] (0.93 min): 148.9 (M+). The NMR spectra in THF-d_8 are in agreement with the previously reported data.[258]

Table S5 Individual yields of 1,3-dimethyl-2,3-dihydro-1*H*-benzo[*d*]imidazole **419**

Experiment	Purity (HPLC, 210 nm)	Yield of 419
1	**94 %**	2.47 g, 15.7 mmol, 78 %
2	**100 %**	2.55 g, 17.2 mmol, 86 %
3	**100 %**	2.58 g, 17.4 mmol, 87 %
Average	**98 %**	2.53 g, 16.8 mmol, 84 %

5.3.3 Preliminary Experiments - Reductive Deiodination

(Corresponds to Chapter 2.2.1).

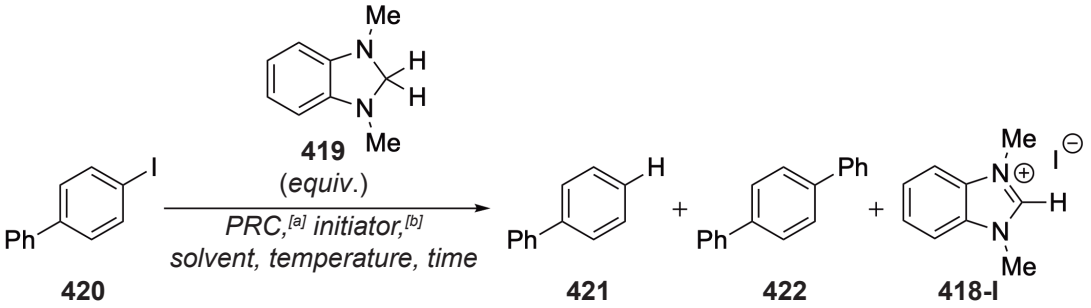

In order to understand the fundamental reactivity of 1,3-dimethyl-2,3-dihydro-1*H*-benzo[*d*]imidazole **419** in radical reactions, the simple deiodination reaction of 4-iodobiphenyl **420** was chosen as a model system. The results are summarised in Table S6 (corresponds to Table 2-1 in the main text).

Conditions for Entry 1 - 2

A pressure tube was charged with 1,3-dimethyl-2,3-dihydro-1*H*-benzo[*d*]imidazole **419** (156 mg, 1.00 mmol, 2.0 equiv.) and brought inside the glove box. Then benzene (5.0 mL) and 4-iodo-1,1'-biphenyl **420** (140 mg, 0.500 mmol, 1.0 equiv.) were added. Finally the initiator (40.0 mg {for dilauroyl peroxide}, 35.0 mg {for dibezoyl peroxide}, 0.100 mmol, 0.2 equiv.) was

added as required and the reaction was heated outside the glove box for 16 h at the specified temperature. The reaction was cooled to room temperature, concentrated in vacuo and analysed by ^{1}H-NMR.

Conditions for Entry 3

A pressure tube was charged with 1,3-dimethyl-2,3-dihydro-1*H*-benzo[*d*]imidazole **419** (156 mg, 1.00 mmol, 2.0 equiv.) and brought inside the glove box. Then benzene (5.0 mL) and 4-iodo-1,1'-biphenyl **420** (140 mg, 0.500 mmol, 1.0 equiv.) were added. Finally the initiator *di-tert*-butyl peroxide (19 µL, 0.10 mmol, 0.2 equiv.) was added and the reaction was heated outside the glove box for 16 h at 130 °C. The reaction was cooled to room temperature, decanted and the precipitate was washed with toluene (3 x 0.5 mL). The precipitate was dried in vacuo to give pure 1,3-dimethyl-1*H*-benzo[*d*]imidazol-3-ium iodide **418-I** (141 mg, 0.513 mmol, 51 %) as a white solid. The NMR spectra were identical to the spectra recorded for the independently synthesised material, vide infra. The organic phase was concentrated *in vacuo*. Purification by flash column chromatography (hexane) gave the pure product biphenyl **421** (50.2 mg, 0.326 mmol, 65 %) as a white solid. **^{1}H-NMR** (400 MHz, Chloroform-*d*) δ 7.65 – 7.60 (m, 4H), 7.50 – 7.44 (m, 4H), 7.40 – 7.35 (m, 2H). **^{13}C-NMR** (101 MHz, Chloroform-*d*) δ 141.4, 128.9, 127.4, 127.3. **GC-MS** [m/z (%)] (10.841 min): 154 (100, M+), 153 (50), 152 (35), 151 (10), 128 (10), 126 (5), 115 (10), 102 (10), 89 (5), 87 (5), 77 (15), 76 (25), 75 (10), 74 (10), 64 (5), 63 (15), 62 (5), 52 (5), 51 (30), 50 (20). **mp** = 65.5 °C - 66 °C (lit. mp = 65 °C - 66 °C).[259] The NMR spectra are in agreement with the previously reported data.[260]

Additionally, *p*-terphenyl **422** (23.1 mg, 0.100 mmol. 20 %) was isolated as a white solid. **^{1}H-NMR** (400 MHz, Chloroform-*d*) δ 7.70 (s, 4H), 7.68 – 7.64 (m, 4H), 7.51 – 7.45 (m, 4H), 7.40 – 7.33 (m, 2H). **^{13}C-NMR** (101 MHz, Chloroform-*d*) δ 140.9, 140.3, 129.0, 127.6, 127.5, 127.2. **GC-MS** [*m/z* (%)] (15.311 min): 230 (100, M+), 229 (10), 228 (15), 227 (5), 226 (10), 202 (10), 153 (5), 152 (15), 151 (5), 115 (15), 78 (10), 77 (20), 63 (5), 51 (15). **mp** = 209 °C - 210 °C (lit. mp = 209 °C - 210 °C).[261] The NMR spectra are in agreement with the previously reported data.[262]

Conditions for Entry 4

A pressure tube was charged with 1,3-dimethyl-2,3-dihydro-1*H*-benzo[*d*]imidazole **419** (62 mg, 0.40 mmol, 2.0 equiv.) and brought inside the glove box. Then 4-iodo-1,1'-biphenyl **420** (56.0 mg, 0.200 mmol, 1.0 equiv.) was added, followed by a solution of the initiator lauroyl peroxide (15.9 mg, 40.0 µmol, 0.2 equiv.) and dodecanethiol (2.4 µL, 10 µmol, 0.05 equiv.) in benzene (2.0 mL). The reaction was heated outside the glove box for 16 h at 70 °C. The reaction was cooled to room temperature and concentrated in vacuo. Purification by flash column chromatography (hexane) gave the pure product biphenyl **421** (27.0 mg, 0.151 mmol, 75 %) as a white solid. The NMR spectra were identical to the previously recorded spectra.

Conditions for Entry 5

A pressure tube was charged with 1,3-dimethyl-2,3-dihydro-1*H*-benzo[*d*]imidazole **419** (62.0 mg, 0.400 mmol, 2.0 equiv.) and brought inside the glove box. Then 4-iodo-1,1'-biphenyl **420** (56.0 mg, 0.200 mmol, 1.0 equiv.) was added, followed by the initiator *di-tert*-butyl peroxide (DTBP) (7.35 µL, 40.0 µmol, 0.2 equiv.) and dodecanethiol (2.4 µL, 10 µmol, 0.05 equiv.) in benzene (2.0 mL). The reaction was heated outside the glove box for 16 h at 130 °C. The reaction was cooled to room temperature, decanted and the precipitate was washed with toluene (3 x 0.5 mL). The precipitate was dried *in vacuo* to give pure 1,3-dimethyl-1*H*-benzo[*d*]imidazol-3-ium iodide **418-I** (39.7 mg, 0.145 mmol, 36 %) as a white solid. The NMR spectra were

identical to the independently synthesised material, vide infra. The organic phase was concentrated in vacuo. Purification by flash column chromatography (hexane) gave the product biphenyl **421** (25.0 mg, 0.162 mmol, 81 %) as a white solid. The NMR spectra were identical to the previously recorded spectra. Additionally, *p*-terphenyl **422** (6.9 mg, 30 µmol, 15 %) was isolated as a white solid. The NMR spectra were identical to the previously recorded spectra.

Conditions for Entry 6

A reaction vessel was charged with 1,3-dimethyl-2,3-dihydro-1*H*-benzo[*d*]imidazole **419** (62.0 mg, 0.400 mmol, 2.0 equiv.) and 4-iodo-1,1'-biphenyl **420** (56.0 mg, 0.200 mmol, 1.0 equiv.). The reaction was stirred at room temperature open to air for 38 h. The reaction was washed and decanted with toluene (3 x 0.5 mL). The precipitate was dried in vacuo to give pure 1,3-dimethyl-1*H*-benzo[*d*]imidazol-3-ium iodide **418-I** (54.1 mg, 0.197 mmol, 49 %) as a white solid. The NMR spectra were identical to the independently synthesised material, vide infra. The organic phase was concentrated in vacuo. Purification by flash column chromatography (hexane) gave the product biphenyl **421** (29.4 mg, 0.181 mmol, 91 %) as a white solid. The NMR spectra were identical to the previously recorded spectra.

Conditions for Entry 7 - 11 and 13 - 22

The reaction vessel was charged with 1,3-dimethyl-2,3-dihydro-1*H*-benzo[*d*]imidazole **419** as required. Then the solvent was added (0.4 mL) as required followed by 4-iodo-1,1'-biphenyl **420** (58 mg, 0.20 mmol, 1.0 equiv.). The reaction was heated to the specified temperature for the specified time while left open to air via a needle. The reaction mixture was cooled to room temperature, diluted to ca. 1 mg/mL of starting material 4-iodobiphenyl **420** and a precisely measured amount of 1-phenylpyrrolidin-2-one (ca. 24.2 mg, 0.100 mmol, 0.5 equiv.) was added as internal standard. An aliquot was analysed by HPLC (biphenyl: 3.209 min).

Conditions for Entry 12

The reaction vessel was charged with 1,3-dimethyl-2,3-dihydro-1*H*-benzo[*d*]imidazole **419** (178 mg, 1.20 mmol, 2.0 equiv.). Then 4-iodo-1,1'-biphenyl **420** (178 mg, 0.600 mmol. 1.0 equiv.) was added, followed by acetonitrile (1.2 mL). The reaction was heated to 55 °C for 4 h open to air via a needle. The reaction mixture was cooled to room temperature, diluted to ca. 1 mg/mL of starting material 4-iodobiphenyl **420** and a precisely measured amount of 1-phenylpyrrolidin-2-one (*ca.* 24.2 mg, 0.100 mmol, 0.5 equiv.) was added (internal standard). An aliquot was analysed by HPLC and the yield was found to equal 99 %. From the same reaction the product was isolated by flash column chromatography (ethyl acetate in heptane, gradient from 0 % to 5 %). Biphenyl **421** (85 mg, 0.55 mmol, 92 %) was obtained as a white solid. The NMR spectra were identical to the previously recorded spectra.

Table S6 - Optimisation of Biphenyl Reduction

Entry	419 (equiv.)	PRC[a] (equiv.)	Initiator[b]	Solvent	Temp.	Time (h:min)	Yield of 421[c]
1	2.0	none	LP	benzene	70 °C	16:00	22 %[d]
2	2.0	none	DBP	benzene	80 °C	16:00	20 %[d]
3	2.0	none	DTBP	benzene	130 °C	16:00	65 %[e,f]
4	2.0	0.05	LP	benzene	70 °C	16:00	75 %[e]
5	2.0	0.05	DTBP	benzene	130 °C	16:00	81 %[e,g]
6	**2.0**	**none**	**air**	**none**	**RT**	**38:00**	**91 %**[e,h]
7	1.1	none	air	none	45 °C	18:00	78 %

Entry	419 (equiv.)	PRC[a] (equiv.)	Initia-tor[b]	Solvent	Temp.	Time (h:min)	Yield of 421[c]
8	1.1	none	air	DMSO	45 °C	18:00	89 %
9	1.1	none	air	ACN	45 °C	18:00	84 %
10	1.5	none	air	ACN	45 °C	6:00	90 %
11	2.0	none	air	ACN	45 °C	6:00	99 %
12	**2.0**	**none**	**air**	**ACN**	**55 °C**	4:00	**99 % (92 %)**[e]
13	1.1	none	air	Acetone	45 °C	18:00	82 %
14	1.1	none	air	1,4-dioxane	45 °C	18:00	76 %
15	1.1	none	air	EtOAc	45 °C	18:00	73 %
16	1.1	none	air	DMF	45 °C	18:00	66 %
17	1.5	none	air	DMF	45 °C	6:00	83 %
18	2.0	none	air	DMF	45 °C	6:00	90 %
19	**2.0**	**none**	**air**	**DMF**	**55 °C**	**4:00**	**95 %**
20	1.1	none	air	DCM	45 °C	18:00	59 %
21	1.1	none	air	Cyclohexane	45 °C	18:00	55 %
22	1.1	none	air	THF[i]	45 °C	18:00	28 %

[a] *n*-Dodecanethiol was used as a polarity reversal catalyst (PRC).

[b] LP: lauroyl peroxide; DBP: dibenzoyl peroxide; DTBP: di-*tert*-butyl peroxide. For all the initiators other than air 0.2 equiv. were used. If air was used as an initiator the reaction was left open to air for the whole reaction period via a needle.

[c] The yield was determined by HPLC vs. 1-phenylpyrrolidin-2-one as internal standard unless mentioned otherwise.

[d] The conversion (product / {product + substrate} x 100 %) was determined by ^{1}H-NMR.

[e] Isolated yield.

[f] Additionally 20 % of *p*-terphenyl **422** and 51 % of **418-I** were isolated.

[g] Additionally 15 % of *p*-terphenyl **422** and 36 % of **418-I** were isolated.

[h] Additionally 49 % of **418-I** was isolated.

[i] THF without stabiliser was used.

5.3.4 Optimisation for Reductive Radical Cyclisation Reactions with 419

(Corresponds to Chapter 2.2.2. For the synthesis of **426** see Chapter 5.3.8).

Optimisation for General Protocol A Based on Synthesis of *tert*-Butyl-3-methylindoline-1-carboxylate 427

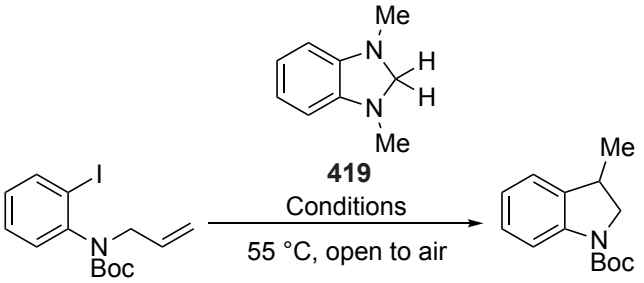

426 **427**

The conditions for 5-*exo*-*trig* reactions with 1,3-dimethyl-2,3-dihydro-1*H*-benzo[*d*]imidazole **419** were optimised for the model substrate *tert*-butyl allyl(2-iodophenyl)carbamate **426**. The results are summarised in Table S7 (corresponds to Table 2-2 in the main text).

Conditions for Entry 1

The reaction vessel was charged with 1,3-dimethyl-2,3-dihydro-1*H*-benzo[*d*]imidazole **419** (356 mg, 2.40 mmol, 2.0 equiv.). Then DMF (2.4 mL) was added followed by *tert*-butyl allyl(2-iodophenyl)carbamate **426** (444 mg, 1.20 mmol, 1.0 equiv.) and a precisely measured amount of internal standard 1-phenylpyrrolidin-2-one (*ca.* 29.0 mg, 0.120 mmol, 0.5 equiv.). All solids were dissolved at room temperature before the reaction was inserted in the pre-heated heat-block. The reaction was heated to 55 °C for 1 h 40 min while left open to air via a needle. Reaction preparation time was < 5 min. The reaction was aliquoted ca. every 10 min. The aliquots were diluted with methanol to ca. 1 mg/mL of substrate and analysed by GC-FID. The reaction was monitored by GC-FID and was found to have reached full conversion after 50 min (the yield vs. the internal standard was found equal to 87 %). The reaction was partitioned between water (66 mL), brine (33 mL) and ethyl acetate (20 mL). The organic phase was extracted with ethyl acetate (3 x 20 mL). The combined organic phases were washed with brine (5 x 20 mL), dried over Na_2SO_4 and concentrated in vacuo. Purification by flash column chromatography (ethyl acetate in heptane, gradient form 0 % to 5 %) gave the product *tert*-butyl 3-methylindoline-1-carboxylate **427** (262 mg, 1.03 mmol, 86 %) as a colourless oil. **^{1}H-NMR** (400 MHz, Chloroform-*d*) δ 7.61 (br m, 1H), 7.20 – 7.14 (m, 1H), 7.14 – 7.11 (m, 1H), 6.95 (ddd, *J* = 7.4, 1.1 Hz, 1H), 4.14 (t, *J* = 10.3 Hz, 1H), 3.57 – 3.46 (m, 1H), 3.45 – 3.31 (m, 1H), 1.57 (s, 9H), 1.32 (d, *J* = 6.8 Hz, 3H). **^{13}C-NMR** (101 MHz, Chloroform-*d*) δ 152.7, 142.0 (br, low intensity), 136.0 (br, low intensity), 127.7, 123.6, 122.4, 114.8, 80.5 (br, low intensity), 55.8, 34.1, 28.6, 20.4. **GC-MS** [*m/z* (%)] (13.312 min): 233 (3, M+), 162 (10), 160 (5), 133 (10), 132 (15), 130 (35), 118 (45), 117 (25), 103 (15), 91 (15), 78 (10), 77 (25), 57 (100). The NMR spectra are in agreement with the previously reported data.[263]

Conditions for Entries 2 - 12

The reaction vessel was charged with 1,3-dimethyl-2,3-dihydro-1*H*-benzo[*d*]imidazole **419** (178 mg, 1.20 mmol, 2.0 equiv.). Solvent (1.2 mL for Entries 2-6 and 9-12 and 6.0 mL for

Entries 7 and 8) was added, followed by dodecanethiol, as required. Then *tert*-butyl allyl(2-iodophenyl)carbamate **426** (221 mg, 0.600 mmol, 1.0 equiv.) and a precisely measured amount of 1-phenylpyrrolidin-2-one (ca. 48.4 mg, 0.300 mmol, 0.5 equiv.), as an internal standard, were added. All solids were dissolved at room temperature before the reaction was inserted in the pre-heated heat-block and left open to air for the whole reaction time. Reaction preparation time was < 5 min. The reactions were aliquoted ca. every 5 min during the first hour. From then on, the reactions were aliquoted ca. every 15 min. The aliquots were diluted with methanol to ca. 1 mg/mL of substrate and analysed by GC-FID. For entry 10, the reaction was repeated on the same scale in the absence of internal standard and the product was isolated: After 2 h of reaction time the reaction was cooled to room temperature. The reaction was partitioned between water (66 mL), brine (33 mL) and ethyl acetate (20 mL). The organic phase was extracted with ethyl acetate (3 x 20 mL). The combined organic phases were washed with brine (5 x 20 mL), dried over Na_2SO_4 and concentrated in vacuo. Purification by flash column chromatography (ethyl acetate in heptane, gradient form 0 % to 5 %) gave the product *tert*-butyl 3-methylindoline-1-carboxylate **427** (91.4 mg, 0.392 mmol, 65 %) as a colourless oil. The NMR spectra were identical to the previously recorded spectra.

Conditions for Entry 13

Preparation of the reagent mixture without reducing agent **419**

The reaction vessel was charged with a precisely measured amount of 1-phenylpyrrolidin-2-one (ca. 48.4 mg, 0.300 mmol, 0.5 equiv.) as an internal standard and *tert*-butyl allyl(2-iodophenyl)carbamate **426** (221 mg, 0.600 mmol, 1.0 equiv.). Then DMF (0.6 mL) was added followed by dodecanethiol (29.3 µL, 0.120 mmol, 0.2 equiv.). The solution was purged with nitrogen for 30 min and pre-heated at 55 °C.

Preparation of a solution of reducing agent **419**

A solution of 1,3-dimethyl-2,3-dihydro-1*H*-benzo[*d*]imidazole **419** (217 mg, 1.46 mmol, 2.4 equiv.) in DMF (0.73 mL) was prepared. The solution was purged with nitrogen for 30 min.

Reaction

From the solution of reducing agent, 0.6 mL were transferred to the pre-heated reaction mixture at 55 °C. The reaction was kept under a flow of nitrogen. Aliquots were taken every 30 min and diluted to ca. 1 mg/mL of substrate with methanol. The diluted aliquots were analysed by GC-FID.

Table S7- Optimisation for General Protocol A

Entry	PRC[a] (equiv.)	Solvent	Concentration	Time[b] (h:min)	Yield of 427[c]
1	**0.2**	**DMF**	**0.5 M**	**0:50**	**87 % (86 %)**[d]
2	0.2	ACN	0.5 M	1:15	75 %
3	0.2	Cyclohexane	0.5 M	4:00	65 %
4	0.2	Toluene	0.5 M	4:00	66 %
5	0.2	THF[e]	0.5 M	3:00	69 %
6	0.2	*t*BuOH	0.5 M	>4:00	46 %[f]
7	0.2	DMF	0.1 M	0:15	77 %
8	1.0	DMF	0.1 M	0:05	81 %
9	0.05	DMF	0.5 M	1:00	76 %
10	none	DMF	0.5 M	2:00	64 % (65 %)[d]

Entry	PRC[a] (equiv.)	Solvent	Concentration	Time[b] (h:min)	Yield of 427[c]
11	0.05	ACN	0.5 M	1:30	69 %
12	none	ACN	0.5 M	2:00	58 %
13[g]	0.2	DMF	0.5 M	>6:00	62 %[h]

[a] *n*-Dodecanethiol was used as a polarity reversal catalyst (PRC).

[b] The reaction progress was monitored by GC-FID and the time when the reaction reached full conversion is given.

[c] Yield determined by GC-FID vs. 1-phenylpyrrolidin-2-one as internal standard unless mentioned otherwise.

[d] Isolated yield in brackets.

[e] THF without stabiliser was used.

[f] Yield of remaining starting material was 45 % by GC-FID vs. 1-phenylpyrrolidin-2-one as internal standard.

[g] The reaction was degassed by purging with nitrogen and was kept under a nitrogen atmosphere.

[h] 22 % of remaining starting material was measured by GC-FID vs. 1-phenylpyrrolidin-2-one as internal standard.

5.3.5 Computational Studies on the Initiation by Oxygen

(Corresponds to Chapter 2.2.3).

All calculations were performed on UM06-2X/6-311++G(d,p)/cpcm(DMF) level of theory. The .log files can be found in the following depository: Https://doi.org/10.15129/deef4cea-f279-4afe-82ca-29b88bd30579 {/Catalytic_Electron_Donor/Initiation}

The structures and corresponding file names for the calculations summarised in Figure 2-2 are listed below (Table S8). It should be noted that Entries 12 - 14 contain supplementary results that have not been discussed in the main text.

Table S8 - File names for structures in Figure 2-2

Entry	Structure	File name	Comment
1	**417**	Benzimidazoyl_radical.log	
2	**419**	Aminal.log	
3	**428**	Aminal_neutral_in_cation_geom.log	Neutral aminal in aminal cation geometry
4	**428**	Aminal_cation.log	
5	**428**	Aminal_cation_in_neutral_geom.log	Aminal cation in neutral aminal geometry
6	**429**	Superoxide_anion.log	Superoxide anion
7	**430**	Hydroxyl_peroxide.log	Hydroxyl peroxide
8	Oxygen	Triplet_oxygen.log	Oxygen
9	Oxygen	TripletOxygen_in_Superoxide_anion_geom.log	Oxygen in superoxide geometry
10	Substrate complex	TS_TripletOxygen_exo_Dihydrobenzimidazole_DMF_M062X_6-311++Gdp_back.log	**419** and oxygen complexed
11	H-abstr. TS	TS_TripletOxygen_exo_Dihydrobenzimidazole_DMF_M062X_6-311++Gdp.log	Transition state for hydrogen abstraction
12	Product complex	TS_TripletOxygen_exo_Dihydrobenzimidazole_DMF_M062X_6-311++Gdp_forward.log	**417** and hydroxyl peroxide complexed

Entry	Structure	File name	Comment
13	Substrate complex (2nd variant)	TS_TripletOxygen_Dihydrobenzimidazole_DMF_M062X_6-311++Gdp_back.log	Analogous to entry 9 with alternative geometry
14	H-abstr. TS (2nd variant)	TS_TripletOxygen_Dihydrobenzimidazole_DMF_M062X_6-311++Gdp.log	Analogous to entry 10 with alternative geometry
15	Product complex (2nd variant)	TS_TripletOxygen_Dihydrobenzimidazole_DMF_M062X_6-311++Gdp_forward.log	Analogous to entry 11 with alternative geometry

Table S9 - File names for structures in Scheme 2-2

Entry	Structure	File name	Comment
1	**419** and **429**	TS_Superoxide_exo_Dihydrobenzimidazole_DMF_M062X_6-311++Gdp_back.log	Substrate complex for hydrogen abstraction by superoxide anion
2	H-abstr. TS	TS_Superoxide_exo_Dihydrobenzimidazole_DMF_M062X_6-311++Gdp_trial_2.log	TS for hydrogen abstraction by superoxide anion
3	**417** and **430**	TS_Superoxide_exo_Dihydrobenzimidazole_DMF_M062X_6-311++Gdp_forward.log	Product complex for hydrogen abstraction by superoxide anion
4	**419** and **430**	TS_Hydroxylperoxide_exo_Dihydrobenzimidazole_DMF_M062X_6-311++Gdp_back.log	Substrate complex for hydrogen abstraction by hydroxyl peroxide
5	H-abstr. TS	TS_Hydroxylperoxide_exo_Dihydrobenzimidazole_DMF_M062X_6-311++Gdp.log	TS for hydrogen abstraction by hydroxyl peroxide
6	**417** and peroxide	TS_Hydroxylperoxide_exo_Dihydrobenzimidazole_DMF_M062X_6-311++Gdp_forward_trial2.log	Product complex for hydrogen abstraction by hydroxyl peroxide
7	Peroxide	Peroxide.log	Hydrogen peroxide

Table S10 - File names for structures in Scheme 2-3

Entry	Structure	File name	Comment
1	**417**	Benzimidazoyl_radical.log	
2	**417**	Benzimidazoyl_radical_in_Benzimidazolium_cation_geom.log	**417** in the geometry of **418**
3	**418**	Benzimidazolium_cation.log	
4	**418**	Benzimidazoium_cation_in_Benzimidazoyl_radical_geom.log	**418** in the geometry of **417**
5	Iodobenzene	Iodobenzene.log	
6	Iodobenzene	Iodobenzene_neutral_in_radical-anion_geom.log	Neutral iodobenzene in geometry of radical anion
7	Iodobenzene radical anion	Iodobenzene_radical-anion_trial2.log	Radical anion of iodobenzene fragmented to phenyl radical and iodide
8	Iodobenzene radical anion	Iodobenzene_radical_anion_in_neutral_geom.log	Radical anion of iodobenzene in the geometry of neutral iodobenzene

5.3.6 Optimisation of the Catalytic Electron Donor Protocol

(Corresponds to Chapter 2.2.4. For the synthesis of **426** see Chapter 5.3.8).

Optimisation for General Protocol B Based on Synthesis of *tert*-Butyl-3-methylindoline-1-carboxylate 427

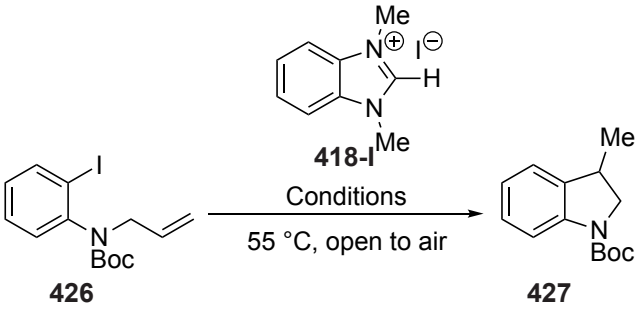

The conditions for 5-*exo*-*trig* reactions with 1,3-dimethyl-1*H*-benzo[*d*]imidazol-3-ium iodide **418-I** as a catalyst were optimised for the model substrate *tert*-butyl allyl(2-iodophenyl)carbamate **426**. The results are summarised in Table S11.

Conditions for Entry 1 and 4 - 18

The reaction vessel was charged with *tert*-butyl allyl(2-iodophenyl)carbamate **426** (73.7 mg, 0.200 mmol, 1.0 equiv.) and 1,3-dimethyl-1*H*-benzo[*d*]imidazol-3-ium iodide **418-I** (11.0 mg, 40.0 µmol, 0.2 equiv.). Then the solvent (0.4 mL) was added as required followed by dodecanethiol as required. Finally, the reducing agent (2.0 equiv.) was added as required and the reaction mixture was inserted in a reaction block, which was pre-heated at 55 °C and was stirred for 4 h. The reaction was left open to air via a needle for the whole reaction time. The reaction mixture was diluted with a solution of 1-phenylpyrrolidin-2-one in methanol (precisely known concentration of *ca.* 1 mg / mL of 1-phenylpyrrolidin-2-one - internal standard) to *ca.* 1 mg / mL of employed substrate and was analysed by GC-FID.

Conditions for Entry 2

The reaction vessel was charged with a precisely measured amount of internal standard dodecane (ca. 38.3 mg, 0.225 mmol, 0.5 equiv.), dodecanethiol (22.0 µL, 90.0 µmol, 0.2 equiv.), *tert*-butyl allyl(2-iodophenyl)carbamate **426** (165 mg, 0.450 mmol, 1.0 equiv.) and the catalyst 1,3-dimethyl-1*H*-benzo[*d*]imidazol-3-ium iodide **418-I** (24.7 mg, 90.0 µmol, 0.2 equiv.). Then DMF (0.9 mL) was added and all solids were dissolved. Then sodium borohydride (34.7 mg, 0.900 mmol, 2.0 equiv.) was added and the reaction was inserted in a reaction block, which was pre-heated at 55 °C. The reaction was left open to air via a needle for the whole reaction time. The reaction was heated at 55 °C for 3 h 40 min. The reaction was monitored by GC-FID and was found to have reached full conversion after 3 h. The yield of product was 91 % by GC-FID. The reaction was partitioned between water (66 mL), brine (33 mL) and ethyl acetate (20 mL). The organic phase was extracted with ethyl acetate (3 x 20 mL). The combined organic phases were washed with brine (5 x 20 mL), dried over Na_2SO_4 and concentrated in vacuo. Purification by flash column chromatography (ethyl acetate in heptane, gradient from 0 % to 5 %) gave the product *tert*-butyl 3-methylindoline-1-carboxylate **427** (90.3 mg, 0.375 mmol, 83 %) as a colourless oil. The NMR spectra were identical to the previously recorded data.

Conditions for Entry 3

The reaction vessel was charged with a precisely measured amount of internal standard 1,3,5-trimethoxybenene (ca. 50.4 mg, 0.300 mmol, 0.5 equiv.), dodecanethiol (29.3 µL, 0.120 mmol, 0.2 equiv.), the substrate *tert*-butyl allyl(2-iodophenyl)carbamate **426** (220 mg, 0.600 mmol, 1.0 equiv.) and the catalyst 1,3-dimethyl-1*H*-benzo[*d*]imidazol-3-ium iodide **418-I** (8.2 mg, 30 µmol, 0.05 equiv.). Then DMF (1.2 mL) was added and all material was dissolved. Then the terminal reducing agent sodium borohydride (46.4 mg, 1.2 mmol, 2.0 equiv.) was added and the reaction was inserted in a reaction block, which was pre-heated at 55 °C. The reaction was left open to air for the whole heating period. An aliquot was taken in regular intervals. The reaction aliquot was partitioned between diethyl ether (1 ml), water (2 mL) and brine (1 mL). The organic phase was passed over $MgSO_4$ and concentrated under a flow of air and dissolved in chloroform-*d*. The aliquot was analysed by ^{1}H-NMR.

Conditions for Entry 19 - 21

The reaction vessel was charged with a precisely measured amount of internal standard *n*-dodecane (ca. 51.1 mg, 0.300 mmol, 0.5 equiv.), dodecanethiol (29.3 µL, 0.120 mmol, 0.2 equiv.), the substrate *tert*-butyl allyl(2-iodophenyl)carbamate **426** (220 mg, 0.600 mmol, 1.0 equiv.) and the catalyst 1,3-dimethyl-1*H*-benzo[*d*]imidazol-3-ium iodide **418-I** (32.9 mg, 0.120 mmol, 0.2 equiv.). Then DMF (1.2 mL) was added and all material was dissolved. Then the terminal reducing agent (Entry 19: $Na(AcO)_3BH$ {1.2 mmol, 262 mg, 2.0 equiv.}; Entry 20: $Na(AcO)_3BH$ {4.8 mmol, 1.05 g, 8.0 equiv.}; Entry 21: $NaBH_3CN$ {1.2 mmol, 79.4 mg, 2.0 equiv.}) was added as required and the reaction was inserted in a reaction block, which was pre-heated at 55 °C. The reaction was left open to air via a needle for the whole reaction time. Aliquots were taken in regular intervals and diluted with methanol to ca. 1 mg / mL of employed substrate. The diluted aliquots were analysed by GC-FID.

Conditions for Entries 22 and 23

The reaction vessel was charged with *tert*-butyl allyl(2-iodophenyl)carbamate **426** (111 mg, 0.300 mmol, 1.0 equiv.). Then DMF (0.6 mL) was added followed by dodecanethiol (Entry 22: 14.7 µL, 60.0 µmol, 0.2 equiv.; Entry 23: 147 µL, 0.600 mmol, 2.0 equiv.) and a precisely measured amount of internal standard 1,3,5-trimethoxybenene (ca. 50.4 mg, 0.300 mmol, 1.0 equiv.). All reactants were dissolved before the addition of sodium borohydride (23.2 mg, 0.600 mmol, 2.0 equiv.). The reaction was heated to 55 °C for the specified time while left open to air via a needle. At the end of the heating period an aliquot was take. The reaction aliquot was partitioned between diethyl ether (1 ml), water (2 mL) and brine (1 mL). The organic phase was passed over $MgSO_4$, and concentrated under a flow of air and dissolved in chloroform-*d*. The aliquot was analysed by ^{1}H-NMR. It was found that the yield of product *tert*-butyl 3-methylindoline-1-carboxylate **427** was 9 % while 87 % of starting material *tert*-butyl allyl(2-iodophenyl)carbamate **426** remained.

Conditions for Entry 24

The reaction vessel was charged with *tert*-butyl allyl(2-iodophenyl)carbamate **426** (111 mg, 0.300 mmol, 1.0 equiv.). Then DMF (0.6 mL) was added followed by a precisely measured amount of internal standard 1,3,5-trimethoxybenene (ca. 50.4 mg, 0.300 mmol, 1.0 equiv.). All reactants were dissolved before the addition of sodium borohydride (23.2 mg, 0.600 mmol, 2.0 equiv.). The reaction was heated to 55 °C for 20 h while left open to air via a needle. A the end of the heating period an aliquot was take. The reaction aliquot was partitioned between diethyl ether (1 ml), water (2 mL) and brine (1 mL). The organic phase was passed over $MgSO_4$, concentrated under a flow of air and dissolved in chloroform-*d*. The aliquot was analysed by

^{1}H-NMR.

Table S11 - Optimisaton for General Protocol A

Entry	Hydride Reducing Agent	Loading of 418-I (equiv.)	PRC (equiv.)[a]	Solvent	Time (h:min)[b]	Yield of 427[c]
1	**$NaBH_4$**	**0.2**	**0.2**	**DMF**	**4:00**	**84 %**
2	**$NaBH_4$**	**0.2**	**0.2**	**DMF**	**3:40**[d]	**83 %**[e]
3	$NaBH_4$	0.05	0.2	DMF	4:00[f]	61 %[g]
4	$NaBH_4$	0.2	none	DMF	4:00	8 %
5	$NaBH_4$	0.2	0.2	ACN	4:00	40 %
6	$NaBH_4$	0.2	none	ACN	4:00	3 %
7	$NaBH_4$	0.2	0.2	*t*BuOH	4:00	20 %
8	$NaBH_4$	0.2	0.2	THF	4:00	18 %
9	$NaBH_4$	0.2	0.2	Toluene/ *t*BuOH	4:00	35 %
10	$NaBH_4$	0.2	0.2	Toluene/ water	4:00	27 %
11	$Na(AcO)_3BH$	0.2	0.2	DMF	4:00	40 %
12	$Na(AcO)_3BH$	0.2	none	DMF	4:00	7 %
13	$Na(AcO)_3BH$	0.2	0.2	ACN	4:00	7 %
14	$Na(AcO)_3BH$	0.2	none	ACN	4:00	1 %
15	$Na(AcO)_3BH$	0.2	0.2	*t*BuOH	4:00	6 %
16	$Na(AcO)_3BH$	0.2	0.2	THF	4:00	5 %
17	$Na(AcO)_3BH$	0.2	0.2	Toluene/ *t*BuOH	4:00	4 %
18	$Na(AcO)_3BH$	0.2	0.2	Toluene/ water	4:00	0 %
19	$Na(AcO)_3BH$	0.2	0.2	DMF	30:00	35 %[h]
20	$Na(AcO)_3BH$[i]	0.2	0.2	DMF	20:00	8 %[j]
21	$NaBH_3CN$	0.2	0.2	DMF	20:00	2 %[k]
22	$NaBH_4$	none	0.2	DMF	20:00	9 %[l]
23	$NaBH_4$	none	2.0	DMF	5:00	64 %
24	$NaBH_4$	none	none	DMF	20:00	0 %[m]

[a] *n*-Dodecanethiol was used as a polarity reversal catalyst (PRC).

[b] Time for which the reaction was heated at 55 °C.

[c] Yield determined by GC-FID vs. 1-phenylpyrrolidin-2-one as an internal standard unless mentioned otherwise.

[d] The reaction reached full conversion after 3 h.

[e] Isolated yield.

[f] The reaction reached full conversion after 4 h.

[g] Yield determined by ^{1}H-NMR vs. 1,3,5-trimethoxybenene as internal standard. No remaining starting material was detected.

[h] Yield of remaining starting material was 65 % by GC-FID vs. *n*-dodecane as internal standard.

[i] 8 equiv. of $Na(AcO)_3BH$ were used.

[j] The reaction was monitored by ^{1}H-NMR. The yield was determined vs. 1,3,5-trimethoxybenene as internal standard. The yield of remaining starting material was 43 % vs. the same internal standard.

[k] Yield of remaining starting material was 98 % by GC-FID vs. *n*-dodecane as internal standard.

[l] Yield determined by ^{1}H-NMR vs. 1,3,5-trimethoxybenene as internal standard. Yield of remaining starting material was 87 % vs. the same internal standard.

[m] The product was not detected by ^{1}H-NMR. Yield of remaining starting material was quantitative vs. 1,3,5-trimethoxybenene as internal standard.

5.3.7 Reductive Radical Cyclisation Reactions

(Corresponds to Chapter 2.3.1. The synthesis of the substrates used in this section is described in Chapter 5.3.8).

***tert*-Butyl 3-isopropylindoline-1-carboxylate 432a**

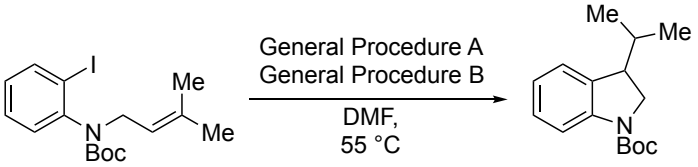

431a **432a**

From substrate **431a** (0.240 g, 0.600 mmol, 1.0 equiv.), according to General Procedure A, the product *tert*-butyl 3-isopropylindoline-1-carboxylate **432a** (105 mg, 0.383 mmol, 64 %) was obtained as a colourless oil after 4 h 30 min (the reaction was monitored by TLC and was found to have reached full conversion after 4 h). According to General Procedure B, the same product *tert*-butyl 3-isopropylindoline-1-carboxylate **432a** (121 mg, 0.464 mmol, 77 %) was obtained as a colourless oil after 3 h (the reaction was monitored by GC-FID and was found to have reached full conversion after 2 h 30 min). The product was purified by flash column chromatography (0 % to 5 % ethyl acetate in heptane). **^{1}H-NMR** (400 MHz, DMSO-d_6, 80 °C) δ 7.59 (d, *J* = 8.1 Hz, 1H), 7.22 – 7.18 (m, 1H), 7.15 (dddd, *J* = 8.1, 1.4, 0.7, 0.7 Hz, 1H), 6.94 (ddd, *J* = 7.5, 1.1, 1.1 Hz, 1H), 3.89 (dd, *J* = 11.5, 9.9 Hz, 1H), 3.71 (dd, *J* = 11.5, 5.2 Hz, 1H), 3.26 (ddd, *J* = 9.8, 4.9, 4.9 Hz, 1H), 2.00 (sepd, *J* = 6.8, 4.5 Hz, 1H), 1.53 (s, 9H), 0.92 (d, *J* = 6.9 Hz, 3H), 0.76 (d, *J* = 6.8 Hz, 3H). **^{13}C-NMR** (101 MHz, DMSO-d_6, 80 °C) δ 151.3, 142.3, 133.3, 126.9, 124.2, 121.5, 113.7, 79.8, 49.4, 44.2, 30.8, 27.7, 19.1, 16.9. **IR** ν_{max} [cm^{-1}]: 3046, 2959, 2930, 2895, 1697, 1601, 1485, 1460, 1389, 1366, 1352, 1325, 1290, 1281, 1256, 1225, 1169, 1130, 1105, 1092, 1042, 1018. **GC-MS** [*m/z* (%)] (14.044 min): 261 (10, M+), 205 (35), 188 (5), 162 (85), 144 (20), 130 (15), 118 (100), 117 (45), 91 (20), 90 (15), 89 (15), 57 (100). **HRMS** (ESI+) [*m/z*]: cacld. for $C_{16}H_{23}NO_2Na$ (M+Na): 284.1621, found: 284.1622.

***tert*-Butyl 3-(acetoxymethyl)indoline-1-carboxylate 432b**

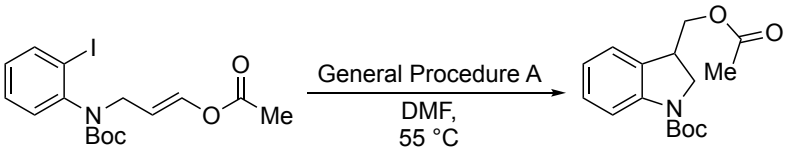

431b **432b**

According to General Procedure A, from substrate **431b** (0.258 g, 0.600 mmol, 1.0 equiv.) the product *tert*-butyl 3-(acetoxymethyl)indoline-1-carboxylate **432b** (38.0 mg, 0.130 mmol, 22 %) was obtained as a colourless oil after 7 h (the reaction was monitored by TLC and was found to have reached full conversion after 4 h). The product was purified by flash column chromatography (20 % ethyl acetate in hexane). **^{1}H-NMR** (400 MHz, Chloroform-d) δ 7.72 (br m, 1H), 7.24 – 7.17 (m, 2H), 6.95 (ddd, *J* = 7.5, 1.1, 1.1 Hz, 1H), 4.28 (dd, *J* = 11.0, 5.8 Hz, 1H), 4.18 – 4.02 (m, 2H), 3.80 (br s, 1H), 3.63 (tt, *J* = 9.8, 5.5 Hz, 1H), 2.08 (s, 3H), 1.57 (s, 9H). **^{13}C-NMR** (101 MHz, Chloroform-d) δ 171.1, 152.6, 134.1, 128.7, 127.5, 124.7 (br) , 122.4, 115.1, 81.0 (br), 66.7, 51.3 (br), 39.2 (br), 28.6, 21.0. **GC-MS** [*m/z* (%)] (15.043 min): 291 (2, M+), 175 (35), 131 (25), 130 (60), 118 (35), 117 (20), 91 (10), 90 (10), 89 (10), 57 (100). The NMR spectra are in agreement with the previously reported data.[264]

***tert*-Butyl 3-(2-methoxy-2-oxoethyl)indoline-1-carboxylate 432c**

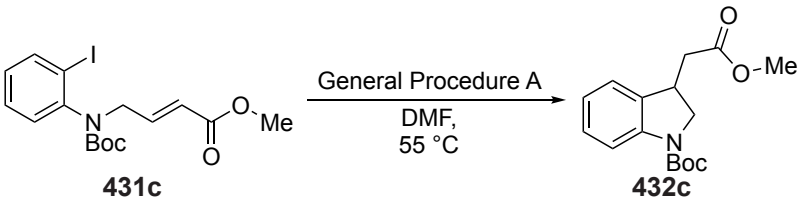

431c **432c**

According to General Procedure A, from substrate **431c** (0.258 g, 0.600 mmol, 1.0 equiv.) the product *tert*-butyl 3-(2-methoxy-2-oxoethyl)indoline-1-carboxylate **432c** (150 mg, 0.515 mmol, 86 %) was obtained as a pale yellow oil after 4 h (the reaction was monitored by TLC and was found to have reached full conversion after 3 h 30 min). The product was purified by flash column chromatography (10 % ethyl acetate in hexane). **^{1}H-NMR** (400 MHz, Chloroform-*d*) δ 7.98 – 7.40 (br m, 1H), 7.18 (ddd, *J* = 7.8, 1.4, 1.4 Hz, 1H), 7.11 (d, *J* = 7.4 Hz, 1H), 6.93 (ddd, *J* = 7.4, 7.4, 1.0 Hz, 1H), 4.19 (dd, *J* = 11.3, 9.4 Hz, 1H), 3.75 (dd, *J* = 10.1, 5.1 Hz, 1H), 3.72 (s, 3H), 3.70 – 3.61 (m, 1H), 2.76 (dd, *J* = 16.4, 4.9 Hz, 1H), 2.55 (dd, *J* = 16.4, 9.4 Hz, 1H), 1.56 (s, 9H). **^{13}C-NMR** (101 MHz, Chloroform-*d*) δ 172.3, 152.5, 142.5 (br), 133.1 (br), 128.3, 123.9 (br), 122.4, 114.9, 80.9 (br), 54.0, 51.9, 40.0, 35.9 (br), 28.5. **GC-MS** [*m/z* (%)] (15.204 min): 291 (4, M+), 235 (10), 191 (10), 176 (5), 162 (5), 161 (5), 158 (5), 131 (10) 130 (50), 118 (70), 117 (50), 103 (10), 91 (10), 90 (10), 89 (10), 77 (10), 59 (15), 57 (100). The NMR spectra are in agreement with the previously reported data.[265]

3-Methyl-2,3-dihydrobenzofuran 432d

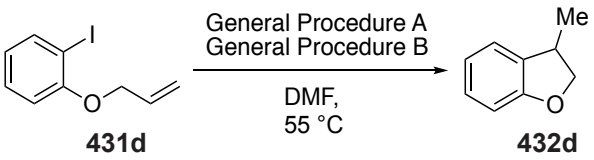

431d **432d**

Due to the volatility of the product, the yield was determined by ^{1}H-NMR *vs.* 1,3,5-trimethoxybenzene as the internal standard. From substrate **431d** (0.159 g, 0.600 mmol, 1.0 equiv.), according to General Procedure A, the product 3-methyl-2,3-dihydrobenzofuran **432d** was formed in 72 % yield after 3 h and according to General Procedure B the same product 3-methyl-2,3-dihydrobenzofuran **432d** was formed in 67 % yield after 22 h. From the reaction performed according to General Procedure B, the product was isolated. Purification by flash column chromatography (2.5 % ethyl acetate in hexane) gave the product 3-methyl-2,3-dihydrobenzofuran **432d** (54 mg, 0.36 mmol, 60 %) as a colourless oil. **^{1}H-NMR** (500 MHz, Chloroform-d) δ 7.16 (ddd, *J* = 7.3, 1.3, 1.3 Hz, 1H), 7.12 (ddd, *J* = 7.6, 7.6, 1.1 Hz, 1H), 6.87 (ddd, *J* = 7.4, 7.4, 1.1 Hz, 1H), 6.79 (d, *J* = 7.9 Hz, 1H), 4.68 (dd, *J* = 8.8, 8.8 Hz, 1H), 4.07 (dd, *J* = 8.5, 7.4 Hz, 1H), 3.55 (app sext, *J* = 7.2 Hz, 1H), 1.34 (d, *J* = 6.9 Hz, 3H). **^{13}C-NMR** (101 MHz, Chloroform-*d*) δ 159.9, 132.4, 128.1, 123.9, 120.6, 109.6, 78.6, 36.6, 19.4. **GC-MS** [*m/z* (%)] (9.015 min): 134 (45, M+), 119 (70), 105 (10), 103 (10), 91 (100), 89 (10), 78 (10), 77 (20), 74 (5), 65 (15), 63 (20), 62 (10). The NMR spectra are in agreement with the previously reported data.[266]

9-(Methylsulfonyl)-2,3,4,4a,9,9a-hexahydro-1*H*-carbazole 435

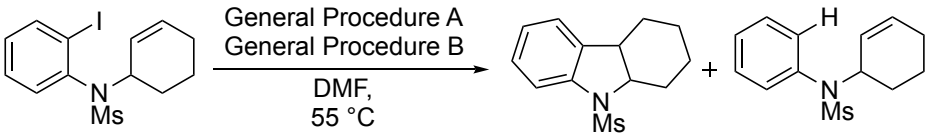

434 **435** **436**

From the substrate **434** (0.233 g, 6.00 mmol, 1.0 equiv.), according to General Procedure A, 9-(methylsulfonyl)-2,3,4,4a,9,9a-hexahydro-1*H*-carbazole **435** (138 mg, 0.519 mmol, 87 %) was obtained as a white solid after 20 h. According to General Procedure B, the same product 9-(methylsulfonyl)-2,3,4,4a,9,9a-hexahydro-1H-carbazole **435** (93.7 mg, 0.373 mmol, 62 %) was obtained as a white solid after 17 h. From the reaction preformed according to General Procedure B, additionally *N*-(cyclohex-2-en-1-yl)-*N*-phenylmethanesulfonamide **436** (17 mg, 66 µmol, 11 %) was isolated as a white solid. The products were purified by flash column chromatography (15 % ethyl acetate in hexane).

9-(Methylsulfonyl)-2,3,4,4a,9,9a-hexahydro-1*H*-carbazole **435**: **^{1}H-NMR** (400 MHz, Chloroform-*d*) δ 7.37 (ddd, *J* = 8.0, 0.8, 0.8 Hz, 1H), 7.24 – 7.15 (m, 2H), 7.08 (ddd, *J* = 7.4, 7.4, 1.1 Hz, 1H), 4.38 (ddd, *J* = 10.1, 7.8, 5.9 Hz, 1H), 3.57 – 3.48 (m, 1H), 2.93 (s, 3H), 2.20 (dddd, *J* = 14.4, 5.5, 3.7, 1.6 Hz, 1H), 2.12 – 2.01 (m, 1H), 1.83 (dddd, *J* = 14.4, 12.2, 5.9, 4.4 Hz, 1H), 1.68 – 1.51 (m, 2H), 1.51 – 1.40 (m, 1H), 1.33 – 1.17 (m, 2H). **^{13}C-NMR** (101 MHz, Chloroform-*d*) δ 141.4, 134.7, 127.9, 124.2, 123.6, 115.5, 64.0, 40.5, 38.6, 28.6, 24.7, 22.2, 20.8. **GC-MS** [*m/z* (%)] (15.254 min): 251 (15, M+), 208 (5), 172 (40), 144 (25), 143 (25), 130 (100),

117 (25), 116 (25), 115 (20), 103 (15), 91 (15), 89 (20), 79 (55), 77 (25), 65 (10), 63 (15). **mp** = 71 °C - 72 °C. The NMR spectra are in agreement with the previously reported data.[94]

N-(Cyclohex-2-en-1-yl)-*N*-phenylmethanesulfonamide **436**: **^{1}H-NMR** (400 MHz, Chloroform-*d*) δ 7.39 – 7.35 (m, 3H), 7.32 – 7.28 (m, 2H), 5.80 – 5.76 (m, 2H), 4.96 – 4.87 (m, 1H), 2.98 (s, 3H), 2.00 (dddd, *J* = 11.1, 5.4, 4.0, 2.9 Hz, 1H), 1.92 – 1.83 (m, 1H), 1.83 – 1.73 (m, 1H), 1.67 – 1.45 (m, 3H). **^{13}C-NMR** (101 MHz, Chloroform-*d*) δ 136.5, 131.9, 131.6, 129.2, 128.8, 128.5, 56.4, 40.9, 29.2, 24.3, 21.4. **IR** ν_{max} [cm^{-1}]: 3034, 2926, 2860, 1593, 1585, 1491, 1449, 1395, 1362, 1323, 1234, 1217, 1200, 1175, 1092, 1076, 1049, 1024, 1011, 995, 966, 893, 826, 766, 733, 700, 658. **GC-MS** [*m/z* (%)] (14.813 min): 251 (0.5, M+), 223 (0.5), 207 (1.5), 171 (60), 143 (30), 130 (15), 117 (25), 104 (15), 92 (50), 81 (55), 79 (90) 77 (100), 65 (35). **HRMS** (ASAP) [*m/z*]: calcd. for $C_{13}H_{18}O_2NS$ (M+H): 252.1058, found: 252.1054. **mp** = 81 °C - 82 °C.

3-Ethylidene-1-(methylsulfonyl)indoline 438a

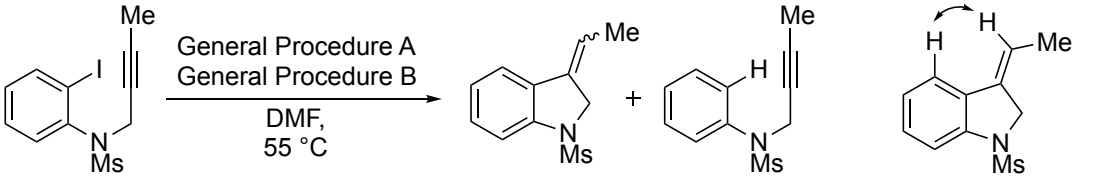

437a **438a** **439a**

Characteristic ^{1}H-^{1}H-NOESY cross-peak for the **438a-*Z*** isomer

From substrate **437a** (0.214 g, 0.600 mmol, 1.0 equiv.), according to General Procedure A, the desired product 3-ethylidene-1-(methylsulfonyl)indoline **438a** (115 mg, 0.504 mmol, 84 %, *E/Z* = 2/8) was obtained as a colourless oil after 20 h. Following General Procedure B, the same product 3-ethylidene-1-(methylsulfonyl)indoline **438a** (83.2 mg, 0.373 mmol, 62 %, *E/Z* = 3/7) was obtained as a colourless oil after 48 h. From the reaction performed following General Procedure B, additionally *N*-(but-2-yn-1-yl)-*N*-phenylmethanesulfonamide **439a** (18.7 mg, 0.0832 mmol, 14 %) was isolated as a colourless oil. The products were purified by flash column chromatography (15 % ethyl acetate in hexane).

3-Ethylidene-1-(methylsulfonyl)indoline **438a**: **^{1}H-NMR** (400 MHz, Chloroform-*d, Z*-isomer) δ 7.49 (ddd, *J* = 8.2, 0.9, 0.9 Hz, 1H), 7.41 (ddd, *J* = 7.7, 0.9, 0.9 Hz, 1H), 7.22 (ddd, *J* = 7.8, 7.8, 1.4 Hz, 1H), 7.06 (ddd, *J* = 7.6, 7.6, 1.0 Hz, 1H), 6.03 (qt, *J* = 7.1, 3.1 Hz, 1H), 4.62 – 4.59 (m, 2H), 2.89 (s, 3H), 1.81 (dt, *J* = 7.2, 2.1 Hz, 3H). **^{13}C-NMR** (101 MHz, Chloroform-*d, Z*-isomer) δ 143.6, 132.9, 130.3, 129.2, 124.0, 120.4, 114.6, 114.3, 53.7, 35.1, 14.9. **GC-MS** [*m/z* (%)] (*Z*-isomer: 14.494 min; *E*-isomer: 14.555 min): 223 (15, M+), 144 (100), 143 (50), 129 (25), 117 (30), 115 (90), 102 (15), 92 (20), 89 (25), 79 (85), 77 (10), 65 (15), 63 (25). The *E*- and *Z*-isomer were distinguished based on the characteristic ^{1}H-^{1}H-NOESY cross-peak for the *Z*-isomer. The NMR spectra are in agreement with the previously reported data.[267]

N-(But-2-yn-1-yl)-*N*-phenylmethanesulfonamide **439**: **^{1}H-NMR** (400 MHz, Chloroform-*d*) δ 7.60 – 7.56 (m, 2H), 7.42 – 7.37 (m, 2H), 7.36 – 7.30 (m, 1H), 4.39 (q, *J* = 2.4 Hz, 2H), 3.02 (s, 3H), 1.88 (t, *J* = 2.4 Hz, 3H). **^{13}C-NMR** (101 MHz, Chloroform-*d*) δ 140.6, 129.5, 128.1, 127.4, 82.3, 74.4, 41.8, 38.9, 3.7. **IR** ν_{max} [cm^{-1}]: 3021, 2922, 2855, 1595, 1491, 1452, 1337, 1215, 1175, 1080, 1063, 1030, 957, 853, 772, 700. **GC-MS** [*m/z* (%)] (13.659 min): 223 (10, M+),

144 (50), 143 (60), 142 (30), 128 (10), 116 (25), 115 (60), 104 (25), 92 (35), 91 (45), 79 (75), 77 (100), 65 (40), 63 (30). **HRMS** (ESI+) [*m/z*]: calcd. for $C_{11}H_{17}N_2O_2S$ (M+NH_4): 241.1005, found: 241.1005.

3-(Cyclohexylmethylene)-1-(methylsulfonyl)indoline 438b

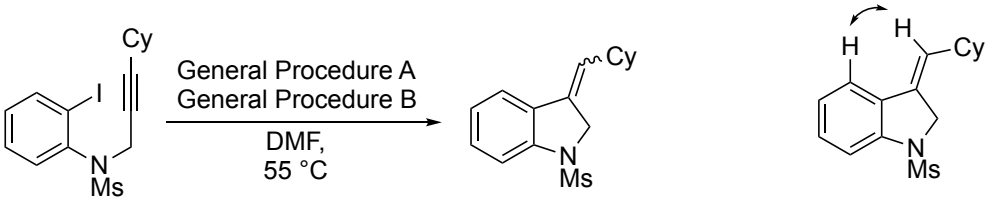

437b **438b**

Characteristic ^{1}H-^{1}H-NOESY cross-peak for the **438b-*Z***.isomer.

From substrate **437b** (0.255 g, 0.600 mmol, 1.0 equiv.), according to General Procedure A, the product 3-(cyclohexylmethylene)-1-(methylsulfonyl)indoline **438b** (126 mg, 0.432 mmol, 90 %, *E/Z* = 3/7) was obtained as a colourless oil after 20 h. According to General Procedure B, the same product 3-(cyclohexylmethylene)-1-(methylsulfonyl)indoline **438b** (145 mg, 0.496 mmol, 83 %, *E/Z* = 2/8) was obtained as a colourless oil after 48 h. The product was purified by flash column chromatography (10 % ethyl acetate in hexane). **^{1}H-NMR** (400 MHz, Chloroform-*d*, *Z*-isomer) δ 7.45 (ddd, *J* = 8.2, 0.9, 0.9 Hz, 1H), 7.40 – 7.37 (m, 1H), 7.19 (ddd, *J* = 8.2, 7.4, 1.3 Hz, 1H), 7.03 (ddd, *J* = 7.5, 7.5, 1.0 Hz, 1H), 5.79 (dt, *J* = 9.6, 3.1 Hz, 1H), 4.60 (d, *J* = 3.0 Hz, 2H), 2.87 (s, 3H), 2.09 (tdt, *J* = 11.6, 10.1, 3.6 Hz, 1H), 1.85 – 1.65 (m, 5H), 1.44 – 1.11 (m, 5H). **^{13}C-NMR** (101 MHz, Chloroform-*d*, *Z*-isomer) δ 143.6, 130.4, 130.0, 129.2, 125.9, 123.9, 120.5, 114.2, 53.4, 39.2, 35.1, 32.5, 26.0, 25.9. **IR** ν_{max} [cm^{-1}]: 3020, 2926, 2851, 1718, 1676, 1605, 1539, 1464, 1447, 1350, 1298, 1279, 1225, 1159, 1126, 1069, 1018, 976, 962, 908, 783, 746, 725, 648. **GC-MS** [*m/z* (%)] (*Z*-isomer: 17.080 min; *E*-isomer: 17.033 min): 291 (10, M+), 208 (10), 168 (20), 167 (10), 156 (10), 154 (20), 130 (100), 128 (25), 115 (15), 79 (35), 67 (10). **HRMS** (ASAP) [*m/z*]: calcd. for $C_{16}H_{22}NO_2S$ (M+H): 292.1371, found: 292.1367. The *E*- and *Z*-isomer were distinguished based the characteristic ^{1}H-^{1}H-NOESY cross-peak for the *Z*-isomer.

***tert*-Butyl 3-(2-((tert-butyldiphenylsilyl)oxy)ethyl)-1*H*-indole-1-carboxylate 441a**

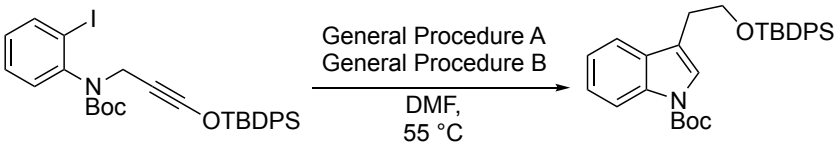

440a **441a**

From substrate **440a** (0.316 g, 0.5 mmol, 1.0 equiv.), according to General Procedure A, the product *tert*-butyl 3-(2-((*tert*-butyldiphenylsilyl)oxy)ethyl)-1*H*-indole-1-carboxylate **441a** (197 mg, 0.395 mmol, 79 %) was obtained as a colourless oil after 3 h 40 min (the reaction was monitored by TLC and was found to have reached full conversion after 2 h 50 min). According to General Procedure B, the same product t*ert*-butyl 3-(2-((*tert*-butyldiphenylsilyl)oxy) ethyl)-1*H*-indole-1-carboxylate **441a** (133 mg, 0.267 mmol, 53 %) was obtained as a colourless oil after 25 h. The product was purified by flash column chromatography (5 % ethyl acetate in hexane). **^{1}H-NMR** (400 MHz, Chloroform-d) δ 7.76 – 7.65 (m, 4H), 7.47 – 7.27 (m, 10H),

6.96 (td, *J* = 7.5, 1.0 Hz, 1H), 4.37 – 4.34 (m, 2H), 4.32 (dt, *J* = 6.1, 2.0 Hz, 2H), 1.55 (s, 9H, major rotamer), 1.52 (s, 9H, minor rotamer), 1.07 (s, 9H). **^{13}C-NMR** (101 MHz, Chloroform-d, major rotamer) δ 151.8, 135.8, 133.8, 133.6, 129.9, 129.6, 129.1, 127.9, 122.4, 120.1, 116.3, 115.4, 115.2, 81.0, 62.2, 29.9, 28.6, 27.0, 19.3. **IR** ν_{max} [cm^{-1}]: 3071, 3049, 2957, 2930, 2857, 1734, 1605, 1589, 1472, 1452, 1427, 1369, 1308, 1254, 1152, 1128, 1105, 1092, 1059, 1016. **LC-(ESI+)-MS** [*m/z*] (11.917 min): 541 (M+ACN+H). **HRMS** (ESI+) [*m/z*]: calcd. for $C_{31}H_{41}N_{23}Si$ (M+NH_4): 517.2881, found: 517.2873.

***tert*-Butyl 3-methyl-1*H*-indole-1-carboxylate 441b**

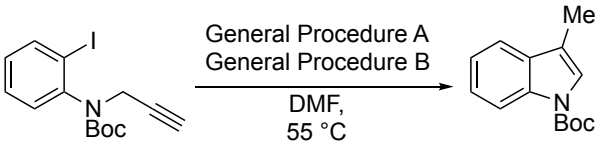

440b **441b**

From substrate **440b** (0.221 g, 0.600 mmol, 1.0 equiv.), according to General Procedure A, the product *tert*-butyl 3-methyl-1*H*-indole-1-carboxylate **441b** (51 mg, 0.21 mmol, 36 %) was obtained as a colourless oil after 24 h. According to General Procedure B, the same product *tert*-butyl 3-methyl-1*H*-indole-1-carboxylate **441b** (52 mg, 0.21 mmol, 36 %) was obtained as a colourless oil after 3 h (the reaction was monitored by TLC and was found to have reached full conversion after 2 h 50 min). The product was purified by flash column chromatography (5 % ethyl acetate in hexane). **^{1}H-NMR** (400 MHz, Chloroform-*d*) δ 8.12 (br d, *J* = 8.2 Hz, 1H), 7.50 (ddd, *J* = 7.6, 1.4, 0.7 Hz, 1H), 7.35 (br s, 1H), 7.31 (ddd, *J* = 8.4, 7.2, 1.4 Hz, 1H), 7.29 – 7.20 (m, 1H), 2.27 (d, *J* = 1.3 Hz, 3H), 1.67 (s, 9H). **^{13}C-NMR** (101 MHz, Chloroform-*d*) δ 150.0, 135.6, 131.6, 124.3, 122.9, 122.4, 119.0, 116.5, 115.3, 83.3, 28.4, 9.7. **GC-MS** [*m/z* (%)] (13.794 min): 231 (15, M+), 176 (10), 175 (65), 174 (30), 158 (10), 131 (35), 130 (100), 129 (20), 128 (15), 103 (35), 102 (25), 77 (45), 57 (95). The NMR spectra are in agreement with the previously reported data.[268]

2-(4-Methoxyphenyl)-4-methyltetrahydrofuran 443

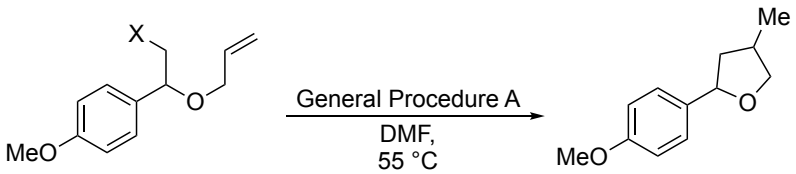

442 **443**

The substrates [**442a** (0.197 g, 0.600 mmol, 1.0 equiv.), **442b** (0.168 mg, 0.600 mmol, 1.0 equiv.), **442c** (0.140 g, 0.600 mmol, 1.0 equiv.)] were reacted according to the General Procedure A. The product 2-(4-methoxyphenyl)-4-methyltetrahydrofuran **443** was purified by flash column chromatography (10 % ethyl acetate in hexane) and obtained as a colourless oil in a diastereomeric ratio of 4:1 in all cases where product was formed. The substrate was treated following General Procedure A. The results are summarised in Table S12 below.

Table S12 - Alkylhalide Substrate Series

Substrate	X	Reaction Time (h:min)	Time to Full Conversion (h:min)	Yield of 443	Recovered Substrate
442a	I	4:30	4:00	100 mg, 0.520 mmol, 87 %	none
442b	Br	7:45	7:15	76.7 mg, 0.399 mmol, 67 %	none
442c	Cl	49:00	not applicable	none	70 %

2-(4-Methoxyphenyl)-4-methyltetrahydrofuran **443**: **^{1}H-NMR** (400 MHz, Chloroform-*d*) δ 7.31 – 7.20 (m, 2H), 6.90 – 6.84 (m, 2H), 4.97 (dd, *J* = 6.9, 6.9 Hz, 1H, major), 4.86 (dd, *J* = 9.9, 5.7 Hz, 1H, minor), 4.25 – 4.18 (m, 1H, major), 4.10 – 4.04 (m, 1H, minor), 3.80 (s, 3H, minor), 3.80 (s, 3H, major), 3.56 (d, *J* = 7.9 Hz, 1H, minor), 3.44 (dd, *J* = 8.2, 6.9 Hz, 1H, major), 2.55 – 2.36 (m, 1H), 2.05 – 1.85 (m, 2H), 1.10 (d, *J* = 6.5 Hz, 3 H, minor), 1.09 (d, *J* = 6.8 Hz, 3H, major). **^{13}C-NMR** (101 MHz, Chloroform-*d*, major diastereoisomer) δ 158.9, 136.0, 127.0, 113.8, 79.9, 75.7, 55.4, 42.7, 33.5, 18.0. **^{13}C-NMR** (101 MHz, Chloroform-*d*, minor diastereoisomer) δ 159.0, 135.5, 127.2, 113.9, 81.5, 75.5, 55.4, 44.0, 35.1, 17.7. **GC-MS** [*m/z* (%)] (12.688 min): 192 (25, M+), 191 (35), 161 (20), 147 (15), 136 (30), 135 (100), 134 (10), 121 (15), 119 (10), 108 (5), 92 (10), 91 (25), 79 (5), 78 (15), 77 (25), 65 (15), 64 (5), 63 (15). The NMR spectra are in agreement with the previously reported data.[6]

***tert*-Butyl 3-(4-methyltetrahydrofuran-3-yl)indoline-1-carboxylate 445a**

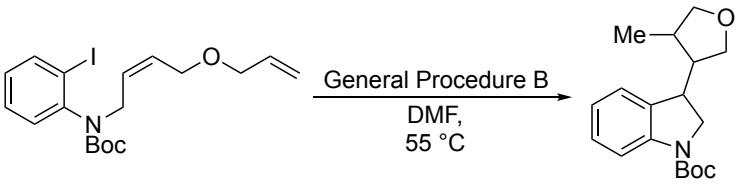

444a **445a**

The substrate **444a** (0.263 g, 0.600 mmol, 1.0 equiv.) was reacted according to General Procedure B. The product *tert*-butyl 3-(4-methyltetrahydrofuran-3-yl)indoline-1-carboxylate **445a** (93.2 mg, 0.307 mmol, 51 %, d.r. = 7:1) was obtained as a colourless oil after 28 h. The product was purified by flash column chromatography (20 % ethyl acetate in hexane). **^{1}H-NMR** (400 MHz, Chloroform-*d*) δ 7.67 (br m, 1H), 7.24 – 7.11 (m, 1H), 6.99 – 6.89 (m, 2H), 4.16 – 3.20 (m, 7H), 2.62 – 2.02 (m, 2H), 1.57 (br s, 9H), 1.17 (d, *J* = 6.8 Hz, 3H, isomer A), 1.06 (d, *J* = 6.7 Hz, 3H, isomer B). **^{13}C-NMR** (101 MHz, Chloroform-*d*, major isomer) δ 152.7, 142.4 (br), 133.7 (br), 128.1, 124.6 (br), 122.3, 115.1, 81.4 (br), 75.6, 70.0, 53.1, 48.5, 38.6 (br), 35.4, 28.6, 14.2. **IR** ν_{max} [cm^{-1}]: 3049, 2967, 2928, 2855, 1697, 1601, 1574, 1483, 1460, 1389, 1366, 1354, 1337, 1317, 1286, 1254, 1223, 1169, 1130, 1098, 1043, 1016. **LC-(ESI+)-MS** [*m/z*] (major isomer: 8.875 min; minor isomer 8.797 min): 304 (M+H). **HRMS** (ESI+) [*m/z*]: calcd. for $C_{18}H_{26}NO_3$ (M+H): 304.1907, found: 304.1909.

3-(4-Methyltetrahydrofuran-3-yl)-2,3-dihydrobenzofuran 445b

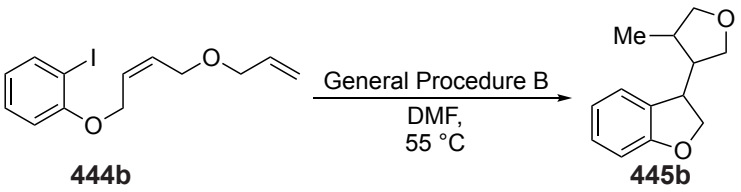

444b **445b**

The substrate **444b** (0.202 g, 0.600 mmol, 1.0 equiv.) was reacted according to General Procedure B. The product 3-(4-methyltetrahydrofuran-3-yl)-2,3-dihydrobenzofuran **445b** (75.6 mg, 0.370 mmol, 62 %, d.r. = 5:2:1:1) was obtained as a colourless oil after 26 h. The product was purified by flash column chromatography (20 % ethyl aceate in hexane). **^{1}H-NMR** (400 MHz, Chloroform-*d*) δ 7.25 – 6.77 (m, 4H), 4.72 – 3.26 (m, 7H), 2.61 – 2.01 (m, 2H), 1.17 (d, *J* = 6.8 Hz, 3H, isomer A), 1.07 (d, *J* = 6.7 Hz, 3H, isomer B), 1.03 (d, *J* = 7.1 Hz, 3H, isomer C), 0.95 – 0.92 (d, *J* = 6.4 Hz, 3H, isomer D). **^{13}C-NMR** (101 MHz, Chloroform-*d*, all isomers) δ 160.4, 160.0, 129.7, 128.9, 128.7, 128.6, 124.9, 124.8, 124.6, 124.6, 120.7, 120.6, 75.9, 75.8, 75.7, 75.7, 75.0, 74.8, 74.1, 71.9, 70.7, 70.1, 69.5, 50.9, 50.8, 48.0, 47.3, 44.1, 43.1, 41.6, 40.9, 37.6, 37.1, 35.3, 35.2, 29.8, 18.2, 17.4, 14.3, 14.3. **IR** ν_{max} [cm^{-1}]: 3048, 2961, 2928, 2870, 2857, 1609, 1595, 1481, 1458, 1385, 1321, 1229, 1165, 1149, 1098, 1074, 1049, 1018. **GC-MS** [*m/z* (%)] (major isomer: §13.642 min): 204 (10, M+), 131 (10), 119 (80), 118 (20), 115 (10), 91 (100), 89 (10), 77 (10), 65 (20), 63 (10), 55 (30). **HRMS** (EI) [*m/z*]: calcd. for $C_{13}H_{16}O_2$ (M+): 204.1150, found: 204.1144.

5.3.8 Substrate Synthesis for Reactions of Chapter 5.3.7

***tert*-Butyl (2-iodophenyl)carbamate 647**

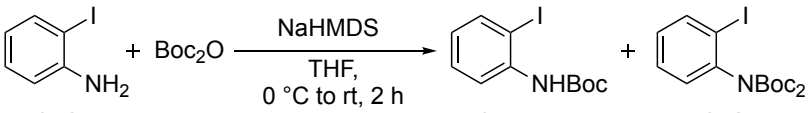

646 **647** **648**

The reaction was kept under nitrogen and anhydrous THF was used. The reaction vessel was charged with THF (58 mL). Then 2-iodoaniline **646** (11.2 g, 50.0 mmol, 1.0 equiv.) was added and the solution was cooled in the ice bath before the slow addition of NaHMDS (110 mL, 1.00 M, 110 mmol, 2.2 equiv.) over *ca.* 15 min. The reaction was stirred at room temperature for 30 min. Then di-*tert*-butyl dicarbonate (12.9 mL, 55.0 mmol, 1.1 equiv.) was added over *ca.* 5 min. A slightly exothermic reaction occurred and a brown solid started to precipitate. The reaction was stirred at room temperature for 1 h 30 min. The reaction was quenched by the addition of aqueous HCl (2.0 M, 110 mL, such that pH = 7) and ethyl acetate (40 mL). The phases were separated and the aqueous phase was extracted with ethyl acetate (3 x 40 mL). The combined organic phases were washed with brine, dried over Na_2SO_4 and concentrated in vacuo to give the crude product as a brown oil. Purification by flash column chromatography (ethyl acetate in hexane, gradient from 0 % to 10 %) gave the desired product *tert*-butyl (2-iodophenyl)carbamate **647** (12.8 g, 40.3 mmol, 81 %) as a pale yellow oil. Additionally, *N,N*-di-(*tert*-butyl-carbamate)-2-iodoaniline **648** (1.13 g, 2.69 mmol, 5.4 %) was isolated as a white solid and remaining starting material 2-iodoaniline **646** (1.32 g, 6.02 mmol, 12 %) was

recovered.

tert-Butyl (2-iodophenyl)carbamate **647**: **^{1}H-NMR** (400 MHz, Chloroform-*d*) δ 8.05 (dd, *J* = 8.3, 1.5 Hz, 1H), 7.75 (dd, *J* = 7.9, 1.5 Hz, 1H), 7.31 (ddd, *J* = 8.5, 7.3, 1.5 Hz, 1H), 6.82 (br, 1H), 6.79 - 6.73 (m, 1H), 1.54 (s, 9H). **^{13}C-NMR** (101 MHz, Chloroform-*d*) δ 152.7, 139.0, 129.3, 124.8, 120.3, 88.9, 81.2, 28.5. **LC-(ESI+)-MS** [*m/z*] (8.923 min): 181 (M+ACN+2H). The NMR spectra are in agreement with the previously reported data.[269]

N,N-di-(*tert*-Butyl-carbamate)-2-iodoaniline **648**: **^{1}H-NMR** (400 MHz, Chloroform-*d*) δ 7.84 (dd, *J* = 7.9, 1.4 Hz, 1H), 7.34 (ddd, *J* = 7.6, 7.6, 1.4 Hz, 1H), 7.20 (dd, *J* = 7.9, 1.6 Hz, 1H), 7.00 (ddd, *J* = 7.6, 7.6, 1.6 Hz, 1H), 1.40 (s, 18H). **^{13}C-NMR** (101 MHz, Chloroform-*d*) δ 150.5, 142.2, 139.2, 129.1, 129.0, 99.9, 83.0, 28.0. **LC-(ESI+)-MS** [*m/z*] (9.200): 442 (M+Na). **mp** = 102 °C - 103 °C. The NMR spectra are in agreement with the previously reported data.[270]

***tert*-Butyl allyl(2-iodophenyl)carbamate 426**

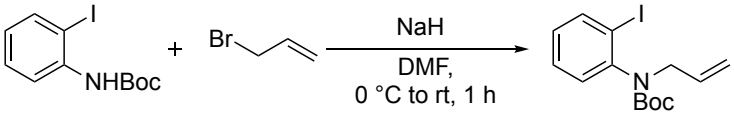

647 **649** **426**

The reaction was kept under nitrogen and anhydrous DMF was used. The reaction vessel was charged with *tert*-butyl (2-iodophenyl)carbamate **647** (6.72 g, 21.1 mmol, 1.0 equiv.). Then DMF (50 mL) was added and the solution was cooled in the ice bath before the careful addition of sodium hydride (926 mg, 23.2 mmol, 1.1 equiv., 60 % suspension in mineral oil). The reaction was stirred at ice bath temperature for 30 min. Then 3-bromoprop-1-ene **649** (3.29 mL, 25.3 mmol, 1.2 equiv.) was added and the reaction was stirred at room temperature for 30 min. The reaction was quenched by the addition of aqueous ammonium chloride (20 mL, sat.), water (500 mL) and *tert*-butylmethyl ether (100 mL). The phases were separated and the aqueous phase was extracted with *tert*-butylmethyl ether (3 x 100 mL). The combined organic phases were washed with water (5 x 50 mL) and brine (1 x 50 mL). Then they were dried over Na_2SO_4 and concentrated *in vacuo* to give the pure product *tert*-butyl allyl(2-iodophenyl)carbamate **426** (7.72 g, 21.1 mmol, quant.) as a pale yellow solid. **^{1}H-NMR** (400 MHz, DMSO-d_6, 80 °C) δ 7.90 (dd, *J* = 7.9, 1.4 Hz, 1H), 7.39 (ddd, *J* = 7.6, 7.6, 1.5 Hz, 1H), 7.23 (dd, *J* = 7.8, 1.6 Hz, 1H), 7.05 (ddd, *J* = 7.6, 7.6, 1.6 Hz, 1H), 5.90 (ddt, *J* = 16.8, 10.4, 6.3 Hz, 1H), 5.09 (m, 2H), 4.35 (dd, *J* = 15.4, 5.8 Hz, 1H), 3.79 (dd, *J* = 15.5, 6.7 Hz, 1H), 1.36 (s, 9H). **^{13}C-NMR** (101 MHz, DMSO-d_6, 80 °C) δ 152.6, 143.8, 138.7, 133.4, 129.6, 128.5, 128.5, 117.0, 100.2, 79.2, 51.5, 27.6. **^{1}H-NMR** (400 MHz, Chloroform-*d*) δ 7.86 (d, *J* = 7.9 Hz, 1H), 7.31 (dd, *J* = 7.5, 7.5 Hz, 1H), 7.22 (d, *J* = 7.5 Hz, 1H, minor rotamer), 7.13 (d, *J* = 7.8 Hz, 1H, major rotamer), 6.97 (ddd, *J* = 7.7, 7.7, 1.6 Hz, 1H), 6.01 – 5.87 (m, 1H), 5.17 – 5.02 (m, 2H), 4.55 – 4.37 (m, 1H), 3.84 – 3.63 (m, 1H), 1.53 (s, 9H, minor rotamer), 1.35 (s, 9H, major rotamer). **^{13}C-NMR** (101 MHz, Chloroform-*d*, major rotamer) δ 154.0, 144.4, 139.5, 133.7, 130.1, 128.8, 128.7, 118.0, 100.7, 80.4, 52.1, 28.4. **GC-MS** [*m/z* (%)] (13.660 min): 359 (0.4, M+), 303 (25), 286 (10), 259 (30), 245 (10), 232 (15), 230 (25), 203 (25), 177 (30), 176 (85), 159 (15), 132 (65), 130 (75), 117 (30), 104 (20), 90 (20), 77 (40), 76 (30), 57 (100). **mp** = 52 °C - 54 °C. The NMR spectra recorded in chloroform-*d* are in agreement with the previously reported data.[271]

***tert*-Butyl (2-iodophenyl)(3-methylbut-2-en-1-yl)carbamate 431a**

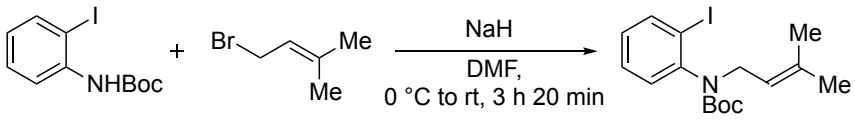

647 **650** **431a**

The reaction was kept under nitrogen and anhydrous DMF was used. The reaction vessel was charged with *tert*-butyl (2-iodophenyl)carbamate **647** (798 mg, 2.50 mmol, 1.0 equiv.). Then DMF (16 mL) was added and the solution was cooled in the ice bath before the careful addition of sodium hydride (110 mg, 2.75 mmol, 1.1 equiv., 60 % suspension in mineral oil). The reaction was stirred at ice bath temperature for 35 min. Then 1-bromo-3-methylbut-2-ene **650** (365 µL, 3.00 mmol, 1.2 equiv.) was added and the reaction was stirred at room temperature for 2 h 45 min. The reaction was monitored by LC-MS and was found to have reached full conversion after 1 h 20 min. The reaction was poured onto water (100 mL), brine (50 mL) and ethyl acetate (20 mL). The phases were separated and the aqueous phase was extracted with ethyl acetate (3 x 20 mL). The combined organic phases were washed with brine (5 x 20 mL), dried over Na_2SO_4 and concentrated *in vacuo*. Purification by flash column chromatography (ethyl acetate in heptane, gradient from 0 % to 5 %) gave *tert*-butyl (2-iodophenyl)(3-methylbut-2-en-1-yl)carbamate **431a** (879 mg, 2.27 mmol, 91 %) as a pale yellow oil. Upon storage on the bench for weeks the material crystallised to give a white solid. **^{1}H-NMR** (400 MHz, DMSO-d_6, 80 °C) δ 7.92 – 7.83 (m, 1H), 7.38 (dd, *J* = 8.4, 6.6 Hz, 1H), 7.24 – 7.13 (m, 1H), 7.03 (dd, *J* = 8.5, 6.6 Hz, 1H), 5.26 (dd, *J* = 6.8, 6.8 Hz, 1H), 4.28 (dd, *J* = 15.0, 6.8 Hz, 1H), 3.87 (dd, *J* = 15.1, 7.5 Hz, 1H), 1.64 (s, 3H), 1.42 (s, 3H), 1.35 (s, 9H). **^{13}C-NMR** (101 MHz, DMSO-d_6, 80 °C, major rotamer) δ 152.7, 143.4, 138.8, 135.2, 129.6, 128.7, 128.6, 119.4, 100.5, 79.0, 45.8, 27.9, 25.2, 17.2. **IR** ν_{max} [cm^{-1}]: 3057, 2986, 2968, 2930, 1687, 1578, 1468, 1449, 1431, 1389, 1366, 1296, 1254, 1160, 1140, 1103, 105, 1032, 1015. **GC-MS** [*m/z* (%)] (14.499 min): 387 (0.1, M+), 331 (15), 263 (15), 245 (5), 230 (5), 219 (10), 204 (15), 203 (5), 162 (15), 158 (10), 144 (10), 136 (20), 118 (10), 90 (10), 69 (40), 57 (100). **HRMS** (ESI+) [*m/z*]: calcd. for $C_{16}H_{23}INO_2$ (M+H): 388.0768, found: 388.0768. **mp** = 40 °C - 41 °C.

***tert*-Butyl (3,3-dimethoxypropyl)(2-iodophenyl)carbamate 652**

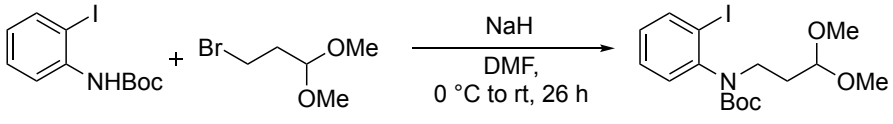

647 **651** **652**

The reaction was kept under nitrogen and anhydrous DMF was used. The reaction vessel was charged with *tert*-butyl (2-iodophenyl)carbamate **647** (4.79 g, 15.0 mmol, 1.0 equiv.). Then DMF (60 mL) was added and the solution was cooled in the ice bath before the careful addition of NaH (660 mg, 16.5 mmol, 1.1 equiv., 60 % emulsion in mineral oil). The reaction was stirred at ice bath temperature for 30 min. Then 3-bromo-1,1-dimethoxypropane **651** (2.96 mL, 19.5 mmol, 1.3 equiv.) was added and the reaction was stirred at room temperature for 26 h. The reaction was quenched by the addition of water (50 mL). The reaction was partitioned

between water (450 mL) and *tert*-butyl methyl ether (100 mL). The phases were separated and the aqueous phase was extracted with *tert*-butyl methyl ether (3 x 100 mL). The combined organic phases were washed with water (5 x 50 mL) and brine (1 x 50 mL). The organic phase was dried over Na_2SO_4 and concentrated *in vacuo*. Purification by flash column chromatography (ethyl acetate in heptane, gradient from 0 % to 15 %) gave the product *tert*-butyl (3,3-dimethoxypropyl)(2-iodophenyl)carbamate **652** (6.06 g, 14.4 mmol, 96 %) as a colourless oil. Upon storage on the bench for weeks, the material crystallised to give a white solid. **^{1}H-NMR** (400 MHz, DMSO-d_6, 80 °C) δ 7.91 (dd, *J* = 7.9, 1.5 Hz, 1H), 7.42 (ddd, *J* = 7.6, 7.6, 1.5 Hz, 1H), 7.28 (dd, *J* = 7.9, 1.6 Hz, 1H), 7.06 (ddd, *J* = 7.6, 7.6, 1.6 Hz, 1H), 4.38 (t, *J* = 5.5 Hz, 1H), 3.72 (ddd, J = 14.0, 9.1, 6.4 Hz, 1H), 3.34 – 3.24 (m, 1H), 3.22 (s, 3H), 3.21 (s, 3H), 1.89 – 1.74 (m, 2H), 1.36 (s, 9H). **^{13}C-NMR** (101 MHz, DMSO-d_6, 80 °C) δ 152.7, 144.1, 138.8, 129.4, 128.6, 128.4, 102.3, 100.0, 79.0, 52.4, 45.0, 31.2, 27.6. **IR** ν_{max} [cm^{-1}]: 2965, 2932, 2830, 1687, 1580, 1470, 1445, 1381, 1362, 1314, 1252, 1223, 1159, 1146, 1123, 1096, 1063, 1049, 1020. **LC-(ESI+)-MS** [*m/z*] (8.884 min): 444 (M+Na). **HRMS** (ESI+) [*m/z*]: calcd. for $C_{16}H_{25}O_4NI$ (M+H): 422.0823, found: 422.0821. **mp** = 34 °C - 35 °C.

***tert*-Butyl (2-iodophenyl)(3-oxopropyl)carbamate 653**

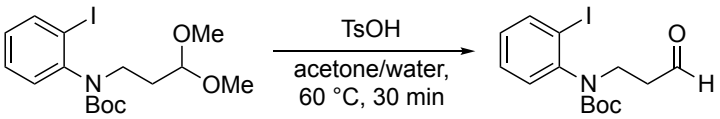

652 **653**

The reaction vessel was charged with *tert*-butyl (3,3-dimethoxypropyl)(2-iodophenyl)carbamate **652** (2.11 g, 5.00 mmol, 1.0 equiv.). Then acetone (150 mL) and water (15 mL) were added followed by 4-methylbenzenesulfonic acid hydrate (1.24 g, 6.50 mmol, 1.3 equiv.). The reaction was stirred at gentle reflux (oil bath at 60 °C) for 30 min. The reaction was monitored by TLC and was found to have reached full conversion after 20 min. The reaction was cooled to room temperature and most of the acetone was evaporated *in vacuo*. The reaction was partitioned between water (100 mL), saturated aqueous $NaHCO_3$ (50 mL) and ethyl acetate (30 mL). The phases were separated and the aqueous phase was extracted with ethyl acetate (3 x 30 mL). The combined organic phases were washed with brine (1 x 30 mL), dried over $MgSO_4$ and concentrated *in vacuo* to give pure *tert*-butyl (2-iodophenyl)(3-oxopropyl)carbamate **653** (1.88 g, 5.00 mmol, quant.) as a pale yellow oil. **^{1}H-NMR** (400 MHz, Chloroform-*d*) δ 9.79 (t, *J* = 1.8 Hz, 1H), 7.87 (d, *J* = 7.9 Hz, 1H), 7.35 (dd, *J* = 7.7, 7.7 Hz, 1H), 7.25 – 7.10 (m, 1H), 6.99 (ddd, *J* = 7.7, 7.7, 1.6 Hz, 1H), 4.13 (dt, *J* = 14.2, 7.1 Hz, 1H), 3.67 (dt, *J* = 14.5, 6.6 Hz, 1H), 2.85 – 2.65 (m, 2H), 1.53 (s, 9H, minor rotamer), 1.34 (s, 9H, major rotamer). **^{13}C-NMR** (101 MHz, Chloroform-*d*, major rotamer) δ 201.0, 154.1, 144.4, 139.7, 129.8, 129.3, 129.1, 100.4, 80.8, 43.6, 43.2, 28.3. **GC-MS** [*m/z* (%)] (14.767 min): 375 (0.02, M+H), 302 (2), 275 (3), 232 (10), 219 (15), 192 (25), 148 (2), 136 (4), 118 (6), 104 (5), 91 (8), 77 (8), 57 (100). The NMR spectra are in agreement with the previously reported data.[272]

(*E*)-3-((*tert*-Butoxycarbonyl)(2-iodophenyl)amino)prop-1-en-1-yl acetate 431b

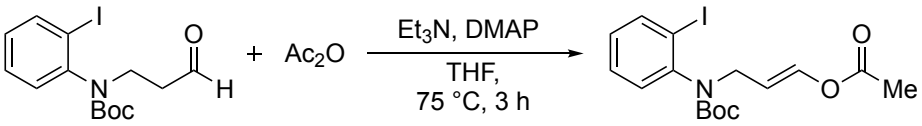

653 **431b**

To the solution of *tert*-butyl (2-iodophenyl)(3-oxopropyl)carbamate **653** (1.69 g, 4.50 mmol, 1.0 equiv.) in THF (25 mL) was added triethylamine (3.2 mL, 23 mmol, 5.0 equiv.) and DMAP (64.8 mg, 0.530 mmol, 0.12 equiv.) followed by acetic anhydride (2.24 mL, 22.5 mmol, 5.0 equiv.). The reaction was gently refluxed (oil bath at 75 °C) for 3 h 25 min. The reaction was monitored by TLC and was found to have reached full conversion after 3 h 15 min. The reaction was cooled to room temperature and most of the solvent was removed *in vacuo*. The residue was poured onto phosphate buffer (50 mL, 1 M, pH = 7.4) and extracted with ethyl acetate (4 x 20 mL). The combined organic phases were washed subsequently with saturated aqueous sodium carbonate (1 x 40 mL) and brine (1 x 40 mL) and were dried over $MgSO_4$. Purification by flash column chromatography (10 % ethyl acetate in hexane) gave the product (*E*)-3-((*tert*-butoxycarbonyl)(2-iodophenyl)amino)prop-1-en-1-yl acetate **431c** (1.48 g, 3.45 mmol, 77 %) as a colourless oil. **^{1}H-NMR** (400 MHz, DMSO-d_6, 80 °C) δ 7.90 (dd, *J* = 7.8, 1.4 Hz, 1H), 7.45 – 7.34 (m, 1H), 7.26 (d, *J* = 8.1 Hz, 1H, minor rotamer), 7.22 (d, *J* = 7.8 Hz, 1H, major rotamer), 7.18 – 6.94 (m, 2H), 5.60 – 5.41 (m, 1H, major rotamer), 5.19 – 5.05 (m, 1H, minor rotamer), 4.39 (ddd, *J* = 15.3, 6.6, 1.5 Hz, 1H, minor rotamer), 4.30 (dd, *J* = 14.9, 7.1 Hz, 1H, major rotamer), 4.10 – 3.68 (m, 1H), 2.09 (br s, 3H, major rotamer), 2.01 (br s, 3H. minor rotamer), 1.47 (s, 9H, minor rotamer), 1.29 (s, 9H. major rotamer). **^{13}C-NMR** (101 MHz, DMSO-d_6, 80 °C, major rotamer) δ 167.1, 152.5, 138.7, 138.0, 135.7, 129.5, 128.6, 128.5, 109.3, 100.3, 79.3, 46.3, 27.6, 19.7. **IR** ν_{max} [cm^{-1}]: 3065, 2974, 2930, 1757, 1697, 1676, 1580, 1472, 1453, 1437, 1366, 1308, 1252, 1204, 1167, 1146, 1101, 1053, 1030, 1018, 1005. **GC-MS** [*m/z* (%)] (15.561 min): 361 (3, M-$C(CH_3)_2CH_2$), 318 (1), 317 (2), 274 (1), 263 (3), 257 (5), 245 (5), 219 (10), 192 (5), 174 (20), 136 (5), 134 (10), 130 (10), 118 (15), 91 (10), 57 (100). **HRMS** (ESI+) [*m/z*]: calcd. for $C_{16}H_{21}INO_4$ (M+H): 418.0515, found: 418.0505.

Methyl (*E*)-4-iodobut-2-enoate 655

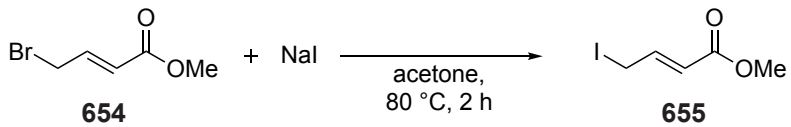

654 **655**

The reaction was kept under nitrogen and shielded from light. Tech. grade methyl (*E*)-4-bromobut-2-enoate **654** was used. The reaction vessel was charged with sodium iodide (6.00 g, 40.0 mmol, 2.0 equiv.) and acetone (45 mL). Then methyl (*E*)-4-bromobut-2-enoate **654** (2.61 mL, 20.0 mmol, 1.0 equiv.) was added and the solution was heated to reflux (metal heating block at 80 °C) for 2 h. The reaction was diluted with *tert*-butyl methyl ether (450 mL). The organic phase was subsequently washed with aqueous sodium thiosulfate (1 M, 50 mL), water (50 mL), and brine (50 mL), dried over Na_2SO_4 and concentrated *in vacuo* (45 °C, > 200

mbar). Purification by flash column chromatography (ethyl acetate in heptane, gradient from 0 % to 10 %) gave the product methyl (*E*)-4-iodobut-2-enoate **655** (3.78 g, 15.9 mmol, 79 %) as a colourless oil. The material was stored in the fridge and shielded from light. **^{1}H-NMR** (400 MHz, Chloroform-*d*) δ 7.06 (dt, *J* = 15.3, 8.3 Hz, 1H), 5.94 (dt, *J* = 15.3, 1.1 Hz, 1H), 3.93 (dd, *J* = 8.3, 1.1 Hz, 2H), 3.75 (s, 3H). **^{13}C-NMR** (101 MHz, Chloroform-*d*) δ 166.1, 143.9, 122.9, 51.9, 0.8. **GC-MS** [*m/z* (%)] (9.895 min): 226 (10, M+), 195 (10), 167 (5), 141 (5), 128 (5), 127 (40), 100 (10), 99 (100), 71 (20), 68 (50), 59 (15). The NMR spectra are in agreement with the previously reported data.[265]

Methyl (*E*)-4-((*tert*-butoxycarbonyl)(2-iodophenyl)amino)but-2-enoate 431c

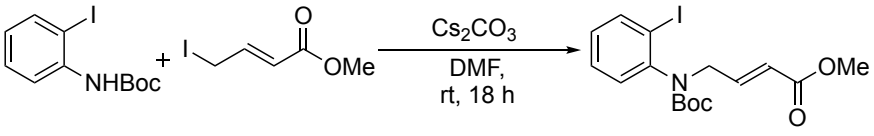

647 **655** **431c**

The reaction was kept under nitrogen. The reaction vessel was charged with *tert*-butyl (2-iodophenyl)carbamate **647** (3.19 g, 10.0 mmol, 1.0 equiv.) and DMF (30 mL). Then Cs_2CO_3 (6.52 g, 20.0 mmol, 2.0 equiv.) was added, followed by a solution of methyl (*E*)-4-iodobut-2-enoate **655** (3.33 g, 14.0 mmol, 1.4 equiv.) in DMF (15 mL). The reaction was stirred at room temperature for 18 h. The reaction was partitioned between water (450 mL), brine (50 mL) and *tert*-butyl methyl ether (50 mL). The aqueous phase was extracted with *tert*-butyl methyl ether (3 x 50 mL). The combined organic phases were washed with brine (3 x 25 mL), dried over Na_2SO_4 and concentrated *in vacuo*. Purification by flash column chromatography (ethyl acetate in heptane, gradient from 0 % to 20 %) gave the product methyl (*E*)-4-((*tert*-butoxycarbonyl)(2-iodophenyl)amino)but-2-enoate **431c** (3.37 g, 7.89 mmol, 79 %) as a colourless oil. Upon storage on the bench for weeks the compound crystallised as a white solid. **^{1}H-NMR** (400 MHz, DMSO-d_6, 80 °C) δ 7.91 (ddd, *J* = 7.7, 1.8, 1.8 Hz, 1H), 7.46 – 7.35 (m, 1H), 7.29 – 7.21 (m, 1H), 7.10 – 7.01 (m, 1H), 6.91 (dt, *J* = 14.3, 6.3 Hz, 1H), 5.95 (dt, *J* = 15.4, 1.7 Hz, 1H), 4.55 – 4.37 (m, 1H), 4.02 (dd, *J* = 16.9, 6.4 Hz, 1H), 3.67 (br s, 3H), 1.37 (s, 9H). **^{13}C-NMR** (101 MHz, DMSO-d_6, 80 °C) δ 165.2, 152.6, 143.8, 143.2, 138.8, 129.2, 128.8, 128.7, 121.9, 100.0, 79.6, 50.8, 50.0, 27.5. **^{1}H-NMR** (400 MHz, Chloroform-*d*) δ 7.86 (d, *J* = 7.9 Hz, 1H), 7.37 – 7.28 (m, 1H), 7.19 (br, 1H), 7.05 – 6.95 (m, 2H), 5.89 (d, *J* = 15.7 Hz, 1H), 4.64 (dt, *J* = 18.4, 9.2 Hz, 1H), 3.91 – 3.80 (m, 1H), 3.75 (s, 3H, minor rotamer), 3.73 (s, 3H, major rotamer), 1.53 (s, 9H, minor rotamer), 1.35 (s, 9H, major rotamer). **^{13}C-NMR** (101 MHz, Chloroform-*d*, major rotamer) δ 166.6, 153.9, 143.5, 139.7, 129.9, 129.2, 129.1 (2C, fortuitous isochrony), 122.9, 100.3, 81.0, 51.7, 50.4, 28.3. **LC-(ESI+)-MS** [*m/z*] (8.813 min): 435 ($M+NH_4$). **mp** = 63 °C - 65 °C. The NMR spectra recorded in chloroform-*d* are in agreement with the previously reported data.[265]

1-(Allyloxy)-2-iodobenzene 431d

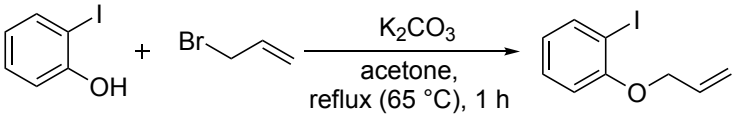

656 **649** **431d**

The reaction vessel was charged with 2-iodophenol **656** (2.25 g, 10.0 mmol, 1.0 equiv.) and potassium carbonate (2.76 g, 20.0 mmol, 2.0 equiv.). Then acetone (2.5 mL) and 3-bromoprop-1-ene **649** (1.43 mL, 11.0 mmol, 1.1 equiv.) were added and the reaction was refluxed for 1 h 40 min (heat block at 65 °C). The reaction was monitored by LC-MS and was found to have reached full conversion after 1 h. The reaction was filtered and concentrated *in vacuo*. Purification by flash column chromatography (ethyl acetate in heptane, gradient from 0 % to 10 %) gave 1-(allyloxy)-2-iodobenzene **431d** (2.09 g, 8.02 mmol, 80 %) as a colourless oil. **^{1}H-NMR** (400 MHz, Chloroform-*d*) δ 7.78 (dd, *J* = 7.7, 1.6 Hz, 1H), 7.32 – 7.23 (m, 1H), 6.81 (dd, *J* = 8.2, 1.3 Hz, 1H), 6.71 (ddd, *J* = 7.6, 7.6, 1.4 Hz, 1H), 6.07 (ddt, *J* = 17.2, 10.4, 4.8 Hz, 1H), 5.53 (ddt, *J* = 17.3, 1.7, 1.7 Hz, 1H), 5.32 (ddt, *J* = 10.6, 1.6, 1.6 Hz, 1H), 4.60 (ddd, *J* = 4.9, 1.7, 1.7 Hz, 2H). **^{13}C-NMR** (101 MHz, Chloroform-*d*) δ 157.3, 139.7, 132.7, 129.5, 122.8, 117.7, 112.7, 86.8, 69.8. **GC-MS** [*m/z* (%)] (11.745 min): 260 (40, M+), 220 (10), 219 (10), 191 (25), 133 (45), 131 (20), 127 (20), 105 (90), 103 (20), 92 (65), 79 (20), 77 (35), 76 (20), 74 (15), 65 (30), 64 (65), 63 (100), 62 (25). The NMR spectra are in agreement with the previously reported data.[266]

***N*-(cyclohex-2-en-1-yl)-*N*-(2-iodophenyl)methanesulfonamide 434**

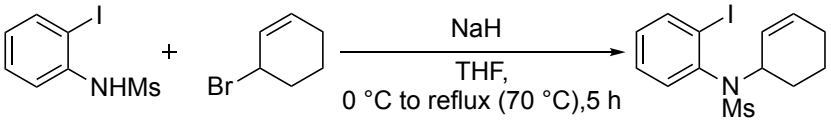

657 **658** **434**

The reaction was kept under nitrogen. The reaction vessel was charged with *N*-(2-iodophenyl)methanesulfonamide **657** (891 mg, 3.00 mmol, 1.0 equiv.) and THF (6.0 mL). The solution was cooled in the ice bath and then sodium hydride (86.4 mg, 3.60 mmol, 1.2 equiv.) was added carefully in several portions. The reaction was stirred at ice bath temperature for 1 h before the addition of 3-bromocyclohex-1-ene **658** (0.46 mL, 4.0 mmol, 1.3 equiv.). Then the reaction was heated to reflux (oil bath at 70 °C). A white precipitate formed after 15 min at reflux temperature. The reaction was monitored by GC-MS and was found to have reached full conversion after 5 h. The reaction was quenched by the addition of aqueous NH_4Cl (10 mL, sat.), water (20 mL) and ethyl acetate (20 mL). The organic phases were separated and the aqueous phase was extracted with ethyl acetate (3 x 20 mL). The combined organic phases were washed with brine, dried over $MgSO_4$ and concentrated *in vacuo*. Purification by flash column chromatography (4 % ethyl acetate in toluene) gave the product *N*-(cyclohex-2-en-1-yl)-*N*-(2-iodophenyl)methanesulfonamide **434** (1.07 g, 2.85 mmol, 95 %) as a white solid. **^{1}H-NMR** (500 MHz, Chloroform-*d*) δ 7.95 (dd, *J* = 8.0, 1.5 Hz, 1H), 7.45 – 7.40 (m, 1H), 7.39 – 7.33 (m, 1H), 7.05 (ddd, *J* = 7.6, 7.6, 1.7 Hz, 1H), 6.07 – 6.00 (m, 1H), 5.88 (ddt, *J* = 10.1,

4.9, 2.5 Hz, 1H, major rotamer), 5.73 (ddt, *J* = 10.2, 3.4 Hz, 1H, minor rotamer), 4.78 – 4.66 (m, 1H), 3.15 (s, 3H, major rotamer), 3.13 (s, 3H, minor rotamer), 2.33 – 2.20 (m, 1H), 1.94 – 1.73 (m, 2H), 1.68 – 1.45 (m, 3H). **^{13}C-NMR** (101 MHz, Chloroform-*d*) δ 140.5, 139.8, 133.2, 132.2, 130.2, 129.0, 128.3, 105.2, 58.8, 42.0, 28.1, 24.4, 21.5. **GC-MS** [*m/z* (%)] (16.625 min): 377 (1.0, M+), 362 (1.0), 349 (1.5), 297 (20), 218 (15), 203 (15), 170 (15), 143 (30), 130 (10), 115 (10), 91 (10), 81 (60), 79 (100), 77 (30), 76 (20), 65 (20), 63 (20). **mp** = 85 °C - 87 °C (lit. mp = 92 °C - 93 °C).[267] The NMR spectra are in agreement with the previously reported data.[6]

***N*-(But-2-yn-1-yl)-*N*-(2-iodophenyl)methanesulfonamide 437a**

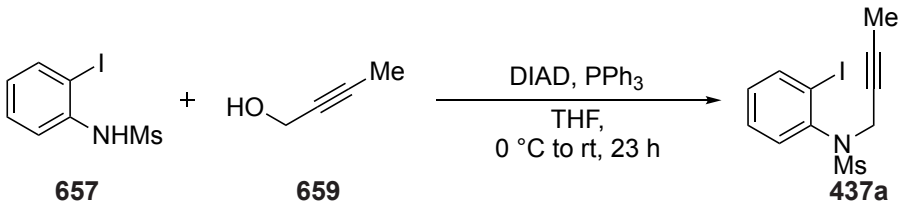

657 **659** **437a**

The reaction vessel was charged with *N*-(2-iodophenyl)methanesulfonamide **657** (891 mg, 3.00 mmol, 1.0 equiv.) and triphenylphosphine (1.18 g, 4.50 mmol, 1.5 equiv.). Then THF (30 mL) was added followed by but-2-yn-1-ol **659** (254 µL, 3.30 mmol, 1.1 equiv.). The solution was cooled in the ice bath and DIAD (0.92 mL, 4.5 mmol, 1.5 equiv.) was added dropwise over ca. 2 min. The reaction was allowed to warm up to room temperature when the addition was finished and was stirred at room temperature for 23 h. The reaction was analysed by TLC and was found to have reached full conversion after that time. The reaction was concentrated *in vacuo*. Purification by flash column chromatography (5 % ethyl acetate in toluene) gave the product *N*-(but-2-yn-1-yl)-*N*-(2-iodophenyl)methanesulfonamide **437a** (1.04 g, 2.97 mmol, 99 %) as a pale yellow oil. **^{1}H-NMR** (400 MHz, Chloroform-*d*) δ 7.97 (dd, *J* = 8.0, 1.5 Hz, 1H), 7.61 (dd, *J* = 7.9, 1.6 Hz, 1H), 7.44 (ddd, *J* = 7.6, 7.6, 1.5 Hz, 1H), 7.12 (ddd, *J* = 7.9, 7.4, 1.6 Hz, 1H), 4.74 – 4.61 (m, 1H), 4.08 – 3.99 (m, 1H), 3.17 (s, 3H), 1.85 (t, *J* = 2.4 Hz, 3H). **^{13}C NMR** (101 MHz, Chloroform-*d*) δ 141.3, 140.4, 131.3, 130.6, 129.3, 102.5, 82.4, 73.5, 41.3, 41.2, 3.6. **LC-ESI(+)-MS** [*m/z*] (7.560 min): 367 ($M+NH_4$). The NMR spectra are in agreement with the previously reported data.[6]

3-Cyclohexylprop-2-yn-1-ol 661

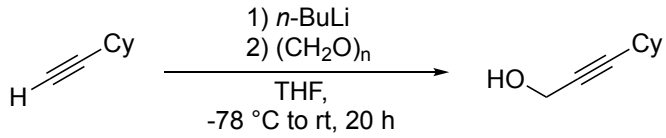

660 **661**

The reaction vessel was charged with THF (10 mL) and ethynylcyclohexane **660** (1.07 mL, 8.00 mmol, 1.0 equiv.) and cooled in an acetone/dry ice cooling bath. Then *n*-butyllithium (7.3 mL, 1.2 M, 8.80 mmol, 1.1 equiv.) was added dropwise followed by paraformaldehyde (343 mg, 11.2 mmol, 1.4 equiv.). The reaction was allowed to warm up to room temperature and was stirred for 20 h. Then the reaction was quenched by the addition of aqueous NH_4Cl

(10 mL, sat.) and water (20 mL). The phases were separated and the aqueous phase was extracted with ethyl acetate (4 x 20 mL). The combined organic phases were washed with brine (20 mL), dried over $MgSO_4$ and carefully concentrated *in vacuo* (100 mbar, 45 °C, 20 min). Purification by flash column chromatography (20 % ethyl acetate in hexane) gave 3-cyclohexylprop-2-yn-1-ol **661** (0.944 g, 6.84 mmol, 85 %) as a colourless oil. **^{1}H-NMR** (400 MHz, Chloroform-*d*) δ 4.26 (dd, *J* = 5.8, 2.0 Hz, 2H), 2.38 (ttt, *J* = 9.6, 3.9, 2.0 Hz, 1H), 1.85 – 1.76 (m, 2H), 1.69 (dddd, *J* = 12.2, 6.5, 4.8, 2.5 Hz, 2H), 1.59 – 1.22 (m, 6H). **^{13}C-NMR** (101 MHz, Chloroform-d) δ 90.8, 78.3, 51.6, 32.8, 29.2, 26.0, 25.0. **GC-MS** [*m/z* (%)] (10.237 min): 138 (5, M+), 110 (5), 109 (15), 117 (10), 105 (20), 97 (15), 96 (10), 95 (35), 94 (20), 93 (10), 92 (30), 91 (50), 83 (20), 81 (75), 79 (100), 77 (45), 70 (35), 67 (90), 65 (40). The NMR spectra are in agreement with the previously reported data.[273]

***N*-(3-Cyclohexylprop-2-yn-1-yl)-*N*-(2-iodophenyl)methanesulfonamide 437b**

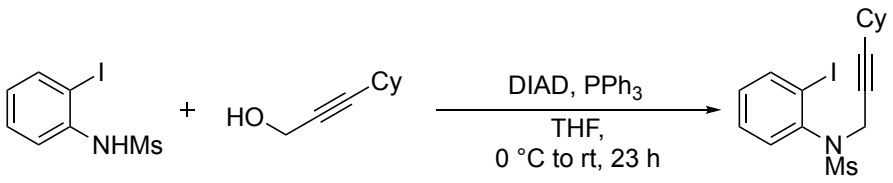

657 **661** **437b**

The reaction vessel was charged with *N*-(2-iodophenyl)methanesulfonamide **657** (891 mg, 3.00 mmol, 1.0 equiv.) and triphenylphosphine (1.18 g, 4.50 mmol, 1.5 equiv.). Then THF (30 mL) was added followed by 3-cyclohexylprop-2-yn-1-ol **661** (539 mg, 3.90 mmol, 1.3 equiv.). The solution was cooled in the ice bath and DIAD (0.93 mL, 4.50 mmol, 1.5 equiv.) was added dropwise over *ca.* 2 min. The reaction was allowed to warm up to room temperature when the addition was finished and was stirred at room temperature for 15 h. The reaction was analysed by TLC and was found to have reached full conversion. The reaction was concentrated *in vacuo*. Purification by flash column chromatography (2.5 % ethyl acetate in toluene) gave the product *N*-(3-cyclohexylprop-2-yn-1-yl)-*N*-(2-iodophenyl)methanesulfonamide **437b** (1.22 g, 2.92 mmol, 97 %) as a colourless oil. **^{1}H-NMR** (400 MHz, Chloroform-*d*) δ 7.94 (dd, *J* = 8.0, 1.5 Hz, 1H), 7.57 (dd, *J* = 7.9, 1.6 Hz, 1H), 7.40 (ddd, *J* = 7.7, 7.7, 1.5 Hz, 1H), 7.09 (ddd, *J* = 7.9, 7.4, 1.6 Hz, 1H), 4.68 (dd, *J* = 18.0, 2.2 Hz, 1H), 4.05 (dd, *J* = 18.0, 2.1 Hz, 1H), 3.15 (s, 3H), 2.42 – 2.30 (m, 1H), 1.80 – 1.71 (m, 2H), 1.70 – 1.60 (m, 2H), 1.57 – 1.45 (m, 1H), 1.44 – 1.20 (m, 5H). **^{13}C-NMR** (101 MHz, Chloroform-*d*) δ 141.3, 140.3, 131.1, 130.6, 129.1, 102.8, 91.1, 74.1, 41.2, 41.2, 32.5, 29.1, 25.8, 24.9. **IR** ν_{max} [cm^{-1}]: 2928, 2853, 2255, 1717, 1576, 1466, 1449, 1344, 1219, 1152, 1074, 1051, 1020, 1007. **LC-ESI(+)-MS** [*m/z*] (9.103 min): 435 ($M+NH_4$). **HRMS** (ESI+) [*m/z*]: calcd. for $C_{16}H_{21}INO_2S$ (M+H): 418.0334, found: 418.0332.

4-((*tert*-Butyldiphenylsilyl)oxy)but-2-yn-1-ol 663

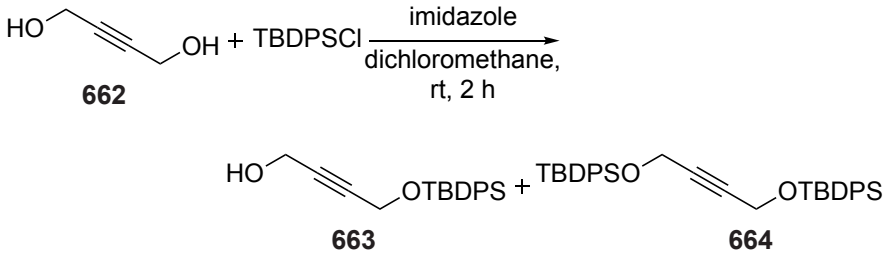

The reaction vessel was charged with but-2-yne-1,4-diol **662** (2.61 g, 30.0 mmol, 2.0 equiv.) and imidazole (1.23 g, 18.0 mmol, 1.2 equiv.) which were suspended in dichloromethane (100 mL). Then *tert*-butylchlorodiphenylsilane (4.02 mL, 15.0 mmol, 1.0 equiv.) was added and the reaction was stirred at room temperature for 2 h 15 min. The reaction was monitored by TLC and was found to have reached full conversion after 1 h 50 min. The reaction was poured onto water (100 mL). The phases were separated and the aqueous phase was extracted with dichloromethane (3 x 20 mL). The combined organic phases were dried over $MgSO_4$ and concentrated *in vacuo*. Purificaction by flash column chromatography (ethyl acetate in hexane, gradient from 5 % to 20 %) gave 4-((*tert*-butyldiphenylsilyl)oxy)but-2-yn-1-ol **663** (1.95 g, 5.72 mmol, 38 %) as a colourless oil. Additionally, 2,2,11,11-tetramethyl-3,3,10,10-tetraphenyl-4,9-dioxa-3,10-disiladodec-6-yne **664** (1.93 g, 3.42 mmol, 46 %) was isolated as a colourless oil.

4-((*tert*-Butyldiphenylsilyl)oxy)but-2-yn-1-ol **663**: **^{1}H-NMR** (400 MHz, Chloroform-*d*) δ 7.77 – 7.67 (m, 4H), 7.47 – 7.37 (m, 6H), 4.37 (t, *J* = 1.8 Hz, 2H), 4.20 (t, *J* = 1.8 Hz, 2H), 1.38 (s, 1H), 1.07 (s, 9H). **^{13}C-NMR** (101 MHz, Chloroform-*d*) δ 135.8, 133.3, 130.0, 127.8, 84.4, 83.6, 52.8, 51.3, 26.9, 19.3. **LC-(ESI+)-MS** [*m/z*] (9.243 min): 342 ($M+NH_4$). The NMR spectra are in agreement with the previously reported data.[274]

2,2,11,11-Tetramethyl-3,3,10,10-tetraphenyl-4,9-dioxa-3,10-disiladodec-6-yne **664**: **^{1}H-NMR** (400 MHz, Chloroform-*d*) δ 7.77 – 7.70 (m, 8H), 7.47 – 7.36 (m, 12H), 4.35 (s, 4H), 1.10 (s, 18H). **^{13}C-NMR** (101 MHz, Chloroform-*d*) δ 135.8, 133.3, 129.9, 127.8, 83.5, 52.9, 26.9, 19.3. **IR** ν_{max} [cm^{-1}]: 3071, 3048, 2957, 2930, 2857, 1472, 1462, 1427, 1369, 1261, 1188, 1138, 1107, 1086, 1057, 1030. **LC-(ESI+)-MS** [*m/z*] (12.771 min): 580 ($M+NH_4$).

((4-Bromobut-2-yn-1-yl)oxy)(tert-butyl)diphenylsilane 665

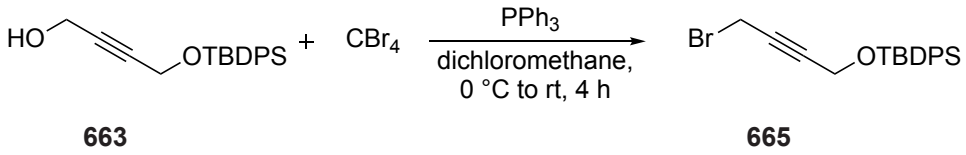

The reaction was kept under argon and shielded from light. Anhydrous dichloromethane was used. To the solution of 4-((*tert*-butyldiphenylsilyl)oxy)but-2-yn-1-ol **663** (669 mg, 2.00 mmol, 1.0 equiv.) in dichloromethane (8.0 mL) was added CBr_4 (670 mg, 2.00 mmol, 1.0 equiv.) and the solution was cooled in the ice bath. Then triphenylphosphine (552 mg, 2.00 mmol, 1.0 equiv.) was added in portions over ca. 3 min. The reaction was allowed to warm up to room

temperature and was stirred at room temperature for 4 h 30 min. The reaction was monitored by TLC and was found to have reached a high degree of conversion after 1 h 40 min. The reaction was quenched by the addition of methanol (2 mL) and was concentrated *in vacuo* and directly purified by flash column chromatography (4 % ethyl acetate in hexane) to give the product ((4-bromobut-2-yn-1-yl)oxy)(*tert*-butyl)diphenylsilane **665** (667 mg, 1.72 mmol, 86 %) as a colourless oil. **^{1}H-NMR** (400 MHz, Chloroform-*d*) δ 7.74 – 7.68 (m, 4H), 7.48 – 7.37 (m, 6H), 4.37 (t, *J* = 2.0 Hz, 2H), 3.89 (t, *J* = 2.0 Hz, 2H), 1.07 (s, 9H). **^{13}C-NMR** (101 MHz, Chloroform-*d*) δ 135.8, 133.1, 130.0, 127.9, 85.4, 80.3, 52.9, 26.8, 19.3, 14.7. **LC-(ESI+)-MS** [*m/z*] (10.253 min): 836 (2M+ACN+Na). The NMR spectra are in agreement with the previously reported data.[275]

tert-Butyl (4-((_tert_-butyldiphenylsilyl)oxy)but-2-yn-1-yl)(2-iodophenyl)carbamate 440a

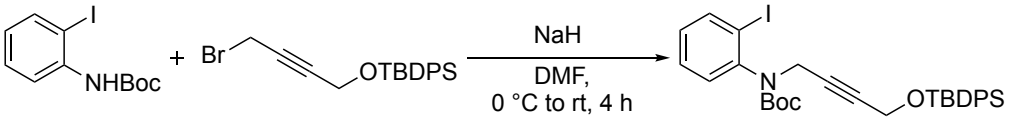

647 **665** **440a**

The reaction was kept under argon and anhydrous dichloromethane was used. The reaction vessel was charged with *tert*-butyl (2-iodophenyl)carbamate **647** (415 mg, 1.30 mmol, 1.0 equiv.). Then DMF (4 mL) was added and the solution was cooled in the ice bath before the careful addition of sodium hydride (31.2 mg, 1.30 mmol, 1.1 equiv.). The reaction was stirred at ice bath temperature for 45 min. Then ((4-bromobut-2-yn-1-yl)oxy)(*tert*-butyl)diphenylsilane **665** (554 mg, 1.43 mmol, 1.1 equiv.) was added and the reaction was stirred at room temperature for 4 h 15 min. The reaction was monitored by TLC and was found to have reached full conversion after 1 h 40 min. The reaction was quenched by the addition of saturated aqueous ammonium chloride (5 mL) and water (100 mL). The phases were separated and the aqueous phase was extracted with ethyl acetate (3 x 20 mL). The combined organic phases were washed with water (3 x 20 mL) and brine (1 x 20 mL), dried over $MgSO_4$ and concentrated *in vacuo*. Purification by flash column chromatography (5 % ethyl acetate in hexane) gave the product *tert*-butyl (4-((tert-butyldiphenylsilyl)oxy)but-2-yn-1-yl)(2-iodophenyl)carbamate **440a** (746 mg, 1.18 mmol, 91 %) as a colourless oil. **^{1}H-NMR** (400 MHz, DMSO-d_6) δ 7.91 (dd, *J* = 7.9, 1.4 Hz, 1H), 7.67 – 7.58 (m, 4H), 7.50 – 7.33 (m, 7H), 7.30 (dd, *J* = 7.9, 1.7 Hz, 1H), 7.08 (ddd, *J* = 7.6, 7.6, 1.8 Hz, 1H), 4.66 – 4.51 (m, 1H), 4.39 – 4.27 (m, 2H), 4.00 – 3.89 (m, 1H), 1.47 (s, 9H, minor rotamer), 1.29 (s, 9H, major rotamer), 0.97 (s, 9H). **^{13}C-NMR** (101 MHz, DMSO-d_6, major rotamer) δ 152.6, 142.9, 139.0, 135.0, 132.5, 129.9, 129.5, 129.4, 128.9, 127.8, 100.8, 82.2, 80.8, 80.0, 52.3, 38.1, 27.8, 26.5, 18.7. **IR** ν_{max} [cm^{-1}]: 3069, 3049, 2959, 2930, 2857, 1736, 1705, 1580, 1472, 1427, 1368, 1298, 1252, 1229, 1153, 1126, 1111, 1063, 1013. **LC-(ESI+)-MS** [*m/z*] (11.241 min): 643 ($M+NH_4$). **HRMS** (ESI+) [*m/z*]: calcd. for $C_{31}H_{40}O_3N_2ISi$ ($M+NH_4$): 643.1847, found: 643.1830.

***tert*-Butyl (2-iodophenyl)(prop-2-yn-1-yl)carbamate 440b**

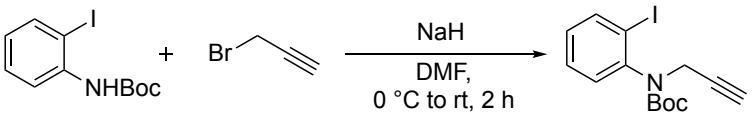

647 **666** **440b**

The reaction was kept under nitrogen and anhydrous DMF was used. The reaction vessel was charged with *tert*-butyl (2-iodophenyl)carbamate **647** (798 mg, 2.50 mmol, 1.0 equiv.). Then DMF (16 mL) was added and the solution was cooled in the ice bath before the careful addition of sodium hydride (110 mg, 2.75 mmol, 1.1 equiv., 60 % suspension in mineral oil). The reaction was stirred at ice bath temperature for 35 min. Then 3-bromoprop-1-yne **666** (334 µL, 3.00 mmol, 1.2 equiv.) was added and the reaction was stirred at room temperature for 2 h 15 min. The reaction was monitored by HPLC and was found to have reached full conversion after 1 h 20 min. The reaction was partitioned between water (100 mL), brine (50 mL) and ethyl acetate (20 mL). The phases were separated and the aqueous phase was extracted with ethyl acetate (3 x 20 mL). The combined organic phases were dried over Na_2SO_4 and concentrated *in vacuo*. Purification by flash column chromatography (ethyl acetate in heptane, gradient from 0 % to 5 %) gave the product *tert*-butyl (2-iodophenyl)(prop-2-yn-1-yl)carbamate **440b** (0.825 g, 2.31 mmol, 92 %) as a pale yellow oil. **^{1}H-NMR** (400 MHz, Chloroform-*d*) δ 7.87 (d, *J* = 7.9 Hz, 1H), 7.48 – 7.33 (m, 2H), 7.02 (ddd, *J* = 8.0, 6.0, 3.1 Hz, 1H), 4.79 (dd, *J* = 17.6, 2.5 Hz, 1H, major rotamer), 4.64 (d, *J* = 17.8 Hz, 1H, minor rotamer), 3.90 (dd, *J* = 17.6, 2.4 Hz, 1H), 2.25 – 2.19 (m, 1H), 1.56 (s, 9H, minor rotamer), 1.36 (s, 9H, major rotamer). **^{13}C-NMR** (101 MHz, Chloroform-*d*, major rotamer) δ 153.6, 143.5, 139.4, 130.3, 129.3, 129.0, 100.2, 81.1, 79.4, 72.6, 39.7, 28.5. **^{1}H-NMR** (400 MHz, DMSO-d_6, 80 °C) δ 7.92 (dd, *J* = 7.9, 1.4 Hz, 1H), 7.48 – 7.41 (m, 1H), 7.36 (dd, *J* = 7.8, 1.7 Hz, 1H), 7.09 (ddd, *J* = 7.6, 7.6, 1.7 Hz, 1H), 4.56 (dd, *J* = 18.0, 2.5 Hz, 1H), 3.99 (dd, *J* = 18.0, 2.5 Hz, 1H), 3.04 (dd, *J* = 2.5 Hz, 1H), 1.37 (s, 9H). **^{13}C-NMR** (101 MHz, DMSO-d_6, 80 °C) δ 152.2, 143.0 (br), 138.7, 129.3, 128.9, 128.6, 100.0, 79.9, 79.0, 74.4, 38.0 (br), 27.6. **GC-MS** [*m/z* (%)] (13.803 min): 357 (0.1, M+), 342 (0.1),314 (0.1), 300 (2), 298 (3), 284 (5), 257 (15), 245 (5), 203 (5), 174 (65), 157 (5), 130 (55), 129 (30), 102 (20), 90 (15), 76 (20), 57 (100). The NMR spectra are in agreement with the previously reported data.[276]

1-(1-(Allyloxy)-2-iodoethyl)-4-methoxybenzene 442a

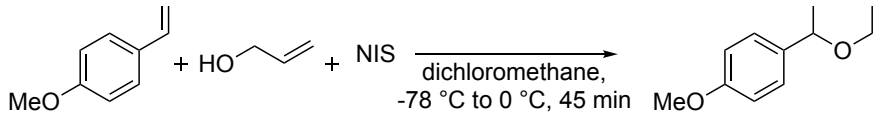

667 **668** **442a**

The reaction was kept under nitrogen and shielded from light. The reaction vessel was charged with dichloromethane (67 mL), prop-2-en-1-ol **668** (1.36 mL, 20.0 mmol, 2.0 equiv.) and 1-methoxy-4-vinylbenzene **667** (1.33 mL, 10.0 mmol, 1.0 equiv.). The solution was cooled in a dry-ice/acetone cooling bath. Then *N*-iodosuccinimide (3.38 g, 15.0 mmol, 1.5 equiv.) was added in one portion. The reaction was stirred in the dry-ice/acetone cooling bath for 15 min. Then it was transferred into a water-ice cooling bath and stirred for 40 min. The reaction was monitored by TLC and was found to have reached full conversion after 30 min. The reaction

was quenched by the addition of a aqueous sodium thiosulfate (1.0 M, 20 mL) at ice bath temperature. Stirring was continued for 10 min. Then the phases were separated and the aqueous phase was extracted with ethyl acetate (3 x 25 mL). The combined organic phases were washed with brine, dried over Na_2SO_4 and concentrated *in vacuo*. Purification by flash column chromatography (ethyl acetate in heptane, gradient from 0 % to 5 %) gave the product **442a** (2.43 g, 7.65 mmol, 77 %) as a pale red oil. The product was stored at 4 °C and shielded from light. **^{1}H-NMR** (400 MHz, Chloroform-*d*) δ 7.26 – 7.21 (m, 2H), 6.92 – 6.87 (m, 2H), 5.92 (dddd, *J* = 17.2, 10.4, 6.2, 5.1 Hz, 1H), 5.28 (dddd, *J* = 17.3, 1.7, 1.7, 1.7 Hz, 1H), 5.18 (dddd, *J* = 10.3, 1.4, 1.4, 1.4 Hz, 1H), 4.43 (dd, *J* = 8.2, 4.8 Hz, 1H), 3.98 (dddd, *J* = 12.8, 5.1, 1.5, 1.5 Hz, 1H), 3.86 – 3.78 (m, 1H), 3.82 (s, 3H), 3.38 (dd, *J* = 10.3, 8.3 Hz, 1H), 3.30 (dd, *J* = 10.3, 4.7 Hz, 1H). **^{13}C-NMR** (101 MHz, Chloroform-*d*) δ 159.8, 134.6, 132.1, 128.0, 117.5, 114.2, 80.7, 70.1, 55.4, 11.0. **GC-MS** [*m/z* (%)] (13.276 min): 318 (3, M+), 261 (1), 191 (2), 177 (100), 149 (10), 135 (55), 134 (45), 121 (50), 119 (20), 91 (25), 77 (20), 65 (20). The NMR spectra are in agreement with the previously reported data.[6]

1-(1-(Allyloxy)-2-bromoethyl)-4-methoxybenzene 442b

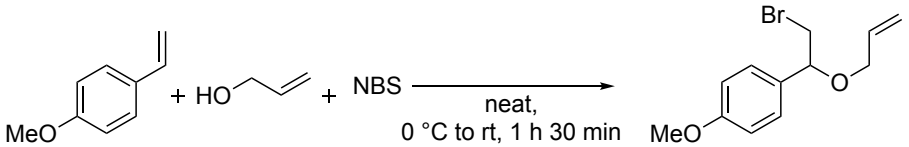

667 **668** **442b**

The reaction was kept under nitrogen. To a mixture of 1-methoxy-4-vinylbenzene **667** (1.33 mL, 10.0 mmol, 1.0 equiv.) and prop-2-en-1-ol **668** (0.680 mL, 10.0 mmol, 1.0 equiv.) was added *N*-bromosuccinimide (1.78 g, 10.0 mmol, 1.0 equiv.) in small portions over ca. 5 min at ice bath temperature. The reaction was cooled for additional 15 min before it was allowed to warm up to room temperature. The reaction was stirred at room temperature for 1 h 30 min. The reaction was monitored by TLC and was found to have reached a high degree of conversion after 10 min. The reaction was diluted with *tert*-butyl methyl ether (40 mL) and washed with aqueous sodium thiosulphate (1 M, 25 mL). The aqueous phase was extracted with *tert*-butyl methyl ether (3 x 25 mL). The combined organic phases were washed with brine, dried over Na_2SO_4 and concentrated *in vacuo*. Purification by flash column chromatography (ethyl acetate in heptane, gradient from 0 % to 5 %) gave the product 1-(1-(allyloxy)-2-bromoethyl)-4-methoxybenzene **442b** (1.22 g, 4.49 mmol, 45 %) as a colourless oil. **^{1}H-NMR** (400 MHz, Chloroform-*d*) δ 7.30 – 7.21 (m, 2H), 6.93 – 6.89 (m, 2H), 5.91 (dddd, *J* = 17.3, 10.4, 6.2, 5.1 Hz, 1H), 5.27 (dddd, *J* = 17.2, 1.7, 1.7, 1.7 Hz, 1H), 5.18 (dddd, *J* = 10.4, 1.4, 1.4, 1.4 Hz, 1H), 4.51 (dd, *J* = 8.1, 4.6 Hz, 1H), 4.00 (dddd, *J* = 12.8, 5.1, 1.5, 1.5 Hz, 1H), 3.89 – 3.78 (m, 1H), 3.82 (s, 3H), 3.56 (dd, *J* = 10.5, 8.1 Hz, 1H), 3.44 (dd, *J* = 10.5, 4.6 Hz, 1H). **^{13}C-NMR** (101 MHz, Chloroform-*d*) δ 159.9, 134.6, 131.4, 128.2, 117.5, 114.2, 80.5, 70.0, 55.4, 36.7. **IR** ν_{max} [cm^{-1}]: 3076, 3001, 2959, 2934, 2905, 2860, 2835, 1609, 1585, 1510, 1462, 1441, 1418, 1337, 1304, 1283, 1242, 1204, 1173, 1009. **GC-MS** [*m/z* (%)] (13.366 min): 272 (2, M+), 270 (2, M+), 215 (5), 213 (5), 177 (100), 149 (10), 135 (90), 134 (65), 121 (60), 119 (30), 91 (45), 77 (35), 65 (25). **HRMS** (ASAP) [*m/z*]: calcd. for $C_{12}H_{14}O_2{}^{79}Br$ (M-H): 269.0177, found: 269.0171.

1-(1-(Allyloxy)-2-chloroethyl)-4-methoxybenzene 442c

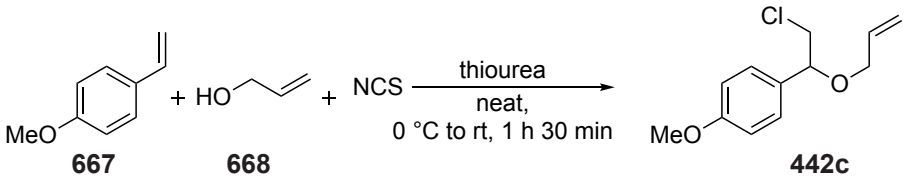

667 **668** **442c**

The reaction was kept under argon. The reaction vessel was charged with 1-methoxy-4-vinylbenzene **667** (0.27 mL, 2.00 mmol, 1.0 equiv.) and prop-2-en-1-ol **668** (2.45 mL, 36.0 mmol, 18 equiv.). Then *N*-chlorosuccinimide (1.07 g, 8.00 mmol, 4.0 equiv.) was added followed by thiourea (15.2 mg, 0.20 mmol, 0.1 equiv.). The suspension was stirred for 13 h at room temperature. The reaction was monitored by TLC and was found to have reached a high degree of conversion after that time. The reaction was partitioned between water (10 mL) and dichloromethane (10 mL). The aqueous phase was extracted with dichloromethane (3x, 10 mL). The combined organic phases were dried over $MgSO_4$ and concentrated *in vacuo*. Purification by flash column chromatography (40% dichloromethane in hexane) gave the product 1-(1-(allyloxy)-2-chloroethyl)-4-methoxybenzene **442c** (0.18 g, 0.79 mmol, 40 %) as a colourless oil. **^{1}H-NMR** (400 MHz, Chloroform-*d*) δ 7.30 – 7.21 (m, 2H), 6.94 – 6.88 (m, 2H), 5.91 (dddd, *J* = 17.2, 10.4, 6.2, 5.1 Hz, 1H), 5.27 (dddd, *J* = 17.2, 1.7, 1.7, 1.7 Hz, 1H), 5.18 (dddd, *J* = 10.4, 1.8, 1.3, 1.3 Hz, 1H), 4.48 (dd, *J* = 7.9, 4.7 Hz, 1H), 4.00 (dddd, *J* = 12.8, 5.1, 1.5, 1.5 Hz, 1H), 3.88 – 3.80 (m, 4H), 3.70 (dd, *J* = 11.3, 7.9 Hz, 1H), 3.56 (dd, *J* = 11.3, 4.7 Hz, 1H). **^{13}C-NMR** (101 MHz, Chloroform-*d*) δ 159.9, 134.6, 131.0, 128.3, 117.5, 114.2, 80.8, 70.0, 55.4, 48.4. **IR** ν_{max} [cm^{-1}]: 3076, 3001, 2953, 2834, 1647, 1610, 1586, 1512, 1461, 1443, 1422, 1305, 1246, 1173, 1093, 1032. **GC-MS** [*m/z* (%)] (12.875 min): 226 (5, M+), 177 (100), 168 (20), 149 (20), 135 (90), 121 (60) 119 (15). **HRMS** (ESI+) [*m/z*]: calcd. for $C_{12}H_{15}O_2$ (M-Cl): 191.1072, found: 191.1067.

***(Z)*-4-(Allyloxy)but-2-en-1-ol 670**

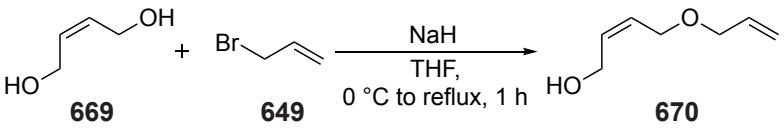

669 **649** **670**

The reaction was kept under argon and anhydrous THF was used. The reaction vessel was charged with THF (20 mL) and *(Z)*-but-2-ene-1,4-diol **669** (5.39 g, 60.0 mmol, 3.0 equiv.). The solution was cooled in the ice bath and NaH (840 mg, 21.0 mmol, 1.05 equiv.) was added over *ca.* 5 min. The reaction was stirred at room temperature for 1 h. Over this time the reaction turned from a slurry into two separate liquid phases. Then 3-bromoprop-1-ene **649** (1.78 mL, 20.0 mmol, 1.0 equiv.) was added carefully and the reaction was stirred at room temperature for 10 min before it was gently refluxed (oil bath at 75 °C) for 1 h. Gradually over the period of refluxing, a light brown precipitate formed. The reaction was poured onto aqueous HCl (1 M, 50 mL) and dichloromethane (20 mL). The phases were separated and the aqueous phase was extracted with dichloromethane (3 x 20 mL). The combined organic phases were dried over $MgSO_4$ and concentrated in vacuo. Purification by flash column chromatography (30 %

ethyl acetate in hexane) gave the product *(Z)*-4-(allyloxy)but-2-en-1-ol **670** (2.00 g, 15.6 mmol, 78 %) as a colourless oil. **^{1}H-NMR** (400 MHz, Chloroform-*d*) δ 5.91 (ddt, *J* = 17.2, 10.4, 5.7 Hz, 1H), 5.82 (dtt, *J* = 11.2, 6.3, 1.3 Hz, 1H), 5.71 (dtt, *J* = 11.3, 6.3, 1.3 Hz, 1H), 5.28 (ddt, *J* = 17.2, 1.6, 1.6 Hz, 1H), 5.20 (ddt, *J* = 10.4, 1.4, 1.4 Hz, 1H), 4.20 (ddt, *J* = 6.4, 1.4, 0.7 Hz, 2H), 4.06 (ddt, *J* = 6.2, 1.5, 0.8 Hz, 2H), 3.99 (ddd, *J* = 5.7, 1.4, 1.4 Hz, 2H), 1.90 (s, 1H). **^{13}C-NMR** (101 MHz, Chloroform-*d*) δ 134.6, 132.4, 128.5, 117.6, 71.5, 65.8, 58.9. **GC-MS** [*m/z* (%)] (8.914 min): 110 (30, M-18), 97 (30), 95 (5), 81 (15), 80 (10), 79 (10), 71 (25), 70 (100), 69 (70), 68 (40), 67 (20), 59 (15), 58 (25), 57 (85), 55 (65), 54 (40), 53 (20). The NMR spectra are in agreement with the previously reported data.[254]

***(Z)*-1-(Allyloxy)-4-bromobut-2-ene 671**

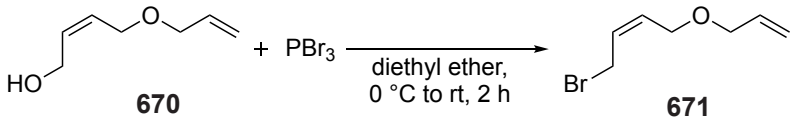

670 **671**

The reaction was shielded from light and kept under argon. Anhydrous diethyl ether was used. The solution of *(Z)*-4-(allyloxy)but-2-en-1-ol **670** (513 mg, 4.00 mmol, 1.0 equiv.) in diethyl ether (8 mL) was cooled in the ice bath. Then PBr_3 (0.15 mL, 1.60 mmol, 0.4 equiv.) was added dropwise over *ca.* 2 min. The reaction was allowed to warm up to room temperature and was stirred at room temperature for 2 h 20 min. The reaction was monitored by TLC and was found to have reached full conversion after 2 h. The reaction was cooled in the ice bath, diluted with diethyl ether (20 mL) and then quenched by the slow addition of water (10 mL). The reaction was poured onto aqueous $NaHCO_3$ (10 mL, sat.). The phases were separated and the aqueous phase was extracted with diethyl ether (3 x 20 mL). The combined organic phases were washed with brine, dried over $MgSO_4$ and carefully concentrated *in vacuo* (45 °C, >200 mbar) to give the product *(Z)*-1-(allyloxy)-4-bromobut-2-ene **671** (0.687 g, 3.56 mmol, 89 %) as a colourless oil. The product was stored at 4 °C and shielded from light. **^{1}H-NMR** (400 MHz, Chloroform-*d*) δ 5.99 – 5.84 (m, 2H), 5.72 (dtt, *J* = 10.9, 6.4, 0.8 Hz, 1H), 5.30 (ddt, *J* = 17.2, 1.6, 1.6 Hz, 1H), 5.21 (ddt, *J* = 10.4, 1.3, 1.3 Hz, 1H), 4.12 (dd, *J* = 6.4, 1.6 Hz, 2H), 4.04 – 3.98 (m, 4H). **^{13}C-NMR** (101 MHz, Chloroform-*d*) δ 134.6, 131.3, 128.4, 117.6, 71.6, 65.1, 26.6. **GC-MS** [*m/z* (%)] (9.440 min): 191 (0.03, M+), 189 (0.03, M+), 162 (0.3), 160 (0.3), 151 (1.5), 149 (1.5), 135 (25), 133 (25), 111 (20), 110 (20), 93 (35), 91 (15), 81 (20), 69 (50), 67 (75), 55 (80), 54 (85), 53 (100). The NMR spectra are in agreement with the previously reported data.[254]

***tert*-Butyl *(Z)*-(4-(allyloxy)but-2-en-1-yl)(2-iodophenyl)carbamate 444a**

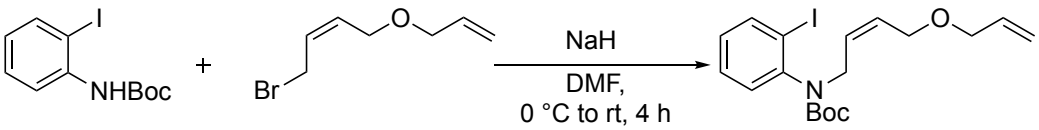

647 **671** **444a**

The reaction was kept under argon and anhydrous DMF was used. The reaction vessel was charged with *tert*-butyl (2-iodophenyl)carbamate **647** (540 mg, 1.69 mmol, 1.0 equiv.). Then DMF (4 mL) was added and the solution was cooled in the ice bath before the careful addition of sodium hydride (74.5 mg, 1.86 mmol, 1.1 equiv.). The reaction was stirred at ice

bath temperature for 30 min. Then *(Z)*-1-(allyloxy)-4-bromobut-2-ene **671** (392 mg, 2.03 mmol, 1.2 equiv.) was added and the reaction was stirred at room temperature for 4 h 20 min. The reaction was monitored by TLC and was found to have reached full conversion after 4 h. The reaction was quenched by the addition of aqueous ammonium chloride (5 mL, sat.) and water (100 mL). The phases were separated and the aqueous phase was extracted with ethyl acetate (3 x 20 mL). The combined organic phases were washed with water (3 x 20 mL) and brine (1 x 20 mL), dried over $MgSO_4$ and concentrated *in vacuo*. Purification by flash column chromatography (10 % ethyl acetate in hexane) gave the product *tert*-butyl *(Z)*-(4-(allyloxy) but-2-en-1-yl)(2-iodophenyl)carbamate **444a** (686 mg, 1.60 mmol, 94 %) as a colourless oil. **^{1}H-NMR** (400 MHz, DMSO-d_6) δ 7.90 (dd, *J* = 8.0, 1.4 Hz, 1H), 7.39 (ddd, *J* = 7.6, 7.6, 1.5 Hz, 1H), 7.25 (dd, *J* = 7.9, 1.6 Hz, 1H), 7.05 (dd, *J* = 7.7, 7.7 Hz, 1H), 5.83 – 5.71 (m, 1H), 5.71 – 5.61 (m, 1H), 5.61 – 5.50 (m, 1H), 5.17 – 5.10 (m, 1H), 5.10 – 5.06 (m, 1H), 4.35 (dd, *J* = 15.5, 6.5 Hz, 1H), 3.96 (dd, *J* = 15.5, 7.4 Hz, 1H), 3.86 – 3.78 (m, 2H), 3.76 – 3.67 (m, 2H), 1.47 (s, 9H, minor isomer), 1.29 (s, 9H, major isomer). **^{13}C-NMR** (101 MHz, DMSO-d_6) δ 152.9, 143.5, 139.0, 135.0, 129.8, 129.6, 129.0, 129.0, 127.6, 116.3, 101.0, 79.5, 69.9, 64.7, 45.4, 27.9. **IR** ν_{max} [cm^{-1}]: 3076, 3003, 2974, 2928, 2853, 1689, 1580, 1472, 1454, 1437, 1379, 1366, 1333, 1298, 1254, 1219, 1167, 1146, 1115, 1082, 1055, 1011. **LC-(ESI+)-MS** [*m/z*] (9.399 min): 430 (M+H). **HRMS** (ESI+) [*m/z*]: calcd. for $C_{18}H_{25}O_3NI$ (M+H): 430.0874, found: 430.0874.

***(Z)*-1-((4-(Allyloxy)but-2-en-1-yl)oxy)-2-iodobenzene 444b**

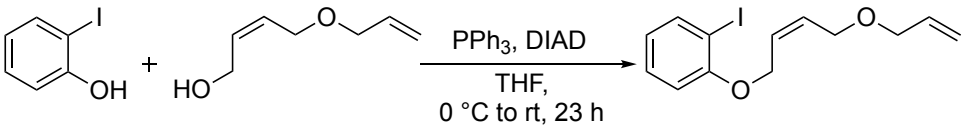

656 **670** **444b**

The reaction was kept under argon and anhydrous THF was used. The reaction vessel was charged with 2-iodophenol **656** (1.57 g, 7.00 mmol, 1.0 equiv.) and triphenylphosphine (2.75 g, 10.5 mmol, 1.5 equiv.). Then THF (45 mL) was added followed by *(Z)*-4-(allyloxy)but-2-en-1-ol **670** (1.02 g, 7.77 mmol, 1.11 equiv.). The solution was cooled in the ice bath and diisopropyl azodicarboxylate (2.2 mL, 10.5 mmol, 1.5 equiv.) was added dropwise over ca. 2 min. Then the reaction was allowed to warm up to room temperature and was stirred for 23 h. The reaction was monitored by TLC and was found to have reached full conversion after that time. The reaction was concentrated *in vacuo*. Purification by flash column chromatography (50 % ethyl acetate in toluene) gave the product as a pale yellow oil, contaminated with 2-iodophenol **656**. The material was dissolved in diethyl ether (30 mL) and extracted with aqueous NaOH (1 M, 5 x 30 mL). The organic phase was washed with brine, dired over $MgSO_4$ and concentrated *in vacuo* to give the pure product *(E)*-1-((4-(allyloxy)but-2-en-1-yl)oxy)-2-iodobenzene **444b** (1.97 g, 5.97 mmol, 85 %) as a pale yellow oil. **^{1}H-NMR** (400 MHz, Chloroform-*d*) δ 7.78 (dd, *J* = 7.8, 1.6 Hz, 1H), 7.28 (ddd, *J* = 8.2, 7.4, 1.6 Hz, 1H), 6.82 (dd, *J* = 8.3, 1.4 Hz, 1H), 6.72 (ddd, *J* = 7.6, 7.6, 1.4 Hz, 1H), 5.98 – 5.86 (m, 2H), 5.86 – 5.78 (m, 1H), 5.30 (ddt, *J* = 17.3, 1.6, 1.6 Hz, 1H), 5.20 (ddt, *J* = 10.4, 1.3, 1.3 Hz, 1H), 4.69 (ddd, *J* = 5.8, 1.2, 1.2 Hz, 2H), 4.16 – 4.12 (m, 2H), 4.01 (ddd, *J* = 5.6, 1.4, 1.4 Hz, 2H). **^{13}C-NMR** (101 MHz, Chloroform-*d*) δ 157.3, 139.7, 134.7, 130.3, 129.5, 127.7, 122.9, 117.5, 112.7, 86.9, 71.5, 66.3, 65.5. **IR** ν_{max} [cm^{-1}]: 3061, 3013, 2978, 2920, 2851, 1645, 1580, 1568, 1470, 1437, 1408, 1331, 1275, 1242,

1227, 1161, 1121, 1080, 1047, 1016. **GC-MS** [*m/z* (%)] (14.651 min): 330 (3, M+), 273 (1), 272 (3), 260 (2), 220 (15), 219 (15), 203 (10), 191 (35), 165 (5), 146 (10), 145 (15), 133 (10), 132 (10), 131 (40), 127 (20), 119 (10), 118 (10), 117 (10), 115 (15), 111 (85), 110 (30), 105 (40), 103 (10), 93 (25), 92 (80), 91 (20), 79 (15), 77 (25), 76 (20), 69 (50), 67 (50), 65 (30), 64 (65), 63 (100), 62 (20), 57 (20), 55 (65), 54 (65), 53 (50). **HRMS** (ASAP) [*m/z*]: calcd. for $C_{13}H_{16}O_2I$ (M+H): 331.0195, found: 331.0192.

5.3.9 Reductive Cleavage of the N-O Bond in Weinreb Amides

(Corresponds to Chapter 2.3.2. The synthesis of the substrates used in this section is described in Chapter 5.3.10).

Reduction of Weinreb Amides 446 to Amides 447

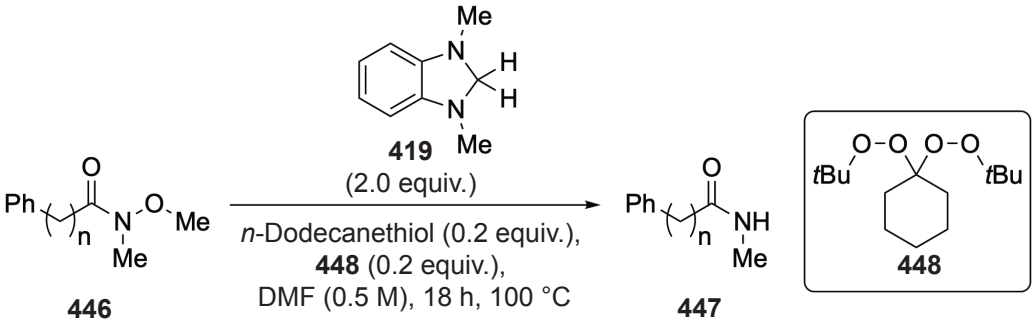

The reaction vessel was charged with 1,3-dimethyl-2,3-dihydro-1H-benzo[d]imidazole **419** (183 mg, 1.20 mmol, 2.0 equiv.). Then *N*-methoxy-*N*-methylbenzamide **446a** (101 mg, 0.600 mmol, 1.0 equiv.) or *N*-methoxy-*N*-methyl-2-phenylacetamide **446b** (110 mg, 0.600 mmol, 1.0 equiv.) as required was added as a solution in DMF (1.2 mL). Then 1,1-bis(*tert*-butylperoxy) cyclohexane **448** (33 µL, 120 µmol, 0.2 equiv.) and *n*-dodecanethiol (29.3 µL, 120 µmol, 0.2 equiv.) were added in this sequence. The reaction was purged with argon for 1 h and then heated to 100 °C for 20 h. The reaction was kept under a positive pressure of argon for the duration of heating. After the heating period, the reaction was poured onto water/brine (100 mL, 2:1) and extracted with ethyl acetate (4 x 20 mL). The combined organic phases were washed with brine (1 x 50 mL). Then a precisely measured amount of 1,3,5-trimethoxybenzene (ca. 50.5 mg, 0.300 mmol, 0.5 equiv.) was added as an internal standard. The solution was dried over $MgSO_4$ and concentrated in vacuo.

The reaction of **446a** was found to have reached full conversion by inspection of the crude product by ^{1}H-NMR spectroscopy. The yield of *N*-methylbenzamide **447a** was calculated to be 93 %. Purification by flash column chromatography (50 % ethyl acetate in hexane) gave *N*-methylbenzamide **447a** (85.7 mg, 0.563 mmol, 94 %) as an off-white solid. **^{1}H-NMR** (400 MHz, Chloroform-d) δ 7.78 – 7.73 (m, 2H), 7.49 – 7.43 (m, 1H), 7.41 – 7.35 (m, 2H), 6.55 (br s, 1H), 2.97 (d, *J* = 4.6 Hz, 3H). **^{13}C-NMR** (101 MHz, Chloroform-d) δ 168.4, 134.7, 131.4, 128.6, 127.0, 26.9. (D314339) **GC-MS** [*m/z* (%)] (11.287 min): 135 (30, M^+), 134 (35), 105 (90), 77 (100), 75 (20), 74 (40). **mp** = 74 °C (lit. mp = 77 °C).[277] The NMR spectra are in agreement with the reported data.[278]

In the reaction of **446b** no product was detected by ^{1}H-NMR spectroscopy. The yield of remaining starting material *N*-methoxy-*N*-methyl-2-phenylacetamide **446b** was calculated to

be 79 %. Also by inspection of the crude reaction product by GC-MS no signal that would be consistent with the structure of **447b** was found.

The reactions with both substrates **446a** and **446b** was repeated under catalytic conditions (conditions **B**). The reaction vessel was charged with *N*-methoxy-*N*-methylbenzamide **446a** (101 mg, 0.600 mmol, 1.0 equiv.) or *N*-methoxy-*N*-methyl-2-phenylacetamide **446b** (110 mg, 0.600 mmol, 1.0 equiv.) as required. Then DMF (1.2 mL) was added followed by 1,3-dimethyl-1H-benzo[d]imidazol-3-ium iodide **418-I** (32.9 mg, 120 µmol, 0.2 equiv.), *n*-dodecanethiol (29.3 µL, 120 µmol, 0.2 equiv.) and sodium borohydride (45.4 mg, 1.20 mmol, 2.0 equiv.). The reaction was heated to 55 °C for 48 h and was left open to air via a needle for the whole reaction period. After the heating period the reaction was poured onto water/brine (100 mL, 2:1) and extracted with ethyl acetate (4 x 20 mL). The combined organic phases were washed with brine (1 x 50 mL). Then a precisely measured amount of 1,3,5-trimethoxybenzene (ca. 50.5 mg, 0.300 mmol, 0.5 equiv.) was added as an internal standard. The solution was dried over $MgSO_4$ and concentrated in vacuo.

The reaction of **446a** gave *N*-methylbenzamide **447a** (11 %), benzyl alcohol (33 % compared against literature data[279] and a commercial sample) and remaining starting material (47 %) as measured by ^{1}H-NMR spectroscopy of the crude reaction product.

The reaction of **446b** gave phenethyl alcohol (31 %, compared against literature data[280]) and remaining starting material (11 %) as measured by ^{1}H-NMR spectroscopy of the crude reaction product. A third, unidentified product was observed by ^{1}H-NMR spectroscopy and GC-MS.

5.3.10 Substrate Synthesis for Reactions in Chapter 5.3.9

1,1-bis(*tert*-Butylperoxy)cyclohexane 448

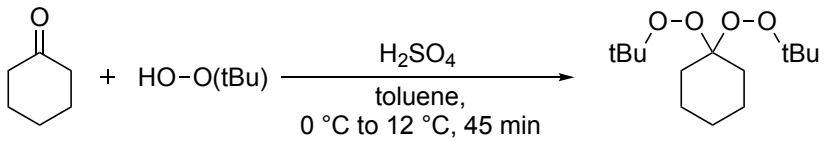

672 **673** **448**

The reaction vessel was charged with toluene (4.5 mL) and cyclohexanone **672** (2.1 mL, 20 mmol, 1.0 equiv.) and cooled in a water-ice/water cooling bath. Then H_2SO_4 (1.3 mL, 16 mmol, 0.8 equiv.) was added dropwise such that the internal temperature of the reaction did not exceed 8 °C. When the addition was finished, the reaction was placed in a water-ice/acetone cooling bath and 2-hydroperoxy-2-methylpropane **673** (5.4 mL, 40 mmol, 2.0 equiv.) was added over 5 min such that the internal temperature of the reaction remained between -3 °C and +3 °C. When the addition was finished the reaction was placed in a +8 °C water bath and stirring was continued for 45 min. The reaction was monitored by TLC and was found to have reached a high degree of conversion after 30 min. The phases were separated. The aqueous phase was extracted with toluene (1 x 5 mL). The combined organic phases were washed with aqueous NaOH (1 x 5 mL, 1 M) and brine (5 mL), dried over $MgSO_4$ and concentrated *in vacuo*. Purification by flash column chromatography (4 % ethyl acetate in hexane) gave the product 1,1-bis(*tert*-butylperoxy)cyclohexane **448** (3.01 g, 11.6 mmol, 58 %) as a colourless oil. The material was stored at 4 °C. **^{1}H-NMR** (400 MHz, Chloroform-*d*) δ 1.81 – 1.76 (m, 4H),

1.58 – 1.49 (m, 4H), 1.44 – 1.37 (m, 2H), 1.25 (s, 18H). **^{13}C-NMR** (101 MHz, Chloroform-*d*) δ 107.1, 79.1, 31.0, 27.0, 25.9, 22.9. Chloroform-*d* was passed over K_2CO_3 before use and the NMR-spectra were recorded immediately. The compound was found to decompose in chloroform-*d* over several hours. **^{1}H-NMR** (400 MHz, DMSO-d_6) δ 1.71 (dd, *J* = 7.4, 4.7 Hz, 4H), 1.51 – 1.43 (m, 4H), 1.42 – 1.33 (m, 2H), 1.20 (s, 18H). **^{13}C-NMR** (101 MHz, DMSO-d_6) δ 106.4, 78.6, 30.4, 26.5, 25.0, 22.2. **LC-(ESI-)-MS** [*m/z*] (10.650 min): 259 (M-H). The NMR spectra are in agreement with the previously reported data (recorded in chloroform-*d*).[265]

***N*-Methoxy-*N*-methylbenzamide 446a**

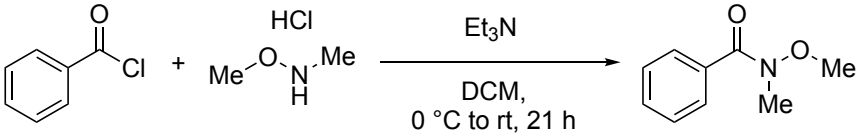

674 **675** **446a**

The reaction was kept under argon and anhydrous dichloromethane was used. The reaction vessel was charged with N,O-dimethylhydroxylamine hydrochloride **675** (1.87 g, 18.8 mmol, 1.25 equiv.) and dichloromethane (45 mL). The solution was cooled in the ice bath before the addition of benzoyl chloride **674** (1.83 mL, 15.0 mmol, 1.0 equiv.) and triethylamine (4.2 mL, 30 mmol, 2.0 equiv.). The reaction was allowed to slowly warm up to room temperature and was stirred for 21 h. The reaction was poured onto aqueous hydrochloric acid (1M, 50 mL). The phases were separated and the aqueous phase was extracted with dichloromethane (3 x 20 mL). The combined organic phases were washed with aqueous $NaHCO_3$ (20 mL), dried over $MgSO_4$ and concentrated in vacuo. Purification by flash column chromatography (40 % ethyl acetate in hexane) gave pure *N*-methoxy-*N*-methylbenzamide **446a** (2.53 g, 15.3 mmol, quant.) as a colourless oil. **^{1}H-NMR** (400 MHz, Chloroform-*d*) δ 7.69 – 7.64 (m, 2H), 7.48 – 7.36 (m, 3H), 3.55 (s, 3H), 3.35 (s, 3H). **^{13}C-NMR** (101 MHz, Chloroform-d) δ 170.1, 134.3, 130.7, 128.3, 128.1, 61.1, 33.9. **GC-MS** [*m/z* (%)] (9.328 min): 165 (2, M^+), 105 (100), 77 (90), 51 (35). The NMR spectra are in agreement with the reported data.[281]

***N*-Methoxy-*N*-methyl-2-phenylacetamide 446b**

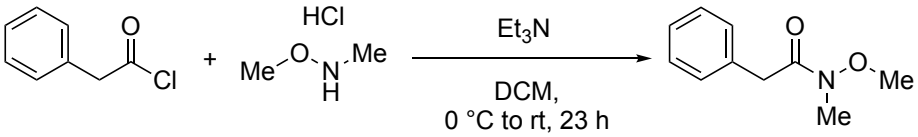

676 **675** **446b**

The reaction was kept under argon and anhydrous dichloromethane was used. The reaction vessel was charged with N,O-dimethylhydroxylamine hydrochloride **675** (1.87 g, 18.8 mmol, 1.25 equiv.) and dichloromethane (45 mL). The solution was cooled in the ice bath before the addition of 2-phenylacetyl chloride **676** (2.04 mL, 15.0 mmol, 1.0 equiv.) and triethylamine (4.2 mL, 30 mmol, 2.0 equiv.). The reaction was allowed to slowly warm up to room temperature and was stirred for 23 h. The reaction was poured onto aqueous hydrochloric acid (1M, 50 mL). The phases were separated and the aqueous phase was extracted with dichloromethane (3 x 20 mL). The combined organic phases were washed with aqueous $NaHCO_3$ (20 mL), dried over $MgSO_4$ and concentrated in vacuo. Purification by flash column chromatography (ethyl

acetate in hexane, gradient from 20 % - 30 %) gave *N*-methoxy-*N*-methyl-2-phenylacetamide **446b** (1.34 g, 7.47 mmol, 50 %) as a pale yellow oil. **^{1}H-NMR** (400 MHz, Chloroform-d) δ 7.39 – 7.20 (m, 5H), 3.78 (s, 2H), 3.60 (s, 3H), 3.19 (s, 3H). **^{13}C-NMR** (101 MHz, Chloroform-d) δ 172.0, 134.5, 128.8, 128.0, 126.3, 60.8, 38.9, 31.8. **GC-MS** [*m/z* (%)] (9.993 min): 179 (2, M^+), 148 (0.5), 118 (20), 91 (100), 89 (10), 65 (25), 61 (10). The NMR spectra are in agreement with the reported data.[282]

5.3.11 Calculations for the Reductive N-O Bond Cleavage Discussed in Chapter 2.3.2

All calculations were performed on UM06-2X/6-311++G(d,p)/cpcm(DMF) level of theory. The .log files can be found in the following depository: Https://doi.org/10.15129/deef4cea-f279-4afe-82ca-29b88bd30579 {/Catalytic_Electron_Donor/Weinreb_Amides}

The structures and corresponding file names for the calculations summarised in Figure 2-2 are listed below (Table S13). It should be noted that the required benzimidazole structures for the Nelsen-four-point calculation can be found in Table S8.

Table S13 - File names for structures in Figure 2-3

Entry	Structure	File name	Comment
1	**446a**	Weinreb_amide_neutral_n-0.log	
2	**446a**	Weinreb_amide_neutral_in_radical-anion_geom_n-0.log	In the geometry of **449a**
3	**449a**	BS_Weinreb_amide_radical-anion_n-0_N-O_bond_cleavage_start.log	
4	**449a**	Weinreb_amide_radical-anion_in_neutral_geom_n-0.log	In the geometry of **446a**
5	**446b**	Weinreb_amide_neutral_n-1.log	
6	**446a**	Weinreb_amide_neutral_in_radical-anion_geom_n-1.log	In the geometry of **449b**
7	**449b**	BS_Weinreb_amide_radical-anion_n-1_N-O_bond_cleavage.log	
8	**449b**	Weinreb_amide_radical-anion_in_neutral_geom_n-1.log	In the geometry of **446b**
9	TS **449a**	TS_Weinreb_amide_radical-anion_n-0_N-O_bond_cleavage.log	TS N-O fragmentation **449a**
10	TS **449b**	TS_Weinreb_amide_radical-anion_n-1_N-O_bond_cleavage.log	TS N-O fragmentation **449b**
11	Product Complex from **449a**	TS_Weinreb_amide_radical-anion_n-0_N-O_bond_cleavage_forward.log	Amide anion of **447a** and methoxyl radical complexed
12	Product Complex from **449b**	TS_Weinreb_amide_radical-anion_n-1_N-O_bond_cleavage_forward.log	Amide anion of **447b** and methoxyl radical complexed
13	**447a**	Amide_n-0_product_anion.log	Amide anion of **447a**
14	**447b**	Amide_n-1_product_anion.log	Amide anion of **447b**
15	Methoxyl radical	Methoxyl_radical_trial2.log	Methoxyl radical
16	Methoxide anion	Methoxylate_anion.log	Alternative, less favourable product
17	Aminyl radical	Amide_n-0_product_radical_trial2.log	Alternative, less favouralbe product

The structures and corresponding .chk file names for the orbital visualisation in Figure 2-4 are listed below (Table S14).

Table S14 - The .chk files required for orbital visualisation in Figure 2-4

Entry	Structure	File name	Comment
1	**446a**	Weinreb_amide_neutral_n-0_trial1.chk	HOMO of **446a**
2	**446b**	Weinreb_amide_neutral_n-1_trial1.chk	HOMO of **446b**
3	**449a**	Weinreb_amide_radical-anion_n-0_N-O_bond_cleavage_start_trial1.chk	SOMO of **449a**
4	**449b**	Weinreb_amide_radical-anion_n-1_N-O_bond_cleavage_start_trial1.chk	SOMO of **449b**

5.3.12 Benchmark

(Corresponds to Chapter 2.3.3. The synthesis of the substrates used in this section is described in Chapter 5.3.10 {for **448**} and Chapter 5.3.13).

Benchmarking the Electron Donor 417 against 4 and 450

In order to be able to compare the reducing power achieved with the new protocol, a series of benchmark reactions was performed (results are summarised in Table S49). The electron donor **417**, derived from 1,3-dimethyl-2,3-dihydro-1*H*-benzo[*d*]imidazole **419**, was compared with *N*^{1},*N*^{1},*N*^{4},*N*^{4}-tetramethylbenzene-1,4-diamine **450** and 14,15-dimethyl-7,8,14,15-tetrahydro-6*H*-benzo[4,5]imidazo[1,2-*a*]benzo[4,5]imidazo[2,1-*c*][1,4]diazepine electron donor **4** (Table S49).

Conditions for Entry 1

This experiment has been reported in Entry 19, Table S6 already. For convenience, the experimental details are printed here again: The reaction vessel was charged with 1,3-dimethyl-2,3-dihydro-1*H*-benzo[*d*]imidazole **419** (59.2 mg, 0.400 mmol, 2.0 equiv.). Then DMF (0.4 mL) was added followed by 4-iodo-1,1'-biphenyl **420** (58 mg, 0.20 mmol, 1.0 equiv.). The reaction was heated to 55 °C for 4 h while open to air via a needle. The reaction mixture was cooled to room temperature, diluted to ca. 1 mg/mL of starting material 4-iodobiphenyl **420** and a precisely measured amount of 1-phenylpyrrolidin-2-one (ca. 24.2 mg, 0.100 mmol, 0.5 equiv.) was added as internal standard. An aliquot was analysed by HPLC (biphenyl: 3.209 min).

Conditions for Entry 2 - 3

The reaction vessel was charged with 1,3-dimethyl-2,3-dihydro-1*H*-benzo[*d*]imidazole **419** (88.9 mg, 0.600 mmol, 2.0 equiv.). Then DMF (0.6 mL) was added followed by 1-bromonaphthalene **451** (64.0 mg, 0.300 mmol, 1.0 equiv.) or 1-bromo-4-methoxybenzene **453** (56.7 mg, 0.300 mmol, 1.0 equiv.) as required. Then dodecanethiol (14.7 µL, 60.0 µmol, 0.2 equiv.) and a precisely measured amount of internal standard 1,3,5-trimethoxybenzene (ca. 25 mg, 0.150 mmol, 0.5 equiv.) were added in this sequence and the reaction mixture was heated to 55 °C for 4 h while left open to air via a needle. An aliquot of the reaction was diluted with methanol to ca. 1 mg / mL of employed starting material and analysed by GC-FID (naphthalene: 10.088 min; anisole: 7.132 min).

Conditions for Entry 4 - 5

The reaction vessel was charged with 1,3-dimethyl-2,3-dihydro-1*H*-benzo[*d*]imidazole **419** (88.9 mg, 0.600 mmol, 2.0 equiv.). Then DMF (0.6 mL) was added followed by 1-bromonaphthalene **451** (64.0 mg, 0.300 mmol, 1.0 equiv.) or 1-bromo-4-methoxybenzene **453** (56.7 mg,

0.300 mmol, 1.0 equiv.) as required. Then 1,1-bis(*tert*-butylperoxy)cyclohexane **448** (16 µL, 60 µmol, 0.2 equiv.) and *n*-dodecanethiol (14.7 µL, 60.0 µmol, 0.2 equiv.) were added in this sequence and the reaction mixture was degassed by purging with argon for 1 h. Then the reaction was heated to 100 °C for 20 h. The reaction was cooled to room temperature and a precisely measured amount of internal standard 1,3,5-trimethoxybenzene (ca. 25 mg, 0.150 mmol, 0.5 equiv.) was added. An aliquot of the reaction was diluted with methanol to ca. 1 mg / mL of employed starting material and analysed by GC-FID (naphthalene: 10.088 min; anisole: 7.132 min). For the reaction with 1-bromonaphthalene **451** (Entry 4) the products were isolated: The reaction was diluted with toluene (3.6 mL). The precipitate was filtered and washed with toluene (2 x 0.5 mL). The filter cake was dried in vacuo to give 1,3-dimethyl-1*H*-benzo[*d*]imidazol-3-ium bromide **418-Br** (141 mg, 0.620 mmol, 52 %). The NMR spectra were identical to the spectra recorded for the independently synthesised material **418-I**, vide infra. The filtrate was poured onto water/brine (2:1, 100 mL) and was extracted with ethyl acetate (4 x 20 mL). The combined organic phases were washed with brine (1 x 50 mL), dried over Mg_2SO_4 and concentrated in vacuo. Purification by flash column chromatography (hexane) gave naphthalene **452** (65.9 mg, 0.442 mmol, 74 %) as a white solid. **^{1}H-NMR** (400 MHz, Chloroform-*d*) δ 7.89 – 7.80 (m, 4H), 7.48 (dd, *J* = 6.3, 3.2 Hz, 4H). **^{13}C-NMR** (101 MHz, Chloroform-*d*) δ 133.6, 128.0, 126.0. **GC-MS** [*m/z* (%)] (9.940 min): 128 (100, M+), 127 (15), 102 (10), 74 (10), 64 (20), 63 (20), 62 (10), 51 (20). **mp** = 73 °C -74 °C (lit. mp = 76 °C - 79 °C).[283] The NMR spectra are in agreement with the previously reported data.[284]

Conditions for Entry 6 - 8

The electron donor **4** was used according to standard procedures,[6] i.e. electron donor **4** was formed in situ by treating the precursor salt **677** with KHMDS as shown below.

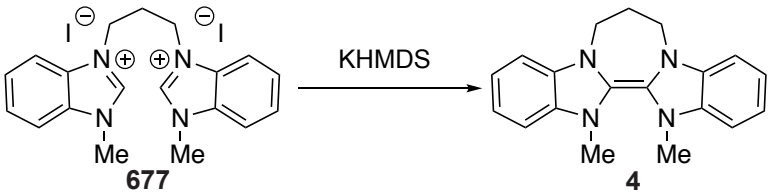

677 **4**

The reaction vessel was charged with the substrate 4-iodo-1,1'-biphenyl **420** (86.6 mg, 0.300 mmol, 1.0 equiv.) or 1-bromonaphthalene **451** (43.3 µL, 0.300 mmol, 1.0 equiv.) or 1-bromo-4-methoxybenzene **453** (37.9 µL, 0.300 mmol, 1.0 equiv.) as required. Then the reaction vessel was brought inside the glove box. Subsequently 3,3'-(propane-1,3-diyl)bis(1-methyl-1*H*-benzo[*d*]imidazol-3-ium) iodide **677** (340 mg, 0.600 mmol, 2.0 equiv.), KHMDS (252 mg, 1.20 mmol, 4.0 equiv.) and DMF (1.2 mL, dried over 3 Å molecular sieves for 1 day and degassed by purging with argon for 30 min) were added. The reaction vessel was sealed and heated to 100 °C for 20 h. The reaction was cooled to room temperature and a precisely measured amount of internal standard 1,3,5-trimethoxybenzene (ca. 25 mg, 0.150 mmol, 0.5 equiv.) was added. An aliquot of the reaction was diluted with methanol to ca. 1 mg / mL of employed starting material and analysed by GC-FID (4-iodobiphenyl: 14.208 min; naphthalene: 10.088 min; anisole: 7.132 min).

Conditions for Entry 9

The reaction vessel was charged with 4-iodo-1,1'-biphenyl **420** (85.7 mg, 0.300 mmol, 1.0 equiv.). Then DMF (0.6 mL) was added, followed by an exactly measured amount of

Table S49 - Comparison of the effective reducing power of three different neutral organic electron donors

Reducing Agents

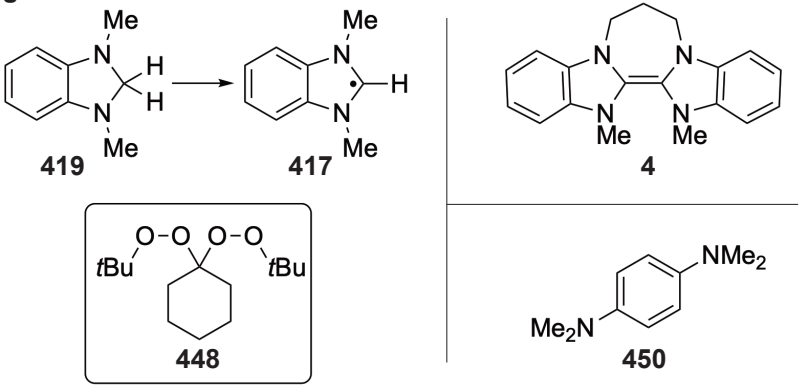

Reference Reactions

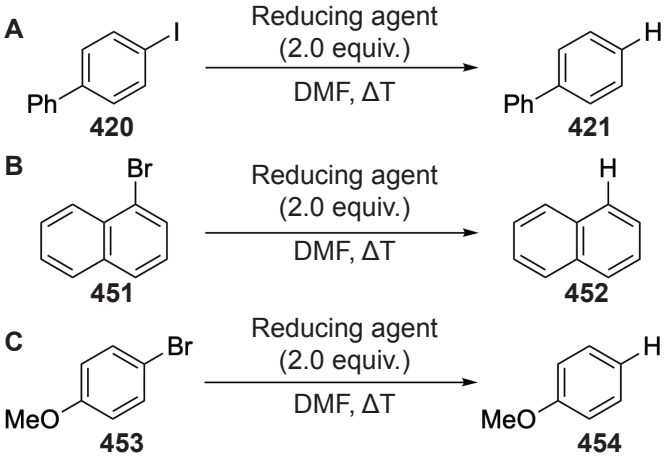

Entry	Reducing Agent	Reaction (substrate)	Initiator	Temp.	Time	Yield of Reduce Product[a]
1	**419**	**A (420)**	air	55 °C	4 h	95 %[b]
2	**419**	**B (451)**	air	55 °C	4 h	80 %
3	**419**	**C (453)**	air	55 °C	4 h	40 %
4	**419**	**B (451)**	**448**	100 °C	20 h	94 % (74 %)[c]
5	**419**	**C (453)**	**448**	100 °C	20 h	42 %
6	**4**	**A (420)**	none	100 °C	20 h	66 %
7	**4**	**B (451)**	none	100 °C	20 h	< 1 %
8	**4**	**C (453)**	none	100 °C	20 h	4 %
9	**450**	**A (420)**	air	55 °C	4 h	not detected

[a] The yield was determined by GC-FID vs. 1,3,5-trimethoxybenezene as internal standard unless mentioned otherwise.

[b] This entry is copied from Table 2-1 Entry 19. The yield was determined by HPLC vs. 1-phenylpyrrolidin-2-one as internal standard.

[c] Isolated yield is given in brackets.

internal standard 1,3,5-trimethoxybenzene (ca. 25 mg, 0.150 mmol, 0.5 equiv.). Then dodecanethiol (14.7 µL, 60.0 µmol, 0.2 equiv.) was added, followed by *N*¹,*N*¹,*N*⁴,*N*⁴-tetramethylbenzene-1,4-diamine **450** (98.5 mg, 0.600 mmol, 2.0 equiv.). The reaction was stirred at 55 °C for 4 h open to air. An aliquot of the reaction was diluted with methanol to ca. 1 mg / mL of employed starting material and analysed by GC-FID (4-iodobiphenyl: 14.208 min).

Attempted reduction of 9-chloroanthracene 118a

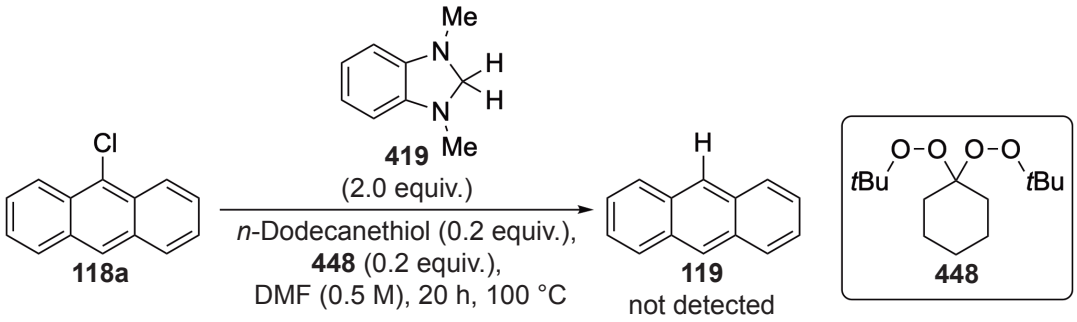

The reaction vessel was charged with 1,3-dimethyl-2,3-dihydro-1H-benzo[d]imidazole **419** (178 mg, 1.20 mmol, 2.0 equiv.). Then DMF (0.6 mL) was added, followed by 9-chloroanthracene **118a** (142 mg, 0.600 mmol, 1.0 equiv.). Another portion of DMF (0.6 mL) was added (used for washing the container of the substrate). Then *n*-dodecanethiol (29.3 µL, 120 µmol, 0.2 equiv.) and 1,1-bis(*tert*-butylperoxy)cyclohexane **448** (33 µL, 120 µmol, 0.2 equiv.) were added in this sequence and the reaction mixture was degassed by five cycles of freeze-pump-thaw. Then the reaction was heated to 100 °C for 20 h while it was kept under a positive pressure of argon. A solid started to precipitate when the reaction was cooled to room temperature. The reaction was diluted with toluene (3.6 mL). The precipitate was filtered and washed with toluene (2 x 0.5 mL). The filter cake was dried in vacuo to give the 1,3-dimethyl-1H-benzo[d] imidazol-3-ium salt **418-X** (29.8 mg, counter cation unknown). The NMR spectra were identical to the independently synthesised material, vide infra. The filtrate was poured on water/brine (2:1, 100 mL) and was extracted with ethyl acetate (4 x 20 mL). The combined organic phases were washed with brine (1 x 50 mL), dried over $MgSO_4$ and concentrated in vacuo. Purification by flash column chromatography (hexane) gave 9-chloroanthracene **118a** (147.8 mg, 0.616 mmol, quant.). The NMR spectra were identical to the spectra of the starting material.

Reduction of 1-bromonaphthalene 451 according to the catalytic protocol (conditions B)

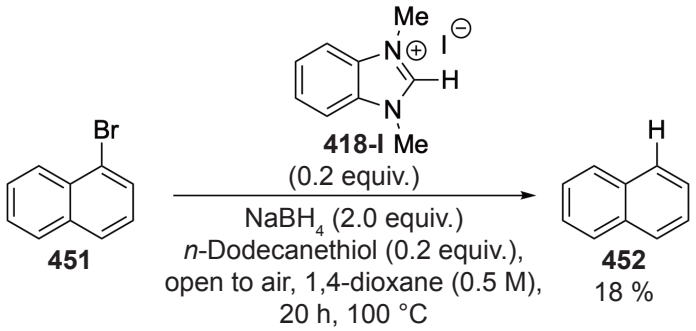

The reaction vessel was charged with 1,3-dimethyl-1*H*-benzo[*d*]imidazol-3-ium iodide **418-I** (32.9 mg, 120 µmol, 0.2 equiv.). Then 1,4-dioxane (0.6 mL) was added followed by 1-bromonaphthalene **451** (128 mg, 0.600 mmol, 1.0 equivl). Another portion of 1,4-dioxane (0.6 mL) was added (used for washing the container of the substrate). Then *n*-dodecanethiol (29.3 µL, 120 µmol, 0.2 equiv.) and $NaBH_4$ (45.4 mg, 1.20 mmol, 2.0 equiv.) were added in this sequence and the reaction mixture was heated to 100 °C for 20 h. The reaction was left open to air via a needle for the whole reaction time. The reaction was poured on water/brine (2:1, 100 mL) and was extracted with ethyl acetate (4 x 20 mL). The combined organic phases were washed with brine (1 x 50 mL), dried over $MgSO_4$ and concentrated in vacuo. Purification by flash column chromatography (hexane) gave 121.7 mg of an inseparable mixture of starting material **451** (0.427 mmol, 71 %) and naphthalene **452** (0.106 mmol, 18 %) as a pale yellow oil.

The reaction was repeated according to the same procedure but without 1,3-dimethyl-1*H*-benzo[*d*]imidazol-3-ium iodide **418-I**. No naphthalene **452** was detected in the crude product of this reaction by ^{1}H-NMR.

5.3.13 Substrate Synthesis for Reactions in Chapter 5.3.12

3,3'-(Propane-1,3-diyl)bis(1-methyl-1*H*-benzo[*d*]imidazol-3-ium) iodide 677

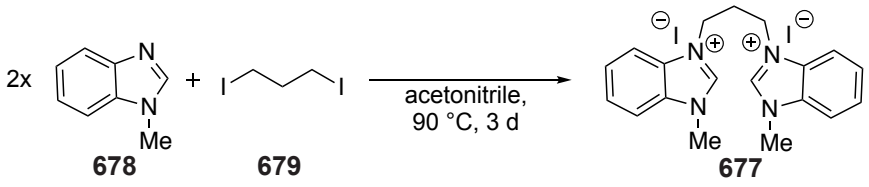

1-Methyl-1*H*-benzo[*d*]imidazole **678** (2.67 g, 20.0 mmol, 4.0 equiv.) was dissolved in acetonitrile and 1,3-diiodopropane **679** (0.580 mL, 5.00 mmol, 1.0 equiv.) was added. The solution was heated to reflux for three days. The solvent was carefully removed and the crude product was washed with diethyl ether (3 x 6 mL) until a white solid was obtained. The material was dried *in vacuo* to give the product 3,3'-(propane-1,3-diyl)bis(1-methyl-1*H*-benzo[*d*]imidazol-3-ium) iodide **677** (2.38 g, 4.25 mmol, 85 %) as a white solid. **^{1}H-NMR** (500 MHz, DMSO-d_6) δ 9.70 (s, 2H), 8.09 - 8.01 (m, 4H), 7.76 – 7.67 (m, 4H), 4.66 (t, *J* = 7.2 Hz, 4H), 4.08 (s, 6H), 2.59 (quint, *J* = 7.3 Hz, 2H). **^{13}C-NMR** (126 MHz, DMSO-d_6) δ 142.8, 131.8, 130.8, 126.6,

126.5, 113.6, 113.4, 43.8, 33.3, 28.0. **LC-(ESI+)-MS** [*m/z*] (0.948 min): 321 (M^{2+}+2ACN). **mp** = 253 °C - 260 °C (decomposition) (lit. mp = 276 °C - 277 °C, decomposition).[6] The NMR spectra are in agreement with the reported data.[6]

5.3.14 Computational Results Presented in Chapter 2.3.3

The .log files can be found in the following depository: Https://doi.org/10.15129/deef4cea-f279-4afe-82ca-29b88bd30579 {/Catalytic_Electron_Donor/Benchmark}

The structures and corresponding file names for the calculations summarised in Figure 2-5. are listed below (Table S15). All calculations were performed on the level of theory as indicated in Figure 2-5. The basis set 6-31+G(d,p) and cpcm(DMF) solvent model was used for all calculations.

Table S15 - File names for structures in Figure 2-5

Entry	Structure	File name	Comment
1	**417**	Benzimidazoyl_Radical_trial1_DMF_6-31+G-dp-.log	With UM06-2X
2	**418**	Benzimidazolium_trial1_DMF_6-31+G-dp-.log	With UM06-2X
3	**417**	Benzimidazoyl_Radical_trial1_DMF_UB3LYP_6-31+G-dp-.log	With B3LYP
4	**418**	Benzimidazolium_trial1_DMF_UB3LYP_6-31+G-dp-.log	With B3LYP
5	**4**	Neutral_BenzimidazoleDonor_trial3.log	With UM06-2X
6	**183 (cation of 4)**	Cation_BenzimidazoleDonor_trial3.log	With UM06-2X
7	**4**	Neutral_BenzimidazoleDonor_B3LYP_trial2.log	With B3LYP
8	**183 (cation of 4)**	Cation_BenzimidazoleDonor_B3LYP_trial2.log	With B3LYP

Oxidation potentials were estimated according to the method described by Nicewicz et al.[214] The ΔG_{ox} values were calculated as $\Delta G_{ox} = G_{298}$(reduced) - G_{298}(oxidised).

The structures used to construct Figure 2-7 can be found in Table S8 - Table S10.

5.3.15 Expanding the Scope of SET Precursors and Catalysts

(Corresponds to Chapter 2.4. The synthesis of the substrates used in this section is described in Chapter 5.3.16).

1,3-Dimethyl-2,3-dihydro-1H-imidazole 220

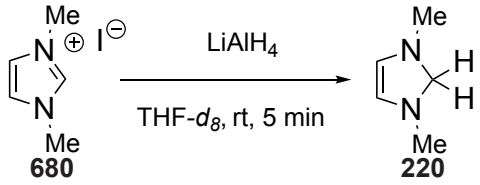

680 **220**

The reaction was performed inside the glove box. The reaction vessel was charged with 1,3-dimethyl-1H-imidazol-3-ium iodide **680** (89.6 mg, 0.4 mmol, 1.0 equiv.) and THF-d_8 (1 mL). Then lithium aluminium hydride (8 mg, 0.2 mmol, 0.5 equiv.) was added and the reaction was stirred for 5 min at room temperature. The solution was decanted and analysed by NMR. **^{1}H-NMR** (400 MHz, THF-d_8) δ 5.34 (s, 2H), 3.66 (s, 2H), 2.36 (s, 6H). **^{13}C-NMR** (101 MHz, THF-d_8) δ 123.8, 81.7, 40.8. Due to the high reactivity of the material it was not possible to obtain further analytical data. The NMR spectra are in agreement with the reported data.[285] Attempts to isolate the material by distillation or careful concentration (in the glove box) led to decomposition of the compound.

Reductive radical cyclisation of 426 with 459

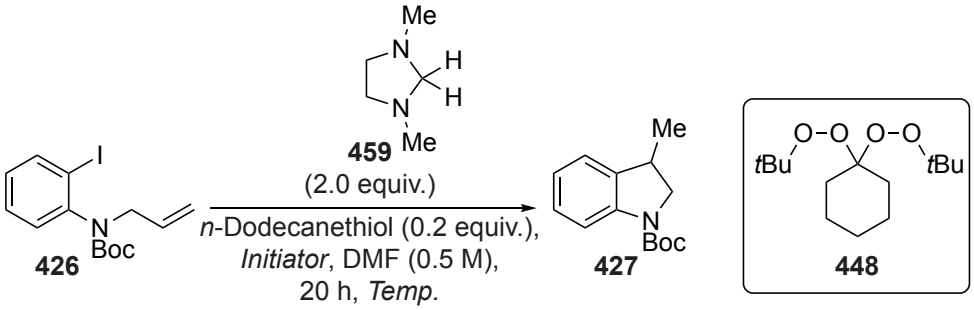

Entry	Initiator	Temp	Yield of 427[a]	Remaining 426[a]
1	Oxygen in the air	55 °C	12 %	72 %
2	**448**	100 °C	93 % (94 %)[b]	not detected

[a] Yields were determined by ^{1}H-NMR vs. 1,3,5-trimethoxybenezene as an internal standard. [b] Isolated yield.

For Entry 1 the reaction was set up on the bench. For Entry 2 the reaction was set up in a nitrogen-filled glove box in a pressure tube.

The reaction vessel was charged with 1,3-dimethylimidazolidine **459** (62.0 mg, 600 µmol, 2.0 equiv.) . Then DMF (0.6 mL) was added followed by *tert*-butyl allyl(2-iodophenyl)carbamate **426** (110 mg, 0.300 mmol, 1.0 equiv.). Then *n*-dodecanethiol (14.7 µL, 60.0 µmol, 0.2 equiv.) and 1,1-bis(*tert*-butylperoxy)cyclohexane **448** (16 µL, 60.0 µmol, 0.2 equiv.) as required were added in this sequence. Finally, a precisely measured amount of 1,3,5-trimethoxybenzene (ca. 50.5 mg, 0.300 mmol, 1.0 equiv.) as internal standard was added. For Entry 1 the reaction was heated to 55 °C for 20 h while left open to air via a needle. For Entry 2 the reaction was heated to 100 °C for 20 h (under inert atmosphere of N_2). The reaction was poured on water/brine (100 mL, 2:1) and extracted with ethyl acetate (4 x 20 mL). The combined organic phases were washed with brine (1 x 50 mL), the solution was dried over $MgSO_4$ and concentrated in vacuo. The crude product was analysed by ^{1}H-NMR. For the reaction of Entry 1 it was found that 12 % of product **427** were formed while 72 % of substrate **426** remained. For the reaction of Entry 2 it was found that 93 % of product **427** were formed while all substrate **426** was consumed. The material from reaction of Entry 2 was purified by flash column chromatography (5 % ethyl acetate in hexane) to give *tert*-butyl 3-methylindoline-1-carboxylate **427** (70.0 mg, 0.282 mmol, 94 %) as a colourless oil. The NMR spectra were identical to the previously recorded spectra.

Attempts to reduce 1-bromonaphthalene 451 with the imidazolium iodide 461 catalyst.

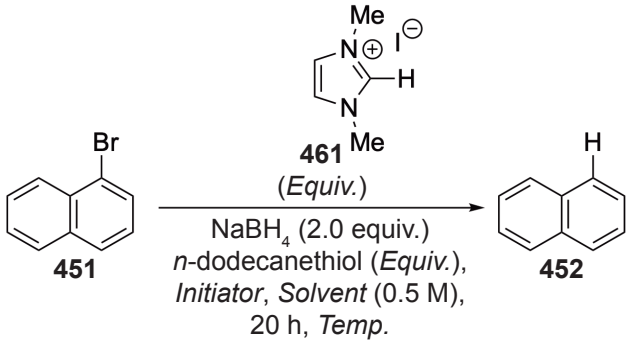

The possibility to use **461** as a catalyst for the reductive debromination reaction of 1-bromonaphthalene **451** was investigated. The results are summarised in Table S16.

Conditions for Entries 1 - 8

The reaction vessel was charged with 1,3-dimethyl-1*H*-imidazol-3-ium iodide **461** (26.9 mg, 120 µmol, 0.2 equiv.) as required. Then the solvent (1.2 mL) was added as required followed by 1-bromonaphthalene **451** (86.5 µL, 0.600 mmol, 1.0 equiv.), a precisely measured amount of internal standard 1,3,5-trimethoxybenezene (ca. 50.5 mg, 0.300 mmol, 0.5 equiv.), *n*-dodecanethiol as required and the initiator 1,1-bis(*tert*-butylperoxy)cyclohexane (33 µL, 120 µmol, 0.2 equiv.) as required. Finally $NaBH_4$ (45.4 mg, 1.20 mmol, 2.0 equiv.) was added. The reaction was heated to the specified temperature for 20 h. The reaction was left open to air for the whole reaction time as required. An aliquot (50 µL) was taken from the reaction and diluted in ethyl acetate (3 mL). The solution was filtered through silica and analysed by GC-FID.

Table S16 - Reactions the imidazolium iodide **461** with 1-bromonaphthalene **451**.

Entry	Solvent	Temp.	461 (equiv.)	PRC (equiv.)	Initiator	Yield of 452
1	DMF	55 °C	0.2	0.2	air	11 %
2	1,4-Dioxane	100 °C	0.2	0.2	**448**	7 %
3	1,4-Dioxane	100 °C	0.2	0.2	air	25 %
4	1,4-Dioxane	75 °C	0.2	0.2	air	19 %
5	1,4-Dioxane	55 °C	0.2	0.2	air	21 %
6	1,4-Dioxane	55 °C	1.0	0.2	air	20 %
7	1,4-Dioxane	55 °C	1.0	1.0	air	30 %
8	1,4-Dioxane	55 °C	none	0.2	air	< 1 %

Attempts to reduce 4-haloanisole substrates with the imidazolium iodide 461 catalyst

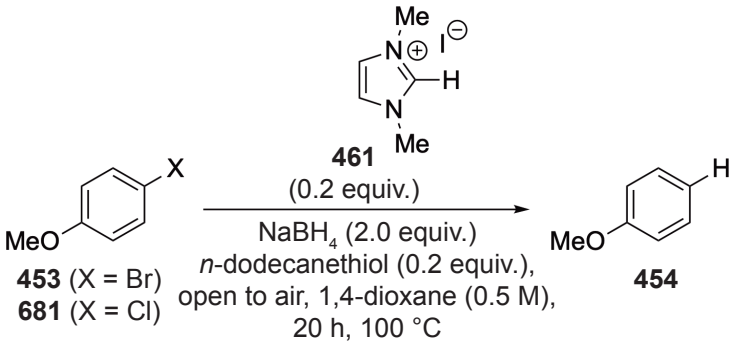

		Yield of 454[a]
453	X = Br	30 %
462	X = Cl	< 1 %

[a] The yield was measured by GC-FID vs 1,3,5-trimethoxybenezene

The reaction vessel was charged with 1,3-dimethyl-1*H*-imidazol-3-ium iodide **461** (26.9 mg, 120 µmol, 0.2 equiv.). Then 1,4-dioxane (1.2 mL) was added followed by 1-bromo-4-methoxybenzene **453** (75.9 µL, 0.600 mmol, 1.0 equiv.) or 1-chloro-4-methoxybenzene (75.0 µL, 0.600 mmol, 1.0 equiv.) as required, a precisely measured amount of internal standard

1,3,5-trimethoxybenezene (ca. 50.5 mg, 0.300 mmol, 0.5 equiv.) and *n*-dodecanethiol. Finally $NaBH_4$ (45.4 mg, 1.20 mmol, 2.0 equiv.) was added. The reaction was heated to 100 °C for 20 h. The reaction was left open to air for the whole reaction time. An aliquot (50 µL) was taken from the reaction and diluted in ethyl acetate (3 mL). The solution was filtered over silica and analysed by GC-FID.

Attempts to use the pyridinium salt 463 as an organocatalyst

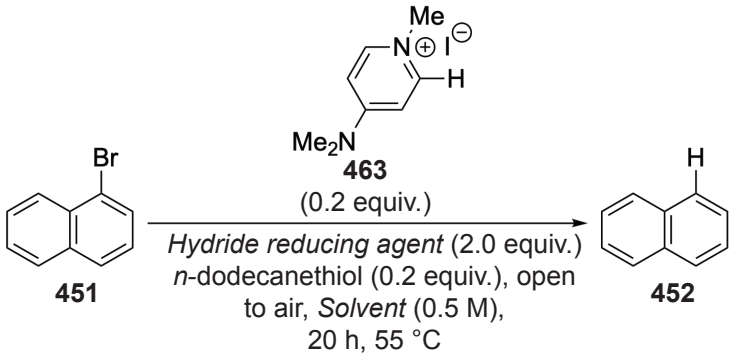

The possibility to use **463** as a catalyst for the reductive debromination reaction of 1-bromonaphthalene **451** was investigated. The results are summarised in Table S17.

Conditions for Entries 1 - 3

The reaction vessel was charged with 4-(dimethylamino)-1-methylpyridin-1-ium iodide **463** (31.7 mg, 120 µmol, 0.2 equiv.). Then the solvent (1.2 mL) was added as required followed by 1-bromonaphthalene **451** (86.5 µL, 0.600 mmol, 1.0 equiv.), a precisely measured amount of internal standard 1,3,5-trimethoxybenezene (ca. 50.5 mg, 0.300 mmol, 0.5 equiv.) and *n*-dodecanethiol. Finally $NaBH_4$ (45.4 mg, 1.20 mmol, 2.0 equiv.) or $LiAlH_4$ (45.5 mg, 1.20 mmol, 2.0 equiv.) was added as required. The reaction was heated to the specified temperature for 20 h. The reaction was left open to air for the whole reaction time as required. An aliquot (50 µL) was taken from the reaction and diluted in ethyl acetate (3 mL). The solution was filtered over silica and analysed by GC-FID.

Table S17 - Reactions the pyridinium iodide **463** with 1-bromonaphthalene **451**.

Entry	Solvent	Hydride reducing agent	Yield of 452
1	DMF	$NaBH_4$	2 %
2	1,4-Dioxane	$LiAlH_4$	63 %
3[a]	1,4-Dioxane	$LiAlH_4$	29 %

[a] Blank reaction without catalyst **463**.

5.3.16 Substrate Synthesis for Reactions in Chapter 5.3.15

1,3-Dimethylimidazolidine 459

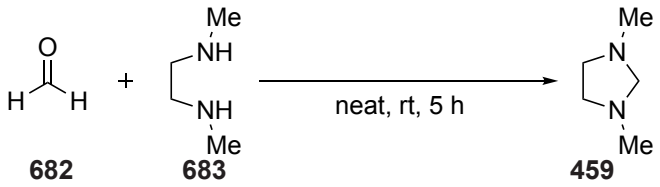

682 **683** **459**

The reaction was kept under argon, no special precaution was taken to exclude humidity. The reaction vessel was charged with *N*[1],*N*[2]-dimethylethane-1,2-diamine (978 µL, 9.00 mmol, 1.0 equiv.). Then polymeric formaldehyde (270 mg, 9.00 mmol, 1.0 equiv.) was added in small portions. The reaction was stirred for 5 h at room temperature until all formaldehyde was dissolved and the reaction was a pale green and clear solution. The reaction was diluted with diethyl ether (0.9 mL), filtered over $MgSO_4$ and NaOH (powder) and carefully concentrated in vacuo (r.t. 200 mbar, 20 min, the product is volatile) to give 1,3-dimethylimidazolidine **459** (0.473 g, 4.33 mmol, 48 %) as a colourless oil. **^{1}H-NMR** (400 MHz, Benzene-d_6) δ 3.21 (s, 2H), 2.57 (s, 4H), 2.22 (s, 6H). **^{13}C-NMR** (101 MHz, Benzene-d_6) δ 80.6, 55.2, 41.8. **MS(ESI+)** [*m/z*] = 101 (M+H). The NMR spectra are in agreement with the reported data.[286]

1,3-Dimethyl-1H-imidazol-3-ium iodide 461

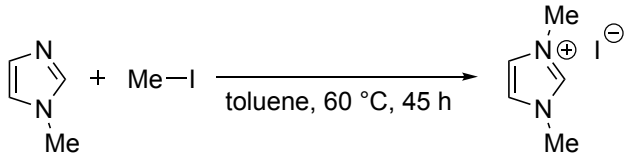

684 **685** **461**

To the solution of 1-methyl-1*H*-imidazole **684** (4.78 mL, 60.0 mmol, 1.0 equiv.) in toluene (200 mL) was added iodomethane (3.74 mL, 60.0 mmol, 1.0 equiv.) . The reaction was heated to 60 °C for 45 h. The reaction was cooled in a water-ice/acetone cooling bath (ca. -15 °C) for 15 min. Then the solvent was carefully decanted and the white solid was washed with diethyl ether (3x, ca. 5 mL) and dried in vacuo (60 °C, 5 h). The product 1,3-dimethyl-1*H*-imidazol-3-ium iodide **461** (13.0 g, 58.0 mmol, 97 %) was obtained as an off-white solid. **^{1}H-NMR** (400 MHz, deuterium oxide) δ 8.76 (s, 1H), 7.52 (d, *J* = 1.9 Hz, 2H), 3.99 (s, 6H). **^{13}C-NMR** (101 MHz, deuterium oxide) δ 136.17, 123.03, 35.55. **^{1}H-NMR** (400 MHz, Chloroform-*d*) δ 10.02 (s, 1H), 7.41 (d, *J* = 1.7 Hz, 2H), 4.10 (s, 6H). **^{13}C-NMR** (101 MHz, Chloroform-*d*)) δ 137.81, 123.52, 37.24. **MS(ESI+)** [*m/z*] = 97 (M-I), 320 (2M-I). **mp** = 85 °C - 86 °C (lit. mp = 84 °C - 86 °C).[287] The NMR spectra are in agreement with the reported data.[288,289]

4-(Dimethylamino)-1-methylpyridin-1-ium iodide 463

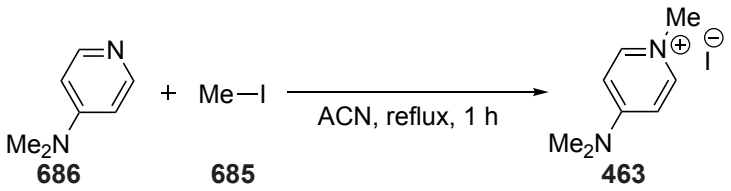

686 **685** **463**

The reaction vessel was charged with *N*,*N*-dimethylpyridin-4-amine **686** (1.22 g, 10.0 mmol, 1.0 equiv.). The material was fully dissolved in acetonitrile (12 mL) before the addition of iodomethane **685** (1.25 mL, 20.0 mmol, 2.0 equiv.). The reaction was stirred at room temperature for 5 min before it was refluxed at 65 °C - 75 °C for 1 h. During the course of the reaction a white precipitate formed. This precipitate was filtered and washed with a small amount of cold acetonitrile (3 x ca. 1 mL). The material was dried in high vacuum (3 mbar) at 100 °C for 14 h to give 4-(dimethylamino)-1-methylpyridin-1-ium iodide **463** (1.71 g, 6.49 mmol, 65 %) as a white solid. The filtrate was concentrated in vacuo and recrystallised from boiling acetonitrile (7 mL). The crystals were filtered and washed with a small amount of acetonitrile (2 x ca. 0.5 mL) to give additional 4-(dimethylamino)-1-methylpyridin-1-ium iodide **463** (301 mg, 1.14 mmol, 11 %) as a white solid. In total 4-(dimethylamino)-1-methylpyridin-1-ium iodide **463 (**2.02 g, 7.63 mmol, 76 %) was obtained. **^{1}H-NMR** (400 MHz, DMSO-d_6) δ 8.26 – 8.20 (m, 2H), 7.05 – 6.99 (m, 2H), 3.92 (s, 3H), 3.18 (s, 6H). **^{13}C-NMR** (101 MHz, DMSO-d_6) δ 155.6, 142.7, 107.4, 44.0, 39.7. **MS(ESI+)** [*m/z*] = 137 (M-I), 401 (2M-I). **mp** = 237 °C (lit. mp = 240 °C - 241 °C).[290] The NMR spectra are in agreement with the reported data.[82]

5.4. Experimental Details for Chapter 3 “The KO*t*Bu-Et$_3$SiH Reagent System”

5.4.1 General Experimental Procedures

General Procedure A - Aryl Ether Cleavage

A pressure tube was charged with the substrate (0.500 mmol, 1.0 equiv.). Then the pressure tube was brought inside the glovebox and triethylsilane (0.240 mL, 1.50 mmol, 3.0 equiv.) and potassium *tert*-butoxide (168 mg, 1.50 mmol, 3.0 equiv.) were added in this sequence. The pressure tube was sealed and the reaction was heated to 130 °C for 18 h. The reaction was quenched by the careful addition of water and partitioned between water (10 mL) and dichloromethane (15 mL). The aqueous phase was acidified with aqueous HCl to pH < 3. The phases were separated and the aqueous phase was extracted with dichloromethane (3 x 15 mL). As required, a precisely measured amount of internal standard 1,3,5-trimethoxybenzene (ca. 25.2 mg, 0.150 mmol, 0.3 equiv.) was added to the organic phase. The combined organic phases were dried over $MgSO_4$ and carefully concentrated in vacuo (45 °C, > 150 mbar, < 15 min) and analysed by ^{1}H-NMR. The reaction products were purified by flash column chromatography, preparative thin-layer chromatography or re-crystallisation as specified.

General Procedure B - Arene Reduction

The reaction vessel was charged with the arene substrate (0.5 mmol, 1.0 equiv.). The reaction vessel was then brought inside the glovebox and triethylsilane (2.40 mL, 15.0 mmol, 30 equiv.) and potassium *tert*-butoxide (1.68 g, 15.0 mmol, 30.0 equiv.) were added in this sequence. The pressure tube was sealed and the reaction was heated to 130 °C for 18 h. The reaction was carefully quenched by the addition of water or deuterium oxide as required until all solid material was dissolved and no more gas evolved. The crude reaction product was partitioned between water (20 mL) and dichloromethane (20 mL). The phases were separated and the aqueous phase was extracted with dichloromethane (3 x 15 mL). The combined organic phases were washed with water (20 mL), dried over $MgSO_4$ and carefully concentrated in vacuo (45 °C, >100 mbar, < 15 min). The reaction products were purified by flash column chromatography, preparative thin-layer chromatography or re-crystallisation as specified.

5.4.2 Reductive Cleavage of Aryl Ethers

(Corresponds to Chapter 3.2.1. The synthesis of the substrates used in this section is described in Chapter 5.4.3).

Reaction of 1-(Benzyloxy)-3,5-dimethylbenzene 469

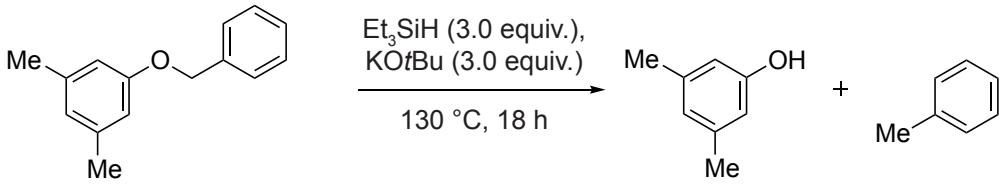

469 **470** **471**

The substrate **469** (106 mg, 0.500 mmol, 1.0 equiv.) was reacted according to the General Procedure A. After the work-up, the internal standard 1,3,5-trimethoxybenzene (ca. 25.2 mg, 0.150 mmol, 0.3 equiv.) was added. The crude reaction product was analysed by ^{1}H-NMR. The signals of the identified products were compared to the signals of a corresponding authentic sample. It was found that **469** (9 %) remained unreacted while **470** (6 %) and **471** (16 %) were formed.

Reaction of 1-((4-Methoxybenzyl)oxy)-3,5-dimethylbenzene 472

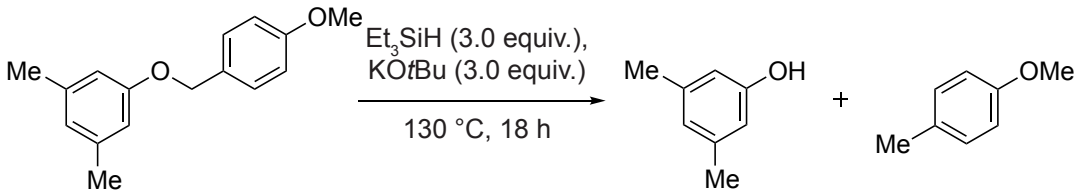

472 **470** **473**

The substrate **472** (121 mg, 0.500 mmol, 1.0 equiv.) was reacted according to the General Procedure A. After the work-up, the internal standard 1,3,5-trimethoxybenzene (ca. 25.2mg, 0.150 mmol, 0.3 equiv.) was added. The crude reaction product was analysed by ^{1}H-NMR. The signals of the identified products were compared to the signals of a corresponding authentic sample. It was found that **472** was fully converted and **470** (5 %) and **473** (12 %) were formed.

Reaction of 2,2'-Oxydinaphthalene 474

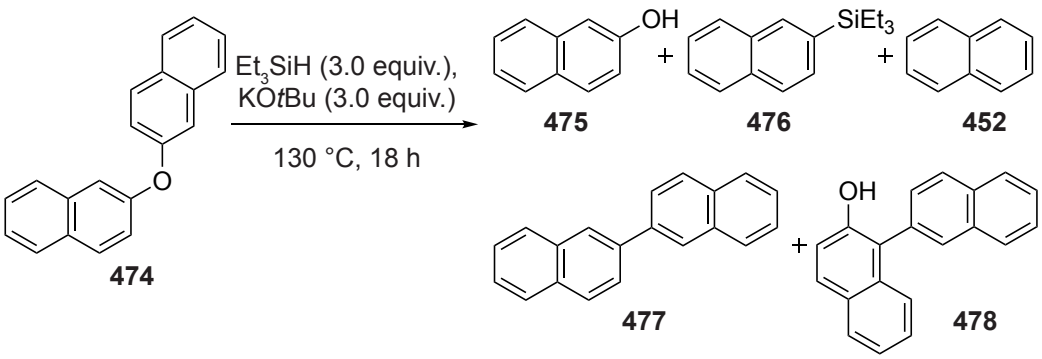

The substrate **474** (137 mg, 0.500 mmol, 1.0 equiv.) was reacted according to the General Procedure A. After the work-up, the internal standard 1,3,5-trimethoxybenzene (ca. 25.2 mg, 0.150 mmol, 0.3 equiv.) was added. The crude reaction product was analysed by ^{1}H-NMR. The signals of the identified products were compared to the signals of a corresponding authentic sample. It was found that **474** was fully converted and **475** (71 %) and **452** (39 %) were formed. Purification by flash column chromatography (ethyl acetate in hexane, gradient from 0 % to 10 %) gave the products naphthalen-2-ol **475** (41.4 mg, 0.235 mmol, 47 %) as a white solid and triethyl(naphthalen-2-yl)silane **476** (7.7 mg, 0.032 mmol, 6 %) as a colourless oil. Additionally, a mixture of compounds was obtained that was further purified by preparative TLC (5 % ethyl acetate in hexane). The two compounds 2,2'-binaphthalene **477** (1.4 mg, 5.5 µmol, 1 %) and [1,2'-binaphthalen]-2-ol **478** (6.4 mg, 0.024 mmol, 5 %) were obtained in pure form as white solids.

Naphthalen-2-ol **475**: **^{1}H-NMR** (600 MHz, Chloroform-d) δ 7.77 (dd, *J* = 9.3, 9.3 Hz, 2H), 7.69 (d, *J* = 8.3 Hz, 1H), 7.44 (dd, *J* = 7.8, 7.8 Hz, 1H), 7.34 (dd, *J* = 7.6, 7.6 Hz, 1H), 7.16 (d, *J* = 3.2 Hz, 1H), 7.11 (dd, *J* = 8.7, 2.7 Hz, 1H), 4.97 (br s, 1H). **^{13}C-NMR** (151 MHz, Chloroform-*d*) δ 153.4, 134.7, 130.0, 129.1, 127.9, 126.7, 126.5, 123.8, 117.9, 109.6. **GC-MS** [*m/z* (%)] (11.956 min): 144 (100, M^{+}), 115 (95), 89 (15), 87 (5), 75 (5). **mp** = 119 °C (lit. mp = 118 °C - 120 °C).[291] The NMR spectra are in agreement with the previously reported data.[292]

Triethyl(naphthalen-2-yl)silane **476**: **^{1}H-NMR** (400 MHz, Chloroform-*d*) δ 7.99 (d, *J* = 1.0 Hz, 1H), 7.88 – 7.79 (m, 3H), 7.58 (dd, *J* = 8.1, 1.2 Hz, 1H), 7.52 – 7.45 (m, 2H), 1.05 – 0.97 (m, 9H), 0.93 – 0.85 (m, 6H). **^{13}C-NMR** (101 MHz, Chloroform-*d*) δ 135.2, 134.9, 133.8, 133.1, 130.7, 128.2, 127.8, 126.9, 126.3, 125.9, 7.6, 3.6. **GC-MS** [*m/z* (%)] (13.999 min): 242 (35), 213 (80), 185 (90), 157 (100), 155 (30), 131 (10), 92 (5), 79 (10). The NMR spectra are in agreement with the previously reported data.[293]

2,2'-Binaphthalene **477**: **^{1}H-NMR** (400 MHz, Chloroform-*d*) δ 8.21 – 8.15 (m, 2H), 8.00 – 7.92 (m, 4H), 7.89 (dd, *J* = 8.5, 1.8 Hz, 4H), 7.57 – 7.47 (m, 4H). **^{13}C-NMR** (101 MHz, Chloroform-*d*) δ 138.6, 133.9, 132.8, 128.7, 128.4, 127.8, 126.5, 126.3, 126.2, 125.9. **GC-MS** [*m/z* (%)] (17.514 min): 254 (100), (252 (50), 250 (15), 126 (25). **mp** = 190 °C (lit. mp = 188 °C).[294] The NMR spectra are in agreement with the previously reported data.[295]

[1,2'-Binaphthalen]-2-ol **478**: **^{1}H-NMR** (400 MHz, Chloroform-*d*) δ 8.07 (ddd, *J* = 8.6, 0.7, 0.7 Hz, 1H), 8.00 – 7.96 (m, 1H), 7.96 – 7.94 (m, 1H), 7.93 – 7.89 (m, 1H), 7.87 – 7.82 (m, 2H), 7.64 – 7.56 (m, 2H), 7.52 (dd, *J* = 8.3, 1.7 Hz, 1H), 7.47 – 7.40 (m, 1H), 7.38 – 7.29 (m, 3H), 5.24 (s, 1H). **^{13}C-NMR** (151 MHz, Chloroform-*d*) δ 150.5, 134.0, 133.5, 133.3, 131.8, 130.3, 129.8, 129.6, 129.1, 129.0, 128.2, 128.2, 128.1, 126.9, 126.9, 126.7, 124.8, 123.5, 121.0,

117.5. **IR** ν_{max} [cm^{-1}]: 3515, 3053, 2940, 2915, 1686, 1677, 1656, 1619, 1598, 1509, 1502, 1376, 1271, 1214, 1169, 1147, 907, 861, 820, 749, 734. **GC-MS** [*m/z* (%)] (17.497 min): 270 (100 M^+), 269 (55), 268 (15), 253 (20), 252 (15), 251 (10), 250 (10), 241 (10), 240 (15), 239 (50), 237 (10), 226 (5), 215 (10), 213 (5), 135 (10), 134 (10), 126 (20), 119 (20), 113 (15). **HRMS** (ESI–) [*m/z*] calcd. for $C_{20}H_{13}O$ ($M\text{-}H^-$): 269.0961, found: 269.0953. **mp** = 132 °C.

A blank reaction was performed in the absence of triethylsilane. The substrate **474** was recovered quantitatively from this reaction.

Reaction of 1-((Naphthalen-2-yloxy)methyl)naphthalene 479

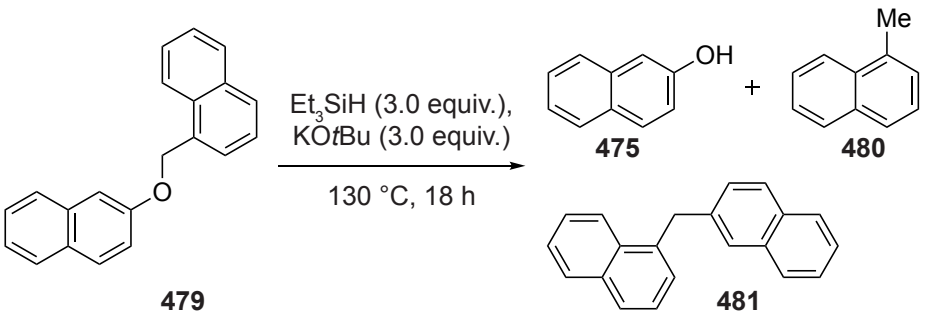

479

The substrate **479** (150 mg, 0.500 mmol, 1.0 equiv.) was reacted according to the General Procedure A. After the work-up, the internal standard 1,3,5-trimethoxybenzene (ca. 25.2 mg, 0.150 mmol, 0.3 equiv.) was added. The crude reaction product was analysed by ^{1}H-NMR. The signals of the identified products were compared to the signals of a corresponding authentic sample. It was found that **479** was fully converted and **475** (56 %) and **480** (34 %) were formed. Purification by flash column chromatography (ethyl acetate in hexane, gradient from 0 % to 10 %) gave the products 1-methylnaphthalene, naphthalene-2-ol and 1-(naphthalen-2-ylmethyl)naphthalene in impure form.

The major impurity in the mixed fractions of 1-methylnaphthalene was found to be *tert*-butoxy triethylsilane **296**. The combined fractions were concentrated in vacuo and redissolved in THF (3 mL). The mixture was then treated with HCl (3 mL, conc. aq). The mixture was left open to air via a needle and stirred at room temperature for 2 days. The reaction was diluted with water (20 mL) and extracted with diethyl ether (4 x 15 mL). The combined organic phases were washed with brine, dried over $MgSO_4$ and concentrated in vacuo. Purification by flash column chromatography (hexane) gave the product 1-methylnaphthalene **480** (15 mg, 0.107 mmol, 21 %) as a colourless oil. **^{1}H-NMR** (600 MHz, Chloroform-*d*) δ 8.02 (d, *J* = 8.3 Hz, 1H), 7.86 (d, *J* = 7.8 Hz, 1H), 7.72 (d, *J* = 8.1 Hz, 1H), 7.54 (ddd, *J* = 8.5, 6.8, 1.6 Hz, 1H), 7.52 – 7.48 (m, 1H), 7.41 – 7.36 (m, 1H), 7.34 (d, *J* = 7.0 Hz, 1H), 2.72 (s, 3H). **^{13}C-NMR** (101 MHz, Chloroform-*d*) δ 134.4, 133.7, 132.7, 128.7, 126.7, 126.5, 125.8, 125.7, 125.7, 124.2, 19.5. GC-MS [*m/z* (%)] (10.778 min): 142 (100, M^+), 141 (75), 139 (10), 115 (40) 63 (5). The NMR spectra are identical to the NMR spectra of a commercial sample.

The mixed fractions of naphthalene-2-ol were combined, concentrated in vacuo and redissolved in hexane/diethyl ether (20 mL, 1:1). The solution was washed with aqueous sodium hydroxide (1 M, 6 x 10 mL). The combined aqueous phases were acidified by the addition of aqueous hydrochloric acid (4 M, 20 mL) and extracted with diethyl ether (4 x 30 mL). The combined organic phases were washed with brine, dried over $MgSO_4$ and concentrated in vacuo to

give pure naphthalen-2-ol **475** (37 mg, 0.234 mmol, 47 %) as a white solid. The NMR spectra were identical to the spectra obtained for the previously isolated material.

The mixed fractions of 1-(naphthalen-2-ylmethyl)naphthalene were combined and concentrated in vacuo. Purification by flash column chromatography (toluene in hexane, gradient from 0 % to 20 %) gave 1-(naphthalen-2-ylmethyl)naphthalene **481** (18 mg, 0.066 mmol, 13 %) as a white solid. **^{1}H-NMR** (600 MHz, Chloroform-*d*) δ 7.96 (d, *J* = 8.2 Hz, 1H), 7.79 (d, *J* = 8.1 Hz, 1H), 7.70 (d, *J* = 8.2 Hz, 2H), 7.68 – 7.65 (m, 1H), 7.62 (d, *J* = 7.3 Hz, 1H), 7.52 (s, 1H), 7.40 – 7.31 (m, 5H), 7.28 (d, *J* = 8.6 Hz, 1H), 7.25 (d, *J* = 7.2 Hz, 1H), 4.53 (s, 2H). **^{13}C-NMR** (151 MHz, Chloroform-*d*) δ 138.3, 136.6, 134.1, 133.8, 132.3, 132.3, 128.8, 128.2, 127.7, 127.7, 127.6, 127.6, 127.4, 127.2, 126.2, 126.1, 125.7, 125.7, 125.5, 124.4, 76.9. **GC-MS** [*m/z* (%)] (17.559 min): 268 (100), 267 (70), 265 (30), 263 (10), 253 (30), 252 (30), 239 (5), 141 (10), 139 (10), 133 (5), 127 (5), 126 (10), 115 (15). **mp** = 105 °C (lit. mp = 89 °C - 91 °C).[296] The NMR spectra are in agreement with the previously reported data.[297]

A blank reaction was performed in the absence of triethylsilane. The substrate **479** was recovered quantitatively from this reaction. An additional blank reaction was performed in the absence of potassium *tert*-butoxide. The substrate **479** (133 mg, 0.467 mmol, 94 %) was recovered from this reaction.

Reaction of 2-(3-Phenylpropoxy)naphthalene 482

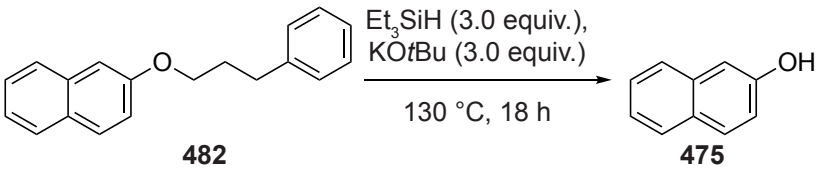

482 **475**

The substrate **482** (131 mg, 0.500 mmol, 1.0 equiv.) was reacted according to the General Procedure A. The crude reaction product was analysed by ^{1}H-NMR. It was found that **482** was fully converted. Purification by flash column chromatography (ethyl acetate in hexane, gradient from 0 % to 10 %) gave the products naphthalene-2-ol (30.7 mg, 0.209 mmol, 42 %) as a white solid. The NMR spectra were identical to the previously recorded spectra.

A blank reaction was performed in the absence of triethylsilane. The substrate **482** was recovered quantitatively from this reaction.

Reaction of 2-(((1*S*,2*R*,5*R*)-2-Isopropyl-5-methylcyclohexyl)oxy)naphthalene 488

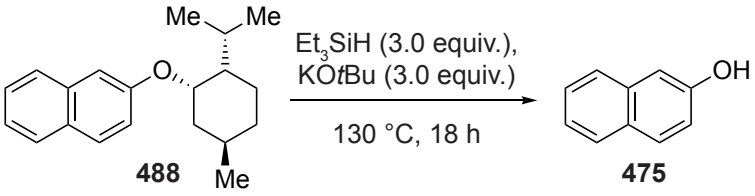

488 **475**

The substrate **488** was reacted according to the General Procedure A on a slightly lower scale. A pressure tube was charged with 2-(((1S,2S,5R)-2-isopropyl-5-methylcyclohexyl)oxy) naphthalene **488** (113 mg, 0.400 mmol, 1.0 equiv.). Then the pressure tube was brought inside the glovebox and triethylsilane (0.192 mL, 1.20 mmol, 3.0 equiv.) and potassium *tert*-butoxide (135 mg, 1.20 mmol, 3.0 equiv.) were added in this sequence. The pressure tube was sealed

and the reaction was heated to 130 °C for 18 h. The reaction was quenched by the careful addition of water and partitioned between water (10 mL) and dichloromethane (15 mL). The aqueous phase was acidified with aqueous HCl to pH < 3. The phases were separated and the aqueous phase was extracted with dichloromethane (3 x 15 mL). The combined organic phases were dried over $MgSO_4$ and carefully concentrated in vacuo (45 °C, > 150 mbar, < 15 min) and analysed by ^{1}H-NMR. Purification by flash column chromatography (ethyl acetate in hexane, gradient from 0 % to 20 %) gave the product naphthalene-2-ol **475** (38.1 mg, 0.264 mmol, 66% yield) as a white solid. The NMR spectra were identical to the spectra obtained for the previously isolated material.

A blank reaction was performed in the absence of triethylsilane. The substrate **488** was recovered quantitatively from this reaction.

Reaction of (((1*R*,2*R*,5*R*)-2-Isopropyl-5-methylcyclohexyl)oxy)benzene 489

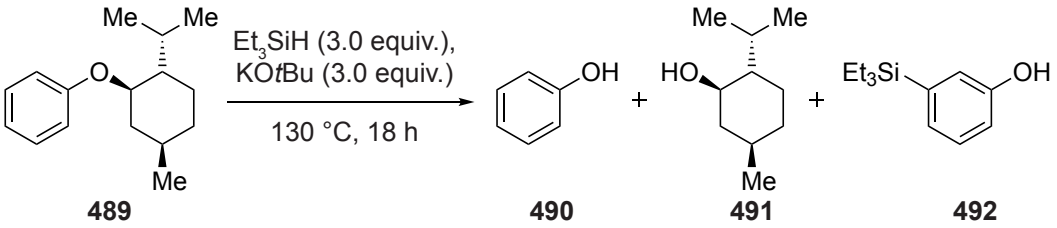

489 **490** **491** **492**

The substrate **489** was reacted according to the General Procedure A on a slightly lower scale. A pressure tube was charged with (((1*R*,2*R*,5*R*)-2-isopropyl-5-methylcyclohexyl)oxy) benzene **489** (105 mg, 0.450 mmol, 1.0 equiv.). Then the pressure tube was brought inside the glovebox and triethylsilane (0.216 mL, 1.35 mmol, 3.0 equiv.) and potassium *tert*-butoxide (151 mg, 1.35 mmol, 3.0 equiv.) were added in this sequence. The pressure tube was sealed and the reaction was heated to 130 °C for 18 h. The reaction was quenched by the careful addition of water and partitioned between water (10 mL) and dichloromethane (15 mL). The aqueous phase was acidified with aqueous HCl to pH < 3. The phases were separated and the aqueous phase was extracted with dichloromethane (3 x 15 mL). The combined organic phases were dried over $MgSO_4$ and carefully concentrated in vacuo (45 °C, > 150 mbar, < 15 min) and analysed by ^{1}H-NMR. Purification by flash column chromatography (ethyl acetate in hexane, gradient from 0 % to 10 %) gave the products phenol **490** (trace amounts), (1*S*,2*S*,5*R*)-2-isopropyl-5-methylcyclohexan-1-ol **491** (9.0 mg, 0.048 mmol, 11 %) as a white solid, 3-(triethylsilyl)phenol **492** (3.3 mg, 0.016 mmol, 4 %) as a colourless oil and recovered starting material (((1*R*,2*R*,5*R*)-2-isopropyl-5-methylcyclohexyl)oxy)benzene **489** (51.7 mg, 0.223 mmol, 50 %) as a white solid.

A blank reaction was performed in the absence of triethylsilane. The substrate **489** was recovered quantitatively from this reaction.

(1*S*,2*S*,5*R*)-2-Isopropyl-5-methylcyclohexan-1-ol **491**: **^{1}H-NMR** (400 MHz, Chloroform-*d*) δ 3.46 – 3.36 (m, 1H), 2.16 (hd, *J* = 7.0, 2.8 Hz, 1H), 1.96 (dddd, *J* = 11.9, 4.2, 3.4, 2.0 Hz, 1H), 1.71 – 1.56 (m, 1H), 1.50 – 1.34 (m, 2H), 1.25 (s, 1H), 1.15 – 1.06 (m, 1H), 1.04 – 0.77 (m, 12H). **^{13}C-NMR** (101 MHz, Chloroform-*d*) δ 71.7, 50.3, 45.2, 34.7, 31.8, 26.0, 23.3, 22.4, 21.2, 16.3. **GC-MS** [*m/z* (%)] (9.449 min): 156 (0.05, M+), 155 (0.3), 154 (0.05), 138 (25), 123 (45), 110 (10), 109 (15), 96 (35), 95 (90), 83 (15), 82 (45), 82 (100), 80 (15), 77 (5), 71 (100), 70 (15) 69 (40), 68 (15), 67 (45), 65 (5), 57 (40), 56 (20), 55 (60), 54 (10), 53 (15). The NMR spectra

are in agreement with the previously reported data.[298]

3-(Triethylsilyl)phenol **492**: **^{1}H-NMR** (400 MHz, Chloroform-*d*) δ 7.26 – 7.20 (m, 1H), 7.05 (ddd, *J* = 7.3, 1.0 Hz, 1H), 6.94 (dd, *J* = 2.8, 0.9 Hz, 1H), 6.81 (ddd, *J* = 8.0, 2.7, 1.0 Hz, 1H), 4.60 (s, 1H), 1.00 – 0.93 (m, 9H), 0.81 – 0.74 (m, 6H). **^{13}C-NMR** (101 MHz, Chloroform-*d*) δ 155.0, 139.8, 129.2, 126.8, 120.8, 115.8, 7.5, 3.5. **GC-MS** [*m/z* (%)] (12.375 min): 208 (20), 179 (70), 151 (100), 123 (90), 121(10), 78 (10), 77 (15). The NMR spectra are in agreement with the previously reported data.[299]

Reaction of (1*R*,2*R*,4*R*)-2-(Cyclohexylmethoxy)-1-isopropyl-4-methylcyclohexane 493

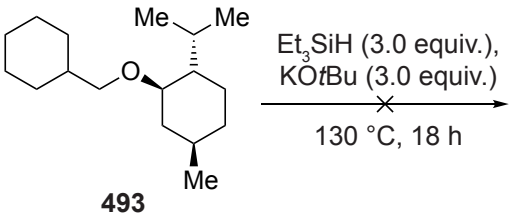

493

The substrate **493** was reacted according to the General Procedure A on a slightly lower scale. A pressure tube was charged with (1*R*,2*R*,4*R*)-2-(cyclohexylmethoxy)-1-isopropyl-4-methylcyclohexane **493** (63 mg, 0.25 mmol, 1.0 equiv.). Then the pressure tube was brought inside the glovebox and triethylsilane (0.12 mL, 0.75 mmol, 3.0 equiv.) and potassium *tert*-butoxide (84 mg, 0.75 mmol, 3.0 equiv.) were added in this sequence. The pressure tube was sealed and the reaction was heated to 130 °C for 18 h. The reaction was quenched by the careful addition of water and partitioned between water (10 mL) and dichloromethane (15 mL). The aqueous phase was acidified with aqueous HCl to pH < 3. The phases were separated and the aqueous phase was extracted with dichloromethane (3 x 15 mL). The combined organic phases were dried over $MgSO_4$ and concentrated in vacuo (45 °C, > 20 mbar, < 15 min) to give back the starting material (1*R*,2*R*,4*R*)-2-(cyclohexylmethoxy)-1-isopropyl-4-methylcyclohexane **493** quantitatively in pure form.

5.4.3 Substrate Synthesis for the Reactions of Chapter 5.4.2

1-(Benzyloxy)-3,5-dimethylbenzene 469

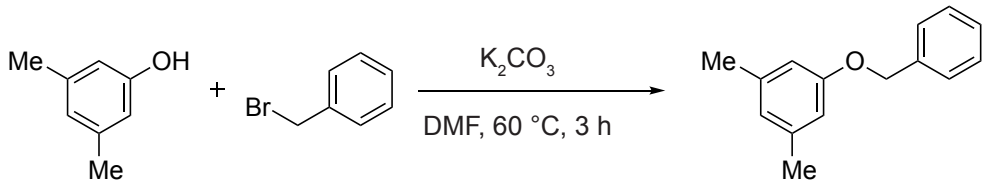

470 **687** **469**

To a solution of 3,5-dimethylphenol **470** (611 mg, 5.00 mmol, 1.0 equiv.) in DMF (9.3 mL) was added potassium carbonate (819 mg, 5.93 mmol, 1.2 equiv.) followed by (bromomethyl) benzene **687** (617 µL, 5.19 mmol, 1.0 equiv.) and the resulting suspension was heated to 60°C for 3 h {15:20 - 18:20}. The reaction was monitored by TLC and was found to have reached a high degree of conversion after 2 h 20 min. The reaction was diluted with diethyl ether (30 mL). The organic phase was washed with water (3 x 30 mL) and brine (1 x 30 mL), dried over

$MgSO_4$ and concentrated in vacuo. Purification by flash column chromatography (ethyl acetate in hexane, gradient from 0 % to 5 %) gave the product 1-(benzyloxy)-3,5-dimethylbenzene **469** (846 mg, 3.99 mmol, 80 %) as a colourless oil. **^{1}H-NMR** (400 MHz, Chloroform-*d*) δ 7.46 – 7.42 (m, 2H), 7.39 (ddd, *J* = 7.9, 6.8, 1.0 Hz, 2H), 7.36 – 7.29 (m, 1H), 6.65 – 6.61 (m, 3H), 5.04 (s, 2H), 2.30 (s, 6H). **^{13}C-NMR** (101 MHz, Chloroform-*d*) δ 159.1, 139.4, 137.5, 128.7, 128.0, 127.6, 122.9, 112.7, 70.0, 21.6. **GC-MS** [*m/z* (%)] (13.544 min): 212 (50, M+), 197 (5), 91 (100), 77 (10), 65 (20). The NMR spectra are in agreement with the previously reported data.[300]

1-((4-Methoxybenzyl)oxy)-3,5-dimethylbenzene 472

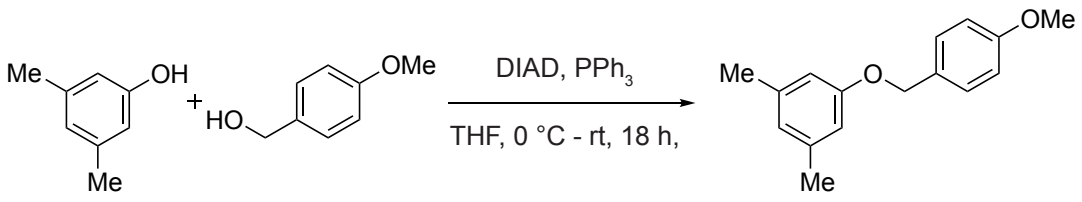

470 **688** **472**

The reaction was kept under a positive pressure of argon. The reaction vessel was charged with triphenylphosphine (1.18 g, 4.50 mmol, 1.5 equiv.) and 3,5-dimethylphenol **470** (367 mg, 3.00 mmol, 1.0 equiv.) which were then dissolved in THF (10 mL). Then (4-methoxyphenyl) methanol **688** (0.42 mL, 3.30 mmol, 1.1 equiv.) was added and the solution was cooled to ice-bath temperature and diisopropyl azodicarboxylate (DIAD) 0.93 mL, 4.50 mmol, 1.5 equiv.) was added dropwise over 20 min. The reaction was stirred at ice bath temperature for 2 h; then the cooing bath was removed and the reaction was allowed to warm up to room temperature over 18 h. Then the reaction was concentrated in vacuo in the presence of silica. Purification by flash column chromatography (33% toluene in hexane) gave the product 1-((4-methoxybenzyl)oxy)-3,5-dimethylbenzene **472** (327 mg, 1.35 mmol, 45 %) as a colourless oil, which crystallised to a white solid after ca. two weeks of storage on the bench. **^{1}H-NMR** (400 MHz, Chloroform-*d*) δ 7.39 – 7.32 (m, 2H), 6.97 – 6.88 (m, 2H), 6.64 – 6.59 (m, 3H), 4.96 (s, 2H), 3.83 (s, 3H), 2.30 (d, *J* = 0.7 Hz, 6H). **^{13}C-NMR** (101 MHz, Chloroform-*d*) δ 159.5, 159.1, 139.3, 129.5, 129.3, 122.8, 114.1, 112.7, 69.8, 55.4, 21.6. **IR** ν_{max} [cm^{-1}]: 3035, 2996, 2949, 2914, 2864, 2834, 1612, 1592, 1514, 1463, 1443, 1376, 1322, 1294, 1246, 1168, 1151, 1112, 1058, 1034, 993, 956, 825, 771, 690. **GC-MS** [*m/z* (%)] (14.882 min): 242 (4, M+), 121 (100), 91 (10), 77 (12). **HRMS** (ESI+) [*m/z*]: calcd. for $C_{16}H_{19}O_2$ (M+H): 243.1380, found: 243.1382. **mp** = 50 °C - 51 °C.

2,2'-Oxydinaphthalene 474

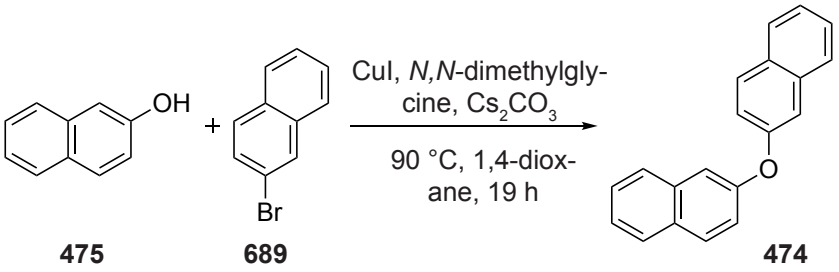

475 **689** **474**

The reaction was kept under a positive pressure of argon. The reaction vessel was charged with 2-bromonaphthalene (1.04 g, 5.00 mmol, 1.0 equiv.), naphthalen-2-ol (1.08 g, 7.50 mmol, 1.5 equiv.) , Cs_2CO_3 (3.26 g, 10.0 mmol, 2.0 equiv.) , copper(I) iodide (95.2 mg, 0.500 mmol, 0.1 equiv.), dimethylglycine (155 mg, 1.50 mmol, 0.3 equiv.) and 1,4-dioxane (12.5 mL) in this sequence. The reaction was heated to 90 °C for 19 h and was monitored by TLC. The reaction was found to have reached a high degree of conversion after that time. **^{1}H-NMR** (400 MHz, Chloroform-*d*) δ 7.91 – 7.82 (m, 4H), 7.75 – 7.69 (m, 2H), 7.51 – 7.40 (m, 4H), 7.39 (d, *J* = 2.4 Hz, 2H), 7.34 (dd, *J* = 8.9, 2.4 Hz, 2H). **^{13}C-NMR** (101 MHz, Chloroform-*d*) δ 155.2, 134.5, 130.4, 130.1, 127.9, 127.3, 126.7, 124.9, 120.3, 114.6. **GC-MS** [*m/z* (%)] (17.541 min): 270 (100), 241 (55), 215 (10), 135 (5), 127 (15), 115 (20). **IR** ν_{max} [cm^{-1}]: 3052, 3027, 2951, 2918, 2849, 1627, 1594, 1579, 1504, 1467, 1441, 1348, 1264, 1251, 1227, 1175, 1140, 1127, 1112, 1017, 959, 879, 851, 822, 807, 738, 718. **HRMS** (ESI+) [*m/z*]: calcd. for $C_{20}H_{15}O$ (M+H) 271.1123, found: 271.1123. **mp** = 101 °C - 103 °C

1-((Naphthalen-2-yloxy)methyl)naphthalene 479

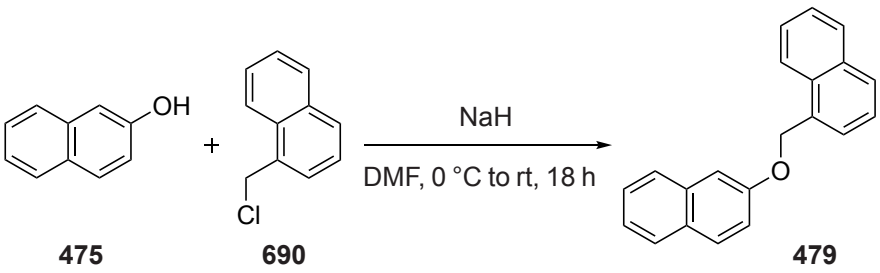

475 **690** **479**

The reaction was kept under a positive pressure of argon. The starting material naphthalen-2-ol **475** (721 mg, 5.00 mmol, 1.0 equiv.) was added slowly as a solid to a suspension of sodium hydride (0.24 g, 6.00 mmol, 1.2 equiv.) in DMF (15 mL) at ice bath temperature. The reaction was stirred for 15 min before 1-(chloromethyl)naphthalene **690** (0.91 mL, 5.50 mmol, 1.1 equiv., 90 %) was added. The reaction was allowed to slowly warm-up to room temperature over 18 h. The reaction was partitioned between water (150 mL) and diethyl ether (50 mL). The organic phase was washed with water (3 x 100 mL) and brine (1 x 50 mL) and dried over $MgSO_4$. The crude material was obtained as a white solid. Recrystallisation from hot hexane/ethyl acetate gave the pure product **479** 1-((naphthalen-2-yloxy)methyl)naphthalene (0.995 g, 3.50 mmol, 70.0 %) as a white solid. A second batch of product **479** 1-((naphthalen-2-yloxy)methyl)naphthalene (131 mg, 0.461 mmol, 9 %) was obtained from the mother liquor of the first crystallisation. In total 1-((naphthalen-2-yloxy)methyl)naphthalene (1.13 g, 3.96 mmol, 79%) was obtained. **^{1}H-NMR** (400 MHz, Chloroform-*d*) δ 8.14 – 8.08 (m, 1H), 7.97 – 7.91 (m,

1H), 7.90 – 7.86 (m, 1H), 7.83 – 7.76 (m, 3H), 7.67 (dd, *J* = 6.9, 1.1 Hz, 1H), 7.60 – 7.52 (m, 2H), 7.52 – 7.44 (m, 2H), 7.40 – 7.33 (m, 2H), 7.29 – 7.24 (m, 1H), 5.63 (s, 2H). **^{13}C-NMR** (101 MHz, Chloroform-*d*) δ 157.0, 134.7, 134.0, 132.4, 131.8, 129.7, 129.3, 129.2, 128.9, 127.8, 127.0, 126.8, 126.6, 126.6, 126.1, 125.5, 123.9, 123.9, 119.2, 107.3, 68.8. **IR** ν_{max} [cm^{-1}]: 3054, 2928, 2876, 1625, 1599, 1509, 1463, 1441, 1383, 1355, 1255, 1214, 1180, 1119, 1063, 1002, 981, 948, 920, 862, 840, 805, 795, 782, 745. **GC-MS** [*m/z* (%)] (18.121 min): 289 (5, M+), 207 (5), 141 (100), 139 (10), 128 (5), 115 (75), 89 (10). **HRMS** (ESI+) [*m/z*]: calcd. for $C_{21}H_{17}O$ (M+H): 285.1274, found: 285.1277. **mp** = 97 °C - 98 °C.

2-(3-Phenylpropoxy)naphthalene 482

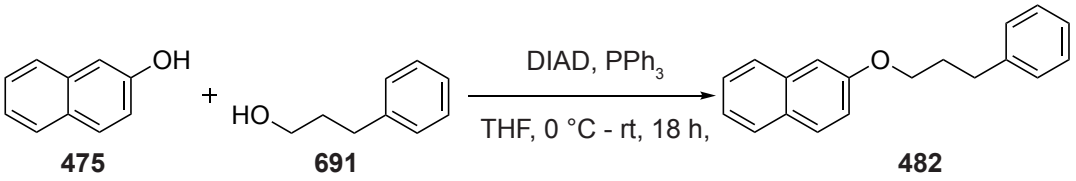

475 **691** **482**

The reaction vessel was charged with triphenylphosphine (1.97 g, 7.50 mmol, 1.5 equiv.) and naphthalen-2-ol **475** (721 mg, 5.00 mmol, 1.0 equiv.), which were then dissolved in THF (20 mL) . Then 3-phenylpropan-1-ol **686** (0.68 mL, 5.00 mmol, 1.0 equiv.) was added and the solution was cooled to ice bath temperature. Diisopropyl azodicarboxylate (DIAD) (1.6 mL, 7.50 mmol, 1.5 equiv.) was added dropwise over 5 min. The reaction was stirred at ice bath temperature for an additional 15 min; then the cooing bath was removed and the reaction was allowed to warm up to room temperature over 18 h. After this period, the reaction was concentrated in vacuo in the presence of silica. Purification by flash column chromatography (25% toluene in hexane) gave the product 2-(3-phenylpropoxy)naphthalene **482** (221 mg, 0.843 mmol, 17 %) as a white solid. **^{1}H-NMR** (400 MHz, Chloroform-*d*) δ 7.80 – 7.73 (m, 2H), 7.71 (dd, *J* = 8.2, 1.0 Hz, 1H), 7.44 (ddd, *J* = 8.2, 6.9, 1.3 Hz, 1H), 7.36 – 7.28 (m, 3H), 7.27 – 7.20 (m, 3H), 7.18 (dd, *J* = 8.9, 2.5 Hz, 1H), 7.11 (d, *J* = 2.5 Hz, 1H), 4.10 (t, *J* = 6.3 Hz, 2H), 2.92-2.82 (m, 2H), 2.25 – 2.13 (m, 2H). **^{13}C-NMR** (101 MHz, Chloroform-*d*) δ 157.1, 141.7, 134.7, 129.5, 129.1, 128.7, 128.6, 127.8, 126.8, 126.4, 126.1, 123.7, 119.1, 106.8, 67.0, 32.4, 30.9. **IR** ν_{max} [cm^{-1}]: 3080, 3056, 3023, 2937, 2868, 1628, 1600, 1511, 1496, 1465, 1390, 1258, 1217, 1182, 1121, 1035, 972, 838, 812, 749, 701. **GC-MS** [*m/z* (%)] (16.426 min): 262 (70), 144 (60), 127 (10), 118 (30), 115 (50), 91 (100), 65 (10). **HRMS** (EI) [*m/z*]: calcd. for $C_{19}H_{18}O$ (M+): 262.1352, found: 262.1345. **mp** = 65 °C.

2-(((1*S*,2*R*,5*R*)-2-Isopropyl-5-methylcyclohexyl)oxy)naphthalene 488

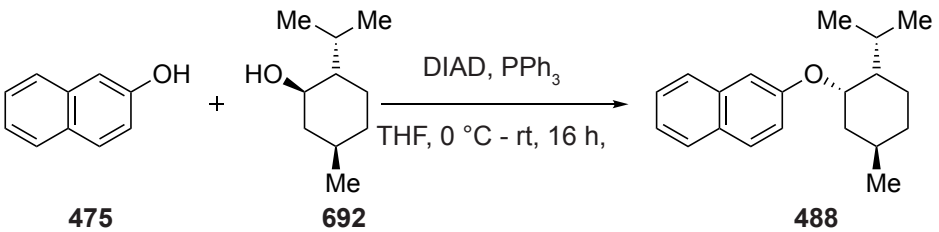

475 **692** **488**

The reaction was kept under a positive pressure of argon. The reaction vessel was charged with triphenylphosphine (1.31 g, 5.00 mmol, 1.0 equiv.) and 2-isopropyl-5-methylcyclohexan-1-ol

692 (781 mg, 5.00 mmol, 1.0 equiv.) , which were then dissolved in THF (25 mL). Then naphthalen-2-ol **475** (721 mg, 5.00 mmol, 1.0 equiv.) was added and the solution was cooled to ice bath temperature and diisopropyl azodicarboxylate (DIAD) (1.0 mL, 5.00 mmol, 1.0 equiv.) was added dropwise over 5 min. The reaction was stirred at ice bath temperature for an additional 10 min. Then the cooing bath was removed and the reaction was allowed to warm up to room temperature over 16 h. The reaction was concentrated in vacuo in the presence of silica. Purification by flash column chromatography (hexane) gave the product 2-((2-isopropyl-5-methylcyclohexyl)oxy)naphthalene **475** (197 mg, 0.691 mmol, 14 %) as a white solid. **^{1}H-NMR** (400 MHz, Chloroform-*d*) δ 7.74 (ddd, *J* = 8.4, 0.9 Hz, 2H), 7.70 (dd, *J* = 8.2, 8.2, 0.9 Hz, 1H), 7.41 (ddd, *J* = 8.2, 6.9, 1.3 Hz, 1H), 7.30 (ddd, *J* = 8.1, 6.8, 1.2 Hz, 1H), 7.19 – 7.10 (m, 2H), 4.85 – 4.70 (m, 1H), 2.23 (ddd, *J* = 13.9, 3.5, 2.3 Hz, 1H), 1.85 – 1.57 (m, 5H), 1.14 – 0.97 (m, 3H), 0.95 (d, *J* = 6.7 Hz, 3H), 0.88 (d, *J* = 6.7 Hz, 3H), 0.82 (d, *J* = 6.6 Hz, 3H). **^{13}C-NMR** (101 MHz, Chloroform-*d*) δ 156.3, 134.9, 129.5, 128.9, 127.7, 126.7, 126.3, 123.4, 119.9, 108.0, 73.4, 48.0, 37.6, 35.2, 29.5, 26.4, 25.1, 22.4, 21.3, 21.0. **IR** ν_{max} [cm^{-1}]: 3054, 3025, 2943, 2921, 2865, 2841, 1628, 1600, 1578, 1509, 1467, 1390, 1368, 1357, 1258, 1216, 1177, 1152, 1119, 1030, 972, 940, 836, 810, 745. **GC-MS** [*m/z* (%)] (15.641 min): 282 (15), 144 (100), 115 (20). **HRMS** (EI) [*m/z*]: calcd. for $C_{20}H_{26}O$ (M+): 282.1978, found: 282.1975. **mp** = 81 °C.

(((1*R*,2*R*,5*R*)-2-Isopropyl-5-methylcyclohexyl)oxy)benzene 489

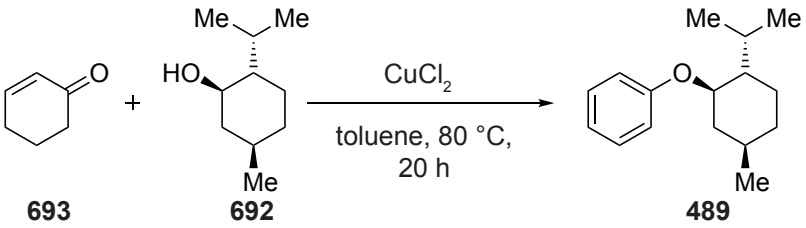

693 **692** **489**

A pressure tube was charged with copper(II) chloride dihydrate (1.28 g, 7.50 mmol, 2.5 equiv.) and (1*R*,2*S*,5*R*)-2-isopropyl-5-methylcyclohexan-1-ol **692** (469 mg, 3.00 mmol, 1.0 equiv.), which were suspended in toluene (6.0 mL) . Then cyclohex-2-en-1-one **693** (0.61 mL, 6.00 mmol, 2.0 equiv.) was added. The pressure tube was sealed and heated to 80 °C for 20 h. The reaction mixture was filtered through a short column of silica with dichloromethane and the crude reaction product was concentrated in vacuo in the presence of silica. Purification by flash column chromatography (hexane) gave the product (((1*R*,2*S*,5*R*)-2-isopropyl-5-methylcyclohexyl)oxy)benzene **489** (162 mg, 0.695 mmol, 23 %) as a white solid. **^{1}H-NMR** (400 MHz, Chloroform-*d*) δ 7.31 – 7.22 (m, 2H), 6.95 – 6.86 (m, 3H), 4.03 (ddd, *J* = 10.6, 10.6, 4.2 Hz, 1H), 2.23 (qd, *J* = 7.0, 2.8 Hz, 1H), 2.16 (dtd, *J* = 12.5, 3.9, 1.9 Hz, 1H), 1.77 – 1.68 (m, 2H), 1.57 – 1.38 (m, 2H), 1.17 – 0.87 (m, 9H), 0.78 (d, *J* = 7.0 Hz, 3H). **^{13}C-NMR** (101 MHz, Chloroform-*d*) δ 158.5, 129.6, 120.5, 116.0, 77.6, 48.2, 40.5, 34.7, 31.6, 26.2, 23.9, 22.3, 20.9, 16.7. **GC-MS** [*m/z* (%)] (12.688 min): 232 (15), 138 (60), 123 (25), 109 (5), 95 (65), 94 (100), 83 (50), 81 (55), 77(20), 69 (25), 67 (20), 65 (15), 55 (50). **mp** = 48 °C - 49 °C. The NMR spectra are in agreement with the previously reported data.[301]

(1*R*,2*R*,4*R*)-2-(Cyclohexylmethoxy)-1-isopropyl-4-methylcyclohexane 493

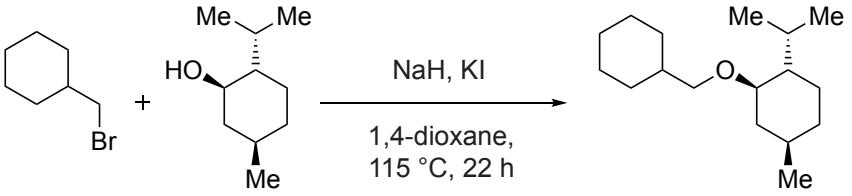

694 **692** **493**

The reaction vessel was charged with (1*R*,2*S*,5*R*)-2-isopropyl-5-methylcyclohexan-1-ol **692** (0.344 g, 2.20 mmol, 1.0 equiv.), which was dissolved in 1,4-dioxane (16.0 mL). Then (bromomethyl)cyclohexane (0.31 mL, 2.20 mmol, 2.2 equiv.) and NaH (98 mg, 2.64 mmol, 1.2 equiv.) were added in this sequence. The reaction was stirred for 25 min at room temperature before it was heated to 115 °C for 16 h. The reaction was monitored by TLC and GC-MS and was found to have not reached full conversion after this time. Therefore potassium iodide (13.0 mg, 0.078 mmol, 0.036 equiv.) was added and heating was continued for 6 h. The reaction was carefully quenched by the addition of water and partitioned between water (100 mL) and diethyl ether (50 mL). The aqueous phase was extracted with diethyl ether (3 x 30 mL). The combined organic phases were washed with brine, dried over $MgSO_4$ and concentrated in vacuo. Purification by flash column chromatography (ethyl acetate in hexane, gradient from 0% to 3%) gave the product (1*S*,2*R*,4*R*)-2-(cyclohexylmethoxy)-1-isopropyl-4-methylcyclohexane **493** (99.0 mg, 0.396 mmol, 17 %) as a colourless oil. **^{1}H-NMR** (500 MHz, Chloroform-*d*) δ 3.42 (dd, *J* = 8.9, 5.9 Hz, 1H), 3.03 (dd, *J* = 8.9, 7.1 Hz, 1H), 2.96 (ddd, *J* = 10.6, 4.1 Hz, 1H), 2.29 – 2.18 (m, 1H), 2.13 – 2.05 (m, 1H), 1.87 – 1.76 (m, 1H), 1.76 – 1.47 (m, 8H), 1.41 – 1.10 (m, 4H), 1.03 – 0.71 (m, 14H). **^{13}C-NMR** (126 MHz, Chloroform-*d*) δ 79.4, 74.9, 48.5, 40.6, 38.7, 34.8, 31.8, 30.6, 30.4, 26.9, 26.1, 26.1, 25.7, 23.5, 22.5, 21.1, 16.3. **GC-MS** [*m/z* (%)] (12.982 min): 252 (2, M+), 237 (1), 167 (65), 138 (65), 123 (20), 97 (70), 95 (30), 83 (35), 81 (50), 71 (85), 55(100). **IR** ν_{max} [cm^{-1}]: 2947, 2917, 2848, 1448, 1385, 1370, 1344, 1320, 1290, 1271, 1240, 1223, 1180, 1151, 1117, 1091, 1071, 1056, 1011, 994, 976, 963, 922, 890, 846. **HRMS** (EI) [*m/z*]: calcd. for $C_{17}H_{32}O$ (M+): 252.2453, found: 252.2454.

5.4.4 Computational Results Presented in Scheme 3-5

The .log files can be found in the following depository: Https://doi.org/10.15129/deef4cea-f279-4afe-82ca-29b88bd30579 {./Aryl_Ether_Cleavage}. All calculations were performed on M06-2X[245]/6-311++G(d,p)/cpcm(triethylamine) level of theory. The silylation reactions were all performed in neat form, i.e. triethylsilane acted as a solvent. Since triethylsilane was not available as a parametrised solvent model triethylamine was chosen as solvent model because its properties match the parameters of triethylsilane best from all the solvents that are included in the Gaussian library.[231]

Table S18 - File names for structures shown in Figure 3-3 for the SET and Fragmentation Pathway (./SET_and_Fragmentation)

Entry	Structure	File name	Comment
1	**494**	Me3SiOtBu_rad.log	-

Entry	Structure	File name	Comment
2	**494** in neutral geometry	Me3SiOtBu_rad-an_in_cat_geom.log	A single point energy calculation was performed on the structure of the neutral counter part of **494** but with the electronic configuration of the radical anion **494**
3	-	Me3SiOtBu_cat.log	Neutral counter part of **494**
4	-	Me3SiOtBu_neutral_in_rad-an_geom.log	A single point energy calculation was performed on the structure of **494** but with the electronic configuration of the neutral counterpart
5	**495**	Two-iPrNp_neutral_M062X_6-311++Gdp.log	-
6	**495** in geometry of **496**	Two-iPrNp_neutral_in_rad-anion_geom_M062X_6-311++Gdp.log	A single point energy calculation was performed on the structure **496** with the electronic configuration of **495**
7	**496**	Two-iPrNp_rad-anion_M062X_6-311++Gdp.log	-
8	**496** in geometry of **495**	Two-iPrNp_rad-anion_in_neutral_geom_M062X_6-311++Gdp.log	A single point energy calculation was performed on the structure **495** with the electronic configuration of **496**
9	TS fragmentation	TS_2-iPrNp_rad-an_fragmentation_M062X_6-311++Gdp.log	Transition state for the carbon-oxygen bond fragmentation in **496**
10	**497** and **498**	TS_2-iPrNp_rad-an_fragmentation_M062X_6-311++Gdp_forward.log	Product complex between **497** and **498**
11	**497**	Two-NpO-anion.log	-
12	**498**	n-prop-2-yl_radical.log	-

Table S19 - File names for structures shown in Figure 3-3 for the Alternative Mechanisms (./Alternative_Mechanisms)

Entry	Structure	File name	Comment
1	**495**	Two-iPrNp_neutral_M062X_6-311++Gdp.log	-
2	Me_3Si-radical	Me3Si-radical.log	-
3	**495** and Me_3Si-radical	Starting_Point_2-iPrNp_Me3Si-radical_attack_M062X_6-311++Gdp_trial2.log	Substrate complex between **495** and Me_3Si-radical
4	TS **499**	TS_2-iPrNp_Me3Si-radical_attack_M062X_6-311++Gdp.log	-
5	2-Naphthoxyl radical and *i*PrSiMe_3	TS_2-iPrNp_Me3Si-radical_attack_M062X_6-311++Gdp_forward.log	Product complex between 2-naphthoxyl radical and *i*PrSiMe_3
6	2-Naphthoxyl radical	Two-NpO-radical.log	-
7	*i*PrSiMe_3	iPrSiMe3.log	-
8	Hydrogen atom	H-atom.log	-
9	**495** and hydrogen atom	TS_2-iPrNp_H-atom_attack_M062X_6-311++Gdp_back_trial4.log	Substrate complex between **495** and hydrogen atom
10	TS **500**	TS_2-iPrNp_H-atom_attack_M062X_6-311++Gdp.log	-
11	2-Naphthoxyl radical and propane	TS_2-iPrNp_H-atom_attack_M062X_6-311++Gdp_forward.log	Product complex between 2-naphthoxyl radical and propane
12	KH	KH.log	Potassium hydride

Entry	Structure	File name	Comment
13	**495** and potassium hydride	Starting_Point_2-iPrNp_KH_attack_var2_M062X_6-311++Gdp_trial2.log	Substrate complex between **495** and potassium hydride
14	TS **501**	TS_2-iPrNp_KH_attack_var2_M062X_6-311++G-dp_trial2.log	-
15	Potassium 2-naphthoxylate and propane	TS_2-iPrNp_KH_attack_var2_M062X_6-311++G-dp_forward.log	Product complex between potassium 2-naphthoxylate and propane
16	Potassium 2-naphthoxylate	Two-NpOK.log	

5.4.5 Arene Reduction

(Corresponds to Chapter 3.2.2. The synthesis of the substrates used in this section is described in Chapter 5.4.6).

Reduction of Anthracene 119

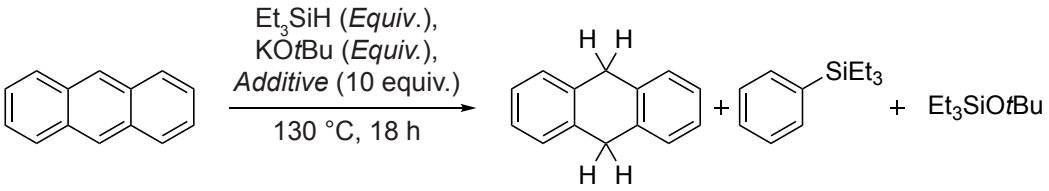

119 **502** **503** **296**

The conditions for the reduction of anthracene **119** to 9,10-dihydroanthracene **502** are investigated. The results of this section are summarised in Table S20 (which corresponds to Table 3-1 in the main text).

Conditions for Entry 1

The reaction vessel was charged with the anthracene **119** (89.1 mg, 0.500 mmol, 1.0 equiv.). The reaction vessel was then brought inside the glovebox and benzene (0.45 mL, 5.00 mmol, 10 equiv.), triethylsilane (2.40 mL, 15.0 mmol, 30 equiv.) and potassium *tert*-butoxide (1.68 g, 15.0 mmol, 30.0 equiv.) were added in this sequence. The pressure tube was sealed and the reaction was heated to 130 °C for 18 h. [Appearance: The colour of the reaction changed from white to deep blue within 6 min at 130 °C (Figure 5-1). The colour stayed deep blue for the rest of the reaction time. When the pressure tube was opened after the heating period, the deep blue colour changed to green within 30 s. A similar evolution of the reaction colour was observed for all other arene reduction reactions]. The reaction was carefully quenched by the addition of water until all solid material was dissolved and no more gas evolved. The crude reaction product was partitioned between water (20 mL) and dichloromethane (20 mL). The phases were separated and the aqueous phase was extracted with dichloromethane (3 x 15 mL). The combined organic phases were washed with water (20 mL), dried over $MgSO_4$ and carefully concentrated in vacuo (45 °C, >100 mbar, < 15 min). In the analysis of the crude reaction product by GC-MS phenyltriethylsilane **503** and *tert*-butoxytriethylsilane **296** were detected as the major reaction components. Purification by flash column chromatography (hexane) gave 9,10-dihydroanthracene **502** (57.2 mg, 0.311 mmol, 62 %) as a white solid, phenyltriethylsilane **503** (342 mg, 1.53 mmol, 31 %, w.r.t. the amount of added benzene) as

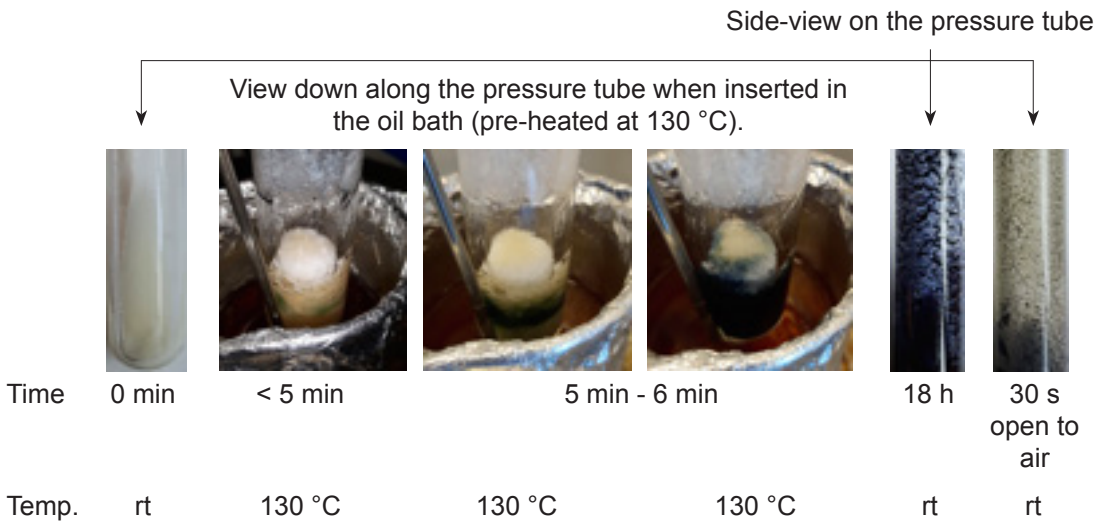

Figure 5-1 Appearance of the reduction reaction of anthracene with the KO*t*Bu-Et_3SiH reagent system.

a colourless oil and recovered anthracene **119** (21.0 mg, 0.101 mmol, 20 %) as a white solid.

A blank reaction was performed in the absence of triethylsilane. The substrate anthracene **119** was recovered quantitatively from this reaction.

9,10-Dihydroanthracene **502**: **^{1}H-NMR** (400 MHz, Chloroform-*d*) δ 7.31 (dd, *J* = 5.5, 3.4 Hz, 4H), 7.21 (dd, *J* = 5.6, 3.3 Hz, 4H), 3.96 (s, 4H). **^{13}C-NMR** (101 MHz, Chloroform-*d*) δ 136.8, 127.5, 126.2, 36.3. **GC-MS** [*m/z* (%)] (13.009 min): 180 (100, M+), 179 (95), 178 (55), 176 (10), 165 (25), 152 (10), 89 (10), 76 (5). **mp** = 116 °C - 118 °C (lit. mp = 108 °C - 111 °C).[302] The NMR spectra are in agreement with the previously reported data.[303]

Phenyltriethylsilane **503**: **^{1}H-NMR** (400 MHz, Chloroform-*d*) δ 7.54 – 7.45 (m, 2H), 7.38 – 7.33 (m, 3H), 1.01 – 0.95 (m, 9H), 0.86 – 0.77 (m, 6H). **^{13}C-NMR** (101 MHz, Chloroform-*d*) δ 137.6, 134.3, 128.8, 127.8, 7.5, 3.5. **GC-MS** [*m/z* (%)] (10.636 min): 192180 (10, M+), 163 (95), 135 (100), 107 (80), 105 (25). The NMR spectra are in agreement with the previously reported data.[304]

Conditions for Entries 2 - 4

The reaction vessel was charged with the anthracene **119** (89.1 mg, 0.500 mmol, 1.0 equiv.). The reaction vessel was then brought inside the glovebox and the additive was added as required [cyclohexene (0.51 mL, 5.00 mmol, 10 equiv.), cyclohexane (0.54 mL, 5.00 mmol, 10 equiv.)] followed by triethylsilane (2.40 mL, 15.0 mmol, 30 equiv.) and potassium *tert*-butoxide (1.68 g, 15.0 mmol, 30.0 equiv.) in this sequence. The pressure tube was sealed and the reaction was heated to 130 °C for 18 h. The reaction was carefully quenched by the addition of water until all solid material was dissolved and no more gas evolved. The crude reaction product was partitioned between water (20 mL) and dichloromethane (20 mL). The phases were separated and the aqueous phase was extracted with dichloromethane (3 x 15 mL). The combined organic phases were washed with water (20 mL), dried over $MgSO_4$ and carefully concentrated in vacuo (45 °C, >100 mbar, < 15 min). Purification by flash column chromatography (hexane) gave 9,10-dihydroanthracene **502** as a white solid and recovered anthracene **502** as a white solid. The NMR spectra of 9,10-dihydroanthracene **502** were identical to the

spectra recorded for the previously isolated material. Additionally, in all three cases *tert*-butoxytriethylsilane **296** was isolated as a colourless oil.

tert-Butoxytriethylsilane **296**: **^{1}H-NMR** (400 MHz, Chloroform-*d*) δ 1.24 (s, 9H), 0.95 (t, *J* = 7.9 Hz, 9H), 0.57 (q, *J* = 8.0 Hz, 6H). **^{13}C-NMR** (101 MHz, Chloroform-*d*) δ 71.6, 32.2, 7.2, 6.8. **GC-MS** [*m/z* (%)] (7.977 min): 188 (0.3, M+), 173 (5), 159 (35), 115 (15), 103 (100), 87 (10), 75 (50). The NMR spectra are in agreement with the previously reported data.[305]

Conditions for Entry 5

The reaction vessel was charged with the anthracene **119** (89.1 mg, 0.500 mmol, 1.0 equiv.). The reaction vessel was then brought inside the glovebox and triethylsilane (0.24 mL, 1.5 mmol, 3.0 equiv.) and potassium *tert*-butoxide (0.168 g, 1.50 mmol, 3.0 equiv.) were added in this sequence. The pressure tube was sealed and the reaction was heated to 130 °C for 18 h. The reaction was carefully quenched by the addition of water until all solid material was dissolved and no more gas evolved. The crude reaction product was partitioned between water (20 mL) and dichloromethane (20 mL). The phases were separated and the aqueous phase was extracted with dichloromethane (3 x 15 mL). The combined organic phases were washed with water (20 mL), dried over $MgSO_4$ and carefully concentrated in vacuo (45 °C, >100 mbar, < 15 min). Purification by flash column chromatography (hexane) gave 9,10-dihydroanthracene **502** (23.3 mg 0.129 mmol, 26 %) as a white solid and recovered anthracene **502** (62.0 mg, 0.306 mmol, 61 %) as a white solid. The NMR spectra of 9,10-dihydroanthracene **502** were identical to the spectra recorded for the previously isolated material.

Table S20 - Reduction of Anthracene with the KO*t*Bu-Et_3SiH Reagent System

Entry	Additive (10 equiv.)	Equiv. of KO*t*Bu and Et_3SiH	Yield of 502	Yield of 119	By-Product (Yield)
1	Benzene	30	62 %	20 %	**503** (31 %)[a,b]
2	Cyclohexene	30	59 %	21 %	**296** (9 %)[c]
3	Cyclohexane	30	80 %	6 %	**296** (21 %)[c]
4	-	30	85 %	5 %	**296** (22 %)[c]
5	-	3	26 %	61 %	-

[a] The yield of **503** was calculated with respect to the amount of benzene.

[b] *tert*-Butoxytriethylsilane **296** was detected by GC-MS analysis of the crude reaction mixture as a major reaction component.

[c] The yield of **296** was calculated with respect to the amount of used Et_3SiH.

Deuterium Oxide Quenching Experiments and i. a. Formation of 502-*(9,10)-d*$_2$

The experiments described in this section correspond to the results presented in Scheme 3-6 in the main text).

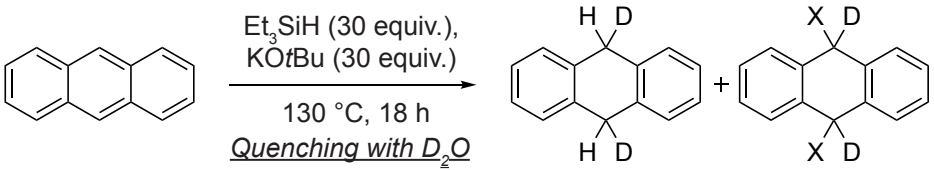

119 **502-*(9,10)-d*$_2$** **502-*(9,9,10)-d*$_3$** **502-*(9,9,10,10)-d*$_4$**

The substrate anthracene **119** (89.1 mg, 0.500 mmol, 1.0 equiv.) was reacted according to the General Procedure B and quenched by the addition of deuterium oxide. A mixture of deuterated compounds **502** (77.9 mg, 0.422 mmol, 85 %) was obtained as a white solid. **^{2}H-NMR** (61 MHz, Chloroform) δ 3.96, 3.92. **^{1}H-NMR** (400 MHz, Chloroform-*d*) δ 7.30 (dd, *J* = 5.4, 3.4 Hz, 4H), 7.23 – 7.17 (m, 4H), 3.95 (s, 4H, non-deuterated compound, ca. 4 %), 3.93 (t, *J* = 2.3 Hz, 2H, di-deuterated compound, ca. 76 %). **^{13}C-NMR** (101 MHz, Chloroform-*d*) δ 136.8, 127.5, 126.2, 36.3 (non-deuterated compound), 35.9 (t, *J* = 19.4 Hz). **GC-MS** [*m/z* (%)] (12.928 min): 184 (15), 183 (50), 182 (100), 181 (85), 180 (55), 179 (25), 178 (15), 167 (20), 166 (10), 153 (10), 90 (20), 77 (10).

The ^{2}H-NMR indicates that deuteration only occurred at the benzylic position and not at the aromatic system. The ^{2}H-NMR also indicates that there are at least two different chemical environments for the deuterium atoms. The ^{1}H-NMR indicates that ca. 4 % of non-deuterated **502** were formed (comparison of the benzylic signal for the non-deuterated compound to the total of aromatic signals). The benzylic proton signal for the di-deuterated compound **502-*d*$_2$** indicates that this compound is formed in ca. 76 % relative abundance. Hence, the combination of non-deuterated **502** and di-deuterated **502-*d*$_2$** can only account for ca. 80 % of the composition of the obtained mixture of deuterated compounds. The GC-MS fragment ion pattern and the HRMS (ASAP) analysis both indicate that higher deuterated analogues such as **502-*(9,9,10)-d*$_3$** and **502-*(9,9,10,10)-d*$_4$** may be contained in the mixture (Figure 5-2).

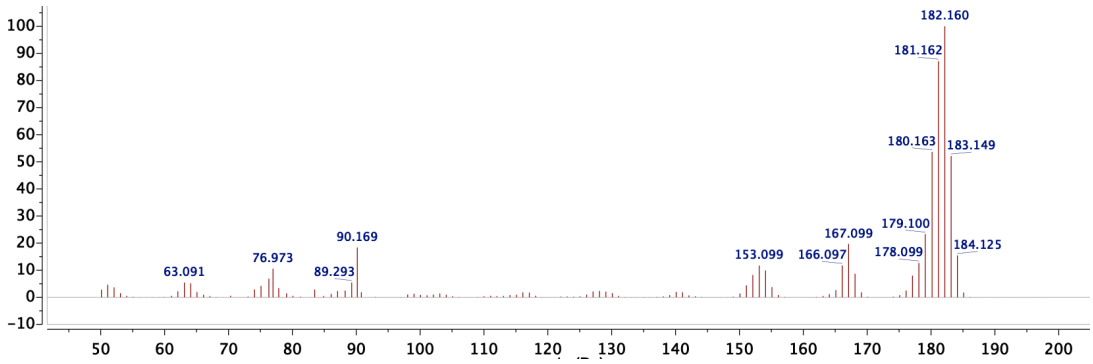

Figure 5-2 LRMS (EI) analysis of the mixture of deuterated analogues obtained from the reaction shown in Scheme 3-6 A. Calculated masses are 180.09 Da for **502**, 182.11 Da for **502-*(9,10)-d*$_2$**, 183.11 Da for **502-*(9,9,10)-d*$_3$**, and 184.12 Da for **502-*(9,9,10,10)-d*$_4$**.

Control Reaction for the Deuterium Oxide Quenching Experiments

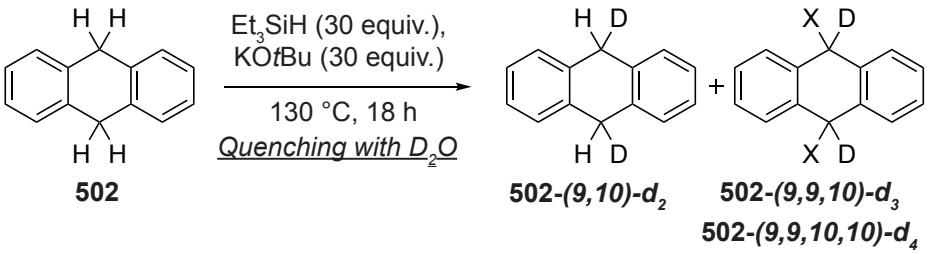

502 **502-*(9,10)*-d_2** **502-*(9,9,10)*-d_3** **502-*(9,9,10,10)*-d_4**

The reaction vessel was charged with 9,10-dihydroanthracene **502** (40.0 mg, 0.222 mmol, 1.0 equiv.). The vessel was then brought inside the glovebox and triethylsilane (1.06 mL, 6.66 mmol, 30 equiv.) and potassium *tert*-butoxide (747 mg, 6.66 mmol. 30 equiv.) were added in this sequence. The pressure tube was sealed and heated to 130 °C for 18 h. The reaction was quenched by the careful addition of deuterium oxide. The reaction mixture was partitioned between water (20 mL) and dichloromethane (20 mL). The phases were separated and the aqueous phase was washed with dichloromethane (3 x 15 mL). The combined organic phases were washed with water (1 x 20 mL), dried over $MgSO_4$ and carefully concentrated in vacuo (45 °C, > 100 mbar, < 10 min). From the crude reaction mixture deuterated **502** (21.5 mg, 0.118 mmol, 53 %) crystallised spontaneously at room temperature as a colourless and transparent material. Further concentration of the mother liquor (70 °C, 20 mbar, 2 h) gave additional deuterated **502** (17.3 mg, 0.093 mmol, 42 %) as an off-white solid. Overall deuterated **502** (38.8 mg, 0.213 mmol, 95 % yield) was obtained. The NMR spectra and GC-MS data of the deuterated **502** were identical to the spectra and GC-MS data recorded for the previously isolated material from the reduction of anthracene **119** and quenching with deuterium oxide.

Reduction of Phenanthrene 508

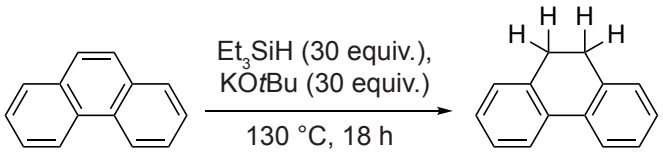

508 **509**

The substrate phenanthrene **508** (89.1 mg, 0.500 mmol, 1.0 equiv.) was reacted according to the General Procedure B and quenched by the addition of water. Inspection of the crude reaction product by ^{1}H-NMR indicated full conversion of the substrate. Purification by flash column chromatography (hexane) gave 9,10-dihydrophenanthrene **509** (24.6 mg, 0.136 mmol, 27 %) as a colourless oil. **^{1}H-NMR** (400 MHz, Chloroform-*d*) δ 7.77 (ddd, *J* = 7.6, 0.9, 0.9 Hz, 2H), 7.32 (ddd, *J* = 7.7, 5.4, 3.5 Hz, 2H), 7.28 – 7.21 (m, 4H), 2.89 (s, 4H). **^{13}C-NMR** (101 MHz, Chloroform-*d*) δ 137.5, 134.6, 128.3, 127.5, 127.1, 123.8, 29.2. **GC-MS** [*m/z* (%)] (13.018): 180 (100, M^+), 179 (75), 178 (50), 176 (15), 165 (40), 152 (15), 151 (10), 89 (20), 88 (5), 76 (10). The NMR spectra are in agreement with the previously reported data.[306]

Reduction of Naphthalene 452

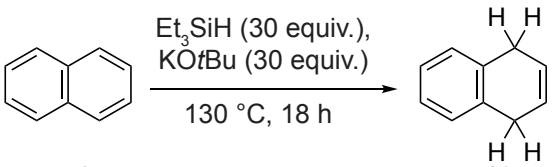

452 **510**

The reaction vessel was charged with naphthalene **452** (64.1 mg, 0.500 mmol, 1.0 equiv.). The vessel was then brought inside the glovebox and triethylsilane (2.40 mL, 15.0 mmol, 30 equiv.) and potassium *tert*-butoxide (1.68 g, 15.0 mmol, 30 equiv.) were added in this sequence. The pressure tube was sealed and heated to 130 °C for 18 h outside the glovebox. The reaction was quenched by the careful addition of water. Then a precisely measure amount of internal standard 1,3,5-trimethoxybenzene (ca. 47 mg, 0.28 mmol, 0.56 equiv.) was added. The reaction mixture was partitioned between water (20 mL) and dichloromethane (20 mL). The phases were separated and the aqueous phase was extracted with dichloromethane (3 x 15 mL). The combined organic phases were washed with water (1 x 20 mL), dried over $MgSO_4$ and carefully concentrated in vacuo (45 °C, > 100 mbar, < 10 min). The crude reaction product was analysed by ^{1}H-NMR. The signals of the identified products were compared to the signals of a corresponding authentic sample. It was found that naphthalene **452** (42 %) remained unreacted while 1,4-dihydronaphthalene **510** (31 %) was formed (the material was synthesised independently, see Chapter 5.4.6).

Reduction of Stilbene 512

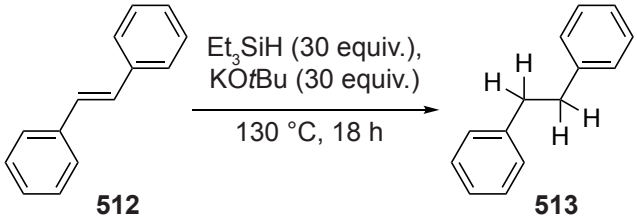

512 **513**

The substrate stilbene **512** (90.1 mg, 0.500 mmol, 1.0 equiv.) was reacted according to the General Procedure B and quenched by the addition of water. Inspection of the crude reaction product by ^{1}H-NMR indicated full conversion of the substrate. Purification by flash column chromatography (hexane) gave 1,2-diphenylethane **513** (83.4 mg, 0.458 mmol, 92 %) as a white solid. **^{1}H-NMR** (400 MHz, Chloroform-*d*) δ 7.32 – 7.26 (m, 4H), 7.23 – 7.17 (m, 6H), 2.93 (s, 4H). **^{13}C-NMR** (101 MHz, Chloroform-*d*) δ 141.9, 128.6, 128.5, 126.1, 38.1. **GC-MS** [*m/z* (%)] (11.885 min): 182 (30, M+), 91 (100), 65 (25), 63 (5), 51 (5). **mp** = 46 °C - 47 °C (lit. mp = 50.5 °C - 51.0 °C).[307] The NMR spectra are in agreement with the previously reported data.[307]

Reduction of Diphenylacetylene 512

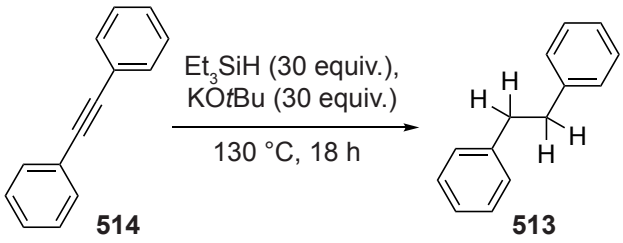

514 **513**

The substrate diphenylacetylene **514** (89.1 mg, 0.500 mmol, 1.0 equiv.) was reacted according to the General Procedure B and quenched by the addition of water. Inspection of the crude reaction product by ^{1}H-NMR indicated full conversion of the substrate. Purification by flash column chromatography (hexane) gave 1,2-diphenylethane **513** (25.1 mg, 0.134 mmol, 27 %) as a white solid. The NMR spectra were identical to the spectra recorded for the previously isolated material.

Reduction of Acridine 515

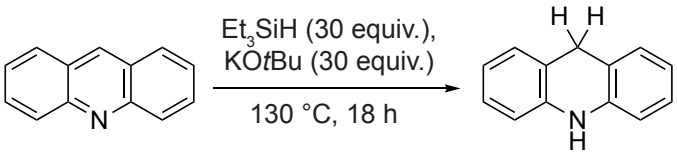

515 **516**

The substrate acridine **515** (89.6 mg, 0.500 mmol, 1.0 equiv.) was reacted according to the General Procedure B and quenched by the addition of water. Inspection of the crude showed that the ratio of acridine **515** to 9,10-dihydroacridine **516** equals 1:13 (which corresponds to 93 % conversion). Purification by flash column chromatography (hexane) gave 9,10-dihydroacridine **516** (70.6 mg, 0.390 mmol, 78 %) as a pale yellow solid. Additionally unreacted acridine **515** (10.9 mg, 57.5 µmol, 12 %) was recovered as a yellow solid.

9,10-Dihydroacridine **516**: **^{1}H-NMR** (400 MHz, Chloroform-*d*) δ 7.14 – 7.06 (m, 4H), 6.86 (ddd, *J* = 7.4, 7.4, 1.2 Hz, 2H), 6.67 (dd, *J* = 7.8, 1.1 Hz, 2H), 5.94 (s, 1H), 4.06 (s, 2H). **^{13}C-NMR** (151 MHz, Chloroform-*d*) δ 140.3, 128.7, 127.1, 120.8, 120.2, 113.6, 31.5. **GC-MS** [*m/z* (%)] (13.516 min): 179 (100, M-2), 178 (25), 177 (10), 152 (10), 151 (10), 150 (5), 126 (5), 89 (10), 75 (10). **mp** = 168 °C - 169 °C (lit. mp = 169 °C - 170 °C).[308] The NMR spectra are in agreement with the previously reported data.[309]

Reduction of Quinoline 517

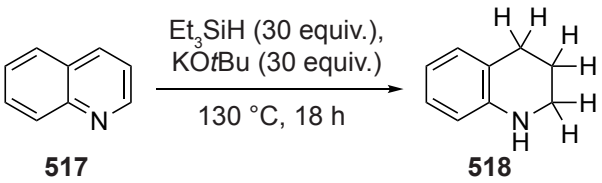

517 **518**

The substrate quinoline **517** (64.6 mg, 0.500 mmol, 1.0 equiv.) was reacted according to the General Procedure B and quenched by the addition of water. Inspection of the crude reaction product by ^{1}H-NMR indicated full conversion of the substrate. Purification by flash column chromatography (ethyl acetate in hexane, gradient from 0 % to 100 %) gave 1,2,3,4-tetrahydroquinoline **518** in impure form. Acidic extraction gave pure 1,2,3,4-tetrahydroquinoline **518** (27.9 mg, 0.199 mmol, 40 %) as a pale yellow oil. **^{1}H-NMR** (400 MHz, Chloroform-*d*) δ 7.02 – 6.93 (m, 2H), 6.64 (ddd, *J* = 7.4, 7.4, 1.2 Hz, 1H), 6.53 (dd, *J* = 7.8, 1.1 Hz, 1H), 3.87 (s, 1H), 3.36 – 3.27 (m, 2H), 2.78 (t, *J* = 6.4 Hz, 2H), 2.00 – 1.92 (m, 2H). **^{13}C-NMR** (151 MHz, Chloroform-*d*) δ 144.4, 129.7, 126.9, 121.9, 117.5, 114.7, 42.1, 27.0, 22.2. **GC-MS** [*m/z* (%)] (10.502 min): 133 (80, M+), 132 (100), 130 (15), 118 (25), 117 (25), 104 (15), 91 (15), 77 (15), 65 (10). The NMR spectra are in agreement with the previously reported data.[310]

Reduction of 9-Cyanoanthracene 521

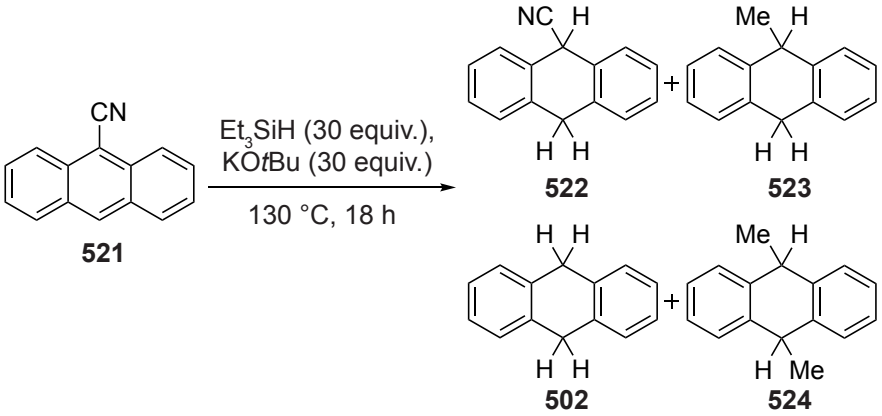

521 **522** **523** **502** **524**

The substrate 9-cyanoanthracene **521** (102 mg, 0.500 mmol, 1.0 equiv.) was reacted according to the General Procedure B and quenched by the addition of water. Inspection of the crude reaction product by ^{1}H-NMR indicated that a small amount of substrate remained unreacted. Purification by flash column chromatography (ethyl acetate in hexane, gradient from 0 % to 100 %) gave impure 9,10-dihydroanthracene-9-carbonitrile **522** and 9-methyl-9,10-dihydroanthracene **523** (35.6 mg, 0.184 mmol, 37 %) as an inseparable mixture with 9,10-dihydroanthracene **502** (3.1 mg, 0.017 mmol, 3.4 %) and 9,10-dihydro-9,10-dimethylanthracene **524** (2.4 mg, 0.011 mmol, 2.3 %) as a white solid. Additionally, starting material 9-cyanoanthracene **521** (12.0 mg, 57.8 µmol, 12 %) was recovered. A second purification of impure 9,10-dihydroanthracene-9-carbonitrile **522** by flash column chromatography (toluene in hexane, gradient from 50 % to 66 %) gave pure 9,10-dihydroanthracene-9-carbonitrile **522** (23 mg, 0.113 mmol, 23 %) as a yellow solid.

The ^{1}H-NMR signals and GC-MS analysis of **523**, **502** and **524** were in agreement with the corresponding data of authentic reference samples:

- For data of **502** see “Reduction of Anthracene **119**” above
- For data of **523** see “Reduction of 9-Methylanthracene **526**” below and
- For data of **524** see “Reduction of 9,10-Dimethylanthracene **527**” below).

9,10-Dihydroanthracene-9-carbonitrile **522**: **^{1}H-NMR** (400 MHz, Chloroform-*d*) δ 7.66 – 7.60 (m, 2H), 7.42 – 7.29 (m, 6H), 5.05 (dd, *J* = 2.4, 1.0 Hz, 1H), 4.10 (d, *J* = 17.8 Hz, 1H), 3.94 (dd, *J* = 17.9, 2.4 Hz, 1H). **^{13}C-NMR** (101 MHz, Chloroform-*d*) δ 136.2, 130.9, 128.4, 128.1, 127.2, 126.7, 118.4, 37.2, 35.7. **GC-MS** [*m/z* (%)] (14.142 min): 205 (100, M+), 204 (85), 203 (35), 190 (40), 179 (10), 178 (50), 177 (20), 176 (25), 175 (10), 152 (10), 151 (10), 150 (10), 102 (5), 89 (15), 88 (15), 76 (10), 75 (5), 63 (5). **mp** = 48 °C. The NMR spectra are in agreement with the previously reported data.[311]

Reduction of Anthracen-9-yl(pyrrolidin-1-yl)methanone 525

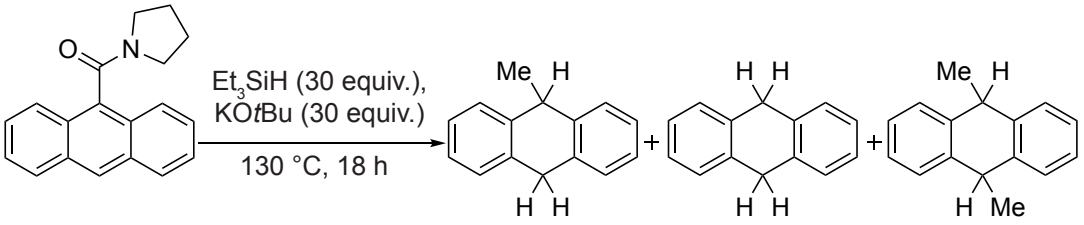

525 **523** **502** **524**

The substrate 9-cyanoanthracene **521** (138 mg, 0.500 mmol, 1.0 equiv.) was reacted according to the General Procedure B and quenched by the addition of water. Inspection of the crude reaction product by ^{1}H-NMR indicated full conversion of the substrate. Purification by flash column chromatography (ethyl acetate in hexane, gradient from 0 % to 100 %) gave 9-methyl-9,10-dihydroanthracene **523** (82.7 mg, 0.426 mmol, 86 %) as an inseparable mixture with 9,10-dihydroanthracene **502** (6.2 mg, 0.0322 mmol, 6.5 %) and 9,10-dihydro-9,10-dimethylanthracene **524** (6.8 mg, 0.0327 mmol, 6.6 %) as a white solid. The ^{1}H-NMR signals and GC-MS analysis of **523**, **502** and **524** were in agreement with the corresponding data of authentic reference samples:

- For data of **502** see “Reduction of Anthracene **119**” above
- For data of **523** see “Reduction of 9-Methylanthracene **526**” below and
- For data of **524** see “Reduction of 9,10-Dimethylanthracene **527**” below).

Reduction of 9-Methylanthracene 526

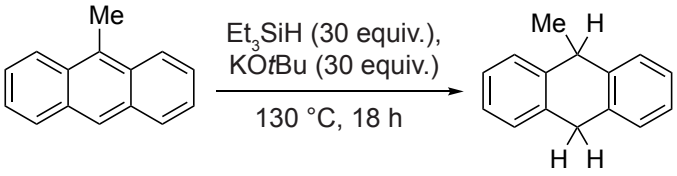

526 **523**

The substrate 9-methylanthracene **526** (96.1 mg, 0.500 mmol, 1.0 equiv.) was reacted according to the General Procedure B and quenched by the addition of water. Inspection of the

crude reaction product by ^{1}H-NMR indicated that the ration of **526** to **523** was equal to 1:99. Importantly, no other reaction products derived from the substrate **526** could be identified. Purification by flash column chromatography (hexane) gave 9-methyl-9,10-dihydroanthracene **523** (94 mg, 0.484 mmol, 97 %) as a white solid. Additionally, 9-methylanthracene **526** (2 mg, 8 µmol, 2 %) was recovered.

9-Methyl-9,10-dihydroanthracene **523**: **^{1}H-NMR** (400 MHz, Chloroform-*d*) δ 7.40 – 7.32 (m, 4H), 7.31 – 7.21 (m, 4H), 4.19 (d, *J* = 18.3 Hz, 1H), 4.10 (q, *J* = 7.3 Hz, 1H), 3.95 (d, *J* = 18.2 Hz, 1H), 1.50 (d, *J* = 7.2 Hz, 3H). **^{13}C-NMR** (101 MHz, Chloroform-*d*) δ 141.9, 135.9, 127.8, 127.0, 126.5, 126.1, 41.2, 35.3, 23.6. **GC-MS** [*m/z* (%)] (12.960 min): 194 (10, M+), 180 (15), 179 (100), 178 (45), 177 (5), 176 (10), 165 (5), 152 (10), 139 (5), 115 (5), 89 (10), 76 (5). **mp** = 118 °C (lit. mp = 62 °C).[312] The NMR spectra are in agreement with the previously reported data.[313]

Reduction of 9,10-Dimethylanthracene 527

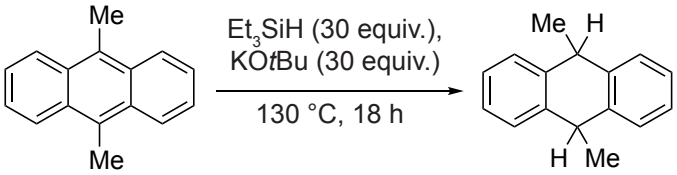

527 **524**

The substrate 9,10-dimethylanthracene **527** (103 mg, 0.500 mmol, 1.0 equiv.) was reacted according to the General Procedure B and quenched by the addition of water. Inspection of the crude reaction product by ^{1}H-NMR indicated that the ratio of **527** to **524** was equal to 4:96. Importantly, no other reaction products derived from the substrate **527** could be identified. Purification by flash column chromatography (hexane) gave 9,10-dimethyl-9,10-dihydroanthracene **524** (68 mg, 0.29 mmol, 59 %, d.r. (*trans:cis*) = 2:8) as a mixture with 9,10-dimethyl-9,10-dihydroanthracene **527** (2 mg, 0.01 mmol, 2 %) as a pale yellow solid. Additionally, pure 9,10-dimethyl-9,10-dihydroanthracene **524** (43 mg, 0.20 mmol, 39 %, d.r. (*trans:cis*) = 7:3) was isolated as a white solid. In total 9,10-dimethyl-9,10-dihydroanthracene **524** (102 mg, 0.490 mmol, 98 %, d.r. (*trans:cis*) = 3:7) was obtained. **^{1}H-NMR** (400 MHz, Chloroform-*d*) δ 7.43 (dd, *J* = 5.6, 3.4 Hz, 2H), 7.34 (dd, *J* = 5.6, 3.4 Hz, 1H), 7.28 (ddd, *J* = 5.3, 3.3 Hz, 4H), 4.19 – 4.09 (m, 2H), 1.68 (d, *J* = 7.2 Hz, 6H, *trans*-isomer), 1.62 (d, *J* = 7.3 Hz, 6H, cis-isomer). **^{13}C-NMR** (101 MHz, Chloroform-*d*, *cis*-isomer) δ 140.6, 127.9, 126.3, 40.1, 28.6. **^{13}C-NMR** (101 MHz, Chloroform-*d*, *trans*-isomer) δ 141.4, 126.3, 125.9, 38.6, 18.9. **GC-MS** [*m/z* (%)] (13.136 min, *cis*-isomer): 208 (10, M+), 193 (100), 191 (10), 189 (10), 178 (90), 165 (10), 152 (10), 115 (5), 96 (5), 89 (15), 76 (5). **mp** = 156 °C (lit. mp = 132 °C).[314] The ^{1}H-NMR[315] and ^{13}C-NMR[316] spectra are in agreement with the previously reported data.

5.4.6 Substrate Synthesis for the Reactions of Chapter 5.4.5

1,4-Dihydronaphthalene 510

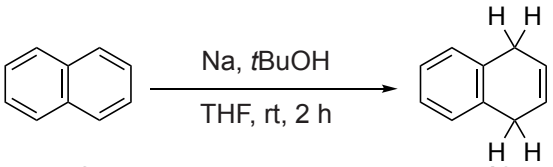

452 **510**

Synthesis of 1,4-dihydronaphthalene **510** as a reference material via a Birch-type reduction. The reaction was kept under a positive pressure of argon. To a solution of naphthalene **452** (1.28 g, 10.0 mmol, 1.0 equiv.) in THF (21 mL) was added sodium metal (575 mg, 25.0 mmol, 2.5 equiv.) in small portions over ca. 2 min. 10 min after the addition was finished, *tert*-butanol (2.4 mL, 25.0 mmol, 2.5 equiv.) was added slowly and the reaction was stirred at room temperature for additional 2 h. Remaining sodium was removed from the reaction by filtration. The crude reaction product was partitioned between water (30 mL) and diethyl ether (30 mL). The phases were separated and the aqueous phase was extracted with diethyl ether (3 x 20 mL). The combined organic phases were washed with brine, dried over $MgSO_4$ and carefully concentrated in vacuo (45 °C, > 100 mbar, < 15 min) to give the crude product as a pale yellow oil. Purification by distillation (69 °C ± 1 °C, 8.5 mbar) gave 1,4-dihydronaphthalene **510** (0.679 g, 5.21 mmol, 52 %) as a colourless oil. **^{1}H-NMR** (400 MHz, Chloroform-*d*) δ 7.19 – 7.11 (m, 4H), 5.96-5.92 (m, 2H), 3.41 (d, *J* = 1.4 Hz, 4H). **^{13}C-NMR** (101 MHz, Chloroform-*d*) δ 134.4, 128.6, 126.0, 124.9, 29.9. **GC-MS** [*m/z* (%)] (9.467 min): 130 (100), 129 (95), 128 (60), 127 (25), 126 (10), 115 (65), 103 (5), 102 (20), 89 (10), 87 (5), 78 (10), 77 (15), 76 (10), 75 (15), 74 (15), 64 (10), 63 (30), 62 (15), 52 (10), 51 (35), 50 (15). The NMR spectra are in agreement with the previously reported data.[317]

Diphenylacetylene 512

695 **696** **514**

The reaction was kept under a positive pressure of argon. The reaction vessel was charged with bis(triphenylphosphine)palladium(II) dichloride (175 mg, 0.250 mmol, 0.05 equiv.) , copper(I) iodide (95.2 mg, 0.500 mmol, 0.1 equiv.) , potassium carbonate (2.07 g, 15.0 mmol, 3.0 equiv.) and DMF (17 mL) . Then iodobenzene (0.56 mL, 5.00 mmol, 1.0 equiv.) and ethynylbenzene (0.55 mL, 5.00 mmol, 0.1 equiv.) were added and the reaction was stirred at room temperature for 5 h. The reaction was monitored by TLC and was found to have reached a high degree of conversion after 4 h. The reaction was partitioned between water (80 mL) and diethyl ether (20 mL). The aqueous phase was extracted with diethyl ether (3 x 20 mL). The combined organic phases were washed with water (50 mL) and brine, dried over $MgSO_4$ and

concentrated in vacuo in the presence of silica. Purification by flash column chromatography (hexane,) gave 1,2-diphenylethyne (0.535 g, 3.00 mmol, 60 %) as a white solid. **^{1}H-NMR** (400 MHz, Chloroform-*d*) δ 7.60 – 7.52 (m, 4H), 7.42 – 7.31 (m, 6H). **^{13}C-NMR** (101 MHz, Chloroform-*d*) δ 131.7, 128.5, 128.4, 123.4, 89.5. **GC-MS** [*m/z* (%)] (12.723 min): 178 (100, M+), 177 (10), 176 (20), 152 (15), 151 (10), 150 (10), 139 (5), 126 (10), 98 (5), 89 (5), 88 (5), 76 (10), 75 (5), 63 (5), 51 (5), 50 (5). **mp** = 57 °C - 58 °C (lit. mp = 57 °C - 58 °C).[318] The NMR spectra are in agreement with the previously reported data.[319]

Anthracen-9-yl(pyrrolidin-1-yl)methanone 525

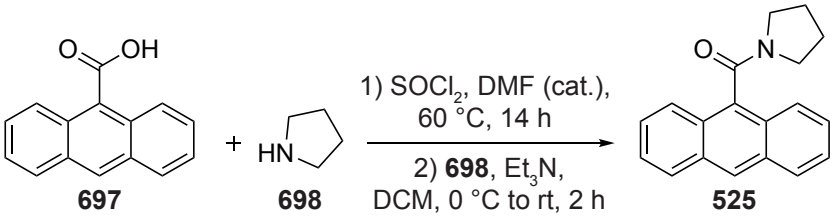

697 **698** **525**

Step 1 The reaction vessel was charged with anthracene-9-carboxylic acid **697** (0.333 g, 1.50 mmol, 1.1 equiv.), thionyl chloride (4.10 mL, 56.2 mmol, 40 equiv.) and a few drops of DMF (cat.). The reaction was heated to 60 °C for 14 h. The reaction was concentrated in vacuo (at 60 °C under a flow of argon). The residue was dissolved in toluene, transferred to a new flask and concentrated further in vacuo (45 °C, 20 mbar). The crude anthracene-9-carbonyl chloride was obtained as a yellow solid and used in the next step without further purification.

Step 2 The reaction vessel was charged with anthracene-9-carbonyl chloride (338 mg, 1.40 mmol, 1.0 equiv.) from Step 1, which was dissolved in DCM (7 mL). The solution was cooled to ice bath temperature and triethylamine (254 µL, 1.83 mmol, 1.3 equiv.) and pyrrolidine **698** (129 µL, 1.54 mmol, 1.1 equiv.) were added sequentially. The reaction was stirred at room temperature for 2 h. The reaction mixture was diluted with dichloromethane (15 mL) and washed with aqueous HCl (3 x 10 mL, 4 M). The organic phase was dried over $MgSO_4$ and concentrated in vacuo (45 °C). The crude product was recrystallised from hot ethyl acetate / hexane to give anthracen-9-yl(pyrrolidin-1-yl)methanone **525** (180 mg, 0.654 mmol, 47 %) as a brown solid. The mother liquor was concentrated and a second recrystallised from hot ethyl acetate / hexane gave additional anthracen-9-yl(pyrrolidin-1-yl)methanone **525** (58.4 mg, 0.212 mmol, 15 %). In total anthracen-9-yl(pyrrolidin-1-yl)methanone **525** (238 mg, 0.866 mmol, 62 %) was isolated. **^{1}H-NMR** (400 MHz, Chloroform-*d*) δ 8.46 (s, 1H), 8.06 – 7.99 (m, 2H), 7.96 – 7.90 (m, 2H), 7.55 – 7.44 (m, 4H), 3.98 (t, *J* = 7.1 Hz, 2H), 2.93 (t, *J* = 6.9 Hz, 2H), 2.05 (tt, *J* = 6.9, 6.9 Hz, 2H), 1.81 (tt, *J* = 6.8, 6.8 Hz, 2H). **^{13}C-NMR** (101 MHz, Chloroform-*d*) δ 168.9, 132.5, 131.4, 128.8, 127.7, 127.4, 126.9, 125.6, 125.0, 47.8, 45.8, 26.1, 24.9. **GC-MS** [*m/z* (%)] (17.532 min): 275 (45, M+), 205 (100), 178 (25), 177 (65), 176 (55), 151 (15), 150 (10), 70 (5). **mp** = 148 °C - 149 °C (lit. mp = 150 °C - 152 °C).[320] The NMR spectra are in agreement with the previously reported data.[320]

5.4.7 Computational Results for Chapter 3.3.1

The .log files can be found in the following depository: Https://doi.org/10.15129/deef4cea-f279-4afe-82ca-29b88bd30579 {/ Silylation_of_Amines/Silylation_of_Amines}. All calculations were performed on M06-2X[245]/6-311++G(d,p)/cpcm(triethylamine) level of theory. The silylation reactions were all performed in neat form, i.e. triethyl silane acted as a solvent. Since triethylsilane was not available as a parametrised solvent model triethylamine was chosen as solvent model because its properties match the parameters of triethylsilane best from all the solvents that are included in the Gaussian library.[231]

Table S21 - File names for structures shown in Figure 3-3 (./Inital_Deprotonation_Aliphatic_Amine)

Entry	Structure	File name	Comment
1	**537**	Me2NH.log	Dimethylamine
2	**287**	tBuOK.log	Potassium *tert*-butoxide
3	**538**	Me2NK.log	Potassium dimethylamide
4	**539**	tBuOH.log	*tert*-Butanol

Table S22 - File names for structures shown in Figure 3-4 (./Formation_of_KH)

Entry	Structure	File name	Comment
1	**543**	Me3SiH.log	Me_3SiH
2	**287**	tBuOK.log	KO*t*Bu
3	Substrate complex	TS_tBuOMe3SiHK_back.log	Substrate complex
4	**TS1**	TS_tBuOMe3SiHK_trial2.log	TS 1 - addition of KO*t*Bu to Me_3SiH
5	Int. 1	TS_tBuOMe3SiHK_forward.log	Intermediate 1 - K^+ coordinating via oxygen
6	Int. 2	TS_KH_formation_Me3SiHOtBuK_back_trial8_freq.log	Intermediate 2 - K^+ coordinating via hydridic hydrogen
7	TS 2	TS_KH_formation_Me3SiHOtBuK_trial2.log	TS 2 - elimination of KH
8	Product complex	TS_KH_formation_Me3SiHOtBuK_forward.log	Product complex
9	**541**	Me3SiOtBu_cat.log	Me_3SiO*t*Bu
10	**467**	KH.log	Potassium hydride

Table S23 - File names for structures shown in Scheme 3-12 and Figure 3-5 (./Silylation_of_Me2NH_with_Me3SiH)

Entry	Structure	File name	Comment
1	**537**	Me2NH.log	Dimethylamine
2	**467**	KH.log	Potassium hydride
3	not shown	TS_H2_Expulsion_KH_back.log	Substrate complex of dimethylamine and potassium hydride
4	not shown	TS_H2_Expulsion_KH.log	TS for deprotonation of dimethylamine with potassium hydride
5	not shown	TS_H2_Expulsion_KH_forward.log	Product complex of potassium dimethylamide and molecular hydrogen
6	H_2	H2.log	Molecular hydrogen
7	**538**	Me2NK.log	Potassium dimethylamide

Entry	Structure	File name	Comment
8	**543**	Me3SiH.log	Trimethylsilane
9	**538** and **543** towards **544a**	TS_Me2NK_Eq_Attack_on_Me3SiH_back.log	Substrate complex of **538** and **543** towards the formation of **544a**
10	TS towards **544a**	TS_Me2NK_Eq_Attack_on_Me3SiH.log	TS for formation of **544a**
11	**544a**	TS_Me2NK_Eq_Attack_on_Me3SiH_forward.log	**544a**
12	**544b**	TS_KH_dissociation_form_Eq_Attack_product_Me2NK_Me3SiH_back.log	**544b**
13	TS KH elimination from **544b**	TS_KH_dissociation_form_Eq_Attack_product_Me2NK_Me3SiH.log	TS for potassium hydride elimination from **544a**
14	**467** and **545**	TS_KH_dissociation_form_Eq_Attack_product_Me2NK_Me3SiH_forward.log	Product complex of potassium hydride and silylated amine **545**
15	**538** and **543** towards **544c**	TS_Me3SiHNMe2K_back.log	Substrate complex of **538** and **543** towards the formation of **544c**
16	TS towards **544a**	TS_Me3SiHNMe2K_trial2.log	TS for formation of **544c**
17	**544c**	TS_Me3SiHNMe2K_forward.log	**544c**
18	**544d**	TS_KH_formation_Me3SiHNMe2K_back.log	**544d**
19	TS KH elimination from **544d**	TS_KH_formation_Me3SiHNMe2K_trial2.log	TS for potassium hydride elimination from **544c**
20	**467** and **545** from **544d**	TS_KH_formation_Me3SiHNMe2K_forward_trial2.log	Product complex of potassium hydride and Me_3SiO*t*Bu derived from **544d**
21	**541**	Me3SiOtBu.log	Me_3SiO*t*Bu
22	**541** and **537**	TS_Me2NK_attacking_Me3SiOtBu_back.log	Substrate complex of **541** and **537**
23	TS towards **546a**	TS_Me2NK_attacking_Me3SiOtBu.log	TS for formation of **546a**
24	**546a**	TS_Me2NK_attacking_Me3SiOtBu_forward.log	**546a**
25	**546a**	TS2_Me2NK_attacking_Me3SiOtBu_back.log	**546b**
26	TS KO*t*Bu elimination from **546a**	TS2_Me2NK_attacking_Me3SiOtBu.log	TS for potassium *tert*-butoxide elimination from **546a**
27	KO*t*Bu and **545**	TS2_Me2NK_attacking_Me3SiOtBu_forward.log	Product complex of potassium *tert*-butoxide **287** and Me_2N-$SiMe_3$ **545**
28	KO*t*Bu **287**	tBuOK.log	Potassium *tert*-butoxide
29	**545**	Me2NSiMe3.log	Product Me_2NSiMe_3 **545**

Table S24 - File names for structures shown in Scheme 3-14 and Figure 3-6 (./Double_Silylation_with_Me3SiH)

Entry	Structure	File name	Comment
1	**467**	KH.log	Potassium hydride
2	**550**	HNMeSiMe3.log	Silylated amine $HN(SiMe_3)Me$ **550**
3	**467** and **550**	TS_H2_expulsion_HNMeSiMe3_KH_back.log	Substrate complex of potassium hydride **467** and amine **550**
4	TS	TS_H2_expulsion_HNMeSiMe3_KH.log	TS for the deprotonation of **550** with potassium hydride **467**

Entry	Structure	File name	Comment
5	**551** and H_2	TS_H2_expulsion_HNMeSiMe3_KH_forward.log	Product complex of potassium aminde **551** and molecular hydrogen
6	**551**	KNMeSiMe3.log	Potassium amide KN($SiMe_3$)Me **551**
7	H_2	H2.log	Molecular hydrogen
8	**543**	Me3SiH.log	Trimethylsilane Me_3SiH **543**
9	**543** and **551** reacting towards **552a**	TS_KNMeSiMe3_attack_on_Me3SiH_back.log	Substrate complex of trimethylsilane **543** and potassium amide **551** leading towards **552a**
10	TS towards **552a**	TS_KNMeSiMe3_attack_on_Me3SiH.log	Attack of potassium amide **551** on trimethyl silane **543** to form **552a**
11	**552a**	TS_KNMeSiMe3_attack_on_Me3SiH_forward.log	-
12	**552b**	TS_KH_expulsion_Me3SiNMeMe3SiHK_back.log	-
13	TS KH expulsion from **552b**	TS_KH_expulsion_Me3SiNMeMe3SiHK.log	-
14	KH and **553** emerging from **552c**	TS_KH_expulsion_Me3SiNMeMe3SiHK_forward.log	Product complex of potassium hydride **467** and silylated amine **553** emerging from intermediate **552c**
15	**543** and **551** reacting towards **552c**	TS_MeMe3SiNK_Eq_Attack_on_Me3SiH_back.log	Substrate complex of trimethylsilane **543** and potassium amide **551** leading towards **552c**
16	TS towards **552c**	TS_MeMe3SiNK_Eq_Attack_on_Me3SiH_trial2.log	Attack of potassium amide **551** on trimethyl silane **543** to form **552c**
17	**552c**	TS_MeMe3SiNK_Eq_Attack_on_Me3SiH_forward.log	-
18	**552d**	TS_KH_elimination_from_Me3SiMeNSiMe3HK_back.log	-
19	TS KH expulsion from **552d**	TS_KH_elimination_from_Me3SiMeNSiMe3HK.log	-
20	KH and **553** emerging from **552d**	TS_KH_elimination_from_Me3SiMeNSiMe3HK_forward.log	Product complex of potassium hydride **467** and silylated amine **553** emerging from intermediate **552d**
21	**553**	MeNSi2Me6.log	Doubly silylated amine product **553**

Table S25 - File names for structures shown in Scheme 3-15 and Figure 3-7 (./Double_Silylation_with_Et3SiH)

Entry	Structure	File name	Comment
1	**467**	KH.log	Potassium hydride
2	**554**	Substrate_Et3SiNHMe_trial2.log	Silylated amine **554**
3	**467** and **554**	TS_H2_expulsion_HNMeSiEt3_KH_back.log	Substrate complex of potassium hydride and amine **554**
4	TS deprotonation	TS_H2_expulsion_HNMeSiEt3_KH.log	Transition state for the deprotonation of **554** by **467**
5	**555** and H_2	TS_H2_expulsion_HNMeSiEt3_KH_forward.log	Product complex between hydrogen and potassium amide **555**
6	**555**	KNMeSiEt3.log	Potassium amide **555**

Entry	Structure	File name	Comment
7	H_2	H2.log	Molecular hydrogen
8	**296**	tBuOK.log	*tert*-Butoxytriethylsilane
9	**284**	Et3SiH.log	Triethylsilane
10	**555** and **284** towards **557a**	TS_KNMeSiEt3_attack_on_Et3SiH_back.log	Substrate complex of **555** and **284** towards the formation of **557a**
11	TS addition towards **557a**	TS_KNMeSiEt3_attack_on_Et3SiH.log	Transition state for the addition of **555** on **284** to form **557a**
12	**557a**	TS_KNMeSiEt3_attack_on_Et3SiH_forward.log	-
13	**557b**	TS_KH_expulsion_Et3SiNMeEt3SiHK_back.log	-
14	TS KH elimination from **557b**	TS_KH_expulsion_Et3SiNMeEt3SiHK.log	Transition state for the elimination of potassium hydride from **557b**
15	**558** and KH from **557b**	TS_KH_expulsion_Et3SiNMeEt3SiHK_forward.log	Product complex of potassium hydride and **558** derived from **557b**
16	**558**	Product_MeNSi2Et6.log	Doubly silylated amine **558**
17	**555** and **284** towards **557c**	TS_MeEt3SiNK_Eq_Attack_on_Et3SiH_back.log	Substrate complex of **555** and **284** towards the formation of **557c**
18	TS addition towards **557c**	TS_MeEt3SiNK_Eq_Attack_on_Et3SiH.log	Transition state for the addition of **555** on **284** to form **557c**
19	**557c**	TS_MeEt3SiNK_Eq_Attack_on_Et3SiH_forward.log	-
20	**557d**	TS_KH_elimination_Et3SiNMeEt3SiHK_back.log	-
21	TS KH elimination from **557d**	TS_KH_elimination_Et3SiNMeEt3SiHK.log	Transition state for the elimination of potassium hydride from **557d**
22	**558** and KH from **557d**	TS_KH_elimination_Et3SiNMeEt3SiHK_forward.log	Product complex of potassium hydride and **558** derived from **557d**
23	**555** and **296**	TS1_MeEt3SiNK_attacking_Et3SiOtBu_back_trial3.log	Substrate complex of **555** and **296** towards the formation of **556a**
24	TS addition towards **556a**	TS1_MeEt3SiNK_attacking_Et3SiOtBu.log	Transition state for the addition of **555** on **296** to form **556a**
25	**556a**	TS1_MeEt3SiNK_attacking_Et3SiOtBu_forward.log	-
26	**556b**	TS2_MeEt3SiNK_attacking_Et3SiOtBu_back.log	-
27	TS elimination of **287** from **556b**	TS2_MeEt3SiNK_attacking_Et3SiOtBu.log	Transition state for the elimination of potassium *tert*-butoxide from **556b**
28	**558** and **287** from **556b**	TS2_MeEt3SiNK_attacking_Et3SiOtBu_forward_trial3.log	Product complex of potassium *tert*-butoxide and **558** derived from **556b**

Table S26 - File names for structures shown in Figure 3-8 (./Double_Silylation_with_Bulky_Amines_and_Et3SiH)

Entry	Structure	File name	Comment
1	**284**	Et3SiH.log	Triethylsilane
2	**559 (R = *n*Pr)**	nPrEt3SiNK_Substrate.log	Potassium amide with R = *n*Pr
3	**559 (R = *n*Pr)** and **284** towards **560a**	TS_KNnPrSiEt3_attack_on_Et3SiH_back_trial2.log	Substrate complex of **559** and **284** towards the formation of **560a**
4	TS towards **560a**	TS_KNnPrSiEt3_attack_on_Et3SiH.log	Transition state for the addition of **555** on **284** to form **560b**
5	**560a**	TS_KNnPrSiEt3_attack_on_Et3SiH_forward.log	-
6	**560b**	TS2_KNnPrSiEt3_attack_on_Et3SiH_back_start.log	-
7	TS elimination of KH from **560b**	TS2_KNnPrSiEt3_attack_on_Et3SiH.log	Transition state for the elimination of potassium hydride from **560b**
8	**562 (R = *n*Pr)** and **467**	TS2_KNnPrSiEt3_attack_on_Et3SiH_forward.log	Product complex of potassium hydride and **562 (R = *n*Pr)** derived from **560b**
9	**467**	KH.log	Potassium hydride
10	**562** (R = *n*Pr)	nPrNSi2Et6_Product.log	Doubly silylated amine **562 (R = *n*Pr)**
11	**559 (R = *n*Pr)** and **284** towards **560c**	TS_nPrEt3SiNK_Eq_Attack_on_Et3SiH_back.log	Substrate complex of **559** and **284** towards the formation of **560c**
12	TS towards **560c**	TS_nPrEt3SiNK_Eq_Attack_on_Et3SiH.log	Transition state for the addition of **555** on **284** to form **560c**
13	**560c**	TS_nPrEt3SiNK_Eq_Attack_on_Et3SiH_forward.log	-
14	**560d**	TS_KH-Expulsion_nPrEt3SiNK_Eq_Attack_on_Et3SiH_back.log	-
15	TS elimination of KH from **560d**	TS_KH-Expulsion_nPrEt3SiNK_Eq_Attack_on_Et3SiH.log	Transition state for the elimination of potassium hydride from **560d**
16	**562 (R = *n*Pr)** and **467**	TS_KH-Expulsion_nPrEt3SiNK_Eq_Attack_on_Et3SiH_forward.log	Product complex of potassium hydride and **562 (R = *n*Pr)** derived from **560d**
17	**559 (R = *i*Pr)**	iPrEt3SiNK_Substrate.log	Potassium amide with R = *i*Pr
18	**559 (R = *i*Pr)** and **284** towards **561a**	TS_KNiPrSiEt3_attack_on_Et3SiH_back_trial2.log	Substrate complex of **559** and **284** towards the formation of **561a**
19	TS towards **561a**	TS_KNiPrSiEt3_attack_on_Et3SiH.log	Transition state for the addition of **555** on **284** to form **561a**
20	**561a**	TS_KNiPrSiEt3_attack_on_Et3SiH_forward.log	-
21	**561b**	TS2_KNiPrSiEt3_attack_on_Et3SiH_back_start.log	-
22	TS elimination of KH from **561b**	TS2_KNiPrSiEt3_attack_on_Et3SiH.log	Transition state for the elimination of potassium hydride from **561b**
23	**562 (R = *i*Pr)** and **467**	TS2_KNiPrSiEt3_attack_on_Et3SiH_forward.log	Product complex of potassium hydride and **562 (R = *i*Pr)** derived from **561b**

Entry	Structure	File name	Comment
24	**562 (R = *i*Pr)**	iPrNSi2Et6_Product.log	Doubly silylated amine **562 (R = *i*Pr)**
25	**559 (R = *i*Pr)** and **284** towards **561c**	TS_iPrEt3SiNK_Eq_Attack_on_Et3SiH_back.log	Substrate complex of **559** and **284** towards the formation of **561c**
26	(**561c**)	BS_iPrEt3SiNK_Eq_Attack_on_Et3SiH.log	Bond scan for the addition of **559 (R = *i*Pr)** on **284** towards **561c**
27	(**561c**)	TS_iPrEt3SiNK_Eq_Attack_on_Et3SiH_forward.log	Attempted optimisation of **561c**

Table S27 - File names for structures shown in Scheme 3-16 and Figure 3-9 (./Silylation_of_Aniline)

Entry	Structure	File name	Comment
1	**542**	KH.log	Potassium hydride
2	**563**	H2NPh.log	Aniline
3	**467** and **563**	TS_H2_Expulsion_H2NPh_KH_back_trial2.log	Substrate complex between potassium hydride and aniline
4	TS deprotonation of **563** with KH	TS_H2_Expulsion_H2NPh_KH.log	Transition state for the deprotonation of aniline with potassium hydride
5	**564** and H_2	TS_H2_Expulsion_H2NPh_KH_forward.log	Product complex between potassium anilide and molecular hydrogen
6	**564**	HKNPh.log	Potassium anilide
7	H_2	H2.log	Molecular hydrogen
8	**287**	tBuOK.log	Potassium *tert*-butoxide
9	**287** and **563**	TS_PhNH2_deprot_with_KOtBu_back.log	Substrate complex between potassium *tert*-butoxide and aniline
10	TS deprotonation of **563** with KO*t*Bu	TS_PhNH2_deprot_with_KOtBu.log	Transition state for the deprotonation of aniline with potassium *tert*-butoxide
11	**564** and HO*t*Bu	TS_PhNH2_deprot_with_KOtBu_forward.log	Product complex between potassium anilide and *tert*-butanol
12	**539**	tBuOH.log	*tert*-Butanol
13	**541**	Me3SiOtBu.log	*tert*-Butoxytrimethylsilane
14	**543**	Me3SiH.log	Trimethylsilane
15	**564** and **543**	TS_Me3SiHNHPhK_back.log	Substrate complex between **564** and **543** leading to intermediate **565a**
16	TS to **565a**	TS_Me3SiHNHPhK_trial2.log	Transition state of the addition of **564** onto **543** leading to **565a**
17	**565a**	TS_Me3SiHNHPhK_forward.log	-
18	**565b**	TS_KH_formation_Me3SiHNHPhK_substrate_complex.log	-
19	TS elimination of KH from **565b**	TS_KH_formation_Me3SiHNHPhK_trial2.log	Transition state for the elimination of potassium hydride from **565b**
20	**567** and KH from **565b**	TS_KH_formation_Me3SiHNHPhK_forward_trial2.log	Product complex of potassium hydride and **567** derived from **565b**
21	**567**	HNPhSiMe3.log	Silylated aniline product **567**

Entry	Structure	File name	Comment
22	**564** and **543** towards **565c**	TS_PhHNK_Eq_Attack_on_Me3SiH_back.log	Substrate complex between **564** and **543** leading to intermediate **565c**
23	TS to **565c**	BS_PhHNK_Eq_Attack_on_Me3SiH_trial2.log	The bond scan for the addition of **564** onto **543** leading to **565c** does not show a local maximum
24	**565c**	TS_PhHNK_Eq_Attack_on_Me3SiH_forward.log	-
25	**565d**	TS_KH_elimination_from_PhHNMe3SiHK_back.log	-
26	TS elimination of KH from **565b**	TS_KH_elimination_from_PhHNMe3SiHK.log	Transition state for the elimination of potassium hydride from **565d**
27	**567** and KH from **565d**	TS_KH_elimination_from_PhHNMe3SiHK_forward.log	Product complex of potassium hydride and **567** derived from **565d**
28	**564** and **541** towards **566a**	TS1_PhHNK_attacking_Me3SiOtBu_back.log	Substrate complex between **564** and **541** leading to intermediate **566a**
29	TS to **566a**	TS1_PhHNK_attacking_Me3SiOtBu.log	Transition state of the addition of **564** onto **541** leading to **566a** does not show a local maximum
30	**566a**	TS1_PhHNK_attacking_Me3SiOtBu_forward.log	-
31	**566b**	TS2_PhHNK_attacking_Me3SiOtBu_back.log	-
32	TS elimination of KO*t*Bu from **566b**	TS2_PhHNK_attacking_Me3SiOtBu_trial2.log	Transition state for the elimination of potassium *tert*-butoxide from **566b**
33	**567** and KO*t*Bu from **566a**	TS2_PhHNK_attacking_Me3SiOtBu_forward.log	Product complex of potassium *tert*-butoxide and **567** derived from **566b**

Table S28 - File names for structures shown in Figure 3-10 (./Double_Silyation_of_Aniline)

Entry	Structure	File name	Comment
1	**568a**	BS_KNMe3SiPh_attack_on_Me3SiH.log	Bond scan towards the formation of **568a** - no local minimum found
2	**568b**	BS_PhMe3SiNK_Eq_Attack_on_Me3SiH_trial2.log	Bond scan towards the formation of **568b** - no local minimum found
3	**569**	BS1_PhMe3SiNK_attacking_Me3SiOtBu_trial2.log	Bond scan towards the formation of **569** - no local minimum found

Table S29- File names for structures shown in Scheme 3-18 and Figure 3-11 (./Cyclisation_and_KMe_Expulsion)

Entry	Structure	File name	Comment
1	**571**	Substrate_Me3Si.log	Three-fold silylated 1,2-diamine
2	**573**	KMe.log	Methyl potassium
3	**571** and **573**	TS_Deprotonation_with_KMe_back.log	Substrate complex between **571** and **573**
4	TS deprotonation of **571** by **573**	TS_Deprotonation_with_KMe.log	Transition state for the deprotonation of **571** by **573**
5	**574** and methane	TS_Deprotonation_with_KMe_forward.log	Product complex between **574** and methane

Entry	Structure	File name	Comment
6	**574**	TS_cyclisation_tri-Me3Si-diaminoethaneK_back.log	Potassium salt of **571**
7	Methane	Methane.log	Methane
8	TS cyclisation	TS_cyclisation_tri-Me3Si-diaminoethaneK.log	Transition state for the cyclisation of **574**
9	**575** (Int. 1)	TS_cyclisation_tri-Me3Si-diaminoethaneK_forward.log	Optimised starting from the transition state for the cyclisation of **574**
10	**575** (Int. 2)	TS_cyclisation_elimination_of_KMe_back_trial2.log	Optimised starting from the transition state for the elimination of methyl potassium
11	TS elimination of KMe	TS_cyclisation_elimination_of_KMe.log	Transition state for the elimination of methyl potassium
12	**576** and **573**	TS_cyclisation_elimination_of_KMe_forward.log	Product complex between **576** and methyl potassium **573**
13	**576**	Cylclised_Product_Me3Si.log	Cyclised product

5.5. Experimental Details for Chapter 4 “Concerted vs. Stepwise S_NAr Mechanism”

The .log files can be found in the following depository: Https://doi.org/10.15129/deef4cea-f279-4afe-82ca-29b88bd30579 {./Concerted_vs_Stepwise_SNAr_Mechanism}.

5.5.1 General Procedure

For all S_NAr reactions reported in this chapter the rate limiting transition state (‘TS1’) was optimised. The transition state geometry was then displaced by 0.05 units along the imaginary vibration mode in both directions. The geometries obtained in this way served as input structure for the optimisation (keyword: opt=calcfc) towards the substrate complex (‘SC’) and the product complex (‘PC’) or Meisenheimer intermediate (‘MI’), respectively. Based on whether the optimisation converged directly to the product complex or to a Meisenheimer intermediate the example was classified as concerted or as stepwise, respectively. This procedure was validated as detailed in the main text (see Section 4.2.2). If a Meisenheimer intermediate was found, the second transition state (‘TS2’) leading to the final product was identified for representative examples as specified.

5.5.2 The Applied σ_p^- Scale

The σ_p^- values were taken form the landmark review by Hansch et al.[238] A selection of *para*-substituents and their associated σ_p^- constants that are used in this chapter are listed in Table S30 below. The less commonly encountered structures are drawn out next to the table.

Table S30 - σ_p^- Values

Entry	*para*-Substituent -R	σ_p^-
1	-NO	1.63
2	$-NO_2$	1.27
3	$-CHC(CN)_2$	1.20
4	$-COCF_3$	1.09
5	-CN	1.00
6	-COMe	0.84
7	$-CO_2Me$	0.75
8	$-CF_3$	0.65
9	-CCH	0.53
10	-NCS	0.34
11	-Cl	0.19
12	-H	0.00
13	-Me	-0.17
14	-OMe	-0.26
15	-NHAc	-0.46
16	$-NP(Ph)_3$	-0.77

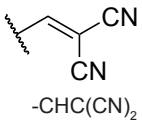

$-CHC(CN)_2$

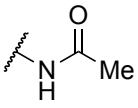

-NHAc

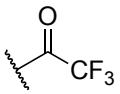

$-COCF_3$

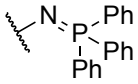

$-NP(Ph)_3$

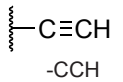

-CCH

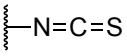

-NCS

Computational Results for Chapter 4.2.1

The .log files can be found in the following depository: Https://doi.org/10.15129/deef4cea-f279-4afe-82ca-29b88bd30579 {./Mechanistic_Transition/Concept}. The calculations for this section were performed on M06-2X[245]/6-311++G(d,p)/cpcm(DMF) level of theory. The names of the .log files are systematically listed in Table S31 below. For each example the substrate complex ('SC'), transition state ('TS'), and product complex ('PC') was calculated.

Table S31 - File names for structures shown in Figure 4-1 (./Mechanistic_Transition/Concept)

Entry	-R (folder name)	Reaction Coordinate[a]	File name
1	-CN	SC	TS_CN_M062X-6311++Gdp_back.log
2	-CN	TS1	TS_CN_M062X-6311++Gdp_trial3.log
3	-CN	MI	TS_CN_M062X-6311++Gdp_forward_trial2.log
4	-CN	TS2	TS2_CN_M062X-6311++Gdp_trial2.log
5	-CN	PC	TS2_CN_M062X-6311++Gdp_forward.log
6	-COMe	SC	TS_COMe_M062X-6311++Gdp_back_trial3.log
7	-COMe	TS	TS_COMe_M062X-6311++Gdp_trial2.log
8	-COMe	MI	TS_COMe_M062X-6311++Gdp_forward.log
9	-COMe	TS2	TS2_COMe_M062X-6311++Gdp_trial2.log
10	-COMe	PC	TS2_COMe_M062X-6311++Gdp_forward_trial2.log
11	$-CO_2Me$	SC	TS_CO2Me_M062X-6311++Gdp_back.log
12	$-CO_2Me$	TS	TS_CO2Me_M062X-6311++Gdp.log

Entry	-R (folder name)	Reaction Coordinate[a]	File name
13	-CO_2Me	MI	TS_CO2Me_M062X-6311++Gdp_forward.log
14	-CO_2Me	TS2	TS2_CO2Me_M062X-6311++Gdp_trial4.log
15	-CO_2Me	PC	TS2_CO2Me_M062X-6311++Gdp_forward.log
16	-CF_3	SC	TS_CF3_M062X-6311++Gdp_back_trial14.log
17	-CF_3	TS	TS_CF3_M062X-6311++Gdp_trial2.log
18	-CF_3	PC	TS_CF3_M062X-6311++Gdp_forward_trial3.log
19	-CCH	SC	TS_CCH_F_MeO_M062X-6311++Gdp_back.log
20	-CCH	TS	TS_CCH_F_MeO_M062X-6311++Gdp.log
21	-CCH	PC	TS_CCH_F_MeO_M062X-6311++Gdp_forward.log

[a] SC: substrate complex; TS1: first transition state; MI: Meisenheimer intermediate; TS2: second transition state; PC: product complex.

5.5.3 Computational Results for Chapter 4.2.2

The calculations of this section were calculated on the level of theory as specified. For all calculations the cpcm solvent model for DMF was used. For each example the substrate complex ('SC'), transition state ('TS'), and product complex ('PC') was calculated.

Benchmarking

The .log files can be found in the following depository: Https://doi.org/10.15129/deef4cea-f279-4afe-82ca-29b88bd30579 {./Mechanistic_Transition/Computational_Model}. The names of the .log files of the calculations used to compile Figure 4-2, Figure 4-3, Table 4-1 and Table 4-2 are systematically listed in Table S32 below.

Table S32- File names for structures shown in Figure 4-2, Figure 4-3, Table 4-1 and Table 4-2 (./Benchmarking)

Entry	Method[a] (folder name)	-R (sub folder name)	Reaction Coordinate[b]	File name
1	MP2_aug-cc-pVTZ	-$COCF_3$	SC	TS_COCF3_MP2_aug-cc-pVTZ_back_trial3.log
2	"	-$COCF_3$	TS1	TS_COCF3_MP2_aug-cc-pVTZ_trial3_freq.log
3	"	-$COCF_3$	MI	TS_COCF3_MP2_aug-cc-pVTZ_forward_freq.log
4	"	-CN	SC	TS_CN_MP2-aug-cc-pVTZ_back_trial2.log
5	"	-CN	TS	TS_CN_MP2-aug-cc-pVTZ
6	"	-CN	MI	TS_CN_MP2-aug-cc-pVTZ_forward_trial5.log
7	"	-COMe	SC	TS_COMe_MP2-aug-cc-pVTZ_back.log
8	"	-COMe	TS	TS_COMe_MP2-aug-cc-pVTZ_trial5_step13_freq.log
9	"	-COMe	PC	TS_COMe_MP2-aug-cc-pVTZ_forward_trial7_freq.log
10	"	-CO_2Me	SC	TS_CO2Me_MP2-aug-cc-pVTZ_back.log
11	"	-CO_2Me	TS	TS_CO2Me_MP2_aug-cc-pVTZ.log
12	"	-CO_2Me	PC	TS_CO2Me_MP2-aug-cc-pVTZ_forward_trial2.log
13	MP2	-$COCF_3$	SC	TS_COCF3_MP2_6311++Gdp_back_trial2.log
14	"	-$COCF_3$	TS1	TS_COCF3_MP2_6311++Gdp_trial4.log
15	"	-$COCF_3$	MI	TS_COCF3_MP2_6311++Gdp_forward.log
16	"	-CN	SC	TS_CN_MP2-6311++Gdp_back.log

Entry	Method[a] (folder name)	-R (sub folder name)	Reaction Coordinate[b]	File name
17	“	-CN	TS	TS_CN_MP2-6311++Gdp_trial3.log
18	“	-CN	MI	TS_CN_MP2-6311++Gdp_forward.log
19	“	-COMe	SC	TS_COMe_MP2-6311++Gdp_back_trial10_freq.log
20	“	-COMe	TS	TS_COMe_MP2-6311++Gdp_trial4_freq.log
21	“	-COMe	PC	TS_COMe_MP2-6311++Gdp_forward_trial2.log
22	“	-CO_2Me	SC	TS_CO2Me_MP2_6311++Gdp_back.log
23	“	-CO_2Me	TS	TS_CO2Me_MP2_6311++Gdp_trial3.log
24	“	-CO_2Me	PC	TS_CO2Me_MP2_6311++Gdp_forward_trial3.log
25	B3PW91	-$COCF_3$	SC	TS_COCF3_B3PW91_6-311++Gdp_back_trial3.log
26	“	-$COCF_3$	TS1	TS_COCF3_B3PW91_6-311++Gdp.log
27	“	-$COCF_3$	MI	TS_COCF3_B3PW91_6-311++Gdp_forward.log
28	“	-CN	SC	TS_CN_B3PW91_6-311++Gdp_back_trial3_freq.log
29	“	-CN	TS	TS_CN_B3PW91_6-311++Gdp.log
30	“	-CN	PC	TS_CN_B3PW91_6-311++Gdp_forward_trial2.log
31	“	-COMe	SC	TS_COMe_B3PW91_6-311++Gdp_back_trial5.log
32	“	-COMe	TS	TS_COMe_B3PW91_6-311++Gdp.log
33	“	-COMe	PC	TS_COMe_B3PW91_6-311++Gdp_forward_trial3.log
34	“	-CO_2Me	SC	TS_CO2Me_B3PW91_6-311++Gdp_back_trial4.log
35	“	-CO_2Me	TS	TS_CO2Me_B3PW91_6-311++Gdp.log
36	“	-CO_2Me	PC	TS_CO2Me_B3PW91_6-311++Gdp_forward_trial2_freq.log
37	B3LYP	-NO2	SC	TS_NO2_F_MeO_B3LYP_back_trial4.log
38	“	-NO2	TS1	TS_NO2_F_MeO_B3LYP_trail2.log
39	“	-NO2	MI	TS_NO2_F_MeO_B3LYP_forward.log
40	“	-$COCF_3$	SC	TS_COCF3_B3LYP-6311++Gdp_back_trial4.log
41	“	-$COCF_3$	TS1	TS_COCF3_B3LYP-6311++Gdp.log
42	“	-$COCF_3$	MI	TS_COCF3_B3LYP-6311++Gdp_forward.log
43	“	-CN	SC	TS_CN_B3LYP-6311++Gdp_back_trial3.log
44	“	-CN	TS	TS_CN_B3LYP-6311++Gdp.log
45	“	-CN	PC	TS_CN_B3LYP-6311++Gdp_forward_trial2.log
46	“	-COMe	SC	TS_COMe_B3LYP-6311++Gdp_back_trial4.log
47	“	-COMe	TS	TS_COMe_B3LYP-6311++Gdp_trial2_freq.log
48	“	-COMe	PC	TS_COMe_B3LYP-6311++Gdp_forward_trial2.log
49	“	-CO_2Me	SC	TS_CO2Me_B3LYP_6-311++Gdp_back_trial5.log
50	“	-CO_2Me	TS	TS_CO2Me_B3LYP_6-311++Gdp.log
51	“	-CO_2Me	PC	TS_CO2Me_B3LYP_6-311++Gdp_forward_trial3.log
52	B3LYP_D3-BJ	-NO2	SC	TS_NO2_F_MeO_B3LYP-D3BJ_back_trial5.log
53	“	-NO2	TS1	TS_NO2_F_MeO_B3LYP-D3BJ.log
54	“	-NO2	MI	TS_NO2_F_MeO_B3LYP-D3BJ_forward.log
55	“	-$COCF_3$	SC	TS_COCF3_B3LYP-D3BJ-6311++Gdp_back_trial4.log
56	“	-$COCF_3$	TS1	TS_COCF3_B3LYP-D3BJ-6311++Gdp_trial4.log
57	“	-$COCF_3$	PC	TS_COCF3_B3LYP-D3BJ-6311++Gdp_forward_trial2.log
58	“	-CN	SC	TS_CN_B3LYP-D3BJ-6311++Gdp_back_trial3.log
59	“	-CN	TS	TS_CN_B3LYP-D3BJ-6311++Gdp.log

Entry	Method[a] (folder name)	-R (sub folder name)	Reaction Coordinate[b]	File name
60	“	-CN	MI	TS_CN_B3LYP-D3BJ-6311++Gdp_forward_trial3.log
61	“	-COMe	SC	TS_COMe_B3LYP-D3BJ-6311++Gdp_back_trial2.log
62	“	-COMe	TS	TS_COMe_B3LYP-D3BJ-6311++Gdp_trial5.log
63	“	-COMe	PC	TS_COMe_B3LYP-D3BJ-6311++Gdp_forward_trial2.log
64	“	-CO_2Me	SC	TS_CO2Me_B3LYP-D3BJ-6311++Gdp_back_trial5.log
65	“	-CO_2Me	TS	TS_CO2Me_B3LYP-D3BJ-6311++Gdp.log
66	“	-CO_2Me	PC	TS_CO2Me_B3LYP-D3BJ-6311++Gdp_forward_trial2_freq.log
67	CAM-B3LYP	-$COCF_3$	SC	TS_COCF3_CAM-B3LYP-6311++Gdp_back_trial2.log
68	“	-$COCF_3$	TS1	TS_COCF3_CAM-B3LYP-6311++Gdp
69	“	-$COCF_3$	MI	TS_COCF3_CAM-B3LYP-6311++Gdp_forward.log
70	“	-CN	SC	TS_CN_CAM-B3LYP-6311++Gdp_back_trial4.log
71	“	-CN	TS	TS_CN_CAM-B3LYP-6311++Gdp.log
72	“	-CN	PC	TS_CN_CAM-B3LYP-6311++Gdp_forward_trial2.log
73	“	-COMe	SC	TS_COMe_CAM-B3LYP-6311++Gdp_back_trail4.log
74	“	-COMe	TS	TS_COMe_CAM-B3LYP-6311++Gdp_trial2.log
75	“	-COMe	PC	TS_COMe_CAM-B3LYP-6311++Gdp_forward_trial2.log
76	“	-CO_2Me	SC	TS_CO2Me_CAM-B3LYP_6-311++Gdp_back.log
77	“	-CO_2Me	TS	TS_CO2Me_CAM-B3LYP_6-311++Gdp.log
78	“	-CO_2Me	PC	TS_CO2Me_CAM-B3LYP_6-311++Gdp_forward_trial2.log
79	BHandHLYP	-$COCF_3$	SC	TS_COCF3_BHandHLYP_6-311++Gdp_back_trial2_freq.log
80	“	-$COCF_3$	TS1	TS_COCF3_BHandHLYP-6-311++Gdp.log
81	“	-$COCF_3$	MI	TS_COCF3_BHandHLYP-6-311++Gdp_forward.log
82	“	-CN	SC	TS_CN_BHandHLYP_6-311++Gdp_back_trial3_freq.log
83	“	-CN	TS	TS_CN_BHandHLYP-6-311++Gdp.log
84	“	-CN	PC	TS_CN_BHandHLYP-6-311++Gdp_forward_trial3.log
85	“	-COMe	SC	TS_COMe_BHandHLYP_6-311++Gdp_back_trial2_freq.log
86	“	-COMe	TS	TS_COMe_BHandHLYP_6-311++Gdp_trial2_freq.log
87	“	-COMe	MI	TS_COMe_BHandHLYP_6-311++Gdp_forward.log
88	“	-CO_2Me	SC	TS_CO2Me_BHandHLYP_6-311++Gdp_back_trial3_freq.log
89	“	-CO_2Me	TS	TS_CO2Me_BHandHLYP_6-311++Gdp.log
90	“	-CO_2Me	PC	TS_CO2Me_BHandHLYP_6-311++Gdp_forward_trial2.log
91	M06L	-$COCF_3$	SC	TS_COCF3_M06L-6311++Gdp_back_trial2.log
92	“	-$COCF_3$	TS1	TS_COCF3_M06L-6311++Gdp.log
93	“	-$COCF_3$	MI	TS_COCF3_M06L-6311++Gdp_forward.log
94	“	-CN	SC	TS_CN_M06L-6311++Gdp_back_trial2.log
95	“	-CN	TS	TS_CN_M06L-6311++Gdp.log
96	“	-CN	PC	TS_CN_M06L-6311++Gdp_forward_trial2.log

Entry	Method[a] (folder name)	-R (sub folder name)	Reaction Coordinate[b]	File name
97	“	-COMe	SC	TS_COMe_M06L-6311++Gdp_back_trial4.log
98	“	-COMe	TS	TS_COMe_M06L-6311++Gdp.log
99	“	-COMe	PC	TS_COMe_M06L-6311++Gdp_forward.log
100	“	-CO_2Me	SC	TS_CO2Me_M06L_6-311++Gdp_back_trial3.log
101	“	-CO_2Me	TS	TS_CO2Me_M06L_6-311++Gdp.log
102	“	-CO_2Me	PC	TS_CO2Me_M06L_6-311++Gdp_forward.log
103	M06	-$COCF_3$	SC	TS_COCF3_M06-6311++Gdp_back.log
104	“	-$COCF_3$	TS1	TS_COCF3_M06-6311++Gdp_trial2.log
105	“	-$COCF_3$	MI	TS_COCF3_M06-6311++Gdp_forward.log
106	“	-CN	SC	TS_CN_M06-6311++Gdp_back_trial2.log
107	“	-CN	TS	TS_CN_M06-6311++Gdp.log
108	“	-CN	PC	TS_CN_M06-6311++Gdp_forward_trial2.log
109	“	-COMe	SC	TS_COMe_M06-6311++Gdp_back_trial4.log
110	“	-COMe	TS	TS_COMe_M06-6311++Gdp_trial2_freq.log
111	“	-COMe	MI	TS_COMe_M06-6311++Gdp_forward.log
112	“	-CO_2Me	SC	TS_CO2Me_M06_6-311++Gdp_back_trial3.log
113	“	-CO_2Me	TS	TS_CO2Me_M06_6-311++Gdp.log
114	“	-CO_2Me	PC	TS_CO2Me_M06_6-311++Gdp_forward_trial3.log
115	M06	-$COCF_3$	SC	TS_COCF3_M062X-6311++Gdp_back_trial5.log
116	“	-$COCF_3$	TS1	TS_COCF3_M062X-6311++Gdp.log
117	“	-$COCF_3$	MI	TS_COCF3_M062X-6311++Gdp_forward.log
118	“	-CN	SC	TS_CN_M062X-6311++Gdp_back.log
119	“	-CN	TS	TS_CN_M062X-6311++Gdp_trial3.log
120	“	-CN	MI	TS_CN_M062X-6311++Gdp_forward_trial2.log
121	“	-COMe	SC	TS_COMe_M062X-6311++Gdp_back_trial3.log
122	“	-COMe	TS	TS_COMe_M062X-6311++Gdp_trial2.log
123	“	-COMe	MI	TS_COMe_M062X-6311++Gdp_forward.log
124	“	-CO_2Me	SC	TS_CO2Me_M062X-6311++Gdp_back.log
125	“	-CO_2Me	TS	TS_CO2Me_M062X-6311++Gdp.log
126	“	-CO_2Me	MI	TS_CO2Me_M062X-6311++Gdp_forward.log
127	“	-CF_3	SC	TS_CF3_M062X-6311++Gdp_back_trial14.log
128	“	-CF_3	TS	TS_CF3_M062X-6311++Gdp_trial2.log
129	“	-CF_3	PC	TS_CF3_M062X-6311++Gdp_forward_trial3.log
130	“	-CCH	SC	TS_CCH_F_MeO_M062X-6311++Gdp_back.log
131	“	-CCH	TS	TS_CCH_F_MeO_M062X-6311++Gdp.log
132	“	-CCH	PC	TS_CCH_F_MeO_M062X-6311++Gdp_forward.log
133	M11	-NO_2	SC	TS_KOMe_NO2_F_M11_6-311++Gdp_back_trial2.log
134	“	-NO_2	TS1	TS_KOMe_NO2_F_M11_6-311++Gdp.log
135	“	-NO_2	MI	TS_KOMe_NO2_F_M11_6-311++Gdp_forward_trial2.log
136	“	-NO_2	TS2	TS2_KOMe_NO2_F_M11_6-311++Gdp_trial8.log
137	“	-NO_2	PC	TS2_KOMe_NO2_F_M11_6-311++Gdp_trial2.log
138	“	-$CHC(CN)_2$	SC	TS_KOMe_CHCCN2_F_M11_6-311++Gdp_back_trial4.log
139	“	-$CHC(CN)_2$	TS1	TS_KOMe_CHCCN2_F_M11_6-311++Gdp.log
140	“	-$CHC(CN)_2$	MI	TS_KOMe_CHCCN2_F_M11_6-311++Gdp_forward.log

Entry	Method[a] (folder name)	-R (sub folder name)	Reaction Coordinate[b]	File name
141	“	-CHC(CN)$_2$	TS2	TS2_KOMe_CHCCN2_F_M11_6-311++Gdp.log
142	“	-CHC(CN)$_2$	PC	TS2_KOMe_CHCCN2_F_M11_6-311++Gdp_forward.log
143	“	-COCF$_3$	SC	TS_COCF3_M11_6-311++Gdp_back_trial2_freq.log
144	“	-COCF$_3$	TS1	TS_COCF3_M11_6-311++Gdp.log
145	“	-COCF$_3$	MI	TS_COCF3_M11_6-311++Gdp_forward.log
146	“	-COCF$_3$	TS2	TS2_COCF3_M11_6-311++Gdp.log
147	“	-COCF$_3$	PC	TS2_COCF3_M11_6-311++Gdp_forward_trial3.log
148	“	-COCF$_3$	IRC+	IRC_TS1_reverse_COCF3_M11_6-311++Gdp.log IRC_TS1_reverse_COCF3_M11_6-311++Gdp_trial2.log IRC_TS1_reverse_COCF3_M11_6-311++Gdp_trial3.log IRC_TS1_reverse_COCF3_M11_6-311++Gdp_trial4.log IRC_TS1_reverse_COCF3_M11_6-311++Gdp_trial5.log IRC_TS1_reverse_COCF3_M11_6-311++Gdp_trial6.log
149	“	-COCF$_3$	IRC-	IRC_TS1_forward_COCF3_M11_6-311++Gdp.log IRC_TS1_forward_COCF3_M11_6-311++Gdp_trial2.log IRC_TS1_forward_COCF3_M11_6-311++Gdp_trial3.log
150	“	-CN	SC	TS_CN_M11_6-311++Gdp_back_trial2.log
151	“	-CN	TS	TS_CN_M11_6-311++Gdp.log
152	“	-CN	PC	TS_CN_M11_6-311++Gdp_forward.log
153	“	-CN	IRC+	IRC_CN_M11_6-311++Gdp_reverse.log IRC_CN_M11_6-311++Gdp_reverse_trial2.log IRC_CN_M11_6-311++Gdp_reverse_trial3.log IRC_CN_M11_6-311++Gdp_reverse_trial4.log
154	“	-CN	IRC-	IRC_CN_M11_6-311++Gdp_forward.log
155	“	-CN	Freq	Intermediate_by_IRC_reverse_CN_M11_6-311++Gdp.log
156	“	-CN	BS	BS2_CN_M11_6-311++Gdp.log BS2_CN_M11_6-311++Gdp_high_res.log
157	“	-COMe	SC	TS_COMe_M11_6-311++Gdp_back_trial2_freq.log
158	“	-COMe	TS	TS_COMe_M11_6-311++Gdp_trial3.log
159	“	-COMe	PC	TS_COMe_M11_6-311++Gdp_forward_trial2.log
160	“	-COMe	IRC+	IRC_COMe_M11_6-311++Gdp_reverse.log IRC_COMe_M11_6-311++Gdp_reverse_trial2.log
161	“	-COMe	IRC-	IRC_COMe_M11_6-311++Gdp_forward.log IRC_COMe_M11_6-311++Gdp_forward_trial2.log
162	“	-COMe	Freq	Intermediate_by_IRC_reverse_COMe_M11_6-311++Gdp.log
163	“	-COMe	BS	BS2_COMe_M11_6-311++Gdp.log BS2_COMe_M11_6-311++Gdp_high_res.log
164	“	-CO$_2$Me	SC	TS_CO2Me_M11_6-311++Gdp_back_trial2.log
165	“	-CO$_2$Me	TS	TS_CO2Me_M11_6-311++Gdp.log
166	“	-CO$_2$Me	PC	TS_CO2Me_M11_6-311++Gdp_forward_trial2.log
167	“	-CO$_2$Me	IRC+	IRC_CO2Me_M11_6-311++Gdp_reverse.log IRC_CO2Me_M11_6-311++Gdp_reverse_trial2.log
168	“	-CO$_2$Me	IRC-	IRC_CO2Me_M11_6-311++Gdp_forward.log
169	PBE0	-COCF$_3$	SC	TS_COCF3_PBE0-6311++Gdp_back_trial4.log
170	“	-COCF$_3$	TS1	TS_COCF3_PBE0-6311++Gdp.log
171	“	-COCF$_3$	MI	TS_COCF3_PBE0-6311++Gdp_forward.log
172	“	-CN	SC	TS_CN_PBE0-6311++Gdp_back_trial3.log

Entry	Method[a] (folder name)	-R (sub folder name)	Reaction Coordinate[b]	File name
173	“	-CN	TS	TS_CN_PBE0-6311++Gdp_trial2.log
174	“	-CN	PC	TS_CN_PBE0-6311++Gdp_forward_trial3.log
175	“	-COMe	SC	TS_COMe_PBE0-6311++Gdp_back_trial4.log
176	“	-COMe	TS	TS_COMe_PBE0-6311++Gdp_trial2_freq.log
177	“	-COMe	PC	TS_COMe_PBE0-6311++Gdp_forward_trial2.log
178	“	-CO_2Me	SC	TS_CO2Me_PBE0_6-311++Gdp_back_trial2.log
179	“	-CO_2Me	TS	TS_CO2Me_PBE0_6-311++Gdp_trial4.log
180	“	-CO_2Me	PC	TS_CO2Me_PBE0_6-311++Gdp_forward_trial3.log
181	PBE0_D3-BJ	-$COCF_3$	SC	TS_COCF3_PBE0-D3BJ_6311++Gdp_back_trial3.log
182	“	-$COCF_3$	TS1	TS_COCF3_PBE0-D3BJ_6311++Gdp.log
183	“	-$COCF_3$	MI	TS_COCF3_PBE0-D3BJ_6311++Gdp_forward.log
184	“	-CN	SC	TS_CN_PBE0-D3BJ_6311++Gdp_back_trial2.log
185	“	-CN	TS	TS_CN_PBE0-D3BJ_6311++Gdp.log
186	“	-CN	PC	TS_CN_PBE0-D3BJ_6311++Gdp_forward_trial2.log
187	“	-COMe	SC	TS_COMe_PBE0-D3BJ_6311++Gdp_back_trial4.log
188	“	-COMe	TS	TS_COMe_PBE0-D3BJ_6311++Gdp_trial2.log
189	“	-COMe	PC	TS_COMe_PBE0-D3BJ_6311++Gdp_back_trial4.log
190	“	-CO_2Me	SC	TS_CO2Me_PBE0-D3BJ_6-311++Gdp_back_trial4.log
191	“	-CO_2Me	TS	TS_CO2Me_PBE0-D3BJ_6-311++Gdp.log
192	“	-CO_2Me	PC	TS_CO2Me_PBE0-D3BJ_6-311++Gdp_forward_trial3.log
193	HSE1PBE	-$COCF_3$	SC	TS_COCF3_HSEH1PBE_6-311++Gdp_back_trial4.log
194	“	-$COCF_3$	TS1	TS_COCF3_HSEH1PBE_6-311++Gdp.log
195	“	-$COCF_3$	MI	TS_COCF3_HSEH1PBE_6-311++Gdp_forward.log
196	“	-CN	SC	TS_HSEH1PBE_6-311++Gdp_back_trial2.log
197	“	-CN	TS	TS_HSEH1PBE_6-311++Gdp.log
198	“	-CN	PC	TS_HSEH1PBE_6-311++Gdp_forward_trial3.log
199	“	-COMe	SC	TS_COMe_HSEH1PBE_6-311++Gdp_back_trial2.log
200	“	-COMe	TS	TS_COMe_HSEH1PBE_6-311++Gdp.log
201	“	-COMe	PC	TS_COMe_HSEH1PBE_6-311++Gdp_forward_trial2.log
202	“	-CO_2Me	SC	TS_CO2Me_HSEH1PBE_6-311++Gdp_back_trial2.log
203	“	-CO_2Me	TS	TS_CO2Me_HSEH1PBE_6-311++Gdp.log
204	“	-CO_2Me	PC	TS_CO2Me_HSEH1PBE_6-311++Gdp_forward_trial2.log
205	B97D	-$COCF_3$	SC	TS_COCF3_B97D_6-311++Gdp_back_trial5.log
206	“	-$COCF_3$	TS1	TS_COCF3_B97D_6-311++Gdp_trial2_freq.log
207	“	-$COCF_3$	PC	TS_COCF3_B97D-6-311++Gdp_forward_trial2.log
208	“	-CN	SC	TS_CN_B97D_6-311++Gdp_back_trial2.log
209	“	-CN	TS	TS_CN_B97D_6-311++Gdp.log
210	“	-CN	PC	TS_CN_B97D_6-311++Gdp_forward_trial2.log
211	“	-COMe	SC	TS_COMe_B97D_6-311++Gdp_back_trial2.log
212	“	-COMe	TS	TS_COMe_B97D_6-311++Gdp.log

Entry	Method[a] (folder name)	-R (sub folder name)	Reaction Coordinate[b]	File name
213	“	-COMe	PC	TS_COMe_B97D_6-311++Gdp_forward_trial2.log
214	“	-CO_2Me	SC	TS_CO2Me_B97D_6-311++Gdp_back_trial2.log
215	“	-CO_2Me	TS	TS_CO2Me_B97D_6-311++Gdp.log
216	“	-CO_2Me	PC	TS_CO2Me_B97D_6-311++Gdp_forward_trial2.log
217	wB97	-$COCF_3$	SC	TS_COCF3_wB97-6-311++Gdp_back.log
218	“	-$COCF_3$	TS1	TS_COCF3_wB97-6-311++Gdp.log
219	“	-$COCF_3$	MI	TS_COCF3_wB97-6-311++Gdp_forward.log
220	“	-CN	SC	TS_CN_wB97_6-311++Gdp_back_trial2_freq.log
221	“	-CN	TS	TS_CN_wB97_6-311++Gdp.log
222	“	-CN	PC	TS_CN_wB97_6-311++Gdp_forward_trial2.log
223	“	-COMe	SC	TS_COMe_wB97_6-311++Gdp_back_trial7.log
224	“	-COMe	TS	TS_COMe_wB97_6-311++Gdp.log
225	“	-COMe	MI	TS_COMe_wB97_6-311++Gdp_forward.log
226	“	-CO_2Me	SC	TS_CO2Me_wB97_6-311++Gdp_back_trial4.log
227	“	-CO_2Me	TS	TS_CO2Me_wB97_6-311++Gdp.log
228	“	-CO_2Me	PC	TS_CO2Me_wB97_6-311++Gdp_forward_trial2.log
229	wB97X	-$COCF_3$	SC	TS_COCF3_wB97X-6-311++Gdp_back_trial4.log
230	“	-$COCF_3$	TS1	TS_COCF3_wB97X-6-311++Gdp.log
231	“	-$COCF_3$	MI	TS_COCF3_wB97X-6-311++Gdp_forward.log
232	“	-CN	SC	TS_CN_wB97X_6-311++Gdp_back_trial2.log
233	“	-CN	TS	TS_CN_wB97X_6-311++Gdp.log
234	“	-CN	PC	TS_CN_wB97X_6-311++Gdp_forward_trial2.log
235	“	-COMe	SC	TS_COMe_wB97X_6-311++Gdp_back_trial2.log
236	“	-COMe	TS	TS_COMe_wB97X_6-311++Gdp.log
237	“	-COMe	PC	TS_COMe_wB97X_6-311++Gdp_forward_trial3.log
238	“	-CO_2Me	SC	TS_CO2Me_wB97X_6-311++Gdp_back_trial2.log
239	“	-CO_2Me	TS	TS_CO2Me_wB97X_6-311++Gdp.log
240	“	-CO_2Me	PC	TS_CO2Me_wB97X_6-311++Gdp_forward.log
241	wB97XD	-$COCF_3$	SC	TS_COCF3_wB97XD-6-311++Gdp_back_trial4.log
242	“	-$COCF_3$	TS1	TS_COCF3_wB97XD-6-311++Gdp.log
243	“	-$COCF_3$	MI	TS_COCF3_wB97XD-6-311++Gdp_forward.log
244	“	-CN	SC	TS_CN_wB97XD-6-311++Gdp_back_trial2.log
245	“	-CN	TS	TS_CN_wB97XD-6-311++Gdp.log
246	“	-CN	PC	TS_CN_wB97XD-6-311++Gdp_forward.log
247	“	-COMe	SC	TS_COMe_wB97XD_6-311++Gdp_back_trial4.log
248	“	-COMe	TS	TS_COMe_wB97XD_6-311++Gdp.log
249	“	-COMe	PC	TS_COMe_wB97XD_6-311++Gdp_forward_trial2.log
250	“	-CO_2Me	SC	TS_CO2Me_wB97XD_6-311++Gdp_back_trial3_freq.log
251	“	-CO_2Me	TS	TS_CO2Me_wB97XD_6-311++Gdp.log
252	“	-CO_2Me	PC	TS_CO2Me_wB97XD_6-311++Gdp_forward_trial2.log

[a] The 6-311++G(d,p) basis set was used unless mentioned otherwise. [b] The reaction coordinate is indicated by the following abbreviations. SC: substrate complex; TS1: first transition state; MI: Meisenheimer intermediate; TS2: second transition state; PC: product complex. Alternatively the type of calculation is stated using the following abbreviation. IRC+: internal reaction coordinate scan towards the products; IRC-: internal reaction coordinate scan

towards the substrates; BS: bond scan; Freq: single point frequency calculation.

Comparison to Literature Reports

The .log files can be found in the following depository: Https://doi.org/10.15129/deef4cea-f279-4afe-82ca-29b88bd30579 {./Mechanistic_Transition/Computational_Model/Comparison_to_Literature_Reports}. The calculations were preformed on M11/6-311++G(d,p)/cpcm(DMF) level of theory.

All files for the calculation shown in Scheme 4-1 are listed in Table S33 below. The activation energy of the S_NAr reaction shown in Scheme 4-1 was calculated with respect to the separated substrates. The counter cation was not included in the computational model. A minor conformational change of the Meisenheimer intermediate was detected along the S_NAr reaction coordinated. The structure 'TS2' in table Table S33 corresponds to the transition state associated with this conformational change.

All files for the calculation shown in Table 4-3 are listed in Table S34 below. If two files are given for the Meisenheimer intermediate (MI) it means that once the MI has been optimised starting form the first transition state (TS1) and once starting from the second transition state (TS2).

Table S33 - File names for structures shown in Scheme 4-1 (./Parker)

Entry	Structure and Comment	Reaction Coordinate[a]	File name
1	Azide anion	-	azide.log
2	**586**	-	Substrate.log
3	Azide anion and **586**	SC	TS_NO2_Azide_back.log
4	Addition of azide on **586**	TS1	TS_NO2_Azide.log
5	-	MI1	TS_NO2_Azide_forward.log
6	Conformational change of MI	TS2	TS2_NO2_Azide_conformation.log
7	-	MI2	TS3_NO2_Azide_back.log
8	Expulsion of fluoride leaving group.	TS3	TS3_NO2_Azide.log
9	Fluoride anion and **588**	PC	TS3_NO2_Azide_forward.log
10	**588**	-	Product.log
11	Fluoride anion	-	fluoride.log

[b] The reaction coordinate is indicated by the following abbreviations. SC: substrate complex; TSx: x^{th} transition state; MIy: Meisenheimer intermediate in conformation y; PC: product complex.

Table S34 - File names for structures shown in Table 4-3 (./Williams)

Entry	Entry in Table 4-3 (Sub Folder)	Reaction Coordinate[a]	File name
1	1 (DMAP-a)	PC	TS_DMAP_4-NO2-PhO_back_trial3.log
2	"	TS1	TS_DMAP_4-NO2-PhO_trial2.log

Entry	Entry in Table 4-3 (Sub Folder)	Reaction Coordinate[a]	File name
3	“	MI	TS_DMAP_4-NO2-PhO_forward.log TS2_DMAP_4-NO2-PhO_back.log
4	“	TS2	TS2_DMAP_4-NO2-PhO_forward.log
5	“	SC	TS2_DMAP_4-NO2-PhO_forward_trial2.log
6	2 (DMAP-a_water)	PC	TS_DMAP_4-NO2-PhO_4_water_back_trial2.log
7	“	TS1	TS_DMAP_4-NO2-PhO_4_water_trial4.log
8	“	MI	TS_DMAP_4-NO2-PhO_4_water_forward_trial2.log TS2_DMAP_4-NO2-PhO_4_water_back.log
9	“	TS2	TS2_DMAP_4-NO2-PhO_4_water_trial2.log
10	“	SC	TS2_DMAP_4-NO2-PhO_4_water_forward.log
11	3 (DMAP-b)	PC	TS_DMAP_4-COH-PhO_back.log
11	“	TS1	TS_DMAP_4-COH-PhO.log
12	“	MI	TS_DMAP_4-COH-PhO_forward.log TS2_DMAP_4-COH-PhO_back.log
13	“	TS2	TS2_DMAP_4-COH-PhO.log
14	“	SC	TS2_DMAP_4-COH-PhO_forward_trial2.log
15	4 (DMAP-c)	PC	TS_DMAP_3-5-di-NO2-PhO_back.log
16	“	TS1	TS_DMAP_3-5-di-NO2-PhO_trial2.log
17	“	MI	TS_DMAP_3-5-di-NO2-PhO_forward.log TS2_DMAP_3-5-di-NO2-PhO_back.log
18	“	TS2	TS2_DMAP_3-5-di-NO2-PhO.log
19	“	SC	TS2_DMAP_3-5-di-NO2-PhO_forward.log
20	5 (Morpholien-a_1)	PC	TS_Morpholine_4-NO2-PhO_back.log
21	“	TS1	TS_Morpholine_4-NO2-PhO.log
22	“	MI	TS_Morpholine_4-NO2-PhO_forward.log TS2_Morpholine_4-NO2-PhO_back.log
23	“	TS2	TS2_Morpholine_4-NO2-PhO.log
24	“	SC	TS2_Morpholine_4-NO2-PhO_forward.log
25	5 (Morpholien-a_1)	PC	TS_Morpholine_4-NO2-PhO_var2_back_trial3.log
26	“	TS1	TS_Morpholine_4-NO2-PhO_var2.log
27	“	MI	TS_Morpholine_4-NO2-PhO_var2_forward.log TS2_Morpholine_4-NO2-PhO_var2_back.log
28	“	TS2	TS2_Morpholine_4-NO2-PhO_var2.log
29	“	SC	TS2_Morpholine_4-NO2-PhO_var2_forward_trial2.log

[a] The reaction coordinate is indicated by the following abbreviations. SC: substrate complex; TS1: first transition state; MI: Meisenheimer intermediate; TS2: second transition state; PC: product complex.

5.5.4 Computational Results for Chapter 4.2.3

The .log files can be found in the following repository: Https://doi.org/10.15129/deef4cea-f279-4afe-82ca-29b88bd30579 {./Mechanistic_Transition/Understanding_the_Mech_Trans}. The calculations of this section were calculated on M11/6-311++G(d,p)/cpcm(DMF) level of theory. For each example the substrate complex (‘SC’), rate limiting transition state (‘TS1’), and product complex (‘PC’) or Meisenheimer intermediate (‘MI’) as appropriate, was calculated. For selected examples also the second transition (‘TS2’) state was calculated.

The .log files for the calculations shown in Figure 4-4 for the displacement of the halides fluoride, chloride, bromide and iodide by potassium methoxide from **595** are listed in below in Table S35 and can be found in the sub directory ./Displacements/KOMe-X.

Table S35- File names for structures shown in Figure 4-4 (./Displacements/KOMe-X)

Entry	X	-R (sub folder)	Reaction Coordinate[a]	File name
1	F	-NO	SC	TS_KOMe_NO_F_M11_6-311++Gdp_back_trial2.log
2	"	"	TS1	TS_KOMe_NO_F_M11_6-311++Gdp.log
3	"	"	MI	TS_KOMe_NO_F_M11_6-311++Gdp_forward.log
4	"	"	TS2	TS2_KOMe_NO_F_M11_6-311++Gdp.log
5	"	"	PC	TS2_KOMe_NO_F_M11_6-311++Gdp_forward.log
6	"	-NO2	SC	TS_KOMe_NO2_F_M11_6-311++Gdp_back_trial2.log
7	"	"	TS1	TS_KOMe_NO2_F_M11_6-311++Gdp.log
8	"	"	MI	TS_KOMe_NO2_F_M11_6-311++Gdp_forward_trial2.log
9	"	"	TS2	TS2_KOMe_NO2_F_M11_6-311++Gdp_trial8.log
10	"	"	PC	TS2_KOMe_NO2_F_M11_6-311++Gdp_trial2.log
11	"	-CHCCN2	SC	TS_KOMe_CHCCN2_F_M11_6-311++Gdp_back_trial4.log
11	"	"	TS1	TS_KOMe_CHCCN2_F_M11_6-311++Gdp.log
12	"	"	MI	TS_KOMe_CHCCN2_F_M11_6-311++Gdp_forward.log
13	"	"	TS2	TS2_KOMe_CHCCN2_F_M11_6-311++Gdp.log
14	"	"	PC	TS2_KOMe_CHCCN2_F_M11_6-311++Gdp_forward.log
15	"	-COCF3	SC	TS_COCF3_M11_6-311++Gdp_back_trial2_freq.log
16	"	"	TS1	TS_COCF3_M11_6-311++Gdp.log
17	"	"	MI	TS_COCF3_M11_6-311++Gdp_forward.log
18	"	"	TS2	TS2_KOMe_NO2_F_M11_6-311++Gdp_trial8.log
19	"	"	PC	TS2_COCF3_M11_6-311++Gdp_forward_trial3.log
20	"	-CN	SC	TS_CN_M11_6-311++Gdp_back_trial2.log
21	"	"	TS1	TS_CN_M11_6-311++Gdp.log
22	"	"	PC	TS_CN_M11_6-311++Gdp_forward.log
23	"	-COMe	SC	TS_COMe_M11_6-311++Gdp_back_trial2_freq.log
24	"	"	TS1	TS_COMe_M11_6-311++Gdp_trial3.log
25	"	"	PC	TS_COMe_M11_6-311++Gdp_forward_trial2.log
26	"	-CO2Me	SC	TS_CO2Me_M11_6-311++Gdp_back_trial2.log
27	"	"	TS1	TS_CO2Me_M11_6-311++Gdp.log
28	"	"	PC	TS_CO2Me_M11_6-311++Gdp_forward_trial2.log
29	"	-CF3	SC	TS_KOMe_CF3_F_M11_6-311++Gdp_back_trial2.log
30	"	"	TS1	TS_KOMe_CF3_F_M11_6-311++Gdp.log
31	"	"	PC	TS_KOMe_CF3_F_M11_6-311++Gdp_forward_trial2.log
32	"	-CCH	SC	TS_KOMe_CCH_F_M11_6-311++Gdp_back_trial2.log
33	"	"	TS1	TS_KOMe_CCH_F_M11_6-311++Gdp.log
34	"	"	PC	TS_KOMe_CCH_F_M11_6-311++Gdp_forward_trial2.log
35	"	-H	SC	TS_KOMe_H_F_M11_6-311++Gdp_back_trial2.log
36	"	"	TS1	TS_KOMe_H_F_M11_6-311++Gdp.log
37	"	"	PC	TS_KOMe_H_F_M11_6-311++Gdp_forward_trial2.log
38	Cl	-NO	SC	TS_KOMe-Cl_NO_M11_6-311++Gdp_back_trial3.log

Entry	X	-R (sub folder)	Reaction Coordinate[a]	File name
39	“	“	TS1	TS_KOMe-Cl_NO_M11_6-311++Gdp.log
40	“	“	PC	TS_KOMe-Cl_NO_M11_6-311++Gdp_forward_trial2.log
41	“	-NO2	SC	TS_KOMe-Cl_NO2_M11_6-311++Gdp_back_trial2.log
42	“	“	TS1	TS_KOMe-Cl_NO2_M11_6-311++Gdp.log
43	“	“	PC	TS_KOMe-Cl_NO2_M11_6-311++Gdp_forward_trial2.log
44	“	-CHCCN2	SC	TS_KOMe-Cl_CHCCN2_M11_6-311++Gdp_back_trial3.log
45	“	“	TS1	TS_KOMe-Cl_CHCCN2_M11_6-311++Gdp.log
46	“	“	PC	TS_KOMe-Cl_CHCCN2_M11_6-311++Gdp_forward_trial2.log
47	“	-COCF3	SC	TS_KOMe-Cl_COCF3_M11_6-311++Gdp_back_trial4_freq.log
48	“	“	TS1	TS_KOMe-Cl_COCF3_M11_6-311++Gdp_trial4.log
49	“	“	PC	TS_KOMe-Cl_COCF3_M11_6-311++Gdp_forward_trial2.log
50	“	-CN	SC	TS_KOMe-Cl_CN_M11_6-311++Gdp_back_trial2_freq.log
51	“	“	TS1	TS_KOMe-Cl_CN_M11_6-311++Gdp.log
52	“	“	PC	TS_KOMe-Cl_CN_M11_6-311++Gdp_forward_trial3.log
53	“	-COMe	SC	TS_KOMe-Cl_COMe_M11_6-311++Gdp_back_trial2.log
54	“	“	TS1	TS_KOMe-Cl_COMe_M11_6-311++Gdp_trial2.log
55	“	“	PC	TS_KOMe-Cl_COMe_M11_6-311++Gdp_forward_trial4.log
56	“	-CO2Me	SC	TS_KOMe-Cl_CO2Me_M11_6-311++Gdp_back_trial2_freq.log
57	“	“	TS1	TS_KOMe-Cl_CO2Me_M11_6-311++Gdp.log
58	“	“	PC	TS_KOMe-Cl_CO2Me_M11_6-311++Gdp_forward_trial2.log
59	“	-CF3	SC	TS_KOMe-Cl_CF3_M11_6-311++Gdp_back_trail2.log
60	“	“	TS1	TS_KOMe-Cl_CF3_M11_6-311++Gdp.log
61	“	“	PC	TS_KOMe-Cl_CF3_M11_6-311++Gdp_forward_trial2.log
62	“	-CCH	SC	TS_KOMe-Cl_CCH_M11_6-311++Gdp_back_trial2.log
63	“	“	TS1	TS_KOMe-Cl_CCH_M11_6-311++Gdp.log
64	“	“	PC	TS_KOMe-Cl_CCH_M11_6-311++Gdp_forward_trial3.log
65	“	-H	SC	TS_KOMe-Cl_H_M11_6-311++Gdp_back_trial2.log
66	“	“	TS1	TS_KOMe-Cl_H_M11_6-311++Gdp.log
67	“	“	PC	TS_KOMe-Cl_H_M11_6-311++Gdp_forward_trial2.log
68	Br	-NO	SC	TS_KOMe-Br_NO_M11_6-311++Gdp_back.log
69	“	“	TS1	TS_KOMe-Br_NO_M11_6-311++Gdp.log
70	“	“	PC	TS_KOMe-Br_NO_M11_6-311++Gdp_forward.log
71	“	-NO2	SC	TS_KOMe-Br_NO2_M11_6-311++Gdp_back.log
72	“	“	TS1	TS_KOMe-Br_NO2_M11_6-311++Gdp.log
73	“	“	PC	TS_KOMe-Br_NO2_M11_6-311++Gdp_forward.log
74	I	-NO	SC	TS_KOMe-I_NO_M11_6-311++Gdp_back.log
75	“	“	TS1	TS_KOMe-I_NO_M11_6-311++Gdp_trial2.log
76	“	“	PC	TS_KOMe-I_NO_M11_6-311++Gdp_forward.log
77	“	-NO2	SC	TS_KOMe-I_NO2_M11_6-311++Gdp_back.log
78	“	“	TS1	TS_KOMe-I_NO2_M11_6-311++Gdp_trial2.log
79	“	“	PC	TS_KOMe-I_NO2_M11_6-311++Gdp_forward.log

[a] The reaction coordinate is indicated by the following abbreviations. SC: substrate complex; TS1: first transition state; MI: Meisenheimer intermediate; TS2: second transition state; PC: product complex.

The .log files for the calculations shown in Table 4-4 for the halide exchange reactions are listed in below in Table S36 and can be found in the sub directory ./Displacements/Halide-Halide.

Table S36- File names for structures shown in Table 4-4 (./Displacements/Halide-Halide)

Entry	KY-X	-R (sub folder)	Reaction Coordinate[a]	File name
1	KF-F	-CO2Me	SC	TS_KF-F_CO2Me_M11_6-311++Gdp_back_trial2.log
2	“	“	TS1	TS_KF-F_CO2Me_M11_6-311++Gdp.log
3	“	“	MI	TS_KF-F_CO2Me_M11_6-311++Gdp_forward.log
4	“	-CF3	SC	TS_KF-F_CF3_M11_6-311++Gdp_back_trial2.log
5	“	“	TS1	TS_KF-F_CF3_M11_6-311++Gdp.log
6	“	“	MI	TS_KF-F_CF3_M11_6-311++Gdp_forward.log
7	“	-CCH	SC	TS_KF-F_CCH_M11_6-311++Gdp_back.log
8	“	“	TS1	TS_KF-F_CCH_M11_6-311++Gdp.log
9	“	“	PC	TS_KF-F_CCH_M11_6-311++Gdp_forward_trial2.log
10	“	-NCS	SC	TS_KF-F_NCS_M11_6-311++Gdp_back.log
11	“	“	TS1	TS_KF-F_NCS_M11_6-311++Gdp.log
11	“	“	PC	TS_KF-F_NCS_M11_6-311++Gdp_forward_trial2.log
12	KF-Cl	-NO	SC	TS_KF-Cl_NO_M11_6-311++Gdp_back.log
13	“	“	TS1	TS_KF-Cl_NO_M11_6-311++Gdp.log
14	“	“	PC	TS_KF-Cl_NO_M11_6-311++Gdp_forward.log
15	“	-NO2	SC	TS_KF-Cl_NO2_M11_6-311++Gdp_back.log
16	“	“	TS1	TS_KF-Cl_NO2_M11_6-311++Gdp.log
17	“	“	PC	TS_KF-Cl_NO2_M11_6-311++Gdp_forward.log
18	KF-Br	-NO	SC	TS_KF-Br_NO_M11_6-311++Gdp_back_trial2.log
19	“	“	TS1	TS_KF-Br_NO_M11_6-311++Gdp.log
20	“	“	PC	TS_KF-Br_NO_M11_6-311++Gdp_forward_trial2.log
21	“	-NO2	SC	TS_KF-Br_NO2_M11_6-311++Gdp_back_trial2.log
22	“	“	TS1	TS_KF-Br_NO2_M11_6-311++Gdp.log
23	“	“	PC	TS_KF-Br_NO2_M11_6-311++Gdp_forward.log
24	KF-I	-NO	SC	TS_KF-I_NO_M11_6-311++Gdp_back_trial2.log
25	“	“	TS1	TS_KF-I_NO_M11_6-311++Gdp.log
26	“	“	PC	TS_KF-I_NO_M11_6-311++Gdp_forward.log
27	“	-NO2	SC	TS_KF-I_NO2_M11_6-311++Gdp_back.log
28	“	“	TS1	TS_KF-I_NO2_M11_6-311++Gdp.log
29	“	“	PC	TS_KF-I_NO2_M11_6-311++Gdp_forward.log
30	KCl-Cl	-NO	SC	TS_KCl-Cl_NO_M11_6-311++Gdp_back.log
31	“	“	TS1	TS_KCl-Cl_NO_M11_6-311++Gdp.log
32	“	“	PC	TS_KCl-Cl_NO_M11_6-311++Gdp_forward_trial2.log
33	“	-NO2	SC	TS_KCl-Cl_NO2_M11_6-311++Gdp_back.log
34	“	“	TS1	TS_KCl-Cl_NO2_M11_6-311++Gdp.log
35	“	“	PC	TS_KCl-Cl_NO2_M11_6-311++Gdp_forward.log
36	KCl-Br	-NO	SC	TS_KCl-Br_NO_M11_6-311++Gdp_back.log
37	“	“	TS1	TS_KCl-Br_NO_M11_6-311++Gdp.log
38	“	“	PC	TS_KCl-Br_NO_M11_6-311++Gdp_forward.log
39	“	-NO2	SC	TS_KCl-Br_NO2_M11_6-311++Gdp_back.log
40	“	“	TS1	TS_KCl-Br_NO2_M11_6-311++Gdp.log

Entry	KY-X	-R (sub folder)	Reaction Coordinate[a]	File name
41	“	“	PC	TS_KCl-Br_NO2_M11_6-311++Gdp_forward_trial2.log
42	KCl-I	-NO	SC	TS_KCl-I_NO_M11_6-311++Gdp_back_trial2.log
43	“	“	TS1	TS_KCl-I_NO_M11_6-311++Gdp.log
44	“	“	PC	TS_KCl-I_NO_M11_6-311++Gdp_forward_trial2.log
45	“	-NO2	SC	TS_KCl-I_NO2_M11_6-311++Gdp_back.log
46	“	“	TS1	TS_KCl-I_NO2_M11_6-311++Gdp.log
47	“	“	PC	TS_KCl-I_NO2_M11_6-311++Gdp_forward_trial2.log
48	KBr-Br	-NO	SC	TS_KBr-Br_NO_M11_6-311++Gdp_back_trial3.log
49	“	“	TS1	TS_KBr-Br_NO_M11_6-311++Gdp.log
50	“	“	PC	TS_KBr-Br_NO_M11_6-311++Gdp_forward_trial2.log
51	“	-NO2	SC	TS_KBr-Br_NO2_M11_6-311++Gdp_back_trial3.log
52	“	“	TS1	TS_KBr-Br_NO2_M11_6-311++Gdp.log
53	“	“	PC	TS_KBr-Br_NO2_M11_6-311++Gdp_forward.log
54	KBr-I	-NO	SC	TS_KBr-I_NO_M11_6-311++Gdp_back_trial2.log
55	“	“	TS1	TS_KBr-I_NO_M11_6-311++Gdp.log
56	“	“	PC	TS_KBr-I_NO_M11_6-311++Gdp_forward.log
57	“	-NO2	SC	TS_KBr-I_NO2_M11_6-311++Gdp_back.log
58	“	“	TS1	TS_KBr-I_NO2_M11_6-311++Gdp.log
59	“	“	PC	TS_KBr-I_NO2_M11_6-311++Gdp_forward.log
60	KI-I	-NO	SC	TS_KI-I_NO2_M11_6-311++Gdp_back.log
61	“	“	TS1	TS_KI-I_NO2_M11_6-311++Gdp.log
62	“	“	PC	TS_KI-I_NO2_M11_6-311++Gdp_forward_trial2.log
63	“	-NO2	SC	TS_KI-I_NO2_M11_6-311++Gdp_back.log
64	“	“	TS1	TS_KI-I_NO2_M11_6-311++Gdp_forward.log
65	“	“	PC	TS_KI-I_NO2_M11_6-311++Gdp.log

[a] The reaction coordinate is indicated by the following abbreviations. SC: substrate complex; TS1: first transition state; MI: Meisenheimer intermediate; TS2: second transition state; PC: product complex.

The .log files for the calculations shown in Table 4-5 for the halide exchange reactions are listed in below in Table S37 and can be found in the sub directory ./Displacements/Chalcogens.

Table S37- File names for structures shown in Table 4-5 (./Displacements/Chalcogens)

Entry	KYMe-XMe	-R (sub folder)	Reaction Coordinate[a]	File name
1	KOMe-OMe	-NHAc	SC	TS_KOMe-OMe_NHCOMe_M11_6-311++Gdp_back
2	“	“	TS1	TS_KOMe-OMe_NHCOMe_M11_6-311++Gdp.log
3	“	“	MI	TS_KOMe-OMe_NHCOMe_M11_6-311++Gdp_forward.log
4	“	-NPPh3	SC	TS_KOMe-OMe_NPPh3_M11_6-311++Gdp_back_trial3.log
5	“	“	TS1	TS_KOMe-OMe_NPPh3_M11_6-311++Gdp_trial2.log
6	“	“	MI	TS_KOMe-OMe_NPPh3_M11_6-311++Gdp_forward.log
7	KOMe-SMe	-CCH	SC	TS_KOMe-SMe_CCH_M11_6-311++Gdp_back.log

Entry	KYMe-XMe	-R (sub folder)	Reaction Coordinate[a]	File name
8	“	“	TS1	TS_KOMe-SMe_CCH_M11_6-311++Gdp.log
9	“	“	MI	TS_KOMe-SMe_CCH_M11_6-311++Gdp_forward.log TS2_KOMe-SMe_CCH_M11_6-311++Gdp_back.log
10	“	“	TS2	TS2_KOMe-SMe_CCH_M11_6-311++Gdp.log
11	“	“	PC	TS2_KOMe-SMe_CCH_M11_6-311++Gdp_forward.log
11	“	-NCS	SC	TS_KOMe-SMe_NCS_M11_6-311++Gdp_back.log
12	“	“	TS1	TS_KOMe-SMe_NCS_M11_6-311++Gdp.log
13	“	“	MI	TS_KOMe-SMe_NCS_M11_6-311++Gdp_forward.log
14	“	-Cl	SC	TS_KOMe-SMe_Cl_M11_6-311++Gdp_back.log
15	“	“	TS1	TS_KOMe-SMe_Cl_M11_6-311++Gdp.log
16	“	“	PC	TS_KOMe-SMe_Cl_M11_6-311++Gdp_forward.log
17	“	-H	SC	TS_KOMe-SMe_H_M11_6-311++Gdp_back_trial2.log
18	“	“	TS1	TS_KOMe-SMe_H_M11_6-311++Gdp.log
19	“	“	PC	TS_KOMe-SMe_H_M11_6-311++Gdp_forward_trial3.log
20	KOMe-SeMe	-NO2	SC	TS_KOMe-SeMe_NO2_M11_6-311++Gdp_back.log
21	“	“	TS1	TS_KOMe-SeMe_NO2_M11_6-311++Gdp.log
22	“	“	MI	TS_KOMe-SeMe_NO2_M11_6-311++Gdp_forward.log
23	“	-CN	SC	TS_KOMe-SeMe_CN_M11_6-311++Gdp_back.log
24	“	“	TS1	TS_KOMe-SeMe_CN_M11_6-311++Gdp.log
25	“	“	MI	TS_KOMe-SeMe_CN_M11_6-311++Gdp_forward.log
26	“	-COMe	SC	TS_KOMe-SeMe_COMe_M11_6-311++Gdp_back.log
27	“	“	TS1	TS_KOMe-SeMe_COMe_M11_6-311++Gdp.log
28	“	“	MI	TS_KOMe-SeMe_COMe_M11_6-311++Gdp_forward.log
29	“	-CO2Me	SC	TS_KOMe-SeMe_CO2Me_M11_6-311++Gdp_back.log
30	“	“	TS1	TS_KOMe-SeMe_CO2Me_M11_6-311++Gdp_trial2.log
31	“	“	MI	TS_KOMe-SeMe_CO2Me_M11_6-311++Gdp_forward.log
32	“	-CCH	SC	TS_KOMe-SeMe_CCH_M11_6-311++Gdp_back_trial2.log
33	“	“	TS1	TS_KOMe-SeMe_CCH_M11_6-311++Gdp.log
34	“	“	PC	TS_KOMe-SeMe_CCH_M11_6-311++Gdp_forward_trial2.log
35	“	-Cl	SC	TS_KOMe-SeMe_Cl_M11_6-311++Gdp_back.log
36	“	“	TS1	TS_KOMe-SeMe_Cl_M11_6-311++Gdp.log
37	“	“	PC	TS_KOMe-SeMe_Cl_M11_6-311++Gdp_forward.log
38	KSMe-SMe	-C6F5	SC	TS_KSMe-SMe_C6F5_M11_6-311++Gdp_back.log
39	“	“	TS1	TS_KSMe-SMe_C6F5_M11_6-311++Gdp_trial2.log
40	“	“	MI	TS_KSMe-SMe_C6F5_M11_6-311++Gdp_forward.log
41	“	-NCS	SC	TS_KSMe-SMe_NCS_M11_6-311++Gdp_back.log
42	“	“	TS1	TS_KSMe-SMe_NCS_M11_6-311++Gdp.log
43	“	“	MI	TS_KSMe-SMe_NCS_M11_6-311++Gdp_forward.log
44	“	-I	SC	TS_KSMe-SMe_I_M11_6-311++Gdp_back.log
45	“	“	TS1	TS_KSMe-SMe_I_M11_6-311++Gdp.log
46	“	“	PC	TS_KSMe-SMe_I_M11_6-311++Gdp_forward.log
47	“	-Cl	SC	TS_KSMe-SMe_Cl_M11_6-311++Gdp_back.sh
48	“	“	TS1	TS_KSMe-SMe_Cl_M11_6-311++Gdp.log
49	“	“	PC	TS_KSMe-SMe_Cl_M11_6-311++Gdp_forward.log

Entry	KYMe-XMe	-R (sub folder)	Reaction Coordinate[a]	File name
50	KSMe-SeMe	-CHCCN2	SC	TS_KSMe-SeMe_CHCCN2_M11_6-311++Gdp_back.log
51	“	“	TS1	TS_KSMe-SeMe_CHCCN2_M11_6-311++Gdp.log
52	“	“	MI	TS_KSMe-SeMe_CHCCN2_M11_6-311++Gdp_forward.log
53	“	-COCF3	SC	TS_KSMe-SeMe_COCF3_M11_6-311++Gdp_back.log
54	“	“	TS1	TS_KSMe-SeMe_COCF3_M11_6-311++Gdp.log
55	“	“	MI	TS_KSMe-SeMe_COCF3_M11_6-311++Gdp_forward.log
56	“	-CN	SC	TS_KSMe-SeMe_CN_M11_6-311++Gdp_back.log
57	“	“	TS1	TS_KSMe-SeMe_CN_M11_6-311++Gdp_forward.log
58	“	“	PC	TS_KSMe-SeMe_CN_M11_6-311++Gdp_forward.log
59	“	-COMe	SC	TS_KSMe-SeMe_COMe_M11_6-311++Gdp_back_trial2.log
60	“	“	TS1	TS_KSMe-SeMe_COMe_M11_6-311++Gdp.log
61	“	“	PC	TS_KSMe-SeMe_COMe_M11_6-311++Gdp_forward.log
62	KSeMe-SeMe	-COMe	SC	TS_KSeMe-SeMe_COMe_M11_6-311++Gdp_back.log
63	“	“	TS1	TS_KSeMe-SeMe_COMe_M11_6-311++Gdp.log
64	“	“	MI	TS_KSeMe-SeMe_COMe_M11_6-311++Gdp_forward.log
65	“	-CO2Me	SC	TS_KSeMe-SeMe_CO2Me_M11_6-311++Gdp_back.log
66	“	“	TS1	TS_KSeMe-SeMe_CO2Me_M11_6-311++Gdp.log
67	“	“	MI	TS_KSeMe-SeMe_CO2Me_M11_6-311++Gdp_forward.log
68	“	-CF3	SC	TS_KSeMe-SeMe_CF3_M11_6-311++Gdp_back.sh
69	“	“	TS1	TS_KSeMe-SeMe_CF3_M11_6-311++Gdp.log
70	“	“	PC	TS_KSeMe-SeMe_CF3_M11_6-311++Gdp_forward_trial2.log
71	“	-CCH	SC	TS_KSeMe-SeMe_CCH_M11_6-311++Gdp_back_trial2.log
72	“	“	TS1	TS_KSeMe-SeMe_CCH_M11_6-311++Gdp.log
73	“	“	PC	TS_KSeMe-SeMe_CCH_M11_6-311++Gdp_forward_trial2.log

[a] The reaction coordinate is indicated by the following abbreviations. SC: substrate complex; TS1: first transition state; MI: Meisenheimer intermediate; TS2: second transition state; PC: product complex.

Effect of the Counter Cation and Explicit Solvation

The .log files for the calculations shown in Figure 4-5 for the halide exchange reactions are listed in below in Table S38 and can be found in the sub directory ./Counter_Cat_and_Expl_Solvent/Counter_Cat.

Table S38- File names for structures shown in Figure 4-5 (./Counter_Cat_and_Expl_Solvent/Counter_Cat)

Entry	Metal M (sub folder)	-R (sub folder)	Reaction Coordinate[a]	File name
1	Li	-NO	SC	TS_LiOMe_NO_F_M11_6-311++Gdp_back_trial2.log
2	“	“	TS1	TS_LiOMe_NO_F_M11_6-311++Gdp.log
3	“	“	MI	TS_LiOMe_NO_F_M11_6-311++Gdp_forward.log

Entry	Metal M (sub folder)	-R (sub folder)	Reaction Coordinate[a]	File name
4	“	-NO2	SC	TS_LiOMe_NO2_F_M11_6-311++Gdp_back_trial2.log
5	“	“	TS1	TS_LiOMe_NO2_F_M11_6-311++Gdp_trial2_freq.log
6	“	“	PC	TS_LiOMe_NO2_F_M11_6-311++Gdp_forward.log
7	“	-CHCCN2	SC	TS_LiOMe_CHCCN2_F_M11_6-311++Gdp_back_trial2.log
8	“	“	TS1	TS_LiOMe_CHCCN2_F_M11_6-311++Gdp.log
9	“	“	MI	TS_LiOMe_CHCCN2_F_M11_6-311++Gdp_forward_trial3.log
10	“	-COCF3	SC	TS_LiOMe_COCF3_M11_6-311++Gdp_back_trial2.log
11	“	“	TS1	TS_LiOMe_COCF3_M11_6-311++Gdp.log
11	“	“	PC	TS_LiOMe_COCF3_M11_6-311++Gdp_forward_trial2.log
12	“	-CN	SC	TS_LiOMe_CN_M11_6-311++Gdp_back_trial2.log
13	“	“	TS1	TS_LiOMe_CN_M11_6-311++Gdp.log
14	“	“	PC	TS_LiOMe_CN_M11_6-311++Gdp_forward_trial2.log
15	“	-COMe	SC	TS_LiOMe_COMe_M11_6-311++Gdp_back_trial2_freq.log
16	“	“	TS1	TS_LiOMe_COMe_M11_6-311++Gdp_trail2.log
17	“	“	PC	TS_LiOMe_COMe_M11_6-311++Gdp_forward.log
18	“	-CO2Me	SC	TS_LiOMe_CO2Me_M11_6-311++Gdp_back_trial3.log
19	“	“	TS1	TS_LiOMe_CO2Me_M11_6-311++Gdp_trial2_freq.log
20	“	“	PC	TS_LiOMe_CO2Me_M11_6-311++Gdp_forward_trial2.log
21	Na	-NO2	SC	TS_NaOMe_NO2_F_M11_6-311++Gdp_back_trial2.log
22	“	“	TS1	TS_NaOMe_NO2_F_M11_6-311++Gdp_trial2_freq.log
23	“	“	MI	TS_NaOMe_NO2_F_M11_6-311++Gdp_forward.log
24	“	-CHCCN2	SC	TS_NaOMe_CHCCN2_F_M11_6-311++Gdp_back_trial3_freq.log
25	“	“	TS1	TS_NaOMe_CHCCN2_F_M11_6-311++Gdp.log
26	“	“	MI	TS_NaOMe_CHCCN2_F_M11_6-311++Gdp_forward.log
27	“	-COCF3	SC	TS_NaOMe_COCF3_M11_6-311++Gdp_back_trial4.log
28	“	“	TS1	TS_NaOMe_COCF3_M11_6-311++Gdp.log
29	“	“	MI	TS_NaOMe_COCF3_M11_6-311++Gdp_forward.log
30	“	-CN	SC	TS_NaOMe_CN_M11_6-311++Gdp_back_trial3.log
31	“	“	TS1	TS_NaOMe_CN_M11_6-311++Gdp.log
32	“	“	PC	TS_NaOMe_CN_M11_6-311++Gdp_forward.log
33	“	-COMe	SC	TS_NaOMe_COMe_M11_6-311++Gdp_back_trial3_freq.log
34	“	“	TS1	TS_NaOMe_COMe_M11_6-311++Gdp_trial3_freq.log
35	“	“	PC	TS_NaOMe_COMe_M11_6-311++Gdp_forward.log
36	“	-CO2Me	SC	TS_NaOMe_CO2Me_M11_6-311++Gdp_back.log
37	“	“	TS1	TS_NaOMe_CO2Me_M11_6-311++Gdp.log
38	“	“	PC	TS_NaOMe_CO2Me_M11_6-311++Gdp_forward.log
39	K	-NO	SC	TS_KOMe_NO_F_M11_6-311++Gdp_back_trial2.log
40	“	“	TS1	TS_KOMe_NO_F_M11_6-311++Gdp.log
41	“	“	MI	TS_KOMe_NO_F_M11_6-311++Gdp_forward.log
42	“	“	TS2	TS2_KOMe_NO_F_M11_6-311++Gdp.log
43	“	“	PC	TS2_KOMe_NO_F_M11_6-311++Gdp_forward.log
44	“	-NO2	SC	TS_KOMe_NO2_F_M11_6-311++Gdp_back_trial2.log
45	“	“	TS1	TS_KOMe_NO2_F_M11_6-311++Gdp.log
46	“	“	MI	TS_KOMe_NO2_F_M11_6-311++Gdp_forward_trial2.log

Entry	Metal M (sub folder)	-R (sub folder)	Reaction Coordinate[a]	File name
47	“	“	TS2	TS2_KOMe_NO2_F_M11_6-311++Gdp_trial8.log
48	“	“	PC	TS2_KOMe_NO2_F_M11_6-311++Gdp_trial2.log
49	“	-CHCCN2	SC	TS_KOMe_CHCCN2_F_M11_6-311++Gdp_back_trial4.log
50	“	“	TS1	TS_KOMe_CHCCN2_F_M11_6-311++Gdp.log
51	“	“	MI	TS_KOMe_CHCCN2_F_M11_6-311++Gdp_forward.log
52	“	“	TS2	TS2_KOMe_CHCCN2_F_M11_6-311++Gdp.log
53	“	“	PC	TS2_KOMe_CHCCN2_F_M11_6-311++Gdp_forward.log
54	“	-COCF3	SC	TS_COCF3_M11_6-311++Gdp_back_trial2_freq.log
55	“	“	TS1	TS_COCF3_M11_6-311++Gdp.log
56	“	“	MI	TS_COCF3_M11_6-311++Gdp_forward.log
57	“	“	TS2	TS2_KOMe_NO2_F_M11_6-311++Gdp_trial8.log
58	“	“	PC	TS2_COCF3_M11_6-311++Gdp_forward_trial3.log
59	“	-CN	SC	TS_CN_M11_6-311++Gdp_back_trial2.log
60	“	“	TS1	TS_CN_M11_6-311++Gdp.log
61	“	“	PC	TS_CN_M11_6-311++Gdp_forward.log
62	“	-COMe	SC	TS_COMe_M11_6-311++Gdp_back_trial2_freq.log
63	“	“	TS1	TS_COMe_M11_6-311++Gdp_trial3.log
64	“	“	PC	TS_COMe_M11_6-311++Gdp_forward_trial2.log
65	“	-CO2Me	SC	TS_CO2Me_M11_6-311++Gdp_back_trial2.log
66	“	“	TS1	TS_CO2Me_M11_6-311++Gdp.log
67	“	“	PC	TS_CO2Me_M11_6-311++Gdp_forward_trial2.log
68	“	-CF3	SC	TS_KOMe_CF3_F_M11_6-311++Gdp_back_trial2.log
69	“	“	TS1	TS_KOMe_CF3_F_M11_6-311++Gdp.log
70	“	“	PC	TS_KOMe_CF3_F_M11_6-311++Gdp_forward_trial2.log
71	“	-CCH	SC	TS_KOMe_CCH_F_M11_6-311++Gdp_back_trial2.log
72	“	“	TS1	TS_KOMe_CCH_F_M11_6-311++Gdp.log
73	“	“	PC	TS_KOMe_CCH_F_M11_6-311++Gdp_forward_trial2.log
74	“	-H	SC	TS_KOMe_H_F_M11_6-311++Gdp_back_trial2.log
75	“	“	TS1	TS_KOMe_H_F_M11_6-311++Gdp.log
76	“	“	PC	TS_KOMe_H_F_M11_6-311++Gdp_forward_trial2.log
77	Rb	-NO	SC	TS_RbOMe_NO_F_M11_6-311++Gdp_back.log
78	“	“	TS1	TS_RbOMe_NO_F_M11_6-311++Gdp.log
79	“	“	MI	TS_RbOMe_NO_F_M11_6-311++Gdp_forward.log
80	“	-NO2	SC	TS_RbOMe_NO2_F_M11_6-311++Gdp_back_trial5.log
81	“	“	TS1	TS_RbOMe_NO2_F_M11_6-311++Gdp.log
82	“	“	MI	TS_RbOMe_NO2_F_M11_6-311++Gdp_forward.log
83	“	-CHCCN2	SC	TS_RbOMe_CHCCN2_F_M11_6-311++Gdp_back_trial8_freq_on_step23.log
84	“	“	TS1	TS_RbOMe_CHCCN2_F_M11_6-311++Gdp.log
85	“	“	MI	TS_RbOMe_CHCCN2_F_M11_6-311++Gdp_forward.log
86	“	-COCF3	SC	TS_RbOMe_COCF3_M11_6-311++Gdp_back_trial3.log
87	“	“	TS1	TS_RbOMe_COCF3_M11_6-311++Gdp.log
88	“	“	MI	TS_RbOMe_COCF3_M11_6-311++Gdp_forward.log
89	“	-CN	SC	TS_RbOMe_CN_M11_6-311++Gdp_back_trial2.log
90	“	“	TS1	TS_RbOMe_CN_M11_6-311++Gdp.log
91	“	“	PC	TS_RbOMe_CN_M11_6-311++Gdp_forward.log

Entry	Metal M (sub folder)	-R (sub folder)	Reaction Coordinate[a]	File name
92	“	-COMe	SC	TS_RbOMe_COMe_M11_6-311++Gdp_back_trial5.log
93	“	“	TS1	TS_RbOMe_COMe_M11_6-311++Gdp_forward_trial2.log
94	“	“	MI	TS_RbOMe_COMe_M11_6-311++Gdp_forward_trial2.log
95	“	-CO2Me	SC	TS_RbOMe_CO2Me_M11_6-311++Gdp_back.log
96	“	“	TS1	TS_RbOMe_CO2Me_M11_6-311++Gdp.log
97	“	“	PC	TS_RbOMe_CO2Me_M11_6-311++Gdp_forward.log
98	“	-CF3	SC	TS_RbOMe_CF3_F_M11_6-311++Gdp_back.log
99	“	“	TS1	TS_RbOMe_CF3_F_M11_6-311++Gdp.log
100	“	“	PC	TS_RbOMe_CF3_F_M11_6-311++Gdp_forward_trial2.log
101	“	-CCH	SC	TS_RbOMe_CCH_F_M11_6-311++Gdp_back.log
102	“	“	TS1	TS_RbOMe_CCH_F_M11_6-311++Gdp.log
103	“	“	PC	TS_RbOMe_CCH_F_M11_6-311++Gdp_forward_trial2.log
104	“	-H	SC	TS_RbOMe_H_F_M11_6-311++Gdp_back_trial2.log
105	“	“	TS1	TS_RbOMe_H_F_M11_6-311++Gdp.log
106	“	“	PC	TS_RbOMe_H_F_M11_6-311++Gdp_forward_trial2.log
107	Cs	-NO	SC	TS_CsOMe_NO_F_M11_6-311++Gdp_back.log
108	“	“	TS1	TS_CsOMe_NO_F_M11_6-311++Gdp_forward.log
109	“	“	MI	TS_CsOMe_NO_F_M11_6-311++Gdp_forward.log
110	“	-NO2	SC	TS_CsOMe_NO2_F_M11_6-311++Gdp_back_trial2.log
111	“	“	TS1	TS_CsOMe_NO2_F_M11_6-311++Gdp.log
112	“	“	MI	TS_CsOMe_NO2_F_M11_6-311++Gdp_forward.log
113	“	-CHCCN2	SC	TS_CsOMe_CHCCN2_F_M11_6-311++Gdp_back_trial2.log
114	“	“	TS1	TS_CsOMe_CHCCN2_F_M11_6-311++Gdp.log
115	“	“	MI	TS_CsOMe_CHCCN2_F_M11_6-311++Gdp_forward.log
116	“	-COCF3	SC	TS_CsOMe_COCF3_M11_6-311++Gdp_back_trial3.log
117	“	“	TS1	TS_CsOMe_COCF3_M11_6-311++Gdp.log
118	“	“	MI	TS_CsOMe_COCF3_M11_6-311++Gdp_forward.log
119	“	-CN	SC	TS_CsOMe_CN_M11_6-311++Gdp_back_trial2.log
120	“	“	TS1	TS_CsOMe_CN_M11_6-311++Gdp_forward_trial3.log
121	“	“	PC	TS_CsOMe_CN_M11_6-311++Gdp_forward_trial3.log
122	“	-COMe	SC	TS_CsOMe_COMe_M11_6-311++Gdp_back.log
123	“	“	TS1	TS_CsOMe_COMe_M11_6-311++Gdp_trial3_freq.log
124	“	“	Mi	TS_CsOMe_COMe_M11_6-311++Gdp_forward.log
125	“	-CO2Me	SC	TS_CsOMe_CO2Me_M11_6-311++Gdp_back.log
126	“	“	TS1	TS_CsOMe_CO2Me_M11_6-311++Gdp.log
127	“	“	PC	TS_CsOMe_CO2Me_M11_6-311++Gdp_forward.log
128	“	-CF3	SC	TS_CsOMe_CF3_F_M11_6-311++Gdp_back.log
129	“	“	TS1	TS_CsOMe_CF3_F_M11_6-311++Gdp.log
130	“	“	PC	TS_CsOMe_CF3_F_M11_6-311++Gdp_forward.log
131	“	-CCH	SC	TS_CsOMe_CCH_F_M11_6-311++Gdp_back.log
132	“	“	TS1	TS_CsOMe_CCH_F_M11_6-311++Gdp.log
133	“	“	PC	TS_CsOMe_CCH_F_M11_6-311++Gdp_forward.log
134	“	-H	SC	TS_CsOMe_H_F_M11_6-311++Gdp_back.log
135	“	“	TS1	TS_CsOMe_H_F_M11_6-311++Gdp.log
136	“	“	PC	TS_CsOMe_H_F_M11_6-311++Gdp_forward_trial2.log
137	none	-COCF3	SC	TS_OMe_COCF3_M11_6-311++Gdp_back_trial2.log

Entry	Metal M (sub folder)	-R (sub folder)	Reaction Coordinate[a]	File name
138	“	“	TS1	TS_OMe_COCF3_M11_6-311++Gdp.log
139	“	“	MI	TS_OMe_COCF3_M11_6-311++Gdp_forward.log
140	“	-CN	SC	TS_OMe_CN_M11_6-311++Gdp_back_trial2.log
141	“	“	TS1	TS_OMe_CN_M11_6-311++Gdp.log
142	“	“	MI	TS_OMe_CN_M11_6-311++Gdp_forward.log
143	“	-COMe	SC	TS_OMe_COMe_M11_6-311++Gdp_back_trial2.log
144	“	“	TS1	TS_OMe_COMe_M11_6-311++Gdp_forward.log
145	“	“	MI	TS_OMe_COMe_M11_6-311++Gdp_forward.log
146	“	-CO2Me	SC	TS_OMe_CO2Me_M11_6-311++Gdp_back_trial4.log
147	“	“	TS1	TS_OMe_CO2Me_M11_6-311++Gdp.log
148	“	“	MI	TS_OMe_CO2Me_M11_6-311++Gdp_forward.log
149	“	-CF3	SC	TS_OMe_CF3_F_M11_6-311++Gdp_back_trial2.log
150	“	“	TS1	TS_OMe_CF3_F_M11_6-311++Gdp.log
151	“	“	MI	TS_OMe_CF3_F_M11_6-311++Gdp_forward_trial2.log
152	“	-CCH	SC	TS_OMe_CCH_F_M11_6-311++Gdp_back.log
153	“	“	TS1	TS_OMe_CCH_F_M11_6-311++Gdp.log
154	“	“	PC	TS_OMe_CCH_F_M11_6-311++Gdp_forward_trial3.log
155	“	-H	SC	TS_OMe_H_F_M11_6-311++Gdp_back.log
156	“	“	TS1	TS_OMe_H_F_M11_6-311++Gdp.log
157	“	“	PC	TS_OMe_H_F_M11_6-311++Gdp_forward_trial2.log

[a] The reaction coordinate is indicated by the following abbreviations. SC: substrate complex; TS1: first transition state; MI: Meisenheimer intermediate; TS2: second transition state; PC: product complex.

The .log files for the calculations with explicit solvent molecules shown in Figure 4-6 are listed in below in Table S39 and can be found in the sub directory ./Counter_Cat_and_Expl_Solvent/Expl_Solvent. For the example without explicit solvation see Table S38.

Table S39 - File names for structures shown in Figure 4-6 (./Counter_Cat_and_Expl_Solvent/Expl_Solvent)

Entry	n (sub folder)	-R (sub folder)	Reaction Coordinate[a]	File name
1	1	-CHCCN2	SC	TS_KOMe-F_CHCCN2_1_DMF_M11_6-311++Gdp_back.log
2	“	“	TS1	TS_KOMe-F_CHCCN2_1_DMF_M11_6-311++Gdp.log
3	“	“	MI	TS_KOMe-F_CHCCN2_1_DMF_M11_6-311++Gdp_forward.log
4	“	-COCF3	SC	TS_KOMe-F_COCF3_1_DMF_M11_6-311++Gdp_back.log
5	“	“	TS1	TS_KOMe-F_COCF3_1_DMF_M11_6-311++Gdp.log
6	“	“	MI	TS_KOMe-F_COCF3_1_DMF_M11_6-311++Gdp_forward.log
7	“	-CN	SC	TS_KOMe-F_CN_1_DMF_M11_6-311++Gdp_back_trial2.log
8	“	“	TS1	TS_KOMe-F_CN_1_DMF_M11_6-311++Gdp_trail2.log
9	“	“	PC	TS_KOMe-F_CN_1_DMF_M11_6-311++Gdp_forward_trial2.log
10	“	-COMe	SC	TS_KOMe-F_COMe_1_DMF_M11_6-311++Gdp_back.log
11	“	“	TS1	TS_KOMe-F_COMe_1_DMF_M11_6-311++Gdp.log

Entry	n (sub folder)	-R (sub folder)	Reaction Coordinate[a]	File name
11	“	“	PC	TS_KOMe-F_COMe_1_DMF_M11_6-311++Gdp_forward_trial2.log
12	2	-CHCCN2	SC	TS_KOMe-F_CHCCN2_2_DMF_M11_6-311++Gdp_back.log
13	“	“	TS1	TS_KOMe-F_CHCCN2_2_DMF_M11_6-311++Gdp_trial2.log
14	“	“	MI	TS_KOMe-F_CHCCN2_2_DMF_M11_6-311++Gdp_forward.log
15	“	-COCF3	SC	TS_KOMe-F_COCF3_2_DMF_M11_6-311++Gdp_back.log
16	“	“	TS1	TS_KOMe-F_COCF3_2_DMF_M11_6-311++Gdp_trial2.log
17	“	“	MI	TS_KOMe-F_COCF3_2_DMF_M11_6-311++Gdp_forward.log
18	“	-CN	SC	TS_KOMe-F_CN_2_DMF_M11_6-311++Gdp_back.log
19	“	“	TS1	TS_KOMe-F_CN_2_DMF_M11_6-311++Gdp_trial4.log
20	“	“	PC	TS_KOMe-F_CN_2_DMF_M11_6-311++Gdp_forward_trial2.log
21	“	-COMe	SC	TS_KOMe-F_COMe_2_DMF_M11_6-311++Gdp_back_trial2.log
22	“	“	TS1	TS_KOMe-F_COMe_2_DMF_M11_6-311++Gdp_trial2.log
23	“	“	MI	TS_KOMe-F_COMe_2_DMF_M11_6-311++Gdp_forward.log
24	“	-CO2Me	SC	TS_KOMe-F_CO2Me_2_DMF_M11_6-311++Gdp_back_trial2.log
25	“	“	TS1	TS_KOMe-F_CO2Me_2_DMF_M11_6-311++Gdp.log
26	“	“	MI	TS_KOMe-F_CO2Me_2_DMF_M11_6-311++Gdp_forward.log
27	“	-CF3	SC	TS_KOMe-F_CF3_2_DMF_M11_6-311++Gdp_back.log
28	“	“	TS1	TS_KOMe-F_CF3_2_DMF_M11_6-311++Gdp.log
29	“	“	PC	TS_KOMe-F_CF3_2_DMF_M11_6-311++Gdp_forward.log
30	“	-CCH	SC	TS_KOMe-F_CCH_2_DMF_M11_6-311++Gdp_back.log
31	“	“	TS1	TS_KOMe-F_CCH_2_DMF_M11_6-311++Gdp.log
32	“	“	PC	TS_KOMe-F_CCH_2_DMF_M11_6-311++Gdp_forward.log

[a] The reaction coordinate is indicated by the following abbreviations. SC: substrate complex; TS1: first transition state; MI: Meisenheimer intermediate; TS2: second transition state; PC: product complex.

Effect of the Nucleophile and the Aromatic System

The .log files for the calculations of different nucleophiles shown in Figure 4-7 are listed in below in Table S40 and can be found in the sub directory ./Nucleophiles/Benzene. For the examples with potassium methoxide as the nucleophile see Table S38.

Table S40 - File names for structures shown in Figure 4-7 (./Nucleophiles/Benzene)

Entry	KNu (sub folder)	-R (sub folder)	Reaction Coordinate[a]	File name
1	KSMe	-NO	SC	TS_KSMe-F_NO_M11-6-311++Gdp_back_trial3.log
2	“	“	TS1	TS_KSMe-F_NO_M11-6-311++Gdp.log
3	“	“	MI	TS_KSMe-F_NO_M11-6-311++Gdp_forward_trial2.log
4	“	-NO2	SC	TS_KSMe-F_NO2_M11-6-311++Gdp_back_trial2.log
5	“	“	TS1	TS_KSMe-F_NO2_M11-6-311++Gdp.log
6	“	“	MI	TS_KSMe-F_NO2_M11-6-311++Gdp_forward_trial2.log

Entry	KNu (sub folder)	-R (sub folder)	Reaction Coordinate[a]	File name
7	“	-CHCCN2	SC	TS_KSMe-F_CHCCN2_M11-6-311++Gdp_back_trial6.log
8	“	“	TS1	TS_KSMe-F_CHCCN2_M11-6-311++Gdp.log
9	“	“	MI	TS_KSMe-F_CHCCN2_M11-6-311++Gdp_forward_trial2.log
10	“	-COCF3	SC	TS_KSMe-F_COCF3_M11-6-311++Gdp_back_trial2.log
11	“	“	TS1	TS_KSMe-F_COCF3_M11-6-311++Gdp.log
11	“	“	MI	TS_KSMe-F_COCF3_M11-6-311++Gdp_forward_trial2.log
12	“	“	TS2	TS2_KSMe-F_COCF3_M11-6-311++Gdp.log
13	“	“	PC	TS2_KSMe-F_COCF3_M11-6-311++Gdp_forward_trial2.log
14	“	-CN	SC	TS_KSMe-F_CN_M11-6-311++Gdp_back_trial3.log
15	“	“	TS1	TS_KSMe-F_CN_M11-6-311++Gdp.log
16	“	“	PC	TS_KSMe-F_CN_M11-6-311++Gdp_forward_tria2.log
17	“	-COMe	SC	TS_KSMe-F_COMe_M11-6-311++Gdp_back_trial2.log
18	“	“	TS1	TS_KSMe-F_COMe_M11-6-311++Gdp.log
19	“	“	PC	TS_KSMe-F_COMe_M11-6-311++Gdp.log
20	“	-CO2Me	SC	TS_KSMe-F_CO2Me_M11-6-311++Gdp_back_trial2.log
21	“	“	TS1	TS_KSMe-F_CO2Me_M11-6-311++Gdp.log
22	“	“	PC	TS_KSMe-F_CO2Me_M11-6-311++Gdp_forward_trial2.log
23	“	-CF3	SC	TS_KSMe-F_CF3_M11-6-311++Gdp_back_trial3.log
24	“	“	TS1	TS_KSMe-F_CF3_M11-6-311++Gdp.log
25	“	“	PC	TS_KSMe-F_CF3_M11-6-311++Gdp_forward_trial2_freq.log TS_KSMe-F_CF3_M11-6-311++Gdp_forward_trial2.log
26	“	-CCH	SC	TS_KSMe-F_CCH_M11-6-311++Gdp_back_trial2_freq.log TS_KSMe-F_CCH_M11-6-311++Gdp_back_trial2.log
27	“	“	TS1	TS_KSMe-F_CCH_M11-6-311++Gdp.log
28	“	“	PC	TS_KSMe-F_CCH_M11-6-311++Gdp_forward_trial2.log
29	“	-H	SC	TS_NaSMe-F_H_M11-6-311++Gdp_back_trial3.log
30	“	“	TS1	TS_NaSMe-F_H_M11-6-311++Gdp.log
31	“	“	PC	TS_NaSMe-F_H_M11-6-311++Gdp_forward_trial3.log
32	KN3	-CHCCN2	SC	TS_KN3-F_CHCCN2_M11_6-311++Gdp_back_trial4.log
33	“	“	TS1	TS_KN3-F_CHCCN2_M11_6-311++Gdp.log
34	“	“	MI	TS_KN3-F_CHCCN2_M11_6-311++Gdp_forward.log
35	“	-COCF3	SC	TS_KN3-F_COCF3_M11-6311++Gdp_back.log
36	“	“	TS1	TS_KN3-F_COCF3_M11-6311++Gdp.log
37	“	“	MI	TS_KN3-F_COCF3_M11-6311++Gdp_forward.log
38	“	“	TS2	TS2_KN3-F_COCF3_M11-6311++Gdp.log
39	“	“	PC	TS2_KN3-F_COCF3_M11-6311++Gdp_forward.log
40	“	-CN	SC	TS_KN3-F_CN_M11-6311++Gdp_back.log
41	“	“	TS1	TS_KN3-F_CN_M11-6311++Gdp.log
42	“	“	PC	TS_KN3-F_CN_M11-6311++Gdp_forward_trial2.log
43	“	-COMe	SC	TS_KN3-F_COMe_M11-6311++Gdp_back_trial2.log
44	“	“	TS1	TS_KN3-F_COMe_M11-6311++Gdp.log
45	“	“	PC	TS_KN3-F_COMe_M11-6311++Gdp_forward_trial2.log
46	“	-CO2Me	SC	TS_KN3-F_CO2Me_M11-6311++Gdp_back_trial3.log

Entry	KNu (sub folder)	-R (sub folder)	Reaction Coordinate[a]	File name
47	“	“	TS1	TS_KN3-F_CO2Me_M11-6311++Gdp.log
48	“	“	PC	TS_KN3-F_CO2Me_M11-6311++Gdp_forward.log
49	**601d (Kacac)**	-CHCCN2	SC	TS_Kacac-F_CHCCN2_M11_6-311++Gdp_back.log
50	“	“	TS1	TS_Kacac-F_CHCCN2_M11_6-311++Gdp.log
51	“	“	MI	TS_Kacac-F_CHCCN2_M11_6-311++Gdp_forward.log
52	“	-COCF3	SC	TS_Kacac-F_COCF3_M11_6-311++Gdp_back.log
53	“	“	TS1	TS_Kacac-F_COCF3_M11_6-311++Gdp.log
54	“	“	MI	TS_Kacac-F_COCF3_M11_6-311++Gdp_forward.log
55	“	“	TS2	TS2_Kacac-F_COCF3_M11_6-311++Gdp.log
56	“	“	PC	TS2_Kacac-F_COCF3_M11_6-311++Gdp_forward.log
57	“	-CN	SC	TS_Kacac-F_CN_M11_6-311++Gdp_back.log
58	“	“	TS1	TS_Kacac-F_CN_M11_6-311++Gdp.log
59	“	“	PC	TS_Kacac-F_CN_M11_6-311++Gdp_forward.log
60	“	-COMe	SC	TS_Kacac-F_COMe_M11_6-311++Gdp_back.log
61	“	“	TS1	TS_Kacac-F_COMe_M11_6-311++Gdp.log
62	“	“	PC	TS_Kacac-F_COMe_M11_6-311++Gdp_forward_trial2.log
63	“	-CO2Me	SC	TS_Kacac-F_CO2Me_M11_6-311++Gdp_back_trial2.log
64	“	“	TS1	TS_Kacac-F_CO2Me_M11_6-311++Gdp.log
65	“	“	PC	TS_Kacac-F_CO2Me_M11_6-311++Gdp_forward_trial2.log
66	**601e (KMeldrum)**	-NO	SC	TS_KMeldrum-F_NO2_M11_6-311++Gdp_back.log
67	“	“	TS1	TS_KMeldrum-F_NO2_M11_6-311++Gdp.log
68	“	“	MI	TS_KMeldrum-F_NO2_M11_6-311++Gdp_forward.log
69	“	-NO2	SC	TS_KMeldrum-F_NO2_M11_6-311++Gdp_back.log
70	“	“	TS1	TS_KMeldrum-F_NO2_M11_6-311++Gdp.log
71	“	“	MI	TS_KMeldrum-F_NO2_M11_6-311++Gdp_forward_trial3.log
72	“	-CHCCN2	SC	TS_KMeldrum-F_CHCCN2_M11_6-311++Gdp_back.log
73	“	“	TS1	TS_KMeldrum-F_CHCCN2_M11_6-311++Gdp.log
74	“	“	MI	TS_KMeldrum-F_CHCCN2_M11_6-311++Gdp_forward.log
75	“	“	TS2	TS2_KMeldrum-F_CHCCN2_M11_6-311++Gdp.log
76	“	“	PC	TS2_KMeldrum-F_CHCCN2_M11_6-311++Gdp_forward_trial2.log
77	“	-COCF3	SC	TS_KMeldrum-F_COCF3_M11_6-311++Gdp_back_trial2.log
78	“	“	TS1	TS_KMeldrum-F_COCF3_M11_6-311++Gdp.log
79	“	“	MI	TS_KMeldrum-F_COCF3_M11_6-311++Gdp_forward_trial3.log
80	“	-CN	SC	TS_KMeldrum-F_CN_M11_6-311++Gdp_back.log
81	“	“	TS1	TS_KMeldrum-F_CN_M11_6-311++Gdp.log
82	“	“	PC	TS_KMeldrum-F_CN_M11_6-311++Gdp_forward.log
83	“	-COMe	SC	TS_KMeldrum-F_COMe_M11_6-311++Gdp_back.log
84	“	“	TS1	TS_KMeldrum-F_COMe_M11_6-311++Gdp.log
85	“	“	PC	TS_KMeldrum-F_COMe_M11_6-311++Gdp_forward.log

[a] The reaction coordinate is indicated by the following abbreviations. SC: substrate

complex; TS1: first transition state; MI: Meisenheimer intermediate; TS2: second transition state; PC: product complex.

The .log files for the calculations of different nucleophiles with 2-fluoropyridines shown in Figure 4-9 are listed in below in Table S41 and can be found in the sub directory ./Nucleophiles/2-Pyridine.

Table S41 - File names for structures shown in Figure 4-9 (./Nucleophiles/2-Pyridine)

Entry	KNu (sub folder)	-R (sub folder)	Reaction Coordinate[a]	File name
1	KOMe	-CHCCN2	SC	TS_KOMe-F_CHCCN2_2Pyr_M11-6311++Gdp_back_trial4.log
2	“	“	TS1	TS_KOMe-F_CHCCN2_2Pyr_M11-6311++Gdp.log
3	“	“	MI	TS_KOMe-F_CHCCN2_2Pyr_M11-6311++Gdp_forward.log
4	“	-COCF3	SC	TS_KOMe-F_COCF3_2Pyr_M11-6311++Gdp_back.log
5	“	“	TS1	TS_KOMe-F_COCF3_2Pyr_M11-6311++Gdp.log
6	“	“	MI	TS_KOMe-F_COCF3_2Pyr_M11-6311++Gdp_forward_trial2.log
7	“	-CN	SC	TS_KOMe-F_COCF3_2Pyr_M11-6311++Gdp_forward_trial2.log
8	“	“	TS1	TS_KOMe-F_CN_2Pyr_M11-6311++Gdp.log
9	“	“	MI	TS_KOMe-F_CN_2Pyr_M11-6311++Gdp_forward.log
10	“	-COMe	SC	TS_KOMe-F_COMe_2Pyr_M11-6311++Gdp_back.log
11	“	“	TS1	TS_KOMe-F_COMe_2Pyr_M11-6311++Gdp_trial2.log
11	“	“	MI	TS_KOMe-F_COMe_2Pyr_M11-6311++Gdp_forward_trial5.log
12	“	-CO2Me	SC	TS_KOMe-F_CO2Me_2Pyr_M11-6311++Gdp_back_trial2.log
13	“	“	TS1	TS_KOMe-F_CO2Me_2Pyr_M11-6311++Gdp.log
14	“	“	MI	TS_KOMe-F_CO2Me_2Pyr_M11-6311++Gdp_forward.log
15	“	-CF3	SC	TS_KOMe-F_CF3_2Pyr_M11-6311++Gdp_back.log
16	“	“	TS1	TS_KOMe-F_CF3_2Pyr_M11-6311++Gdp.log
17	“	“	PC	TS_KOMe-F_CF3_2Pyr_M11-6311++Gdp_forward.log
18	“	-CCH	SC	TS_KOMe-F_CCH_2Pyr_M11-6311++Gdp_back_trial2.log
19	“	“	TS1	TS_KOMe-F_CCH_2Pyr_M11-6311++Gdp.log
20	“	“	PC	TS_KOMe-F_CCH_2Pyr_M11-6311++Gdp_forward.log
21	KSMe	-CHCCN2	SC	TS_KSMe-F_CHCCN2_2Pyr_M11-6311++Gdp_back.log
22	“	“	TS1	TS_KSMe-F_CHCCN2_2Pyr_M11-6311++Gdp.log
23	“	“	MI	TS_KSMe-F_CHCCN2_2Pyr_M11-6311++Gdp_forward.log
24	“	-COCF3	SC	TS_KSMe-F_COCF3_2Pyr_M11-6311++Gdp_back.log
25	“	“	TS1	TS_KSMe-F_COCF3_2Pyr_M11-6311++Gdp_trial3.log
26	“	“	MI	TS_KSMe-F_COCF3_2Pyr_M11-6311++Gdp_forward_trial5.log
27	“	-CN	SC	TS_KSMe-F_CN_2Pyr_M11-6311++Gdp_back.log
28	“	“	TS1	TS_KSMe-F_CN_2Pyr_M11-6311++Gdp.log
29	“	“	PC	TS_KSMe-F_CN_2Pyr_M11-6311++Gdp_forward_trial2.log
30	“	-COMe	SC	TS_KSMe-F_COMe_2Pyr_M11-6311++Gdp_back.log

Entry	KNu (sub folder)	-R (sub folder)	Reaction Coordinate[a]	File name
31	“	“	TS1	TS_KSMe-F_COMe_2Pyr_M11-6311++Gdp.log
32	“	“	PC	TS_KSMe-F_COMe_2Pyr_M11-6311++Gdp_forward_trial2.log
33	KN3	-CHCCN2	SC	TS_KN3-F_CHCCN2_2Pyr_M11-6311++Gdp_back.log
34	“	“	TS1	TS_KN3-F_CHCCN2_2Pyr_M11-6311++Gdp_trial2.log
35	“	“	MI	TS_KN3-F_CHCCN2_2Pyr_M11-6311++Gdp_forward.log
36	“	-COCF3	SC	TS_KN3-F_COCF3_2Pyr_M11-6311++Gdp_back.log
37	“	“	TS1	TS_KN3-F_COCF3_2Pyr_M11-6311++Gdp.log
38	“	“	MI	TS_KN3-F_COCF3_2Pyr_M11-6311++Gdp_forward.log
39	“	-CN	SC	TS_KN3-F_CN_2Pyr_M11-6311++Gdp_back_trial2.log
40	“	“	TS1	TS_KN3-F_CN_2Pyr_M11-6311++Gdp.log
41	“	“	PC	TS_KN3-F_CN_2Pyr_M11-6311++Gdp_forward_trial2.log
42	“	-COMe	SC	TS_KN3-F_COMe_2Pyr_M11-6311++Gdp_back_trial2.log
43	“	“	TS1	TS_KN3-F_COMe_2Pyr_M11-6311++Gdp.log
44	“	“	PC	TS_KN3-F_COMe_2Pyr_M11-6311++Gdp_forward_trial3.log
45	“	-CO2Me	SC	TS_KN3-F_CO2Me_2Pyr_M11-6311++Gdp_back.log
46	“	“	TS1	TS_KN3-F_CO2Me_2Pyr_M11-6311++Gdp.log
47	“	“	PC	TS_KN3-F_CO2Me_2Pyr_M11-6311++Gdp_forward.log
48	**601d (Kacac)**	-CHCCN2	SC	TS_Kacac-F_CHCCN2_2Pyr_M11-6311++Gdp_back.log
49	“	“	TS1	TS_Kacac-F_CHCCN2_2Pyr_M11-6311++Gdp.log
50	“	“	MI	TS_Kacac-F_CHCCN2_2Pyr_M11-6311++Gdp_forward.log
51	“	-COCF3	SC	TS_Kacac-F_COCF3_2Pyr_M11-6311++Gdp_back.log
52	“	“	TS1	TS_Kacac-F_COCF3_2Pyr_M11-6311++Gdp.log
53	“	“	MI	TS_Kacac-F_COCF3_2Pyr_M11-6311++Gdp_forward.log
54	“	-CN	SC	TS_Kacac-F_CN_2Pyr_M11-6311++Gdp_back.log
55	“	“	TS1	TS_Kacac-F_CN_2Pyr_M11-6311++Gdp.log
56	“	“	MI	TS_Kacac-F_CN_2Pyr_M11-6311++Gdp_forward.log
57	“	-COMe	SC	TS_Kacac-F_COMe_2Pyr_M11-6311++Gdp_back.log
58	“	“	TS1	TS_Kacac-F_COMe_2Pyr_M11-6311++Gdp.log
59	“	“	PC	TS_Kacac-F_COMe_2Pyr_M11-6311++Gdp_forward_trial2.log
60	“	-CO2Me	SC	TS_Kacac-F_CO2Me_2Pyr_M11-6311++Gdp_back.log
61	“	“	TS1	TS_Kacac-F_CO2Me_2Pyr_M11-6311++Gdp.log
62	“	“	PC	TS_Kacac-F_CO2Me_2Pyr_M11-6311++Gdp_forward.log

[a] The reaction coordinate is indicated by the following abbreviations. SC: substrate complex; TS1: first transition state; MI: Meisenheimer intermediate; TS2: second transition state; PC: product complex.

The .log files for the calculations of different nucleophiles with naphthalene shown in Figure 4-10 are listed in below in Table S42 and can be found in the sub directory ./Nucleophiles/Naphthalene.

Table S42 - File names for structures shown in Figure 4-10 (./Nucleophiles/Naphthalene)

Entry	KNu (sub folder)	-R (sub folder)	Reaction Coordinate[a]	File name
1	KOMe	-CHCCN2	SC	TS_KOMe-F_CHCCN2_Np_M11_6-311++Gdp_back.log
2	“	“	TS1	TS_KOMe-F_CHCCN2_Np_M11_6-311++Gdp.log
3	“	“	MI	TS_KOMe-F_CHCCN2_Np_M11_6-311++Gdp_forward.log
4	“	-COCF3	SC	TS_KOMe-F_COCF3_Np_M11_6-311++Gdp_back.log
5	“	“	TS1	TS_KOMe-F_COCF3_Np_M11_6-311++Gdp.log
6	“	“	MI	TS_KOMe-F_COCF3_Np_M11_6-311++Gdp_back.log
7	“	-CN	SC	TS_KOMe-F_CN_Np_M11_6-311++Gdp_back_trial2.log
8	“	“	TS1	TS_KOMe-F_CN_Np_M11_6-311++Gdp.log
9	“	“	MI	TS_KOMe-F_CN_Np_M11_6-311++Gdp_forward.log
10	“	-COMe	SC	TS_KOMe-F_COMe_Np_M11_6-311++Gdp_back.log
11	“	“	TS1	TS_KOMe-F_COMe_Np_M11_6-311++Gdp.log
11	“	“	MI	TS_KOMe-F_COMe_Np_M11_6-311++Gdp_forward.log
12	“	-CO2Me	SC	TS_KOMe-F_CO2Me_Np_M11_6-311++Gdp_back.log
13	“	“	TS1	TS_KOMe-F_CO2Me_Np_M11_6-311++Gdp.log
14	“	“	MI	TS_KOMe-F_CO2Me_Np_M11_6-311++Gdp_forward.sh
15	“	-CF3	SC	TS_KOMe-F_CF3_Np_M11_6-311++Gdp_back_trial2.log
16	“	“	TS1	TS_KOMe-F_CF3_Np_M11_6-311++Gdp_trial2.log
17	“	“	PC	TS_KOMe-F_CF3_Np_M11_6-311++Gdp_forward_trial2.log
18	“	-CCH	SC	TS_KOMe-F_CCH_Np_M11_6-311++Gdp_back.log
19	“	“	TS1	TS_KOMe-F_CCH_Np_M11_6-311++Gdp.log
20	“	“	PC	TS_KOMe-F_CCH_Np_M11_6-311++Gdp_forward.log
21	KSMe	-CHCCN2	SC	TS_KSMe-F_CHCCN2_Np_M11-6-311++Gdp_back.log
22	“	“	TS1	TS_KSMe-F_CHCCN2_Np_M11-6-311++Gdp.log
23	“	“	MI	TS_KSMe-F_CHCCN2_Np_M11-6-311++Gdp_forward.log
24	“	-COCF3	SC	TS_KSMe-F_COCF3_Np_M11-6-311++Gdp_back_trail3.log
25	“	“	TS1	TS_KSMe-F_COCF3_Np_M11-6-311++Gdp.log
26	“	“	MI	TS_KSMe-F_COCF3_Np_M11-6-311++Gdp_forward_trial2.log
27	“	-CN	SC	TS_KSMe-F_CN_Np_M11-6-311++Gdp_back.log
28	“	“	TS1	TS_KSMe-F_CN_Np_M11-6-311++Gdp.log
29	“	“	PC	TS_KSMe-F_CN_Np_M11-6-311++Gdp_forward_trial3.log
30	“	-COMe	SC	TS_KSMe-F_COMe_Np_M11-6-311++Gdp_back.log
31	“	“	TS1	TS_KSMe-F_COMe_Np_M11-6-311++Gdp.log
32	“	“	MI	TS_KSMe-F_COMe_Np_M11-6-311++Gdp_forward.log
33	“	-CO2Me	SC	TS_KSMe-F_CO2Me_Np_M11-6-311++Gdp_back.log
34	“	“	TS1	TS_KSMe-F_CO2Me_Np_M11-6-311++Gdp_forward.log
35	“	“	PC	TS_KSMe-F_CO2Me_Np_M11-6-311++Gdp_forward.log
36	“	-CF3	SC	TS_KSMe-F_CF3_Np_M11-6-311++Gdp_back.log
37	“	“	TS1	TS_KSMe-F_CF3_Np_M11-6-311++Gdp.log
38	“	“	PC	TS_KSMe-F_CF3_Np_M11-6-311++Gdp_back.log
39	“	-CCH	SC	TS_KSMe-F_CCH_Np_M11-6-311++Gdp_back.log
40	“	“	TS1	TS_KSMe-F_CCH_Np_M11-6-311++Gdp.log
41	“	“	PC	TS_KSMe-F_CCH_Np_M11-6-311++Gdp_forward_trial2.log

Entry	KNu (sub folder)	-R (sub folder)	Reaction Coordinate[a]	File name
42	KN3	-COMe	SC	TS_KN3-F_COMe_Np_M11-6311++Gdp_back.log
43	“	“	TS1	TS_KN3-F_COMe_Np_M11-6311++Gdp_trial2.log
44	“	“	MI	TS_KN3-F_COMe_Np_M11-6311++Gdp_forward.log
45	“	-CO2Me	SC	TS_KN3-F_CO2Me_Np_M11-6311++Gdp_back.log
46	“	“	TS1	TS_KN3-F_CO2Me_Np_M11-6311++Gdp.log
47	“	“	PC	TS_KN3-F_CO2Me_Np_M11-6311++Gdp_forward.log
48	“	-CF3	SC	TS_KN3-F_CF3_Np_M11-6311++Gdp_back.log
49	“	“	TS1	TS_KN3-F_CF3_Np_M11-6311++Gdp.log
50	“	“	PC	TS_KN3-F_CF3_Np_M11-6311++Gdp_forward.log
51	“	-CCH	SC	TS_KN3-F_CCH_Np_M11-6311++Gdp_back.log
52	“	“	TS1	TS_KN3-F_CCH_Np_M11-6311++Gdp.log
53	“	“	PC	TS_KN3-F_CCH_Np_M11-6311++Gdp_forward.log
54	**601d (Kacac)**	-COMe	SC	TS_Kacac-F_COMe_Np_M11_6-311++Gdp_back_trial3.log
55	“	“	TS1	TS_Kacac-F_COMe_Np_M11_6-311++Gdp.log
56	“	“	MI	TS_Kacac-F_COMe_Np_M11_6-311++Gdp_forward.log
57	“	-CO2Me	SC	TS_Kacac-F_CO2Me_Np_M11_6-311++Gdp_back.log
58	“	“	TS1	TS_Kacac-F_CO2Me_Np_M11_6-311++Gdp.log
59	“	“	MI	TS_Kacac-F_CO2Me_Np_M11_6-311++Gdp_forward.log
60	“	-CF3	SC	TS_Kacac-F_CF3_Np_M11_6-311++Gdp_back.log
61	“	“	TS1	TS_Kacac-F_CF3_Np_M11_6-311++Gdp.log
62	“	“	MI	TS_Kacac-F_CF3_Np_M11_6-311++Gdp_forward.log
63	“	-CCH	SC	TS_Kacac-F_CCH_Np_M11_6-311++Gdp_back.log
64	“	“	TS1	TS_Kacac-F_CCH_Np_M11_6-311++Gdp.log
65	“	“	MI	TS_Kacac-F_CCH_Np_M11_6-311++Gdp_forward.log
66	“	-NCS	SC	TS_Kacac-F_NCS_Np_M11_6-311++Gdp_back.log
67	“	“	TS1	TS_Kacac-F_NCS_Np_M11_6-311++Gdp.log
68	“	“	MI	TS_Kacac-F_NCS_Np_M11_6-311++Gdp_forward.log
69	“	-Cl	SC	TS_Kacac-F_Cl_Np_M11_6-311++Gdp_back.log
70	“	“	TS1	TS_Kacac-F_Cl_Np_M11_6-311++Gdp.log
71	“	“	MI	TS_Kacac-F_Cl_Np_M11_6-311++Gdp_forward.log
72	“	-H	SC	TS_Kacac-F_H_Np_M11_6-311++Gdp_back.log
73	“	“	TS1	TS_Kacac-F_H_Np_M11_6-311++Gdp_trial2.log
74	“	“	PC	TS_Kacac-F_H_Np_M11_6-311++Gdp_forward.log
75	“	-Me	SC	TS_Kacac-F_Me_Np_M11_6-311++Gdp_back.log
76	“	“	TS1	TS_Kacac-F_Me_Np_M11_6-311++Gdp.log
77	“	“	MI	TS_Kacac-F_Me_Np_M11_6-311++Gdp_forward.log
78	“	-OMe	SC	TS_Kacac-F_OMe_Np_M11_6-311++Gdp_back.log
79	“	“	TS1	TS_Kacac-F_OMe_Np_M11_6-311++Gdp.log
80	“	“	PC	TS_Kacac-F_OMe_Np_M11_6-311++Gdp_forward.log
81	“	-NHAc	SC	TS_Kacac-F_NHAc_Np_M11_6-311++Gdp_back.log
82	“	“	TS1	TS_Kacac-F_NHAc_Np_M11_6-311++Gdp.log
83	“	“	MI	TS_Kacac-F_NHAc_Np_M11_6-311++Gdp_forward.log

[a] The reaction coordinate is indicated by the following abbreviations. SC: substrate complex; TS1: first transition state; MI: Meisenheimer intermediate; TS2: second transition state; PC: product complex.

The .log files for the calculations of different aromatic systems with the potassium methoxide nucleophile shown in Figure 4-11 are listed in below in Table S43 and can be found in the sub directory ./Nucleophiles. For the examples with the aromatic systems **580**, **603** and **604** see Table S40, Table S41 and Table S42, respectively.

Table S43 - File names for structures shown in Figure 4-11 (./Nucleophiles/)

Entry	Aromatic system (sub folder)	-R (sub folder)	Reaction Coordinate[a]	File name
1	**605 (Pyrimidine)**	-COMe	SC	TS_KOMe-F_COMe_Pyrm_M11-6311++Gdp_back.log
2	“	“	TS1	TS_KOMe-F_COMe_Pyrm_M11-6311++Gdp.log
3	“	“	MI	TS_KOMe-F_COMe_Pyrm_M11-6311++Gdp_forward.log
4	“	-CO2Me	SC	TS_KOMe-F_CO2Me_Pyrm_M11-6311++Gdp_back.log
5	“	“	TS1	TS_KOMe-F_CO2Me_Pyrm_M11-6311++Gdp.log
6	“	“	MI	TS_KOMe-F_CO2Me_Pyrm_M11-6311++Gdp_forward.log
7	“	-CF3	SC	TS_KOMe-F_CF3_Pyrm_M11-6311++Gdp_back.log
8	“	“	TS1	TS_KOMe-F_CF3_Pyrm_M11-6311++Gdp.log
9	“	“	MI	TS_KOMe-F_CF3_Pyrm_M11-6311++Gdp_back.log
10	“	-CCH	SC	TS_KOMe-F_CCH_Pyrm_M11-6311++Gdp_back.log
11	“	“	TS1	TS_KOMe-F_CCH_Pyrm_M11-6311++Gdp.log
11	“	“	MI	TS_KOMe-F_CCH_Pyrm_M11-6311++Gdp_forward.log
12	“	-NCS	SC	TS_KOMe-F_NCS_Pyrm_M11-6311++Gdp_back.log
13	“	“	TS1	TS_KOMe-F_NCS_Pyrm_M11-6311++Gdp.log
14	“	“	MI	TS_KOMe-F_NCS_Pyrm_M11-6311++Gdp_forward.log
15	“	-H	SC	TS_KOMe-F_H_Pyrm_M11-6311++Gdp_back_trial2.log
16	“	“	TS1	TS_KOMe-F_H_Pyrm_M11-6311++Gdp.log
17	“	“	PC	TS_KOMe-F_H_Pyrm_M11-6311++Gdp_forward_trial2.log
18	“	-Me	SC	TS_KOMe-F_Me_Pyrm_M11-6311++Gdp_back.log
19	“	“	TS1	TS_KOMe-F_Me_Pyrm_M11-6311++Gdp_trial2.log
20	“	“	PC	TS_KOMe-F_Me_Pyrm_M11-6311++Gdp_forward.log
21	**606 (Anthracene)**	-CO2Me	SC	TS_KOMe-F_CO2Me_Ant_M11_6-311++Gdp_back.log
22	“	“	TS1	TS_KOMe-F_CO2Me_Ant_M11_6-311++Gdp.log
23	“	“	MI	TS_KOMe-F_CO2Me_Ant_M11_6-311++Gdp_back.log
24	“	-CF3	SC	TS_KOMe-F_CF3_Ant_M11_6-311++Gdp_back.log
25	“	“	TS1	TS_KOMe-F_CF3_Ant_M11_6-311++Gdp_trial4.log
26	“	“	MI	TS_KOMe-F_CF3_Ant_M11_6-311++Gdp_forward.log
27	“	-CCH	SC	TS_KOMe-F_CCH_Ant_M11_6-311++Gdp_back.log
28	“	“	TS1	TS_KOMe-F_CCH_Ant_M11_6-311++Gdp.log
29	“	“	MI	TS_KOMe-F_CCH_Ant_M11_6-311++Gdp_forward.log
30	“	-NCS	SC	TS_KOMe-F_NCS_Ant_M11_6-311++Gdp_back.log
31	“	“	TS1	TS_KOMe-F_NCS_Ant_M11_6-311++Gdp.log
32	“	“	MI	TS_KOMe-F_NCS_Ant_M11_6-311++Gdp_forward.log
33	“	-H	SC	TS_KOMe-F_H_Ant_M11_6-311++Gdp_back.log
34	“	“	TS1	TS_KOMe-F_H_Ant_M11_6-311++Gdp.log

Entry	Aromatic system (sub folder)	-R (sub folder)	Reaction Coordinate[a]	File name
35	“	“	PC	TS_KOMe-F_H_Ant_M11_6-311++Gdp_forward_trial2.log
36	“	-Me	SC	TS_KOMe-F_Me_Ant_M11_6-311++Gdp_back.log
37	“	“	TS1	TS_KOMe-F_Me_Ant_M11_6-311++Gdp.log
38	“	“	PC	TS_KOMe-F_Me_Ant_M11_6-311++Gdp_forward.log

[a] The reaction coordinate is indicated by the following abbreviations. SC: substrate complex; TS1: first transition state; MI: Meisenheimer intermediate; TS2: second transition state; PC: product complex.

Steric Effects

The .log files for the calculations shown in Figure 4-12 are listed in below in Table S44 and can be found in the sub directory ./Sterics. For the examples with the aromatic system **580** see Table S40.

Table S44 - File names for structures shown in Figure 4-12 (./Sterics)

Entry	KNu/Ar (sub folder)	-R (sub folder)	Reaction Coordinate[a]	File name
1	KN3/**607** (Me)	-NO2	SC	TS_KN3-F_NO2_ortho-Me_M11-6311++Gdp_back_trial2.log
2	“	“	TS1	TS_KN3-F_NO2_ortho-Me_M11-6311++Gdp.log
3	“	“	MI	TS_KN3-F_NO2_ortho-Me_M11-6311++Gdp_forward_trial3.log
4	“	-CHCCN2	SC	TS_KN3-F_CHCCN2_ortho-Me_M11_6-311++Gdp_back_trial2.log
5	“	“	TS1	TS_KN3-F_CHCCN2_ortho-Me_M11_6-311++Gdp.log
6	“	“	MI	TS_KN3-F_CHCCN2_ortho-Me_M11_6-311++Gdp_forward.log
7	“	-COCF3	SC	TS_KN3-F_COCF3_ortho_Me_M11-6311++Gdp_back_trial2.log
8	“	“	TS1	TS_KN3-F_COCF3_ortho_Me_M11-6311++Gdp.log
9	“	“	MI	TS_KN3-F_COCF3_ortho_Me_M11-6311++Gdp_forward.log
10	“	-CN	SC	TS_KN3-F_CN_ortho-Me_M11-6311++Gdp_back_trial7.log
11	“	“	TS1	TS_KN3-F_CN_ortho-Me_M11-6311++Gdp.log
11	“	“	PC	TS_KN3-F_CN_ortho-Me_M11-6311++Gdp_forward.log
12		-COMe	SC	TS_KN3-F_COMe_ortho-Me_M11-6311++Gdp_back_trial3.log
13		“	TS1	TS_KN3-F_COMe_ortho-Me_M11-6311++Gdp.log
14		“	PC	TS_KN3-F_COMe_ortho-Me_M11-6311++Gdp_forward.log
15	KN3/ **608** (di-Me)	-NO2	SC	TS_KN3-F_NO2_ortho-di-Me_M11-6311++Gdp_back.log
16	“	“	TS1	TS_KN3-F_NO2_ortho-di-Me_M11-6311++Gdp.log
17	“	“	MI	TS_KN3-F_NO2_ortho-di-Me_M11-6311++Gdp_forward.log
18	“	-CHCCN2	SC	TS_KN3-F_CHCCN2_ortho-di-Me_M11_6-311++Gdp_back.log

Entry	KNu/Ar (sub folder)	-R (sub folder)	Reaction Coordinate[a]	File name
19	“	“	TS1	TS_KN3-F_CHCCN2_ortho-di-Me_M11_6-311++Gdp.log
20	“	“	MI	TS_KN3-F_CHCCN2_ortho-di-Me_M11_6-311++Gdp_forward_trial2.log
21	“	-COCF3	SC	TS_KN3-F_COCF3_ortho_di-Me_M11-6311++Gdp_back.log
22	“	“	TS1	TS_KN3-F_COCF3_ortho_di-Me_M11-6311++Gdp.log
23	“	“	MI	TS_KN3-F_COCF3_ortho_di-Me_M11-6311++Gdp_forward_trial2.log
24	“	-CN	SC	TS_KN3-F_CN_ortho-di-Me_M11-6311++Gdp_back.log
25	“	“	TS1	TS_KN3-F_CN_ortho-di-Me_M11-6311++Gdp.log
26	“	“	PC	TS_KN3-F_CN_ortho-di-Me_M11-6311++Gdp_forward.log
27	“	-COMe	SC	TS_KN3-F_COMe_ortho-di-Me_M11-6311++Gdp_back_trial2.log
28	“	“	TS1	TS_KN3-F_COMe_ortho-di-Me_M11-6311++Gdp.log
29	“	“	PC	TS_KN3-F_COMe_ortho-di-Me_M11-6311++Gdp_forward.log
30	**601d (Kacac)/ 607** (Me)	-CHCCN2	SC	TS_Kacac-F_CHCCN2_ortho-Me_M11_6-311++Gdp_back.log
31	“	“	TS1	TS_Kacac-F_CHCCN2_ortho-Me_M11_6-311++Gdp.log
32	“	“	MI	TS_Kacac-F_CHCCN2_ortho-Me_M11_6-311++Gdp_forward.log
33	“	-COCF3	SC	TS_Kacac-F_COCF3_ortho-Me_M11_6-311++Gdp_back.log
34	“	“	TS1	TS_Kacac-F_COCF3_ortho-Me_M11_6-311++Gdp.log
35	“	“	MI	TS_Kacac-F_COCF3_ortho-Me_M11_6-311++Gdp_forward.log
36	“	-CN	SC	TS_Kacac-F_ortho-Me_CN_M11_6-311++Gdp_back.log
37	“	“	TS1	TS_Kacac-F_ortho-Me_CN_M11_6-311++Gdp.log
38	“	“	PC	TS_Kacac-F_ortho-Me_CN_M11_6-311++Gdp_forward.log
39	“	-COMe	SC	TS_Kacac-F_COMe_ortho-Me_M11_6-311++Gdp_back.log
40	“	“	TS1	TS_Kacac-F_COMe_ortho-Me_M11_6-311++Gdp.log
41	“	“	PC	TS_Kacac-F_COMe_ortho-Me_M11_6-311++Gdp_forward_trial2.log
42	**601d (Kacac)/ 607** (di-Me)	-COCF3	SC	TS_Kacac-F_COCF3_ortho-di-Me_M11_6-311++Gdp_back.log
43	“	“	TS1	TS_Kacac-F_COCF3_ortho-di-Me_M11_6-311++Gdp_forward.log
44	“	“	MI	TS_Kacac-F_COCF3_ortho-di-Me_M11_6-311++Gdp_forward.log
45	“	-CN	SC	TS_Kacac-F_ortho-di-Me_CN_M11_6-311++Gdp_back.log
46	“	“	TS1	TS_Kacac-F_ortho-di-Me_CN_M11_6-311++Gdp.log
47	“	“	MI	TS_Kacac-F_ortho-di-Me_CN_M11_6-311++Gdp_forward.log

Entry	KNu/Ar (sub folder)	-R (sub folder)	Reaction Coordinate[a]	File name
48	“	-COMe	SC	TS_Kacac-F_COMe_ortho-di-Me_M11_6-311++Gdp_back.log
49	“	“	TS1	TS_Kacac-F_COMe_ortho-di-Me_M11_6-311++Gdp.log
50	“	“	Mi	TS_Kacac-F_COMe_ortho-di-Me_M11_6-311++Gdp_forward.log
51	“	-CO2Me	SC	TS_Kacac-F_CO2Me_ortho-di-Me_M11_6-311++Gdp_back.log
52	“	“	TS1	TS_Kacac-F_CO2Me_ortho-di-Me_M11_6-311++Gdp.log
53	“	“	MI	TS_Kacac-F_CO2Me_ortho-di-Me_M11_6-311++Gdp_forward.log
54	“	-CF3	SC	TS_Kacac-F_CF3_ortho-di-Me_M11_6-311++Gdp_back.log
55	“	“	TS1	TS_Kacac-F_CF3_ortho-di-Me_M11_6-311++Gdp.log
56	“	“	MI	TS_Kacac-F_CF3_ortho-di-Me_M11_6-311++Gdp_forward.log
57	“	-CCH	SC	TS_Kacac-F_CCH_ortho-di-Me_M11_6-311++Gdp_back.log
58	“	“	TS1	TS_Kacac-F_CCH_ortho-di-Me_M11_6-311++Gdp.log
59	“	“	MI	TS_Kacac-F_CCH_ortho-di-Me_M11_6-311++Gdp_forward.log
60	“	-NCS	SC	TS_Kacac-F_NCS_ortho-di-Me_M11_6-311++Gdp_back.log
61	“	“	TS1	TS_Kacac-F_NCS_ortho-di-Me_M11_6-311++Gdp.log
62	“	“	MI	TS_Kacac-F_NCS_ortho-di-Me_M11_6-311++Gdp_forward.log
63	“	-Cl	SC	TS_Kacac-F_Cl_ortho-di-Me_M11_6-311++Gdp_back.log
64	“	“	TS1	TS_Kacac-F_Cl_ortho-di-Me_M11_6-311++Gdp.log
65	“	“	MI	TS_Kacac-F_Cl_ortho-di-Me_M11_6-311++Gdp_forward.log
66	“	-H	SC	TS_Kacac-F_H_ortho-di-Me_M11_6-311++Gdp_back.log
67	“	“	TS1	TS_Kacac-F_H_ortho-di-Me_M11_6-311++Gdp.log
68	“	“	MI	TS_Kacac-F_H_ortho-di-Me_M11_6-311++Gdp_forward.log
69	“	-Me	SC	TS_Kacac-F_Me_ortho-di-Me_M11_6-311++Gdp_back.log
70	“	“	TS1	TS_Kacac-F_Me_ortho-di-Me_M11_6-311++Gdp.log
71	“	“	PC	TS_Kacac-F_Me_ortho-di-Me_M11_6-311++Gdp_forward.log
72	“	-OMe	SC	TS_Kacac-F_OMe_ortho-di-Me_M11_6-311++Gdp_back.log
73	“	“	TS1	TS_Kacac-F_OMe_ortho-di-Me_M11_6-311++Gdp.log
74	“	“	PC	TS_Kacac-F_OMe_ortho-di-Me_M11_6-311++Gdp_forward_trial2.log

[a] The reaction coordinate is indicated by the following abbreviations. SC: substrate complex; TS1: first transition state; MI: Meisenheimer intermediate; TS2: second transition state; PC: product complex.

The .log files for the calculations shown in Figure 4-13 and Figure 4-14 can be found in Table S36 and Table S40.

5.5.5 Computational Results for Chapter 4.3

All calculations were performed on M06-2X/6-311++G(d,p) level of theory with the cpcm solvent model for the appropriate solvent. The .log files can be found in the following depository: Https://doi.org/10.15129/deef4cea-f279-4afe-82ca-29b88bd30579 {./Complex_Case_Study}.

The .log files for the calculations shown in Table 4-6 are listed in below in Table S45 and can be found in the sub directory ./SNAr.

Table S45 - File names for structures shown in Table 4-6 (./SNAr/)

Entry	Example	X	Reaction Coordinate[a]	File name
1	A	F	SC	TS_F_back.log
2	“	“	TS1	TS_F.log
3	“	“	PC	TS_F_forward.log
4	“	Cl	SC	TS_Cl_back.log
5	“	“	TS1	TS_Cl.log
6	“	“	PC	TS_Cl_forward.log
7	“	Br	SC	TS_Br_back_trial2.log
8	“	“	TS1	TS_Br.log
9	“	“	PC	TS_Br_forward.log
10	“	I	SC	TS_I_back.log
11	“	“	TS1	TS_I.log
11	“	“	PC	TS_I_forward.log
12	B	F	SC	TS_cSnAr_F_K_back.log
13	“	“	TS1	TS_cSnAr_F_K.log
14	“	“	PC	TS_cSnAr_F_K_forward.log
15	“	Cl	SC	TS_cSnAr_Cl_K_back.log
16	“	“	TS1	TS_cSnAr_Cl_K.log
17	“	“	PC	TS_cSnAr_Cl_K_forward.log
18	“	Br	SC	TS_cSnAr_Br_K_back.log
19	“	“	TS1	TS_cSnAr_Br_K.log
20	“	“	PC	TS_cSnAr_Br_K_forward.log
21	“	I	SC	TS_cSnAr_I_K_back.log
22	“	“	TS1	TS_cSnAr_I_K.log
23	“	“	PC	TS_cSnAr_I_K_forward.log
24	C	F	SC	TS_F_back.log
25	“	“	TS1	TS_F.log
26	“	“	PC	TS_F_forward_trail2.log
27	“	Cl	SC	TS_Cl_back.log
28	“	“	TS1	TS_Cl.log
29	“	“	PC	TS_Cl_forward.log
30	“	Br	SC	TS_Br_back.log
31	“	“	TS1	TS_Br.log
32	“	“	PC	TS_Br_forward.log
33	“	I	SC	TS_I_back.log
34	“	“	TS1	TS_I.log
35	“	“	PC	TS_I_forward.log

[a] The reaction coordinate is indicated by the following abbreviations. SC: substrate complex; TS1: first transition state; PC: product complex.

The .log files for the calculations shown in Table 4-7 are listed in below in Table S46 and can be found in the sub directory ./Benzyne.

Table S46 - File names for structures shown in Table 4-7 (./Benzyne/)

Entry	Example	X	Comment[a]	File name
1	A	F	KOH	KOH.log
2	“	“	SC	TS_F_benzyneformation_K_back.log
3	“	“	TS1	TS_F_benzyneformation_K_trial6.log
4	“	“	I	TS_F_benzyneformation_K_forward.log
5	“	“	TS2	TS2_F_benzyneformation_K_trial2.log
6	“	“	PC	TS2_F_benzyneformation_K_forward.log
7	“	“	KF	KF.log
8	“	Cl	SC	TS_Cl_benzyneformation_K_back.log
9	“	“	TS1	TS_Cl_benzyneformation_K_trial3.log
10	“	“	I	TS_Cl_benzyneformation_K_forward.log
11	“	“	TS2	TS2_Cl_benzyneformation_K.log
11	“	“	PC	TS2_Cl_benzyneformation_K_forward.log
12	“	“	KCl	KCl.log
13	“	Br	SC	TS_Br_benzyneformation_K_back_trial2.log
14	“	“	TS1	TS_Br_benzyneformation_K.log
15	“	“	I	TS_Br_benzyneformation_K_forward.log
16	“	“	TS2	TS2_Br_benzyneformation_K.log
17	“	“	PC	TS2_Br_benzyneformation_K_forward_trial2.log
18	“	“	KBr	KBr.log
19	“	I	SC	TS_I_benzyneformation_K_back.log
20	“	“	TS1	TS_I_benzyneformation_K_trial2.log
21	“	“	I	TS_I_benzyneformation_K_forward.log
22	“	“	TS2	TS2_I_benzyneformation_K_trial4.log
23	“	“	PC	TS2_I_benzyneformation_K_forward.log
24	“	“	KI	KI.log
25	“	Cyclisation	Substrate	TS_cyclisation_benzyne_Bolm2011_back.log
26	“	“	TS1	TS_cyclisation_benzyne_Bolm2011.log
27	“	“	Product	TS_cyclisation_benzyne_Bolm2011_forward.log
28	A	F	SC	TS_F_K_benzynefromation_of_enolate_back_trial8.log
29	“	“	TS1	TS_F_K_benzynefromation_of_enolate_trail2.log
30	“	“	I	TS_F_K_benzynefromation_of_enolate_forward.log
31	“	“	TS2	TS2_F_K_benzynefromation_of_enolate_trial2.log
32	“	“	PC	TS2_F_K_benzynefromation_of_enolate_forward_trial3.log
33	“	Cl	SC	TS_Cl_K_benzynefromation_of_enolate_back.log
34	“	“	TS1	TS_Cl_K_benzynefromation_of_enolate_trial3.log
35	“	“	I	TS_Cl_K_benzynefromation_of_enolate_forward.log
36	“	“	TS2	TS2_Cl_K_benzynefromation_of_enolate.log
37	“	“	PC	TS2_Cl_K_benzynefromation_of_enolate_forward.log
38	“	Br	SC	TS_Br_K_benzynefromation_of_enolate_back.log
39	“	“	TS1	TS_Br_K_benzynefromation_of_enolate_trial2.log

Entry	Example	X	Comment[a]	File name
40	“	“	I	TS_Br_K_benzynefromation_of_enolate_forward.log
41	“	“	TS2	TS2_Br_K_benzynefromation_of_enolate.log
42	“	“	PC	TS2_Br_K_benzynefromation_of_enolate_forward.log
43	“	I	SC	TS_I_K_benzynefromation_of_enolate_back.log
44	“	“	TS1	TS_I_K_benzynefromation_of_enolate_trial2.log
45	“	“	I	TS_I_K_benzynefromation_of_enolate_forward.log
46	“	“	TS2	TS2_I_K_benzynefromation_of_enolate.log
47	“	“	PC	TS2_I_K_benzynefromation_of_enolate_forward_trial2.log TS2_I_K_benzynefromation_of_enolate_proton_shift_trial3.log
48	A	F	SC	TS_F_Benzyne_formationK_back.log
49	“	“	TS1	TS_F_Benzyne_formationK_trial4.log
50	“	“	I	TS_F_Benzyne_formation_forward.log
51	“	“	TS2	TS2_F_Benzyne_formationK.log
52	“	“	PC	TS2_F_Benzyne_formationK_forward.log
53	“	Cl	SC	TS_Cl_Benzyne_formationK_back.log
54	“	“	TS1	TS_Cl_Benzyne_formationK_trial11.log
55	“	“	I	TS_Cl_Benzyne_formationK_forward_trial5.log
56	“	“	TS2	TS2_Cl_Benzyne_formationK.log
57	“	“	PC	TS2_Cl_Benzyne_formationK_forward_trial2.log
58	“	Br	SC	TS_Br_Benzyne_formationK_back.log
59	“	“	TS1	TS_Br_Benzyne_formationK_trial4.log
60	“	“	I	TS_Br_Benzyne_formationK_forward.log
61	“	“	TS2	TS2_Br_Benzyne_formationK.log
62	“	“	PC	TS2_Br_Benzyne_formationK_forward_trial3.log
63	“	I	SC	TS_I_Benzyne_formationK_back.log
64	“	“	TS1	TS_I_Benzyne_formationK.log
65	“	“	I	TS_I_Benzyne_formationK_forward.log
66	“	“	TS2	TS2_I_Benzyne_formationK.log
67	“	“	PC	TS2_I_Benzyne_formationK_forward_trial3_freq.log TS2_I_Benzyne_formationK_forward_trial3_freq.log
68	“	Cyclisation	Substrate	TS_NH_addition_on_benzyne_back.log
69	“	“	TS1	TS_NH_addition_on_benzyne.log
70	“	“	Product	TS_NH_addition_on_benzyne_forward.log

[a] The reaction coordinate is indicated by the following abbreviations. SC: substrate complex; TS1: first transition state; I: Intermediate; TS2: second transition state; PC: product complex.

The .log files for the calculations shown in Table 4-8 are listed in below in Table S47 and can be found in the sub directory ./BHAS_and_SRN1.

Table S47 - File names for structures shown in Table 4-7 (./BHAS_and_SRN1/)

Entry	Example	Step (X)	Comment[a]	File name
1	A	1 (F)	SET	Sbstrt_X-F_neutral.log
2	“	“	SET	Sbstrt_X-F_rad-anion.log
3	“	“	SET	Sbstrt_X-F_neutral_in_rad-anion_geom.log
4	“	“	SET	Sbstrt_X-F_rad-anion_in_neutral_geom.log

Entry	Example	Step (X)	Comment[a]	File name
5	“	“	TS1	TS_F_rad-anion_conformation.log
6	“	“	I	TS_F_rad-anion_conformation_forward.log TS_F_rad-anion_fragmentation_back.log
7	“	“	TS2	TS_F_rad-anion_fragmentation.log
8	“	“	PC	TS_F_rad-anion_fragmentation_forward.log
9	“	1 (Cl)	SET	Sbstrt_X-Cl_neutral.log
10	“	“	SET	Sbstrt_X-Cl_rad-anion_trial4.log
11	“	“	SET	Sbstrt_X-Cl_rad-anion_in_neutral_geom.log
11	“	“	SET	Sbstrt_X-Cl_neutral_in_rad-anion_geom.log
12	“	“	TS1	TS_Cl_rad-anion_fragmentation.log
13	“	“	PC	TS_Cl_rad-anion_fragmentation_forward_trial3.log
14	“	1 (Br)	SET	Sbstrt_X-Br_neutral.log
15	“	“	SET	Sbstrt_X-Br_rad-anion.log
16	“	“	SET	Sbstrt_X-Br_rad-anion_in_neutral_geom.log
17	“	“	SET	Sbstrt_X-Br_neutral_in_rad-anion_geom.log
18	“	1 (I)	SET	Sbstrt_X-I_neutral.log
19	“	“	SET	Sbstrt_X-I_rad-anion_trial3.log
20	“	“	SET	Sbstrt_X-I_rad-anion_in_neutral_geom.log
21	“	“	SET	Sbstrt_X-I_neutral_in_rad-anion_geom.log
22	“	1 (Product)	SET	Product_neutral.log
23	“	“	SET	Product_rad-anion.log
24	“	“	SET	Product_rad-anion_in_neutral_geom.log
25	“	“	SET	Product_neutral_in_rad-anion_geom.log
26	“	2	Substrate	TS_H-abstr_back.log
27	“	“	TS1	TS_H-abstr.log
28	“	“	Product	TS_H-abstr_forward.log
29	“	3	Substrate	TS_Ndot_on_Ph_back.log
30	“	“	TS1	TS_Ndot_on_Ph_trial2.log
31	“	“	Product	TS_Ndot_on_Ph_forward.log
32	“	4	Substrate	TS_deprot_KOH_back.log
33	“	“	TS1	TS_deprot_KOH.log
34	“	“	Product	TS_deprot_KOH_forward.log
35	“	5	(TS1-barrier less)	BS_Deprotonation_Bolm11_trial2.log
36	“	“	PC	TS_Deprotonation_Bolm11_back.log
37	“	6	Substrate	TS_Ar-radical_adding_on_anion_back.log
38	“	“	TS1	TS_Ar-radical_adding_on_anion.log
39	“	“	Product	TS_Ar-radical_adding_on_anion_forward.log
40	B	1 (F)	SET	F_neutral.log
41	“	“	SET	F_rad-anion.log
42	“	“	SET	F_rad-anion.log
43	“	“	SET	F_rad-anion_in_neutral_geom.log
44	“	“	TS1	TS_F_rad-anion_conformation.log
45	“	“	I	TS_F_rad-anion_conformation_forward.log TS_F_rad-anion_fragmentation_back.log
46	“	“	TS2	TS_F_rad-anion_fragmentation.log
47	“	“	PC	TS_F_rad-anion_fragmentation_forward.log
48	“	1 (Cl)	SET	Cl_neutral.log

Entry	Example	Step (X)	Comment[a]	File name
49	“	“	SET	Cl_rad-anion.log
50	“	“	SET	Cl_neutral_in_rad-anion_geom.log
51	“	“	SET	Cl_rad-anion_in_neutral_geom.log
52	“	“	TS1	no TS could be located
53	“	“	PC	TS_Cl_rad-anion_fragmentation_trial3_forward.log
54	“	1 (Br)	SET	Br_neutral.log
55	“	“	SET	Br_rad-anion.log
56	“	“	SET	Br_rad-anion_in_neutral_geom.log
57	“	“	SET	Br_neutral_in_rad-anion_geom.log
58	“	1 (I)	SET	I_neutral.log
59	“	“	SET	I_rad-anion.log
60	“	“	SET	I_rad-anion_in_neutral_geom.log
61	“	“	SET	I_neutral_in_rad-anion_geom.log
62	“	1 (Product)	SET	Product_neutral.log
63	“	“	SET	Product_rad-anion.log
64	“	“	SET	Product_rad-anion_in_neutral_geom.log
65	“	“	SET	Product_neutral_in_rad-anion_geom.log
66	“	2	Substrate	TS_H-abstr_back.log
67	“	“	TS1	TS_H-abstr.log
68	“	“	Product	TS_H-abstr_forward.log
69	“	3	Substrate	TS_Cdot_on_Ph_back.log
70	“	“	TS1	TS_Cdot_on_Ph.log
71	“	“	Product	TS_Cdot_on_Ph_forward.log
72	“	4	Substrate	TS_deprot_KOtBu_back.log
73	“	“	TS1	TS_deprot_KOtBu.log
74	“	“	Product	TS_deprot_KOtBu_forward.log
75	“	5	SC	TS_Deprotonation_SRN1_Bolm12_back.log
76	“	“	TS1	
77	“	“	PC	TS_Deprotonation_SRN1_Bolm12_forward.log
78	“	6	Substrate	TS_Ar-radical_adding_onto_enolate_back.log
79	“	“	(TS1 - barri-er-less)	BS_Ar-radical_adding_onto_enolate_trial2.log
80	“	“	Product	TS_Ar-radical_adding_onto_enolate_forward.log
81	C	1 (F)	SET	Sbstrt_X-F_neutral.log
82	“	“	SET	Sbstrt_X-F_rad-anion.log
83	“	“	SET	Sbstrt_X-F_rad-an_in_neutral_geom.log
84	“	“	SET	Sbstrt_X-F_neutral_in_rad-anion_geom.log
85	“	“	TS1	TS_F_rad-anion_conformation.log
86	“	“	I	TS_F_rad-anion_conformation_forward.log TS_F_rad-anion_fragmentation_back.log
87	“	“	TS2	TS_F_rad-anion_fragmentation_trial3.log
88	“	“	PC	TS_F_rad-anion_fragmentation_forward.log
89	“	1 (Cl)	SET	Sbstrt_X-Cl_neutral.log
90	“	“	SET	Sbstrt_X-Cl_rad-anion.log
91	“	“	SET	Sbstrt_X-Cl_rad-an_in_neutral_geom.log
92	“	“	SET	Sbstrt_X-Cl_neutral_in_rad-anion_geom.log
93	“	“	TS1	TS_Cl_rad-anion_fragmentation_trial3.log
94	“	“	PC	TS_Cl_rad-anion_fragmentation_forward_trial10.log

Entry	Example	Step (X)	Comment[a]	File name
95	“	1 (Br)	SET	Sbstrt_X-Br_neutral.log
96	“	“	SET	Sbstrt_X-Br_rad-anion.log
97	“	“	SET	Sbstrt_X-Br_rad-an_in_neutral_geom.log
98	“	“	SET	Sbstrt_X-Br_neutral_in_rad-anion_geom.log
99	“	“	TS1	TS_Br_rad-anion_fragmentation.log
100	“	“	PC	TS_Br_rad-anion_fragmentation_forward.log
101	“	1 (I)	SET	Sbstrt_X-I_neutral.log
102	“	“	SET	Sbstrt_X-I_rad-anion.log
103	“	“	SET	Sbstrt_X-I_rad-anion.log
104	“	“	SET	Sbstrt_X-I_neutral_in_rad-anion_geom.log
105	“	“	TS1	TS_I_rad-anion_fragmentation.log
106	“	“	PC	TS_I_rad-anion_fragmentation_forward_trial2.log
107	“	1 (Product)	SET	Product_neutral.log
108	“	“	SET	Product_rad-anion.log
109	“	“	SET	Product_rad-an_in_neutral_geom.log
110	“	“	SET	Product_neutral_in_rad-anion_geom.log
111	“	2	Substrate	TS_H-abstr_back.log
112	“	“	TS1	TS_H-abstr.log
113	“	“	Product	TS_H-abstr_forward.log
114	“	3	Substrate	TS_Ndot_on_Ph_back.log
115	“	“	TS1	TS_Ndot_on_Ph.log
116	“	“	Product	TS_Ndot_on_Ph_forward.log
117	“	4	Substrate	TS_deprot_KOH_back.log
118	“	“	TS1	TS_deprot_KOH.log
119	“	“	Product	TS_deprot_KOH_forward_trial2.log
120	“	5	(TS1 - barrier less)	BS_SRN1_Deprotonation_Bolm14_trial2.log
121	“	“	PC	TS_SRN1_Deprotonation_Bolm14_back.log
122		6	Substrate	TS_Ar-radical_adding_onto_anion_back.log
123		“	(TS1 - barrier-less)	TS_Ar-radical_adding_onto_anion.log
124		“	Product	TS_Ar-radical_adding_onto_anion_forward.log

[a] The reaction coordinate is indicated by the following abbreviations. SC: substrate complex; TS1: first transition state; I: Intermediate; TS2: second transition state; PC: product complex.

The .log files for the calculations of the electron donor structures presented in Table 4-9 are listed below in Table S48 and can be found in the sub directory ./Initiation. For the relevant .log files of the electron acceptor structures see Table S47.

Table S48 - File names for structures shown in Table 4-9 (./Initiation/)

Entry	Electron Donor (sub folder)	File name
1	**628 (Dimsyl)**	DMSO_anion.log
2	“	DMSO_radical.log
3	“	DMSO_rad_in_anion_geom.log
4	“	DMSO_anion_in_radical_geom.log

Entry	Electron Donor (sub folder)	File name
5	**629 (DMF)**	DMF_dimer_2K.log
6	“	DMF_dimer_2K_radical_cation_trial2.log
7	“	DMF_dimer_2K_rad-cat_in_neutral_geom.log
8	“	DMF_dimer_2K_neutral_in_radical_cation_geom.log
9	**630 (A)**	Sbstrat_X-I_anion.log
10	“	Sbstrt_X-I_radical.log
11	“	Sbstrat_X-I_radical_in_anion_geom.log
11	“	Sbstrt_X-I_anion_in_radical_geom.log
12	**631 (B)**	TS_cSnAr_I_K_back_anion.log
13	“	TS_cSnAr_I_K_back_radical_trial2.log
14	“	TS_cSnAr_I_K_back_radical_in_anion_geom.log
15	“	TS_cSnAr_I_K_back_anion_in_neutral_radical_geom.log
16	**632 (C)**	Sbstrt_X-I_anion.log
17	“	Sbstrt_X-I_radical_trial2.log
18	“	Sbstrt_X-I_radical_in_anion_geom.log
19	“	Sbstrt_X-I_anion_in_radical_geom.log

6. References

[1] C. K. Prier, D. A. Rankic, D. W. C. MacMillan, *Chem. Rev.* **2013**, *113*, 5322–5363.

[2] J. Broggi, T. Terme, P. Vanelle, *Angew. Chem. Int. Ed*. **2014**, *53*, 384–413.

[3] J. A. Murphy, F. Rasheed, S. J. Roome, K. A. Scott, N. Lewis, *J. Chem. Soc., Perkin Trans. 1* **1998**, 2331–2340.

[4] M. Médebielle, W. R. Dolbier Jr., *J. Fluorine Chem.* **2008**, *129*, 930–942.

[5] M. Mahesh, J. A. Murphy, F. LeStrat, H. P. Wessel, *Beilstein J. Org. Chem.* **2009**, *5*, 1–12.

[6] J. A. Murphy, T. A. Khan, S.-Z. Zhou, D. W. Thomson, M. Mahesh, *Angew. Chem. Int. Ed.* **2005**, *44*, 1356–1360.

[7] J. A. Murphy, J. Garnier, S. R. Park, F. Schoenebeck, S.-Z. Zhou, A. T. Turner, *Org. Lett.* **2008**, *10*, 1227–1230.

[8] P. I. Jolly, N. Fleary-Roberts, S. O'Sullivan, E. Doni, S.-Z. Zhou, J. A. Murphy, *Org. Biomol. Chem.* **2012**, *10*, 5807–5810.

[9] S. S. Hanson, E. Doni, K. T. Traboulsee, G. Coulthard, J. A. Murphy, C. A. Dyker, *Angew. Chem. Int. Ed.* **2015**, *54*, 11236–11239.

[10] K. K. Barnes, C. K. Mann, *J. Org. Chem.* **1967**, *32*, 1474–1479.

[11] N. L. Weinberg, H. R. Weinberg, *Chem. Rev.* **1968**, *68*, 449–523.

[12] T. M. McKinney, D. H. Geske, *J. Am. Chem. Soc.* **1965**, *87*, 3013–3014.

[13] G. S. Weiss, A. S. Parkes, E. R. Nixon, R. E. Hughes, *J. Chem. Phys.* **1964**, *41*, 3759–3767.

[14] J. K. Nimmo, B. W. Lucas, *Acta Crystallogr. Sect. B Struct. Sci.* **1976**, *32*, 348–353.

[15] S. F. Nelsen, J. M. Buschek, *J. Am. Chem. Soc.* **1974**, *96*, 7930–7934.

[16] G. Balakrishnan, T. Keszthelyi, R. Wilbrandt, J. M. Zwier, A. M. Brouwer, W. J. Buma, *J. Phys. Chem. A* **2000**, *104*, 1834–1841.

[17] Z.-R. Zheng, D. H. Evans, S. F. Nelsen, *J. Org. Chem.* **2000**, *65*, 1793–1798.

[18] J. L. Jeffrey, F. R. Petronijević, D. W. C. MacMillan, *J. Am. Chem. Soc.* **2015**, *137*, 8404–8407.

[19] J. P. Barham, M. P. John, J. A. Murphy, *J. Am. Chem. Soc.* **2016**, *138*, 15482–15487.

[20] D. Jérome, *Chem. Rev.* **2004**, *104*, 5565–5592.

[21] F. Wudl, G. M. Smith, E. J. Hufnagel, *Chem. Commun.* **1970**, 1452–1453.

[22] S. Hünig, H. Schlaf, G. Kiesslich, D. Scheutzow, *Tetrahedron Lett.* **1969**, *10*, 2271–2274.

[23] Y. Yamashita, Y. Kobayashi, T. Miyashi, *Angew. Chem. Int. Ed.* **1989**, *28*, 1052–1053.

[24] M. Sato, M. V. Lakshmikantham, M. P. Cava, A. F. Garito, *J. Org. Chem.* **1978**, *43*, 2084–2085.

[25] R. L. Pruett, J. T. Barr, K. E. Rapp, C. T. Bahner, J. D. Gibson, R. H. Lafferty, *J. Am.*

Chem. Soc. **1950**, *72*, 3646–3650.
[26] H. W. Wanzlick, E. Schikora, *Angew. Chem.* **1960**, *72*, 494–494.
[27] H. W. Wanzlick, *Angew. Chem. Int. Ed.* **1962**, *1*, 75–80.
[28] N. Wiberg, *Angew. Chem. Int. Ed.* **1968**, *7*, 766–779.
[29] R. W. Alder, M. E. Blake, L. Chaker, J. N. Harvey, F. Paolini, J. Schütz, *Angew. Chem. Int. Ed.* **2004**, *43*, 5896–5911.
[30] C. Burkholder, W. R. Dolbier, M. Médebielle, *J. Org. Chem.* **1998**, *63*, 5385–5394.
[31] K. Kuwata, D. H. Geske, *J. Am. Chem. Soc.* **1964**, *86*, 2101–2105.
[32] J. A. Murphy, S.-Z. Zhou, D. W. Thomson, F. Schoenebeck, M. Mahesh, S. R. Park, T. Tuttle, L. E. A. Berlouis, *Angew. Chem. Int. Ed.* **2007**, *46*, 5178–5183.
[33] J. R. Ames, M. A. Houghtaling, D. L. Terrian, T. P. Mitchell, *Can. J. Chem*. **1997**, *75*, 28–36.
[34] R. P. Thummel, V. Goulle, B. Chen, *J. Org. Chem.* **1989**, *54*, 3057–3061.
[35] P. I. Jolly, S.-Z. Zhou, D. W. Thomson, J. Garnier, J. A. Parkinson, T. Tuttle, J. A. Murphy, *Chem. Sci.* **2012**, *3*, 1675–1679.
[36] Z. Shi, V. Goulle, R. P. Thummel, *Tetrahedron Lett.* **1996**, *37*, 2357–2360.
[37] Z. Han, T. P. Vaid, A. L. Rheingold, *J. Org. Chem.* **2008**, *73*, 445–450.
[38] T. M. Bockman, J. K. Kochi, *J. Org. Chem.* **1990**, *55*, 4127–4135.
[39] K. Takahashi, T. Nihira, K. Akiyama, Y. Ikegami, E. Fukuyo, *Chem. Commun.* **1992**, 620–622.
[40] W. W. Porter, T. P. Vaid, A. L. Rheingold, *J. Am. Chem. Soc.* **2005**, *127*, 16559–16566.
[41] H. S. Farwaha, G. Bucher, J. A. Murphy, *Org. Biomol. Chem.* **2013**, *11*, 8073–8081.
[42] J. Casado, S. Patchkovskii, M. Z. Zgierski, L. Hermosilla, C. Sieiro, M. Moreno Oliva, J. T. López Navarrete, *Angew. Chem. Int. Ed.* **2008**, *47*, 1443–1446.
[43] G. Gryn'ova, M. L. Coote, C. Corminboeuf, *Wiley Interdiscip. Rev. Comput. Mol. Sci*. **2015**, *5*, 440–459.
[44] J. Garnier, A. R. Kennedy, L. E. A. Berlouis, A. T. Turner, J. A. Murphy, *Beilstein J. Org. Chem.* **2010**, *6*, 1–8.
[45] S. S. Hanson, N. A. Richard, C. A. Dyker, *Chem. Eur. J.* **2015**, *21*, 8052–8055.
[46] A. Peters, E. Kaifer, H.-J. Himmel, *Eur. J. Org. Chem.* **2008**, *2008*, 5907–5914.
[47] S.-Z. Zhou, H. Farwaha, J. A. Murphy, *Chimia* **2012**, *66*, 418–424.
[48] T. P. Vaid, *J. Am. Chem. Soc.* **2011**, *133*, 15838–15841.
[49] Y. Wang, B. Quillian, P. Wei, C. S. Wannere, Y. Xie, R. B. King, H. F. Schaefer, P. V. R. Schleyer, G. H. Robinson, *J. Am. Chem. Soc.* **2007**, *129*, 12412–12413.
[50] P. Bissinger, H. Braunschweig, A. Damme, C. Hörl, I. Krummenacher, T. Kupfer, *Angew. Chem. Int. Ed.* **2014**, *54*, 359–362.
[51] L. Zhang, L. Jiao, *Chem. Sci.* **2018**, *9*, 2711–2722.
[52] K. Tanaka, K. Yoshida, T. Ishida, A. Kobayashi, T. Nogami, *Adv. Mater*. **2000**, *12*, 661–664.
[53] K. Lerstrup, D. Talham, A. Bloch, T. Poehler, D. Cowan, *J. Chem. Soc, Chem. Commun.* **1982**, 336–337.
[54] S. Hünig, H. Schlaf, G. Kießlich, D. Scheutzow, *Tetrahedron Lett.* **1969**, *10*, 2271–2274.
[55] R. W. Hoffmann, J. Schneider, *Chem. Ber.* **1967**, *100*, 3689–3697.

[56] T. Nogami, K. Tanaka, T. Ishida, A. Kobayashi, *Synth. Met.* **2001**, *120*, 755–756.
[57] J. W. Kamplain, V. M. Lynch, C. W. Bielawski, *Org. Lett*. **2007**, *9*, 5401–5404.
[58] G. N. Reddy, S. Giri, *Phys. Chem. Chem. Phys.* **2016**, *18*, 24356–24360.
[59] P. W. Antoni, T. Bruckhoff, M. M. Hansmann, *J. Am. Chem. Soc.* **2019**, 141, 9701–9711.
[60] B. Eberle, O. Hübner, A. Ziesak, E. Kaifer, H.-J. Himmel, *Chem. Eur. J.* 2015, 21, 8578–8590.
[61] R. A. Marcus, *Pure Appl. Chem.* **1997**, *69*, 13–29.
[61] R. A. Marcus, *Pure Appl. Chem.* **1997**, *69*, 13–29.
[62] J. A. Murphy, *J. Org. Chem.* **2014**, *79*, 3731–3746.
[63] L. Pause, M. Robert, J.-M. Savéant, *J. Am. Chem. Soc.* **1999**, *121*, 7158–7159.
[64] G. M. Anderson, I. Cameron, J. A. Murphy, T. Tuttle, *RSC Adv.* **2016**, *6*, 11335–11343.
[65] J. Garnier, D. W. Thomson, S.-Z. Zhou, P. I. Jolly, L. E. A. Berlouis, J. A. Murphy, *Beilstein J. Org. Chem.* **2012**, *8*, 994–1002.
[66] C. P. Andrieux, J. Pinson, *J. Am. Chem. Soc.* **2003**, *125*, 14801–14806.
[67] P. P. Romańczyk, G. Rotko, S. S. Kurek, *Electrochem. Commun.* **2014**, *48*, 21–23.
[68] H. Ishibashi, S. Haruki, M. Uchiyama, O. Tamura, J.-I. Matsuo, *Tetrahedron Lett.* **2006**, *47*, 6263–6266.
[69] T. Taniguchi, K. Ryota, H. Ishibashi, *Arkivoc* **2008**, *(xiv)*, 7–16.
[70] H. Ishibashi, T. Taniguchi, M. Sasaki, *Heterocycles* **2010**, *80*, 657–6.
[71] T. Taniguchi, T. Fujii, A. Idota, H. Ishibashi, *Org. Lett.* **2009**, *11*, 3298–3301.
[72] A. Skiebe, A. Hirsch, H. Klos, B. Gotschy, *Chem. Phys. Lett.* **1994**, *220*, 138–140.
[73] Y. Nishiyama, H. Kawabata, A. Kobayashi, T. Nishino, N. Sonoda, *Tetrahedron Lett.* **2005**, *46*, 867–869.
[74] G. W. Gribble, *Indole Ring Synthesis: From Natural Products to Drug Discovery*, Wiley-VCH, **2016**, ISBN: 978-0-470-51218-0.
[75] R. J. Fletcher, C. Lampard, J. A. Murphy, N. Lewis, *J. Chem. Soc., Perkin Trans. 1* **1995**, 623–633.
[76] J. A. Murphy, *The Radical-Polar Crossover Reaction* in *Radicals in Organic Synthesis*, Ed. M. P. Sibi, P. Renaud, Wiley-VCH, **2001**, 298-314, https://doi.org/10.1002/9783527618293.ch15.
[77] N. Bashir, J. A. Murphy, *Chem. Commun.* **2000**, 627–628.
[78] C. Lampard, J. A. Murphy, N. Lewis, *J. Chem. Soc., Chem. Commun.* **1993**, 295–297.
[79] M. J. Begley, J. A. Murphy, S. J. Roome, *Tetrahedron Lett.* **1994**, *35*, 8679–8682.
[80] T. Koizumi, N. Bashir, A. R. Kennedy, J. A. Murphy, *J. Chem. Soc., Perkin Trans. 1*, **1999**, 3637–3643.
[81] E. Doni, J. A. Murphy, *Chem. Commun.* **2014**, *50*, 6073–6087.
[82] J. Garnier, *A New Approach to Highly Reductive Neutral Organic Molecules*, Ph.D. Thesis, University of Strathclyde, Dept. of Pure and Applied Chemistry, **2008**.
[83] J. Broggi, M. Rollet, J.-L. Clément, G. Canard, T. Terme, D. Gigmes, P. Vanelle, *Angew. Chem. Int. Ed.* **2016**, *55*, 5994–5999.
[84] F. Schoenebeck, J. A. Murphy, S.-Z. Zhou, Y. Uenoyama, Y. Miclo, T. Tuttle, *J. Am. Chem. Soc.* **2007**, *129*, 13368–13369.
[85] S. P. Y. Cutulic, J. A. Murphy, H. Farwaha, S.-Z. Zhou, E. Chrystal, *Synlett* **2008**, *2008*, 2132–2136.

[86] S. P. Y. Cutulic, N. J. Findlay, S.-Z. Zhou, E. J. T. Chrystal, J. A. Murphy, *J. Org. Chem.* **2009**, *74*, 8713–8718.
[87] J. A. Murphy, F. Schoenebeck, N. J. Findlay, D. W. Thomson, S.-Z. Zhou, J. Garnier, *J. Am. Chem. Soc.* **2009**, *131*, 6475–6479.
[88] R. Sword, L. A. Baldwin, J. A. Murphy, *Org. Biomol. Chem.* **2011**, *9*, 3560–3570.
[89] H. Fischer, *J. Am. Chem. Soc.* **1986**, *108*, 3925–3927.
[90] A. Studer, *Chem. Eur. J.* **2001**, *7*, 1159–1164.
[91] M. Li, S. Berritt, L. Matuszewski, G. Deng, A. Pascual-Escudero, G. B. Panetti, M. Poznik, X. Yang, J. J. Chruma, P. J. Walsh, *J. Am. Chem. Soc.* **2017**, *139*, 16327–16333.
[92] Y. Lei, J. Yang, R. Qi, S. Wang, R. Wang, Z. Xu, *Chem. Commun.* **2018**, *54*, 11881–11884.
[93] S. R. Graham, J. A. Murphy, D. Coates, *Tetrahedron Lett.* **1999**, *40*, 2415–2416.
[94] T. A. Khan, R. Tripoli, J. J. Crawford, C. G. Martin, J. A. Murphy, *Org. Lett*. **2003**, *5*, 2971–2974.
[95] M. R. Heinrich, A. Gansäuer, Eds., *Radicals in Synthesis III*, Springer Berlin Heidelberg, **2012**.
[96] T. Kawamoto, I. Ryu, *Org. Biomol. Chem.* **2014**, *12*, 9733–9742.
[97] A. Dewanji, C. Mück-Lichtenfeld, A. Studer, *Angew. Chem. Int. Ed.* **2016**, *55*, 6749–6752.
[98] D. Rottschäfer, B. Neumann, H.-G. Stammler, M. van Gastel, D. M. Andrada, R. S. Ghadwal, *Angew. Chem. Int. Ed.* **2018**, *57*, 4765–4768.
[99] C.-H. Lim, S. Ilic, A. Alherz, B. T. Worrell, S. S. Bacon, J. T. Hynes, K. D. Glusac, C. B. Musgrave, *J. Am. Chem. Soc.* **2018**, *141*, 272–280.
[100] H. Chikashita, M. Miyazaki, K. Itoh, *J. Chem. Soc., Perkin Trans. 1* **1987**, 699–706.
[101] H. Chikashita, K. Itoh, *Bull. Chem. Soc. Jpn.*, **1986**, *59*, 1747–1752.
[102] H. Chikashita, H. Ide, K. Itoh, *J. Org. Chem.* **1986**, *51*, 5400–5405.
[103] D. D. Tanner, J. J. Chen, *J. Org. Chem.* **1989**, *54*, 3842–3846.
[104] D. D. Tanner, H. K. Singh, A. Kharrat, A. R. Stein, *J. Org. Chem.* **1987**, *52*, 2142–2146.
[105] D. D. Tanner, A. R. Stein, *J. Org. Chem.* **1988**, *53*, 1642–1646.
[106] J. Chen, D. D. Tanner, *J. Org. Chem.* **1988**, *53*, 3897–3900.
[107] D. D. Tanner, J. J. Chen, L. Chen, C. Luelo, *J. Am. Chem. Soc.* **1991**, *113*, 8074–8081.
[108] D. D. Tanner, P. M. Peters, J. J. Chen, C. Luelo, *J. Am. Chem. Soc.* **1992**, *114*, 713–717.
[109] D. D. Tanner, J. J. Chen, *J. Org. Chem.* **1992**, *57*, 662–666.
[110] M. K. Denk, N. S. Milutinović, K. M. Marczenko, N. M. Sadowski, A. Paschos, *Chem. Sci.* **2017**, *8*, 1883–1887.
[111] E. Rabe, H.-W. Wanzlick, *Liebigs Ann*. **1973**, *1973*, 40–44.
[112] M. K. Denk, N. S. Milutinović, *Chemosphere* **2018**, *191*, 408–411.
[113] X.-Q. Zhu, M.-T. Zhang, A. Yu, C.-H. Wang, J.-P. Cheng, *J. Am. Chem. Soc.* **2008**, *130*, 2501–2516.
[114] E. Hasegawa, S.-Y. Takizawa, *Aust. J. Chem.* **2015**, *68*, 1640–1647.
[115] E. Hasegawa, T. Ohta, S. Tsuji, K. Mori, K. Uchida, T. Miura, T. Ikoma, E. Tayama, H.

Iwamoto, S.-Y. Takizawa, S. Murata, *Tetrahedron* **2015**, *71*, 5494–5505.
[116] E. Hasegawa, N. Izumiya, T. Fukuda, K. Nemoto, H. Iwamoto, S.-Y. Takizawa, S. Murata, *Tetrahedron* **2016**, *72*, 7805–7812.
[117] E. Hasegawa, N. Izumiya, T. Miura, T. Ikoma, H. Iwamoto, S.-Y. Takizawa, S. Murata, *J. Org. Chem.* **2018**, *83*, 3921–3927.
[118] E. Hasegawa, Y. Nagakura, N. Izumiya, K. Matsumoto, T. Tanaka, T. Miura, T. Ikoma, H. Iwamoto, K. Wakamatsu, *J. Org. Chem.* **2018**, *83*, 10813–10825.
[119] M. A. Syroeshkin, F. Kuriakose, E. A. Saverina, V. A. Timofeeva, M. P. Egorov, I. V. Alabugin, *Angew. Chem. Int. Ed.* **2018**, *58*, 5532–5550.
[120] A. Studer, D. P. Curran, *Nat. Chem.* **2014**, *6*, 765–773.
[121] M. A. Syroeshkin, I. B. Krylov, A. M. Hughes, I. V. Alabugin, D. V. Nasybullina, M. Y. Sharipov, V. P. Gul'Tyai, A. O. Terent'ev, *J. Phys. Org. Chem.* **2017**, *30*:e3744. https://doi.org/ 10.1002/poc.3744.
[122] E. Hayon, M. Simic, *Acc. Chem. Res.* **1974**, *7*, 114–121.
[123] J. C. Walton, *J. Phys. Chem. A* **2017**, *121*, 7761–7767.
[124] R. A. Rossi, A. B. Pierini, A. B. Peñéñory, *Chem. Rev.* **2003**, *103*, 71–168.
[125] A. Studer, D. P. Curran, *Angew. Chem. Int. Ed.* **2011**, *50*, 5018–5022.
[126] S.-Z. Zhou, G. M. Anderson, B. Mondal, E. Doni, V. Ironmonger, M. Kranz, T. Tuttle, J. A. Murphy, *Chem. Sci.* **2014**, *5*, 476–482.
[127] S.-Z. Zhou, E. Doni, G. M. Anderson, R. G. Kane, S. W. MacDougall, V. M. Ironmonger, T. Tuttle, J. A. Murphy, *J. Am. Chem. Soc.* **2014**, *136*, 17818–17826.
[128] L. Zhang, H. Yang, L. Jiao, *J. Am. Chem. Soc.* **2016**, *138*, 7151–7160.
[129] T. Hokamp, A. Dewanji, M. Lübbesmeyer, C. Mück-Lichtenfeld, E.-U. Würthwein, A. Studer, *Angew. Chem. Int. Ed.* **2017**, *56*, 13275–13278.
[130] N. L. Bauld, D. J. Bellville, B. Harirchian, K. T. Lorenz, R. A. Pabon, D. W. Reynolds, D. D. Wirth, H. S. Chiou, B. K. Marsh, *Acc. Chem. Res.* **1987**, *20*, 371–378.
[131] T. Broese, A. F. Roesel, A. Prudlik, R. Francke, *Org. Lett.* **2018**, *20*, 7483–7487.
[132] S. Chiniforoush, C. J. Cramer, *ChemRxiv Preprint* **2018**, DOI 10.26434/chemrxiv.7471223.v1.
[133] A. Fedorov, A. A. Toutov, N. A. Swisher, R. H. Grubbs, *Chem. Sci.* **2013**, *4*, 1640–1645.
[134] A. A. Toutov, W.-B. Liu, K. N. Betz, A. Fedorov, B. M. Stoltz, R. H. Grubbs, *Nature* **2015**, 518, 80–84.
[135] A. A. Toutov, W.-B. Liu, B. M. Stoltz, R. H. Grubbs, *Org. Synth.* **2016**, 263–271.
[136] A. A. Toutov, W.-B. Liu, K. N. Betz, B. M. Stoltz, R. H. Grubbs, *Nat. Protoc.* **2015**, *10*, 1897–1903.
[137] A. A. Toutov, K. N. Betz, D. P. Schuman, W.-B. Liu, A. Fedorov, B. M. Stoltz, R. H. Grubbs, *J. Am. Chem. Soc.* **2017**, *139*, 1668–1674.
[138] A. A. Toutov, M. Salata, A. Fedorov, Y.-F. Yang, Y. Liang, R. Cariou, K. N. Betz, E. P. A. Couzijn, J. W. Shabaker, K. N. Houk, R. H. Grubbs, *Nat. Energy* **2017**, *2*, 17008–17014.
[139] D. Yang, D. D. Tanner, *J. Org. Chem.* **1986**, *51*, 2267–2270.
[140] S. Rendler, M. Oestreich, *Synthesis* **2005**, 1727–1747.
[141] B. Becker, R. Corriu, C. Guérin, B. Henner, Q. Wang, *J. Organomet. Chem.* **1989**, *359*, C33–C35.

[142] R. Corriu, C. Guérin, B. Henner, Q. Wang, *J. Organomet. Chem.* **1989**, *365*, C7–C10.
[143] W.-B. Liu, D. P. Schuman, Y.-F. Yang, A. A. Toutov, Y. Liang, H. F. T. Klare, N. Nesnas, M. Oestreich, D. G. Blackmond, S. C. Virgil, S. Banerjee, R. N. Zare, R. H. Grubbs, K. N. Houk, B. M. Stoltz, *J. Am. Chem. Soc.* **2017**, *139*, 6867–6879.
[144] S. Banerjee, Y.-F. Yang, I. D. Jenkins, Y. Liang, A. A. Toutov, W.-B. Liu, D. P. Schuman, R. H. Grubbs, B. M. Stoltz, E. H. Krenske, K. N. Houk, R. N. Zare, *J. Am. Chem. Soc.* **2017**, *139*, 6880–6887.
[145] P. Asgari, Y. Hua, A. Bokka, C. Thiamsiri, W. Prasitwatcharakorn, A. Karedath, X. Chen, S. Sardar, K. Yum, G. Leem, B. S. Pierce, K. Nam, J. Gao, J. Jeon, *Nat. Catal.* **2019**, *2*, 164–173.
[146] R. N. Meals, *J. Am. Chem. Soc.* **1946**, *68*, 1880–1881.
[147] A. Causero, G. Ballmann, J. Pahl, H. Zijlstra, C. Färber, S. Harder, *Organometallics* **2016**, *35*, 3350–3360.
[148] F. Buch, J. Brettar, S. Harder, *Angew. Chem. Int. Ed.* **2006**, *45*, 2741–2745.
[149] F. Buch, S. Harder, *Organometallics* **2007**, *26*, 5132–5135.
[150] K. Takaki, M. Kurioka, T. Kamata, K. Takehira, Y. Makioka, Y. Fujiwara, *J. Org. Chem.* **1998**, *63*, 9265–9269.
[151] K. Takaki, T. Kamata, Y. Miura, T. Shishido, K. Takehira, *J. Org. Chem.* **1999**, *64*, 3891–3895.
[152] J. F. Dunne, S. R. Neal, J. Engelkemier, A. Ellern, A. D. Sadow, *J. Am. Chem. Soc.* **2011**, *133*, 16782–16785.
[153] M. S. Hill, D. J. Liptrot, D. J. MacDougall, M. F. Mahon, T. P. Robinson, *Chem. Sci.* **2013**, *4*, 4212–4222.
[154] C. Bellini, J.-F. Carpentier, S. Tobisch, Y. Sarazin, *Angew. Chem. Int. Ed.* **2015**, *54*, 7679–7683.
[155] W. Fink, *Helv. Chim. Acta* **1966**, *49*, 1408–1415.
[156] W. Fink, *Chem. Ber.* **1966**, *99*, 2267–2274.
[157] W. Fink, *Helv. Chim. Acta* **1969**, *52*, 1841–1847.
[158] D. Seyferth, G. H. Wiseman, *J. Am. Ceram. Soc.* **1984**, *67*, C-132–C-133.
[159] R. J. P. Corriu, D. Leclercq, P. H. Mutin, J. M. Planeix, A. Vioux, *J. Organomet. Chem.* **1991**, *406*, C1–C4.
[160] K. Kikushima, M. Grellier, M. Ohashi, S. Ogoshi, *Angew. Chem. Int. Ed*. **2017**, *56*, 16191–16196.
[161] K. Kuciński, G. Hreczycho, *ChemCatChem* **2017**, *9*, 1868–1885.
[162] J. F. Bunnett, R. E. Zahler, *Chem. Rev.* **1951**, *49*, 273–412.
[163] J. Meisenheimer, *Liebigs Ann.* **1902**, *323*, 205–246.
[164] O. Y. Borbulevych, A. Y. Kovalevsky, O. V. Shishkin, Y. M. Atroschenko, E. N. Alifanova, S. S. Gitis, A. Y. Kaminsky, E. Y. Tarasova, *Monatsh. Chem.* **1998**, *129*, 467–472.
[165] G. A. Artamkina, M. P. Egorov, I. P. Beletskaya, *Chem. Rev.* **1982**, *82*, 427–459.
[166] W. Koch, M. C. Holthausen *A Chemist's Guide to Density Functional Theory*, **2000**, *2nd Ed.* Wiley-VCH, DOI:10.1002/3527600043.
[167] A. H. M. Renfrew, J. A. Taylor, J. M. J. Whitmore, A. Williams, *J. Chem. Soc., Perkin Trans. 2* **1993**, 1703–1704.
[168] A. Hunter, M. Renfrew, J. A. Taylor, D. Rettura, J. M. J. Whitmore, A. Williams, *J. Am. Chem. Soc.* **1995**, *117*, 5484–5491.

[169] J. Shakes, C. Raymond, D. Rettura, A. Williams, *J. Chem. Soc., Perkin Trans. 2* **1996**, 1553–1557.
[170] N. R. Cullum, D. Rettura, J. M. J. Whitmore, A. Williams, *J. Chem. Soc., Perkin Trans. 2* **1996**, 1559–1563.
[171] J. Miller, *Aust. J. Chem.* **1956**, 9, 61–73.
[172] S. E. Fry, N. J. Pienta, *J. Am. Chem. Soc.* **1985**, *107*, 6399–6400.
[173] J. Miller, W. Kai-Yan, *J. Chem. Soc. D* **1963**, 3492–3494.
[174] R. Y. Sung, H. Choi, J. P. Lee, J. K. Park, K. Yang, I. S. Koo, *Bull. Korean Chem. Soc.* **2009**, *30*, 1579–1582.
[175] D. Y. Ong, C. Tejo, K. Xu, H. Hirao, S. Chiba, *Angew. Chem. Int. Ed.* **2017**, *56*, 1840–1844.
[176] D. J. Leonard, J. W. Ward, J. Clayden, *Nature* **2018**, *562*, 105–109.
[177] N. Chéron, D. Jacquemin, P. Fleurat-Lessard, *Phys. Chem. Chem. Phys.* **2012**, *14*, 7170–7175.
[178] E. E. Kwan, Y. Zeng, H. A. Besser, E. N. Jacobsen, *Nat. Chem.* **2018**, *10*, 917–923.
[179] A. J. J. Lennox, *Angew. Chem. Int. Ed.* **2018**, *57*, 14686–14688.
[180] M. N. Glukhovtsev, R. D. Bach, S. Laiter, *J. Org. Chem.* **1997**, *62*, 4036–4046.
[181] I. Fernández, G. Frenking, E. Uggerud, *J. Org. Chem.* **2010**, *75*, 2971–2980.
[182] H. Sun, S. G. DiMagno, *Angew. Chem. Int. Ed.* **2006**, *45*, 2720–2725.
[183] J. R. Pliego, D. Piló-Veloso, *Phys. Chem. Chem. Phys.* **2008**, *10*, 1118–1124.
[184] D. R. Silva, J. R. Pliego, *Struct. Chem.* **2018**, *36*, 234–242.
[185] Y.-J. Zheng, T. C. Bruice, *J. Am. Chem. Soc.* **1997**, *119*, 3868–3877.
[186] a) K. Tanaka, M. Deguchi, S. Iwata, *J. Chem. Res., Synop.* **1999**, 528–529. b) K. Tanaka, M. Deguchi, S. Iwata, *J. Chem. Res. Miniprint* **1999**, 2279–2294.
[187] A. G. Cairns, H. M. Senn, M. P. Murphy, R. C. Hartley, *Chem. Eur. J.* **2014**, *20*, 3742–3751.
[188] P. Tang, W. Wang, T. Ritter, *J. Am. Chem. Soc.* **2011**, *133*, 11482–11484.
[189] C. N. Neumann, J. M. Hooker, T. Ritter, *Nature* **2016**, *534*, 369–373.
[190] C. N. Neumann, T. Ritter, *Acc. Chem. Res.* **2017**, *50*, 2822–2833.
[191] K. Miyazaki, *Tetrahedron Lett.* **1968**, *9*, 2793–2798.
[192] A. Kaji, Y. Araki, K. Miyazaki, *Bull. Chem. Soc. Jpn.* **1971**, *44*, 1393–1399.
[193] G. Lloyd-Jones, J. Moseley, J. Renny, *Synthesis* **2008**, 661–689.
[194] H. Jacobsen, J. P. Donahue, *Can. J. Chem.* **2006**, *84*, 1567–1574.
[195] V. Albrow, K. Biswas, A. Crane, N. Chaplin, T. Easun, S. Gladiali, B. Lygo, S. Woodward, *Tetrahedron: Asymmetry* **2003**, *14*, 2813–2819.
[196] A. J. Perkowski, C. L. Cruz, D. A. Nicewicz, *J. Am. Chem. Soc.* **2015**, *137*, 15684–15687.
[197] S. K. Pedersen, A. Ulfkjær, M. N. Newman, S. Yogarasa, A. U. Petersen, T. I. Sølling, M. Pittelkow, *J. Org. Chem.* **2018**, *83*, 12000–12006.
[198] H. Sun, J. Li, D. Zhang, C. Ma, C. Liu, *J. Phys. Org. Chem.* **2008**, *21*, 215–218.
[199] Y. Zhao, Y. Wu, J. Jia, D. Zhang, C. Ma, *J. Org. Chem.* **2012**, *77*, 8501–8506.
[200] J. Reyes-González, R. M. Gómez, F. Cortés-Guzmán, *J. Phys. Org. Chem.* **2012**, *25*, 230–238.
[201] B. Yang, X. Tan, R. Guo, S. Chen, Z. Zhang, X. Chu, C. Xie, D. Zhang, C. Ma, *J. Org. Chem.* **2014**, *79*, 8040–8048.

[202] L. Legnani, A. Porta, P. Caramella, L. Toma, G. Zanoni, G. Vidari, *J. Org. Chem.* **2015**, *80*, 3092–3100.
[203] F. Nawaz, K. Mohanan, L. Charles, M. Rajzmann, D. Bonne, O. Chuzel, J. Rodriguez, Y. Coquerel, *Chem. Eur. J.* **2013**, *19*, 17578–17583.
[204] G. Tintori, P. Nabokoff, R. Buhaibeh, D. Bergé-Lefranc, S. Redon, J. Broggi, P. Vanelle, *Angew. Chem. Int. Ed.* **2018**, *57*, 3148–3153.
[205] AkzoNobel Product Data Sheets, all accessed on 7. Feb. 2019, a) for LP: http://www.pcpds.akzonobel.com/PolymerChemicalsPDS/showPDF.aspx?pds_id=988; b) for DBP: http://www.pcpds.akzonobel.com/PolymerChemicalsPDS/showPDF.aspx?pds_id=1096; c) for DTBP: http://www.pcpds.akzonobel.com/PolymerChemicalsPDS/showPDF.aspx?pds_id=1695.
[206] B. P. Roberts, *Chem. Soc. Rev.* **1999**, *28*, 25–35.
[207] H. S. Dang, M. R. J. Elsegood, K. M. Kirn, B. P. Roberts, *J. Chem. Soc., Perkin Trans. 1* **1999**, 2061–2068.
[208] A. J. Fielding, B. P. Roberts, *Tetrahedron Lett.* **2001**, *42*, 4061–4064.
[209] S. F. Nelsen, S. C. Blackstock, Y. Kim, *J. Am. Chem. Soc.* **1987**, *109*, 677–682.
[210] R. A. Marcus, *J. Chem. Phys.* **1965**, *43*, 679–701.
[211] A. L. J. Beckwith, C. H. Schiesser, *Tetrahedron* **1985**, *41*, 3925–3941.
[212] C. H. Schiesser, M. A. Skidmore *Calculations: a Useful Tool for Synthetic Chemists* in *Radicals in Organic Synthesis*, Ed. M. P. Sibi, P. Renaud, Wiley-VCH, **2001** 337-359.
[213] AkzoNobel Product Data Sheets, accessed on 13. Feb. 19, https://polymerchemistry.nouryon.com/globalassets/inriver/resources/pds-trigonox-22-c80-polymer-production-glo-en-201812190837.pdf
[214] H. Roth, N. Romero, D. A. Nicewicz, *Synlett* **2016**, *27*, 714–723.
[215] A. J. Bard, L. R. Faulkner *Electrochemical Methods - Fundamentals and Applications*, Wiley-VCH, **2001** (2^{end} Ed.).
[216] L. Pause, M. Robert, J.-M. Savéant, *J. Am. Chem. Soc.* **1999**, *121*, 7158–7159.
[217] A. A. Isse, P. R. Mussini, A. Gennaro, *J. Phys. Chem. C* **2009**, *113*, 14983–14992.
[218] A. A. Isse, S. Gottardello, C. Durante, A. Gennaro, *Phys. Chem. Chem. Phys.* **2008**, *10*, 2409–2416.
[219] S. Shimizu, H. Osato, Y. Imamura, Y. Satou, *Org. Process Res. Dev.* **2010**, *14*, 1518–1520.
[220] K. Schank, G. Bouillon, M. Fünfrocken, C. Lick, R. Lieder, *Helv. Chim. Acta* **2002**, *85*, 1295–1326.
[221] J. W. Runyon, O. Steinhof, H. V. R. Dias, J. C. Calabrese, W. J. Marshall, A. J. Arduengo, *Aust. J. Chem.* **2011**, *64*, 1165–1172.
[222] E. Lee, D. V. Yandulov, *J. Organomet. Chem.* **2011**, *696*, 4095–4103.
[223] M. V. Mirkin, H. J. Yang, A. J. Bard, *J. Electrochem. Soc.* **1992**, *139*, 2212–2217.
[224] D. M. F. Santos, C. A. C. Sequeira, *Electrochim. Acta* **2010**, *55*, 6775–6781.
[225] A. Greenwood, M. Nierenstein, *J. Chem. Soc., Trans.* **1920**, *117*, 1594–1599.
[226] R. K. Razdan, H. G. Pars, W. R. Thompson, F. E. Granche, *Tetrahedron Lett.* **1974**, *15*, 4315–4318.
[227] A. Maercker, *Angew. Chem. Int. Ed* **1987**, *26*, 972–989.
[228] P. K. Choudhury, J. Almena, F. Foubelo, M. Yus, *Tetrahedron* **1997**, *53*, 17373–17382.
[229] U. Azzena, M. Carraro, C. Meloni, I. Murgia, L. Pisano, M. Pittalis, R. Luisi, B. Musio,

L. Degennaro, *Tetrahedron: Asymmetry* **2014**, *25*, 1550–1554.
[230] H.-S. Wang, unpublished results, **2017**, at the University of Strathclyde.
[231] A. J. Smith, A. Young, S. Rohrbach, E. F. O'Connor, M. Allison, H.-S. Wang, D. L. Poole, T. Tuttle, J. A. Murphy, *Angew. Chem. Int. Ed.* **2017**, *56*, 13747–13751.
[232] J.-F. Lohier, K. Wright, C. Peggion, F. Formaggio, C. Toniolo, M. Wakselman, J.-P. Mazaleyrat, *Tetrahedron* **2006**, *62*, 6203–6213.
[233] T. V. RajanBabu, D. F. Eaton, T. Fukunaga, *J. Org. Chem.* **1983**, *48*, 652–657.
[234] F. Palumbo, S. Rohrbach, J. A. Murphy, *Manuscript in Preparation*, **2019**, *Pure and Applied Chemistry*, University of Strathclyde.
[235] http://evans.rc.fas.harvard.edu/pdf/evans_pKa_table.pdf, 19:11 14 March 2019.
[236] A. H. M. Renfrew, J. A. Taylor, J. M. J. Whitmore, A. Williams, *J. Chem. Soc., Perkin Trans. 2* **1994**, 2383–2384.
[237] N. R. Cullum, D. Rettura, A. Williams, A. H. Renfrew, J. A. Taylor, J. M. Whitmore, *J. Am. Chem. Soc.* **1995**, *117*, 9200–9205.
[238] C. Hansch, A. Leo, R. W. Taft, *Chem. Rev.* **1991**, *91*, 165–195.
[239] B. G. Cox, A. J. Parker, *J. Am. Chem. Soc.* **1973**, *95*, 408–410.
[240] D. F. Shriver, P. W. Atkins, C. H. Langford *"Inorganic Chemistry"*, 2nd Ed., **1995**, Oxford University Press.
[241] G. Glockler, *J. Phys. Chem.* **1959**, *63*, 828–832.
[242] A. Beyer, C. M. M. Reucher, C. Bolm, *Org. Lett.* **2011**, *13*, 2876–2879.
[243] A. Beyer, J. Buendia, C. Bolm, *Org. Lett.* **2012**, *14*, 3948–3951.
[244] H. Baars, A. Beyer, S. V. Kohlhepp, C. Bolm, *Org. Lett.* **2014**, *16*, 536–539.
[245] M. E. Budén, J. I. Bardagí, M. Puiatti, R. A. Rossi, *J. Org. Chem.* **2017**, *82*, 8325–8333.
[245] Y. Zhao, D. G. Truhlar, *Theor. Chem. Acc.* **2008**, *120*, 215–241.
[246] J. P. Barham, G. Coulthard, K. J. Emery, E. Doni, F. Cumine, G. Nocera, M. P. John, L. E. A. Berlouis, T. McGuire, T. Tuttle, J. A. Murphy, *J. Am. Chem. Soc.* **2016**, *138*, 7402–7410.
[247] Gaussian 09, (both Revisions, A.02 or D.01, were used), M. J. Frisch, G. W. Trucks, H. B. Schlegel, G. E. Scuseria, M. A. Robb, J. R. Cheeseman, G. Scalmani, V. Barone, G. A. Petersson, H. Nakatsuji, X. Li, M. Caricato, A. Marenich, J. Bloino, B. G. Janesko, R. Gomperts, B. Mennucci, H. P. Hratchian, J. V. Ortiz, A. F. Izmaylov, J. L. Sonnenberg, D. Williams-Young, F. Ding, F. Lipparini, F. Egidi, J. Goings, B. Peng, A. Petrone, T. Henderson, D. Ranasinghe, V. G. Zakrzewski, J. Gao, N. Rega, G. Zheng, W. Liang, M. Hada, M. Ehara, K. Toyota, R. Fukuda, J. Hasegawa, M. Ishida, T. Nakajima, Y. Honda, O. Kitao, H. Nakai, T. Vreven, K. Throssell, J. A. Montgomery, Jr., J. E. Peralta, F. Ogliaro, M. Bearpark, J. J. Heyd, E. Brothers, K. N. Kudin, V. N. Staroverov, T. Keith, R. Kobayashi, J. Normand, K. Raghavachari, A. Rendell, J. C. Burant, S. S. Iyengar, J. Tomasi, M. Cossi, J. M. Millam, M. Klene, C. Adamo, R. Cammi, J. W. Ochterski, R. L. Martin, K. Morokuma, O. Farkas, J. B. Foresman, and D. J. Fox, Gaussian, Inc., Wallingford CT, **2016**.
[248] GaussView, Version 5, Roy Dennington, Todd A. Keith, and John M. Millan, Semichem Inc., Shawnee Mission, KS, **2016**.
[249] R. Krishnan, J. S. Binkley, R. Seeger, J. A. Pople, *J. Chem. Phys.* **1980**, *72*, 650–654.
[250] A. D. McLean, G. S. Chandler, *J. Chem. Phys.* **1980**, *72*, 5639–5648.

[251] T. Clark, J. Chandersekhar, G. W. Spitznagel, P. V. Schleyer, *J. Comput. Chem.* **1983**, *4*, 294–301.
[252] M. J. Frisch, J. A. Pople, J. S. Binkley, *J. Chem. Phys.* **1984**, *80*, 3265–3269.
[253] A. Bergner, M. Dolg, W. Küchle, H. Stoll, H. Preuß, *Mol. Phys.* **1993**, *80*, 1431–1441.
[254] a) V. Barone, M. Cossi, *J. Phys. Chem. A* **1998**, *102*, 1995–2001.b) M. Cossi, N. Rega, G. Scalmani, V. Barone, *J. Comput. Chem.* **2003**, *24*, 669–681.
[255] M. Cossi, N. Rega, G. Scalmani, V. Barone, *J. Comput. Chem.* **2003**, *24*, 669–681.
[256] A. Kena Diba, C. Noll, M. Richter, M. T. Gieseler, M. Kalesse, *Angew. Chem. Int. Ed.* **2010**, *49*, 8367–8369.
[257] G. de Robillard, C. H. Devillers, D. Kunz, H. Cattey, E. Digard, J. Andrieu, *Org. Lett.* **2013**, *15*, 4410–4413.
[258] G. Jin, C. G. Werncke, Y. Escudié, S. Sabo-Etienne, S. Bontemps, *J. Am. Chem. Soc.* **2015**, *137*, 9563–9566.
[259] X.-H. Fan, L.-M. Yang, *Eur. J. Org. Chem.* **2010**, 2457–2460.
[260] S. Sobhani, Z. M. Falatooni, S. Asadi, M. Honarmand, *Catal. Letters* **2016**, *146*, 255–268.
[261] J.-F. Wei, J. Jiao, J.-J. Feng, J. Lv, X.-R. Zhang, X.-Y. Shi, Z.-G. Chen, *J. Org. Chem.* **2009**, *74*, 6283–6286.
[262] Q. Song, D. Zhang, Q. Zhu, Y. Xu, *Org. Lett.* **2014**, *16*, 5272–5274.
[263] A. Minatti, S. L. Buchwald, *Org. Lett.* **2008**, *10*, 2721–2724.
[264] S. Chandrasekhar, D. Basu, C. R. Reddy, *Synthesis* **2007**, 1509–1512.
[265] D. B. Guthrie, D. P. Curran, *Org. Lett.* **2009**, *11*, 249–251.
[266] W. R. Bowman, S. L. Krintel, M. B. Schilling, *Synlett* **2004**, 1215–1218.
[267] R. Lhermet, M. Durandetti, J. Maddaluno, *Beilstein J. Org. Chem.* **2013**, *9*, 710–716.
[268] G. Özüduru, T. Schubach, M. M. K. Boysen, *Org. Lett.* **2012**, *14*, 4990–4993.
[269] H. Song, Y. Liu, Y. Liu, Q. Wang, *Org. Lett.* **2014**, *16*, 3240–3243.
[270] H. Kamisaki, T. Nanjo, C. Tsukano, Y. Takemoto, *Chem. Eur. J.* **2011**, *17*, 626–633.
[271] T. Adler, J. Bonjoch, J. Clayden, M. Font-Bardía, M. Pickworth, X. Solans, D. Solé, L. Vallverdú, *Org. Biomol. Chem.* **2005**, *3*, 3173–3183.
[272] D. Solé, F. Mariani, I. Fernández, M. A. Sierra, *J. Org. Chem.* **2012**, *77*, 10272–10284.
[273] A. D. Worthy, C. L. Joe, T. E. Lightburn, K. L. Tan, *J. Am. Chem. Soc.* **2010**, *132*, 14757–14759.
[274] B. M. Trost, R. C. Livingston, *J. Am. Chem. Soc.* **2008**, *130*, 11970–11978.
[275] Y. Kita, H. Nambu, N. G. Ramesh, G. Anilkumar, M. Matsugi, *Org. Lett.* **2001**, *3*, 1157–1160.
[276] S. He, R. P. Hsung, W. R. Presser, Z.-X. Ma, B. J. Haugen, *Org. Lett.* **2014**, *16*, 2180–2183.
[277] E. K. Harvill, R. M. Herbst, E. C. Schreiner, C. W. Roberts, *J. Org. Chem.* **1950**, *15*, 662–670.
[278] C. Bai, X. Yao, Y. Li, *ACS Catal.* **2015**, *5*, 884–891.
[279] Y. Sawama, M. Masuda, S. Asai, R. Goto, S. Nagata, S. Nishimura, Y. Monguchi, H. Sajiki, *Org. Lett.* **2015**, *17*, 434–437.
[280] M. Szostak, M. Spain, A. J. Eberhart, D. J. Procter, *J. Org. Chem.* **2014**, *79*, 11988–12003.
[281] W. J. Kerr, A. J. Morrison, M. Pazicky, T. Weber, *Org. Lett.* **2012**, *14*, 2250–2253.

[282] M. K. Gupta, Z. Li, T. S. Snowden, *Org. Lett.* **2014**, *16*, 1602–1605.
[283] L. A. Rothman, E. I. Becker, *J. Org. Chem.* **1960**, *25*, 2203–2206.
[284] A. V. Iosub, S. S. Stahl, *J. Am. Chem. Soc.* **2015**, *137*, 3454–3457.
[285] E. Lee, D. V. Yandulov, *J. Organomet. Chem.* **2011**, *696*, 4095–4103.
[286] M. K. Denk, S. Gupta, J. Brownie, S. Tajammul, A. J. Lough, *Chem. Eur. J.* **2001**, *7*, 4477–4486.
[287] I. Antonini, G. Cristalli, P. Franchetti, M. Grifantini, U. Gulini, S. Martelli, *J. Heterocyclic Chem.* **1978**, *15*, 1201–1203.
[288] T. L. Amyes, S. T. Diver, J. P. Richard, F. M. Rivas, K. Toth, *J. Am. Chem. Soc.* **2004**, *126*, 4366–4374.
[289] H. Zhao, F. W. Foss, R. Breslow, *J. Am. Chem. Soc.* **2008**, *130*, 12590–12591.
[290] H. Rollema, E. A. Johnson, R. G. Booth, P. Caldera, P. Lampen, S. K. Youngster, A. J. Trevor, N. Naiman, N. Castagnoli, *J. Med. Chem.* **1990**, *33*, 2221–2230.
[291] H. J. J. Loozen, *J. Org. Chem.* **1975**, *40*, 520–521.
[292] B. Y.-H. Tan, Y.-C. Teo, *Synlett* **2016**, *27*, 1814–1819.
[293] C. Zarate, R. Martin, *J. Am. Chem. Soc.* **2014**, *136*, 2236–2239.
[294] C. F. Nising, U. K. Schmid, M. Nieger, S. Bräse, *J. Org. Chem.* **2004**, *69*, 6830–6833.
[295] Y. Miyake, M. Wu, M. J. Rahman, Y. Kuwatani, M. Iyoda, *J. Org. Chem.* **2006**, *71*, 6110–6117.
[296] B. Inés, I. Moreno, R. SanMartin, E. Domínguez, *J. Org. Chem.* **2008**, *73*, 8448–8451.
[297] M. Tobisu, A. Yasutome, H. Kinuta, K. Nakamura, N. Chatani, *Org. Lett.* **2014**, *16*, 5572–5575.
[298] T. Iwasaki, K. Agura, Y. Maegawa, Y. Hayashi, T. Ohshima, K. Mashima, *Chem. Eur. J.* **2010**, *16*, 11567–11571.
[299] Y. Yamanoi, H. Nishihara, *J. Org. Chem.* **2008**, *73*, 6671–6678.
[300] S. Sueki, Y. Kuninobu, *Org. Lett.* **2013**, *15*, 1544–1547.
[301] N. Sakurai, K. Ikegai, T. Mukaiyama, *Arkivoc* **2007**, *7*, 254–264.
[302] H. Gilman, O. L. Marrs, *J. Org. Chem.* **1962**, *27*, 1879–1881.
[303] S. Kitagaki, M. Kajita, S. Narita, C. Mukai, *Org. Lett.* **2012**, *14*, 1366–1369.
[304] C. Zarate, M. Nakajima, R. Martin, *J. Am. Chem. Soc.* **2017**, *139*, 1191–1197.
[305] L. D. Field, B. A. Messerle, M. Rehr, L. P. Soler, T. W. Hambley, *Organometallics* **2003**, *22*, 2387–2395.
[306] O. Lebedev, U. Mäeorg, *Organometallics* **2014**, *33*, 188–193.
[307] K. Sato, Y. Inoue, T. Mori, A. Sakaue, A. Tarui, M. Omote, I. Kumadaki, A. Ando, *Org. Lett.* **2014**, *16*, 3756–3759.
[308] L. J. Sargent, L. Small, *J. Org. Chem.* **1948**, *13*, 447–454.
[309] P. Eisenberger, A. M. Bailey, C. M. Crudden, *J. Am. Chem. Soc.* **2012**, *134*, 17384–17387.
[310] S. Kyasa, R. N. Meier, R. A. Pardini, T. K. Truttmann, K. T. Kuwata, P. H. Dussault, *J. Org. Chem.* **2015**, *80*, 12100–12114.
[311] N. J. Findlay, S. R. Park, F. Schoenebeck, E. Cahard, S.-Z. Zhou, L. E. A. Berlouis, M. D. Spicer, T. Tuttle, J. A. Murphy, *J. Am. Chem. Soc.* **2010**, *132*, 15462–15464.
[312] A. Sieglitz, R. Marx, *Ber. Dtsch. Chem. Ges.* **1923**, *56B*, 1619–1640.
[313] M. Szostak, M. Spain, D. J. Procter, *J. Org. Chem.* **2014**, *79*, 2522–2537.
[314] R. Gerdil, E. A. C Lueken, *Helv. Chim. Acta* **1961**, 1966–1978.

[315] D. T. Glatzhofer, Y. Liang, M. A. Khan, *Organometallics* **1993**, *12*, 624–632.
[316] M. Nir, R. E. Hoffman, I. O. Shapiro, M. Rabinovitz, *J. Chem. Soc., Perkin Trans. 2* **1995**, 1433–1442.
[317] F. Nador, Y. Moglie, C. Vitale, M. Yus, F. Alonso, G. Radivoy, *Tetrahedron* **2010**, *66*, 4318–4325.
[318] M. B. Thathagar, G. Rothenberg, *Org. Biomol. Chem.* **2006**, *4*, 111–115.
[319] M.-P. Guo, S.-W. Liu, S.-B. Chen, Y.-J. Wen, H. Liang, M.-Y. Lv, *Synth. Commun.* **2015**, *45*, 777–787.
[320] J. Karthikeyan, N. Yoshikai, *Org. Lett.* **2014**, 16, 4224–4227.

Was kann ich für die Heimat tun
Bevor ich geh' im Grabe ruhn?
Was geb ich, das dem Tod enflieht?
Vielleicht ein Wort, vielleicht ein Lied,
Ein kleines stilles Leuchten!

Conrad Ferdinand Meyer, Firnelicht

Mechanistic Studies on Three Areas of Organic Chemistry -

A Combined Computational and Experimental Approach

–

Appendix

Simon Rohrbach

1,3-Dimethyl-1*H*-benzo[*d*]imidazol-3-ium iodide 418-I

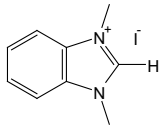

^{1}H NMR (400 MHz, DMSO-d_6) δ 9.67 (s, 1H), 8.05 – 7.98 (m, 2H), 7.73 – 7.67 (m, 2H), 4.09 (d, J = 0.6 Hz, 6H).

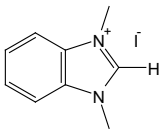

^{13}C NMR (101 MHz, DMSO) δ 143.06, 131.59, 126.35, 113.37, 33.22.

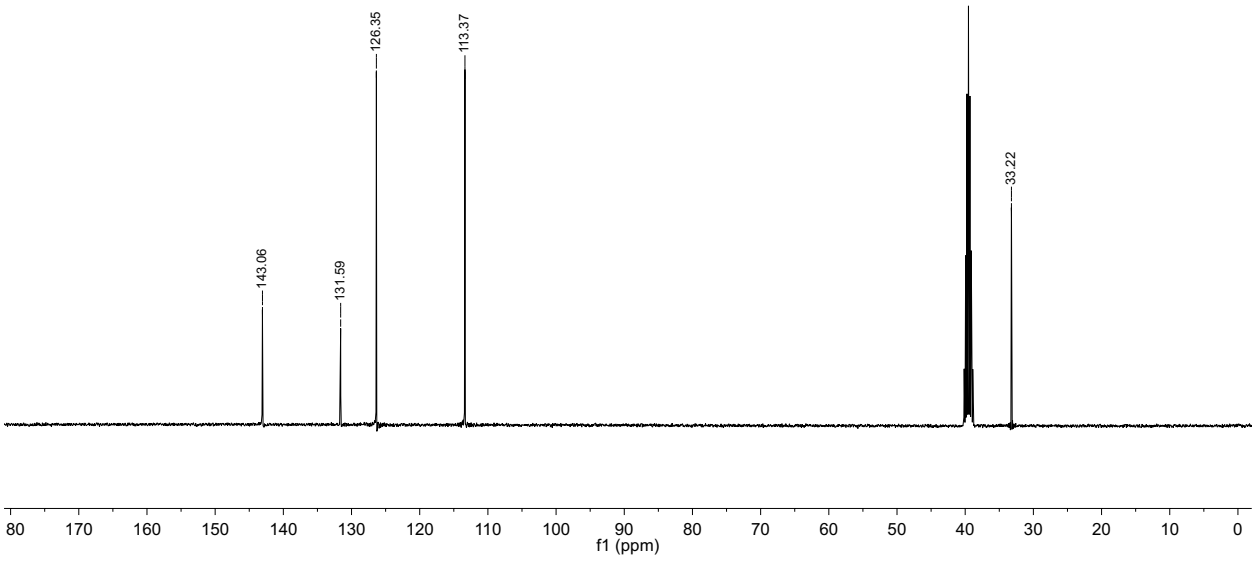

1,3-Dimethyl-1*H*-benzo[*d*]imidazol-3-ium iodide 418-I

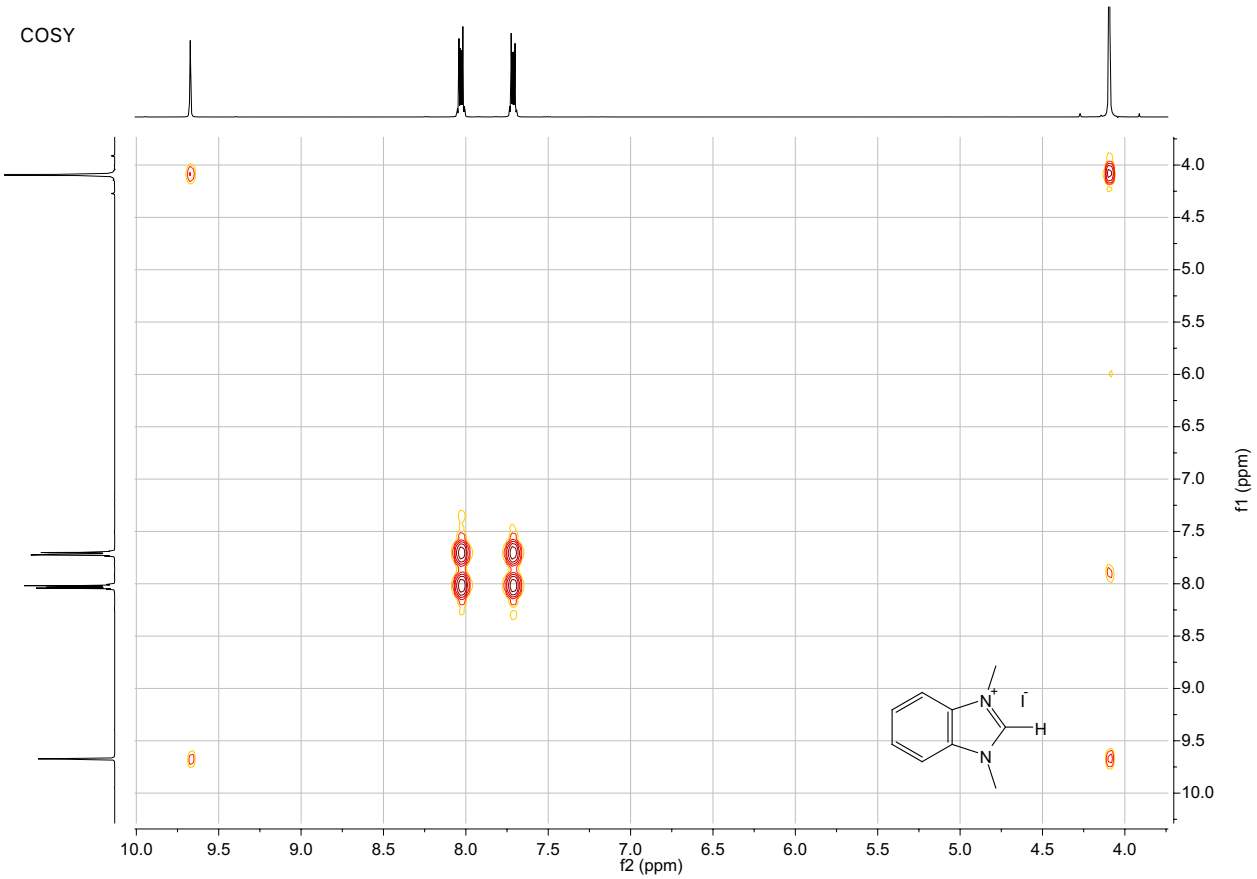

1,3-Dimethyl-2,3-dihydro-1*H*-benzo[*d*]imidazole 419

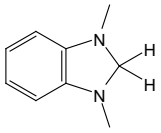

^{1}H NMR (400 MHz, THF-d_8) δ 6.52 (dd, J = 5.5, 3.2 Hz, 2H), 6.32 (dd, J = 5.4, 3.2 Hz, 2H), 4.24 (s, 2H), 2.66 (s, 6H).

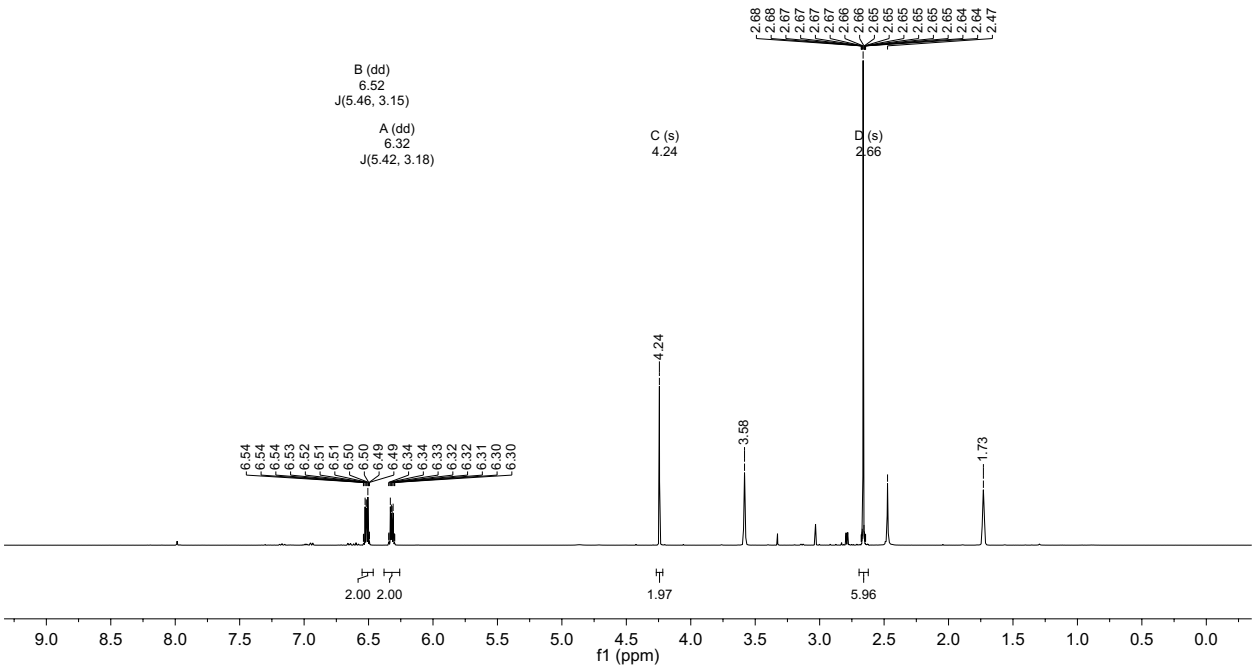

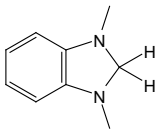

^{13}C NMR (101 MHz, THF) δ 144.55, 119.65, 106.66, 81.32, 34.69.

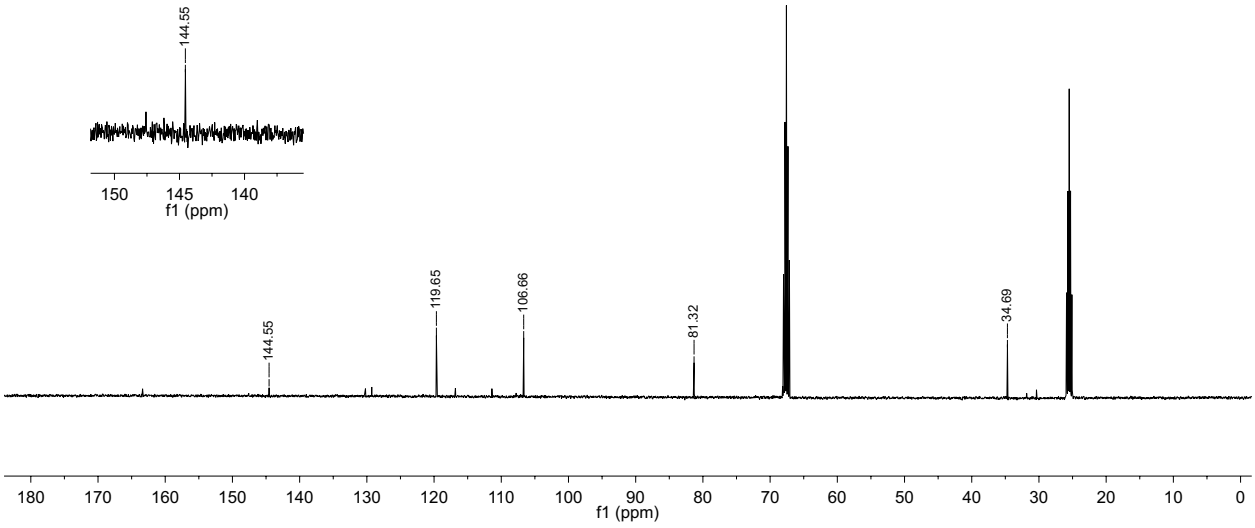

1,3-Dimethyl-2,3-dihydro-1*H*-benzo[*d*]imidazole 419

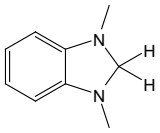

^{1}H NMR (400 MHz, DMSO-d_6) δ 6.54 (dd, J = 5.4, 3.2 Hz, 2H), 6.40 (dd, J = 5.4, 3.2 Hz, 2H), 4.24 (s, 3H), 2.65 (s, 7H).

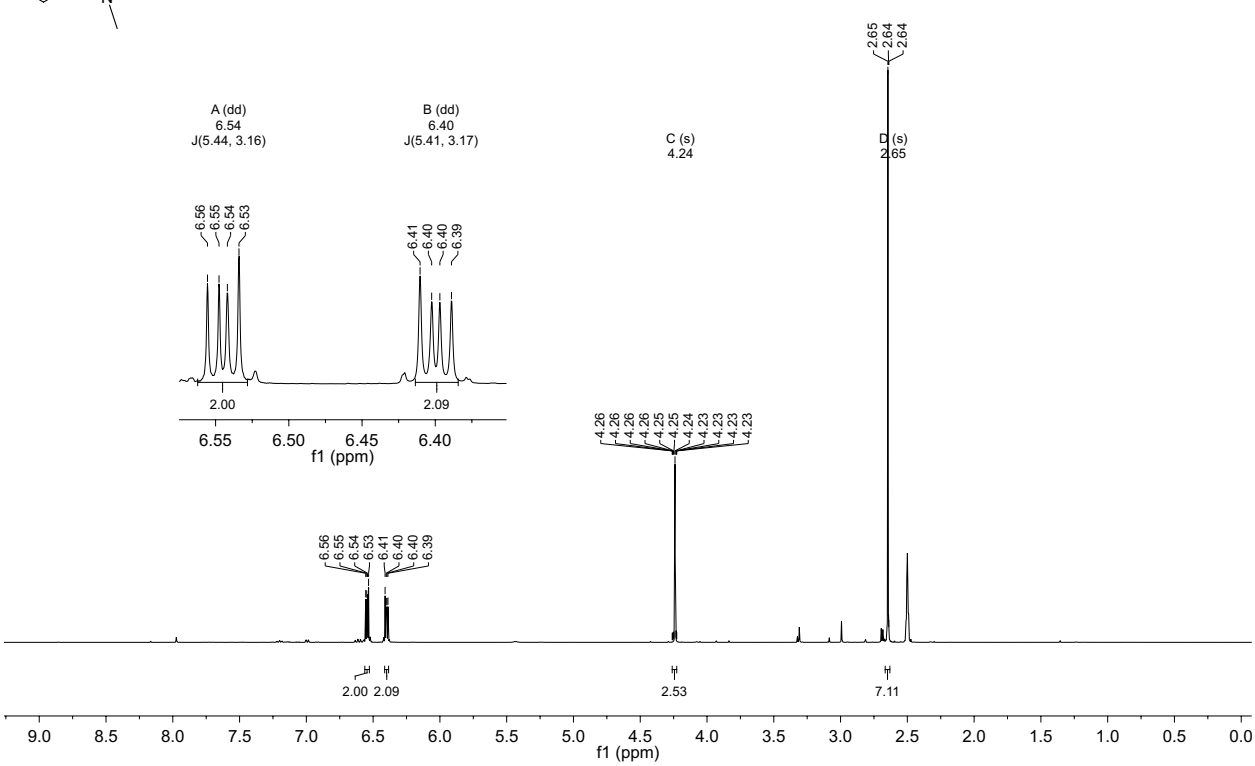

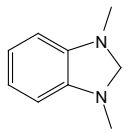

^{13}C NMR (101 MHz, DMSO-d_6) δ 143.2, 118.6, 105.9, 79.6, 34.1.

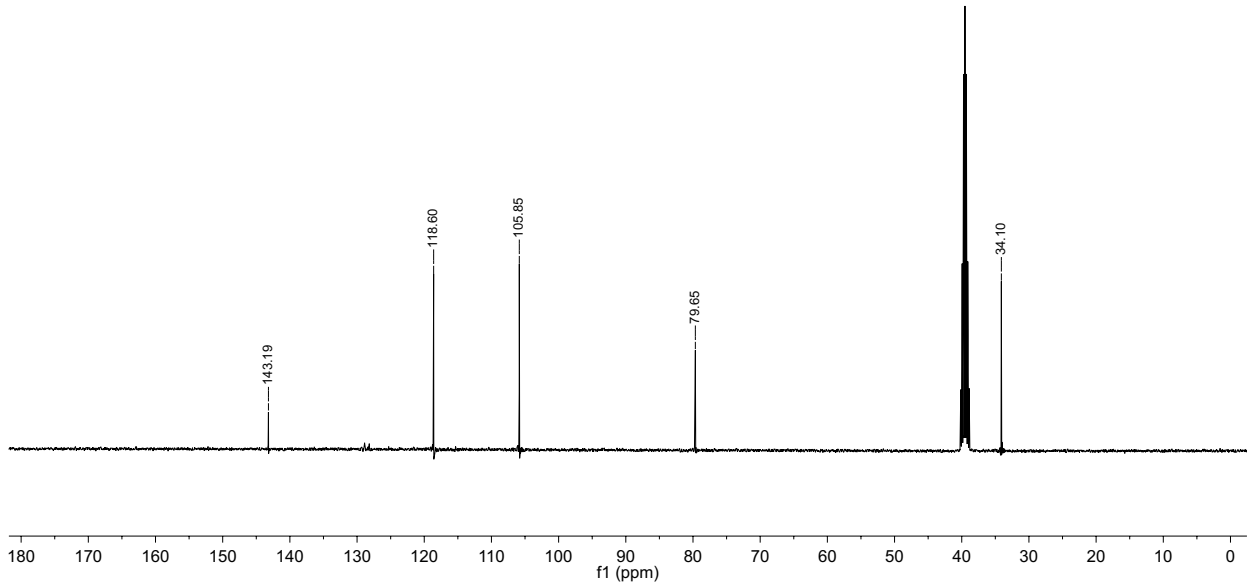

1,3-Dimethyl-2,3-dihydro-1*H*-benzo[*d*]imidazole 419

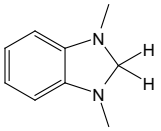

^{1}H NMR (400 MHz, Chloroform-*d*) δ 6.71 – 6.65 (m, 2H), 6.43 (dd, *J* = 5.4, 3.2 Hz, 2H), 4.34 (s, 2H), 2.74 (s, 6H).

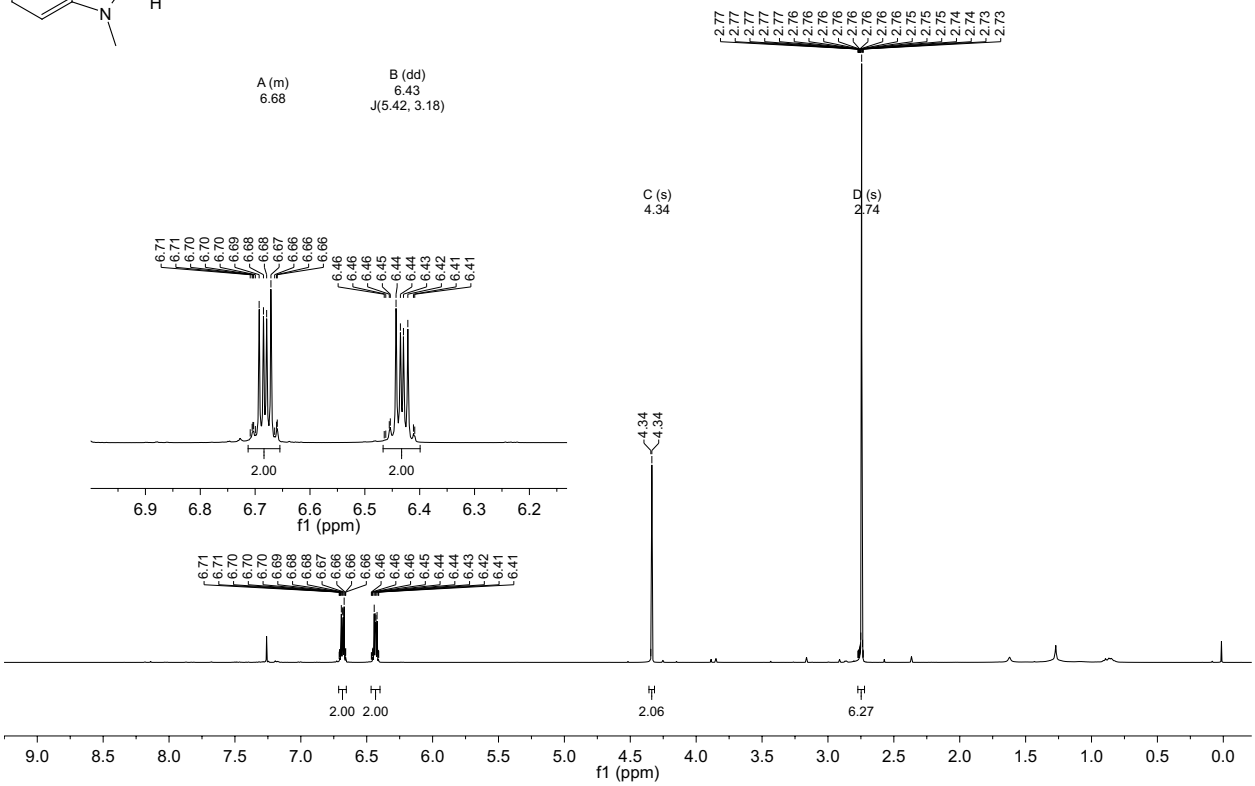

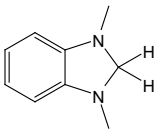

^{13}C NMR (101 MHz, Chloroform-*d*) δ 143.3, 119.3, 106.3, 80.4, 34.6.

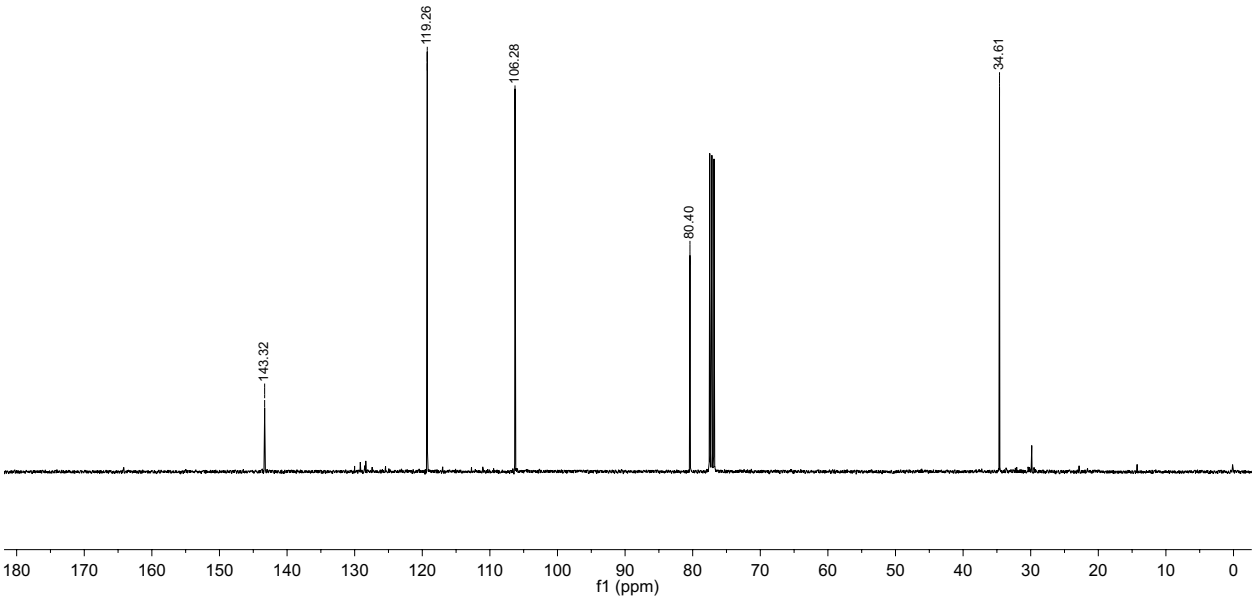

Biphenyl 421

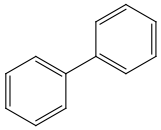

^{1}H NMR (400 MHz, Chloroform-*d*) δ 7.65 – 7.60 (m, 4H), 7.50 – 7.44 (m, 4H), 7.40 – 7.35 (m, 2H).

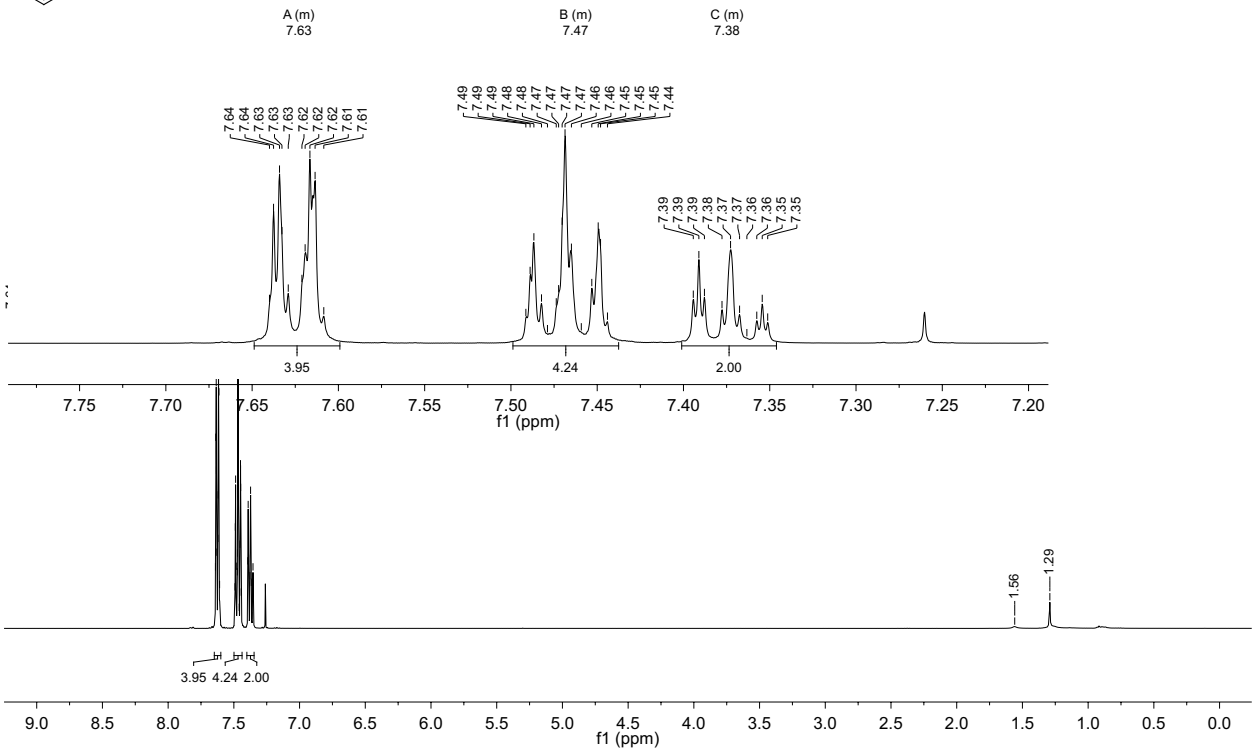

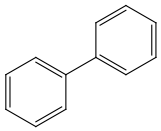

^{13}C NMR (101 MHz, $CDCl_3$) δ 141.39, 128.89, 127.39, 127.31.

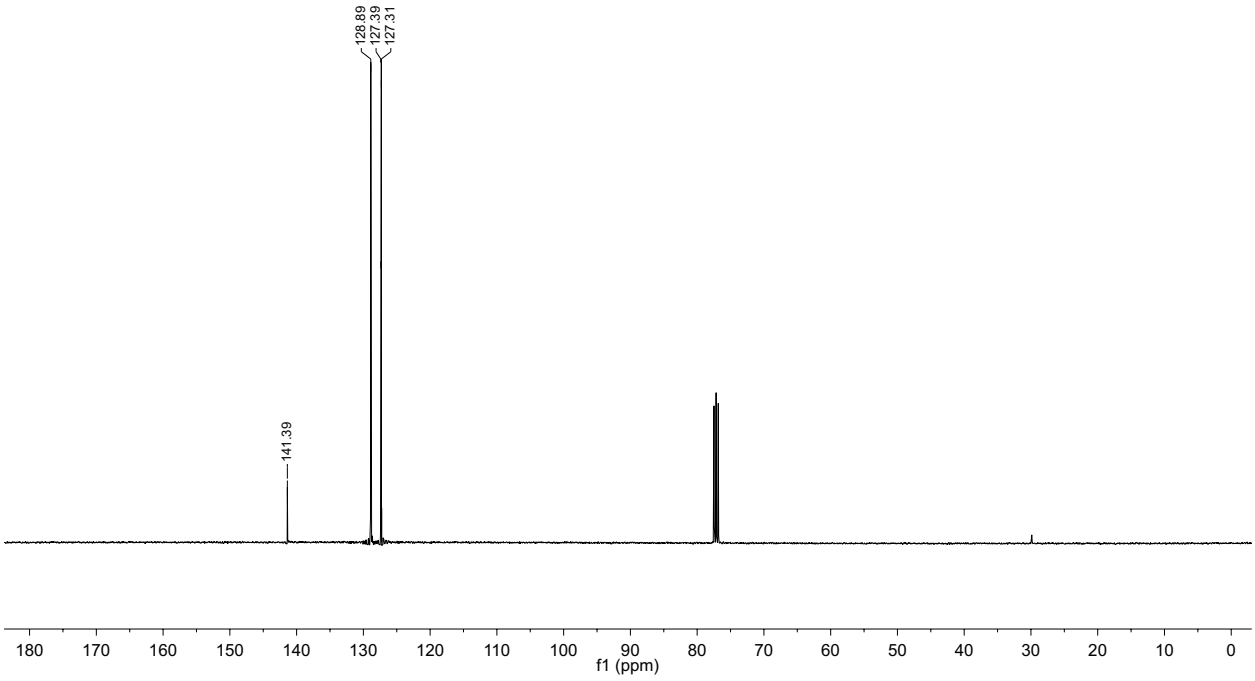

p-Terphenyl 422

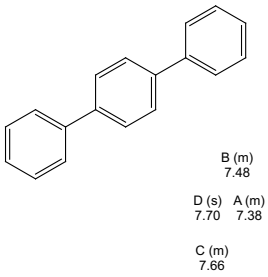

^{1}H NMR (400 MHz, Chloroform-*d*) δ 7.70 (s, 4H), 7.68 – 7.64 (m, 4H), 7.51 – 7.45 (m, 4H), 7.40 – 7.33 (m, 2H).

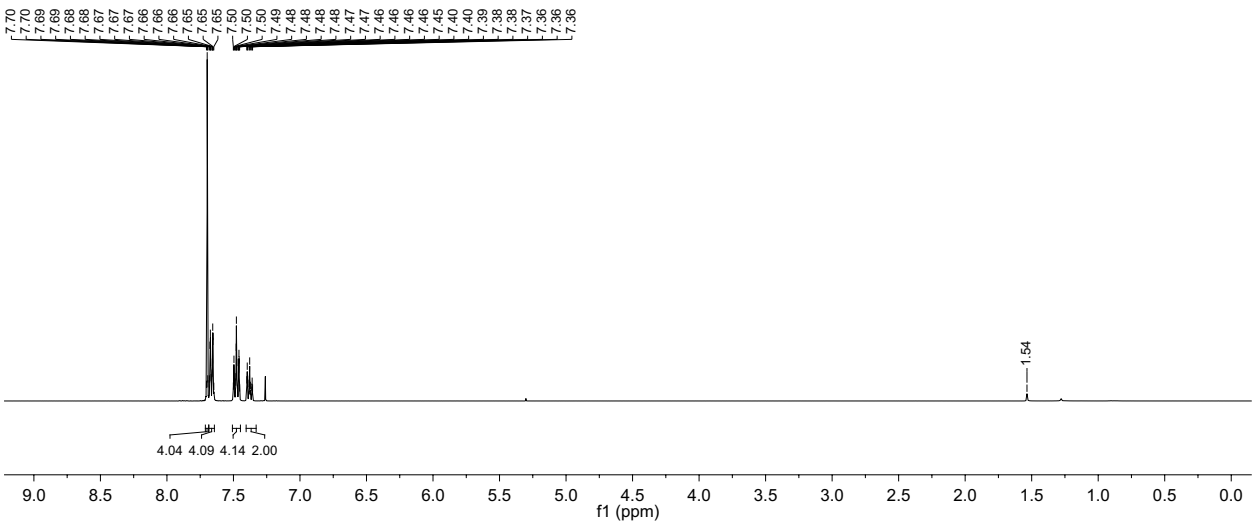

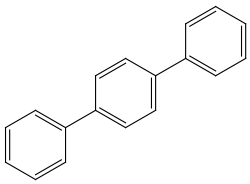

^{13}C NMR (101 MHz, $CDCl_3$) δ 140.86, 140.27, 128.96, 127.64, 127.49, 127.20.

tert-Butyl-3-methylindoline-1-carboxylate 427

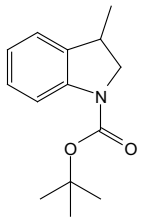

^{1}H NMR (400 MHz, Chloroform-*d*) δ 7.61 (br m, 1H), 7.20 – 7.14 (m, 1H), 7.14 – 7.11 (m, 1H), 6.95 (ddd, *J* = 7.4, 1.1 Hz, 1H), 4.14 (t, *J* = 10.3 Hz, 1H), 3.57 – 3.46 (m, 1H), 3.45 – 3.31 (m, 1H), 1.57 (s, 9H), 1.32 (d, *J* = 6.8 Hz, 3H).

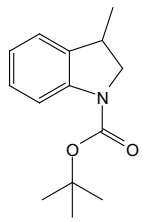

^{13}C NMR (101 MHz, Chloroform-*d*) δ 152.7, 142.0, 136.0, 127.7, 123.6, 122.4, 114.8, 80.5, 55.8, 34.1, 28.6, 20.4.

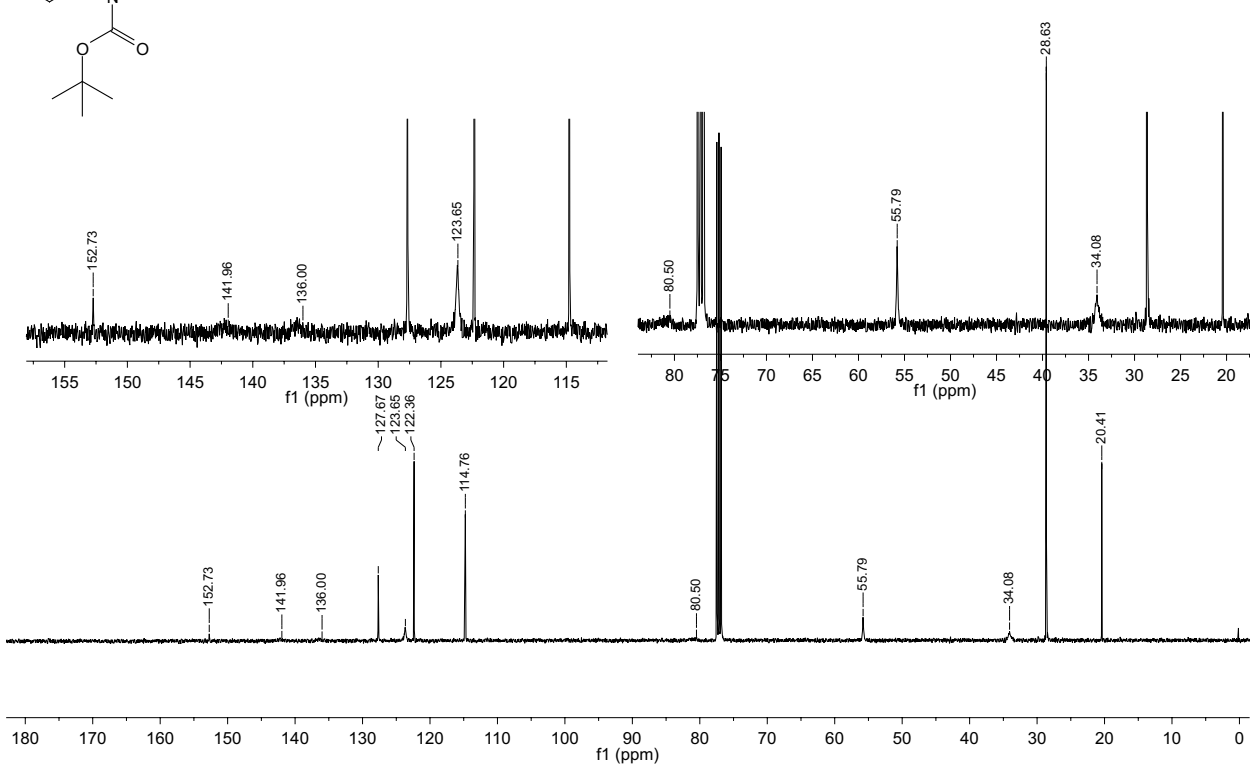

***tert*-Butyl 3-isopropylindoline-1-carboxylate 432a**

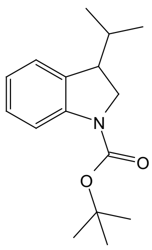

[1]H NMR (400 MHz, DMSO-d_6) δ 7.59 (d, J = 8.1 Hz, 1H), 7.22 – 7.18 (m, 1H), 7.15 (dddd, J = 8.1, 1.4, 0.7 Hz, 1H), 6.94 (ddd, J = 7.5, 1.1 Hz, 1H), 3.89 (dd, J = 11.5, 9.9 Hz, 1H), 3.71 (dd, J = 11.5, 5.2 Hz, 1H), 3.26 (ddd, J = 9.8, 4.9 Hz, 1H), 2.00 (hd, J = 6.8, 4.5 Hz, 1H), 1.53 (s, 9H), 0.92 (d, J = 6.9 Hz, 3H), 0.76 (d, J = 6.8 Hz, 3H).

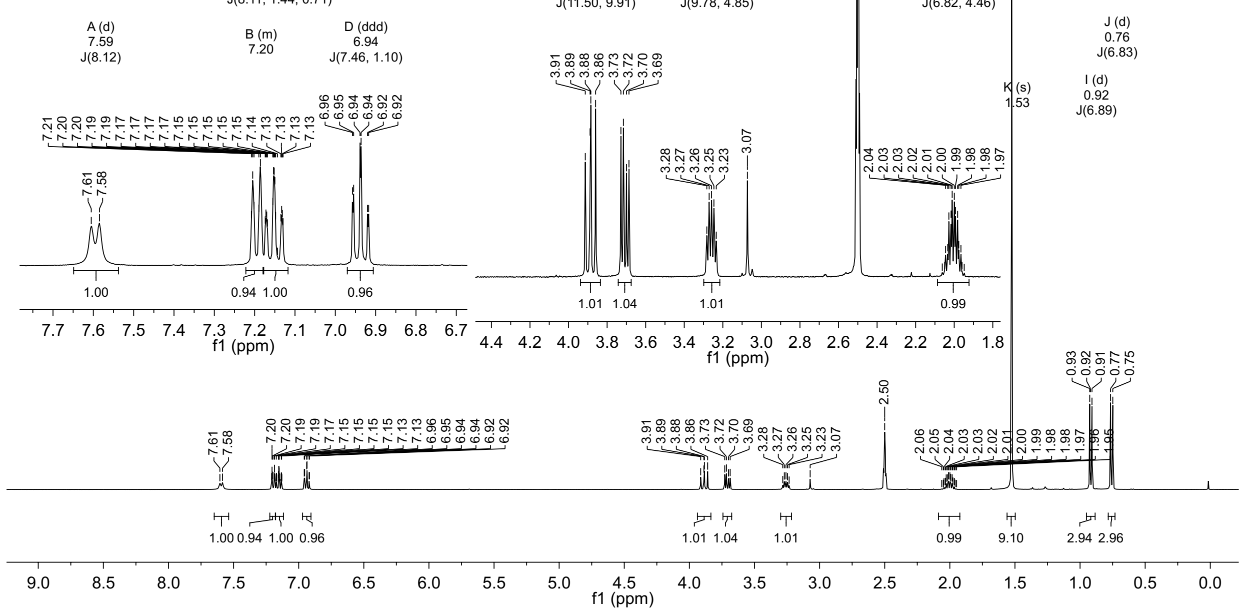

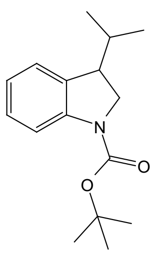

[13]C NMR (101 MHz, DMSO-d_6) δ 151.3, 142.3, 133.3, 126.9, 124.2, 121.5, 113.7, 79.8, 49.4, 44.2, 30.8, 27.7, 19.1, 16.9.

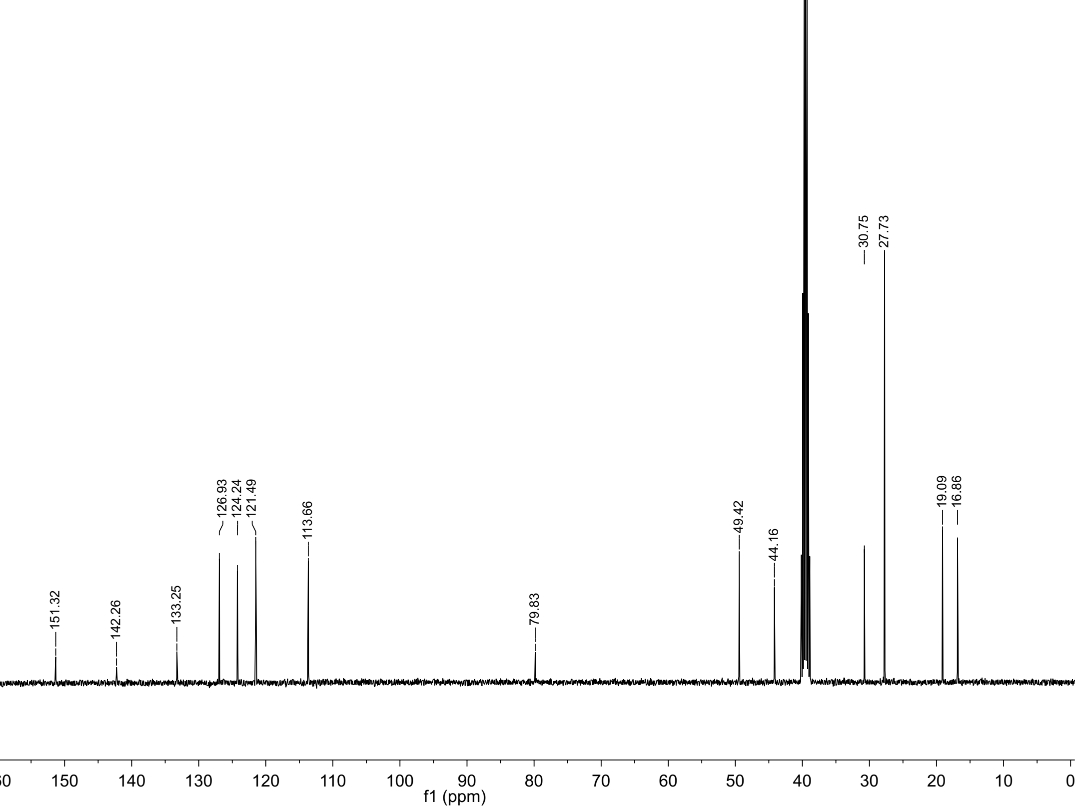

tert-Butyl 3-(acetoxymethyl)indoline-1-carboxylate 432b

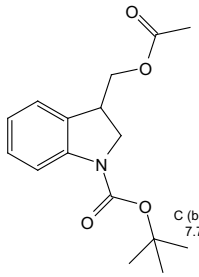

^{1}H NMR (400 MHz, Chloroform-*d*) δ 7.72 (br m, 1H), 7.24 – 7.17 (m, 2H), 6.95 (ddd, *J* = 7.5, 1.1 Hz, 1H), 4.28 (dd, *J* = 11.0, 5.8 Hz, 1H), 4.18 – 4.02 (m, 2H), 3.80 (br s, 1H), 3.63 (tt, *J* = 9.8, 5.5 Hz, 1H), 2.08 (s, 3H), 1.57 (s, 9H).

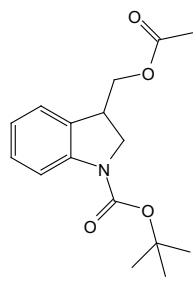

^{13}C NMR (101 MHz, Chloroform-*d*) δ 171.1, 152.6, 134.1, 128.7, 127.5, 124.7 (br) , 122.4, 115.1, 81.0 (br), 66.7, 51.3 (br), 39.2 (br), 28.6, 21.0.

tert-Butyl 3-(2-methoxy-2-oxoethyl)indoline-1-carboxylate 432c

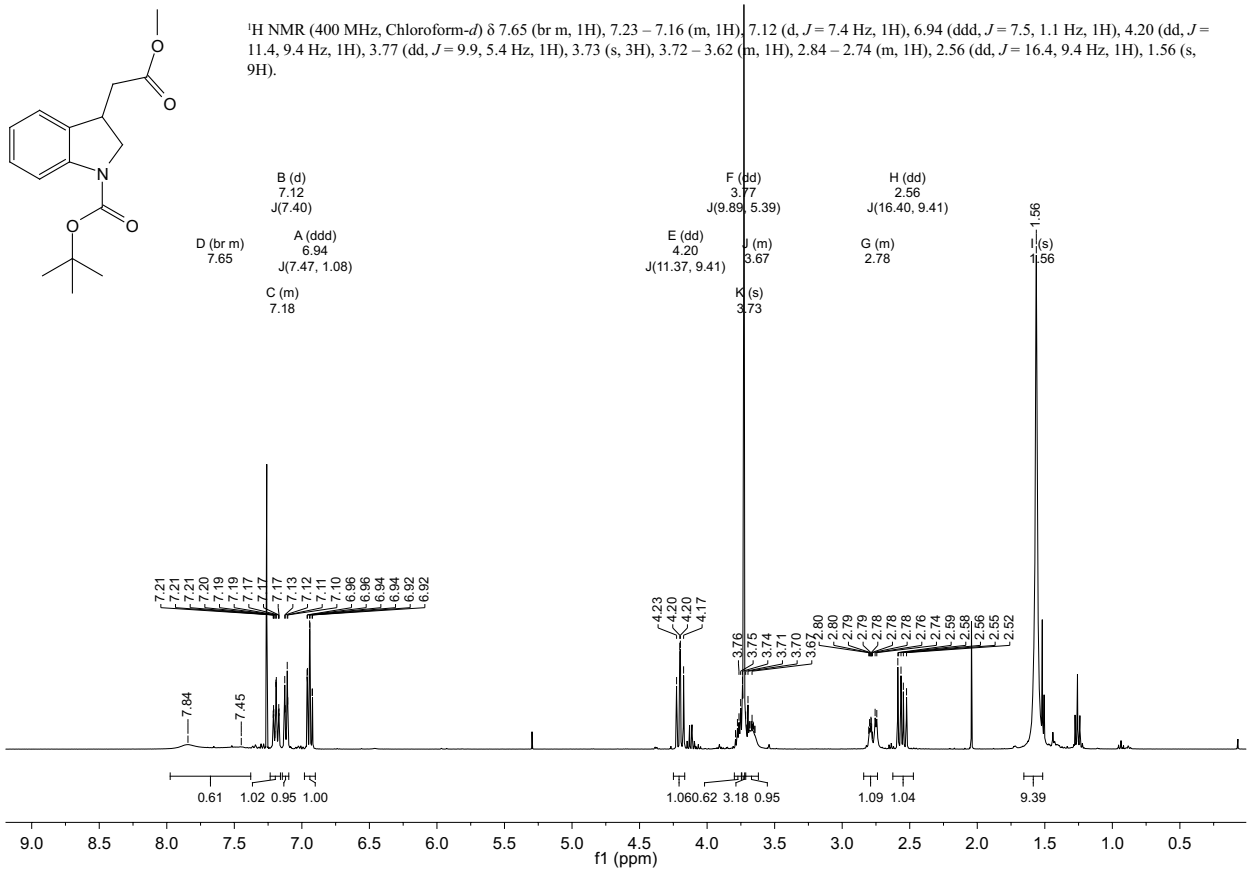

^{1}H NMR (400 MHz, Chloroform-*d*) δ 7.65 (br m, 1H), 7.23 – 7.16 (m, 1H), 7.12 (d, *J* = 7.4 Hz, 1H), 6.94 (ddd, *J* = 7.5, 1.1 Hz, 1H), 4.20 (dd, *J* = 11.4, 9.4 Hz, 1H), 3.77 (dd, *J* = 9.9, 5.4 Hz, 1H), 3.73 (s, 3H), 3.72 – 3.62 (m, 1H), 2.84 – 2.74 (m, 1H), 2.56 (dd, *J* = 16.4, 9.4 Hz, 1H), 1.56 (s, 9H).

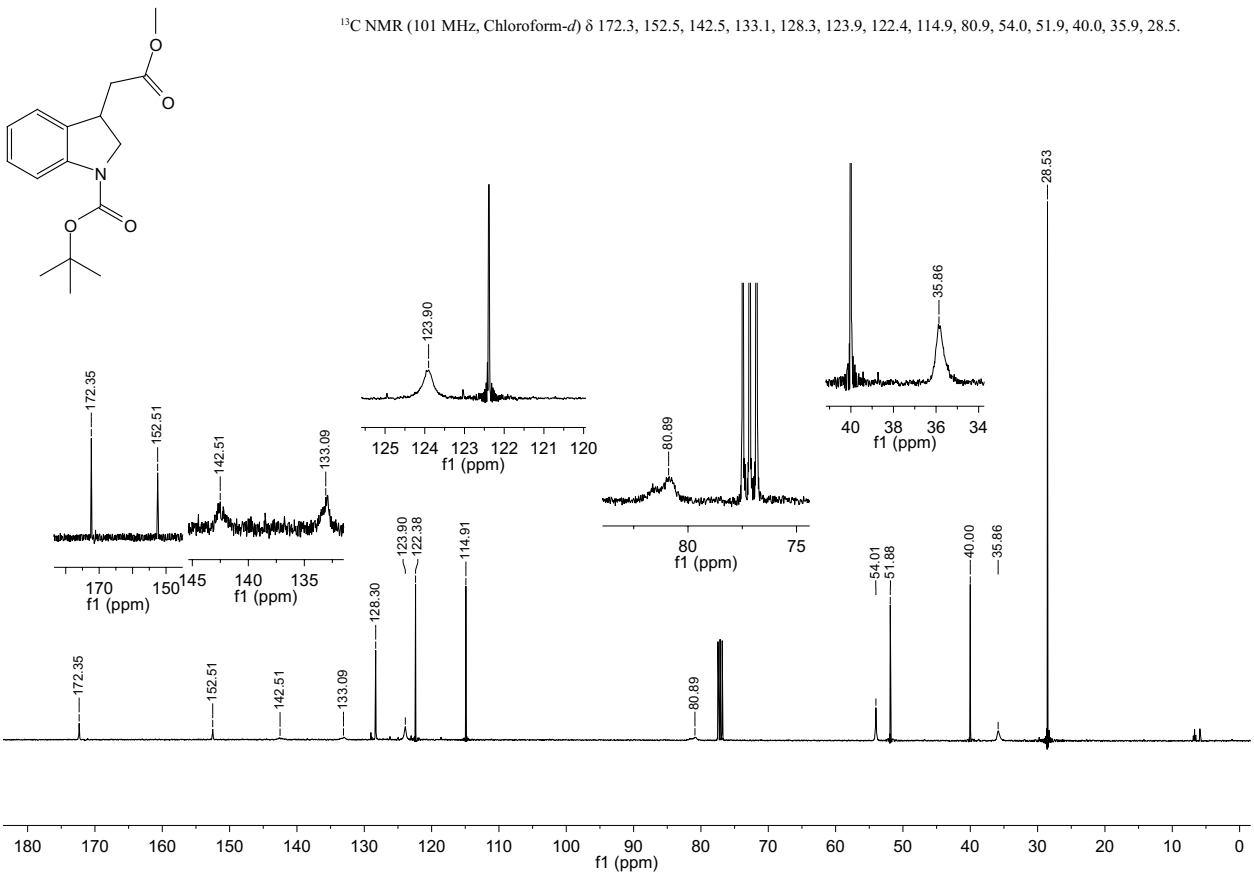

^{13}C NMR (101 MHz, Chloroform-*d*) δ 172.3, 152.5, 142.5, 133.1, 128.3, 123.9, 122.4, 114.9, 80.9, 54.0, 51.9, 40.0, 35.9, 28.5.

3-Methyl-2,3-dihydrobenzofuran 432d

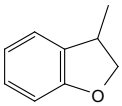

^{1}H NMR (500 MHz, Chloroform-*d*) δ 7.16 (ddd, *J* = 7.3, 1.3 Hz, 1H), 7.12 (ddd, *J* = 7.6, 1.1 Hz, 1H), 6.87 (ddd, *J* = 7.4, 1.1 Hz, 1H), 6.79 (d, *J* = 7.9 Hz, 1H), 4.68 (dd, *J* = 8.8 Hz, 1H), 4.07 (dd, *J* = 8.5, 7.4 Hz, 1H), 3.55 (app h, *J* = 7.2 Hz, 1H), 1.34 (d, *J* = 6.9 Hz, 3H).

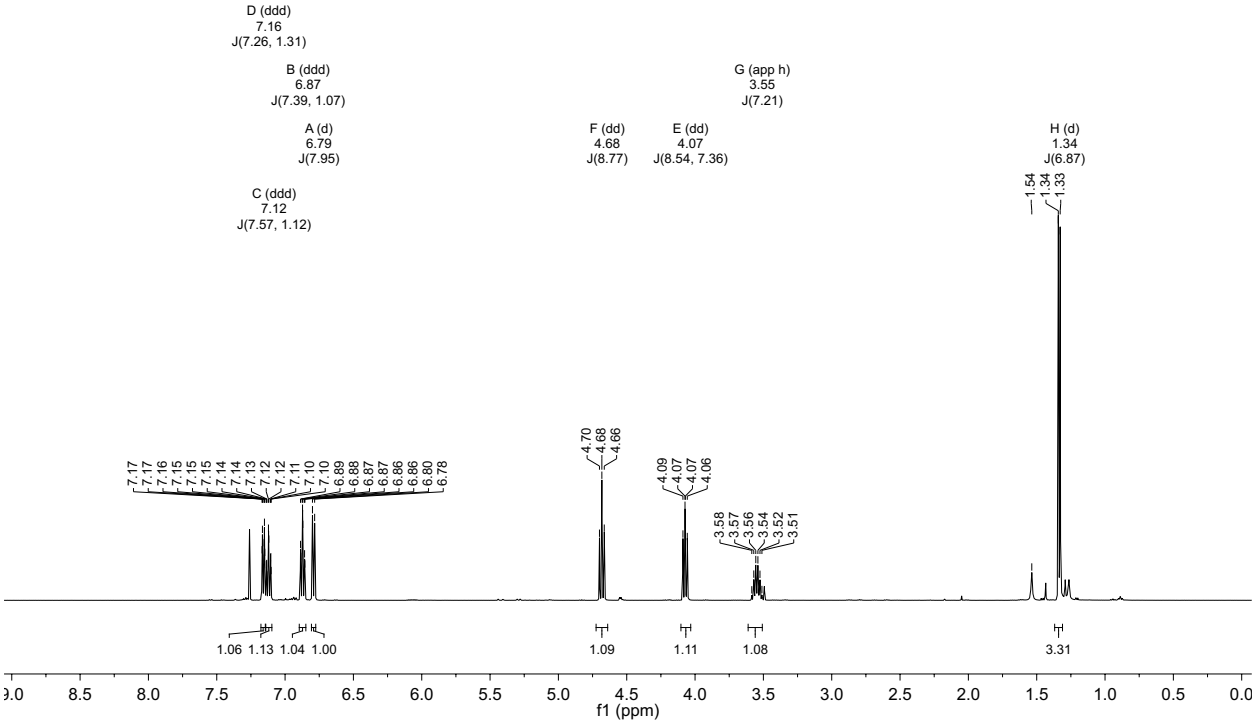

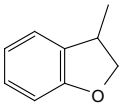

^{13}C NMR (101 MHz, Chloroform-*d*) δ 159.9, 132.4, 128.1, 123.9, 120.6, 109.6, 78.6, 36.6, 19.4.

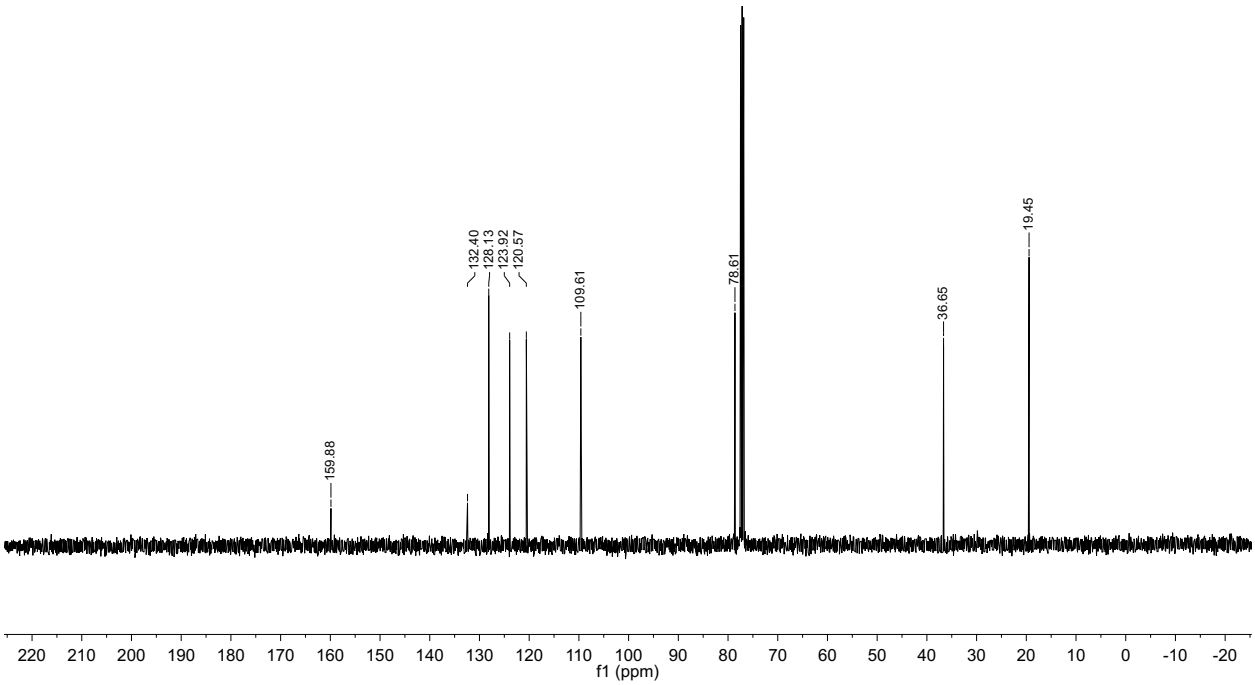

9-(methylsulfonyl)-2,3,4,4a,9,9a-hexahydro-1*H*-carbazole 435

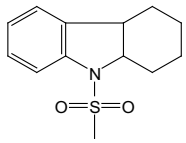

^{1}H NMR (400 MHz, Chloroform-*d*) δ 7.37 (ddd, *J* = 8.0, 0.8 Hz, 1H), 7.24 – 7.15 (m, 2H), 7.08 (ddd, *J* = 7.4, 1.1 Hz, 1H), 4.38 (ddd, *J* = 10.1, 7.8, 5.9 Hz, 1H), 3.57 – 3.48 (m, 1H), 2.93 (s, 3H), 2.20 (dddd, *J* = 14.4, 5.5, 3.7, 1.6 Hz, 1H), 2.12 – 2.01 (m, 1H), 1.83 (dddd, *J* = 14.4, 12.2, 5.9, 4.4 Hz, 1H), 1.68 – 1.51 (m, 2H), 1.51 – 1.40 (m, 1H), 1.33 – 1.17 (m, 2H).

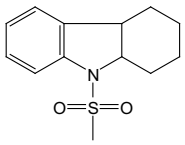

^{13}C NMR (101 MHz, Chloroform-*d*) δ 141.4, 134.7, 127.9, 124.2, 123.6, 115.5, 64.0, 40.5, 38.6, 28.6, 24.7, 22.2, 20.8.

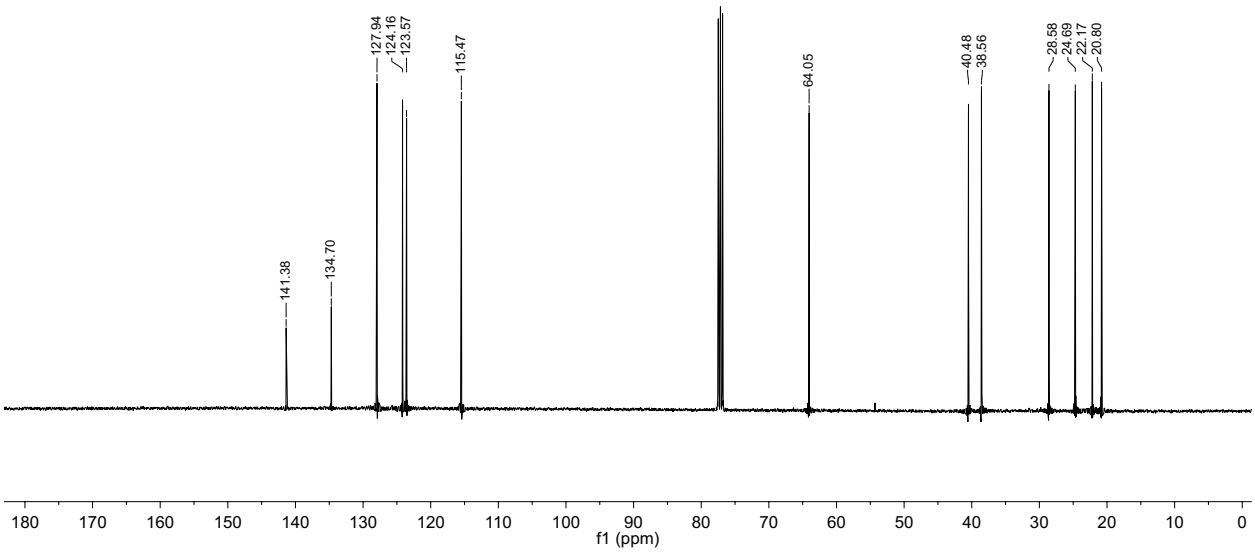

N-(Cyclohex-2-en-1-yl)-*N*-phenylmethanesulfonamide 436

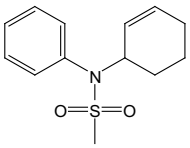

^{1}H NMR (400 MHz, Chloroform-*d*) δ 7.39 – 7.35 (m, 3H), 7.32 – 7.28 (m, 2H), 5.80 – 5.76 (m, 2H), 4.96 – 4.87 (m, 1H), 2.98 (s, 3H), 2.00 (dddd, *J* = 11.1, 5.4, 4.0, 2.9 Hz, 1H), 1.92 – 1.83 (m, 1H), 1.83 – 1.73 (m, 1H), 1.67 – 1.45 (m, 3H).

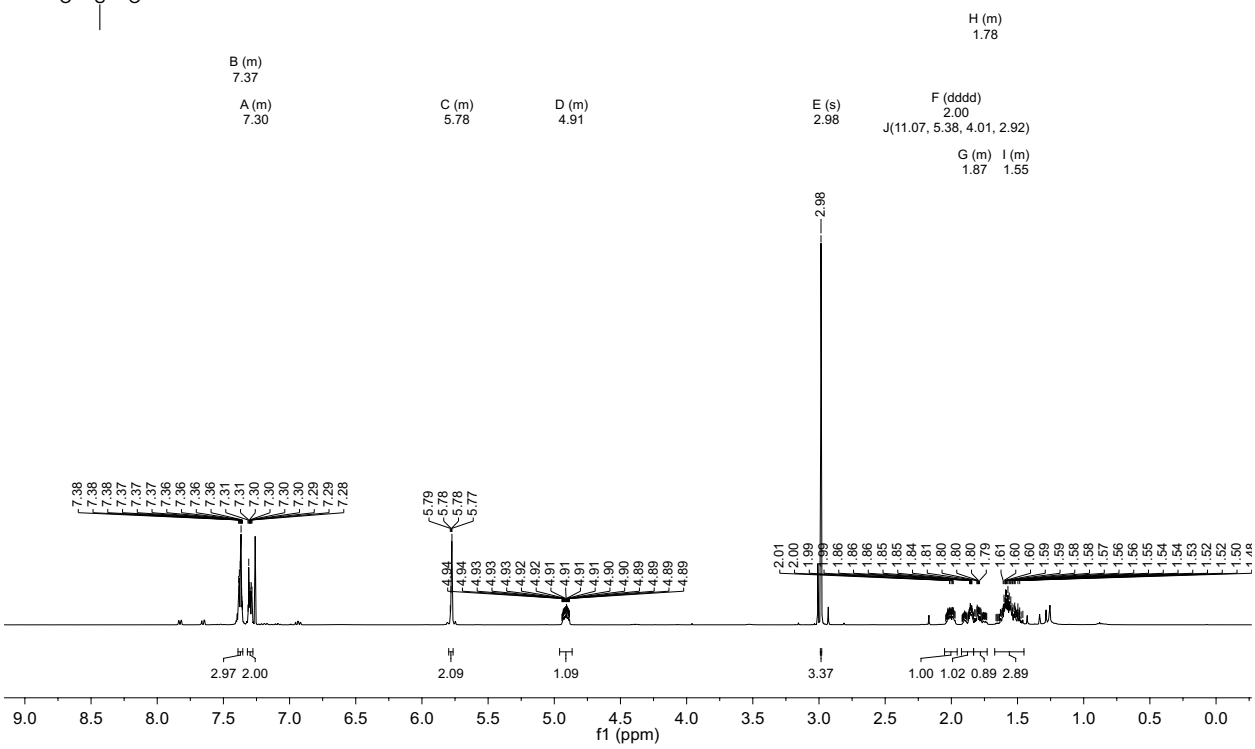

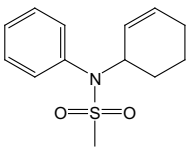

^{13}C NMR (101 MHz, Chloroform-*d*) δ 136.5, 131.9, 131.6, 129.2, 128.8, 128.5, 56.4, 40.9, 29.2, 24.3, 21.4.

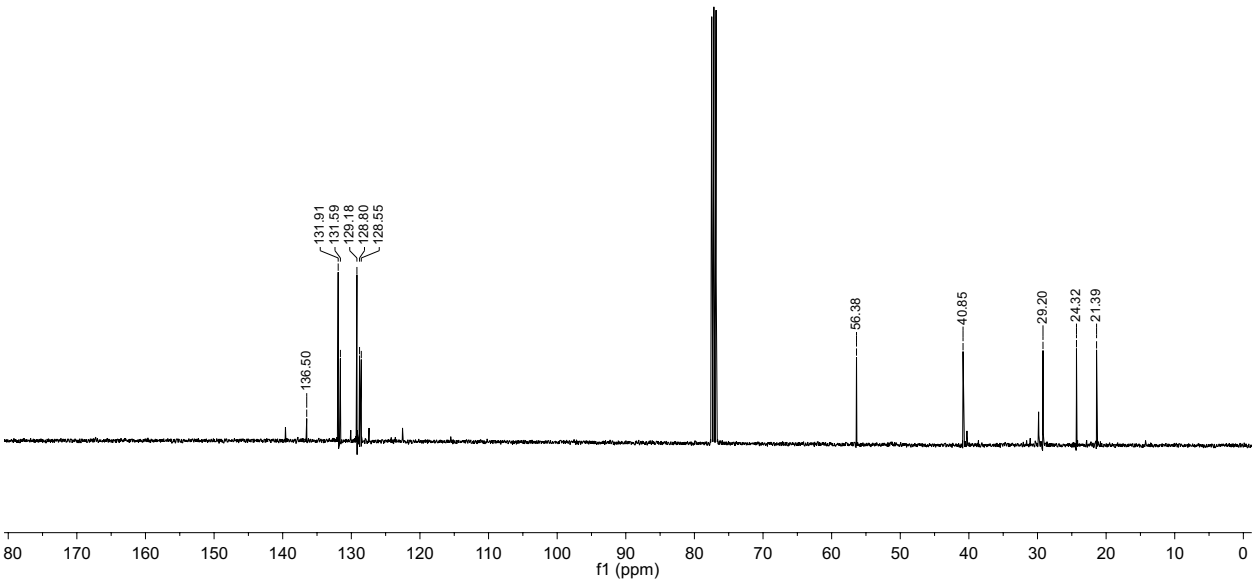

N-(Cyclohex-2-en-1-yl)-*N*-phenylmethanesulfonamide 436

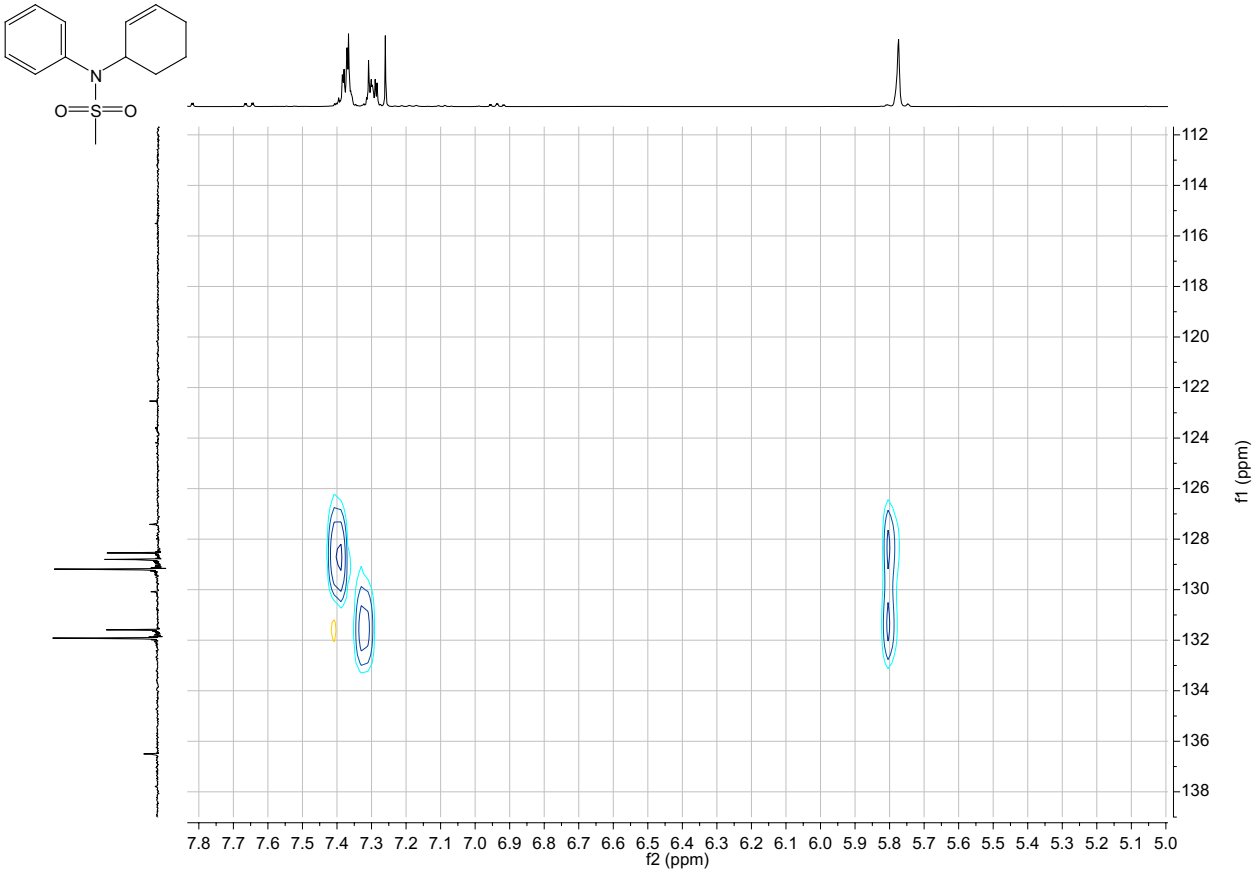

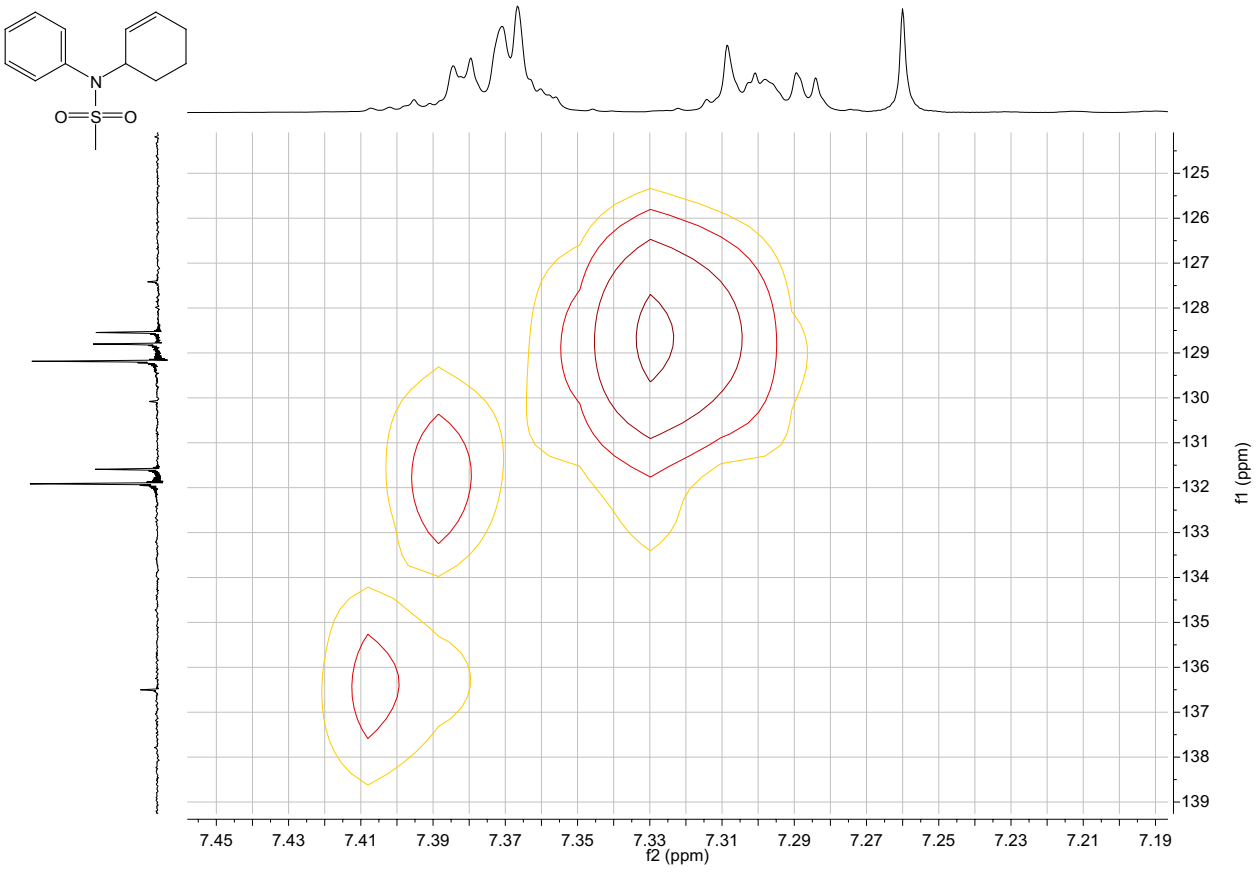

3-Ethylidene-1-(methylsulfonyl)indoline 438a

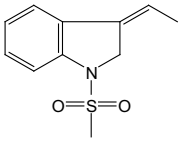

Major Isomer: ^{1}H NMR (400 MHz, Chloroform-*d*) δ 7.49 (ddd, *J* = 8.2, 0.9 Hz, 1H), 7.41 (ddd, *J* = 7.7, 0.9 Hz, 1H), 7.22 (ddd, *J* = 7.8, 1.4 Hz, 1H), 7.06 (ddd, *J* = 7.6, 1.0 Hz, 1H), 2.92 – 2.87 (m, 4H), 6.03 (qt, *J* = 7.1, 3.1 Hz, 1H), 4.62 – 4.59 (m, 2H), 2.89 (s, 3H), 1.81 (dt, *J* = 7.2, 2.1 Hz, 3H).

Minor Isomer

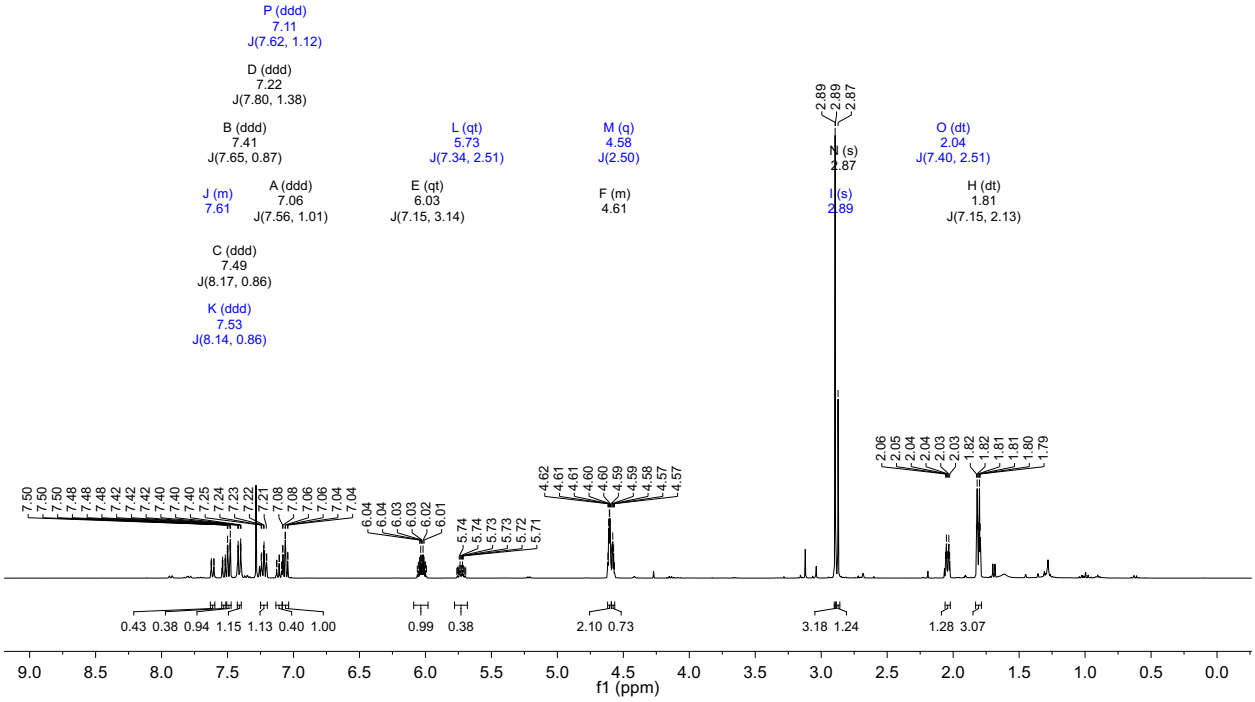

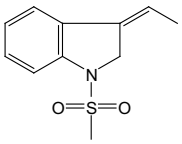

Major Isomer: ^{13}C NMR (101 MHz, Chloroform-*d*) δ 143.6, 132.9, 130.3, 129.2, 124.0, 120.4, 114.6, 114.3, 53.7, 35.1, 14.9.

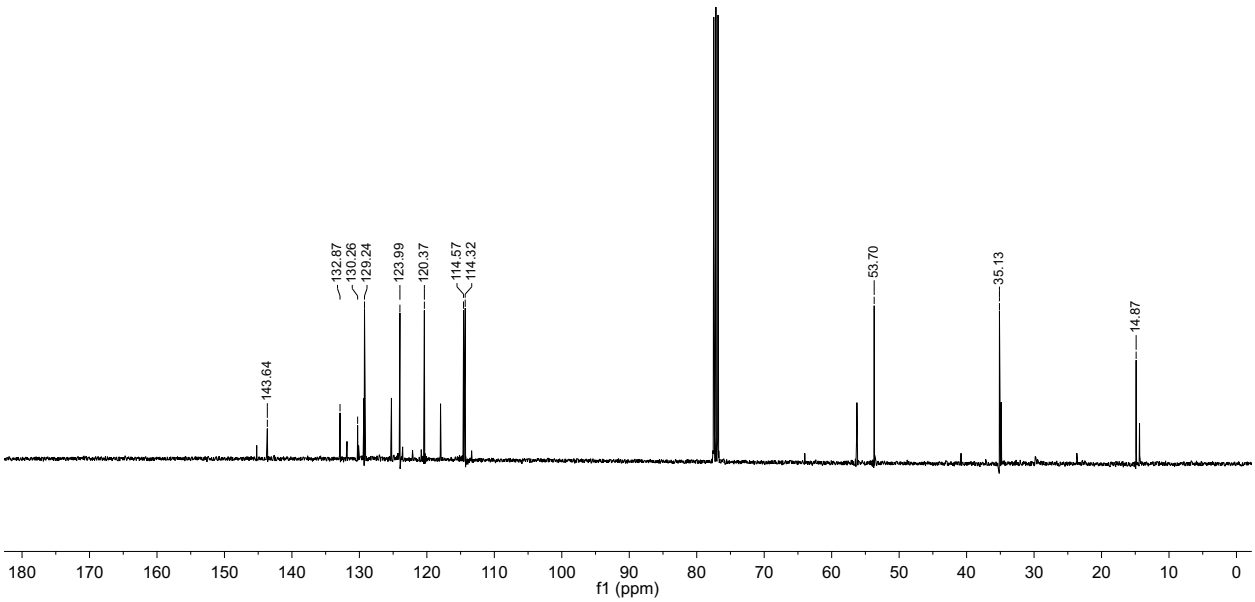

3-Ethylidene-1-(methylsulfonyl)indoline 438a

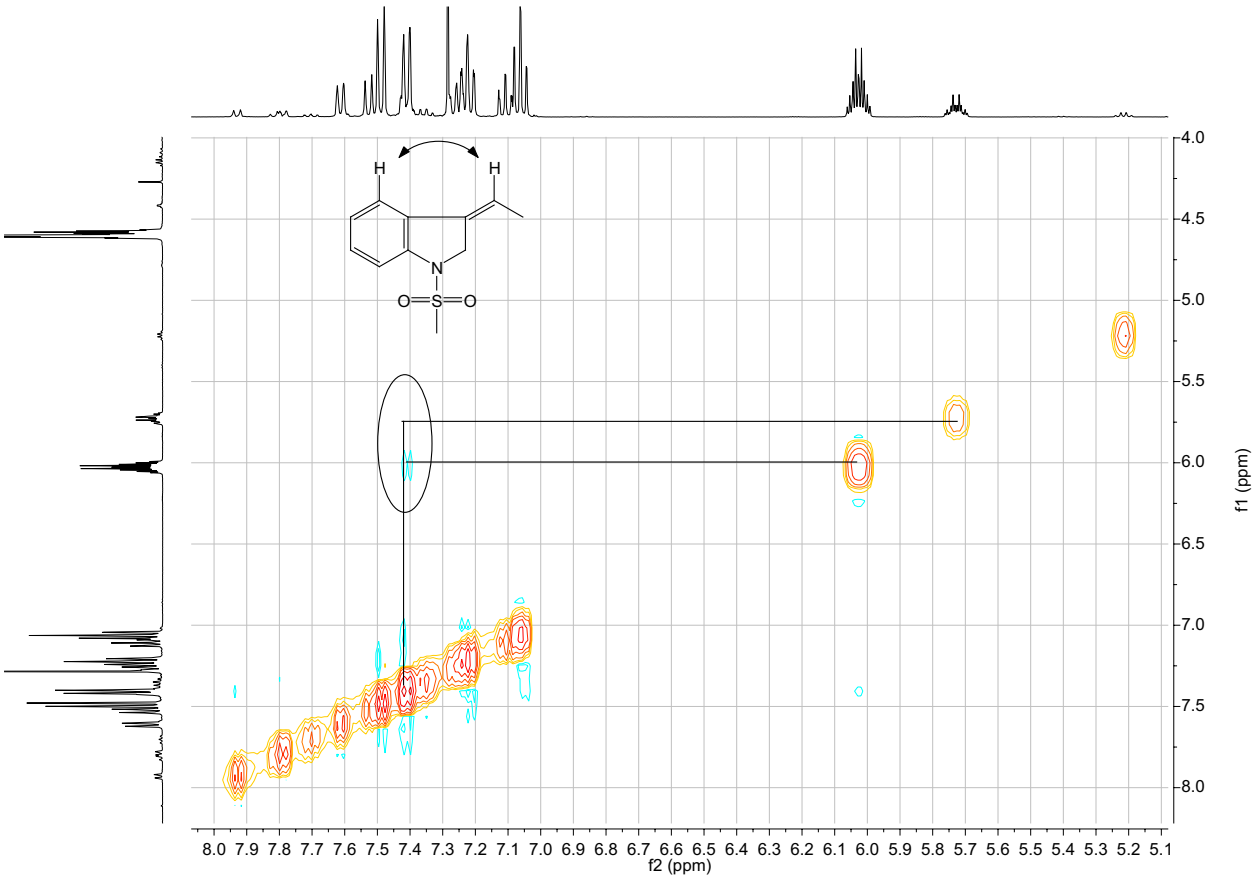

N-(But-2-yn-1-yl)-*N*-phenylmethanesulfonamide 439a

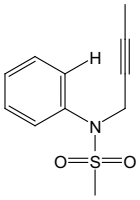

^{1}H NMR (400 MHz, Chloroform-*d*) δ 7.60 – 7.56 (m, 2H), 7.42 – 7.37 (m, 2H), 7.36 – 7.30 (m, 1H), 4.39 (q, *J* = 2.4 Hz, 2H), 3.02 (s, 3H), 1.88 (t, *J* = 2.4 Hz, 3H).

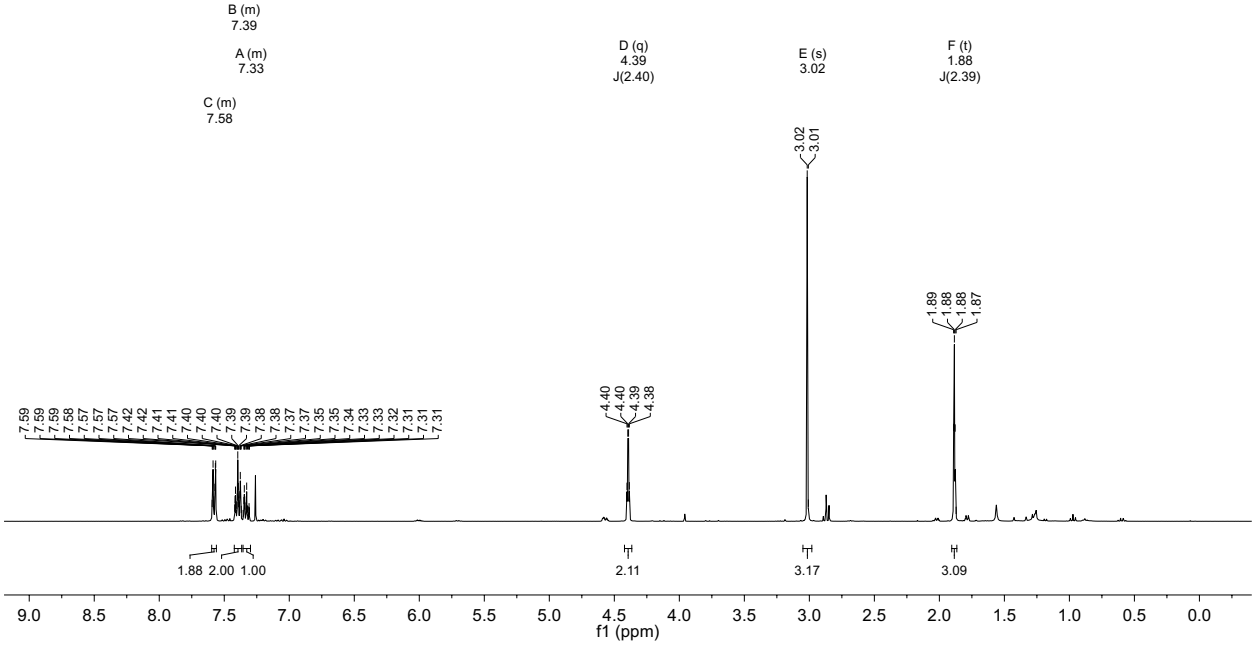

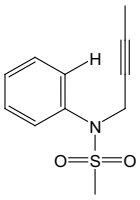

^{13}C NMR (101 MHz, Chloroform-*d*) δ 140.6, 129.5, 128.1, 127.4, 82.3, 74.4, 41.8, 38.9, 3.7.

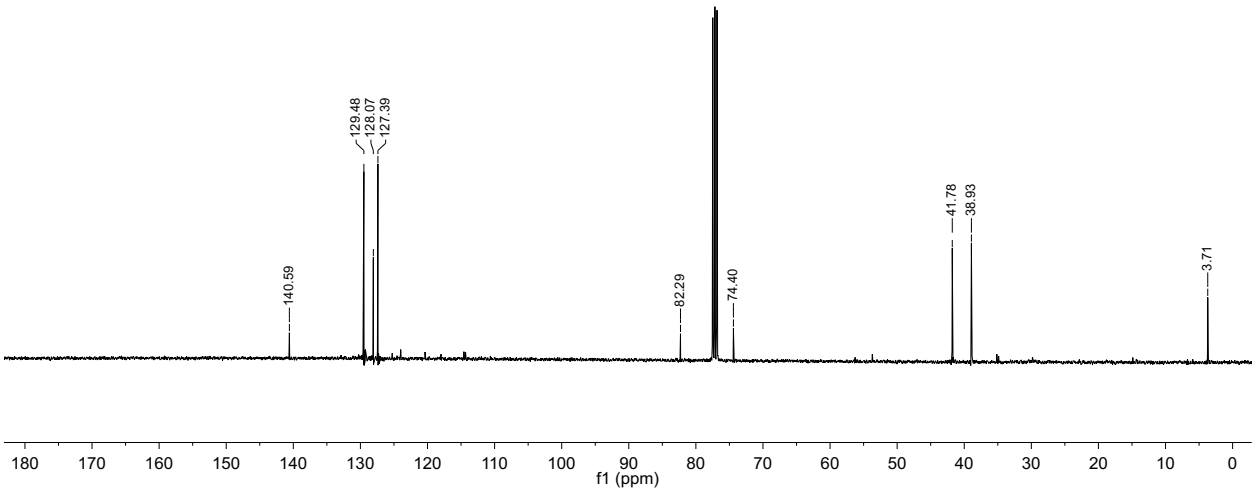

3-(Cyclohexylmethylene)-1-(methylsulfonyl)indoline 438b

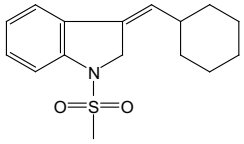

Major Isomer: ^{1}H NMR (400 MHz, Chloroform-*d*) δ 7.45 (ddd, *J* = 8.2, 0.9 Hz, 1H), 7.40 – 7.37 (m, 1H), 7.19 (ddd, *J* = 8.2, 7.4, 1.3 Hz, 1H), 7.03 (ddd, *J* = 7.5, 1.0 Hz, 1H), 5.79 (dt, *J* = 9.6, 3.1 Hz, 1H), 4.60 (d, *J* = 3.0 Hz, 2H), 2.87 (s, 3H), 2.09 (tdt, *J* = 11.6, 10.1, 3.6 Hz, 1H), 1.85 – 1.65 (m, 6H), 1.44 – 1.11 (m, 6H).
Minor Isomer

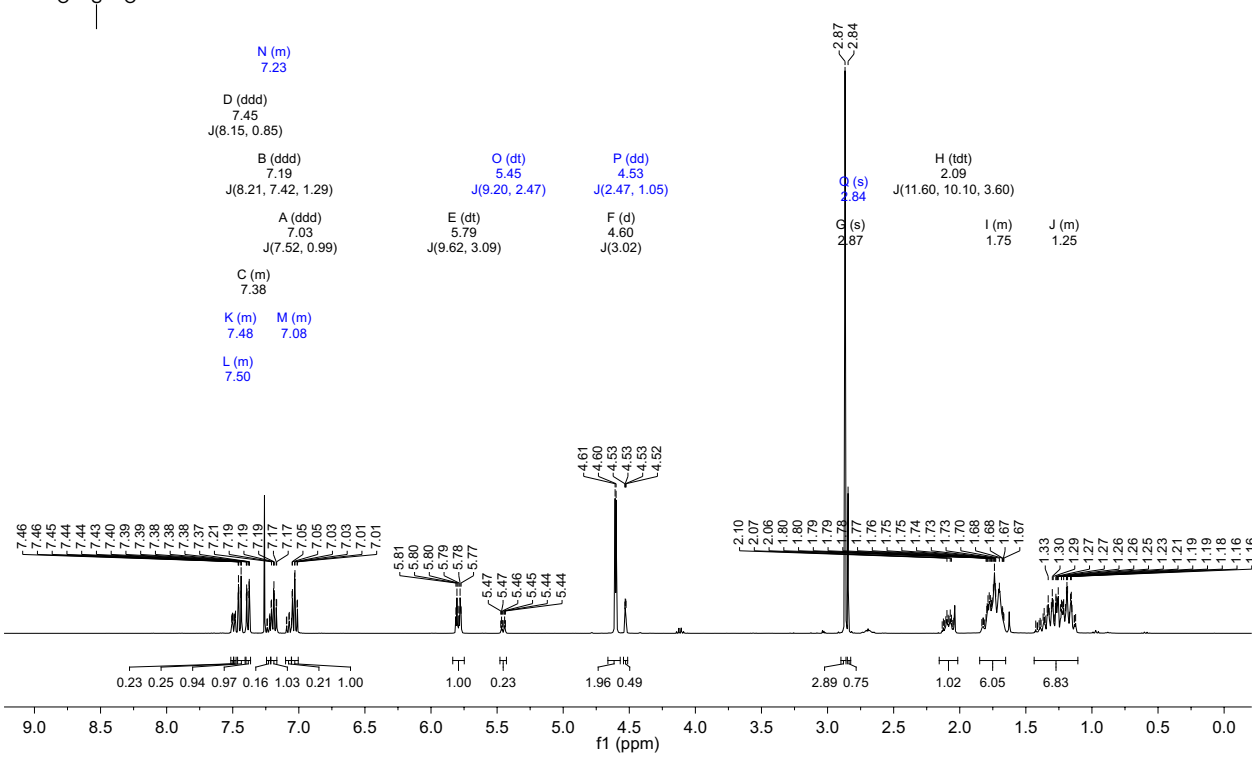

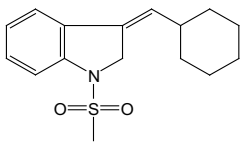

Major Isomer: ^{13}C NMR (101 MHz, $CDCl_3$) δ 143.6, 130.4, 130.0, 129.2, 125.9, 123.9, 120.5, 114.2, 53.4, 39.2, 35.1, 32.5, 26.0, 25.9.
Minor Isomer: ^{13}C NMR (101 MHz, Chloroform-*d*) δ 145.3, 130.2, 129.4, 129.3, 124.9, 124.0, 120.5, 114.4, 56.3, 37.2, 34.8, 32.8, 26.1, 25.9.

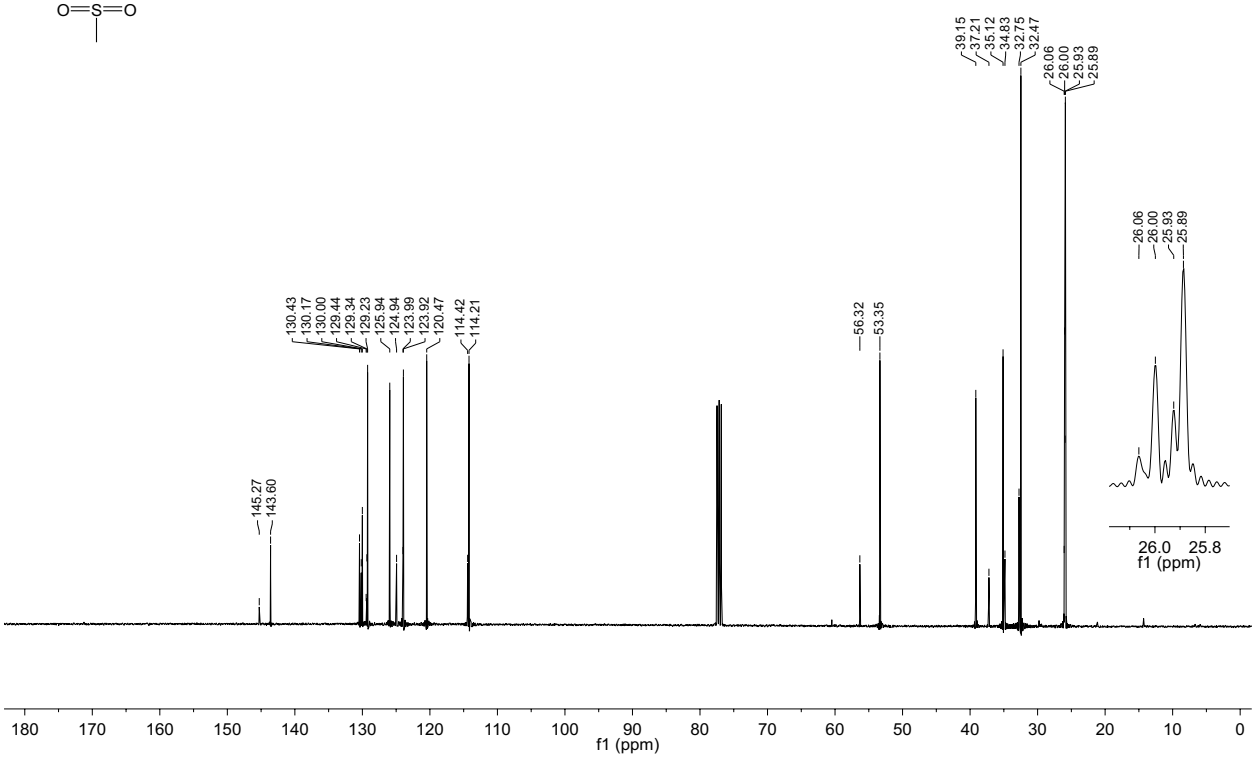

3-(Cyclohexylmethylene)-1-(methylsulfonyl)indoline 438

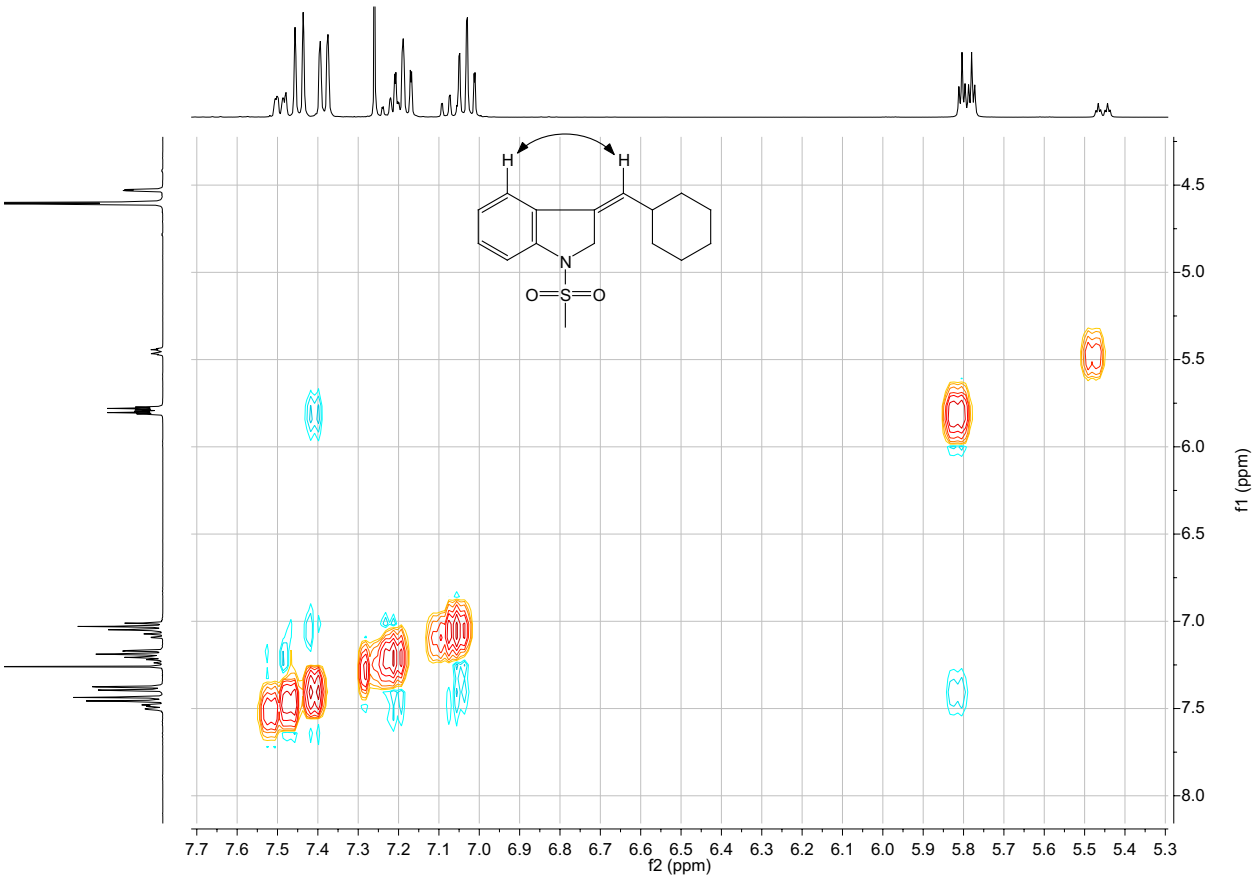

tert-Butyl 3-(2-((tert-butyldiphenylsilyl)oxy)ethyl)-1*H*-indole-1-carboxylate 441a

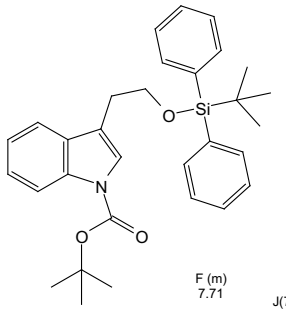

^{1}H NMR (400 MHz, Chloroform-*d*) δ 7.76 – 7.65 (m, 4H), 7.47 – 7.27 (m, 10H), 6.96 (td, *J* = 7.5, 1.0 Hz, 1H), 4.37 – 4.34 (m, 2H), 4.32 (dt, *J* = 6.1, 2.0 Hz, 2H), 1.55 (s, 9H, major rotamer), 1.52 (s, 9H, minor rotamer), 1.07 (s, 9H).

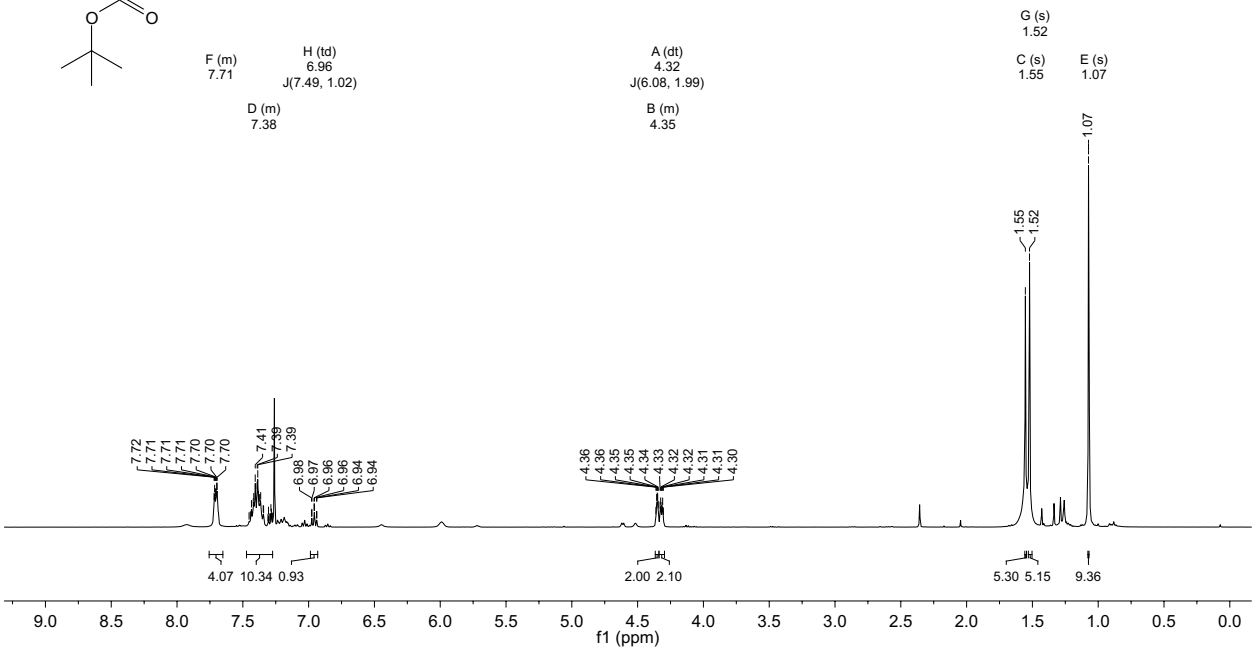

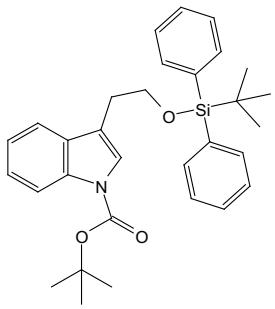

^{13}C NMR (101 MHz, Chloroform-*d*) δ 151.8, 135.8, 133.8, 133.6, 129.9, 129.6, 129.1, 127.9, 122.4, 120.1, 116.3, 115.4, 115.2, 62.2, 61.3, 29.9, 28.6, 27.0, 19.3.

tert-Butyl 3-methyl-1*H*-indole-1-carboxylate 441b

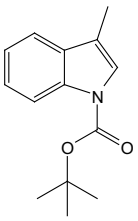

^{1}H NMR (400 MHz, Chloroform-*d*) δ 8.12 (br d, *J* = 8.2 Hz, 1H), 7.50 (ddd, *J* = 7.6, 1.4, 0.7 Hz, 1H), 7.35 (br s, 1H), 7.31 (ddd, *J* = 8.4, 7.2, 1.4 Hz, 1H), 7.29 – 7.20 (m, 1H), 2.27 (d, *J* = 1.3 Hz, 3H), 1.67 (s, 9H).

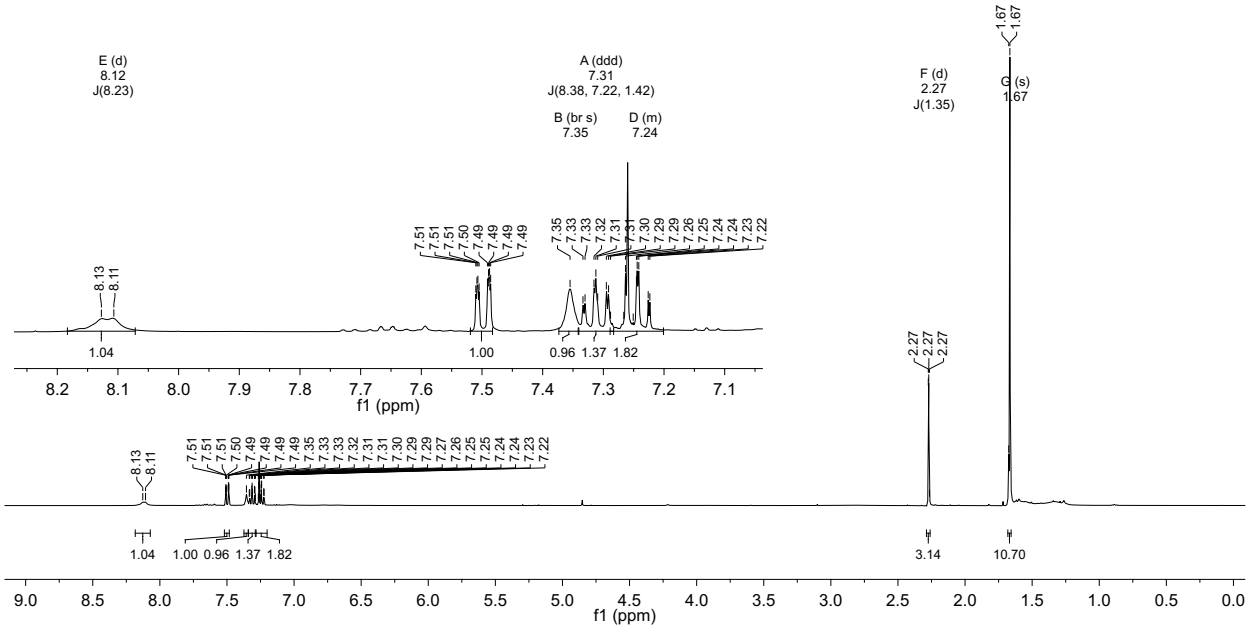

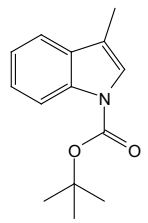

^{13}C NMR (101 MHz, Chloroform-*d*) δ 150.0, 135.6, 131.6, 124.3, 122.9, 122.4, 119.0, 116.5, 115.3, 83.3, 28.4, 9.7.

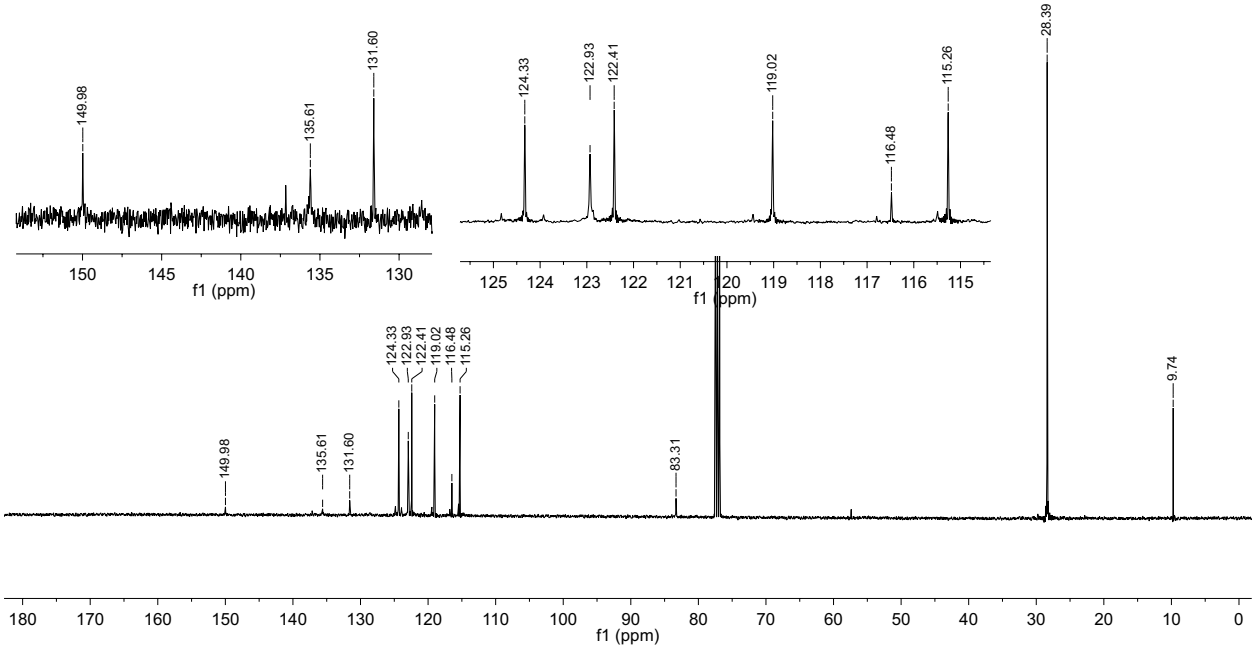

2-(4-Methoxyphenyl)-4-methyltetrahydrofuran 443

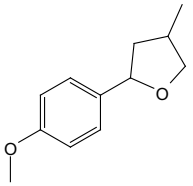

^{1}H NMR (400 MHz, Chloroform-*d*) δ 7.31 – 7.20 (m, 2H), 6.90 – 6.84 (m, 2H), 4.97 (dd, *J* = 6.9 Hz, 1H, major), 4.86 (dd, *J* = 9.9, 5.7 Hz, 1H, minor), 4.25 – 4.18 (m, 1H, major), 4.10 – 4.04 (m, 1H, minor), 3.80 (s, 3H, minor), 3.80 (s, 3H, major), 3.56 (d, *J* = 7.9 Hz, 1H, minor), 3.44 (dd, *J* = 8.2, 6.9 Hz, 1H, major), 2.55 – 2.36 (m, 1H), 2.05 – 1.85 (m, 2H), 1.10 (d, *J* = 6.5 Hz, 3 H, minor), 1.09 (d, *J* = 6.8 Hz, 3H, major).

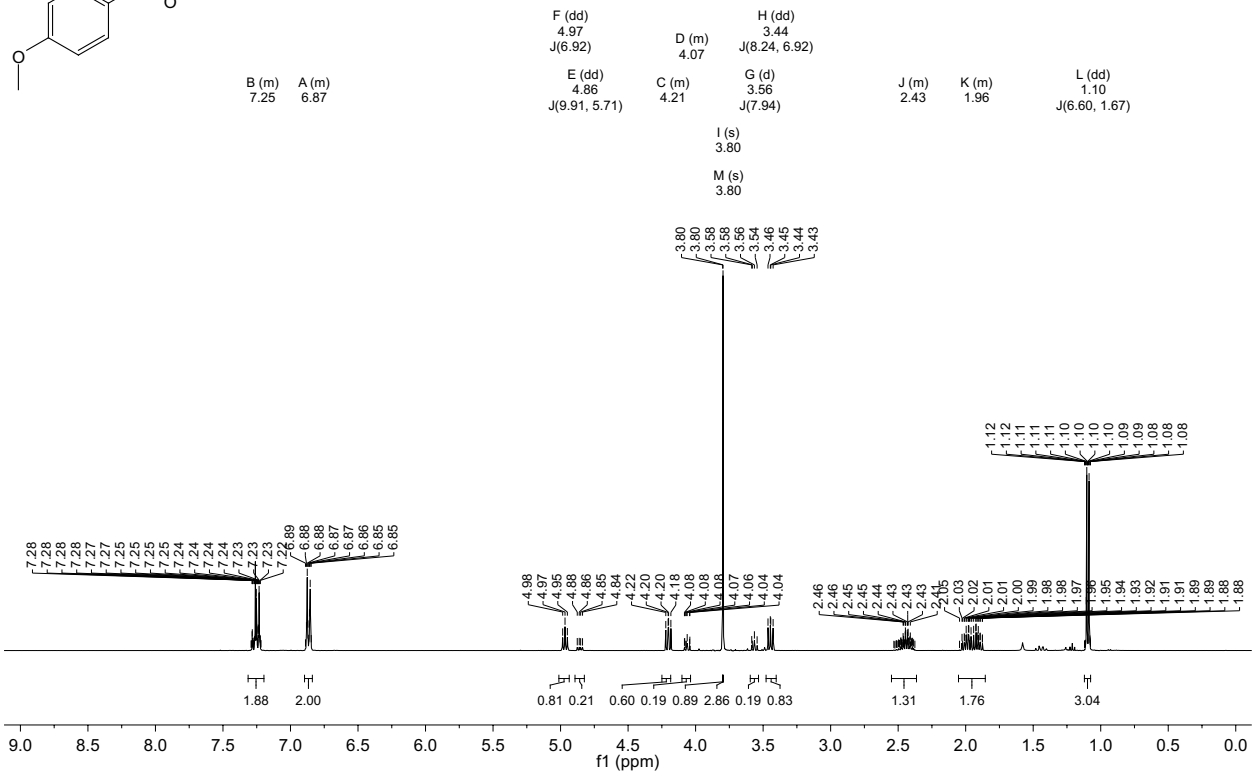

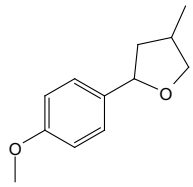

^{13}C NMR (101 MHz, Chloroform-*d,* major) δ 158.9, 136.0, 127.0, 113.8, 79.9, 75.7, 55.4, 42.7, 33.5, 18.0.
^{13}C NMR (101 MHz, Chloroform-*d,* minor) δ 159.00, 135.45, 127.15, 113.87, 81.53, 75.46, 55.43, 43.95, 35.06, 17.67.

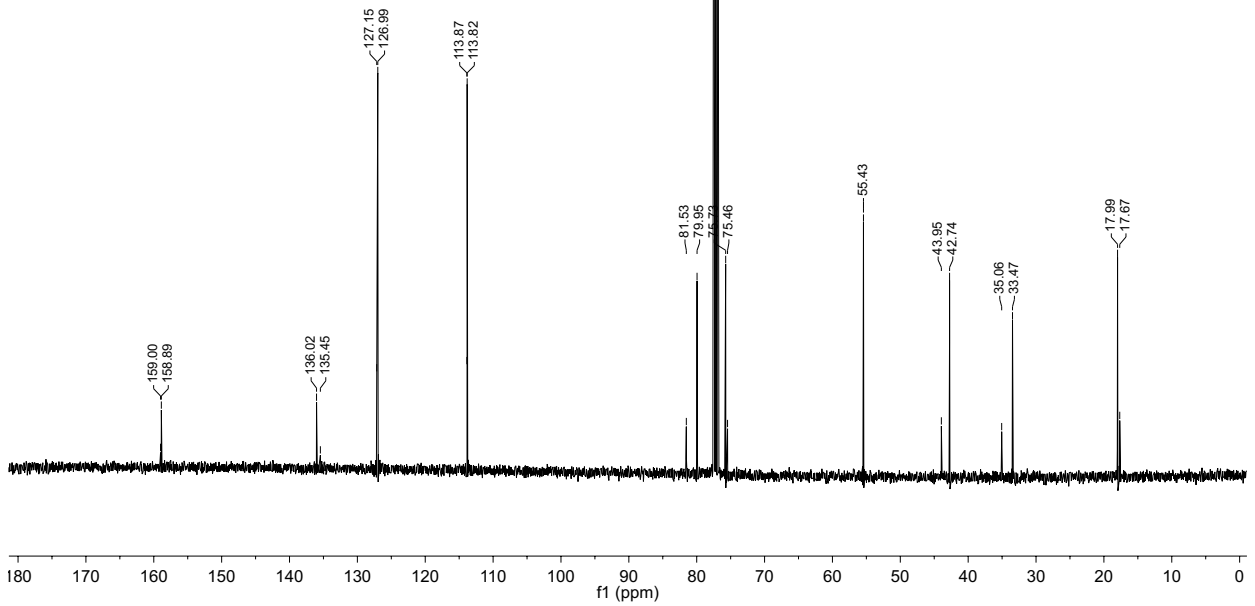

tert-Butyl 3-(4-methyltetrahydrofuran-3-yl)indoline-1-carboxylate 445a

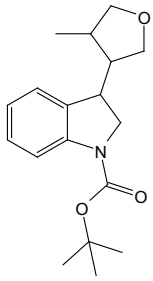

^{1}H NMR (400 MHz, Chloroform-*d*) δ 7.67 (br m, *J* = 147.3 Hz, 1H), 7.24 – 7.11 (m, 1H), 6.99 – 6.89 (m, 2H), 4.16 – 3.20 (m, 7H), 2.62 – 2.02 (m, 2H), 1.57 (br s, 9H), 1.17 (d, *J* = 6.8 Hz, 3H, isomer A), 1.06 (d, *J* = 6.7 Hz, 3H, isomer B).

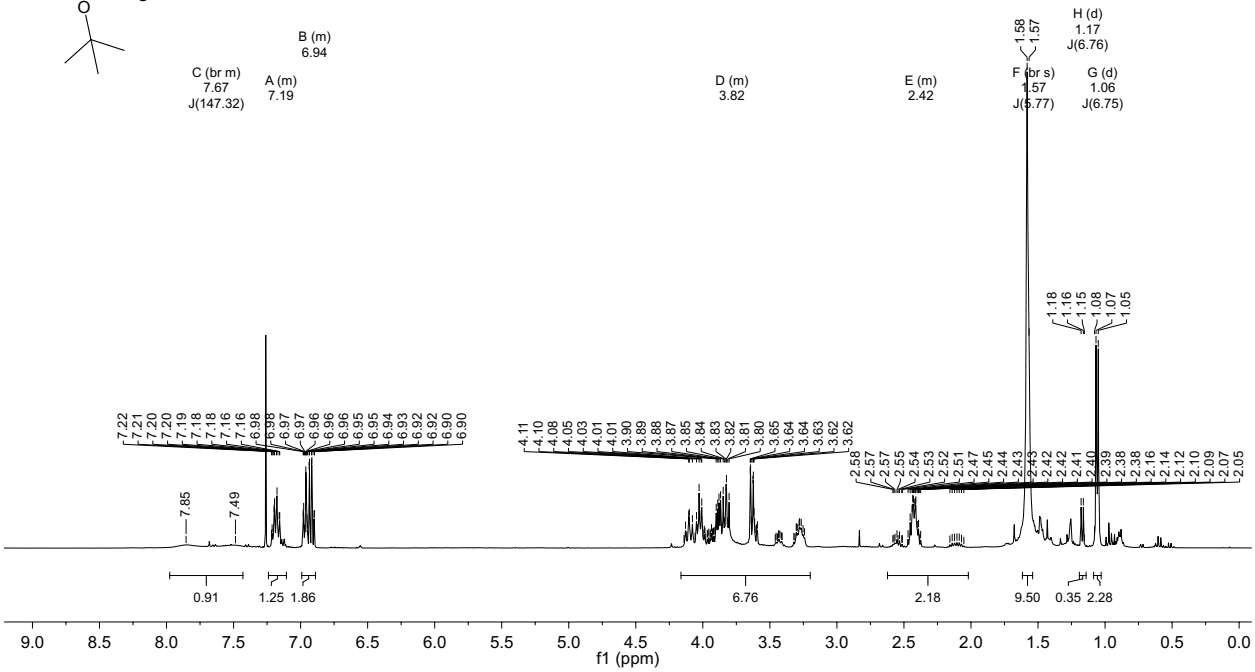

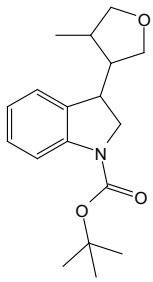

^{13}C NMR (101 MHz, Chloroform-*d*) δ 152.7, 142.4, 133.7, 128.1, 124.6, 122.3, 115.1, 81.4, 75.6, 70.0, 53.1, 48.5, 38.6, 35.4, 28.6, 14.2.

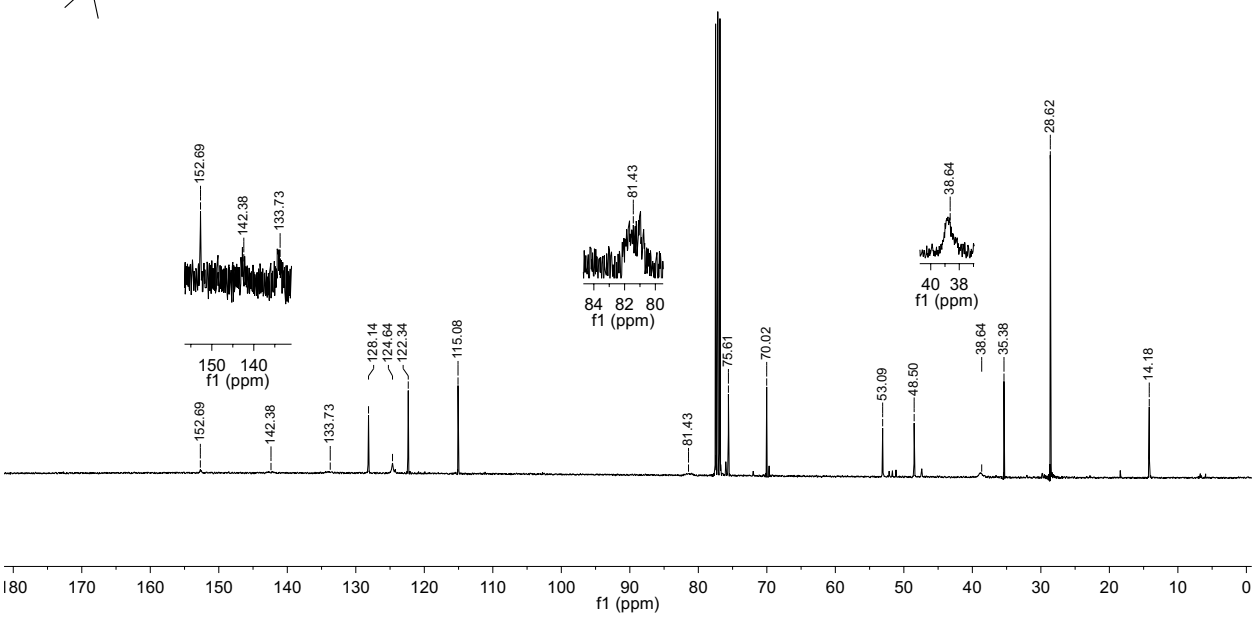

tert-Butyl 3-(4-methyltetrahydrofuran-3-yl)indoline-1-carboxylate 445a

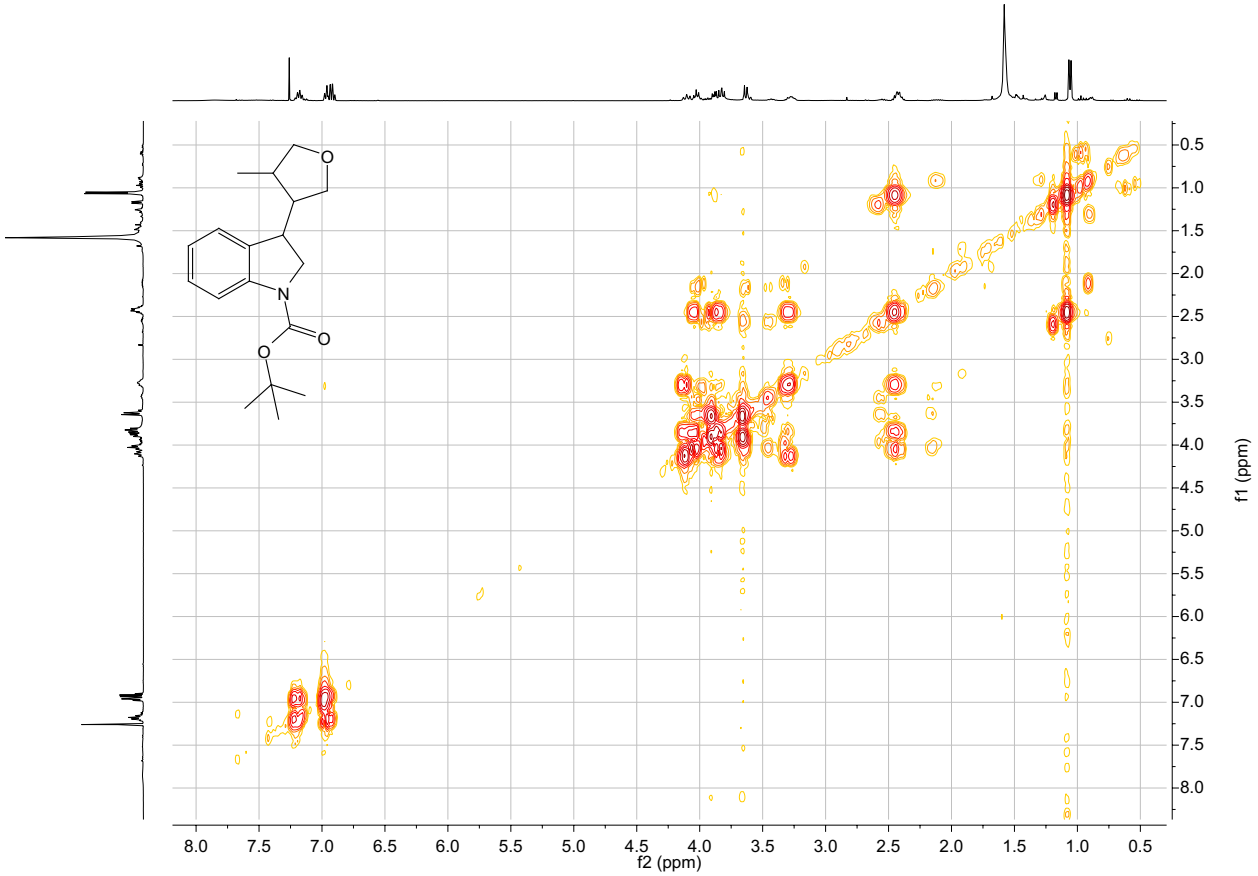

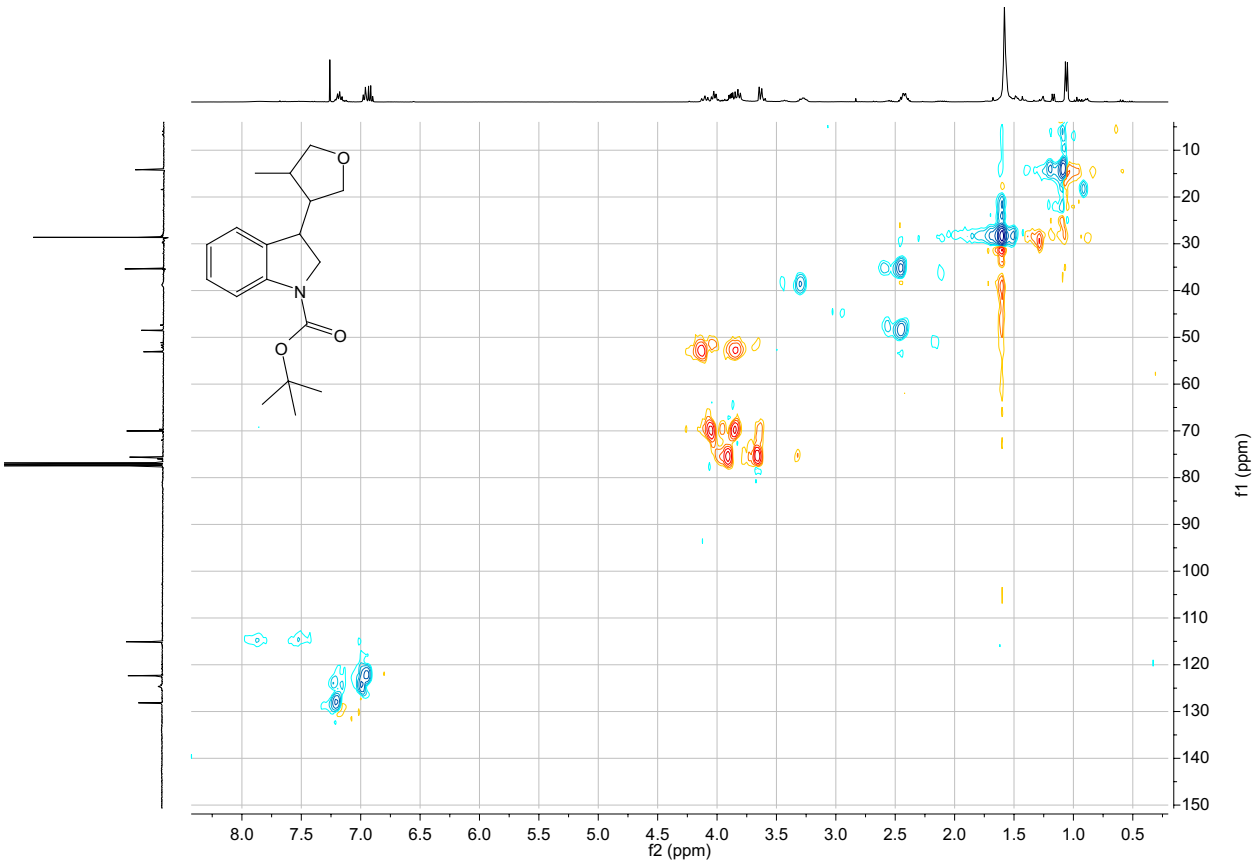

3-(4-Methyltetrahydrofuran-3-yl)-2,3-dihydrobenzofuran 445b

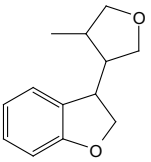

^{1}H NMR (400 MHz, Chloroform-*d*) δ 7.25 – 6.77 (m, 4H), 4.72 – 3.26 (m, 7H), 2.61 – 2.01 (m, 2H), 1.17 (d, *J* = 6.8 Hz, 3H, isomer A), 1.07 (d, *J* = 6.7 Hz, 3H, isomer B), 1.03 (d, *J* = 7.1 Hz, 3H, isomer C), 0.95 – 0.92 (m, 3H, isomer D).

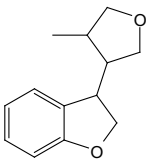

^{13}C NMR (101 MHz, Chloroform-*d*) δ 160.4, 160.0, 129.7, 128.9, 128.7, 128.6, 124.9, 124.8, 124.6, 124.6, 120.7, 120.6, 75.9, 75.8, 75.7, 75.7, 75.0, 74.8, 74.1, 71.9, 70.7, 70.1, 69.5, 50.9, 50.8, 48.0, 47.3, 44.1, 43.1, 41.6, 40.9, 37.6, 37.1, 35.3, 35.2, 29.8, 18.2, 17.4, 14.3, 14.3.

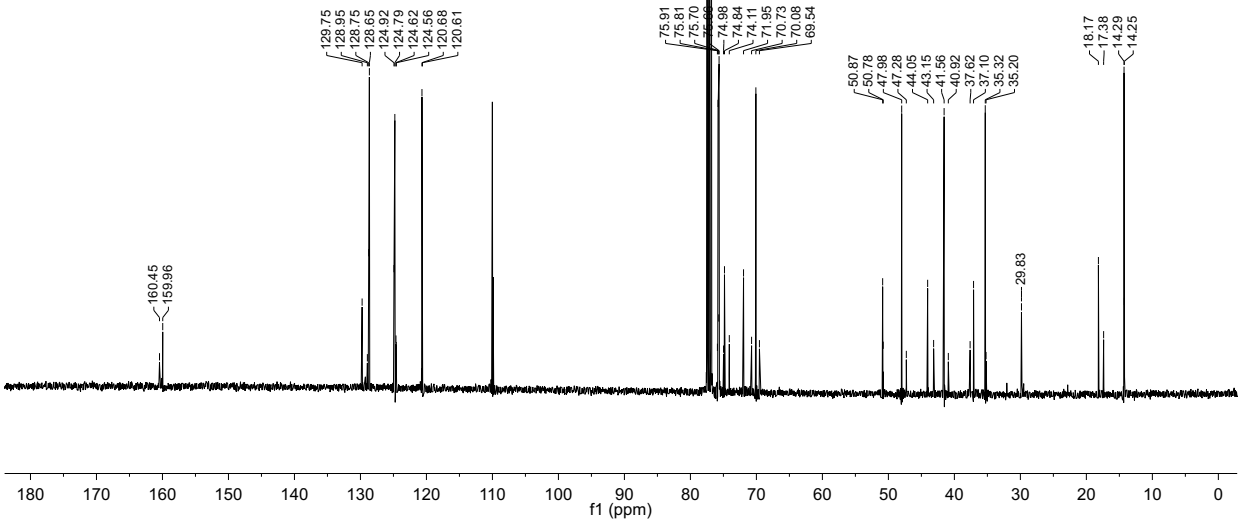

3-(4-Methyltetrahydrofuran-3-yl)-2,3-dihydrobenzofuran 445b

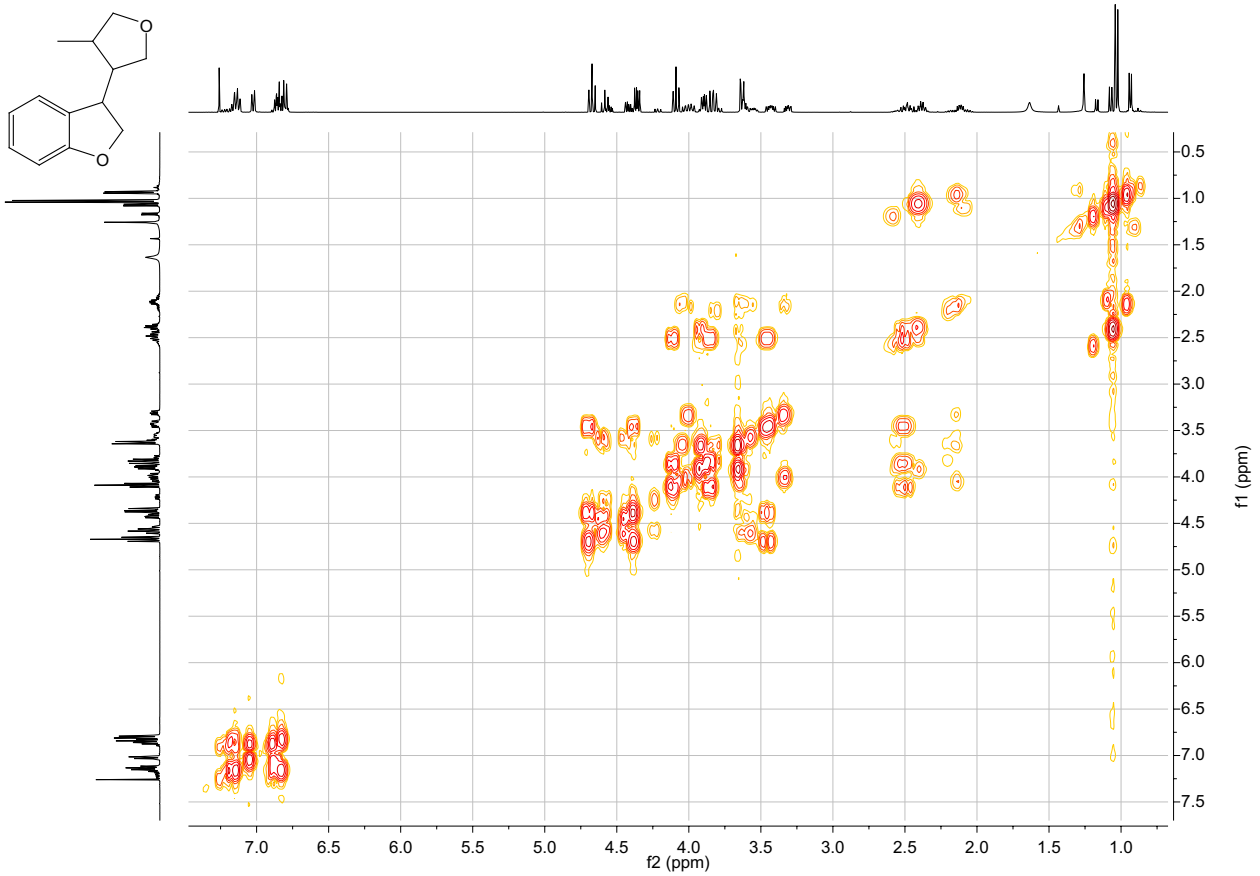

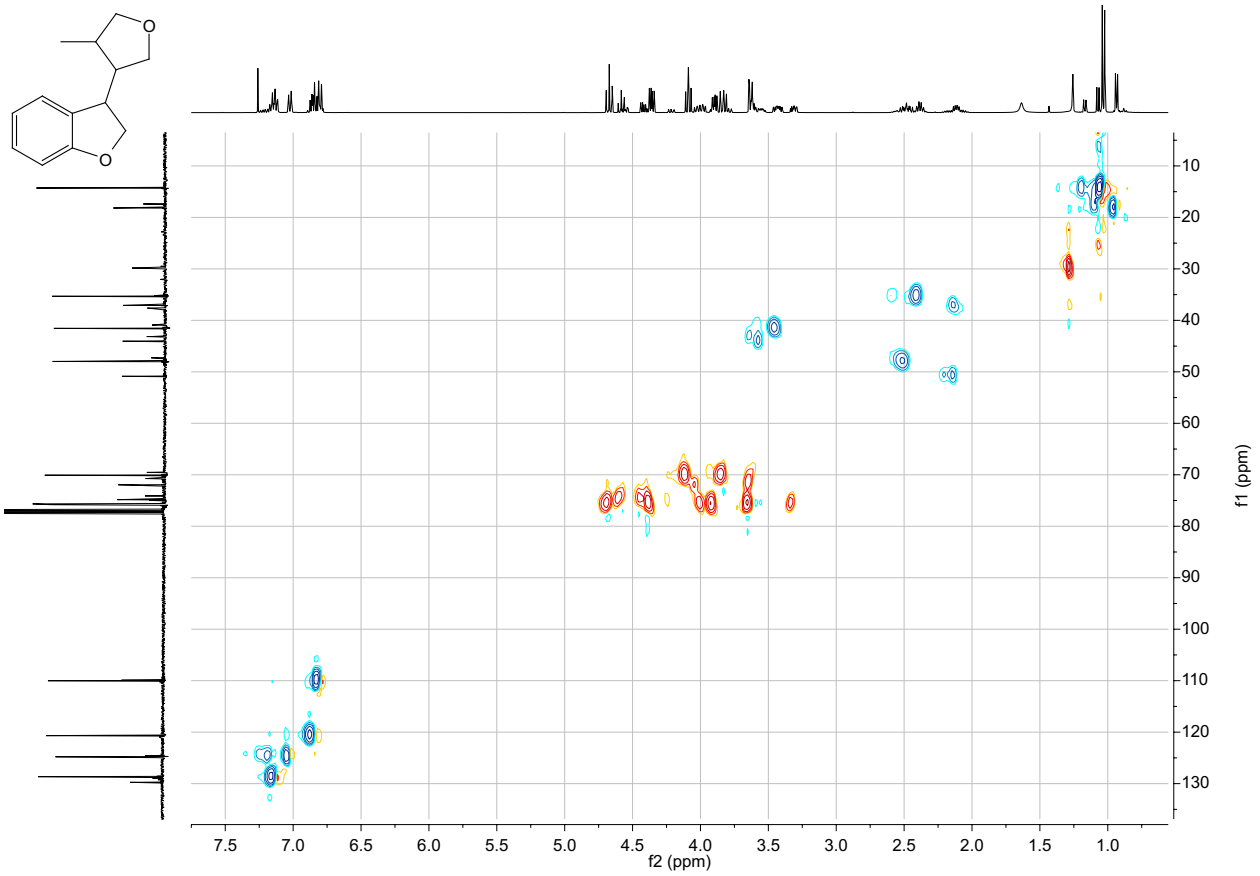

tert-Butyl (2-iodophenyl)carbamate 647

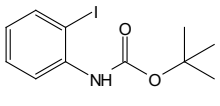

^{1}H NMR (400 MHz, Chloroform-*d*) δ 8.05 (dd, *J* = 8.4, 1.5 Hz, 1H), 7.74 (dd, *J* = 8.0, 1.5 Hz, 1H), 7.35 – 7.29 (m, 1H), 6.82 (br s, 1H), 6.76 (ddd, *J* = 7.9, 7.3, 1.6 Hz, 1H), 1.54 (s, 9H).

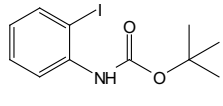

^{13}C NMR (101 MHz, Chloroform-*d*) δ 152.7, 139.0, 129.3, 124.8, 120.3, 88.9, 81.2, 28.5.

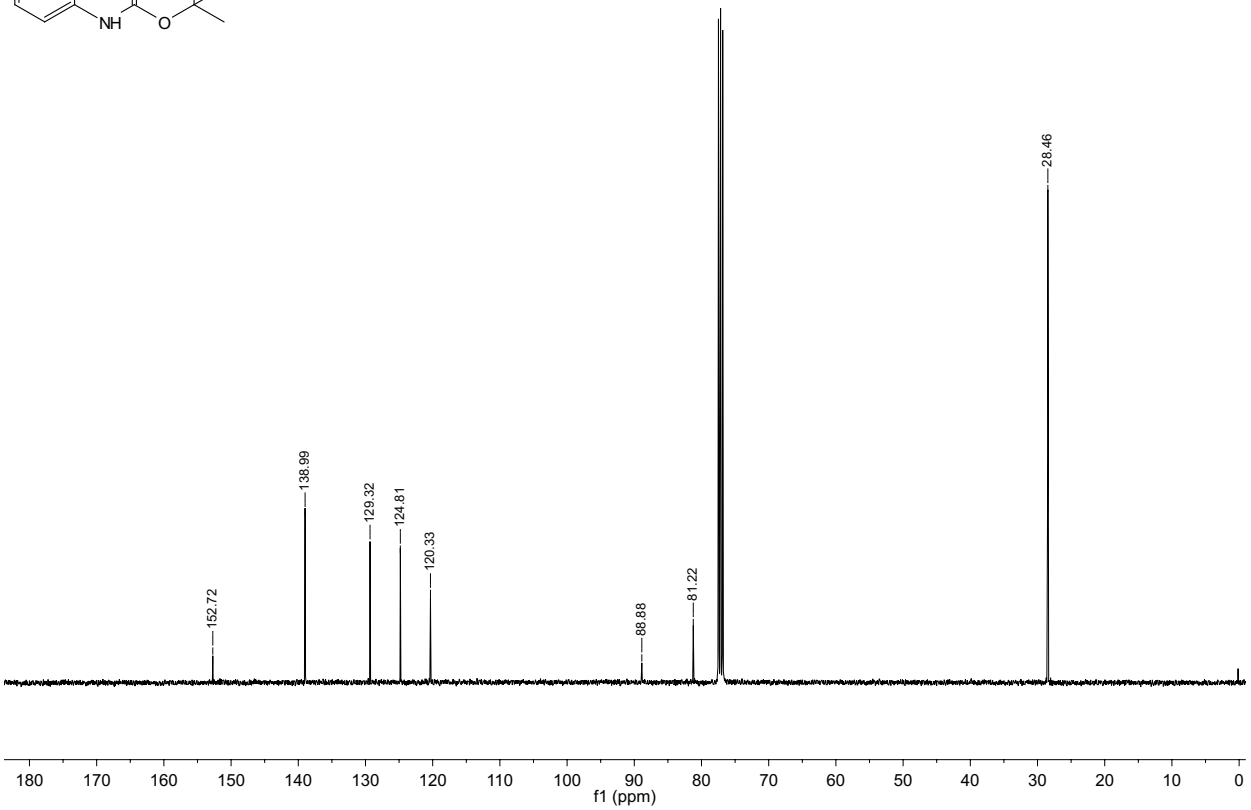

N,N-di-(*tert*-Butyl-carbamate)-2-iodoaniline 648

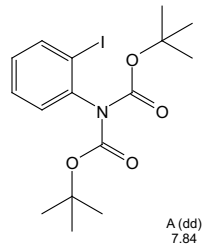

^{1}H NMR (400 MHz, Chloroform-*d*) δ 7.84 (dd, *J* = 7.9, 1.4 Hz, 1H), 7.34 (ddd, *J* = 7.6, 1.4 Hz, 1H), 7.20 (dd, *J* = 7.9, 1.6 Hz, 1H), 7.00 (ddd, *J* = 7.6, 1.6 Hz, 1H), 1.40 (s, 18H).

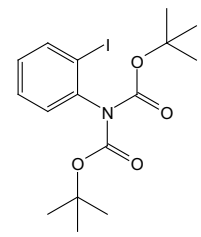

^{13}C NMR (101 MHz, Chloroform-*d*) δ 150.5, 142.2, 139.2, 129.1, 129.0, 99.9, 83.0, 28.0.

tert-Butyl allyl(2-iodophenyl)carbamate 426

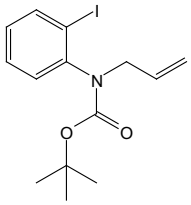

^{1}H NMR (400 MHz, DMSO-d_6) δ 7.90 (dd, J = 7.9, 1.4 Hz, 1H), 7.39 (ddd, J = 7.6, 7.6, 1.5 Hz, 1H), 7.23 (dd, J = 7.8, 1.6 Hz, 1H), 7.05 (ddd, J = 7.7, 7.6, 1.6 Hz, 1H), 5.90 (ddt, J = 16.8, 10.4, 6.3, 6.3 Hz, 1H), 5.09 (m, 2H), 4.35 (dd, J = 15.4, 5.8 Hz, 1H), 3.79 (dd, J = 15.5, 6.7 Hz, 1H), 1.36 (s, 9H).

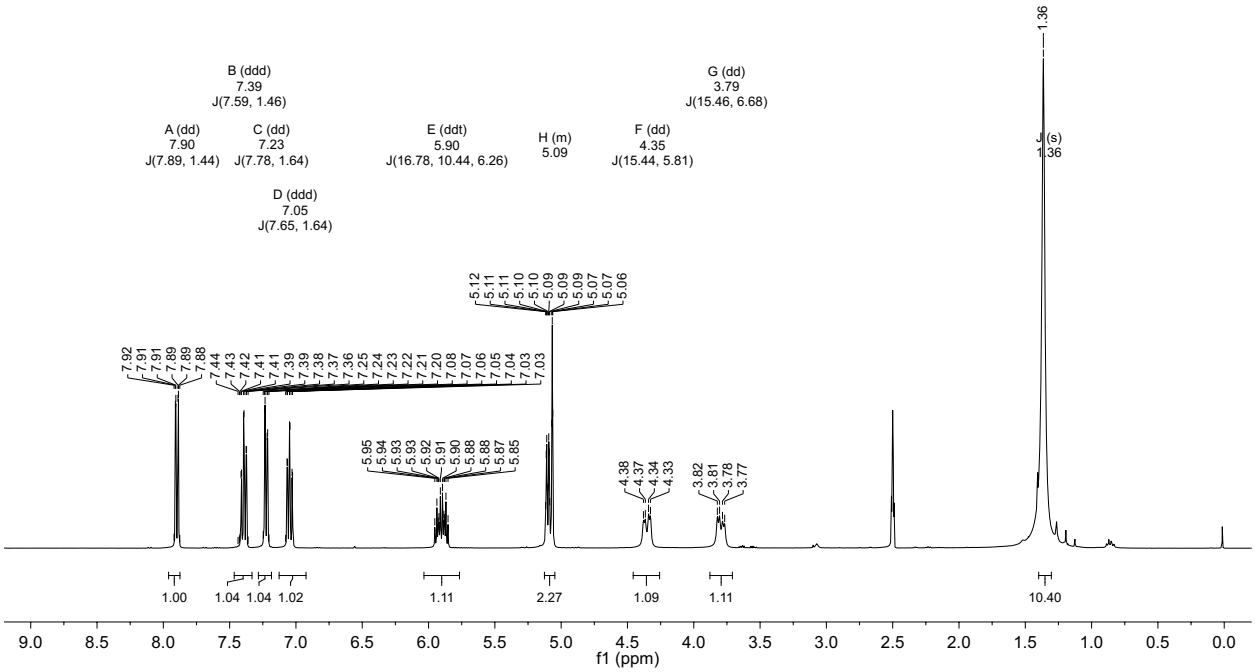

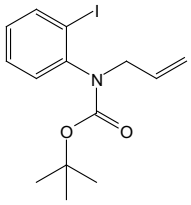

^{1}H NMR (400 MHz, DMSO-d_6) δ 7.90 (dd, J = 7.9, 1.4 Hz, 1H), 7.39 (ddd, J = 7.6, 7.6, 1.5 Hz, 1H), 7.23 (dd, J = 7.8, 1.6 Hz, 1H), 7.05 (ddd, J = 7.7, 7.6, 1.6 Hz, 1H), 5.90 (ddt, J = 16.8, 10.4, 6.3, 6.3 Hz, 1H), 5.10 (ddt, J = 7.5, 1.5, 1.5, 1.5 Hz, 1H), 5.07 (dd, J = 1.5 Hz, 1H), 4.35 (dd, J = 15.4, 5.8 Hz, 1H), 3.79 (dd, J = 15.5, 6.7 Hz, 1H), 1.36 (s, 9H).

tert-Butyl allyl(2-iodophenyl)carbamate 426

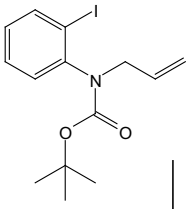

^{1}H NMR (400 MHz, Chloroform-*d*) δ 7.86 (d, *J* = 7.9 Hz, 1H), 7.31 (dd, *J* = 7.5 Hz, 1H), 7.22 (d, *J* = 7.5 Hz, 1H, minor rotamer), 7.13 (d, *J* = 7.8 Hz, 1H, major rotamer), 6.97 (ddd, *J* = 7.7, 1.6 Hz, 1H), 6.01 – 5.87 (m, 1H), 5.17 – 5.02 (m, 2H), 4.55 – 4.37 (m, 1H), 3.84 – 3.63 (m, 1H), 1.53 (s, 9H, minor rotamer), 1.35 (s, 9H, major rotamer).

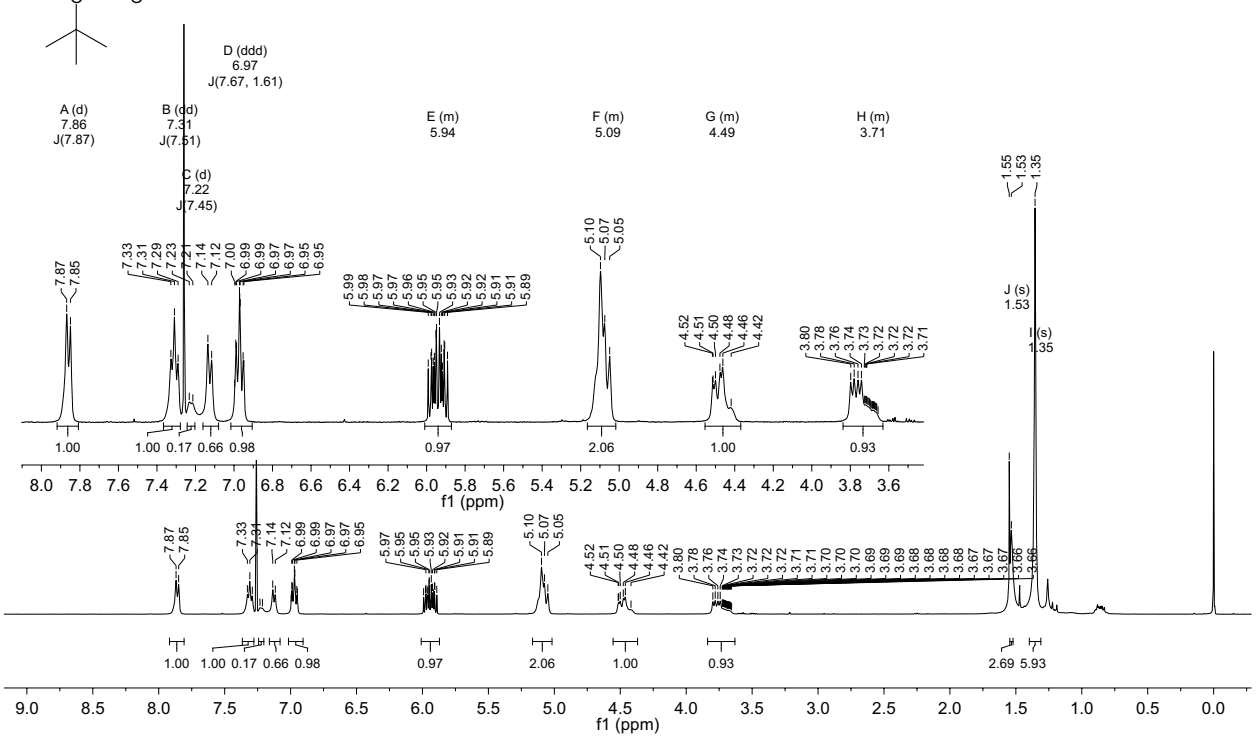

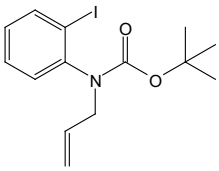

^{13}C NMR (101 MHz, Chloroform-*d*, major rotamer) δ 154.0, 144.4, 139.5, 133.7, 130.1, 128.8, 128.7, 118.0, 100.7, 80.4, 52.1, 28.4.

tert-Butyl (2-iodophenyl)(3-methylbut-2-en-1-yl)carbamate 431a

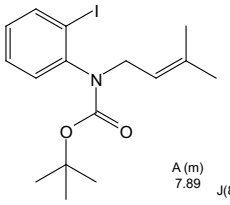

^{1}H NMR (400 MHz, DMSO-d_6) δ 7.92 – 7.83 (m, 1H), 7.38 (dd, J = 8.4, 6.6 Hz, 1H), 7.24 – 7.13 (m, 1H), 7.03 (dd, J = 8.5, 6.6 Hz, 1H), 5.26 (t, J = 6.8 Hz, 1H), 4.28 (dd, J = 15.0, 6.8 Hz, 1H), 3.87 (dd, J = 15.1, 7.5 Hz, 1H), 1.64 (s, 3H), 1.42 (s, 3H), 1.35 (s, 9H).

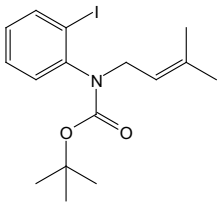

^{13}C NMR (101 MHz, DMSO-d_6) δ 152.7, 143.4, 138.8, 135.2, 129.6, 128.7, 128.6, 119.4, 100.5, 79.0, 45.8, 27.9, 25.2, 17.2.

tert-Butyl (2-iodophenyl)(3-oxopropyl)carbamate 652

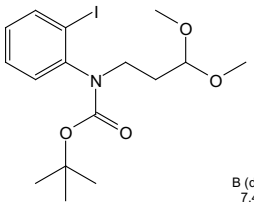

^{1}H NMR (400 MHz, DMSO-d_6, 80 °C) δ 7.91 (dd, J = 7.9, 1.4 Hz, 1H), 7.42 (ddd, J = 7.4, 1.5 Hz, 1H), 7.28 (dd, J = 7.8, 1.6 Hz, 1H), 7.06 (ddd, J = 7.9, 7.4, 1.6 Hz, 1H), 4.38 (t, J = 5.5 Hz, 1H), 3.73 (ddd, J = 14.0, 9.1, 6.4 Hz, 1H), 3.30 (ddd, J = 14.4, 9.0, 6.2 Hz, 1H), 3.23 (s, 3H), 3.22 (s, 3H), 1.89 – 1.74 (m, 2H), 1.36 (s, 9H).

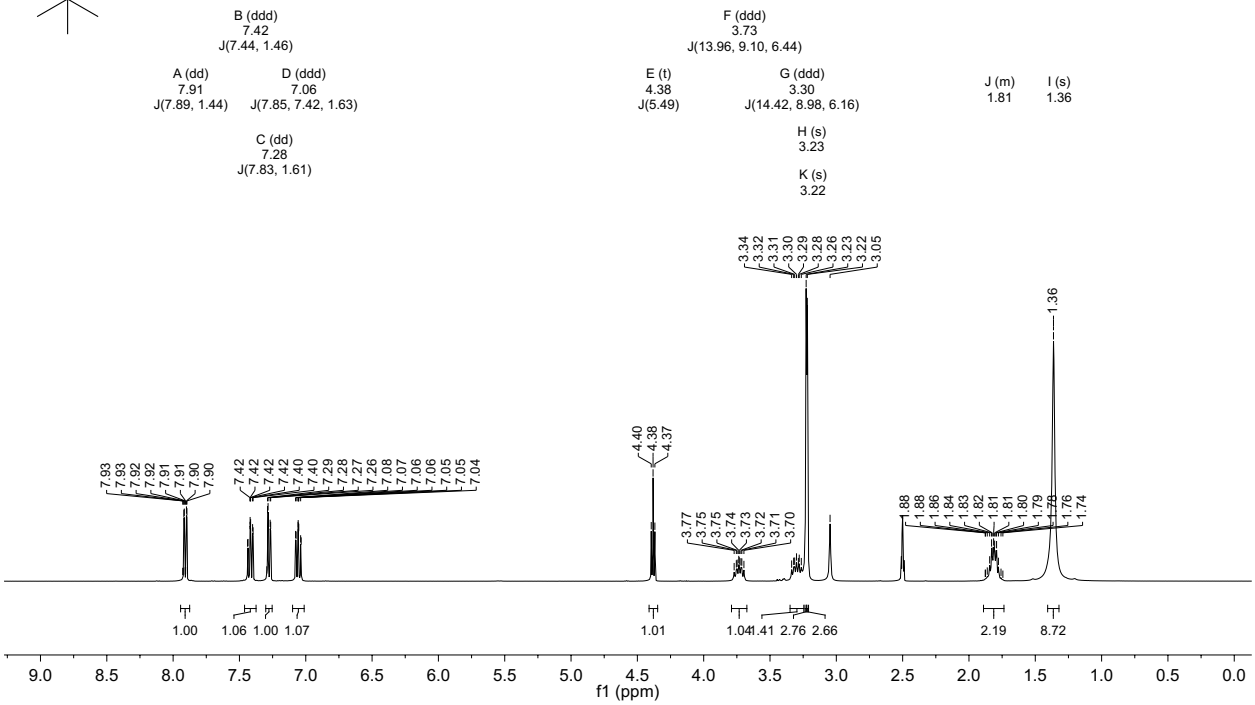

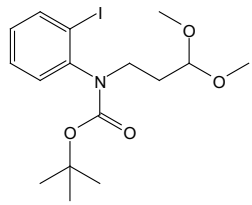

^{13}C NMR (101 MHz, DMSO-d_6) δ 152.7, 144.1, 138.8, 129.4, 128.6, 128.4, 102.3, 100.0, 79.0, 52.4, 45.0, 31.2, 27.6.

tert-Butyl (2-iodophenyl)(3-oxopropyl)carbamate 653

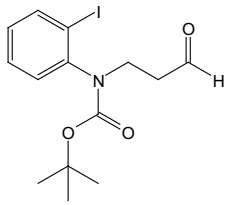

^{1}H NMR (400 MHz, Chloroform-*d*) δ 9.79 (t, *J* = 1.8 Hz, 1H), 7.87 (d, *J* = 7.9 Hz, 1H), 7.35 (dd, *J* = 7.7 Hz, 1H), 7.25 – 7.10 (m, 1H), 6.99 (ddd, *J* = 7.7, 1.6 Hz, 1H), 4.13 (dt, *J* = 14.2, 7.1 Hz, 1H), 3.67 (dt, *J* = 14.5, 6.6 Hz, 1H), 2.85 – 2.65 (m, 2H), 1.53 (s, 9H, minor rotamer), 1.34 (s, 9H, major rotamer).

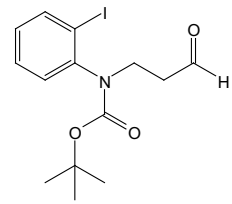

^{13}C NMR (101 MHz, Chloroform-*d*) δ 201.0, 154.1, 144.4, 139.7, 129.8, 129.3, 129.1, 100.4, 80.8, 43.6, 43.2, 28.3.

(*E*)-3-((*tert*-Butoxycarbonyl)(2-iodophenyl)amino)prop-1-en-1-yl acetate 431c

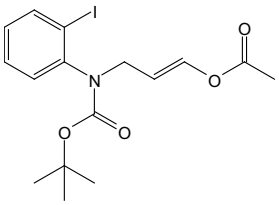

^{1}H NMR (400 MHz, DMSO-d_6, 80 °C) δ 7.90 (dd, J = 7.8, 1.4, 1H), 7.45 – 7.34 (m, 1H), 7.26 (d, J = 8.1 Hz, 1H, minor), 7.22 (d, J = 7.8 Hz, 1H, major), 7.18 – 6.94 (m, 2H), 5.60 – 5.41 (m, 1H, major), 5.19 – 5.05 (m, 1H, minor), 4.39 (ddd, J = 15.3, 6.6, 1.5 Hz, 1H, minor), 4.30 (dd, J = 14.9, 7.1 Hz, 1H, major), 4.10 – 3.68 (m, 1H), 2.09 (br s, 3H, major), 2.01 (br s, 3H. minor), 1.47 (s, 9H, minor), 1.29 (s, 9H. major).

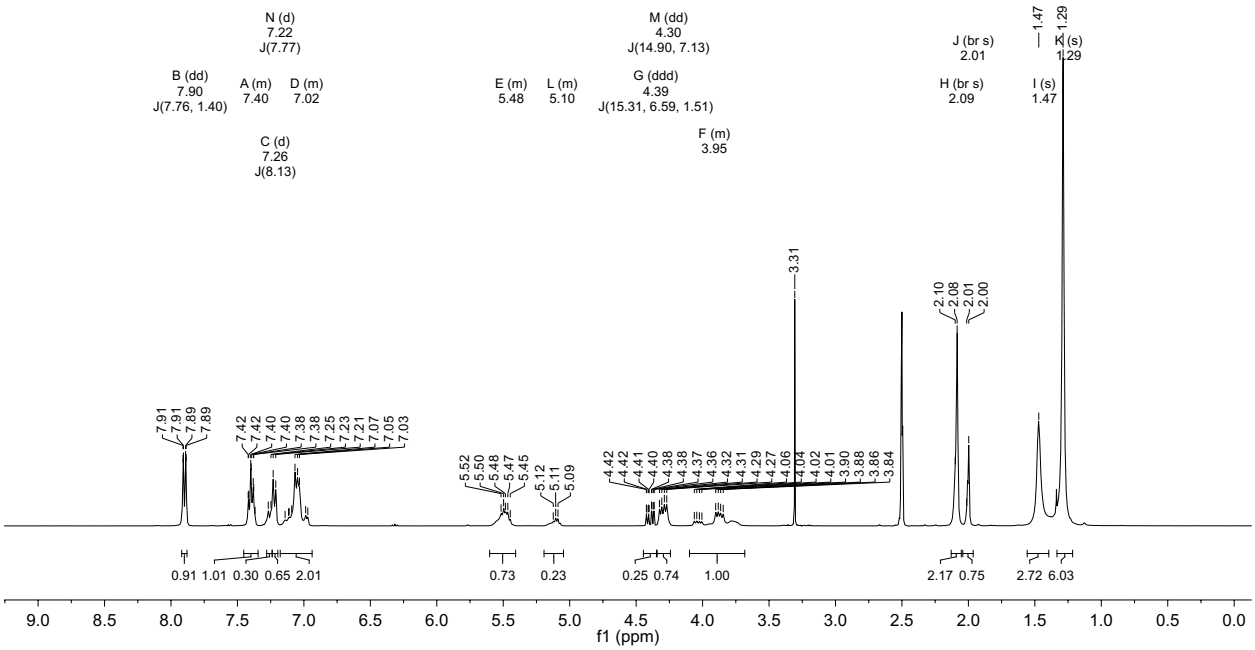

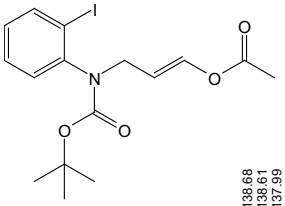

^{13}C NMR (101 MHz, DMSO-d_6, 80 °C) δ 167.1 (major), 166.7 (minor), 152.5, 138.7 (major), 138.6 (minor), 138.0, 135.7, 129.5 (major), 129.4 (minor), 128.6, 128.5, 109.3 (major), 108.8 (minor), 100.3 (major), 100.0 (minor), 79.3, 46.3, 27.6, 19.7 (major), 19.6 (minor).

Methyl (*E*)-4-iodobut-2-enoate 655

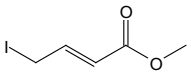

^{1}H NMR (400 MHz, Chloroform-*d*) δ 7.06 (dt, *J* = 15.3, 8.3 Hz, 1H), 5.94 (dt, *J* = 15.3, 1.1 Hz, 1H), 3.93 (dd, *J* = 8.3, 1.1 Hz, 2H), 3.75 (s, 3H).

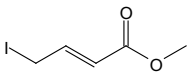

^{13}C NMR (101 MHz, Chloroform-*d*) δ 166.1, 143.9, 122.9, 51.9, 0.8.

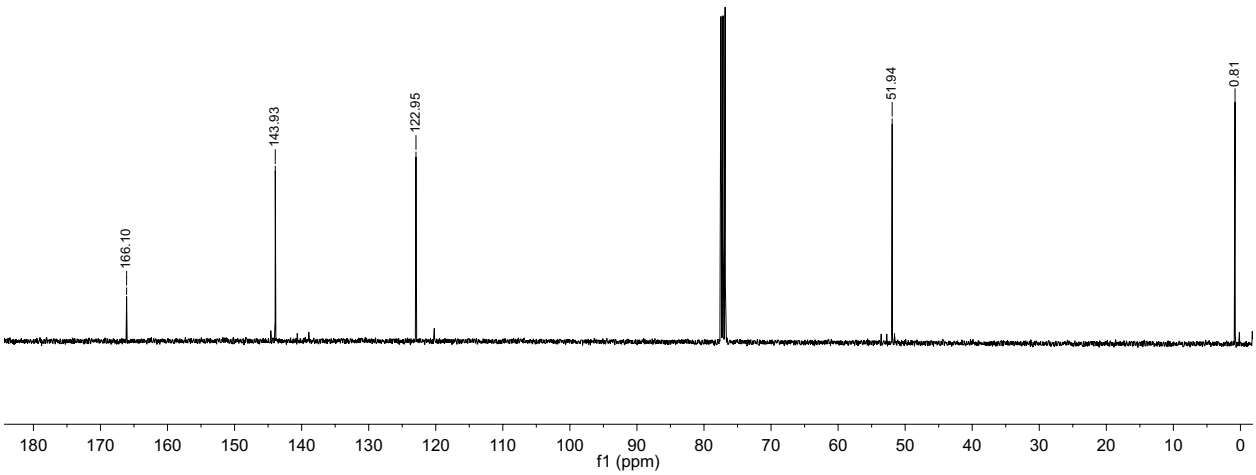

Methyl (*E*)-4-((*tert*-butoxycarbonyl)(2-iodophenyl)amino)but-2-enoate 431c

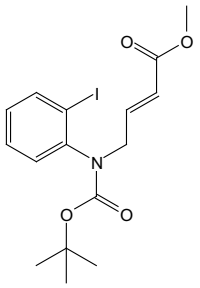

^{1}H NMR (400 MHz, DMSO-d_6) δ 7.91 (ddd, J = 7.7, 1.8 Hz, 1H), 7.46 – 7.35 (m, 1H), 7.29 – 7.21 (m, 1H), 7.10 – 7.01 (m, 1H), 6.91 (dt, J = 14.3, 6.3 Hz, 1H), 5.95 (dt, J = 15.4, 1.7 Hz, 1H), 4.55 – 4.37 (m, 1H), 4.02 (dd, J = 16.9, 6.4 Hz, 1H), 3.67 (br s, J = 1.8 Hz, 3H), 1.37 (s, 9H).

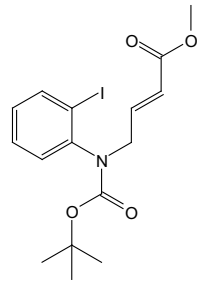

^{13}C NMR (101 MHz, DMSO-d_6) δ 165.2, 152.6, 143.8, 143.2, 138.8, 129.2, 128.8, 128.7, 121.9, 100.0, 79.6, 50.8, 50.0, 27.5.

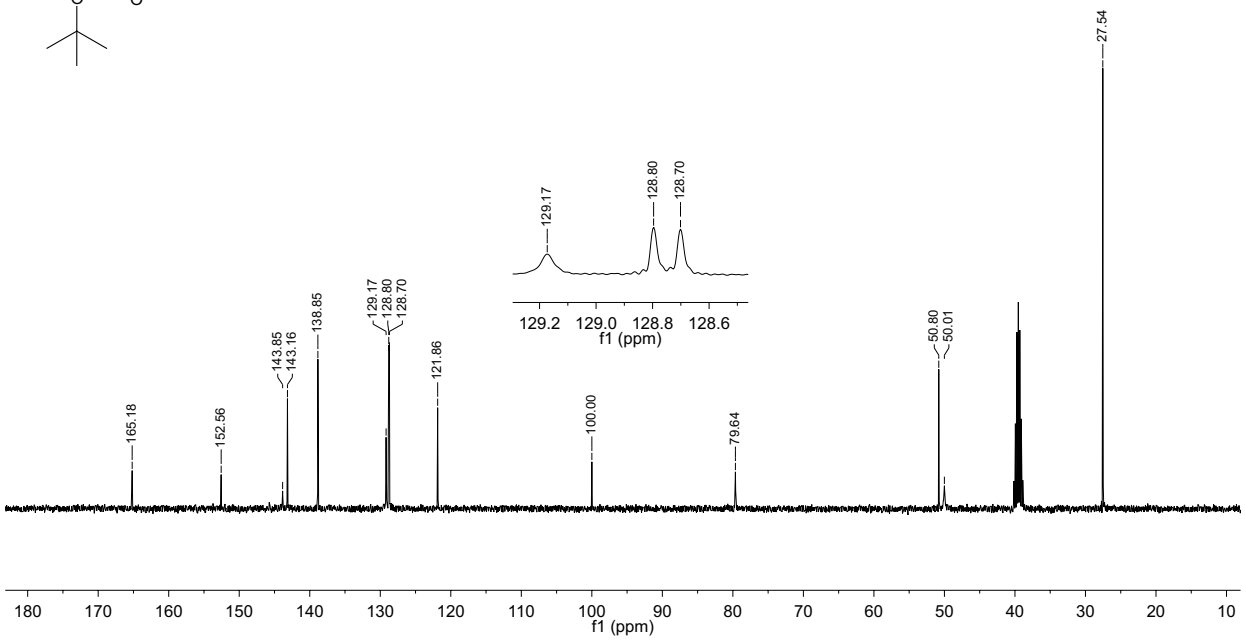

Methyl (*E*)-4-((*tert*-butoxycarbonyl)(2-iodophenyl)amino)but-2-enoate 431c

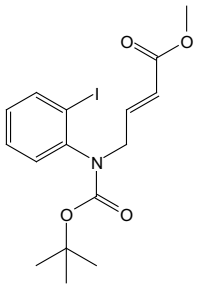

^{1}H NMR (400 MHz, Chloroform-*d*) δ 7.86 (d, *J* = 7.9 Hz, 1H), 7.37 – 7.28 (m, 1H), 7.19 (dd, *J* = 35.4, 7.7 Hz, 1H), 7.05 – 6.95 (m, 2H), 5.89 (d, *J* = 15.7 Hz, 1H), 4.64 (dt, *J* = 18.4, 9.2 Hz, 1H), 3.91 – 3.80 (m, 1H), 3.75 (s, 3H, minor rotamer), 3.73 (s, 3H, major rotamer), 1.53 (s, 9H, minor rotamer), 1.35 (s, 9H, major rotamer).

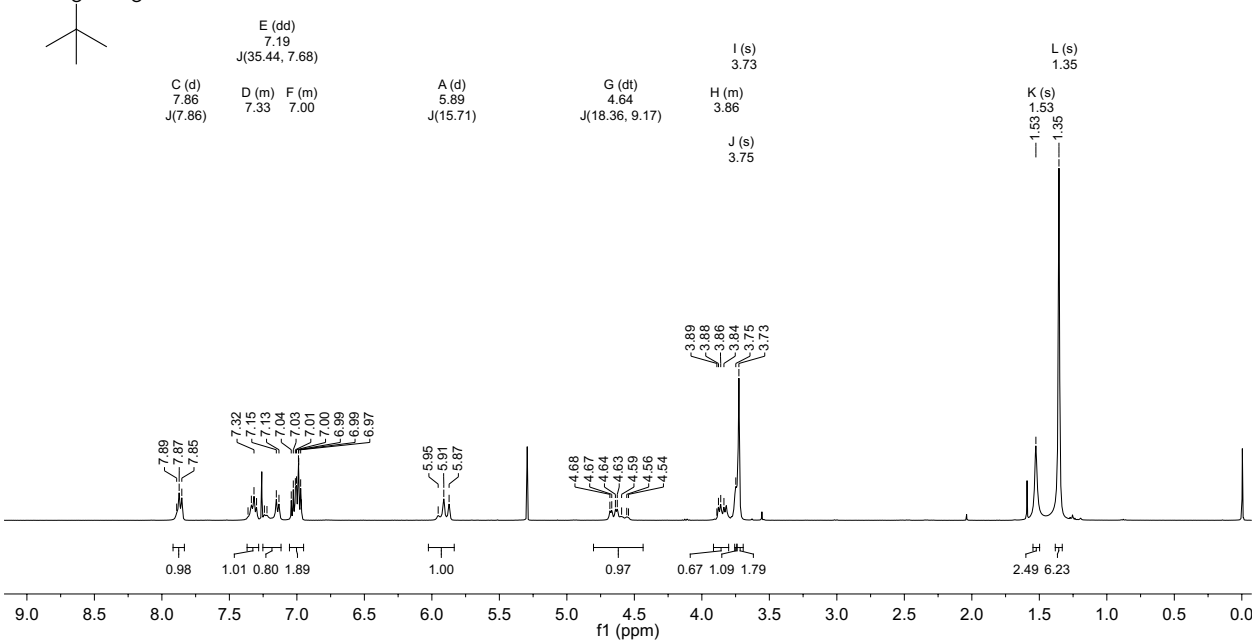

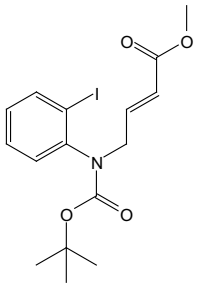

^{13}C NMR (101 MHz, Chloroform-*d*) δ 166.6, 153.9, 143.5, 139.7, 129.9, 129.2, 129.1 (2C, accidential isochrony), 122.9, 100.3, 81.0, 51.7, 50.4, 28.3.

1-(Allyloxy)-2-iodobenzene 431d

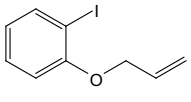

^{1}H NMR (400 MHz, Chloroform-*d*) δ 7.78 (dd, *J* = 7.7, 1.6 Hz, 1H), 7.32 – 7.23 (m, 1H), 6.81 (dd, *J* = 8.2, 1.3 Hz, 1H), 6.71 (ddd, *J* = 7.6, 1.4 Hz, 1H), 6.07 (ddt, *J* = 17.2, 10.4, 4.8 Hz, 1H), 5.53 (ddt, *J* = 17.3, 1.7 Hz, 1H), 5.32 (ddt, *J* = 10.6, 1.6 Hz, 1H), 4.60 (dt, *J* = 4.9, 1.7 Hz, 2H).

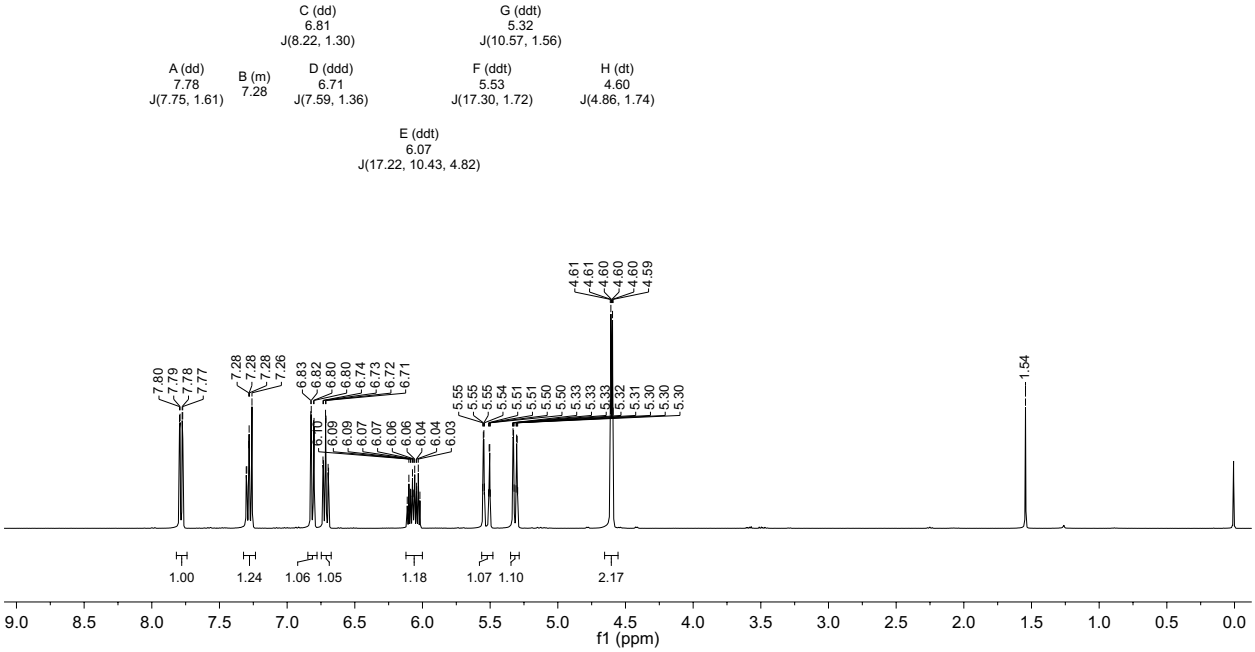

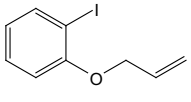

^{13}C NMR (101 MHz, Chloroform-*d*) δ 157.3, 139.7, 132.7, 129.5, 122.8, 117.7, 112.7, 86.8, 69.8.

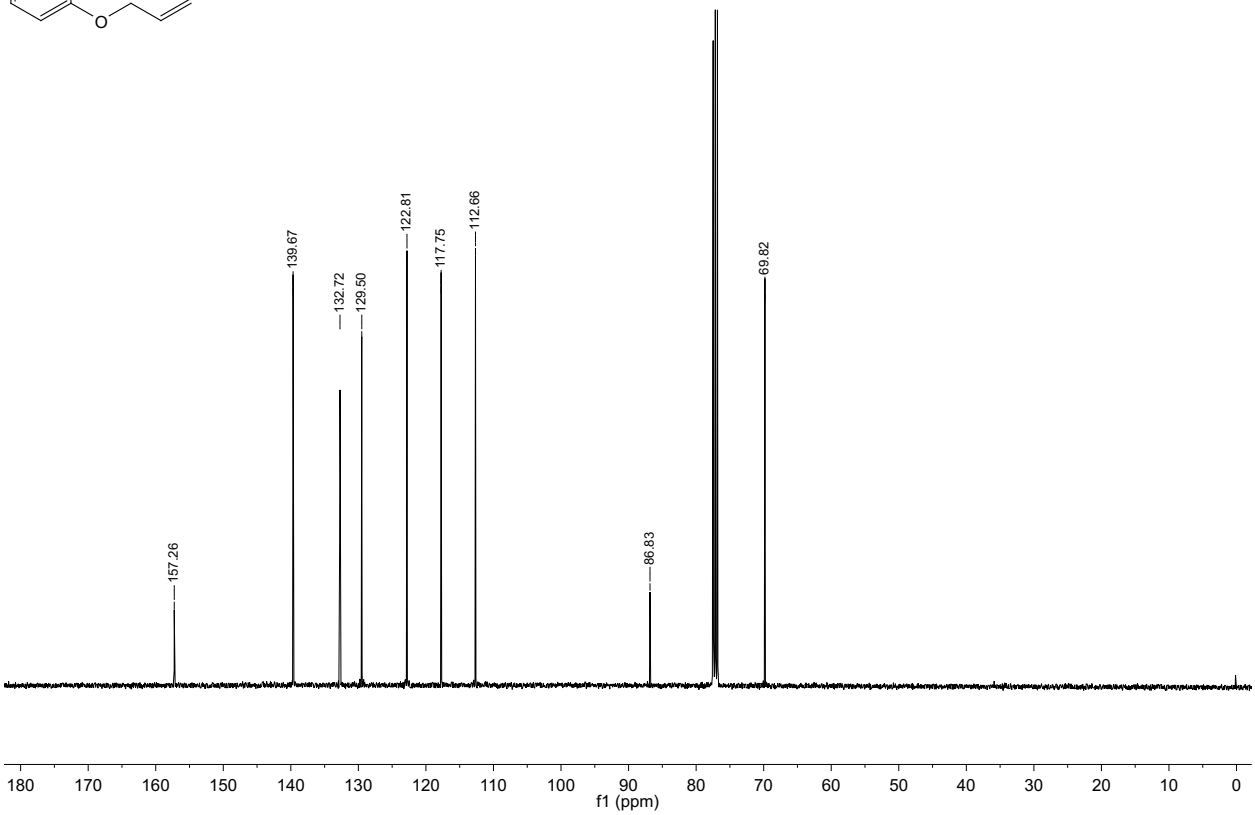

N-(cyclohex-2-en-1-yl)-*N*-(2-iodophenyl)methanesulfonamide 434

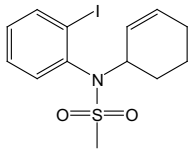

^{1}H NMR (500 MHz, Chloroform-*d*) δ 7.95 (dd, *J* = 8.0, 1.5 Hz, 1H), 7.45 – 7.40 (m, 1H), 7.39 – 7.33 (m, 1H), 7.05 (ddd, *J* = 7.6, 1.7 Hz, 1H), 6.07 – 6.00 (m, 1H), 5.88 (ddt, *J* = 10.1, 4.9, 2.5 Hz, 1H, major conformer), 5.73 (ddt, *J* = 10.2, 3.4 Hz, 1H, minor conformer), 4.78 – 4.66 (m, 1H), 3.15 (s, 2H), 3.13 (s, 1H), 2.33 – 2.20 (m, 1H), 1.94 – 1.73 (m, 2H), 1.68 – 1.45 (m, 3H).

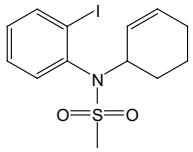

^{13}C NMR (101 MHz, Chloroform-*d*) δ 140.5, 139.8, 133.2, 132.2, 130.2, 129.0, 128.3, 105.2, 58.8, 42.0, 28.1, 24.4, 21.5.

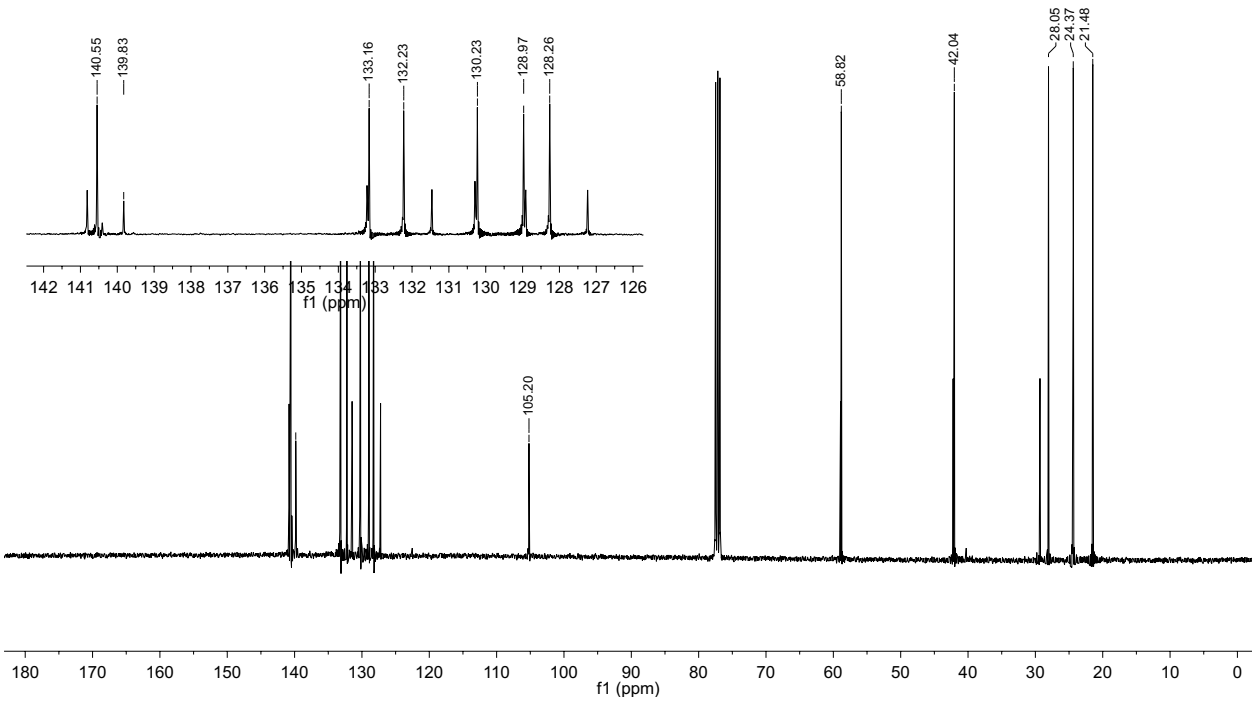

N-(But-2-yn-1-yl)-*N*-(2-iodophenyl)methanesulfonamide 437a

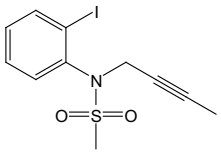

^{1}H NMR (400 MHz, Chloroform-*d*) δ 7.97 (dd, *J* = 8.0, 1.5 Hz, 1H), 7.61 (dd, *J* = 7.9, 1.6 Hz, 1H), 7.44 (ddd, *J* = 7.6, 1.5 Hz, 1H), 7.12 (ddd, *J* = 7.9, 7.4, 1.6 Hz, 1H), 4.74 – 4.61 (m, 1H), 4.08 – 3.99 (m, 1H), 3.17 (s, 3H), 1.85 (t, *J* = 2.4 Hz, 3H).

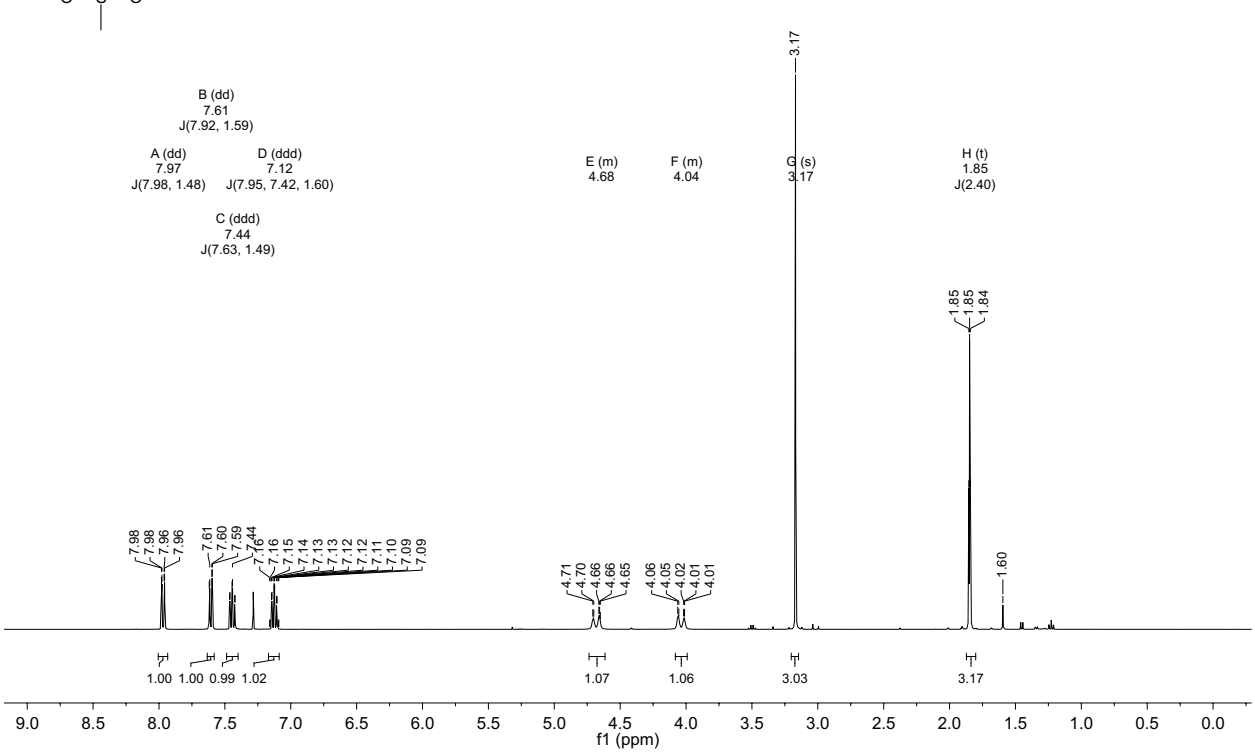

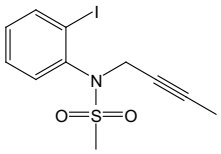

^{13}C NMR (101 MHz, Chloroform-*d*) δ 141.3, 140.4, 131.3, 130.6, 129.3, 102.5, 82.4, 73.5, 41.3, 41.2, 3.6.

3-Cyclohexylprop-2-yn-1-ol 661

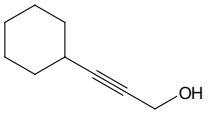

^{1}H NMR (400 MHz, Chloroform-*d*) δ 4.26 (dd, *J* = 5.8, 2.0 Hz, 2H), 2.38 (ttt, *J* = 9.6, 3.9, 2.0 Hz, 1H), 1.85 – 1.76 (m, 2H), 1.69 (dddd, *J* = 12.2, 6.5, 4.8, 2.5 Hz, 2H), 1.59 – 1.22 (m, 6H).

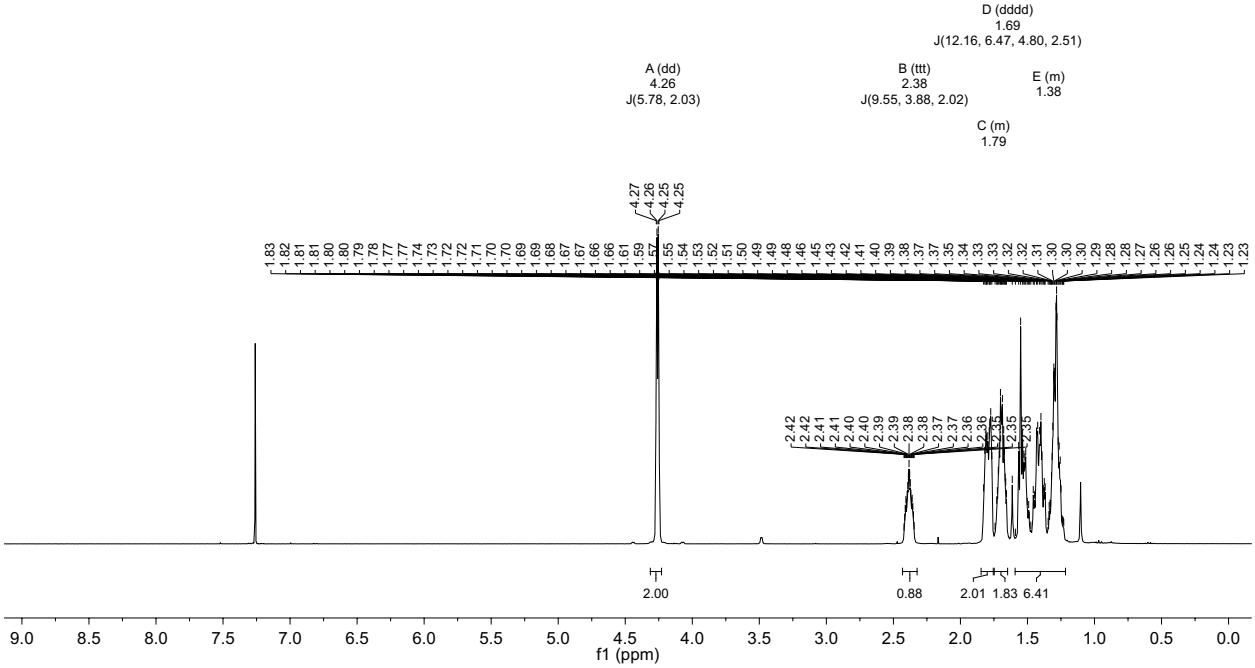

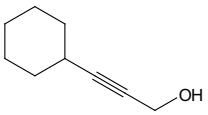

^{13}C NMR (101 MHz, Chloroform-*d*) δ 90.8, 78.3, 51.6, 32.8, 29.2, 26.0, 25.0.

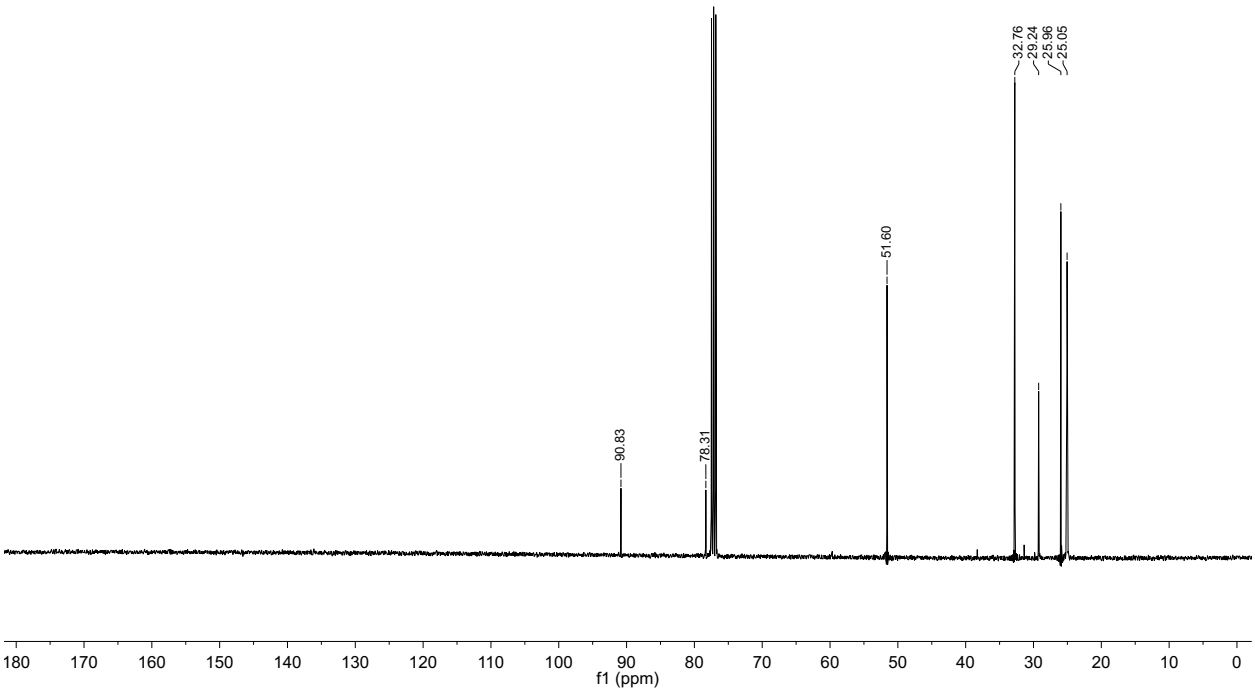

N-(3-Cyclohexylprop-2-yn-1-yl)-*N*-(2-iodophenyl)methanesulfonamide 437b

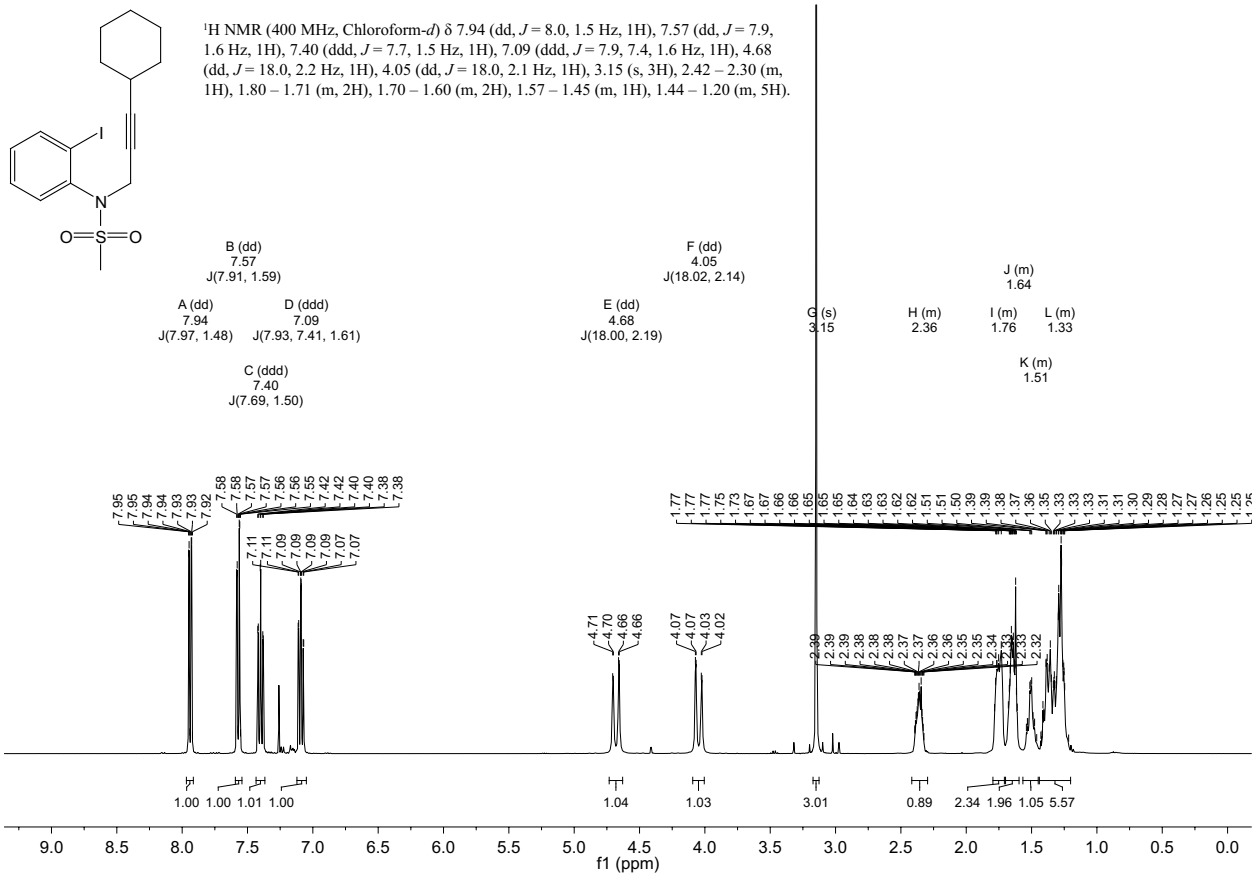

[1]H NMR (400 MHz, Chloroform-*d*) δ 7.94 (dd, *J* = 8.0, 1.5 Hz, 1H), 7.57 (dd, *J* = 7.9, 1.6 Hz, 1H), 7.40 (ddd, *J* = 7.7, 1.5 Hz, 1H), 7.09 (ddd, *J* = 7.9, 7.4, 1.6 Hz, 1H), 4.68 (dd, *J* = 18.0, 2.2 Hz, 1H), 4.05 (dd, *J* = 18.0, 2.1 Hz, 1H), 3.15 (s, 3H), 2.42 – 2.30 (m, 1H), 1.80 – 1.71 (m, 2H), 1.70 – 1.60 (m, 2H), 1.57 – 1.45 (m, 1H), 1.44 – 1.20 (m, 5H).

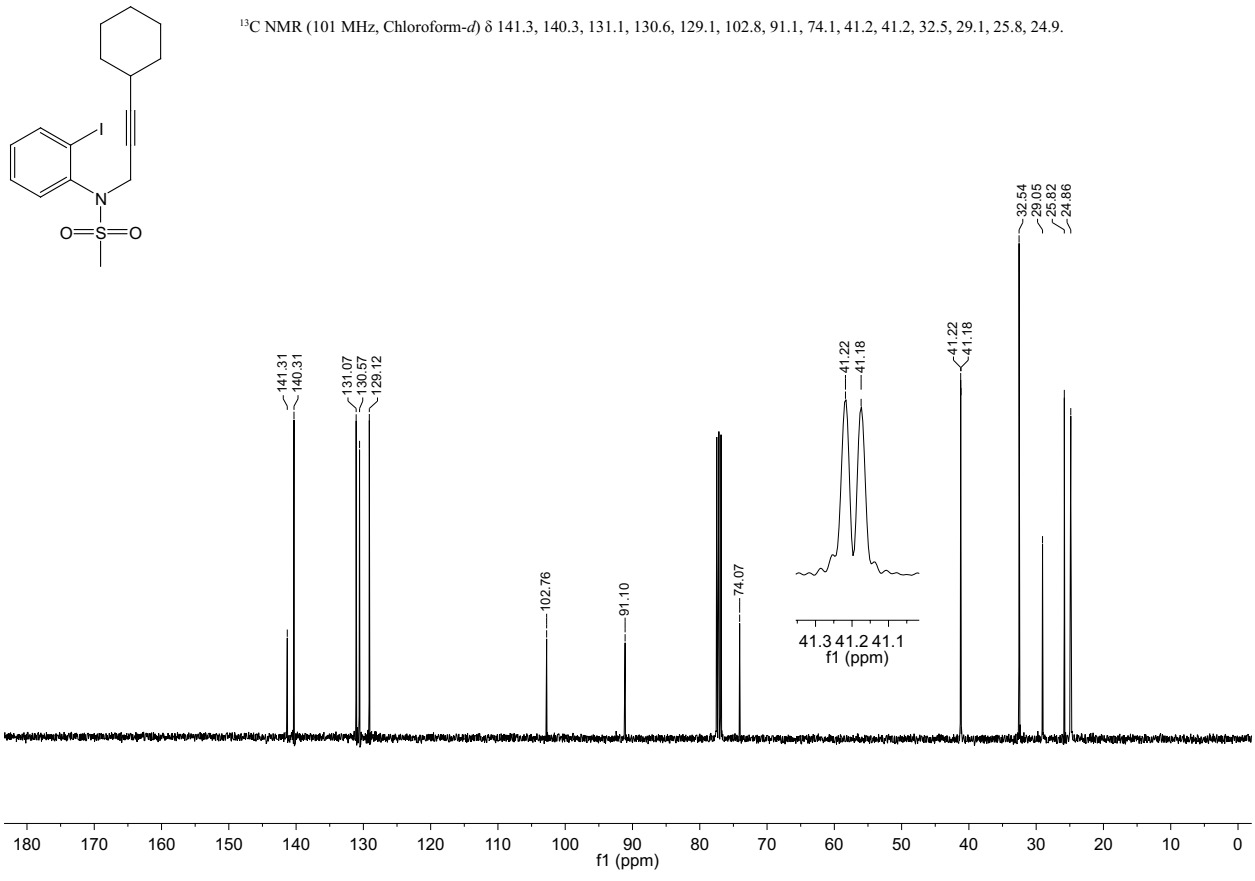

[13]C NMR (101 MHz, Chloroform-*d*) δ 141.3, 140.3, 131.1, 130.6, 129.1, 102.8, 91.1, 74.1, 41.2, 41.2, 32.5, 29.1, 25.8, 24.9.

4-((*tert*-Butyldiphenylsilyl)oxy)but-2-yn-1-ol 663

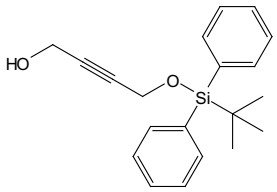

^{1}H NMR (400 MHz, Chloroform-*d*) δ 7.77 – 7.67 (m, 4H), 7.47 – 7.37 (m, 6H), 4.37 (t, *J* = 1.8 Hz, 2H), 4.20 (t, *J* = 1.8 Hz, 2H), 1.38 (s, 1H), 1.07 (s, 9H).

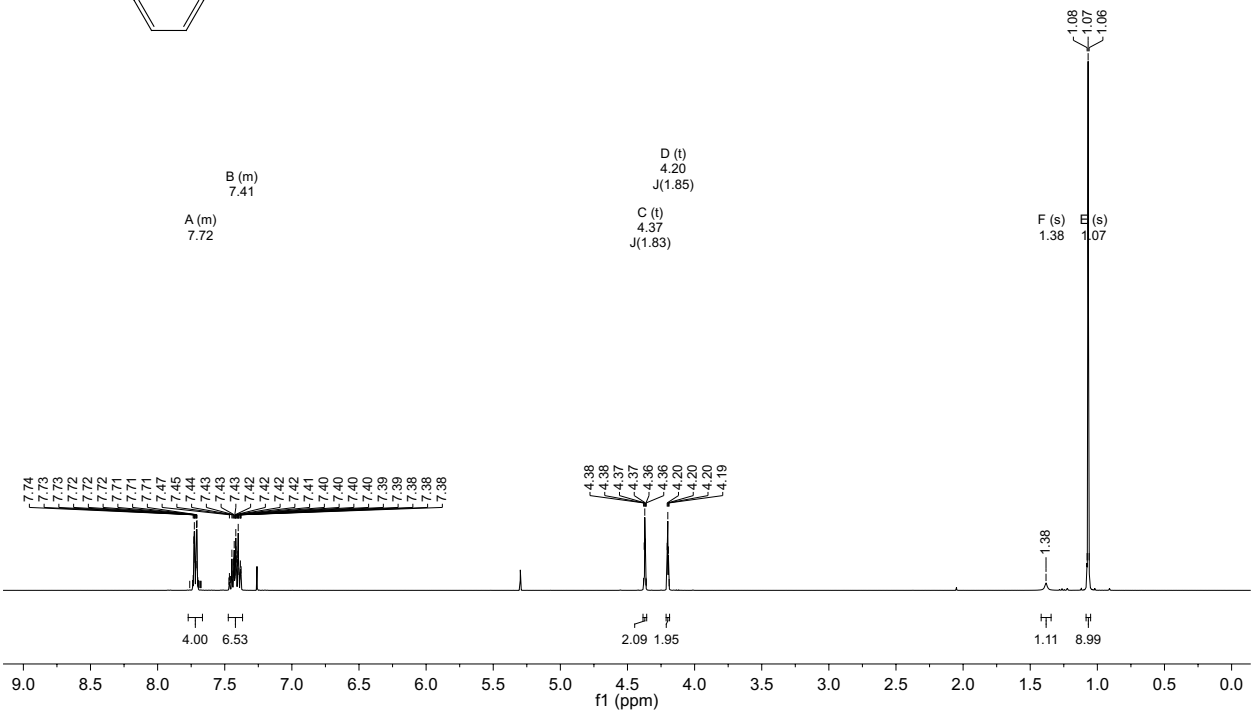

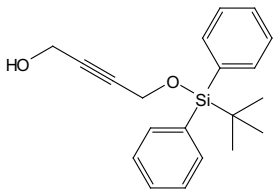

^{13}C NMR (101 MHz, Chloroform-*d*) δ 135.8, 133.3, 130.0, 127.8, 84.4, 83.6, 52.8, 51.3, 26.9, 19.3.

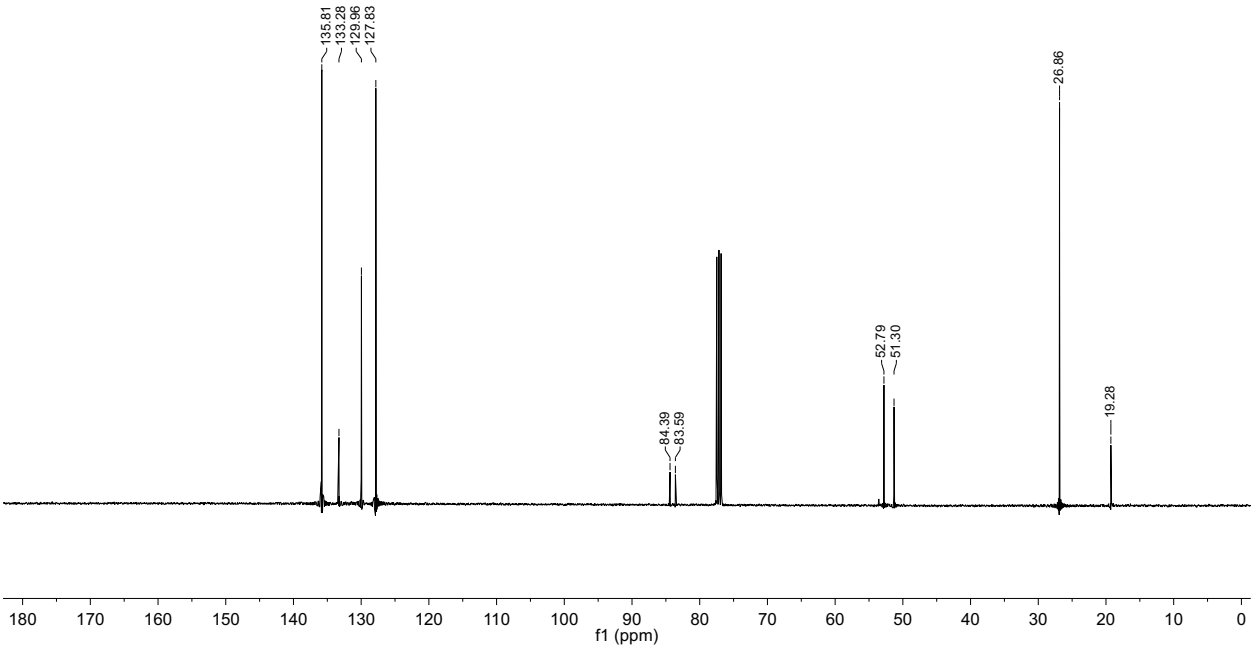

2,2,11,11-Tetramethyl-3,3,10,10-tetraphenyl-4,9-dioxa-3,10-disiladodec-6-yne 664

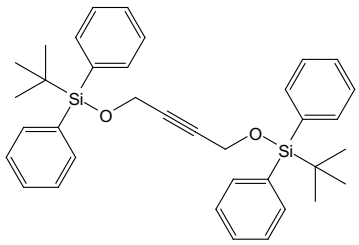

^{1}H NMR (400 MHz, Chloroform-*d*) δ 7.77 – 7.70 (m, 8H), 7.47 – 7.36 (m, 12H), 4.35 (s, 4H), 1.10 (s, 18H).

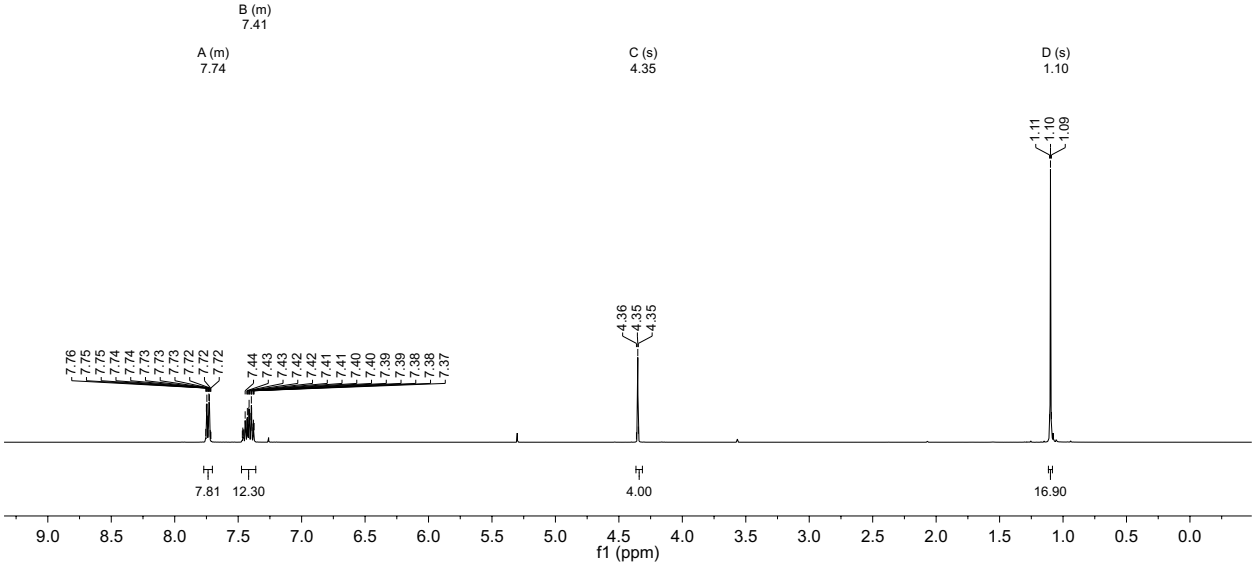

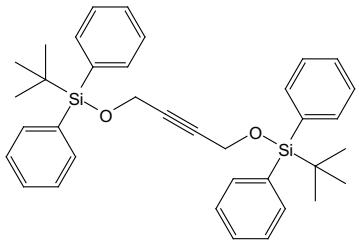

^{13}C NMR (101 MHz, Chloroform-*d*) δ 135.8, 133.3, 129.9, 127.8, 83.5, 52.9, 26.9, 19.3.

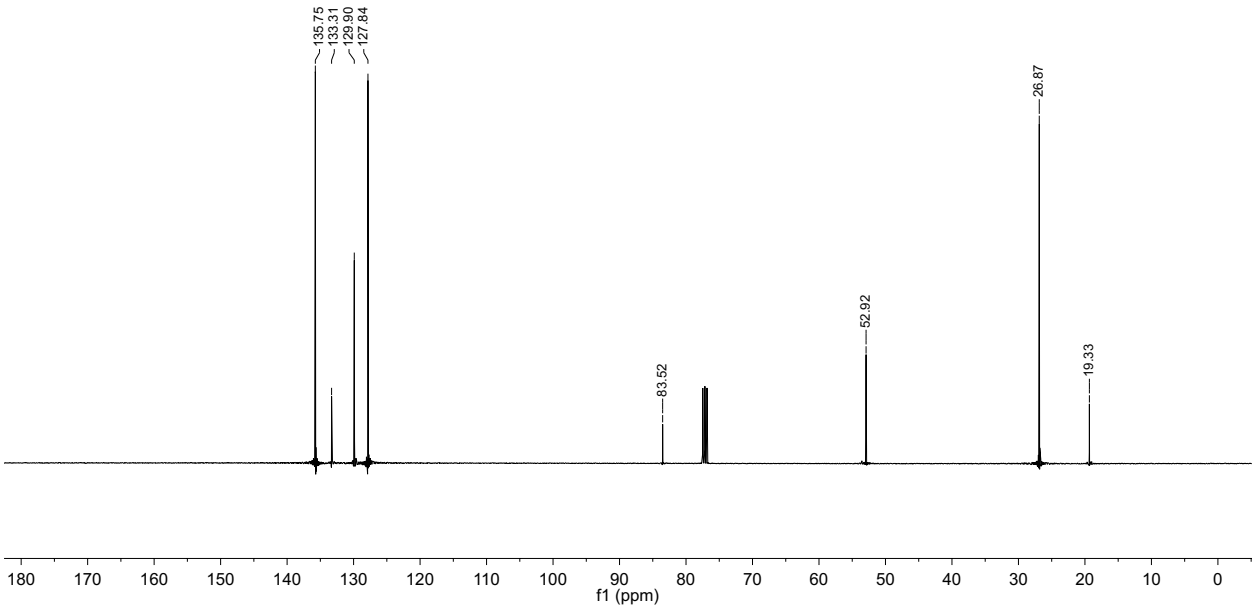

((4-Bromobut-2-yn-1-yl)oxy)(tert-butyl)diphenylsilane 665

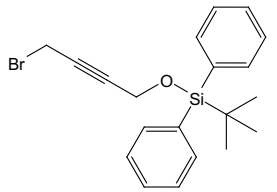

^{1}H NMR (400 MHz, Chloroform-*d*) δ 7.74 – 7.68 (m, 4H), 7.48 – 7.37 (m, 6H), 4.37 (t, *J* = 2.0 Hz, 2H), 3.89 (t, *J* = 2.0 Hz, 2H), 1.07 (s, 9H).

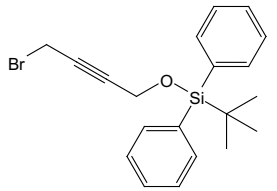

^{13}C NMR (101 MHz, Chloroform-*d*) δ 135.8, 133.1, 130.0, 127.9, 85.4, 80.3, 52.9, 26.8, 19.3, 14.7.

tert-Butyl (4-((*tert*-butyldiphenylsilyl)oxy)but-2-yn-1-yl)(2-iodophenyl)carbamate 440a

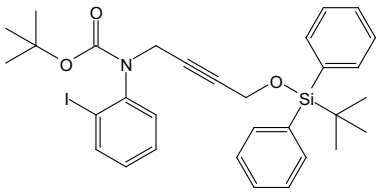

^{1}H NMR (400 MHz, DMSO-d_6) δ 7.91 (dd, J = 7.9, 1.4 Hz, 1H), 7.67 – 7.58 (m, 4H), 7.50 – 7.33 (m, 7H), 7.30 (dd, J = 7.9, 1.7 Hz, 1H), 7.08 (ddd, J = 7.6, 1.8 Hz, 1H), 4.66 – 4.51 (m, 1H), 4.39 – 4.27 (m, 2H), 4.00 – 3.89 (m, 1H), 1.47 (s, 9H, minor), 1.29 (s, 9H, major), 0.97 (s, 9H).

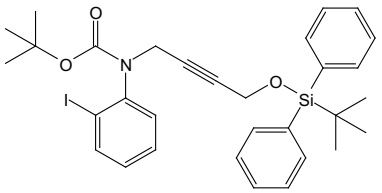

^{13}C NMR (101 MHz, DMSO-d_6) δ 152.6, 142.9, 139.0, 135.0, 132.5, 129.9, 129.5 (minor), 129.5 (major), 129.4, 128.9, 127.8, 100.8, 82.2, 80.8, 80.0, 52.3, 38.1, 27.8, 26.5, 18.7.

tert-Butyl (2-iodophenyl)(prop-2-yn-1-yl)carbamate 440b

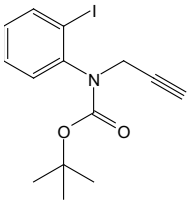

^{1}H NMR (400 MHz, Chloroform-*d*) δ 7.87 (d, *J* = 7.9 Hz, 1H), 7.48 – 7.33 (m, 2H), 7.02 (ddd, *J* = 8.0, 6.0, 3.1 Hz, 1H), 4.79 (dd, *J* = 17.6, 2.5 Hz, 1H, major), 4.64 (d, *J* = 17.8 Hz, 1H, minor), 3.90 (dd, *J* = 17.6, 2.4 Hz, 1H), 2.25 – 2.19 (m, 1H), 1.56 (s, 9H, minor), 1.36 (s, 9H, major).

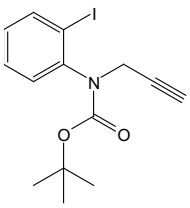

^{13}C NMR (101 MHz, Chloroform-*d*) δ 153.6, 143.5, 139.7 (minor), 139.4 (major), 130.5 (minor), 130.3 (major), 129.6 (minor), 129.4 (minor), 129.3 (major), 129.0 (major), 100.2, 81.1, 79.4, 72.6 (major), 72.2 (minor), 39.7 (major), 38.3 (minor), 28.5 (major), 28.3 (minor).

tert-Butyl (2-iodophenyl)(prop-2-yn-1-yl)carbamate 440a

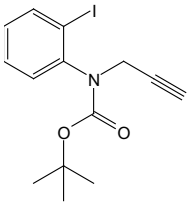

^{1}H NMR (400 MHz, DMSO-d_6, 80 °C) δ 7.92 (dd, J = 7.9, 1.4 Hz, 1H), 7.48 – 7.41 (m, 1H), 7.36 (dd, J = 7.8, 1.7 Hz, 1H), 7.09 (ddd, J = 7.6, 1.7 Hz, 1H), 4.56 (dd, J = 18.0, 2.5 Hz, 1H), 3.99 (dd, J = 18.0, 2.5 Hz, 1H), 3.04 (dd, J = 2.5 Hz, 1H), 1.37 (s, 9H).

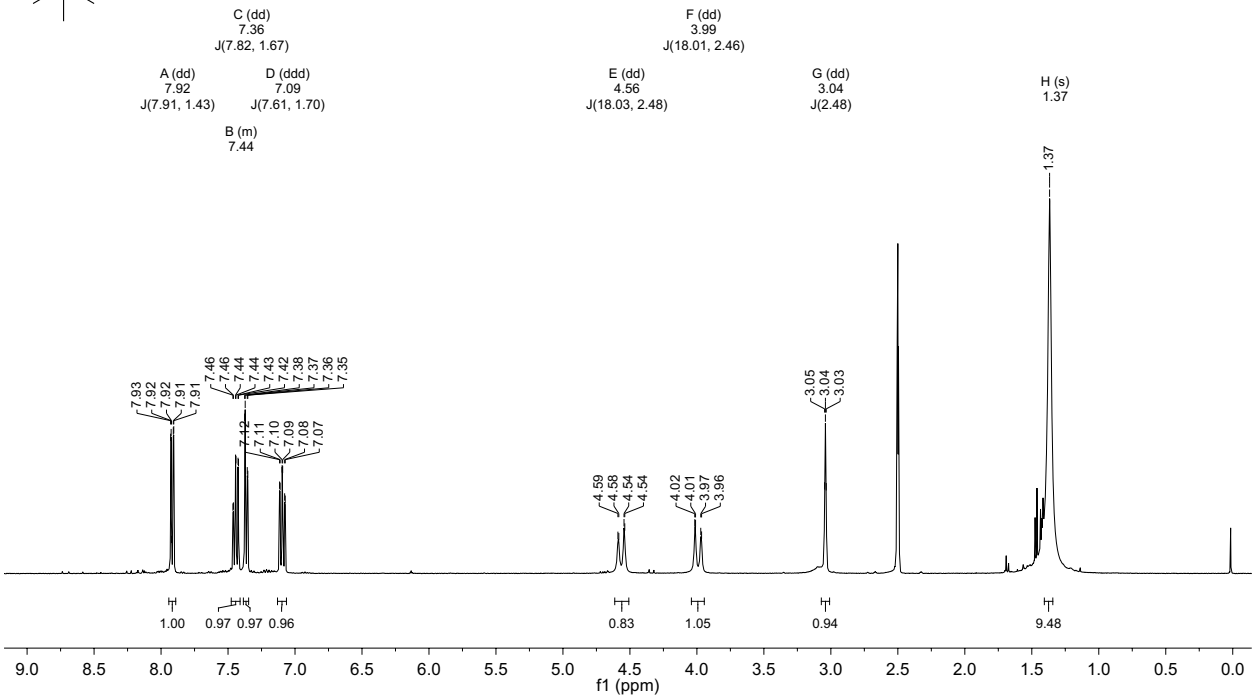

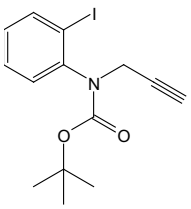

^{13}C NMR (101 MHz, DMSO-d_6, 80 °C) δ 152.2, 143.0 (br), 138.7, 129.3, 128.9, 128.6, 100.0, 79.9, 79.0, 74.4, 38.0 (br), 27.6.

1-(1-(Allyloxy)-2-iodoethyl)-4-methoxybenzene 442a

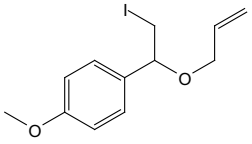

^{1}H NMR (400 MHz, Chloroform-*d*) δ 7.26 – 7.21 (m, 2H), 6.92 – 6.87 (m, 2H), 5.92 (dddd, *J* = 17.2, 10.4, 6.2, 5.1 Hz, 1H), 5.28 (dq, *J* = 17.3, 1.7 Hz, 1H), 5.18 (dq, *J* = 10.3, 1.4 Hz, 1H), 4.43 (dd, *J* = 8.2, 4.8 Hz, 1H), 3.98 (dddd, *J* = 12.8, 5.1, 1.5 Hz, 1H), 3.86 – 3.78 (m, 1H), 3.82 (s, 3H), 3.38 (dd, *J* = 10.3, 8.3 Hz, 1H), 3.30 (dd, *J* = 10.3, 4.7 Hz, 1H).

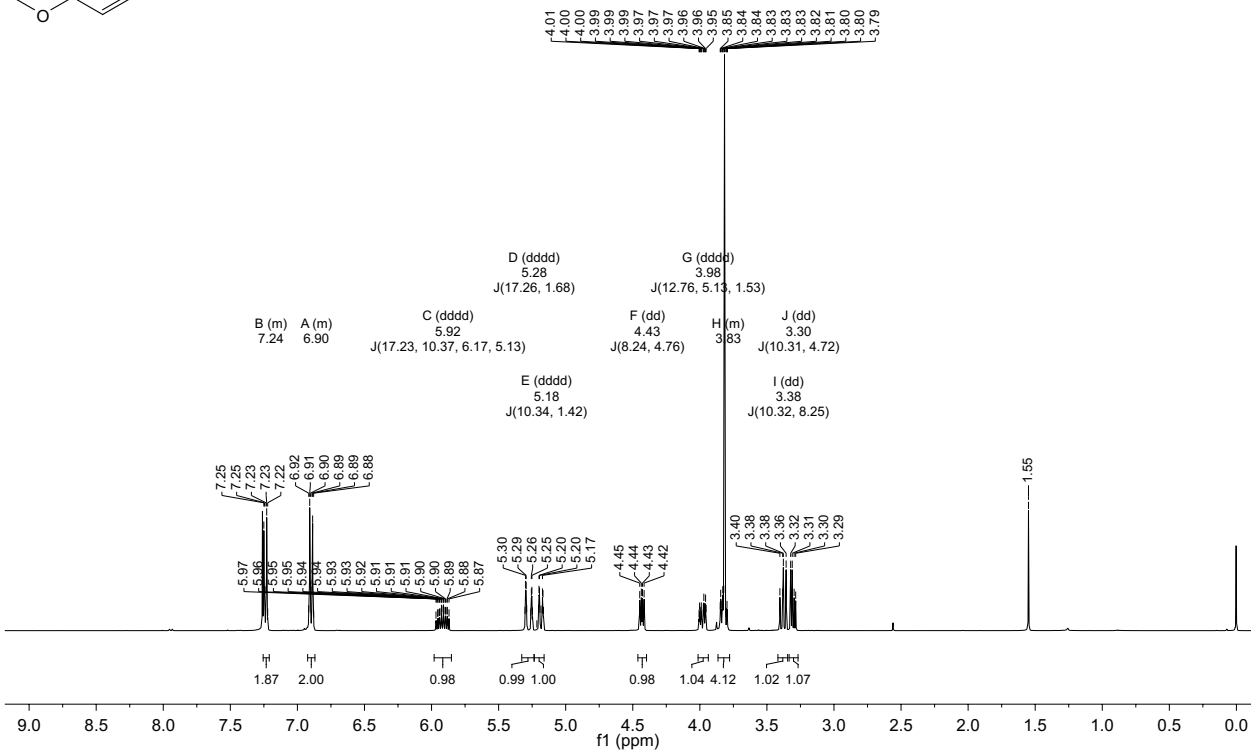

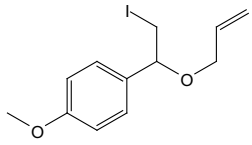

^{13}C NMR (101 MHz, Chloroform-*d*) δ 159.8, 134.6, 132.1, 128.0, 117.5, 114.2, 80.7, 70.1, 55.4, 11.0.

1-(1-(Allyloxy)-2-bromoethyl)-4-methoxybenzene 442b

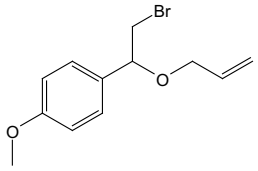

^{1}H NMR (400 MHz, Chloroform-*d*) δ 7.30 – 7.21 (m, 2H), 6.93 – 6.89 (m, 2H), 5.91 (dddd, *J* = 17.3, 10.4, 6.2, 5.1 Hz, 1H), 5.27 (ddt, *J* = 17.2, 1.7 Hz, 1H), 5.18 (ddt, *J* = 10.4, 1.4 Hz, 1H), 4.51 (dd, *J* = 8.1, 4.6 Hz, 1H), 4.00 (dddd, *J* = 12.8, 5.1, 1.5 Hz, 1H), 3.89 – 3.78 (m, 1H), 3.82 (s, 3H), 3.56 (dd, *J* = 10.5, 8.1 Hz, 1H), 3.44 (dd, *J* = 10.5, 4.6 Hz, 1H).

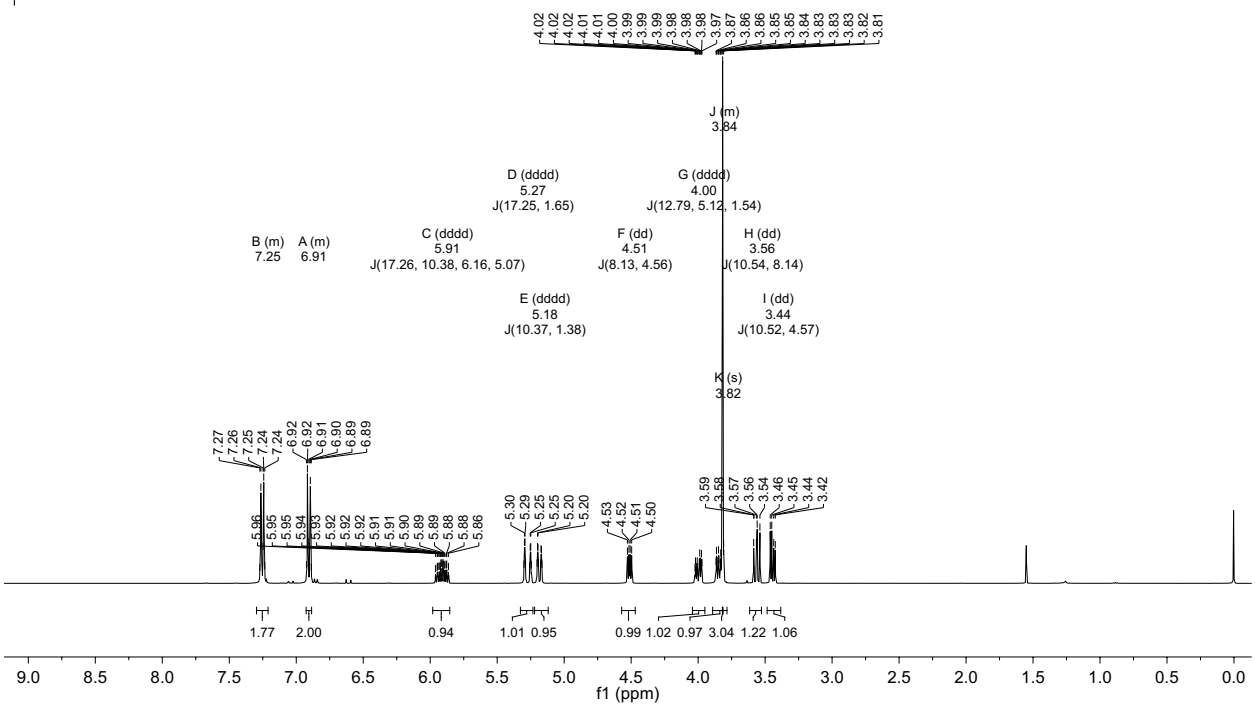

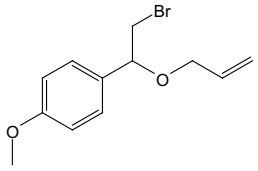

^{13}C NMR (101 MHz, Chloroform-*d*) δ 159.9, 134.6, 131.4, 128.2, 117.5, 114.2, 80.5, 70.0, 55.4, 36.7.

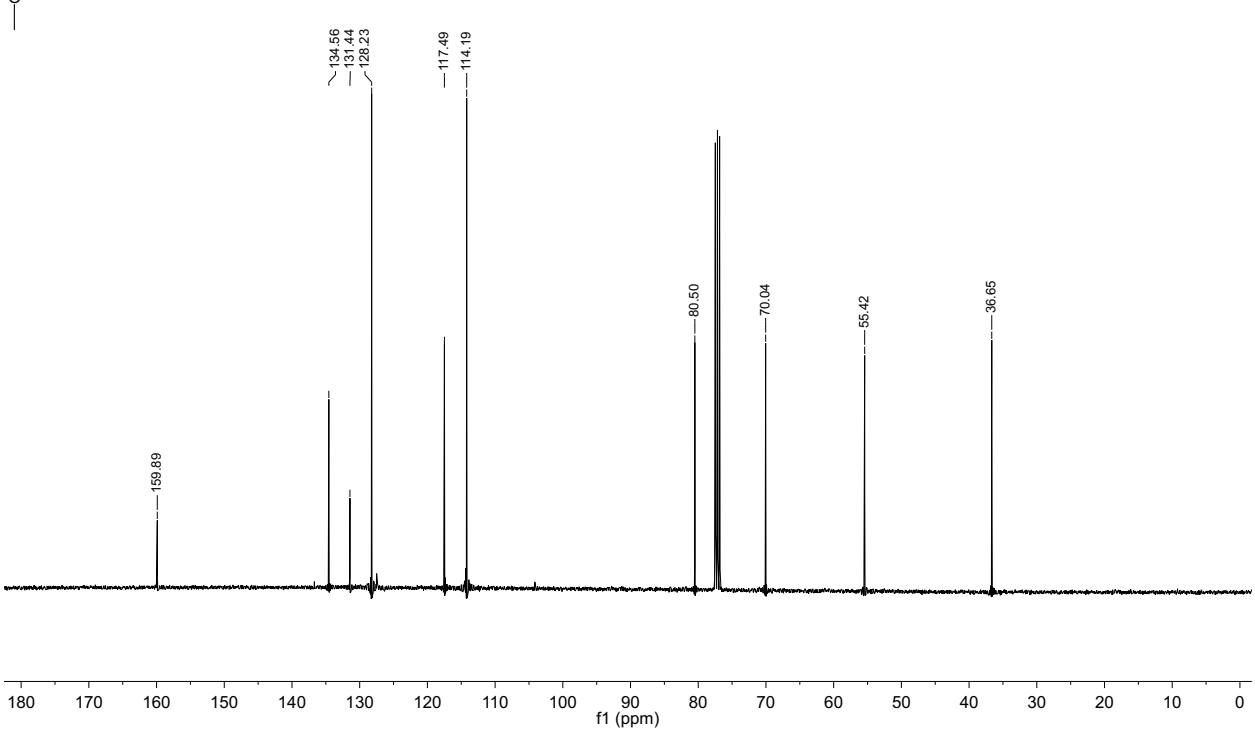

1-(1-(Allyloxy)-2-chloroethyl)-4-methoxybenzene 442c

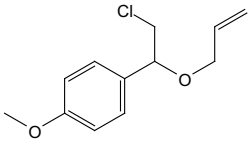

^{1}H NMR (400 MHz, Chloroform-*d*) δ 7.30 – 7.21 (m, 2H), 6.94 – 6.88 (m, 2H), 5.91 (dddd, *J* = 17.2, 10.4, 6.2, 5.1 Hz, 1H), 5.27 (dq, *J* = 17.2, 1.7 Hz, 1H), 5.18 (ddt, *J* = 10.4, 1.8, 1.3 Hz, 1H), 4.48 (dd, *J* = 7.9, 4.7 Hz, 1H), 4.00 (ddt, *J* = 12.8, 5.1, 1.5 Hz, 1H), 3.88 – 3.80 (m, 4H), 3.70 (dd, *J* = 11.3, 7.9 Hz, 1H), 3.56 (dd, *J* = 11.3, 4.7 Hz, 1H).

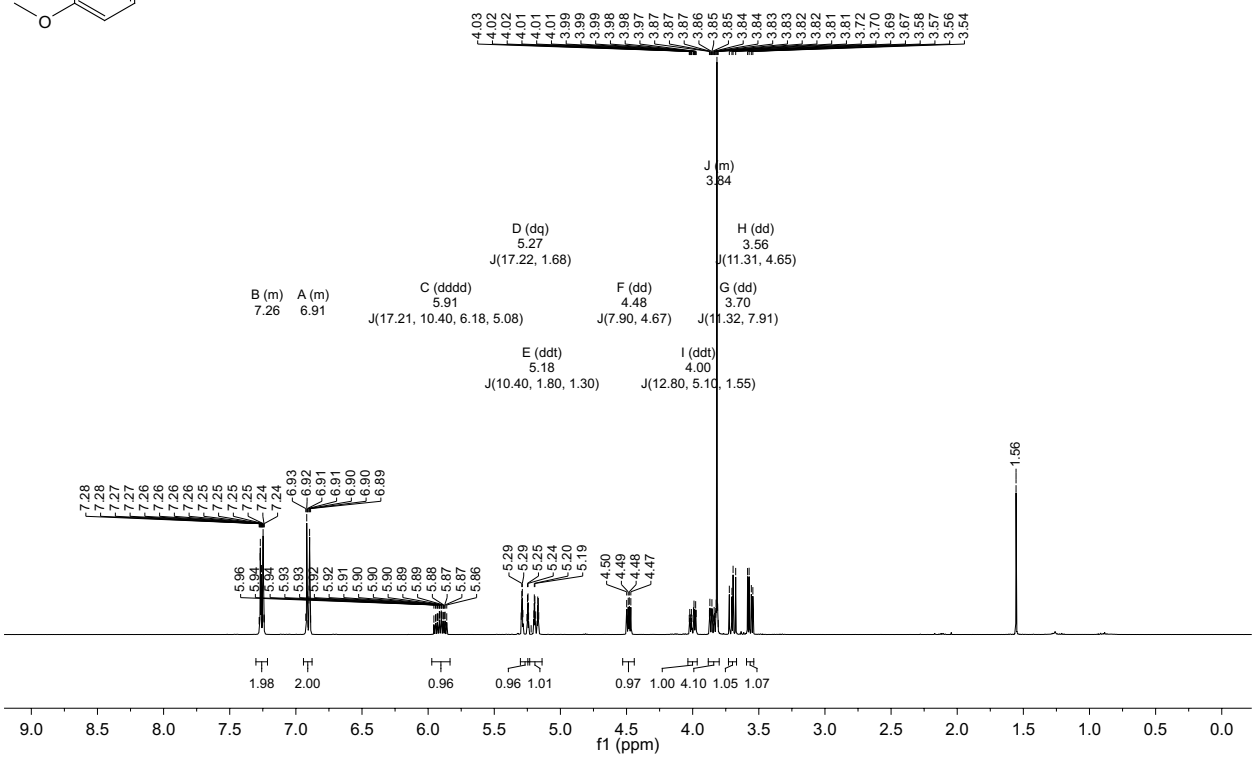

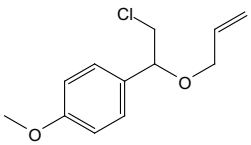

^{13}C NMR (101 MHz, Chloroform-*d*) δ 159.9, 134.6, 131.0, 128.3, 117.5, 114.2, 80.8, 70.0, 55.4, 48.4.

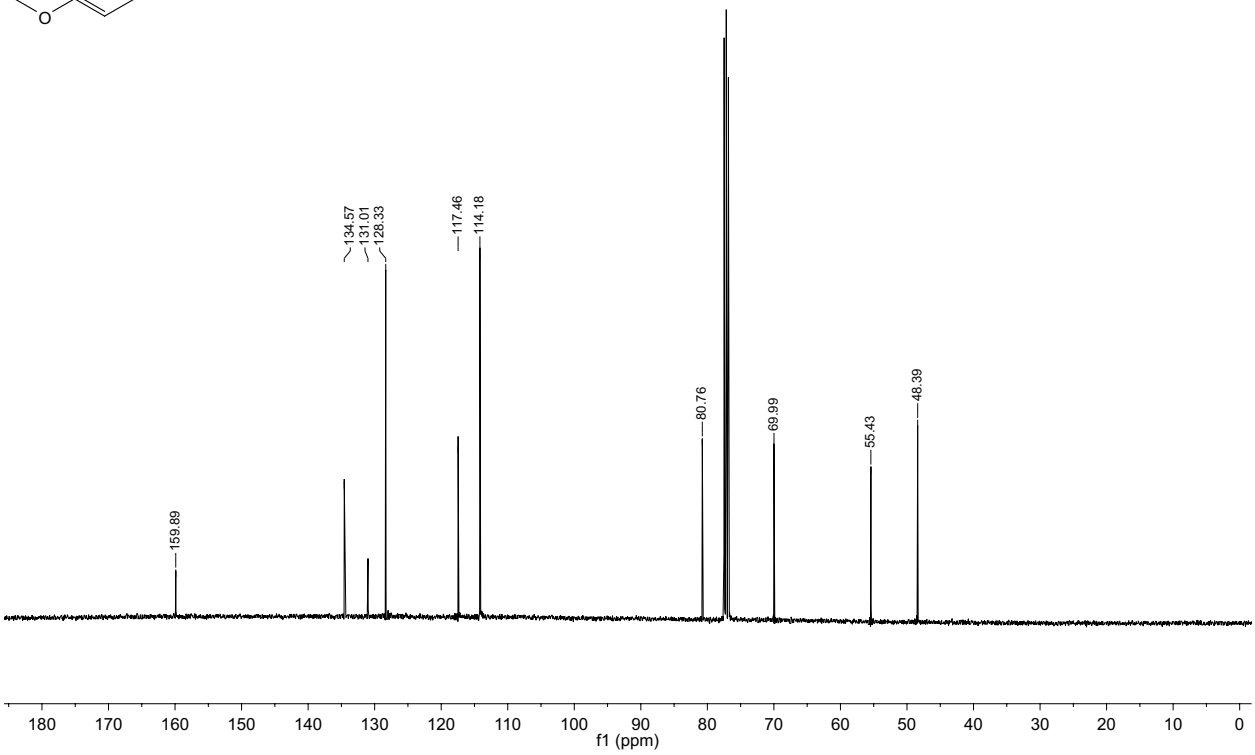

(Z)-4-(Allyloxy)but-2-en-1-ol 670

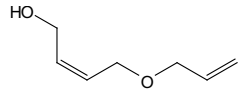

^{1}H NMR (400 MHz, Chloroform-*d*) δ 5.91 (ddt, *J* = 17.2, 10.4, 5.7 Hz, 1H), 5.82 (dtt, *J* = 11.2, 6.3, 1.3 Hz, 1H), 5.71 (dtt, *J* = 11.3, 6.3, 1.3 Hz, 1H), 5.28 (ddt, *J* = 17.2, 1.6 Hz, 1H), 5.20 (ddt, *J* = 10.4, 1.4 Hz, 1H), 4.20 (ddt, *J* = 6.4, 1.4, 0.7 Hz, 2H), 4.06 (ddt, *J* = 6.2, 1.5, 0.8 Hz, 2H), 3.99 (ddd, *J* = 5.7, 1.4 Hz, 2H), 1.90 (s, 1H).

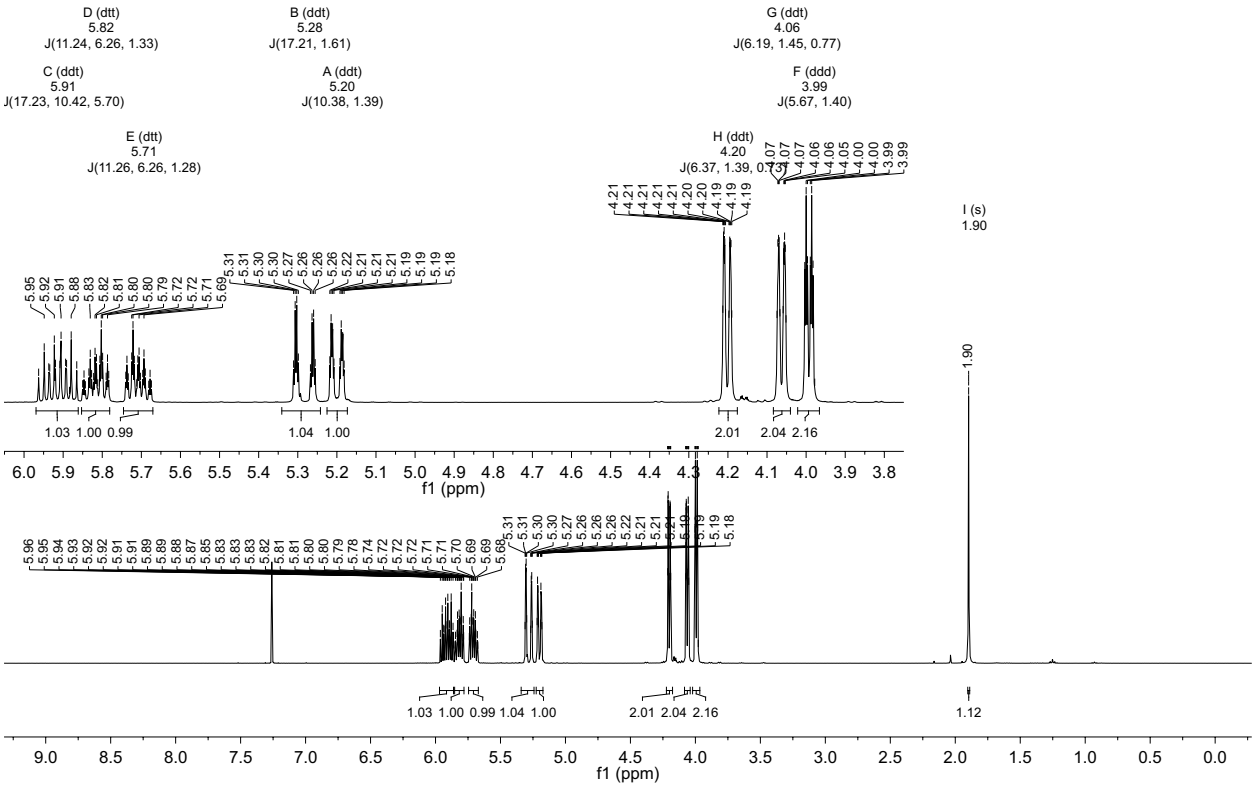

^{13}C NMR (101 MHz, Chloroform-*d*) δ 134.6, 132.4, 128.5, 117.6, 71.5, 65.8, 58.9.

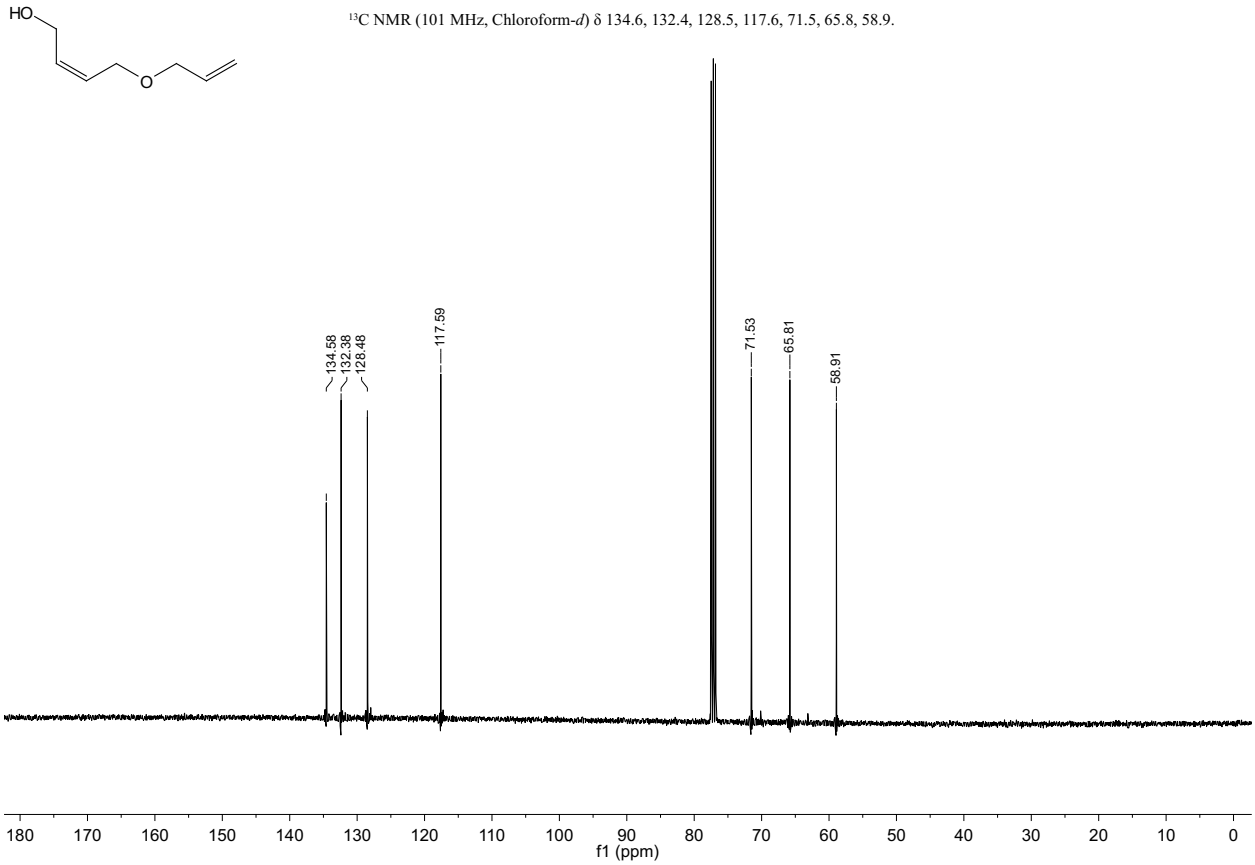

(Z)-1-(Allyloxy)-4-bromobut-2-ene 671

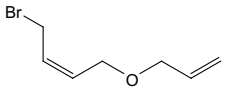

^{1}H NMR (400 MHz, Chloroform-*d*) δ 5.99 – 5.83 (m, 2H), 5.72 (dtt, *J* = 10.9, 6.4, 0.8 Hz, 1H), 5.30 (ddt, *J* = 17.3, 1.6 Hz, 1H), 5.21 (ddt, *J* = 10.4, 1.4 Hz, 1H), 4.12 (dd, *J* = 6.3, 1.6 Hz, 2H), 4.03 – 3.98 (m, 4H).

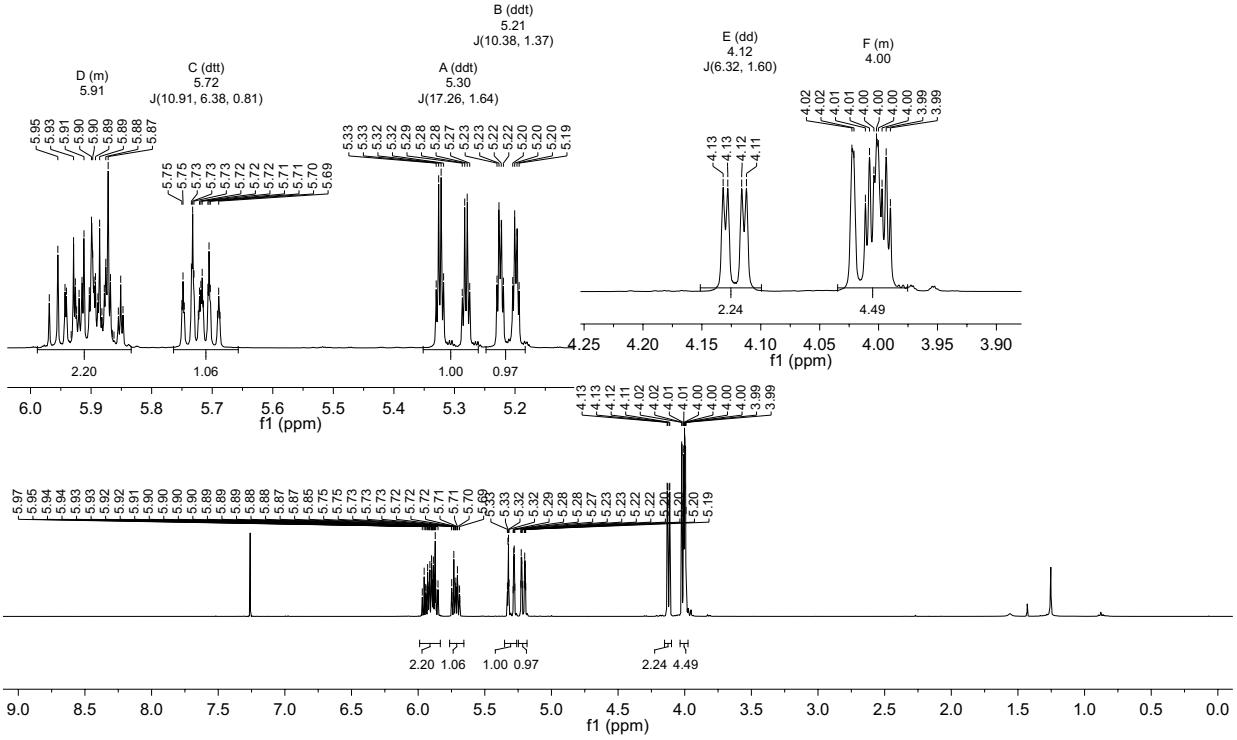

^{13}C NMR (101 MHz, Chloroform-*d*) δ 134.6, 131.3, 128.4, 117.6, 71.6, 65.1, 26.6.

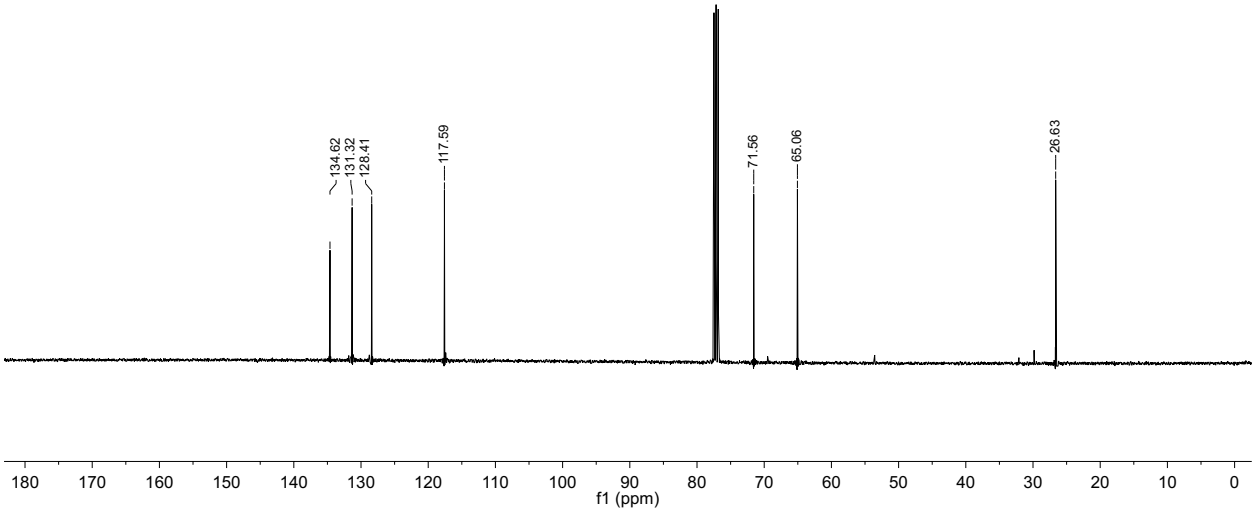

tert-Butyl *(Z)*-(4-(allyloxy)but-2-en-1-yl)(2-iodophenyl)carbamate 444a

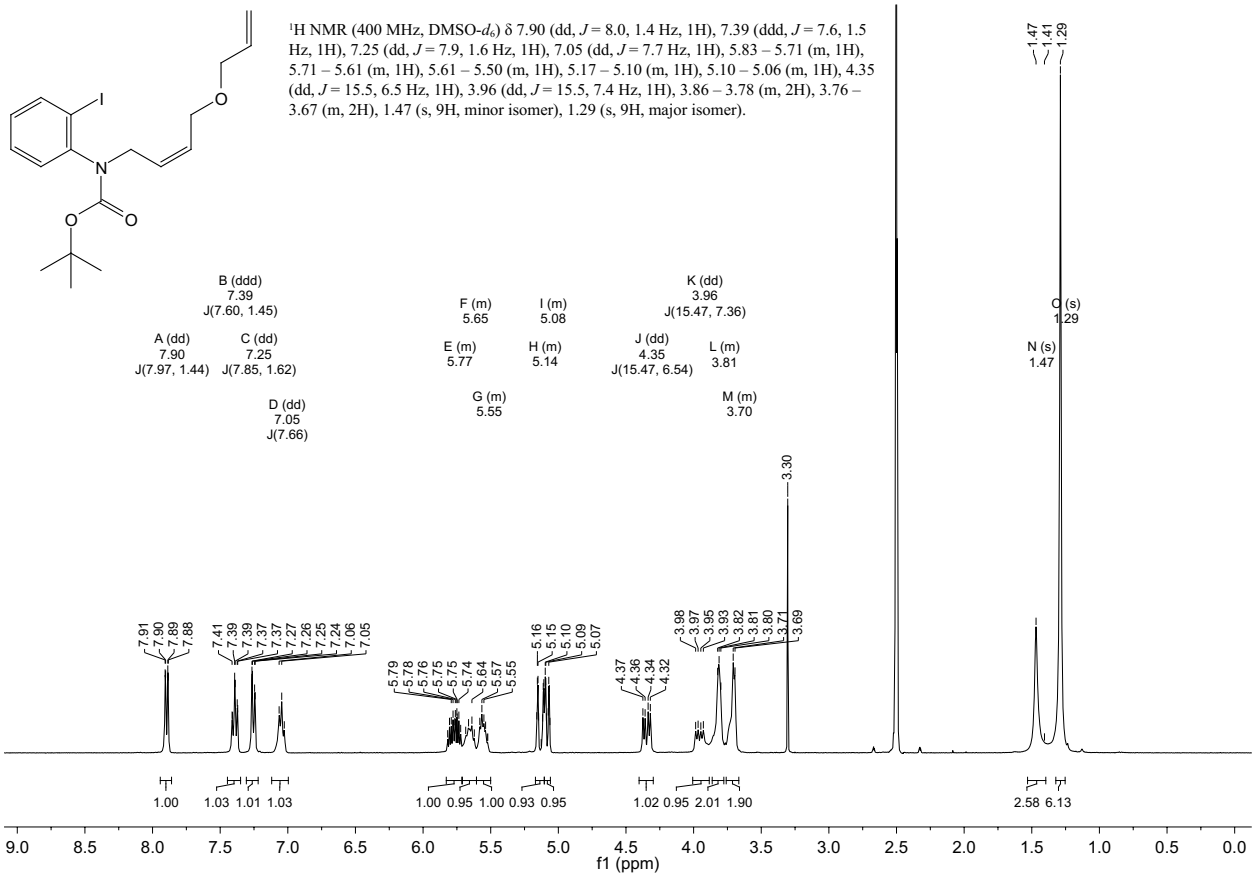

^{1}H NMR (400 MHz, DMSO-d_6) δ 7.90 (dd, J = 8.0, 1.4 Hz, 1H), 7.39 (ddd, J = 7.6, 1.5 Hz, 1H), 7.25 (dd, J = 7.9, 1.6 Hz, 1H), 7.05 (dd, J = 7.7 Hz, 1H), 5.83 – 5.71 (m, 1H), 5.71 – 5.61 (m, 1H), 5.61 – 5.50 (m, 1H), 5.17 – 5.10 (m, 1H), 5.10 – 5.06 (m, 1H), 4.35 (dd, J = 15.5, 6.5 Hz, 1H), 3.96 (dd, J = 15.5, 7.4 Hz, 1H), 3.86 – 3.78 (m, 2H), 3.76 – 3.67 (m, 2H), 1.47 (s, 9H, minor isomer), 1.29 (s, 9H, major isomer).

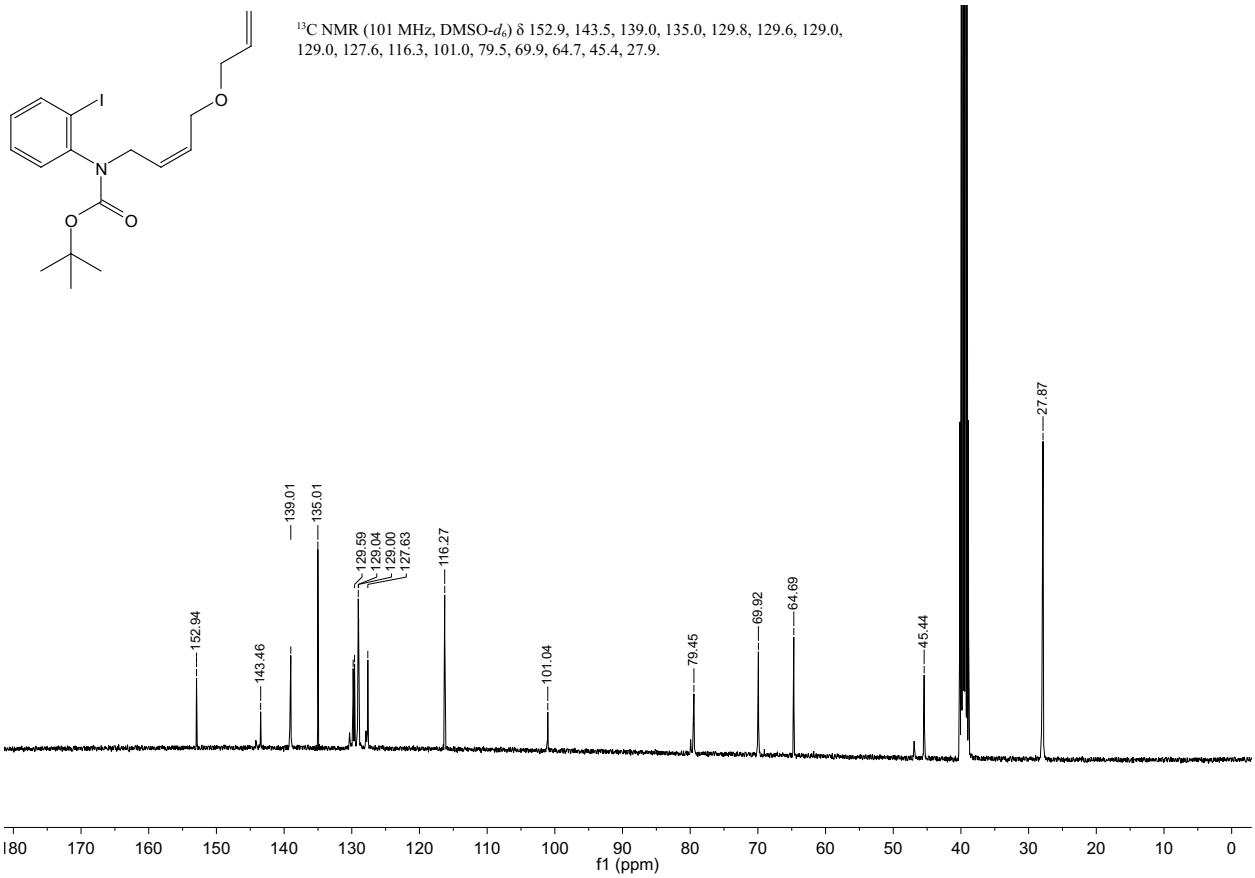

^{13}C NMR (101 MHz, DMSO-d_6) δ 152.9, 143.5, 139.0, 135.0, 129.8, 129.6, 129.0, 129.0, 127.6, 116.3, 101.0, 79.5, 69.9, 64.7, 45.4, 27.9.

(Z)-1-((4-(Allyloxy)but-2-en-1-yl)oxy)-2-iodobenzene 444b

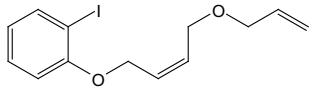

^{1}H NMR (400 MHz, Chloroform-*d*) δ 7.78 (dd, *J* = 7.8, 1.6 Hz, 1H), 7.28 (ddd, *J* = 8.2, 7.4, 1.6 Hz, 1H), 6.82 (dd, *J* = 8.3, 1.4 Hz, 1H), 6.72 (ddd, *J* = 7.6, 1.4 Hz, 1H), 5.98 – 5.86 (m, 2H), 5.86 – 5.78 (m, 1H), 5.30 (ddt, *J* = 17.3, 1.6 Hz, 1H), 5.20 (ddt, *J* = 10.4, 1.3 Hz, 1H), 4.69 (ddd, *J* = 5.8, 1.2 Hz, 2H), 4.16 – 4.12 (m, 2H), 4.01 (ddd, *J* = 5.6, 1.4 Hz, 2H).

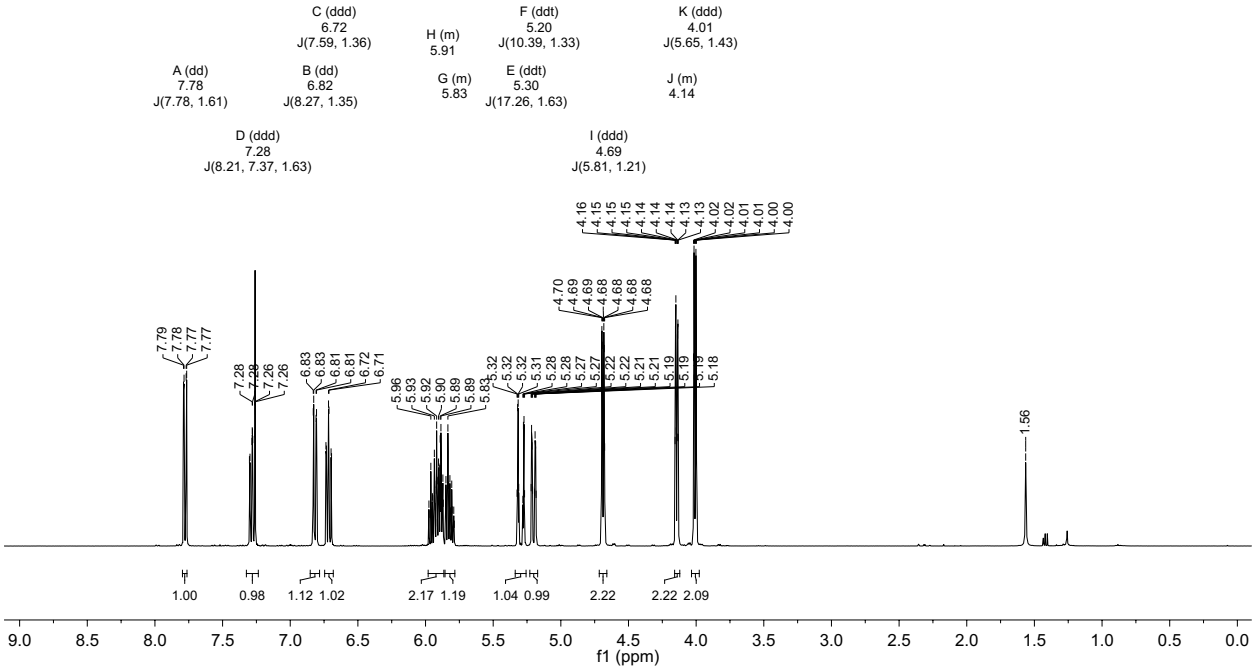

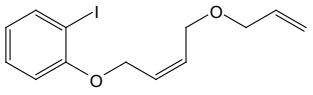

^{13}C NMR (101 MHz, Chloroform-*d*) δ 157.3, 139.7, 134.7, 130.3, 129.5, 127.7, 122.9, 117.5, 112.7, 86.9, 71.5, 66.3, 65.5.

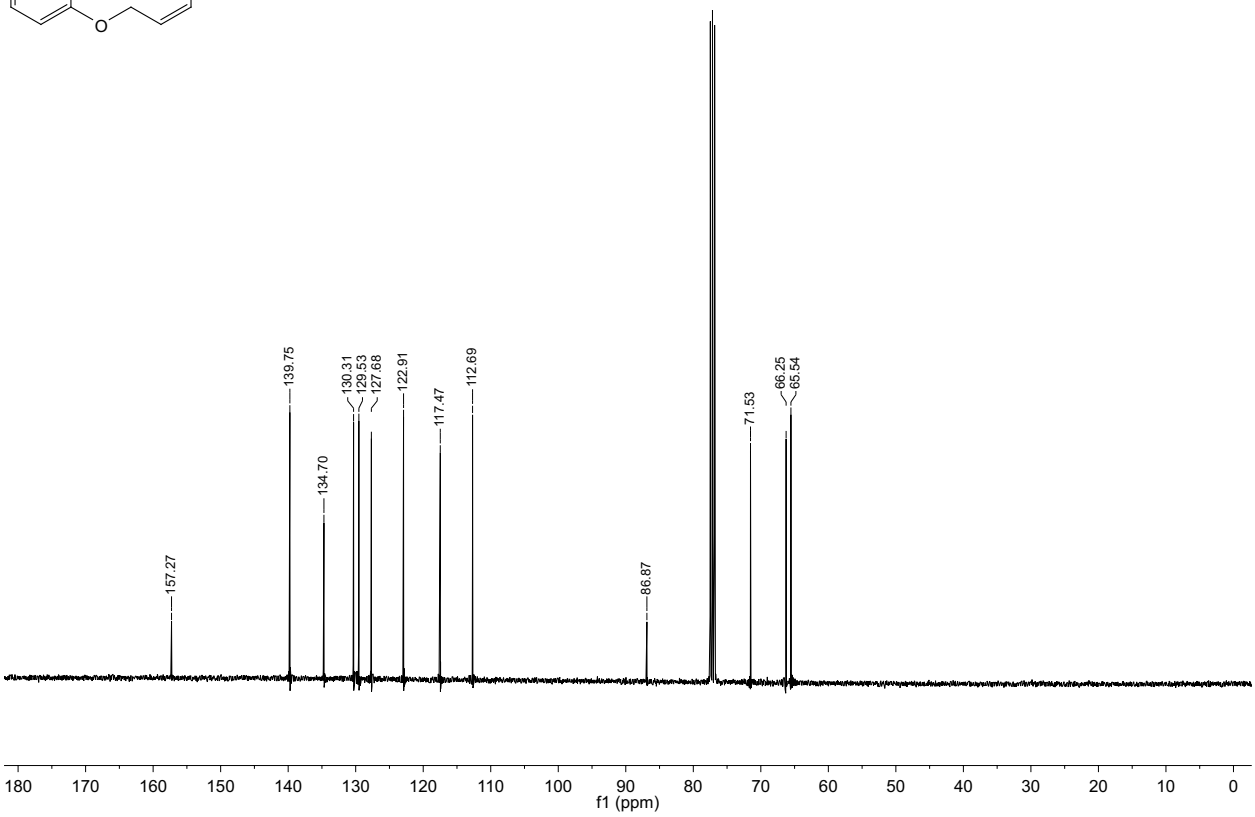

N-methylbenzamide 447a

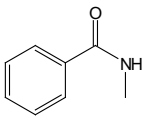

^{1}H NMR (400 MHz, Chloroform-*d*) δ 7.78 – 7.73 (m, 2H), 7.49 – 7.43 (m, 1H), 7.41 – 7.35 (m, 2H), 6.55 (br s, 1H), 2.97 (d, *J* = 4.6 Hz, 3H).

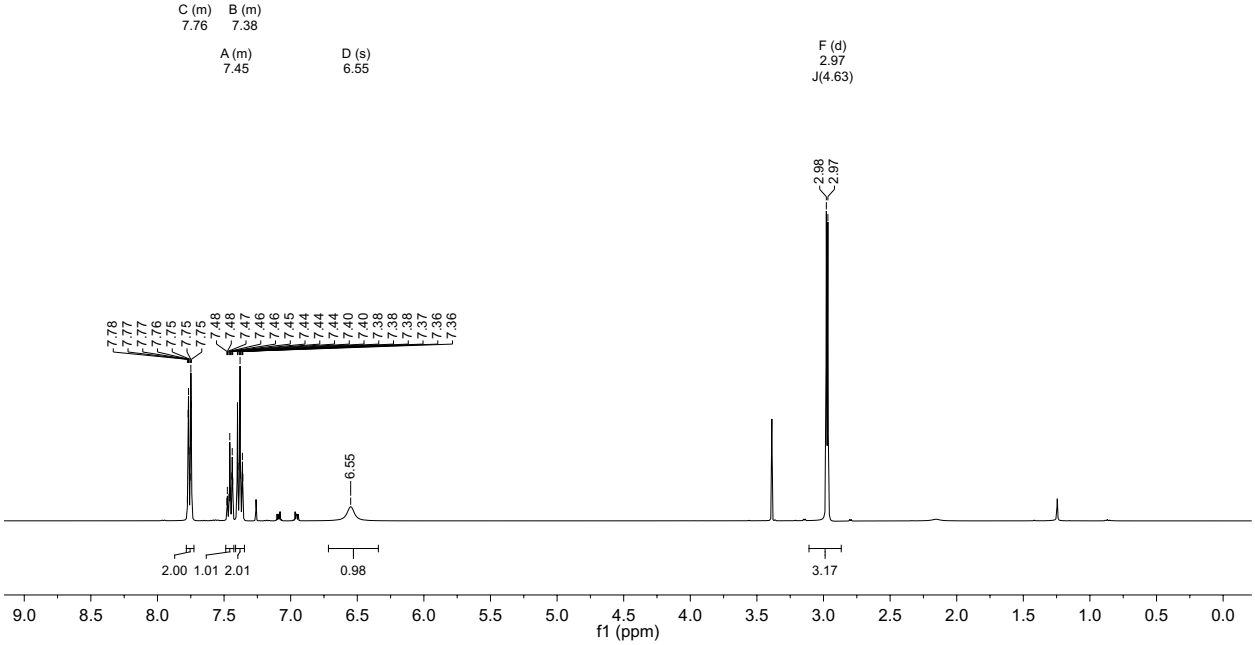

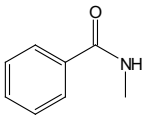

^{13}C NMR (101 MHz, Chloroform-*d*) δ 168.4, 134.7, 131.4, 128.6, 127.0, 26.9.

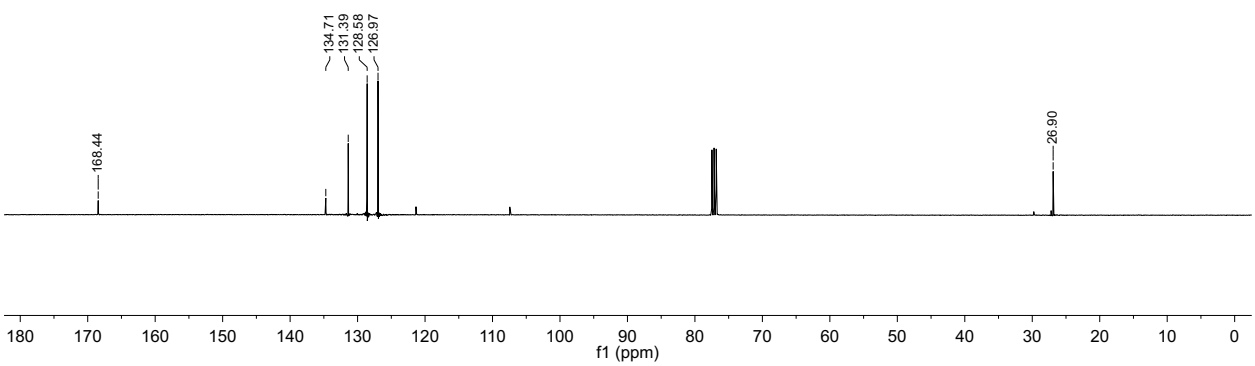

1,1-Bis(*tert*-butylperoxy)cyclohexane 448

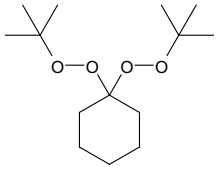

^{1}H NMR (400 MHz, Chloroform-*d*) δ 1.81 – 1.76 (m, 4H), 1.58 – 1.49 (m, 4H), 1.44 – 1.37 (m, 2H), 1.25 (s, 18H).

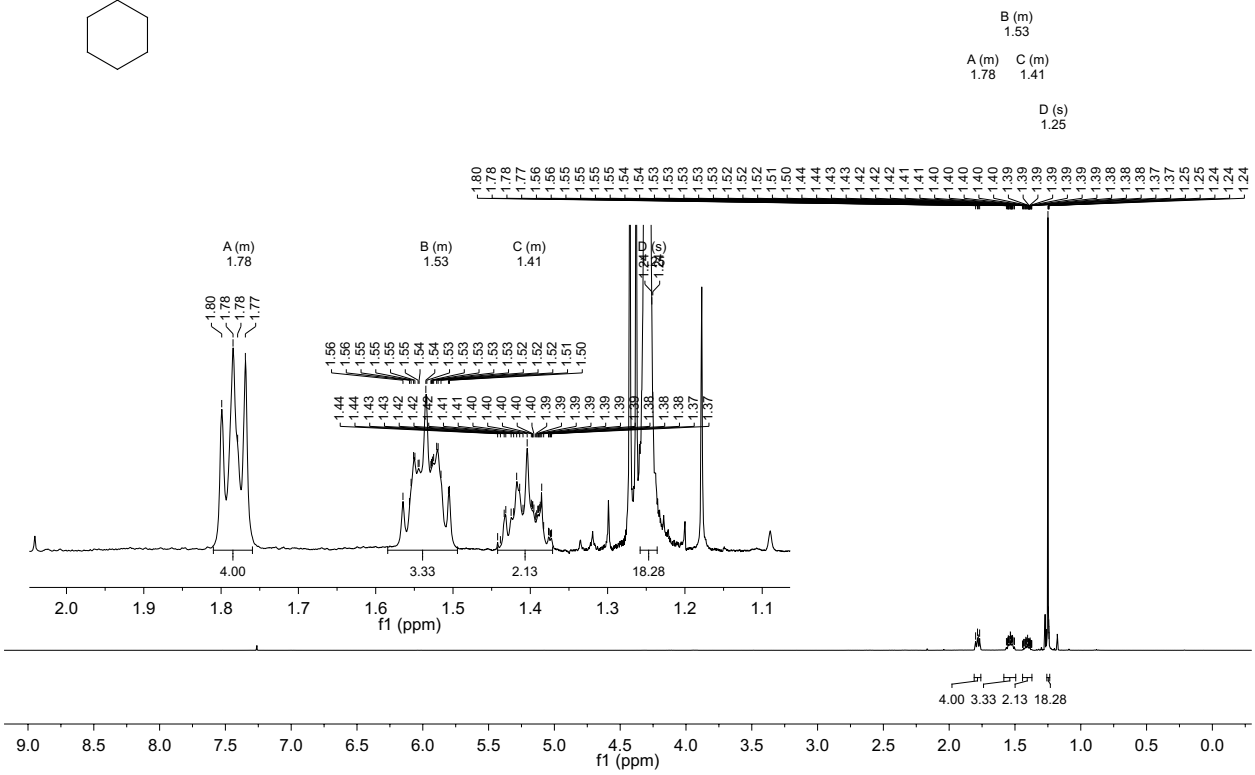

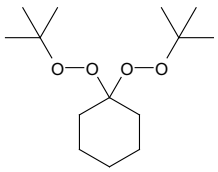

^{13}C NMR (101 MHz, Chloroform-*d*) δ 107.1, 79.1, 31.0, 27.0, 25.9, 22.9.

1,1-Bis(*tert*-butylperoxy)cyclohexane 38

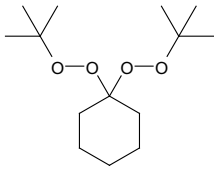

^{1}H NMR (400 MHz, DMSO-d_6) δ 1.71 (dd, J = 7.4, 4.7 Hz, 4H), 1.51 – 1.43 (m, 4H), 1.42 – 1.33 (m, 2H), 1.20 (s, 18H).

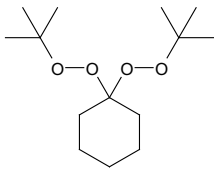

^{13}C NMR (101 MHz, DMSO-d_6) δ 106.4, 78.6, 30.4, 26.5, 25.0, 22.2.

N-Methoxy-*N*-methylbenzamide 446a

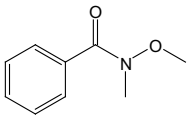

^{1}H NMR (400 MHz, Chloroform-*d*) δ 7.69 – 7.64 (m, 2H), 7.48 – 7.36 (m, 3H), 3.55 (s, 3H), 3.35 (s, 3H).

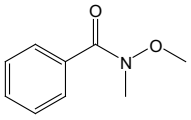

^{13}C NMR (101 MHz, Chloroform-*d*) δ 170.1, 134.3, 130.7, 128.3, 128.1, 61.1, 33.9.

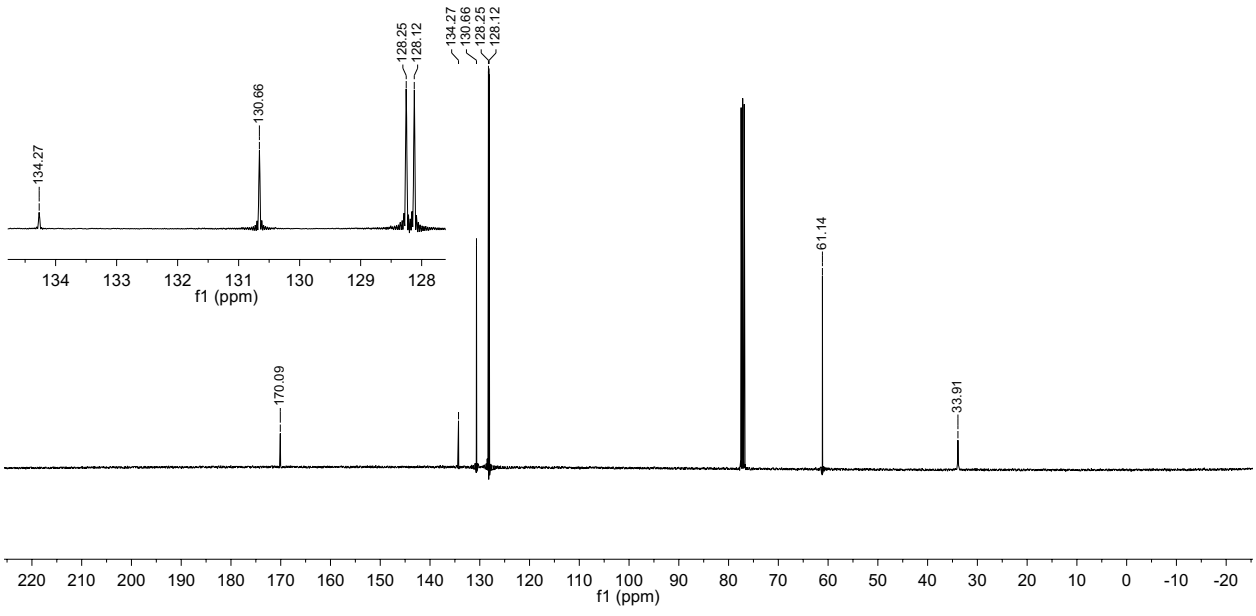

N-Methoxy-*N*-methyl-2-phenylacetamide 446b

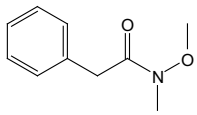

^{1}H NMR (400 MHz, Chloroform-*d*) δ 7.39 – 7.20 (m, 5H), 3.78 (s, 2H), 3.60 (s, 3H), 3.19 (s, 3H).

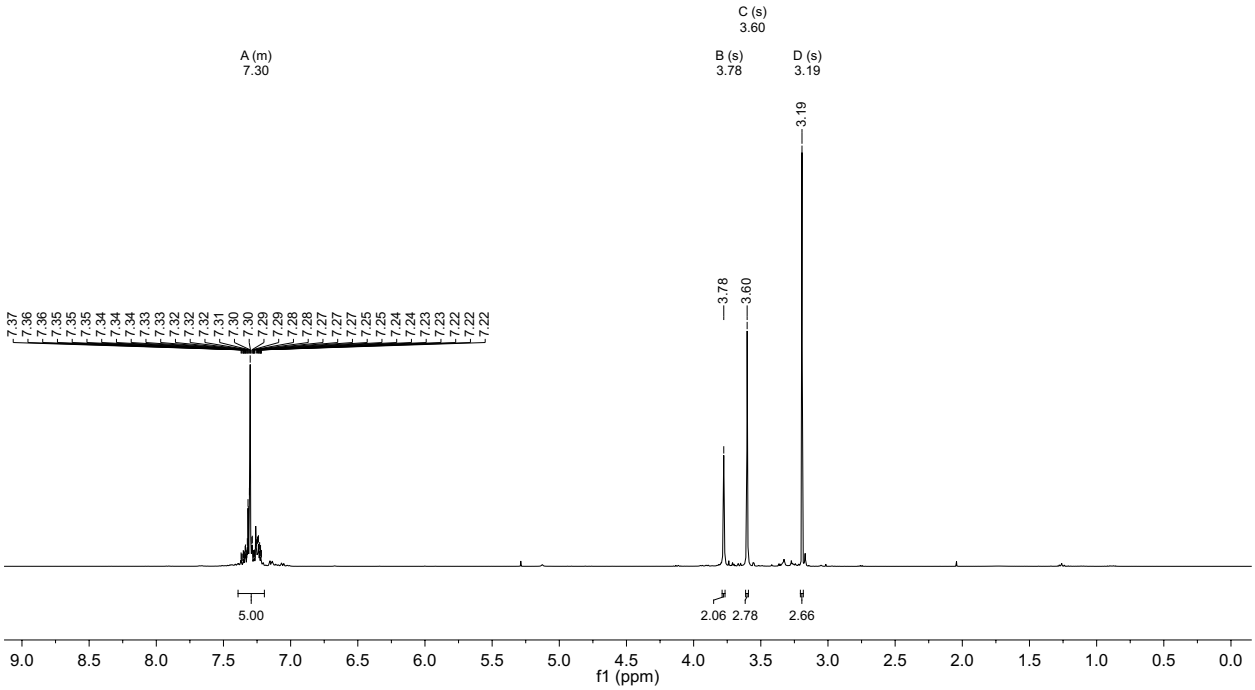

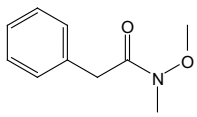

^{13}C NMR (101 MHz, Chloroform-*d*) δ 172.0, 134.5, 128.8, 128.0, 126.3, 60.8, 38.9, 31.8.

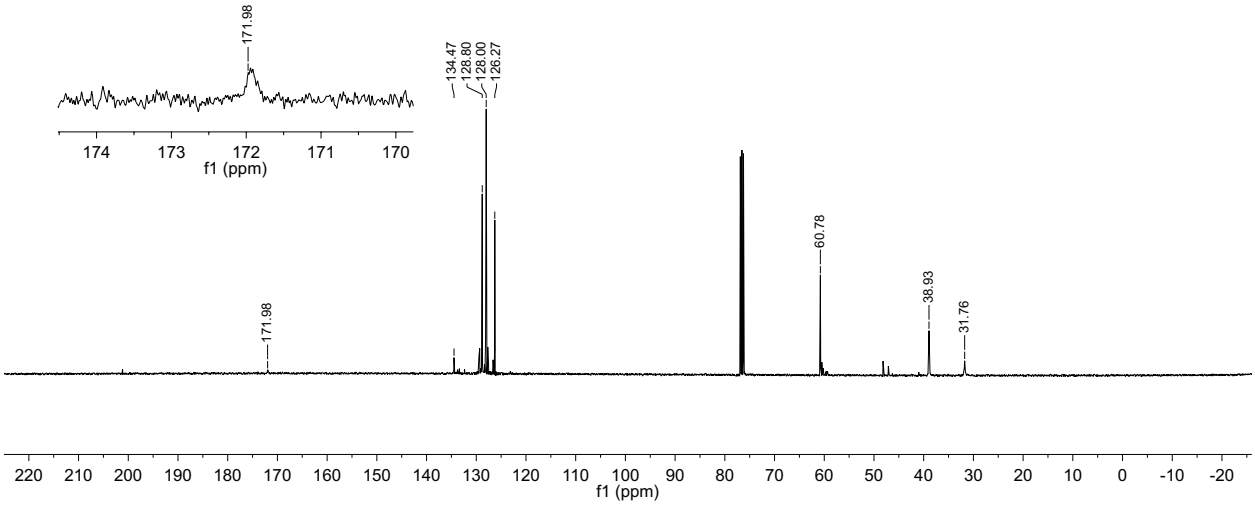

Naphthalene 39

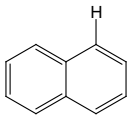

^{1}H NMR (400 MHz, Chloroform-*d*) δ 7.89 – 7.80 (m, 4H), 7.48 (dd, *J* = 6.3, 3.2 Hz, 4H).

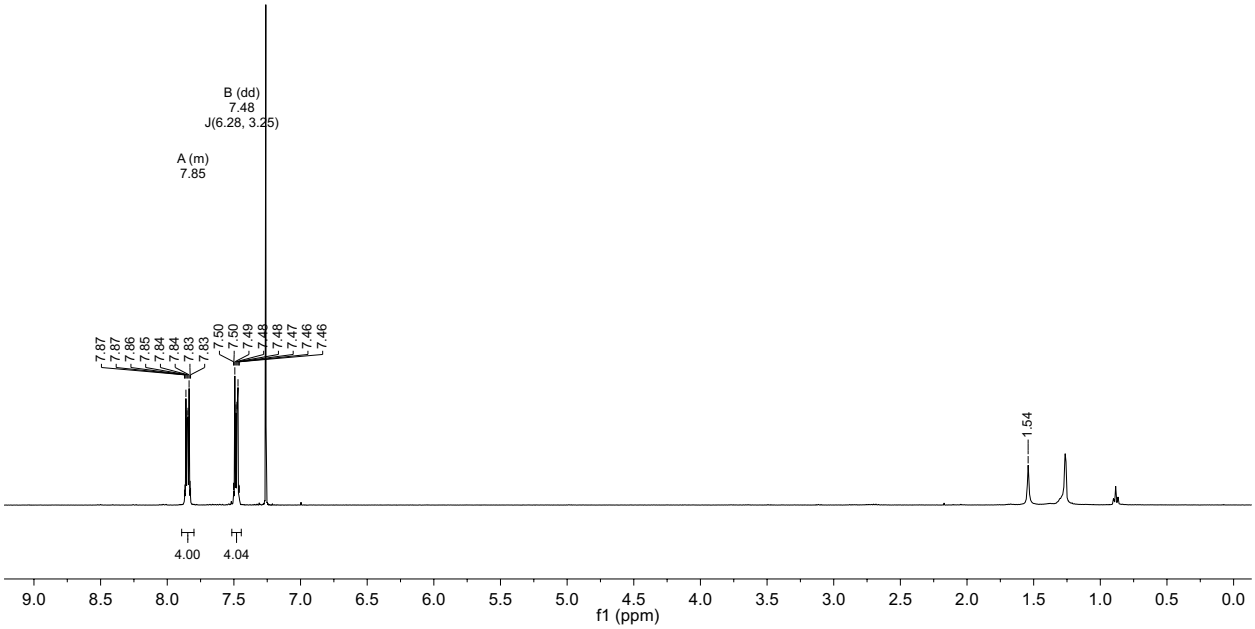

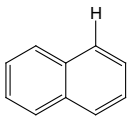

^{13}C NMR (101 MHz, Chloroform-*d*) δ 133.6, 128.0, 126.0.

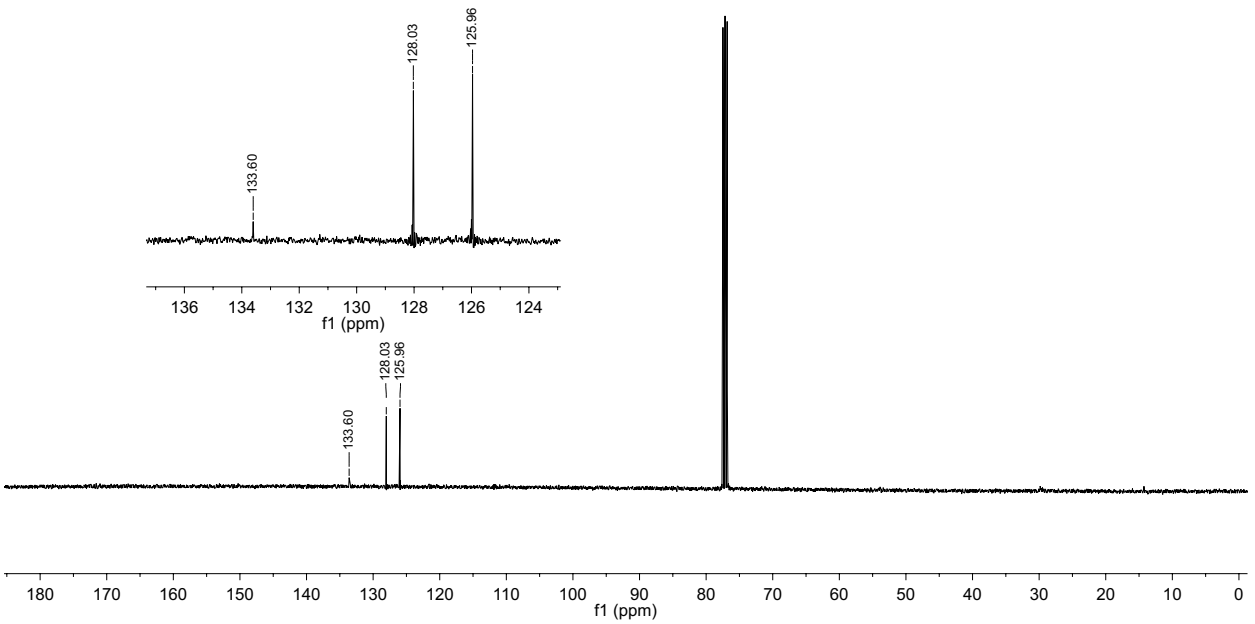

3,3'-(Propane-1,3-diyl)bis(1-methyl-1*H*-benzo[*d*]imidazol-3-ium) iodide 41

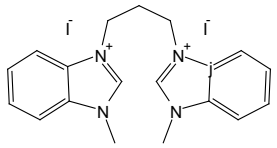

^{1}H NMR (500 MHz, DMSO-d_6) δ 9.70 (s, 2H), 8.05 (ddd, J = 7.0, 3.0 Hz, 4H), 7.76 – 7.67 (m, 4H), 4.66 (t, J = 7.2 Hz, 4H), 4.08 (s, 6H), 2.59 (p, J = 7.3 Hz, 2H).

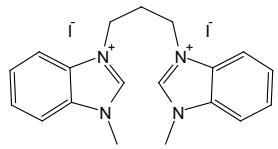

^{13}C NMR (126 MHz, DMSO) δ 142.80, 131.80, 130.82, 126.56, 126.50, 113.62, 113.41, 43.82, 33.33, 28.04.

1,3-Dimethyl-2,3-dihydro-1H-imidazole 220

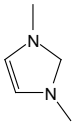

^{1}H NMR (400 MHz, THF-d_8) δ 5.34 (s, 2H), 3.66 (s, 2H), 2.36 (s, 6H).

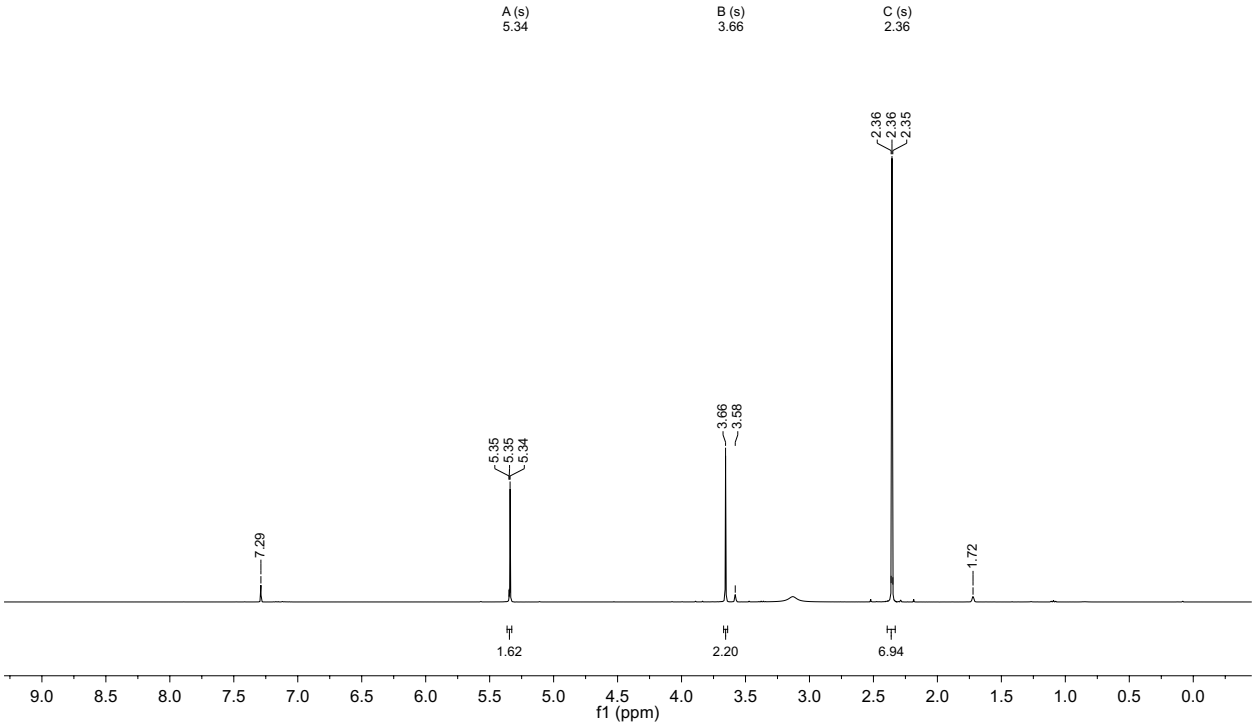

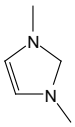

^{13}C NMR (101 MHz, THF) δ 123.82, 81.73, 40.84.

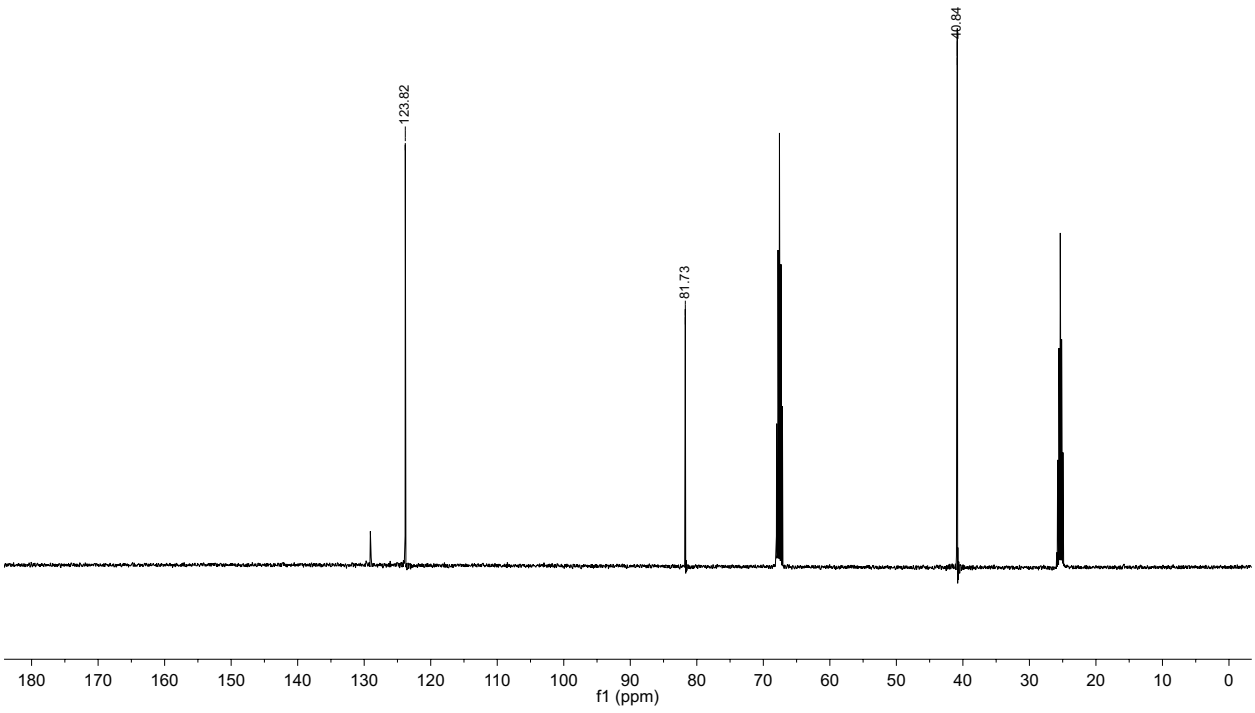

1,3-Dimethylimidazolidine 459

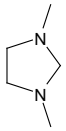

^{13}C NMR (101 MHz, Benzene-d_6) δ 80.6, 55.2, 41.8.

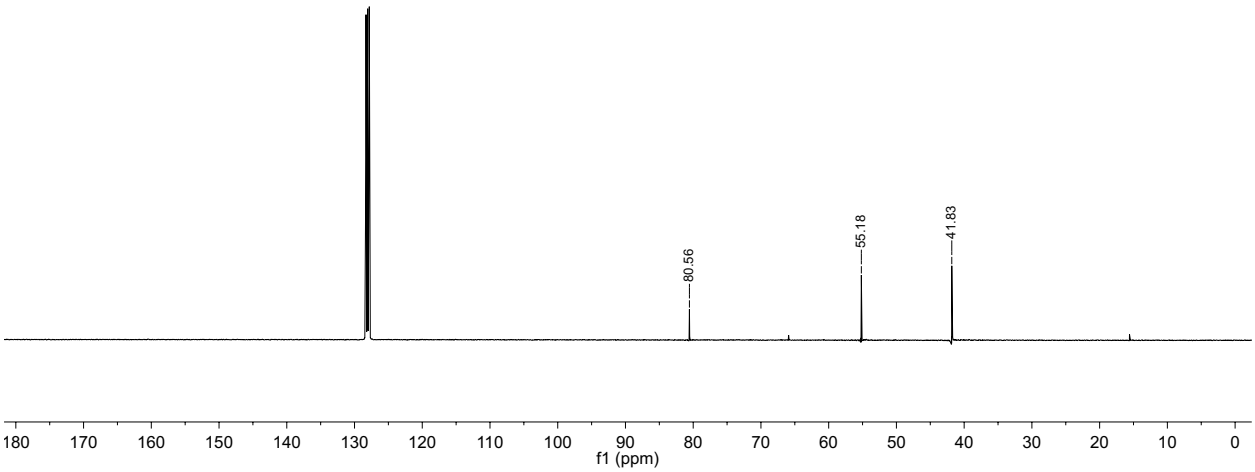

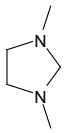

^{13}C NMR (101 MHz, Benzene-d_6) δ 80.6, 55.2, 41.8.

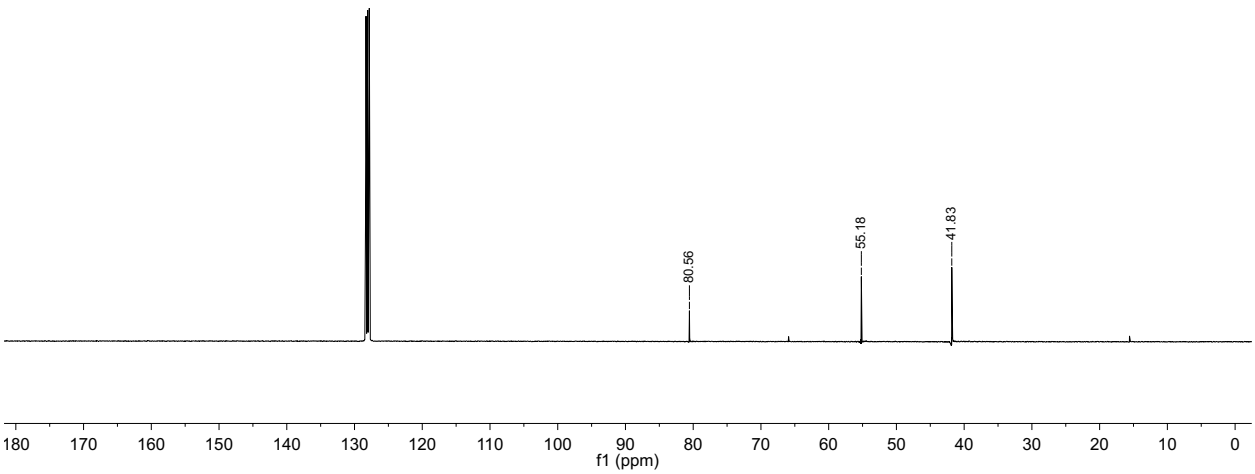

1,3-Dimethyl-1H-imidazol-3-ium iodide 461

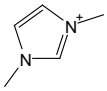

^{1}H NMR (400 MHz, Deuterium Oxide) δ 8.76 (s, 1H), 7.52 (d, *J* = 1.9 Hz, 2H), 3.99 (s, 7H).

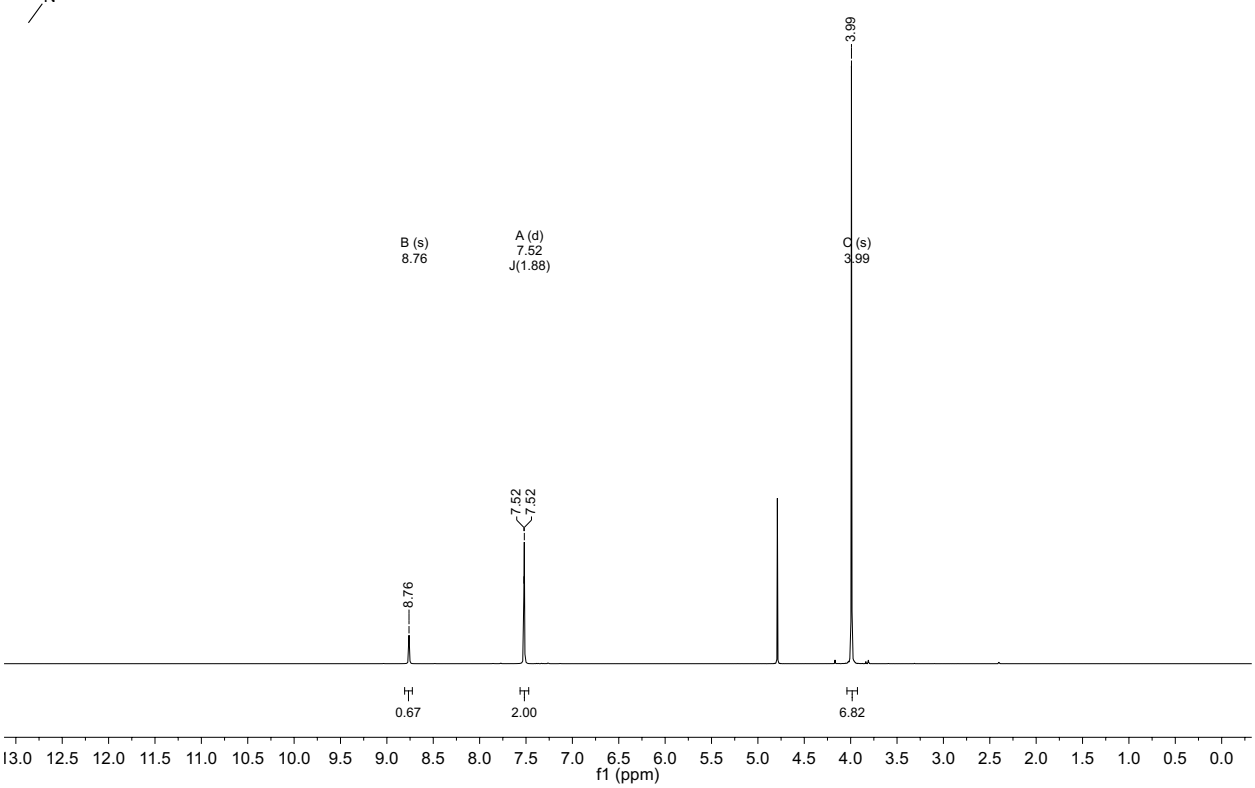

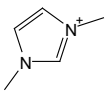

^{13}C NMR (101 MHz, D_2O) δ 136.17, 123.03, 35.55.

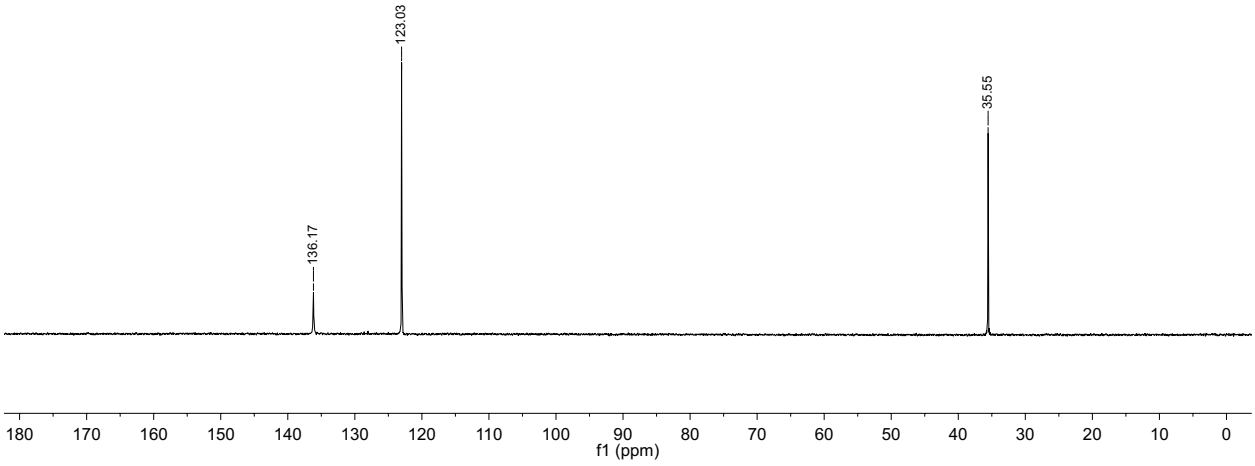

1,3-Dimethyl-1H-imidazol-3-ium iodide 461

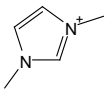

^{1}H NMR (400 MHz, Chloroform-*d*) δ 10.02 (s, 1H), 7.41 (d, *J* = 1.7 Hz, 2H), 4.10 (s, 6H).

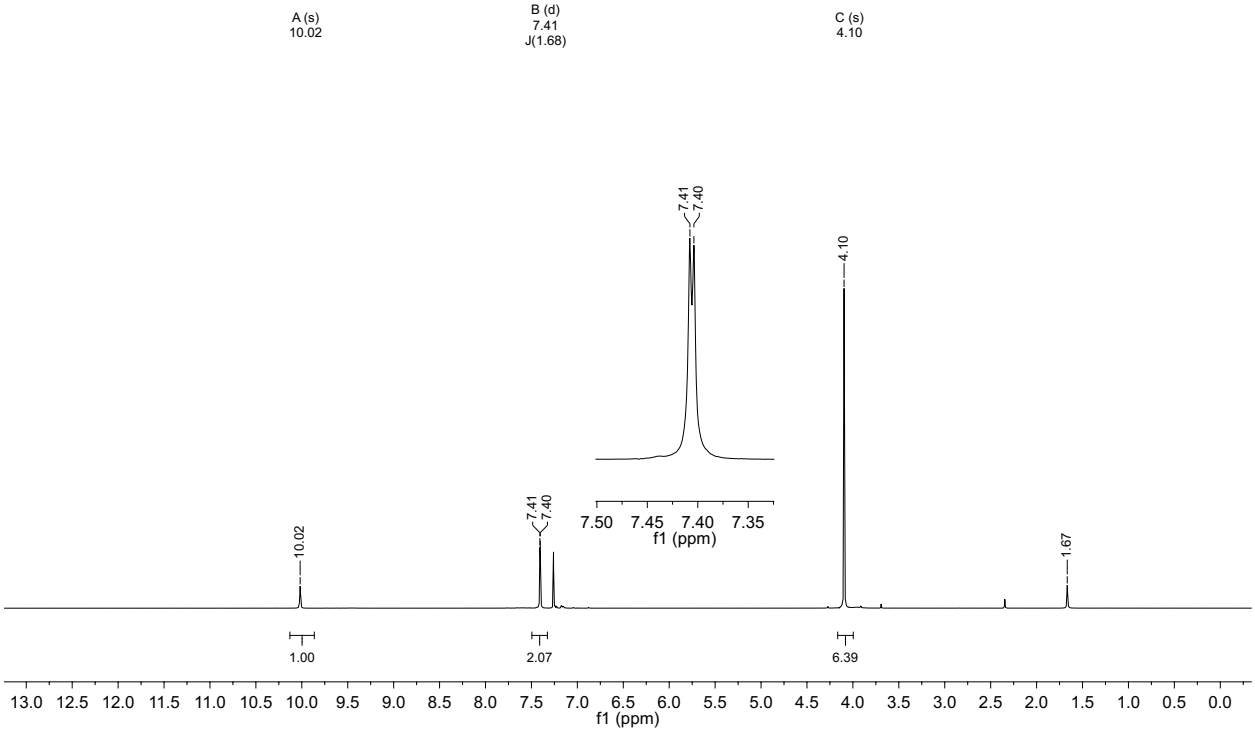

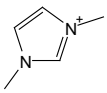

^{13}C NMR (101 MHz, $CDCl_3$) δ 137.81, 123.52, 37.24.

4-(Dimethylamino)-1-methylpyridin-1-ium iodide 463

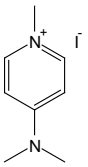

^{1}H NMR (400 MHz, DMSO-d_6) δ 8.26 – 8.20 (m, 2H), 7.05 – 6.99 (m, 2H), 3.92 (s, 3H), 3.18 (s, 6H).

A (m)	B (m)	C (s)	D (s)
8.23	7.02	3.92	3.18

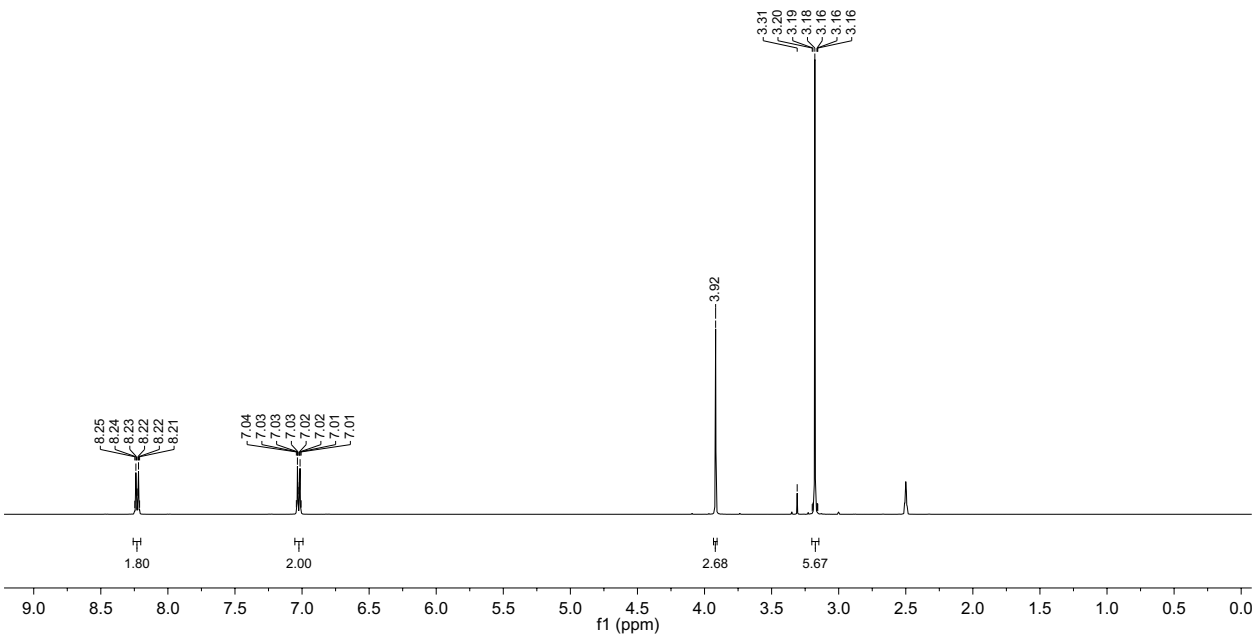

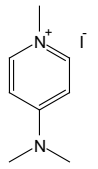

^{13}C NMR (101 MHz, DMSO-d_6) δ 155.6, 142.7, 107.4, 44.0, 39.7.

Naphthalen-2-ol 475

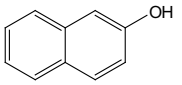

^{1}H NMR (600 MHz, Chloroform-*d*) δ 7.77 (dd, *J* = 9.3 Hz, 2H), 7.69 (d, *J* = 8.3 Hz, 1H), 7.44 (dd, *J* = 7.8 Hz, 1H), 7.34 (dd, *J* = 7.6 Hz, 1H), 7.16 (d, *J* = 3.2 Hz, 1H), 7.11 (dd, *J* = 8.7, 2.7 Hz, 1H), 4.97 (s, 1H).

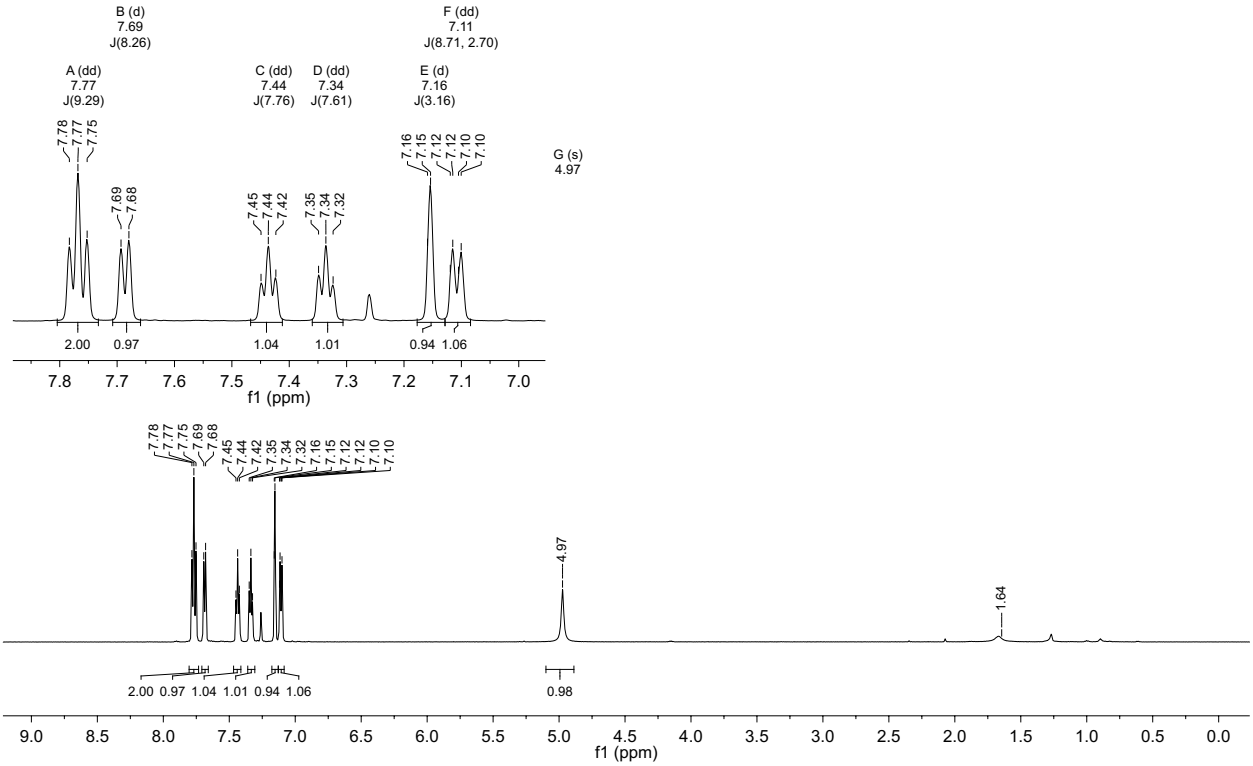

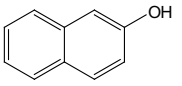

^{13}C NMR (151 MHz, Chloroform-*d*) δ 153.4, 134.7, 130.0, 129.1, 127.9, 126.7, 126.5, 123.8, 117.9, 109.6.

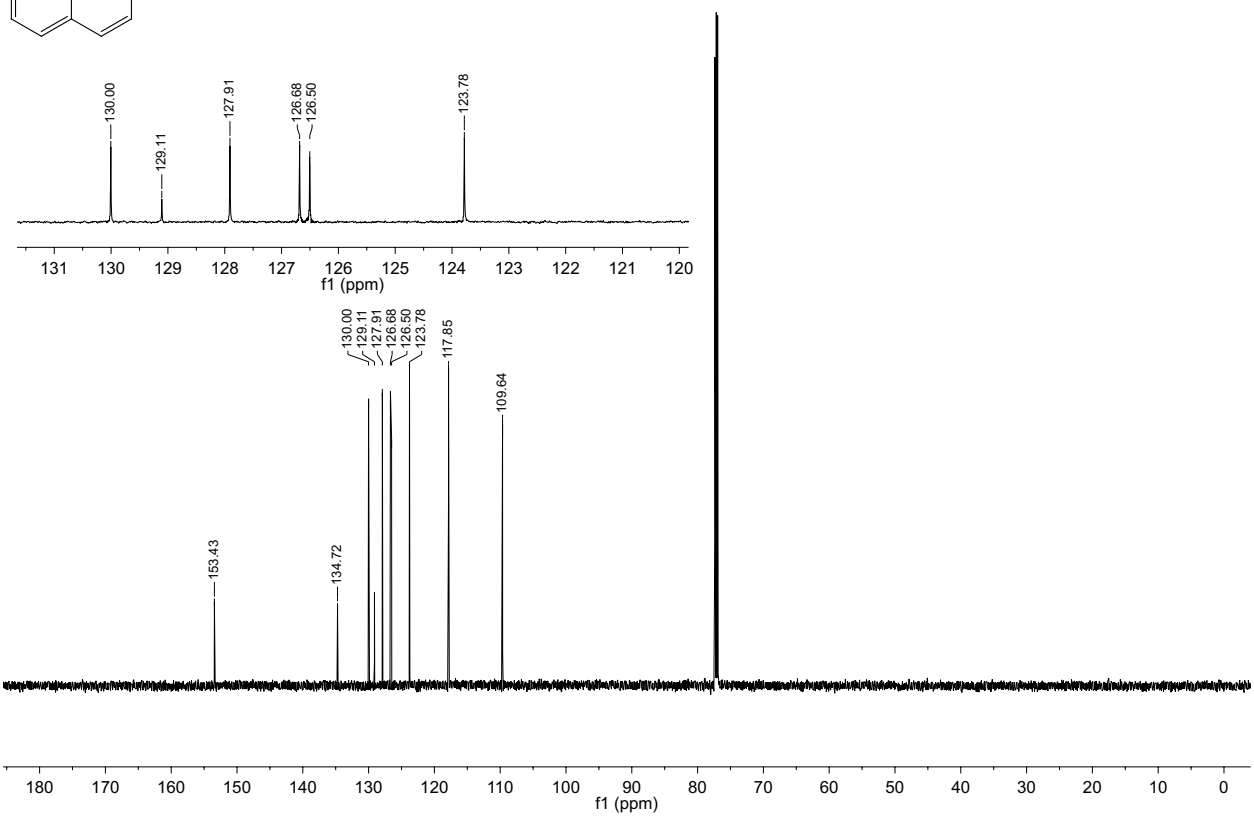

Triethyl(naphthalen-2-yl)silane 476

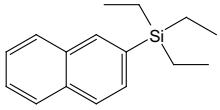

^{1}H NMR (400 MHz, Chloroform-*d*) δ 7.99 (d, *J* = 1.0 Hz, 1H), 7.88 – 7.79 (m, 3H), 7.58 (dd, *J* = 8.1, 1.2 Hz, 1H), 7.52 – 7.45 (m, 2H), 1.05 – 0.97 (m, 9H), 0.93 – 0.85 (m, 6H).

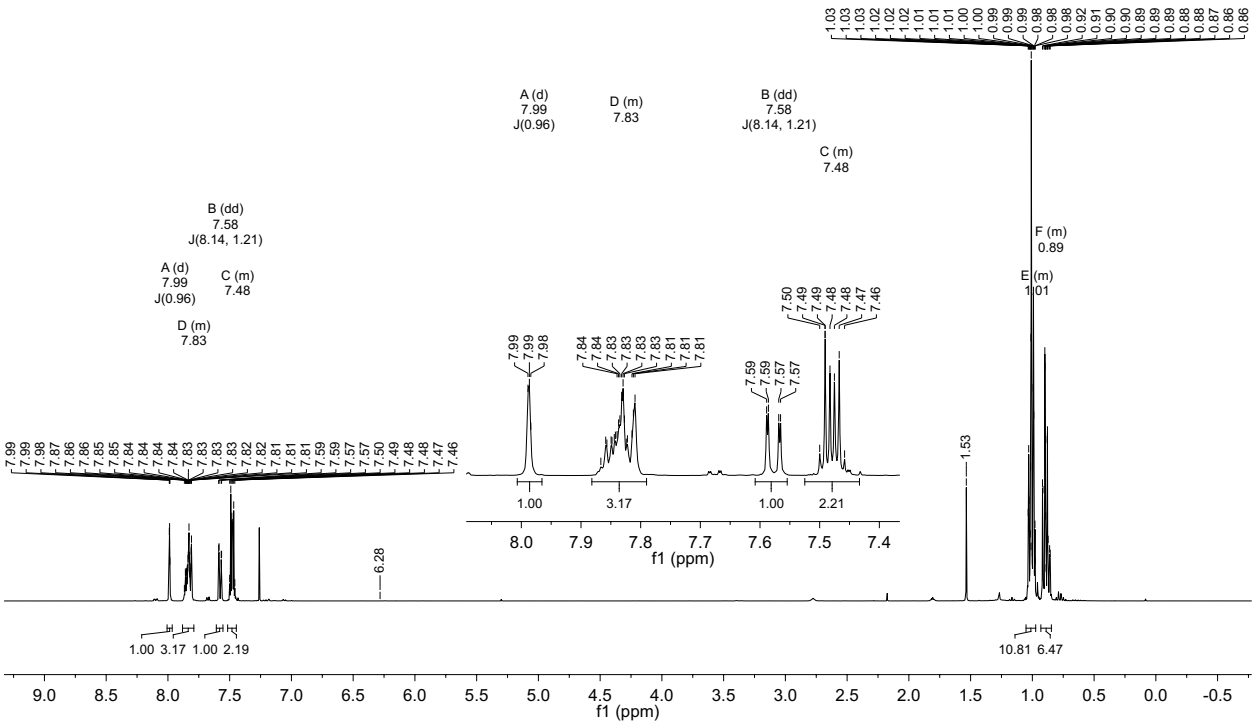

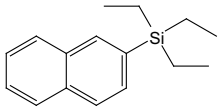

^{13}C NMR (101 MHz, Chloroform-*d*) δ 135.2, 134.9, 133.8, 133.1, 130.7, 128.2, 127.8, 126.9, 126.3, 125.9, 7.6, 3.6.

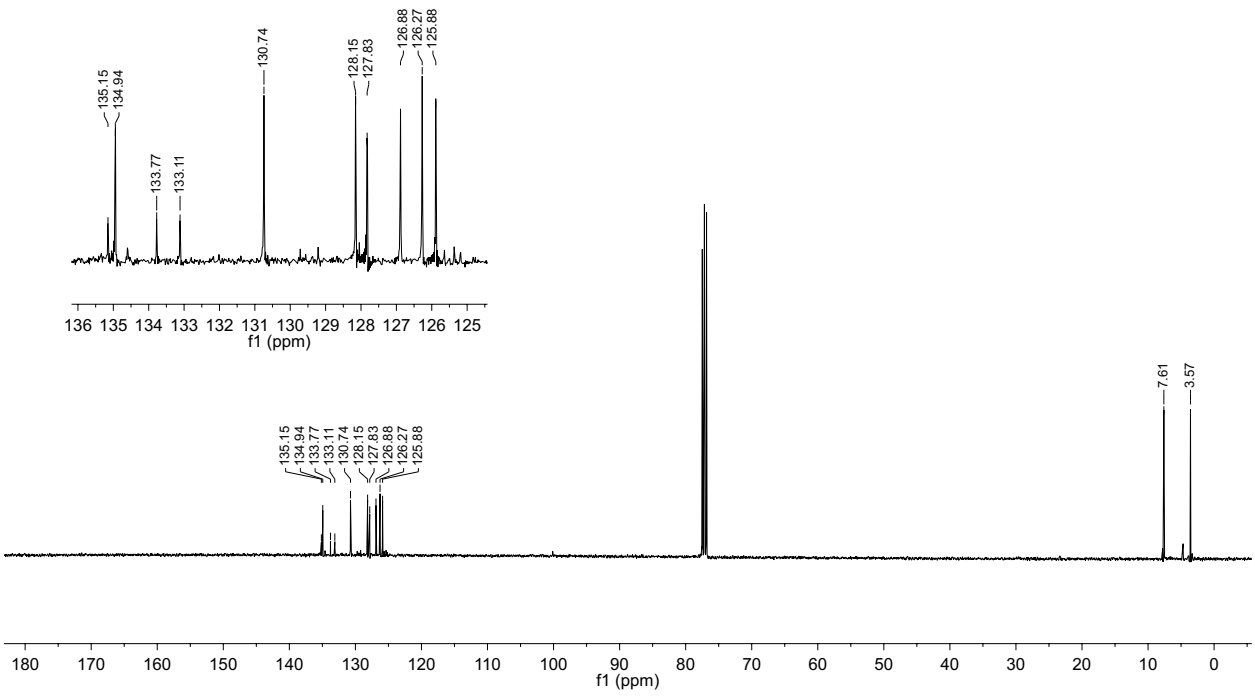

2,2'-Binaphthalene 477

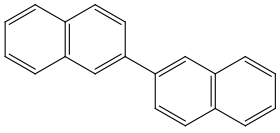

^{1}H NMR (400 MHz, Chloroform-*d*) δ 8.21 – 8.15 (m, 2H), 8.00 – 7.92 (m, 4H), 7.89 (dd, *J* = 8.5, 1.8 Hz, 4H), 7.57 – 7.47 (m, 4H).

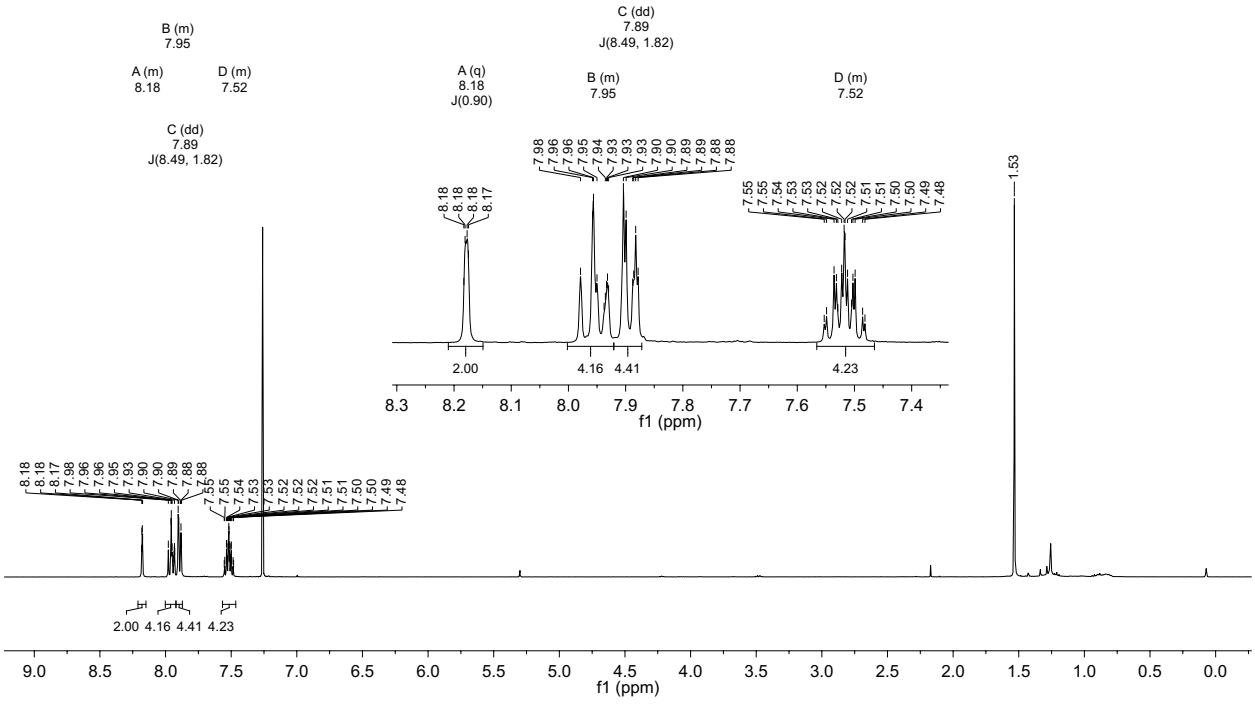

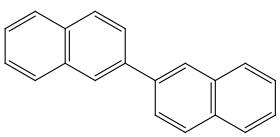

^{13}C NMR (101 MHz, Chloroform-*d*) δ 138.6, 133.9, 132.8, 128.7, 128.4, 127.8, 126.5, 126.3, 126.2, 125.9.

[1,2'-Binaphthalen]-2-ol 478

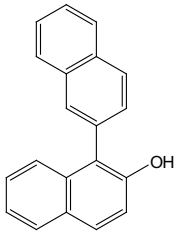

^{1}H NMR (400 MHz, Chloroform-*d*) δ 8.07 (ddd, *J* = 8.6, 0.7 Hz, 1H), 8.00 – 7.96 (m, 1H), 7.96 – 7.94 (m, 1H), 7.93 – 7.89 (m, 1H), 7.87 – 7.82 (m, 2H), 7.64 – 7.56 (m, 2H), 7.52 (dd, *J* = 8.3, 1.7 Hz, 1H), 7.47 – 7.40 (m, 1H), 7.38 – 7.29 (m, 3H), 5.24 (s, 1H).

^{13}C NMR (151 MHz, Chloroform-*d*) δ 150.5, 134.0, 133.5, 133.3, 131.8, 130.3, 129.8, 129.6, 129.1, 129.0, 128.2, 128.2, 128.1, 126.9, 126.9, 126.7, 124.8, 123.5, 121.0, 117.5.

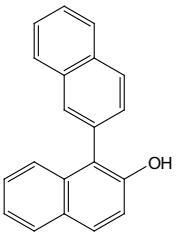

[1,2'-Binaphthalen]-2-ol 478

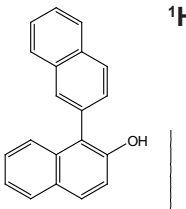

^{1}H-^{1}H-COSY

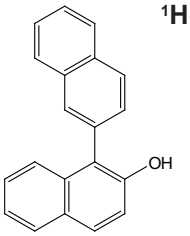

^{1}H-^{1}H-NOE

NOE: OH irradiated

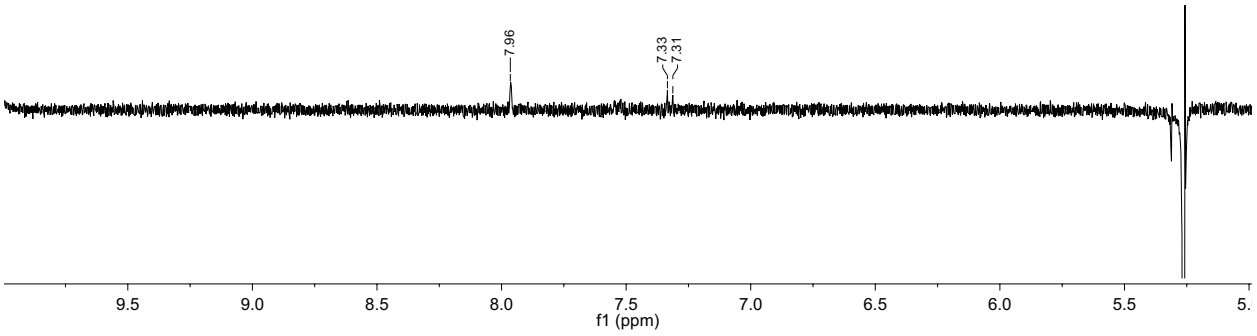

1-Methylnaphthalene 480

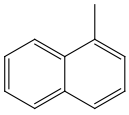

^{1}H NMR (600 MHz, Chloroform-*d*) δ 8.02 (d, *J* = 8.3 Hz, 1H), 7.86 (d, *J* = 7.8 Hz, 1H), 7.72 (d, *J* = 8.1 Hz, 1H), 7.54 (ddd, *J* = 8.5, 6.8, 1.6 Hz, 1H), 7.52 – 7.48 (m, 1H), 7.41 – 7.36 (m, 1H), 7.34 (d, *J* = 7.0 Hz, 1H), 2.72 (s, 3H).

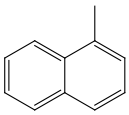

^{13}C NMR (101 MHz, Chloroform-*d*) δ 134.4, 133.7, 132.7, 128.6, 126.7, 125.9, 125.8, 125.7, 125.7, 124.2, 19.5.

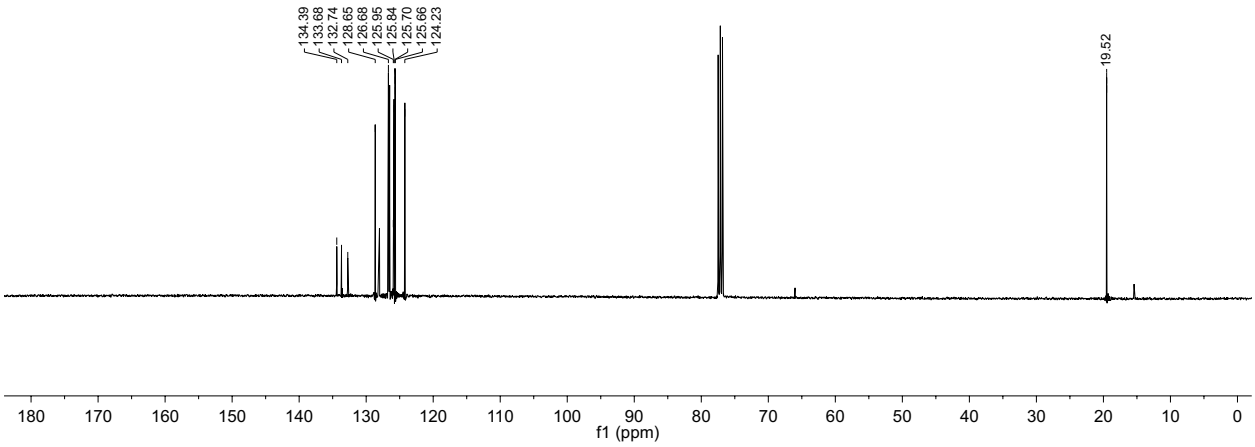

1-(Naphthalen-2-ylmethyl)naphthalene 481

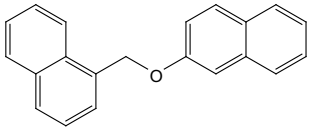

^{1}H NMR (400 MHz, Chloroform-*d*) δ 8.14 – 8.08 (m, 1H), 7.97 – 7.91 (m, 1H), 7.90 – 7.86 (m, 1H), 7.83 – 7.76 (m, 3H), 7.67 (dd, *J* = 6.9, 1.1 Hz, 1H), 7.60 – 7.52 (m, 2H), 7.52 – 7.44 (m, 2H), 7.40 – 7.33 (m, 2H), 7.29 – 7.24 (m, 1H), 5.63 (s, 2H).

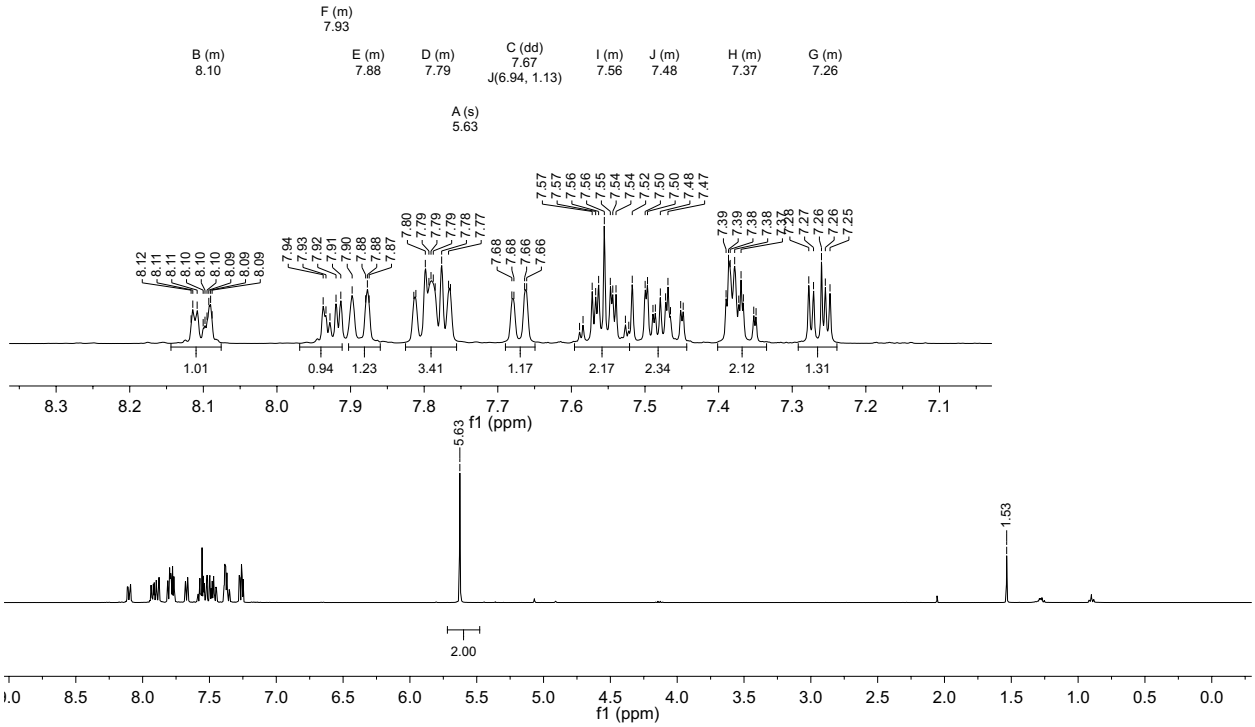

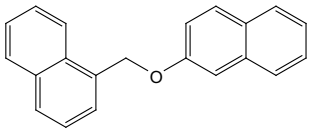

^{13}C NMR (101 MHz, Chloroform-*d*) δ 157.0, 134.7, 134.0, 132.4, 131.8, 129.7, 129.3, 129.2, 128.9, 127.8, 127.0, 126.8, 126.6, 126.6, 126.1, 125.5, 123.9, 123.9, 119.2, 107.3, 68.8.

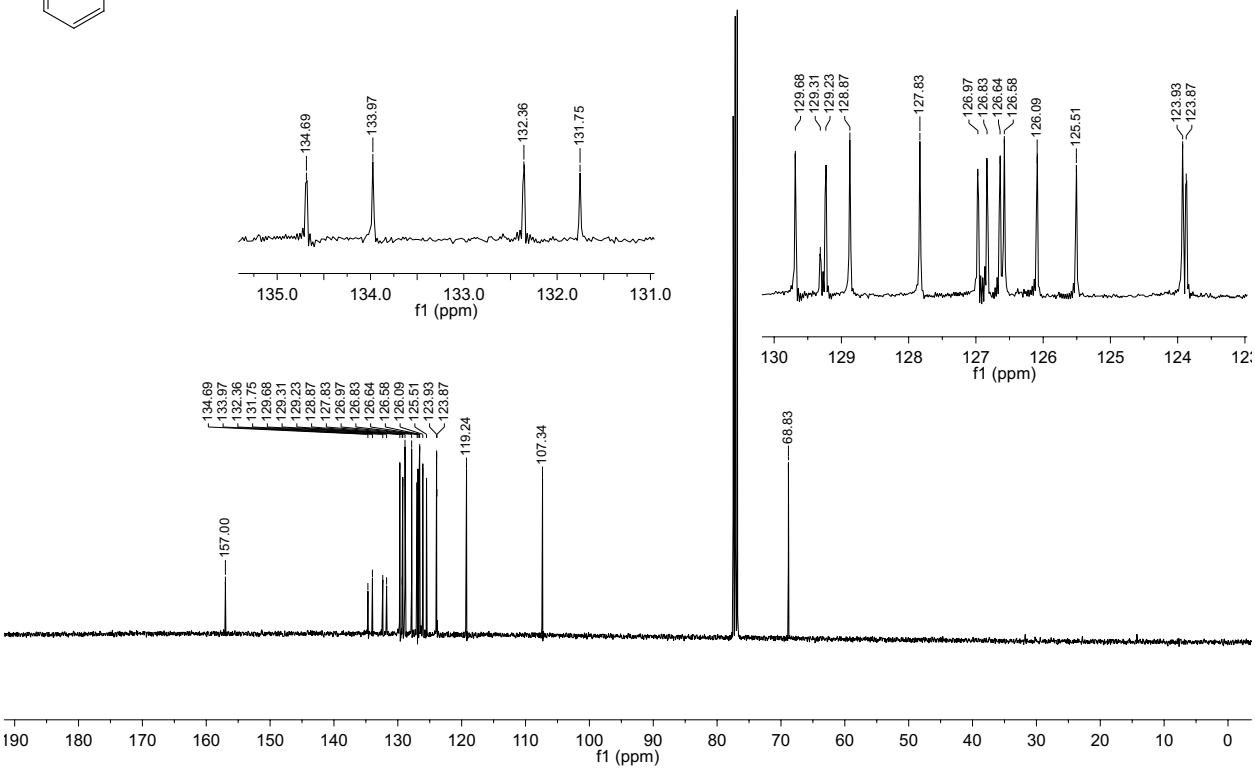

(1*S*,2*S*,5*R*)-2-Isopropyl-5-methylcyclohexan-1-ol 491

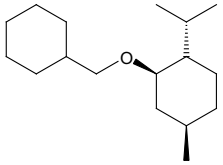

^{1}H NMR (500 MHz, Chloroform-*d*) δ 3.42 (dd, *J* = 8.9, 5.9 Hz, 1H), 3.03 (dd, *J* = 8.9, 7.1 Hz, 1H), 2.96 (ddd, *J* = 10.6, 4.1 Hz, 1H), 2.29 – 2.18 (m, 1H), 2.13 – 2.05 (m, 1H), 1.87 – 1.76 (m, 1H), 1.76 – 1.47 (m, 8H), 1.41 – 1.10 (m, 5H), 1.03 – 0.71 (m, 15H).

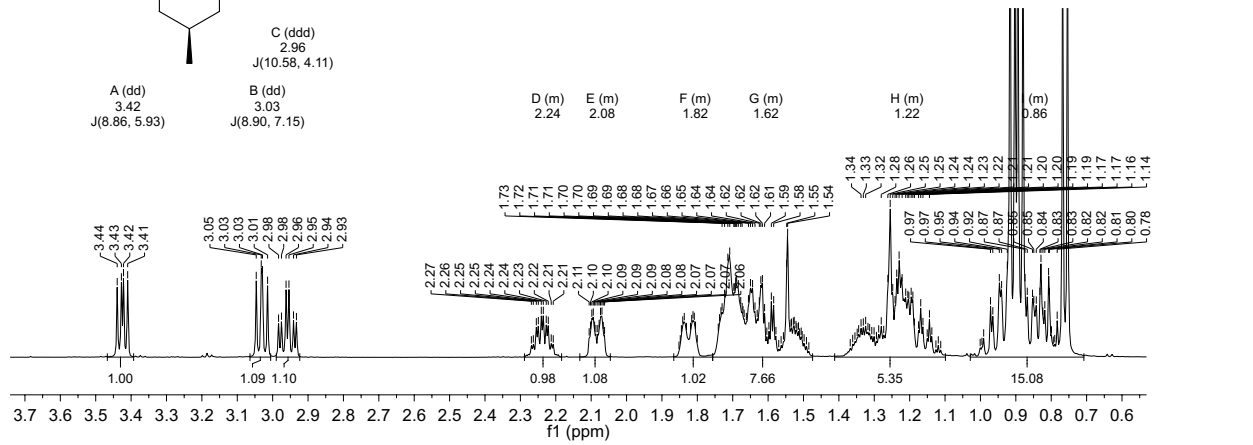

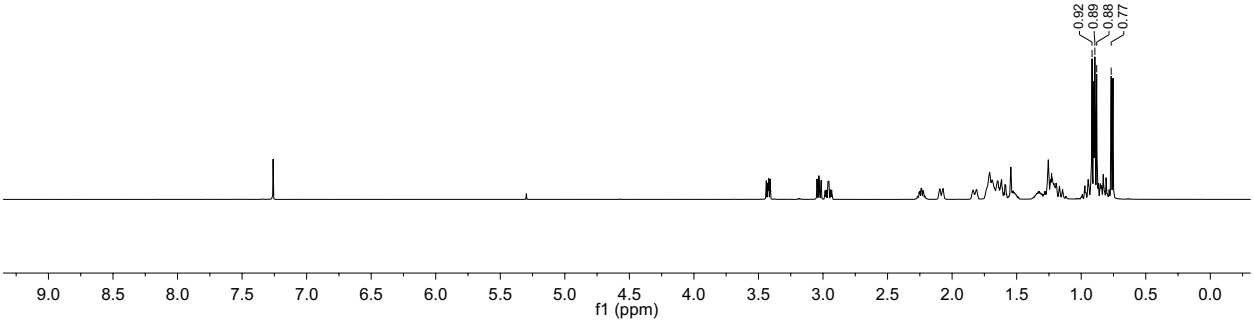

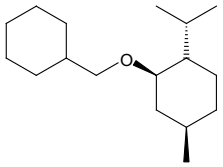

^{13}C NMR (126 MHz, Chloroform-*d*) δ 79.4, 74.9, 48.5, 40.6, 38.7, 34.8, 31.8, 30.6, 30.4, 26.9, 26.1, 26.1, 25.7, 23.5, 22.5, 21.1, 16.3.

3-(Triethylsilyl)phenol 492

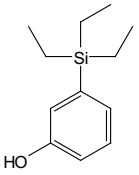

^{1}H NMR (400 MHz, Chloroform-*d*) δ 7.26 – 7.20 (m, 1H), 7.05 (ddd, *J* = 7.3, 1.0 Hz, 1H), 6.94 (dd, *J* = 2.8, 0.9 Hz, 1H), 6.81 (ddd, *J* = 8.0, 2.7, 1.0 Hz, 1H), 4.60 (s, 1H), 1.00 – 0.93 (m, 9H), 0.81 – 0.74 (m, 6H).

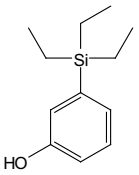

^{13}C NMR (101 MHz, Chloroform-*d*) δ 155.0, 139.8, 129.2, 126.8, 120.8, 115.8, 7.5, 3.5.

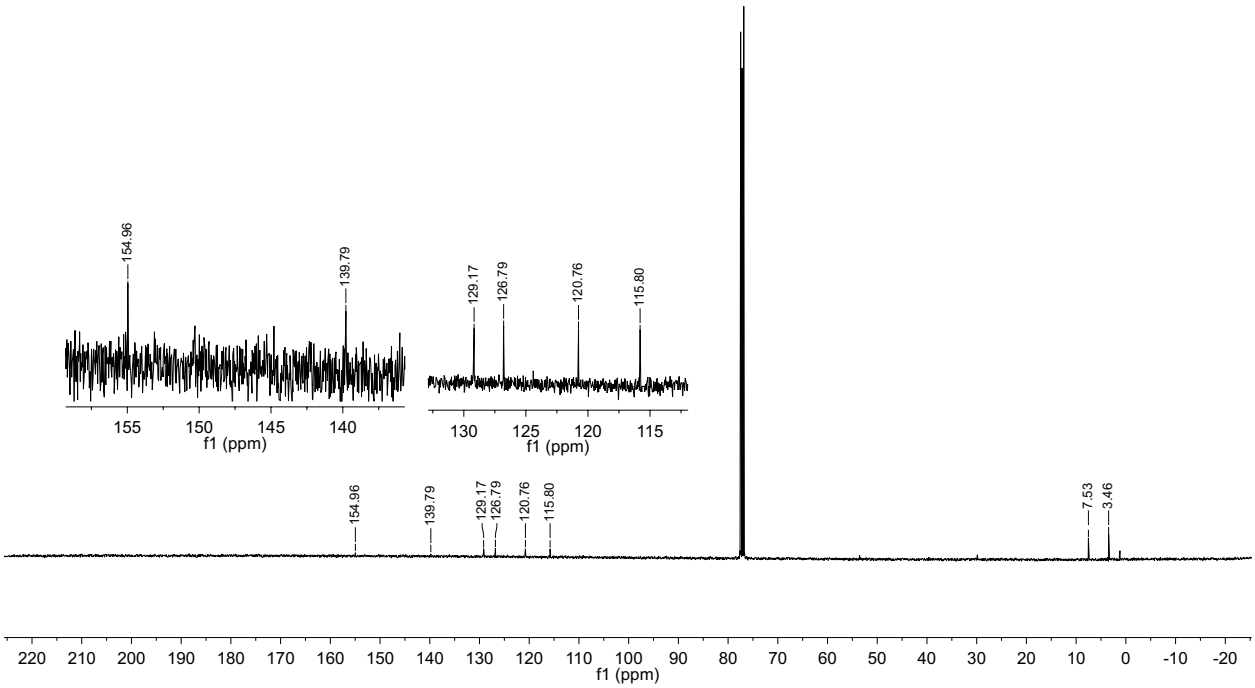

1-(Benzyloxy)-3,5-dimethylbenzene 469

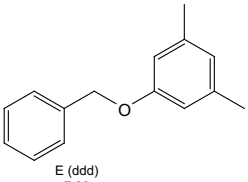

^{1}H NMR (400 MHz, Chloroform-*d*) δ 7.46 – 7.42 (m, 2H), 7.39 (ddd, *J* = 7.9, 6.8, 1.0 Hz, 2H), 7.36 – 7.29 (m, 1H), 6.65 – 6.61 (m, 3H), 5.04 (s, 2H), 2.30 (q, *J* = 0.6 Hz, 6H).

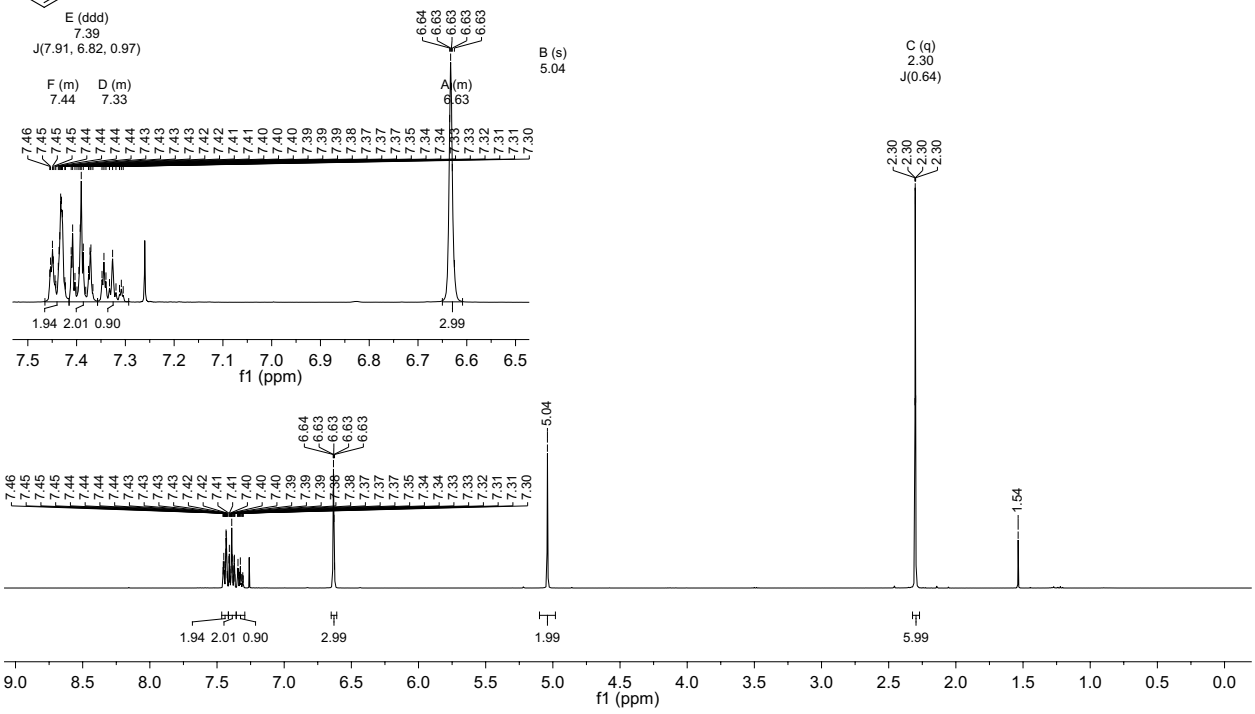

^{13}C NMR (101 MHz, Chloroform-*d*) δ 159.1, 139.4, 137.5, 128.7, 128.0, 127.6, 122.9, 112.7, 70.0, 21.6.

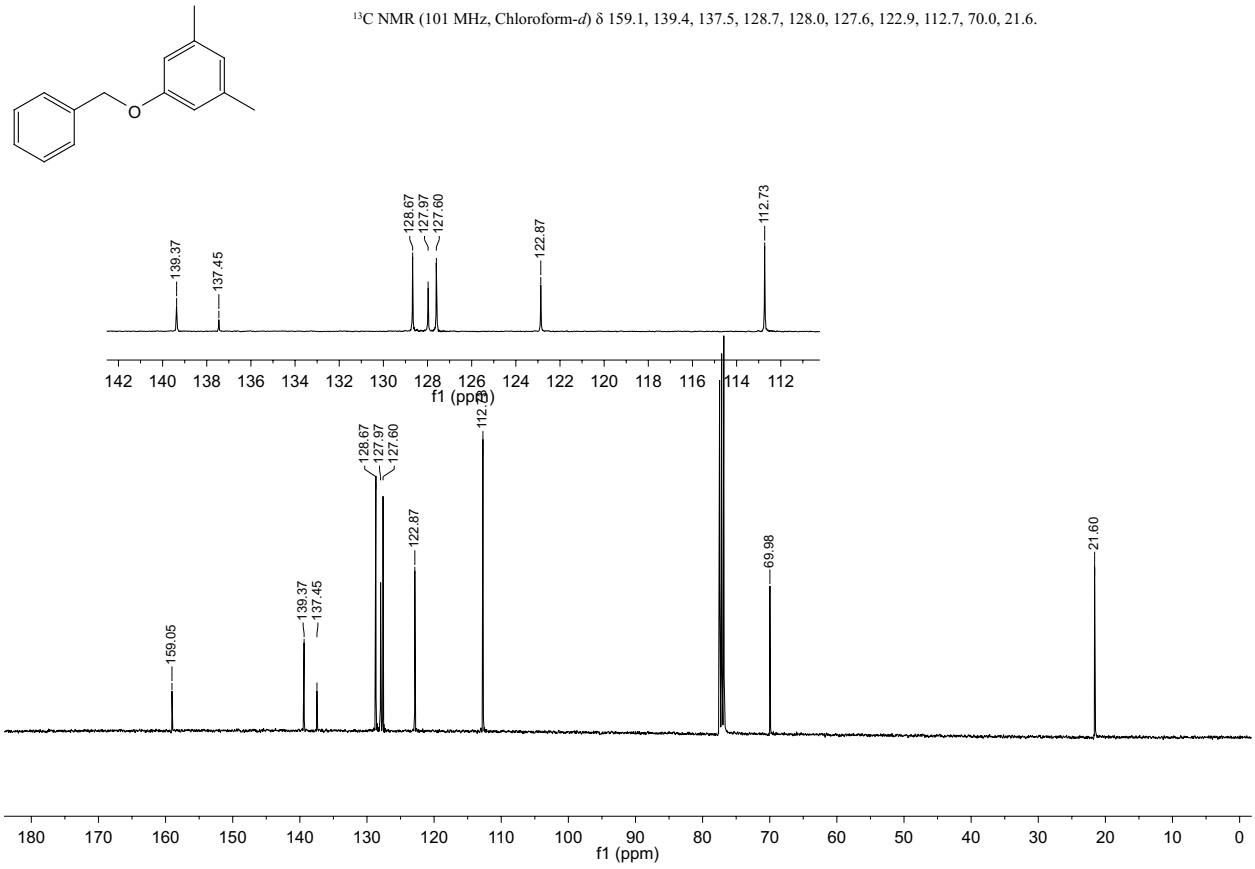

1-((4-Methoxybenzyl)oxy)-3,5-dimethylbenzene 472

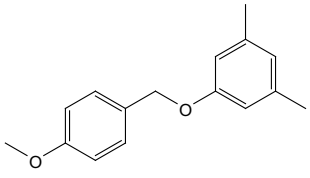

^{1}H NMR (400 MHz, Chloroform-*d*) δ 7.39 – 7.32 (m, 2H), 6.97 – 6.88 (m, 2H), 6.64 – 6.59 (m, 3H), 4.96 (s, 2H), 3.83 (s, 3H), 2.30 (d, *J* = 0.7 Hz, 6H).

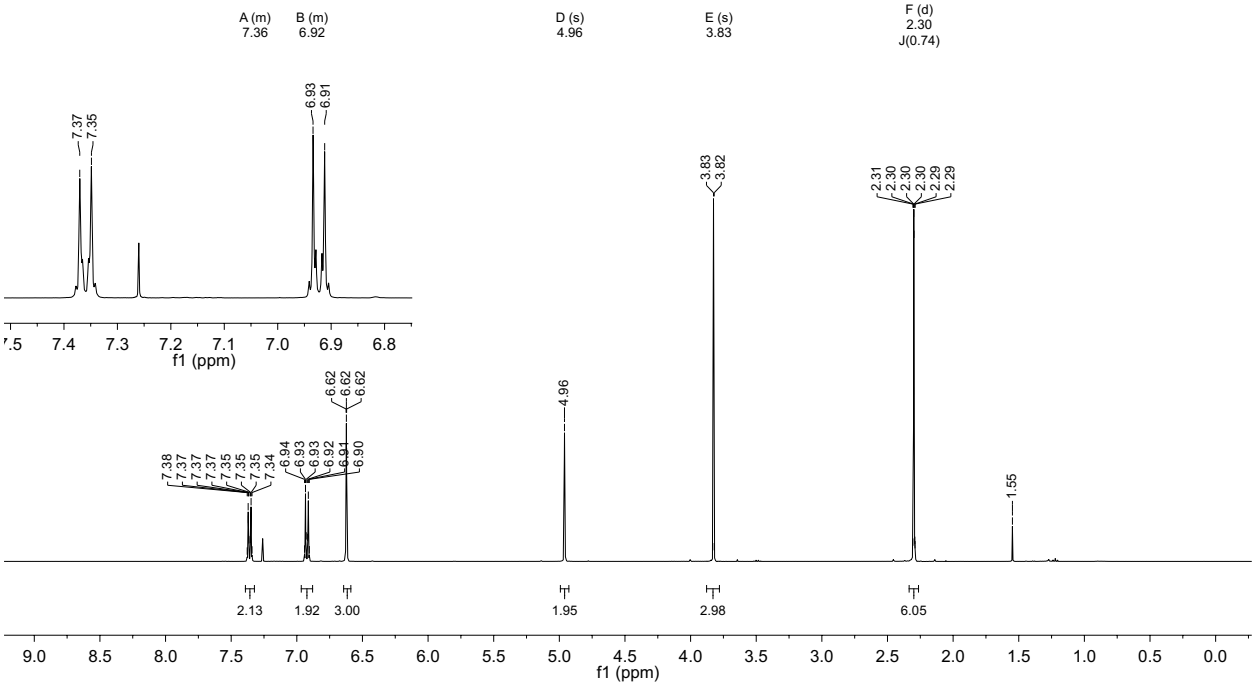

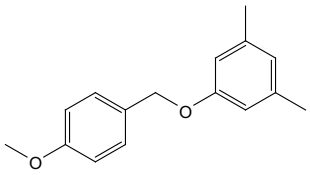

^{13}C NMR (101 MHz, Chloroform-*d*) δ 159.5, 159.1, 139.3, 129.5, 129.3, 122.8, 114.1, 112.7, 69.8, 55.4, 21.6.

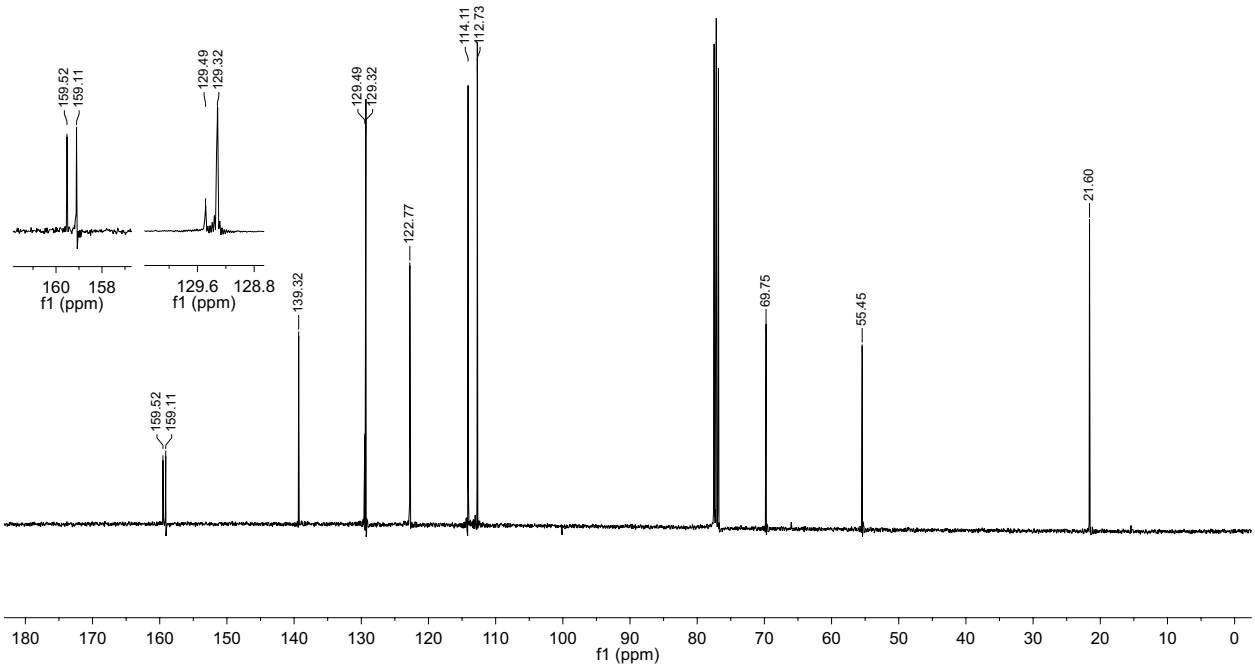

2,2'-Oxydinaphthalene 474

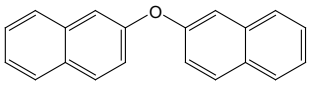

^{1}H NMR (400 MHz, Chloroform-*d*) δ 7.91 – 7.82 (m, 4H), 7.75 – 7.69 (m, 2H), 7.51 – 7.40 (m, 4H), 7.39 (d, *J* = 2.4 Hz, 2H), 7.34 (dd, *J* = 8.9, 2.4 Hz, 2H).

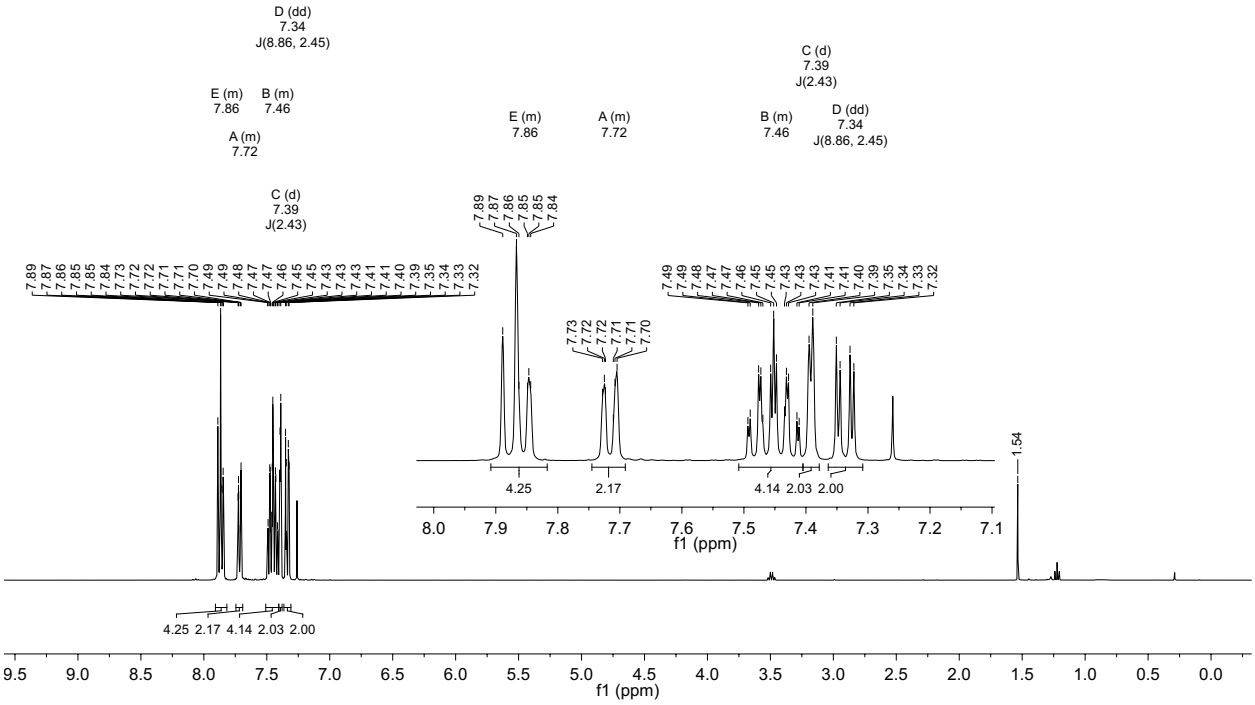

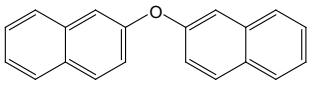

^{13}C NMR (101 MHz, Chloroform-*d*) δ 155.2, 134.5, 130.4, 130.1, 127.9, 127.3, 126.7, 124.9, 120.3, 114.6.

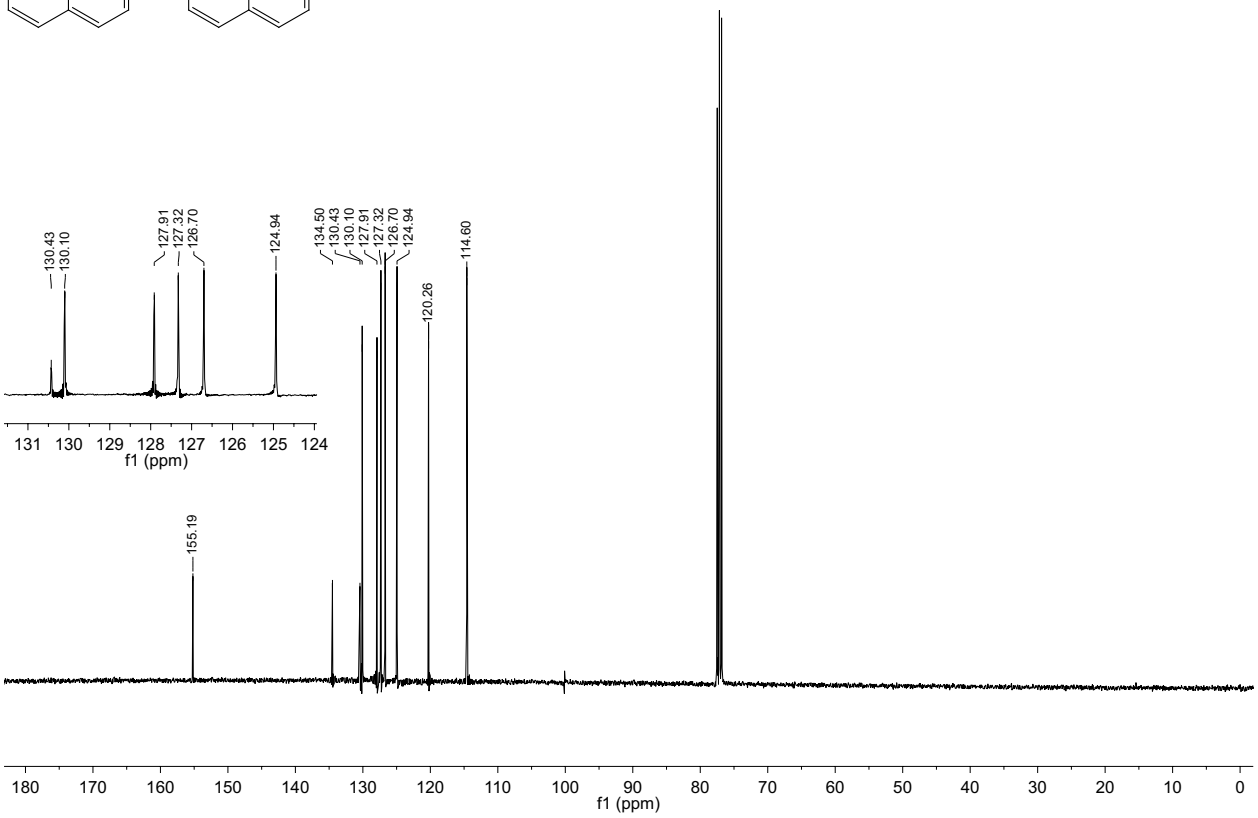

1-((Naphthalen-2-yloxy)methyl)naphthalene 479

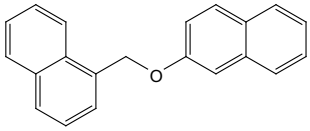

^{1}H NMR (400 MHz, Chloroform-*d*) δ 8.14 – 8.08 (m, 1H), 7.97 – 7.91 (m, 1H), 7.90 – 7.86 (m, 1H), 7.83 – 7.76 (m, 3H), 7.67 (dd, *J* = 6.9, 1.1 Hz, 1H), 7.60 – 7.52 (m, 2H), 7.52 – 7.44 (m, 2H), 7.40 – 7.33 (m, 2H), 7.29 – 7.24 (m, 1H), 5.63 (s, 2H).

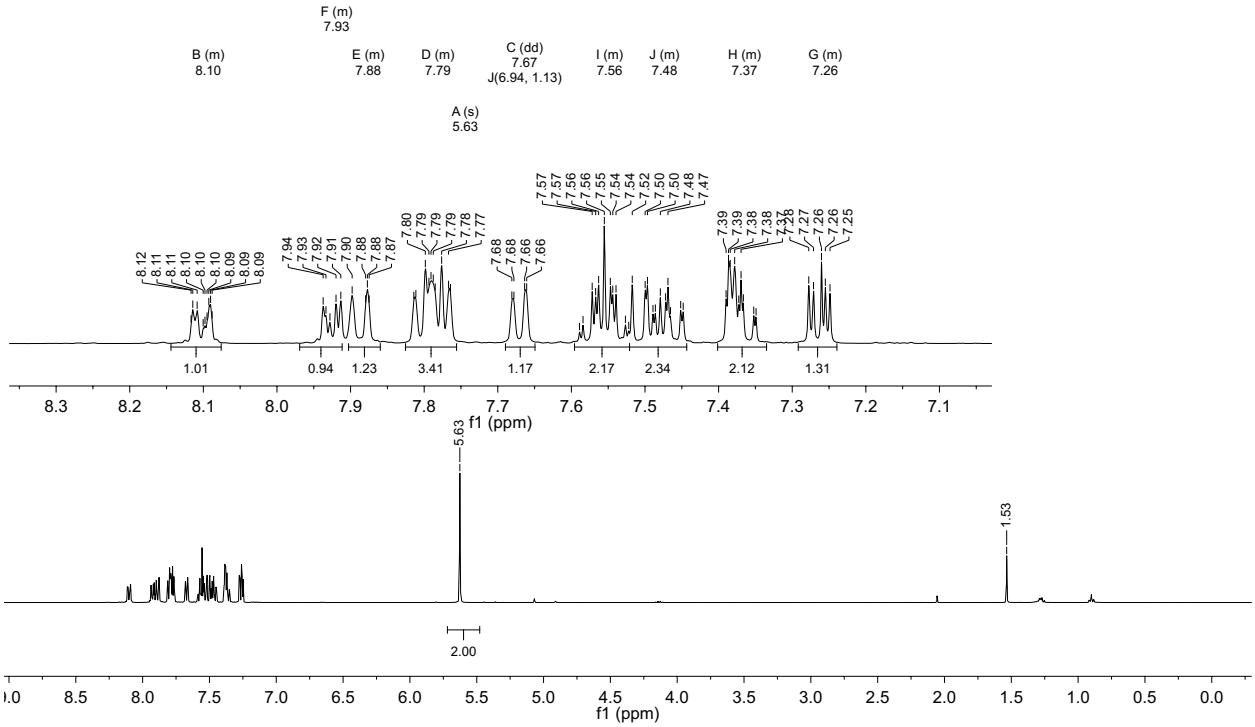

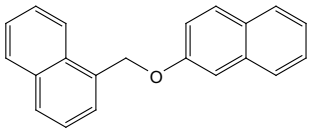

^{13}C NMR (101 MHz, Chloroform-*d*) δ 157.0, 134.7, 134.0, 132.4, 131.8, 129.7, 129.3, 129.2, 128.9, 127.8, 127.0, 126.8, 126.6, 126.6, 126.1, 125.5, 123.9, 123.9, 119.2, 107.3, 68.8.

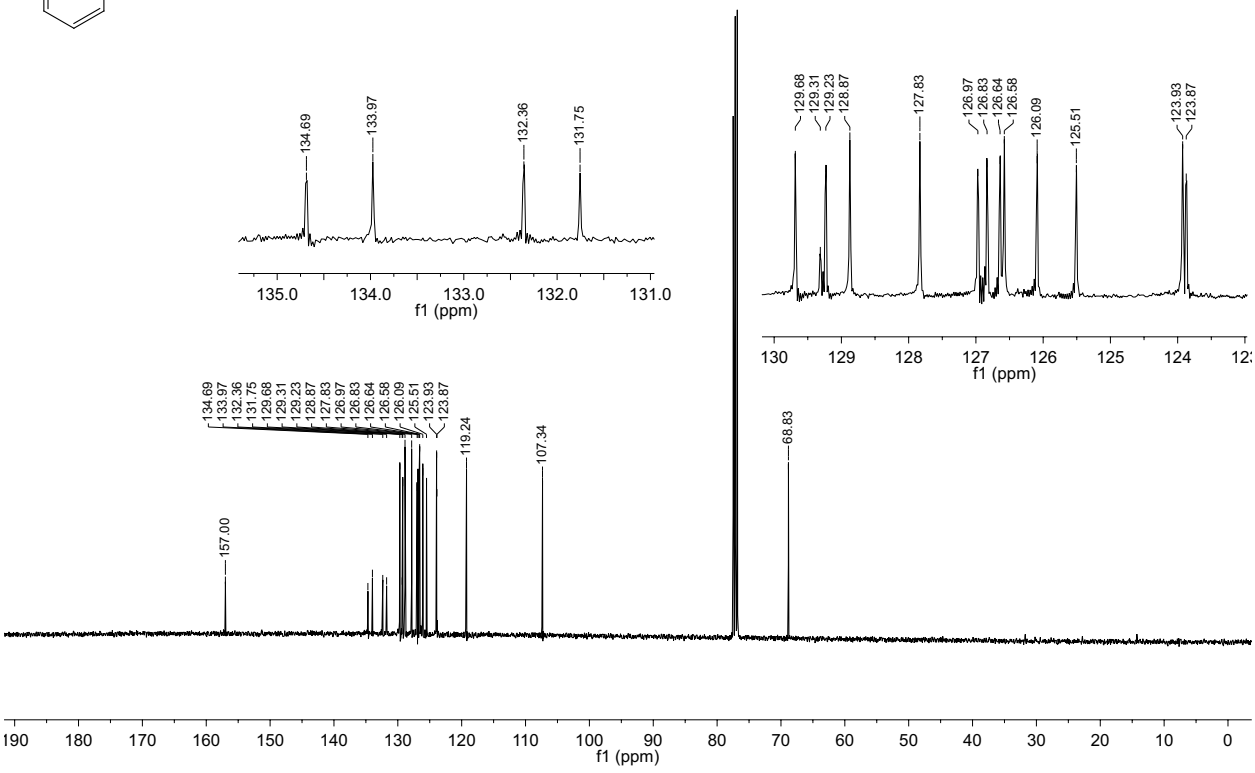

2-(3-Phenylpropoxy)naphthalene 482

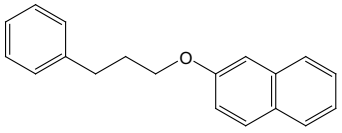

^{1}H NMR (400 MHz, Chloroform-*d*) δ 7.80 – 7.73 (m, 2H), 7.71 (dd, *J* = 8.2, 1.0 Hz, 1H), 7.44 (ddd, *J* = 8.2, 6.9, 1.3 Hz, 1H), 7.36 – 7.28 (m, 3H), 7.27 – 7.20 (m, 3H), 7.18 (dd, *J* = 8.9, 2.5 Hz, 1H), 7.11 (d, *J* = 2.5 Hz, 1H), 4.10 (t, *J* = 6.3 Hz, 2H), 2.88 (dd, *J* = 8.3, 6.8 Hz, 2H), 2.25 – 2.13 (m, 2H).

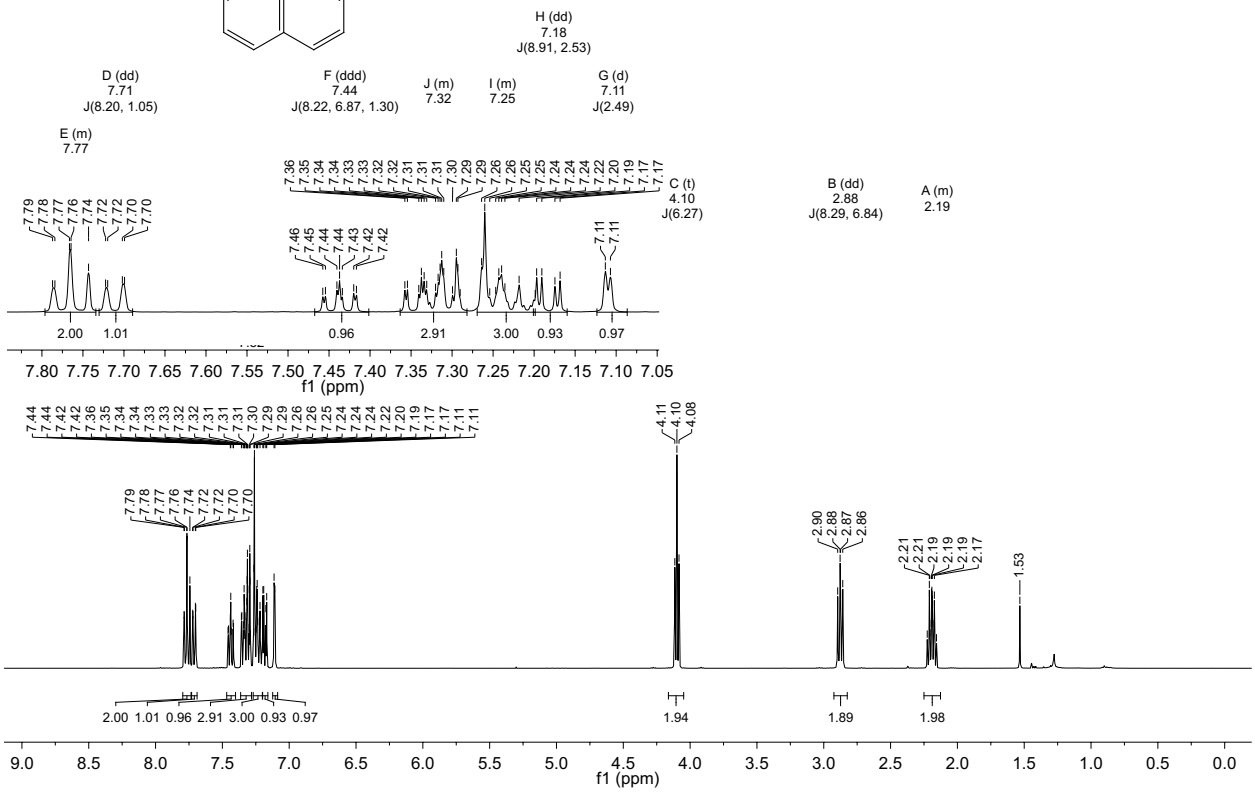

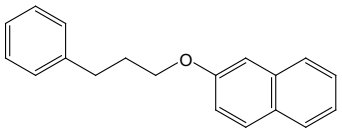

^{13}C NMR (101 MHz, Chloroform-*d*) δ 157.1, 141.7, 134.7, 129.5, 129.1, 128.7, 128.6, 127.8, 126.8, 126.4, 126.1, 123.7, 119.1, 106.8, 67.0, 32.4, 30.9.

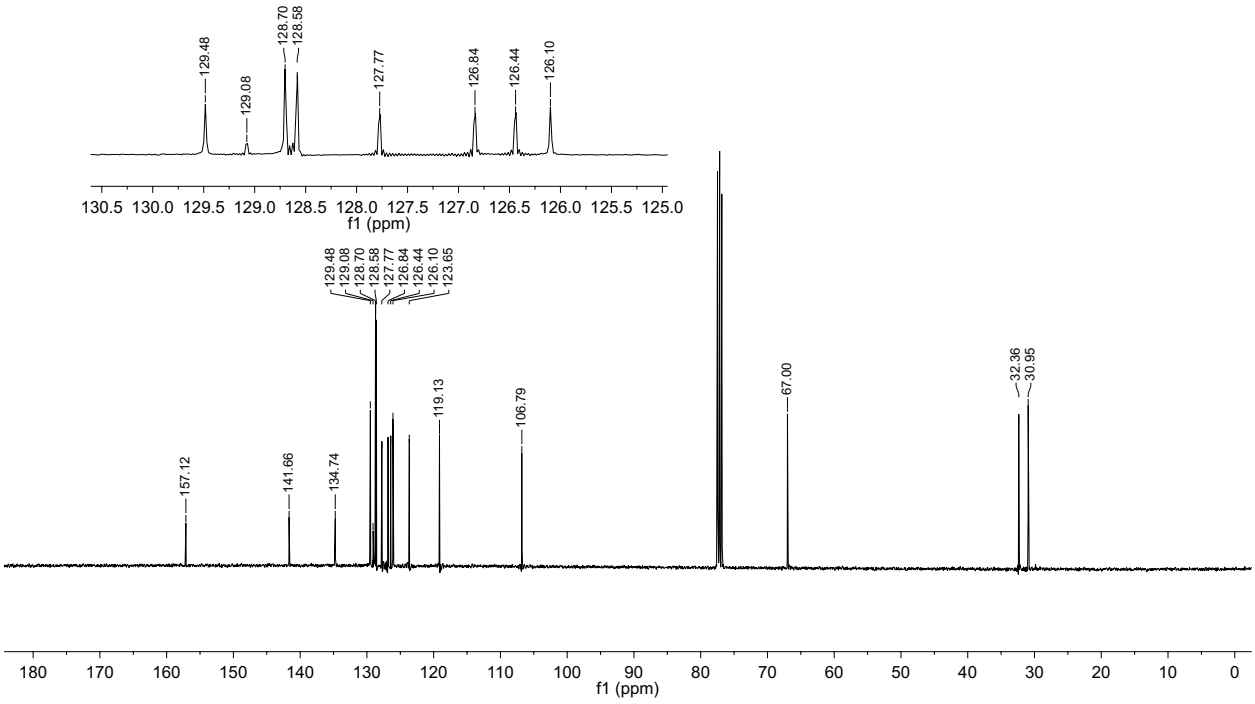

2-(((1*S*,2*R*,5*R*)-2-Isopropyl-5-methylcyclohexyl)oxy)naphthalene 488

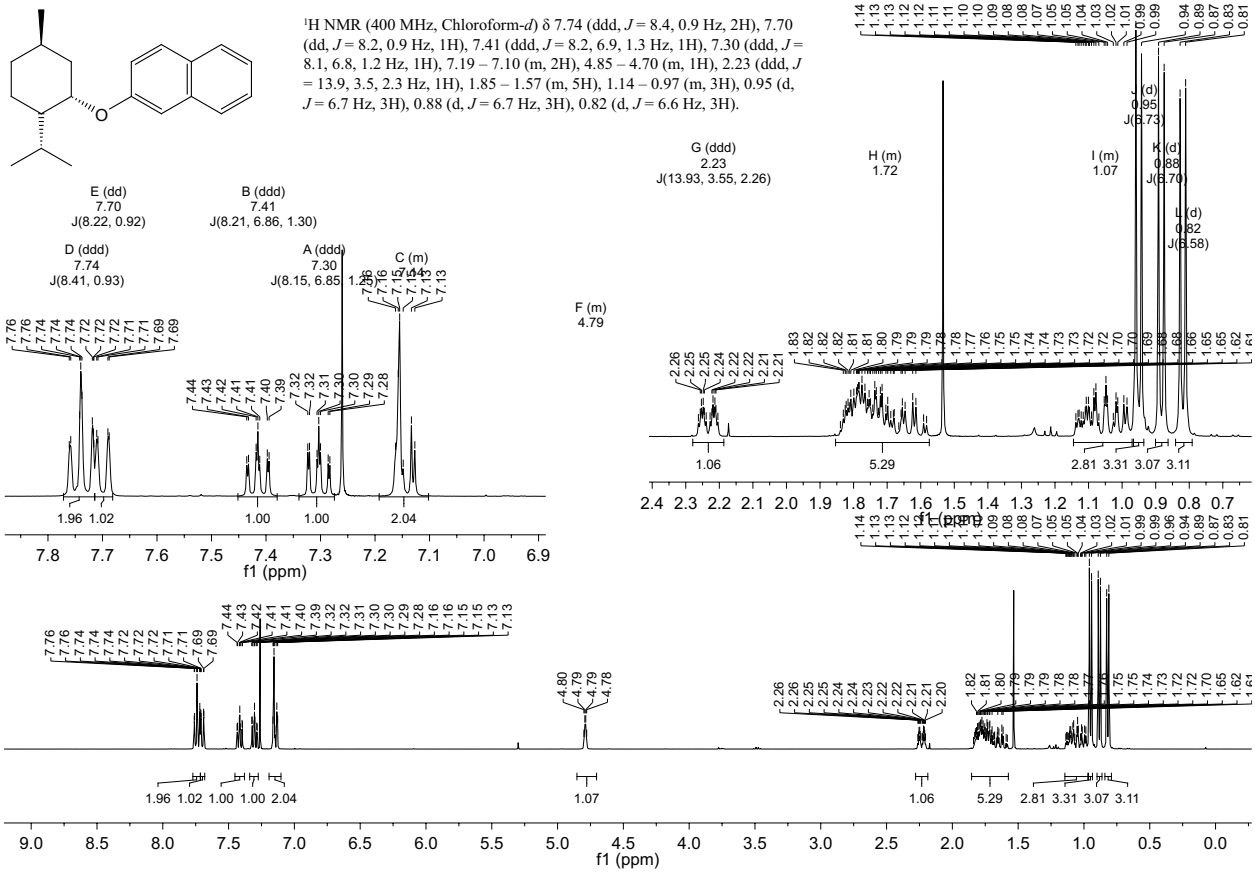

^{1}H NMR (400 MHz, Chloroform-*d*) δ 7.74 (ddd, *J* = 8.4, 0.9 Hz, 2H), 7.70 (dd, *J* = 8.2, 0.9 Hz, 1H), 7.41 (ddd, *J* = 8.2, 6.9, 1.3 Hz, 1H), 7.30 (ddd, *J* = 8.1, 6.8, 1.2 Hz, 1H), 7.19 – 7.10 (m, 2H), 4.85 – 4.70 (m, 1H), 2.23 (ddd, *J* = 13.9, 3.5, 2.3 Hz, 1H), 1.85 – 1.57 (m, 5H), 1.14 – 0.97 (m, 3H), 0.95 (d, *J* = 6.7 Hz, 3H), 0.88 (d, *J* = 6.7 Hz, 3H), 0.82 (d, *J* = 6.6 Hz, 3H).

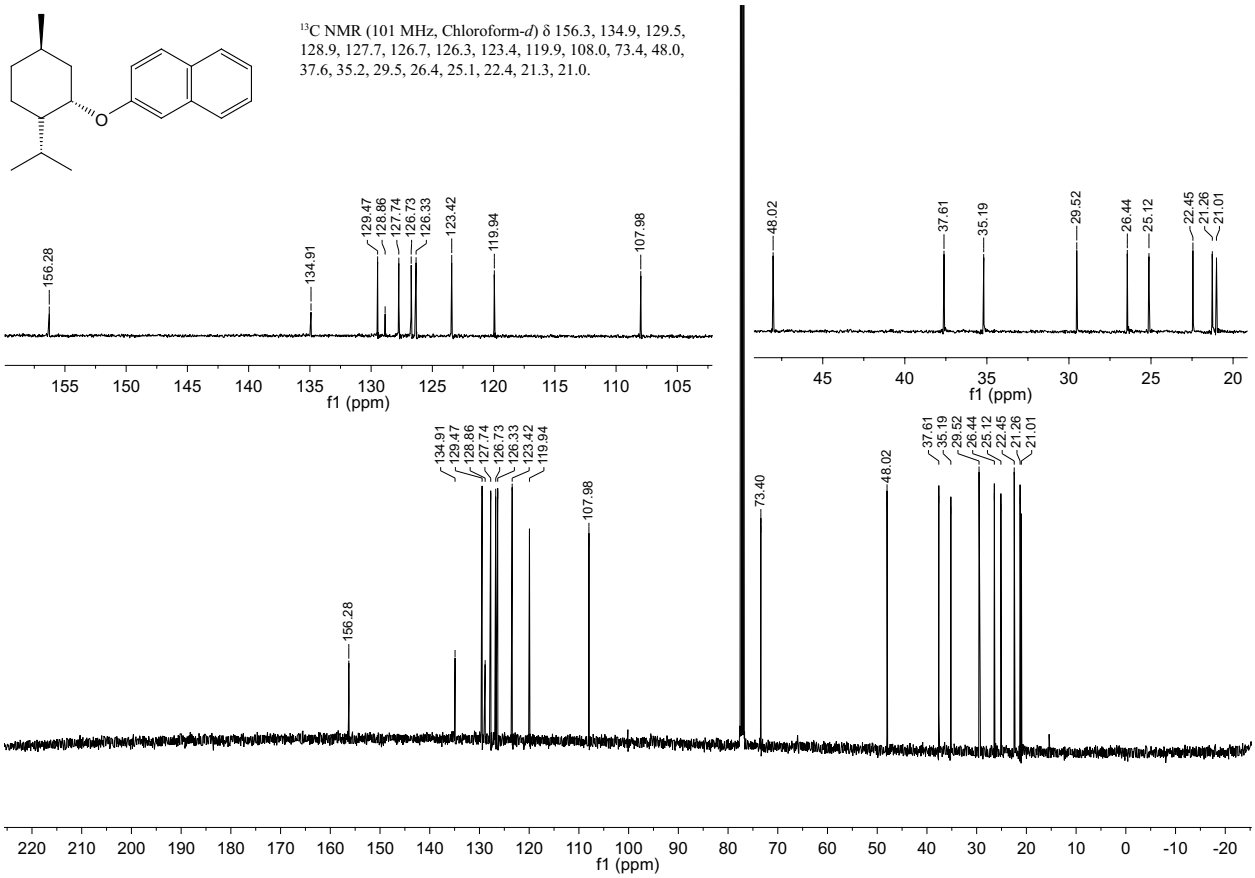

^{13}C NMR (101 MHz, Chloroform-*d*) δ 156.3, 134.9, 129.5, 128.9, 127.7, 126.7, 126.3, 123.4, 119.9, 108.0, 73.4, 48.0, 37.6, 35.2, 29.5, 26.4, 25.1, 22.4, 21.3, 21.0.

(((1*R*,2*R*,5*R*)-2-Isopropyl-5-methylcyclohexyl)oxy)benzene 489

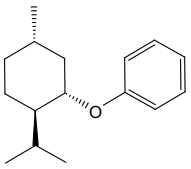

^{1}H NMR (400 MHz, Chloroform-*d*) δ 7.31 – 7.22 (m, 2H), 6.95 – 6.86 (m, 3H), 4.03 (ddd, *J* = 10.6, 4.2 Hz, 1H), 2.23 (qd, *J* = 7.0, 2.8 Hz, 1H), 2.16 (dtd, *J* = 12.5, 3.9, 1.9 Hz, 1H), 1.77 – 1.68 (m, 2H), 1.57 – 1.38 (m, 2H), 1.17 – 0.87 (m, 9H), 0.78 (d, *J* = 7.0 Hz, 3H).

^{13}C NMR (101 MHz, Chloroform-*d*) δ 158.5, 129.6, 120.5, 116.0, 77.6, 48.2, 40.5, 34.7, 31.6, 26.2, 23.9, 22.3, 20.9, 16.7.

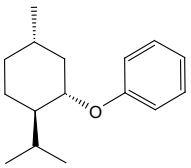

(1*R*,2*R*,4*R*)-2-(Cyclohexylmethoxy)-1-isopropyl-4-methylcyclohexane 493

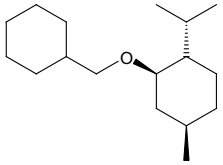

^{1}H NMR (500 MHz, Chloroform-*d*) δ 3.42 (dd, *J* = 8.9, 5.9 Hz, 1H), 3.03 (dd, *J* = 8.9, 7.1 Hz, 1H), 2.96 (ddd, *J* = 10.6, 4.1 Hz, 1H), 2.29 – 2.18 (m, 1H), 2.13 – 2.05 (m, 1H), 1.87 – 1.76 (m, 1H), 1.76 – 1.47 (m, 8H), 1.41 – 1.10 (m, 5H), 1.03 – 0.71 (m, 15H).

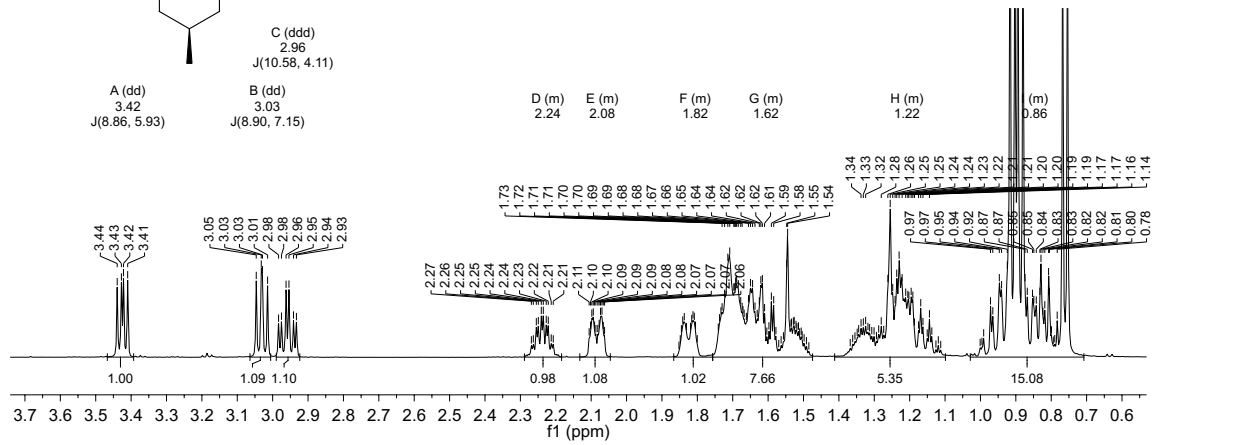

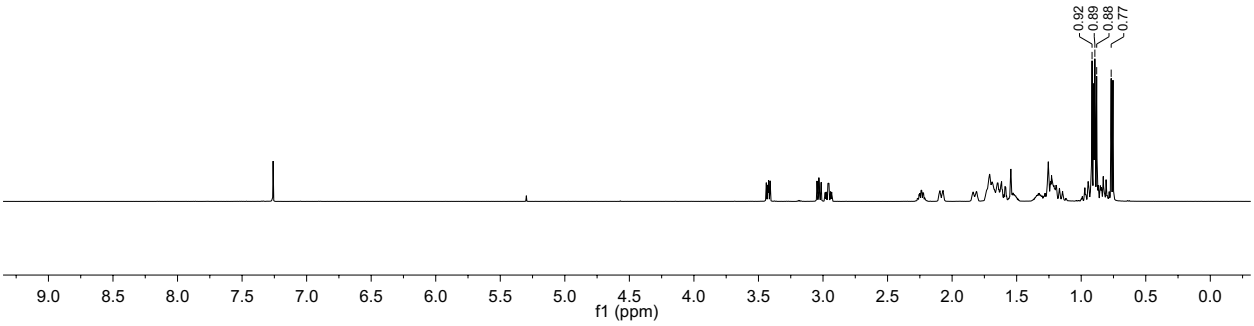

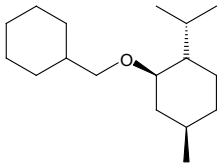

^{13}C NMR (126 MHz, Chloroform-*d*) δ 79.4, 74.9, 48.5, 40.6, 38.7, 34.8, 31.8, 30.6, 30.4, 26.9, 26.1, 26.1, 25.7, 23.5, 22.5, 21.1, 16.3.

9,10-Dihydroanthracene 502

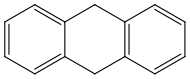

^{1}H NMR (400 MHz, Chloroform-*d*) δ 7.31 (dd, *J* = 5.5, 3.4 Hz, 4H), 7.21 (dd, *J* = 5.6, 3.3 Hz, 4H), 3.96 (s, 4H).

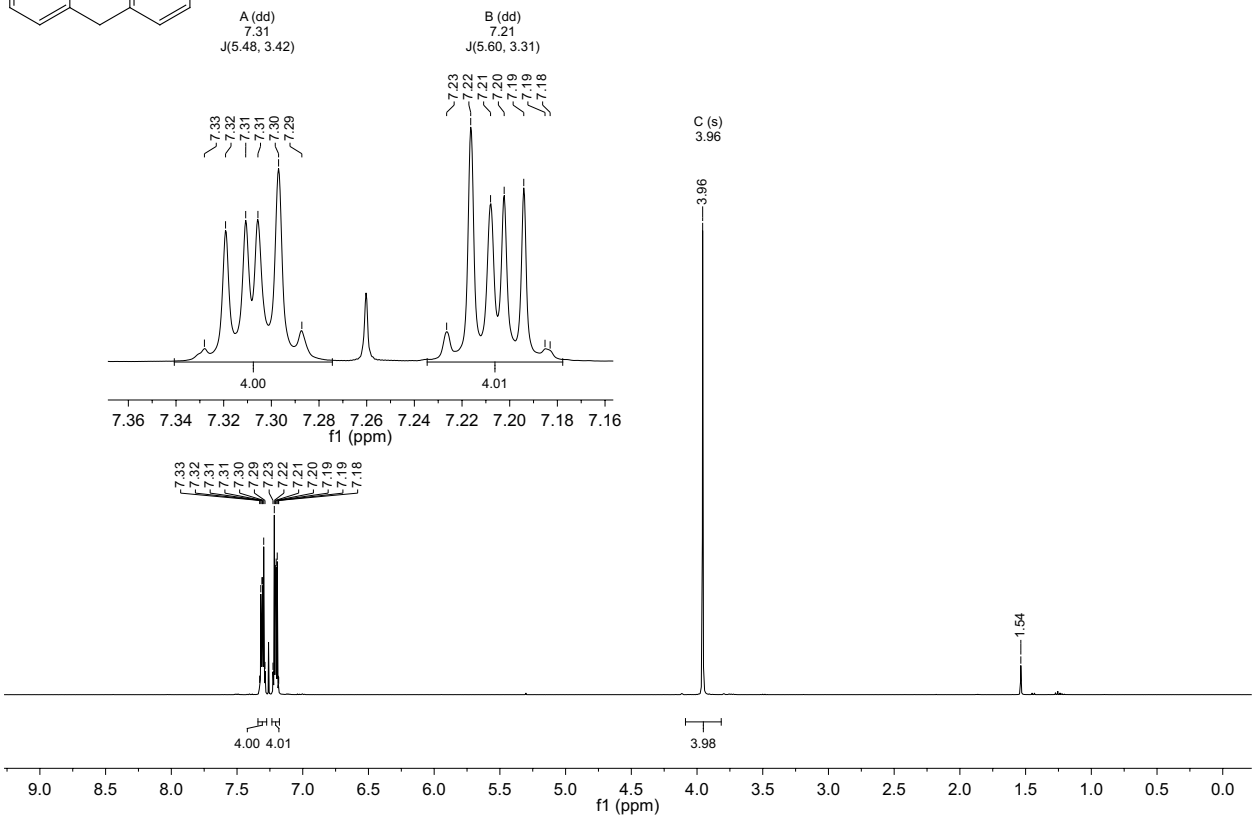

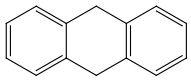

^{13}C NMR (101 MHz, Chloroform-*d*) δ 136.8, 127.5, 126.2, 36.3.

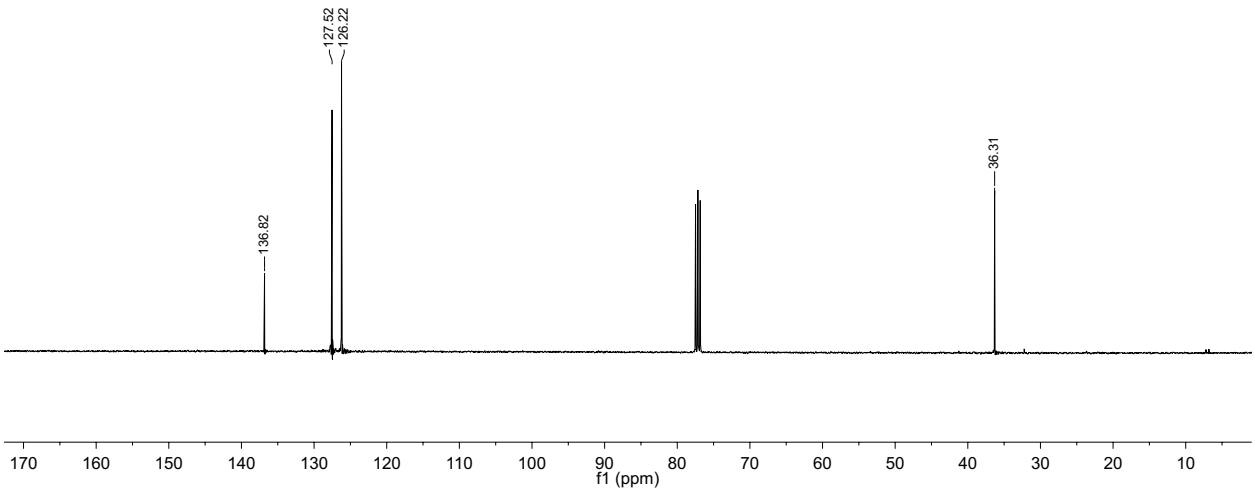

Phenyltriethylsilane 503

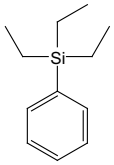

^{1}H NMR (400 MHz, Chloroform-*d*) δ 7.54 – 7.45 (m, 2H), 7.38 – 7.33 (m, 3H), 1.01 – 0.95 (m, 9H), 0.86 – 0.77 (m, 6H).

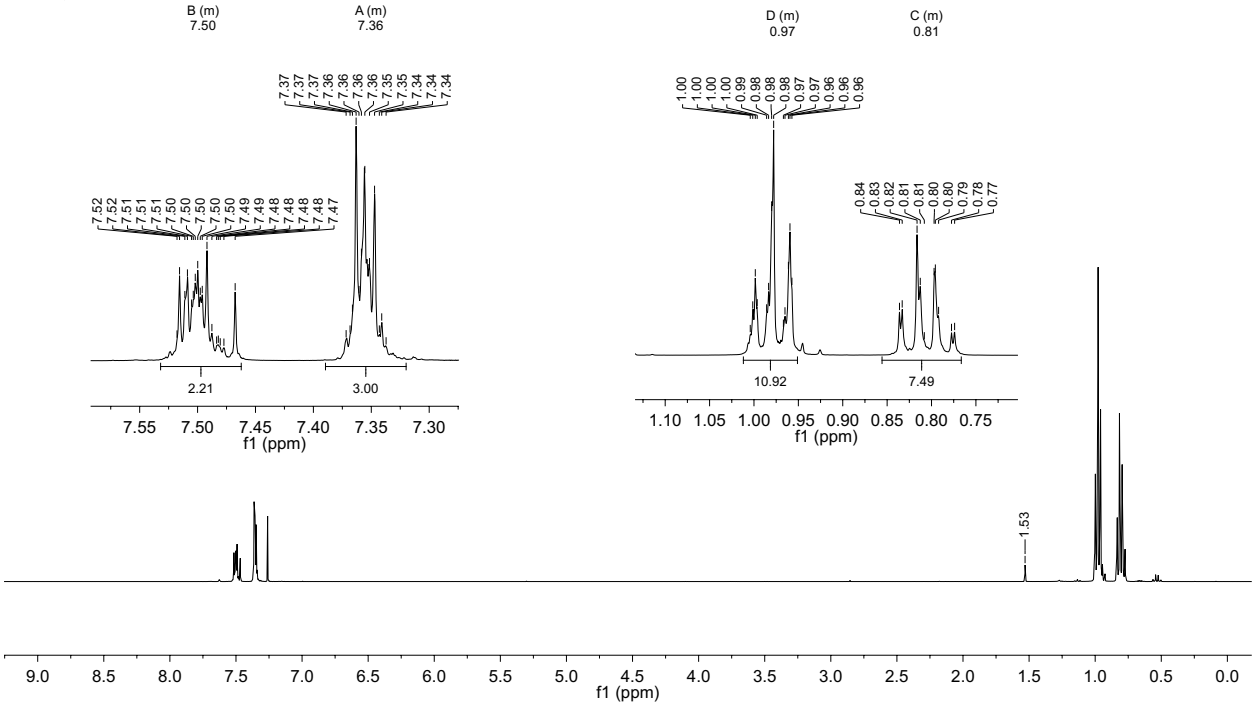

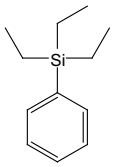

^{13}C NMR (101 MHz, Chloroform-*d*) δ 137.6, 134.3, 128.8, 127.8, 7.5, 3.5.

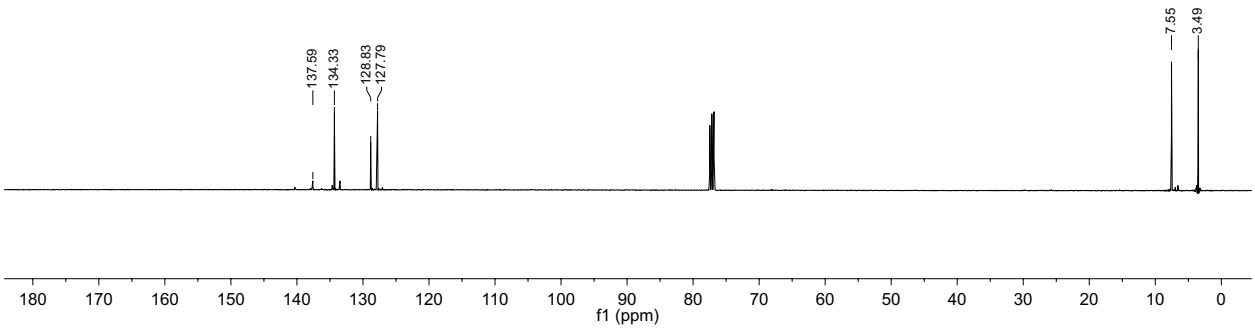

tert-Butoxytriethylsilane 296

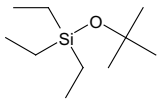

^{1}H NMR (400 MHz, Chloroform-*d*) δ 1.24 (s, 9H), 0.95 (t, *J* = 7.9 Hz, 9H), 0.57 (q, *J* = 8.0 Hz, 6H).

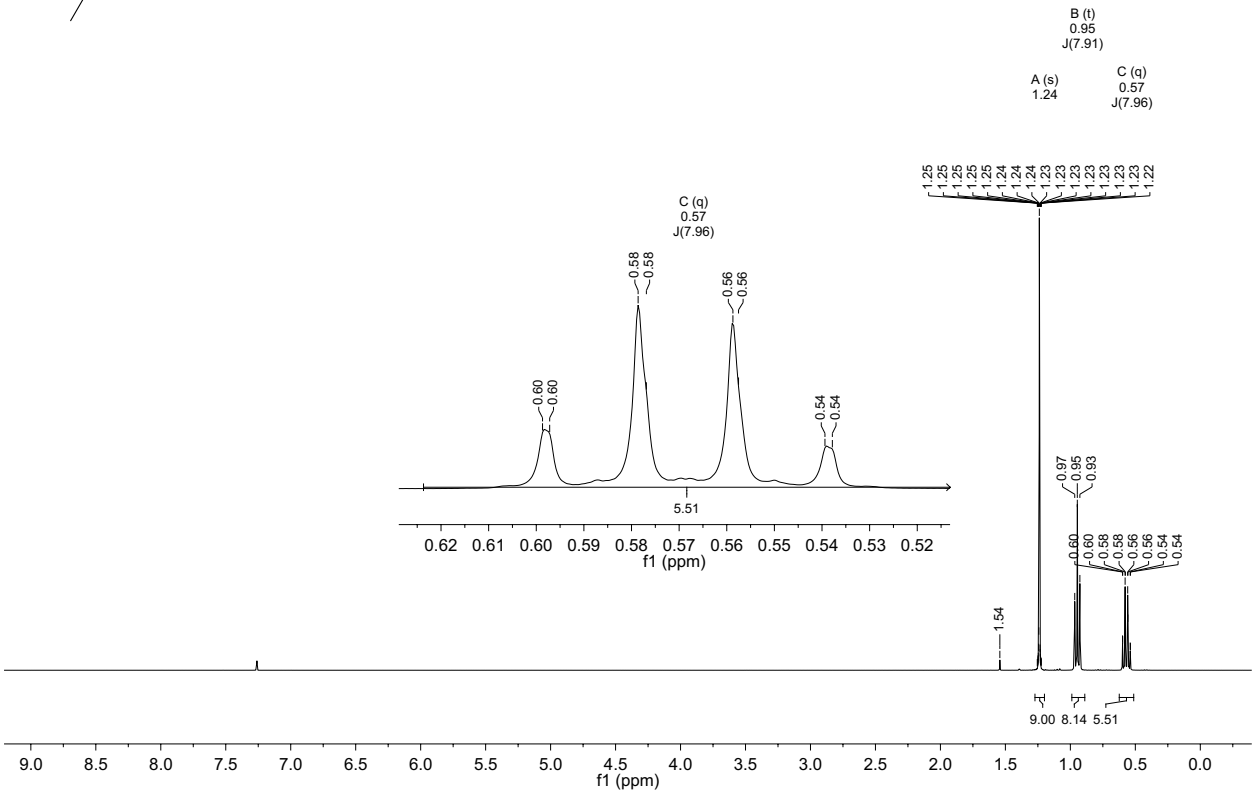

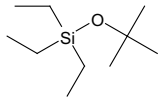

^{13}C NMR (101 MHz, Chloroform-*d*) δ 71.6, 32.2, 7.2, 6.8.

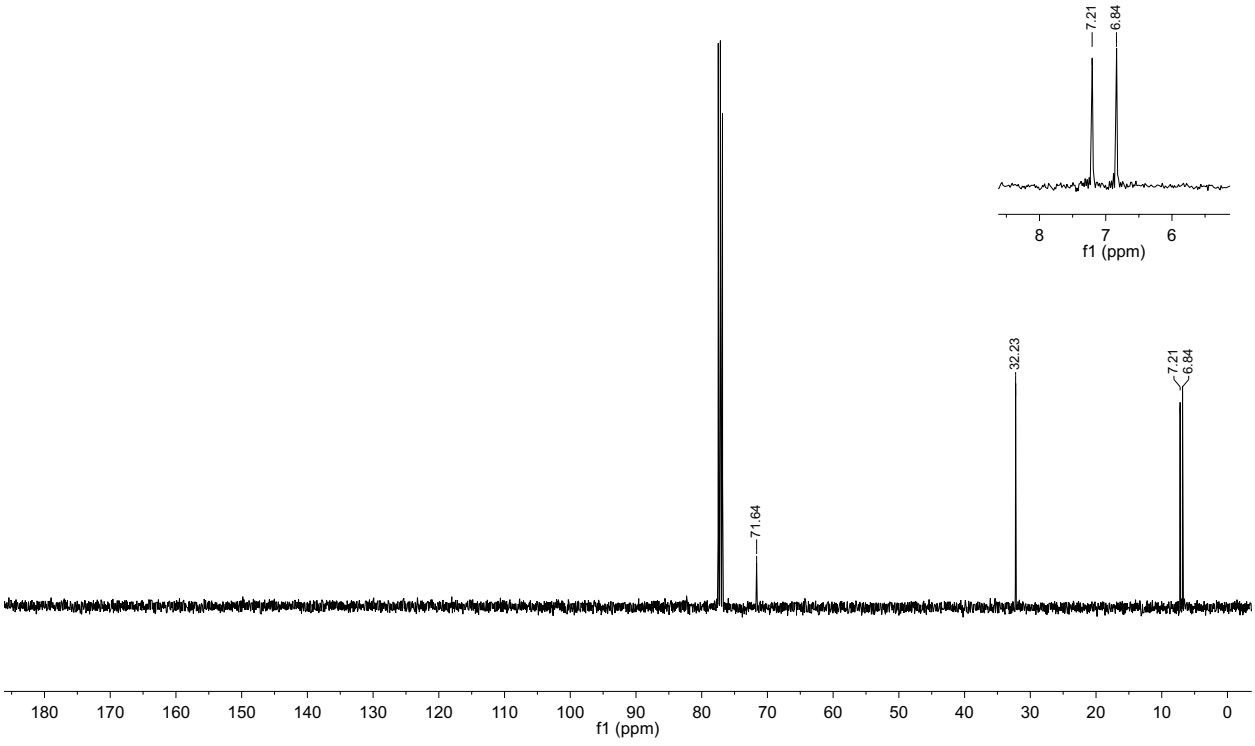

9,10-Dihydroanthracene-*(9,10)*-d_2 502-*(9,10)*-d_2

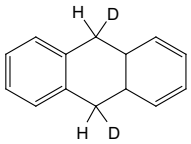

^{1}H NMR (400 MHz, Chloroform-*d*) δ 7.30 (dd, *J* = 5.4, 3.4 Hz, 4H), 7.23 – 7.17 (m, 4H), 3.95 (s, 0.16H), 3.93 (t, *J* = 2.3 Hz, 1.51H).

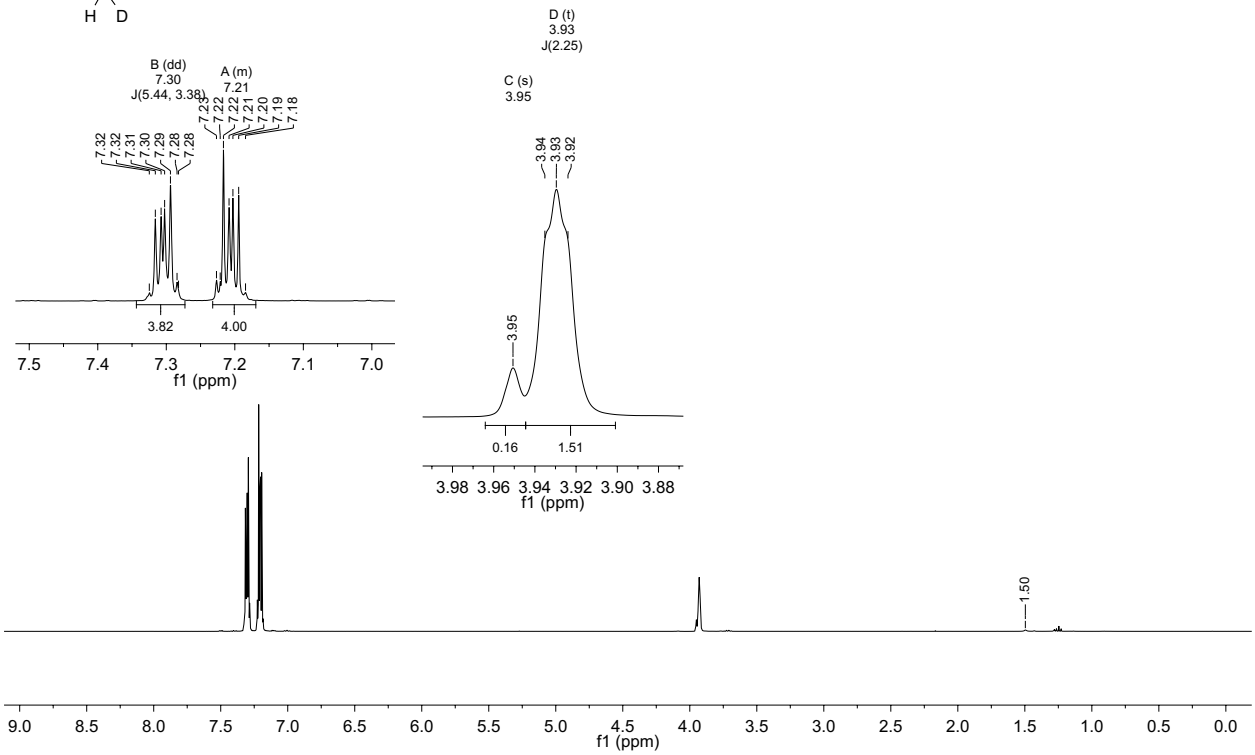

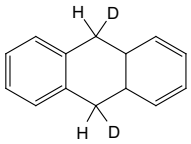

^{13}C NMR (101 MHz, $CDCl_3$) δ 136.78, 127.51, 126.21, 36.29 (non-deuterated compound), 35.9 (t, J = 19.4 Hz).

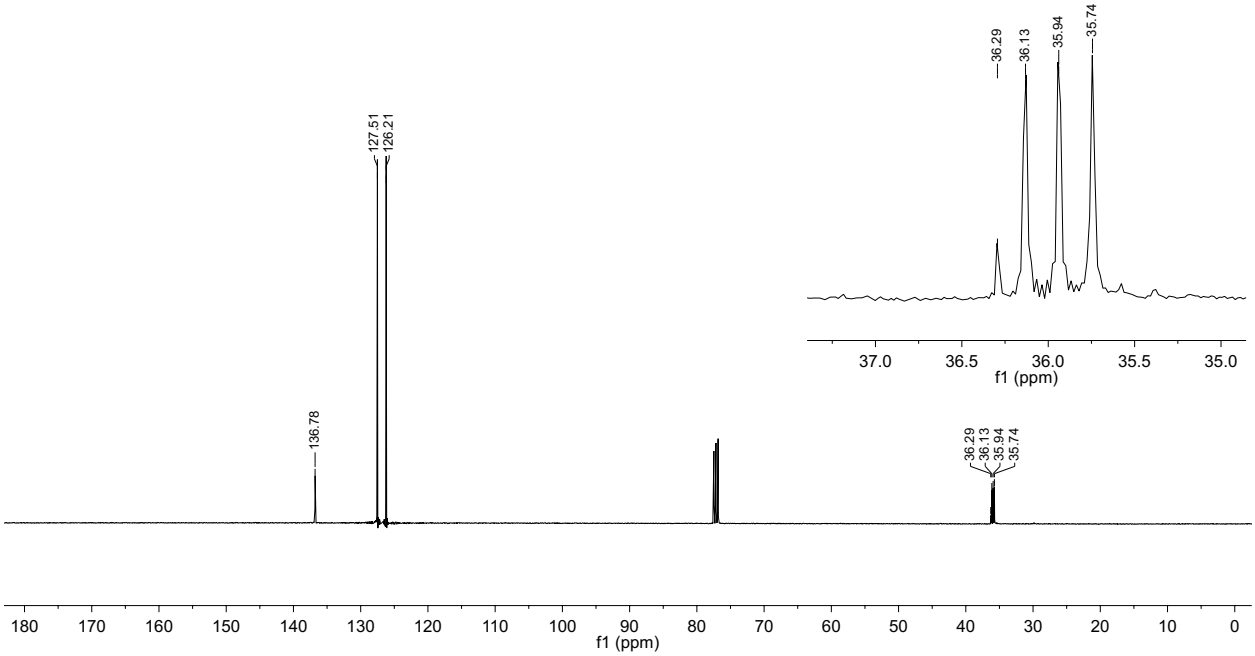

9,10-Dihydroanthracene-*(9,10)*-d_2 502-*(9,10)*-d_2

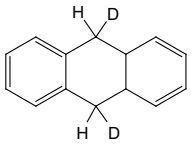

^{2}H NMR (61 MHz,) δ 3.96, 3.92.

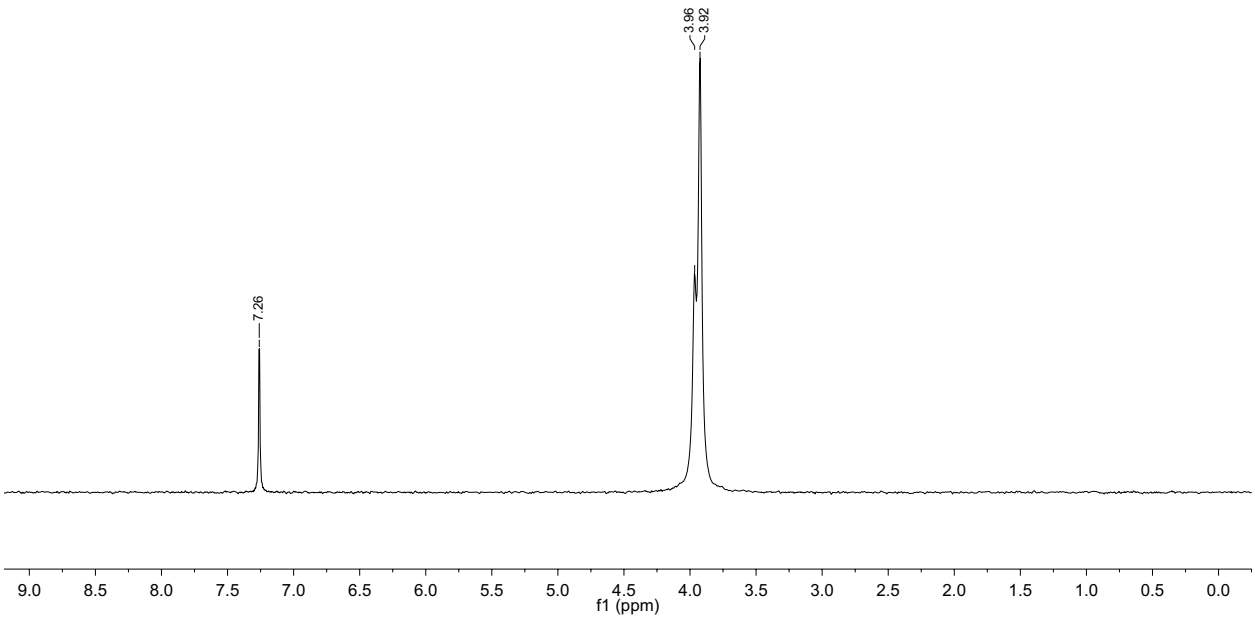

9,10-Dihydrophenanthrene 509

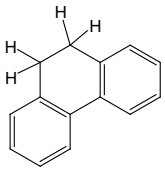

^{1}H NMR (400 MHz, Chloroform-*d*) δ 7.77 (ddd, *J* = 7.6, 0.9 Hz, 2H), 7.32 (ddd, *J* = 7.7, 5.4, 3.5 Hz, 2H), 7.28 – 7.21 (m, 4H), 2.89 (s, 4H).

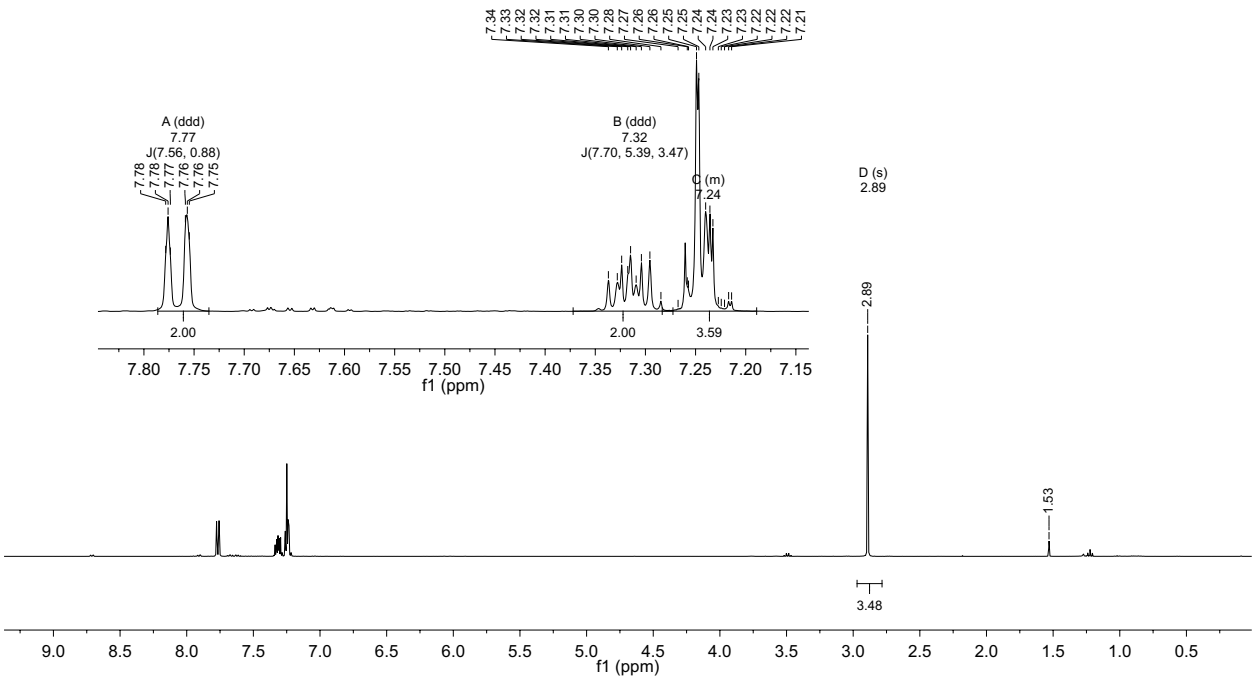

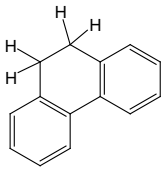

^{13}C NMR (101 MHz, Chloroform-*d*) δ 137.5, 134.6, 128.3, 127.5, 127.1, 123.8, 29.2.

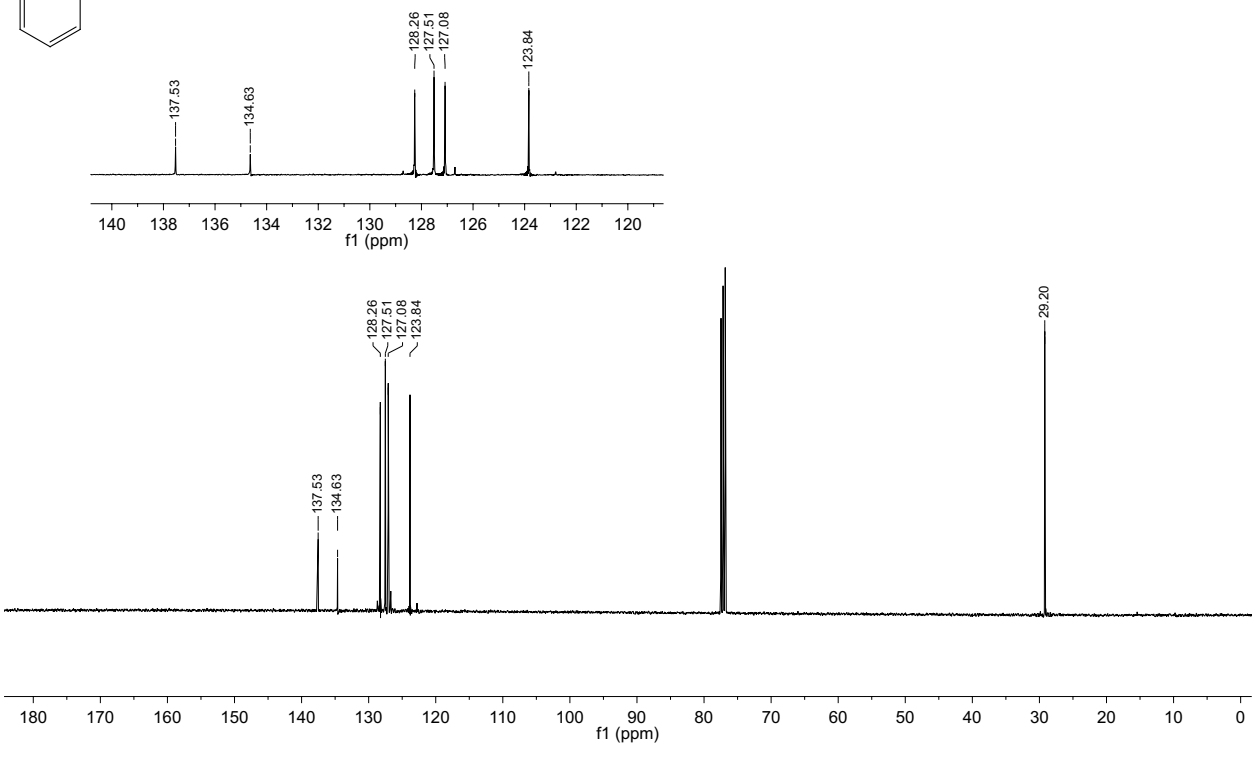

1,2-Diphenylethane 513

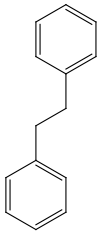

^{1}H NMR (400 MHz, Chloroform-*d*) δ 7.32 – 7.26 (m, 4H), 7.23 – 7.17 (m, 6H), 2.93 (s, 4H).

/Users/Simon1/Documents/Documents/1_PhD/Strathclyde/Research/1_Analysis/_NMR/2/2212-D280080/2/fid

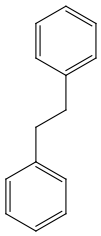

^{13}C NMR (101 MHz, Chloroform-*d*) δ 141.9, 128.6, 128.5, 126.1, 38.1.

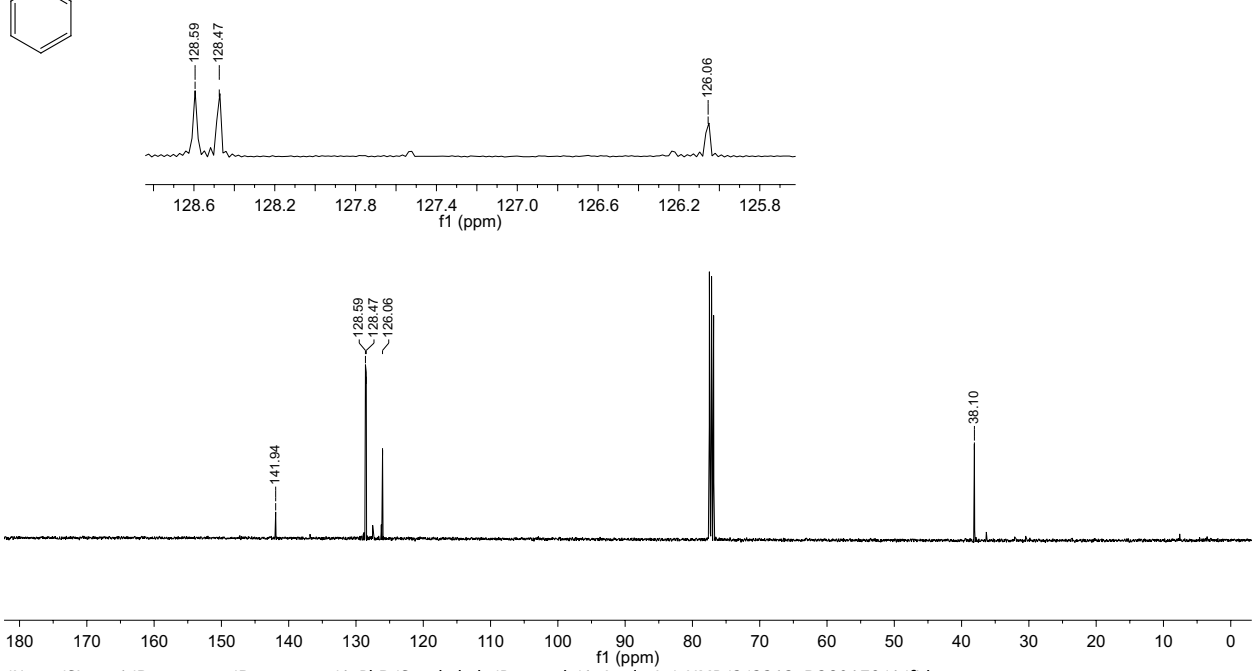

/Users/Simon1/Documents/Documents/1_PhD/Strathclyde/Research/1_Analysis/_NMR/2/2212-D280179/1/fid

9,10-Dihydroacridine 516

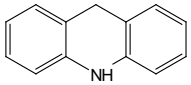

^{1}H NMR (400 MHz, Chloroform-*d*) δ 7.14 – 7.06 (m, 4H), 6.86 (ddd, *J* = 7.4, 7.4, 1.2 Hz, 2H), 6.67 (dd, *J* = 7.8, 1.1 Hz, 2H), 5.94 (s, 1H), 4.06 (s, 2H).

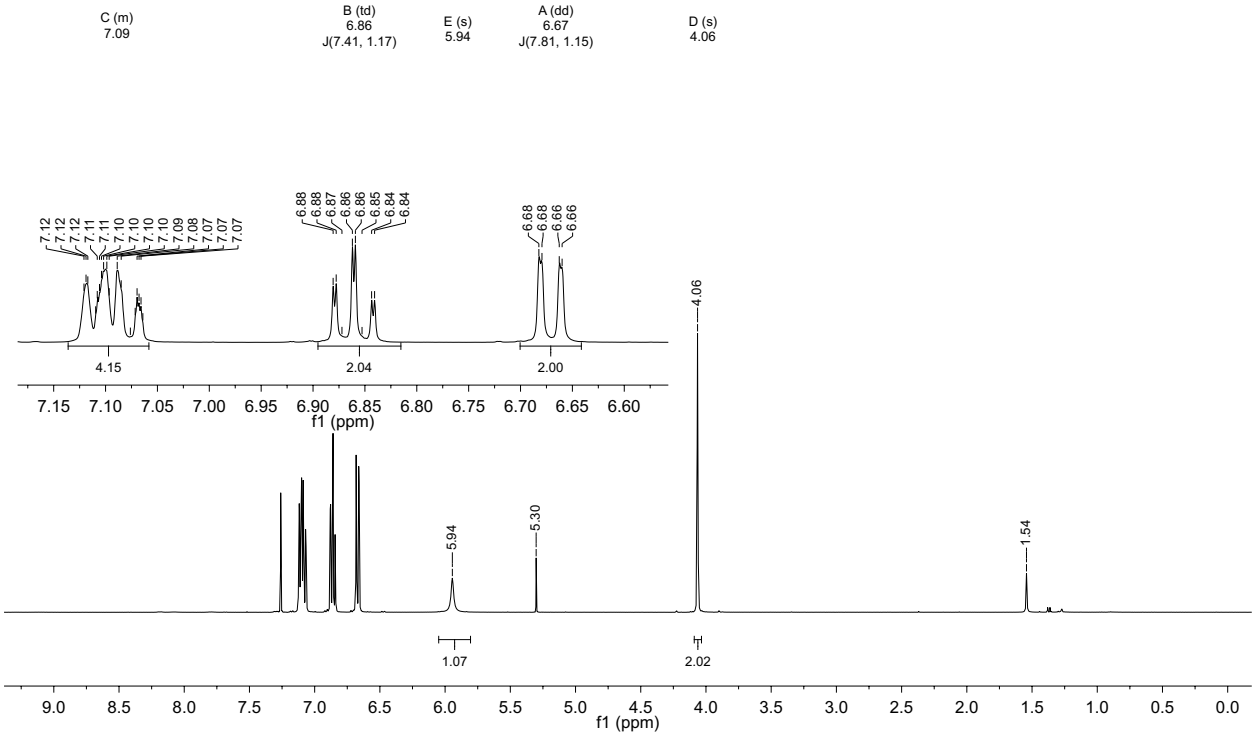

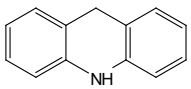

^{13}C NMR (151 MHz, Chloroform-*d*) δ 140.3, 128.7, 127.1, 120.8, 120.2, 113.6, 31.5.

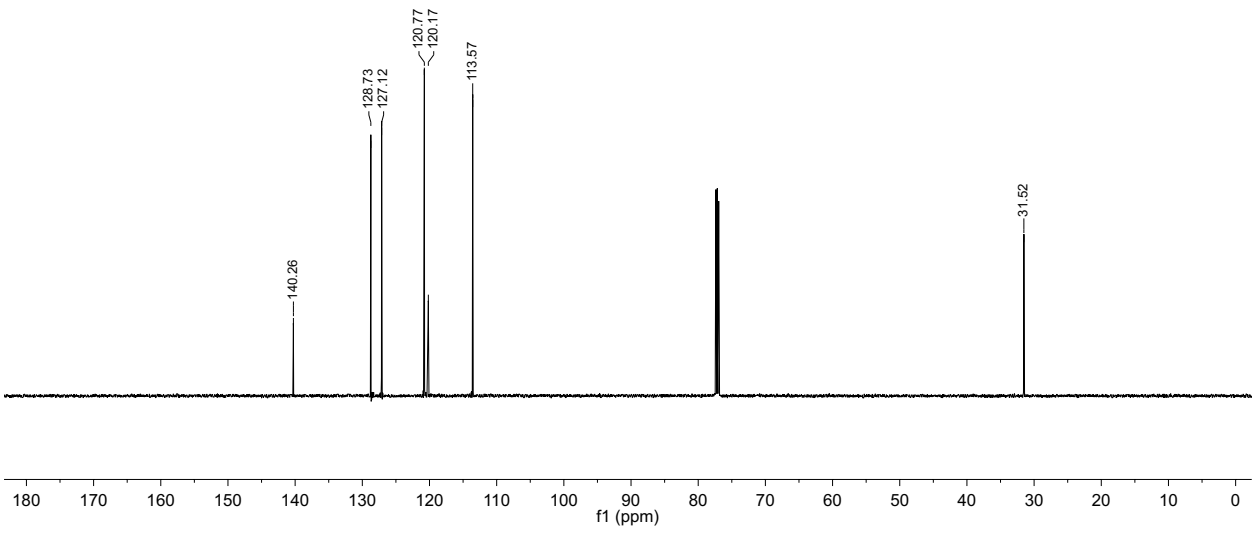

1,2,3,4-Tetrahydroquinoline 518

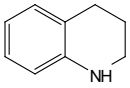

^{1}H NMR (400 MHz, Chloroform-*d*) δ 7.02 – 6.93 (m, 2H), 6.64 (ddd, *J* = 7.4, 7.4, 1.2 Hz, 1H), 6.53 (dd, *J* = 7.8, 1.1 Hz, 1H), 3.87 (s, 1H), 3.36 – 3.27 (m, 2H), 2.78 (t, *J* = 6.4 Hz, 2H), 2.00 – 1.92 (m, 2H).

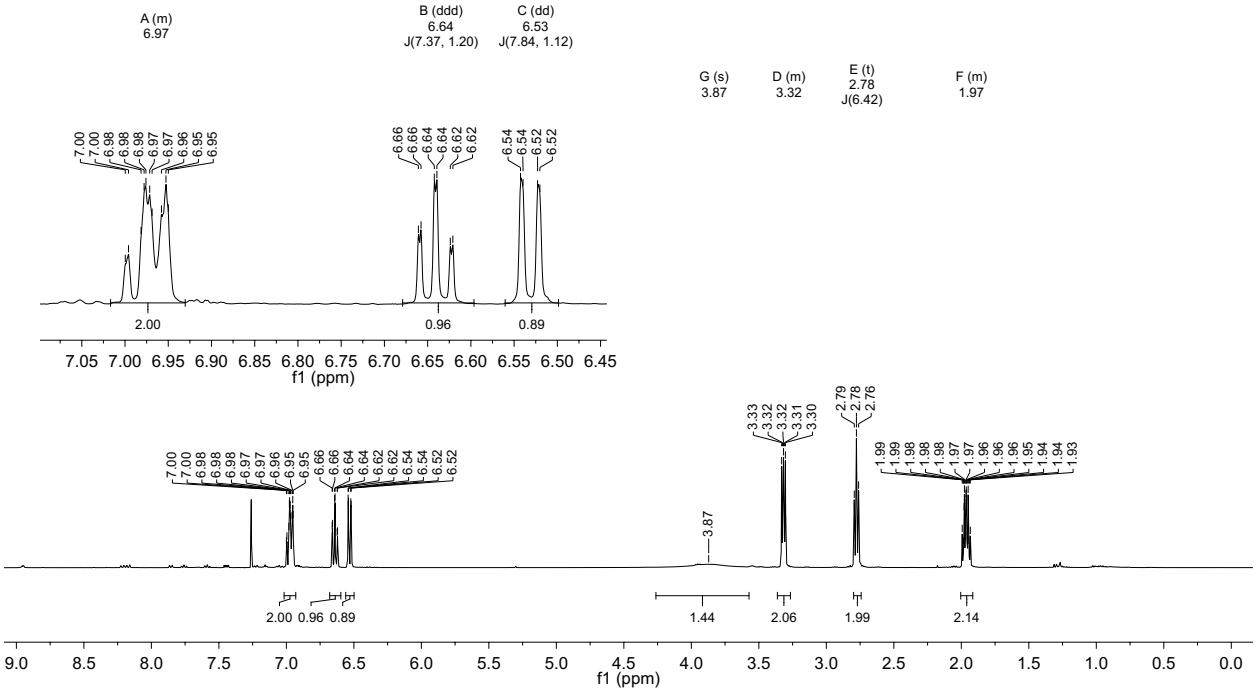

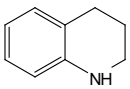

^{13}C NMR (151 MHz, Chloroform-*d*) δ 144.4, 129.7, 126.9, 121.9, 117.5, 114.7, 42.1, 27.0, 22.2.

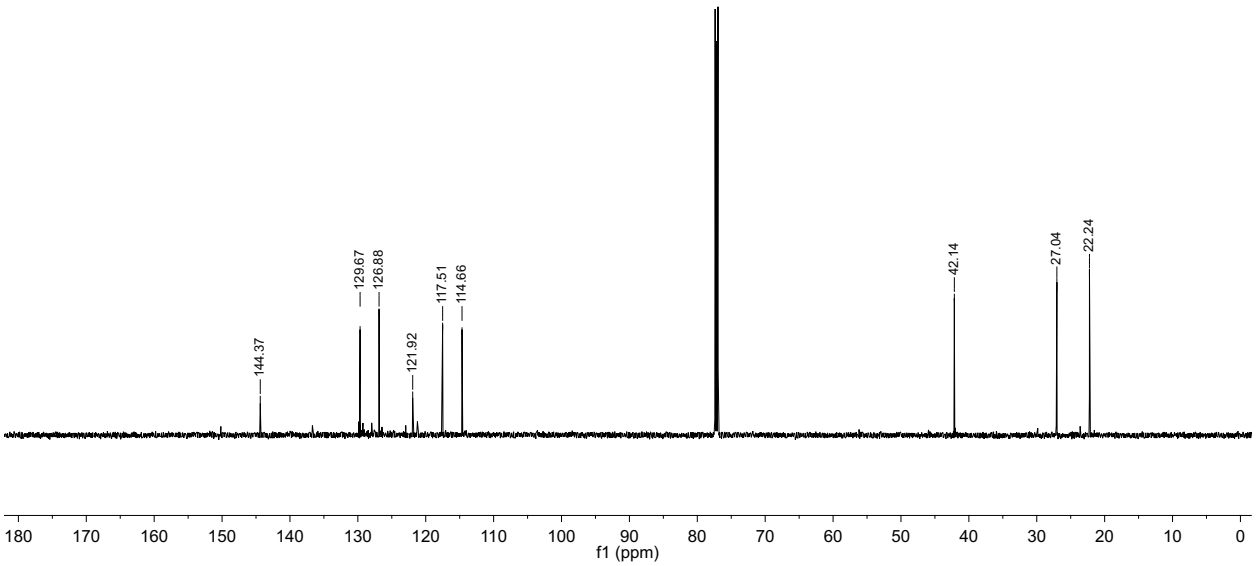

9,10-Dihydroanthracene-9-carbonitrile 522

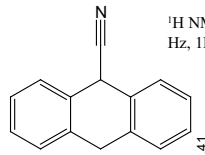

^{1}H NMR (400 MHz, Chloroform-*d*) δ 7.66 – 7.60 (m, 2H), 7.42 – 7.29 (m, 6H), 5.05 (dd, *J* = 2.4, 1.0 Hz, 1H), 4.10 (d, *J* = 17.8 Hz, 1H), 3.94 (dd, *J* = 17.9, 2.4 Hz, 1H).

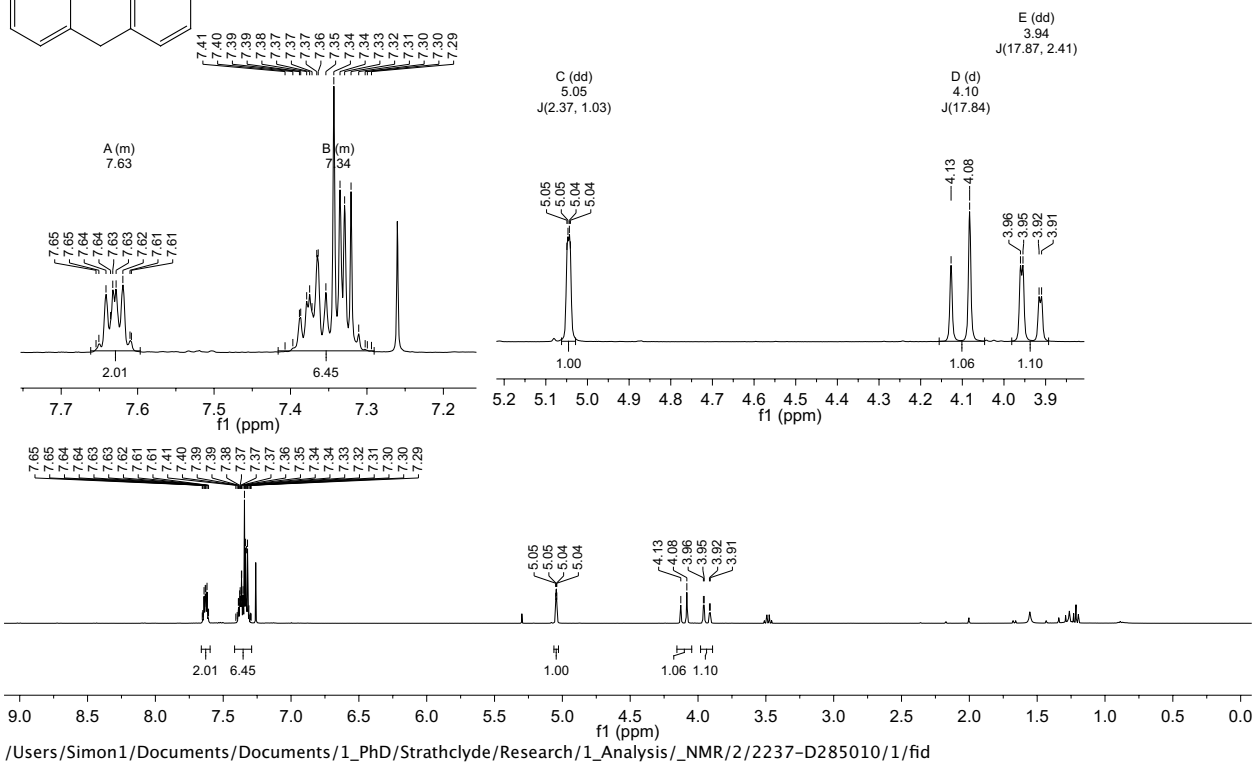

/Users/Simon1/Documents/Documents/1_PhD/Strathclyde/Research/1_Analysis/_NMR/2/2237-D285010/1/fid

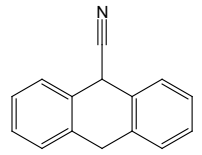

^{13}C NMR (101 MHz, Chloroform-*d*) δ 136.2, 130.9, 128.4, 128.1, 127.2, 126.7, 118.4, 37.2, 35.7.

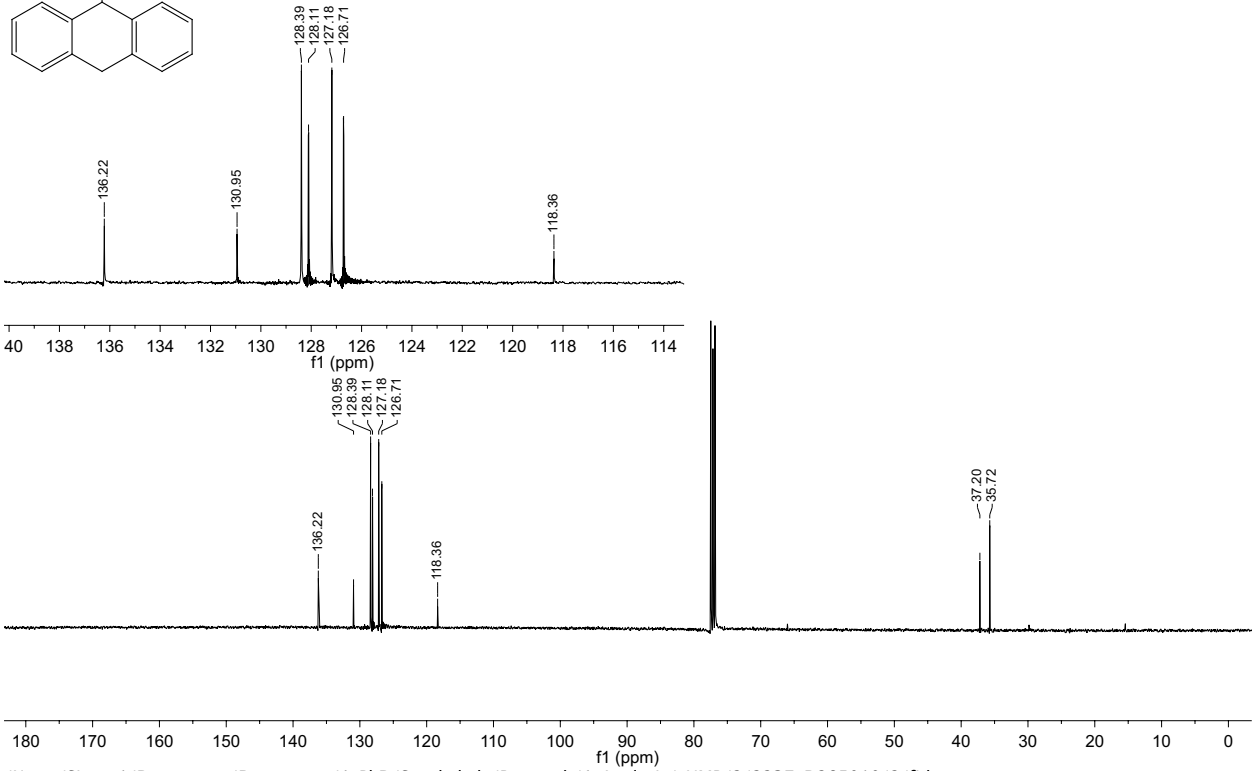

/Users/Simon1/Documents/Documents/1_PhD/Strathclyde/Research/1_Analysis/_NMR/2/2237-D285010/2/fid

9-Methyl-9,10-dihydroanthracene 523

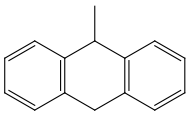

^{1}H NMR (400 MHz, Chloroform-*d*) δ 7.40 – 7.31 (m, 4H), 7.31 – 7.21 (m, 4H), 4.19 (d, *J* = 18.3 Hz, 1H), 4.10 (q, *J* = 7.2 Hz, 1H), 3.95 (d, *J* = 18.2 Hz, 1H), 1.50 (d, *J* = 7.2 Hz, 3H).

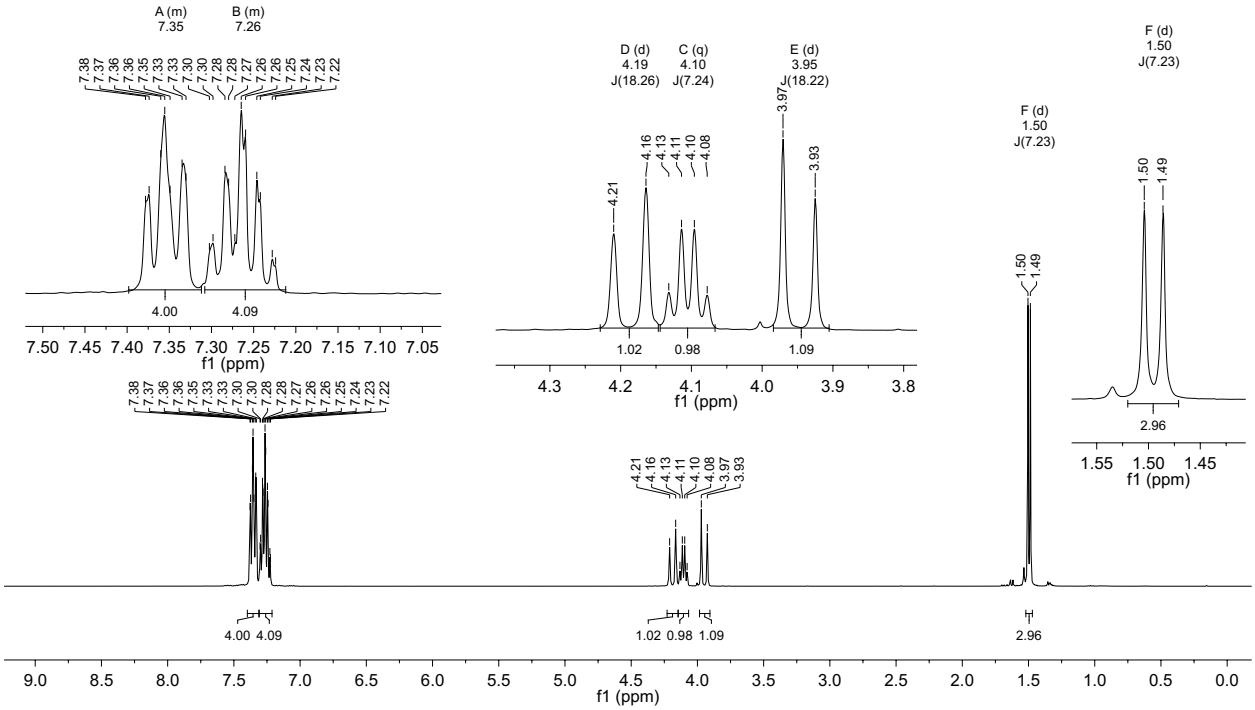

^{13}C NMR (101 MHz, Chloroform-*d*) δ 141.9, 135.9, 127.8, 127.0, 126.5, 126.1, 41.2, 35.3, 23.6.

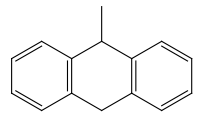

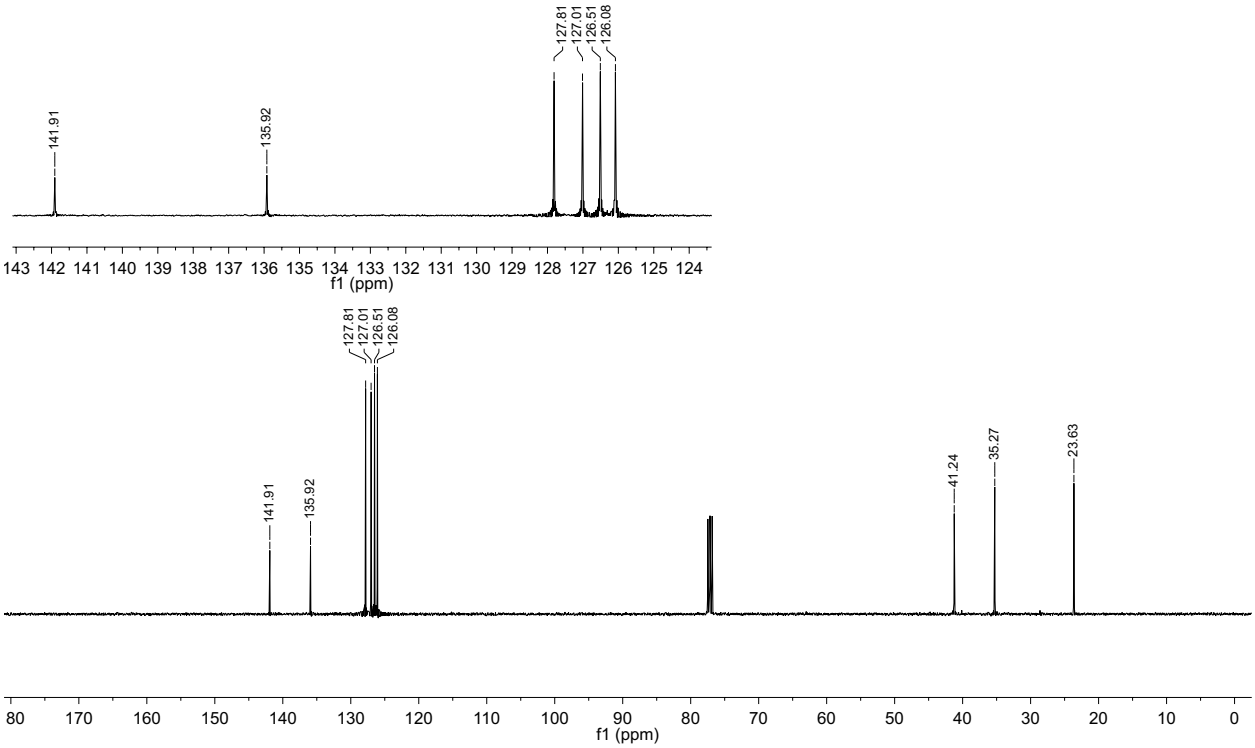

9,10-Dimethyl-9,10-dihydroanthracene 524

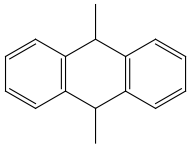

^{1}H NMR (400 MHz, Chloroform-*d*) δ 7.43 (dd, *J* = 5.6, 3.4 Hz, 2H), 7.34 (dd, *J* = 5.6, 3.4 Hz, 1H), 7.28 (ddd, *J* = 5.3, 3.3 Hz, 4H), 4.19 – 4.09 (m, 2H), 1.68 (d, *J* = 7.2 Hz, 6H, trans-isomer), 1.62 (d, *J* = 7.3 Hz, 6H, cis-isomer).

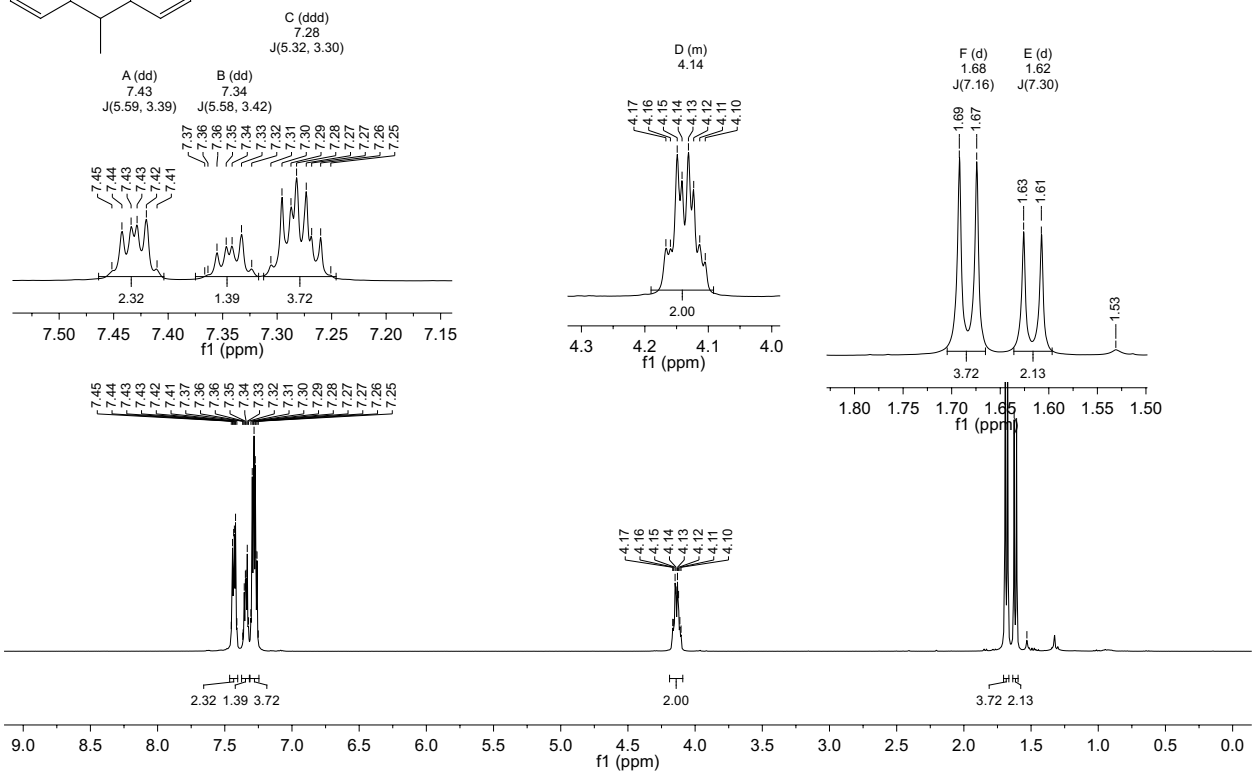

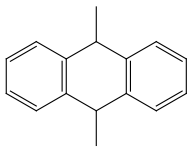

^{13}C NMR (101 MHz, Chloroform-*d*) δ 141.4, 140.6, 127.9, 126.3, 126.3, 125.9, 40.1, 38.6, 28.6, 18.9.

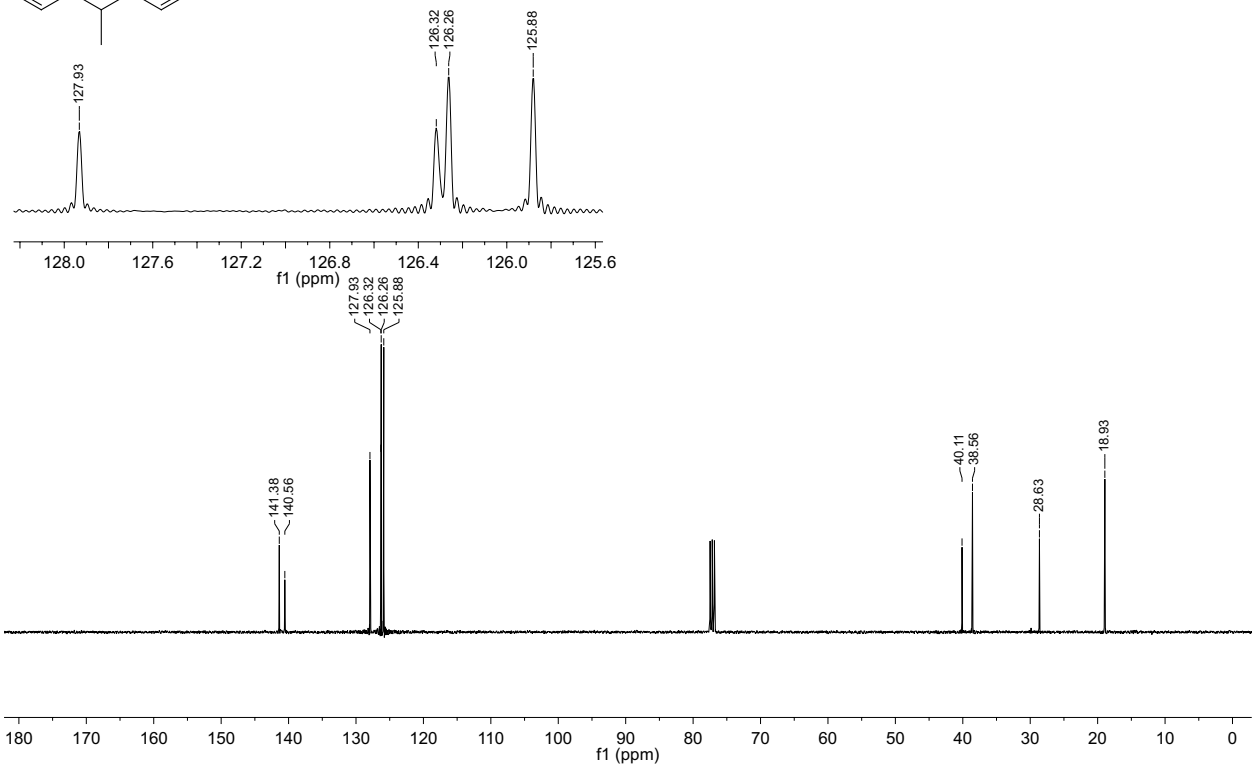

1,4-Dihydronaphthalene 510

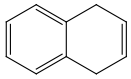

^{1}H NMR (400 MHz, Chloroform-*d*) δ 7.19 – 7.11 (m, 4H), 5.94 (q, *J* = 1.5 Hz, 2H), 3.41 (d, *J* = 1.4 Hz, 4H).

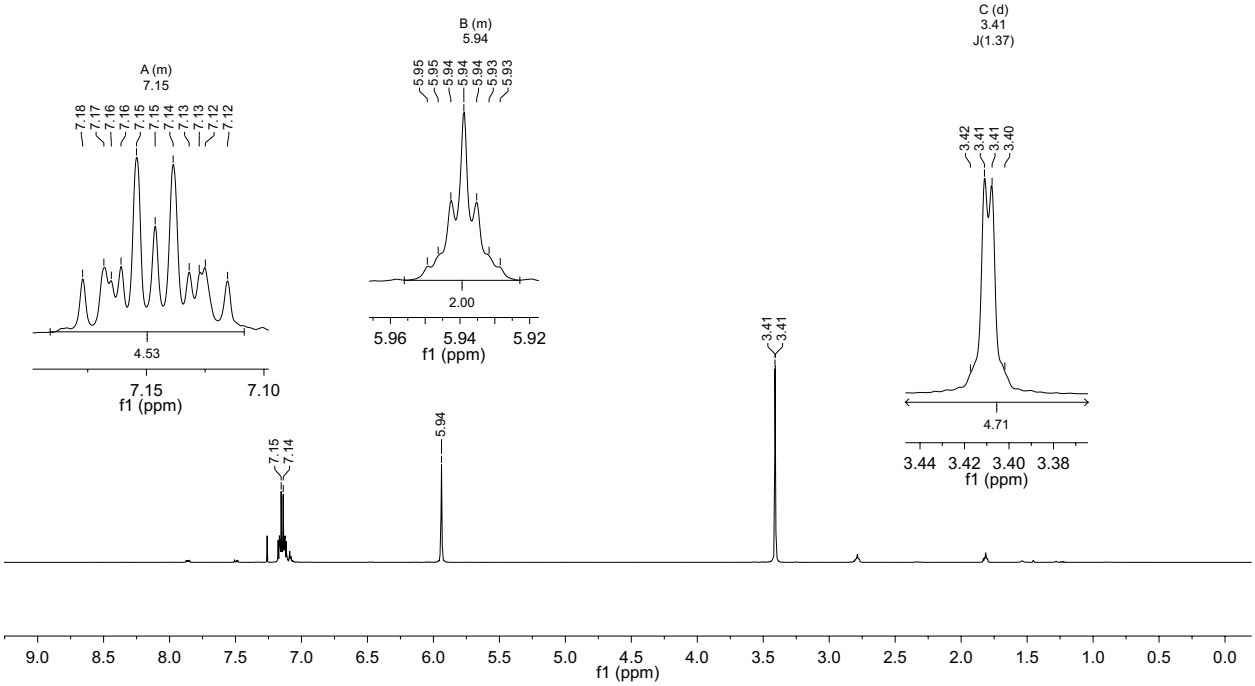

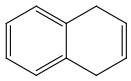

^{13}C NMR (101 MHz, Chloroform-*d*) δ 134.4, 128.6, 126.0, 124.9, 29.9.

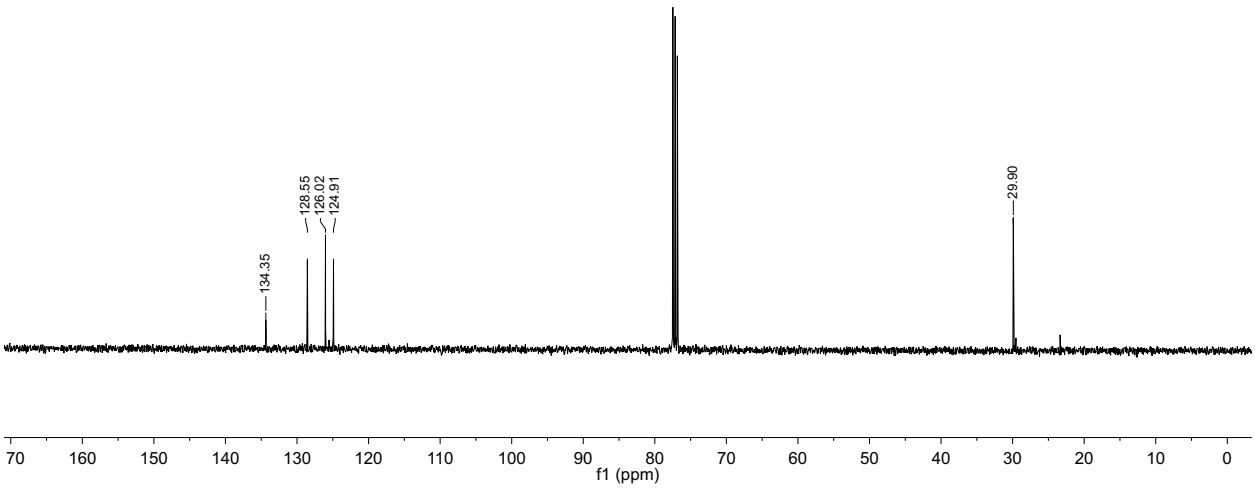

Diphenylacetylene 512

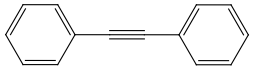

^{1}H NMR (400 MHz, Chloroform-*d*) δ 7.60 – 7.52 (m, 4H), 7.42 – 7.31 (m, 6H).

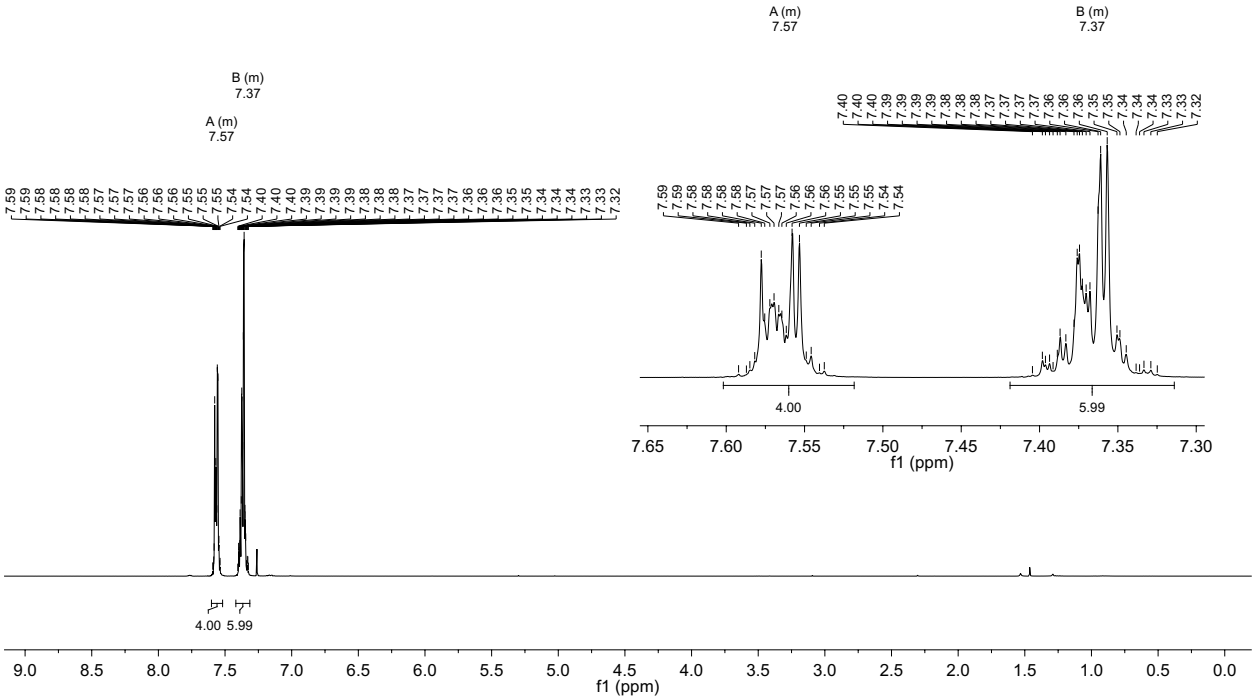

^{13}C NMR (101 MHz, Chloroform-*d*) δ 131.7, 128.5, 128.4, 123.4, 89.5.

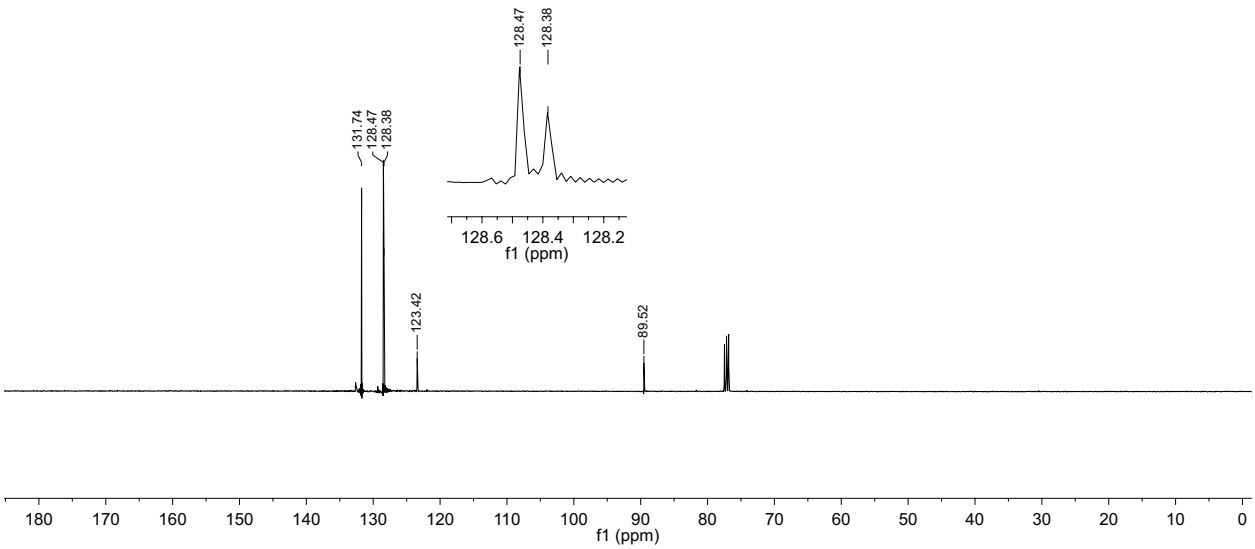

Anthracen-9-yl(pyrrolidin-1-yl)methanone 525

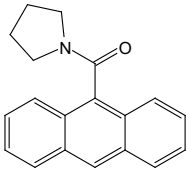

^{1}H NMR (400 MHz, Chloroform-*d*) δ 8.46 (s, 1H), 8.06 – 7.99 (m, 2H), 7.96 – 7.90 (m, 2H), 7.55 – 7.44 (m, 4H), 3.98 (t, *J* = 7.1 Hz, 2H), 2.93 (t, *J* = 6.9 Hz, 2H), 2.05 (tt, *J* = 6.9, 6.9 Hz, 2H), 1.81 (tt, *J* = 6.8, 6.8 Hz, 2H).

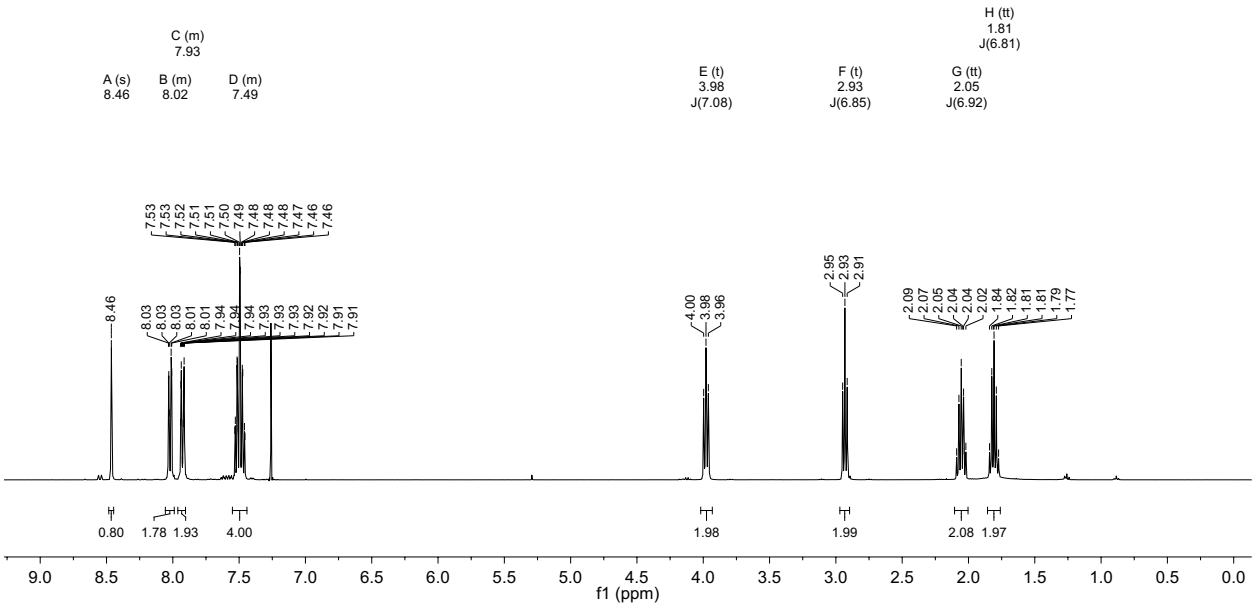

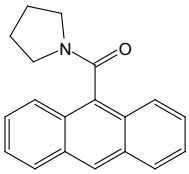

^{13}C NMR (101 MHz, Chloroform-*d*) δ 168.9, 132.5, 131.4, 128.8, 127.7, 127.4, 126.9, 125.6, 125.0, 47.8, 45.8, 26.1, 24.9.

Da steh’ ich nun, ich armer Tor! Und bin so klug als wie zuvor.

Johann Wofgang von Goethe, Faust: Der Tragödie Erster Teil